UNIVERSITY OF SOUTHERN QUEENSLAND

Faculty of Health, Engineering and Sciences

SCALING EFFECTS ON LANDSCAPE FUNCTION ANALYSIS OF RANGELANDS USING REMOTELY SENSED IMAGERY

A thesis submitted by

John Ernest Dunwoody
Qld. Dip. Hort. UQ., B. Agr. Sc. UQ.,
M. Envir. Mgmt. UQ., M. Spat. Sci. Tech. USQ.

In fulfilment of the requirements of

Doctor of Philosophy

2015

ABSTRACT

The declining productivity and loss of ecosystem condition of arid and semi-arid lands is a worldwide concern and a major problem in Australia. Ecosystem condition can be assessed with the help of satellite imagery to measure the loss of basic resources (leakiness) from these areas. Leakiness has been shown to depend on the amount, type and position of vegetation cover in the landscape. It is well established that image scale (the observation scale) strongly affects the detection of landscape patterns and that rescaling changes these observed patterns through change in the structure of image features. Determining the relationship between leakiness calculated from images at different scales may assist in comparing results from the newer satellites with data from older long-duration time-series satellites such as Landsat and MODIS.

This research investigated the effect of different image resolutions on the calculation of leakiness (CSIRO Leakiness Calculator) from a savannah grazing catchment in North Queensland, Australia. Temporally and spatially coincident images from SPOT, Landsat and MODIS satellites were analysed for 11 vegetation indices. These were used in the Leakiness Calculator (LC) to calculate catchment leakiness.

Catchment and sub-catchments were defined from DEMs at scales matching the imagery. A high resolution DEM matching the SPOT resolution was extracted from an aerial photograph stereo model. The SRTM 1s DEM and the GEODATA 9s DEM were each rescaled to match the Landsat and MODIS image scales. Rescaling was by cubic convolution in ArcGIS and other image adjustments were done using ERDAS Imagine, SAGA and ERMapper software. Image structure was analysed by variogram analysis using FETEX 2 software in an ENVI IDL environment.

This study found that the amount of vegetation cover varied with the type of analysis method and the spatial resolution. There was no clear pattern of cover values, except that the 25m Ground Cover Index (GCI) had the highest values. The usual measure of catchment leakiness, Calculated Leakiness (Lcalc) was nominally higher at higher resolutions. This is because it is influenced by the number of cells in the analysis area. A new measure of leakiness, the Adjusted Average Leakiness (AAL) was formulated to be insensitive to cell number and to cell size.

AAL responded inversely to amount of vegetation cover for a given vegetation index but there was no consistent relationship between AAL and type of vegetation index. AAL from Perpendicular Distance Indices (PDI) correlated negatively with cover (as expected) but AAL from the Soil Adjusted Vegetation Index (SAVI) and the Normalised Difference Vegetation Index (NDVI) correlated positively with amount of cover (unexpected). Other vegetation indices had irregular correlations between amount of cover and AAL.

Leakiness scaling functions for calculating both types of leakiness between 10 – 250m resolutions were developed (Resolution Scalograms). Lcalc scalograms took the form of linear reciprocal squared relationships for leakiness from SAVI and the Stress Related Vegetation Index (STVI) and a cubic reciprocal squared relationship for leakiness from the Perpendicular Distance of red-over-green band index (PDrg). AAL scalograms were simpler and took the form of simple linear relationships for leakiness from SAVI and STVI, but cubic for leakiness from PDrg. The high correlation between sill variance and resolution allowed the development of Variance Leakiness Scalograms (VLS). VLS for SAVI and STVI were positive logarithmic relationships and the PDrg VLS was a positive linear relationship.

Analysis of the structure (variance) of observation scale images of the catchment showed they had bounded natural logarithmic variograms. This structure decayed with progressive upscaling. Both observation scale and upscaled images had higher variances at lower a resolution. This is substantially different from previously reported findings. Three-dimensional (3D) models of the variance surfaces showed the effect of upscaling on image structure for different vegetation indices. The PDrg image variance response was the most complex. These models identified the optimal image resolution at which SAVI, STVI and PDrg features are expressed. Correlation between leakiness and conventional variogram indices and indices developed by the Universidad Politecnica de Valencia (UPV) was used to analyse for relationships between image structure and resolution. DEM variograms behaved differently. They had unbounded quadratic variograms and retained their form when upscaled.

The effect of vegetation cover in different areas of the catchment was tested by increasing SAVI and PDrg vegetation cover at different locations relative to major catchment features such as streamlines, elevation, slope, aspect, topographic feature and amount of pre-existing cover. Leakiness decreased the most when cover was added to zones distant from streams, at higher elevations, on lower slopes, on the crest of rises, on the top of ridge lines and in areas with the lowest amount of pre-existing cover. It is acknowledged that these findings are not entirely consistent with each other. There is mixed support for them in the literature. Smaller amounts of cover reduced leakiness more per unit of added cover than larger amounts of cover in all situations.

CERTIFICATION OF DISSERTATION

I certify that the ideas, experimental work, results, analyses, software and conclusions reported in this dissertation are entirely my own efforts, except where otherwise acknowledged. I also certify that the work is original and has not been previously submitted for any other award, except where otherwise acknowledged.

Signature of Candidate	Date

ENDORSEMENT

Signature of Principal Supervisor	Date
Signature of Associate Supervisor	Date

ACKNOWLEDGEMENTS

A thesis is not possible without the help of many people but most of all I would like to express my sincere appreciation to my supervisors. First and foremost to Associate Professor Armando Apan who both introduced me to GIS and Remote Sensing in the beginning through his very capable teaching skills and who has stood by me, ever ready to assist me throughout this thesis. He helped me realise a design that was only a vague idea in the beginning, helped me formulate the approach, the analysis methods and finally the interpretation of the findings. His forbearance with the idiosyncrasies of a senior student is acknowledged and very much appreciated. Dr Xiaoye Liu, my co-supervisor, has been quietly involved in all aspects of this work as she was with my Master's Thesis. She has been someone I could always depend on for ideas or whenever a difficult processing step was encountered. Individually and collectively, I thank both my supervisors.

This work required access to many resources without which it would not have been possible. Firstly, I acknowledge the USQ resources that were made available including computing resources of the ICT Department and the field mapping equipment provided by the Department of Civil Engineering and Surveying. I especially appreciate the help of Mr Clinton Caudell in overcoming many practical problems associated with fieldwork. A financial travel grant from the National Climate Change Adaptation Research Facility (NCCARF) was particularly helpful with costs associated with conferring with established researchers at CSIRO and the Queensland Department of Agriculture, Fisheries and Forestry (QDAFF).

Mr Lee Blacklock of the Queensland Natural Resources Management Groups Cooperative was very helpful in making SPOT imagery available along with Mr Doug Willis of the North Queensland Dry Tropics Natural Resources Management Group. The Government of the USA also deserves credit for continuing to make GPS data signals and Landsat and MODIS imagery available free of cost to the user.

Many people gave freely of their time and technical advice, especially Queensland State Government agency staff. Special acknowledgement is given to Mr Adrian Neal, Mr Mehedi Etemadi, Ms Jasmine Muir, Dr Peter Scarth and Dr Robert Karfs for their counsel and advice. No work of this type could be done without the pioneering work of CSIRO investigators and special acknowledgement is given to Mr David Tongway, Dr Adam Liedloff, Mr John Ludwig, Dr Brett Abbott, Mrs Vanessa Chewings and Dr Gary Bastin each of whom gave very useful and helpful advice. I also acknowledge the patient and helpful processing advice of two fellow students, Mr Govinda Baral and Mr Rodolfo Espada.

All fieldwork has a “home in the bush” somewhere and it fell to the lot of four friendly graziers to let me tramp throughout their properties collecting data. Without release of confidentiality, I am very thankful for the goodwill of Brian and Molly Christensen of Jesmond Station, Jennifer and Robert Laurie of Powlathanga station, Ian and Pam Berryman of Fifteen Mile Station and David Berryman and Rita Parker of Mt Windsor Station for allowing me open access for collecting a suite of field records. These were essential for correctly georegistering the imagery and ground-truthing image values.

PUBLICATIONS RELATED TO THIS THESIS

1. Dunwoody, E., A. Apan, and X. Liu (2013). *Effects of spatial resolution on measurement of landscape function using the landscape leakiness calculator*. In: Proceedings of the Surveying and Spatial Sciences Conference (SSSC 2013): 17-19 April 2013, Canberra, Australia
2. Dunwoody, E., A. Apan, and X. Liu (2013). *Use of satellite imagery to optimize selection of revegetation sites for increased ecosystem function*. In: Proceedings of the Queensland State Landcare Conference, 27-29 September, 2013 Warwick, Queensland.
3. Dunwoody, E., A. Apan, and X. Liu (in preparation). Effect of image scale on catchment Leakiness analysis. To be submitted to the Journal of Ecological Applications, Ecological Society of America, Washington DC.
4. Dunwoody, E., A. Apan, and X. Liu (in preparation). Effect of resampling on image structure for landscape function analysis. To be submitted to the International Journal of Remote Sensing, Remote Sensing and Photogrammetry Society, Taylor and Francis Pty Ltd.
5. Dunwoody, E., A. Apan, and X. Liu (in preparation). Not all bare spots are the same: Use of the Leakiness Calculator to rank revegetation areas in a watershed. To be submitted to journal of Applied Geography, Elsevier Pty. Ltd. Cambridge MA.

TABLE OF CONTENTS

Abstract iii
Certification of Dissertation...v
Acknowledgements..vii
Publications related to this Thesis ix
Table of Contents...xi
Table of Figures xix
List of Tables xxix
Photographs..xxxiii
Appendices xxxv
Abbreviations xxxvii

CHAPTER 1

INTRODUCTION

1.1. Introduction 1
1.2. Statement of the Problem 3
1.3. Aim 5
1.4. Objectives.. 5
1.5. Significance of this Research 5
1.6. Limitations of the Study 8
1.7. Conclusion.. 9

CHAPTER 2

LITERATURE REVIEW

2.1. Overview 11
2.2. Rangeland Condition Monitoring 13
2.3. Ecosystem Condition Monitoring 16
2.4. Landscape Function Indices (LFI) 18
2.4.1. Directional Leakiness Index (DLI) 20
2.4.2. Cover-based Directional Leakiness Index (CDLI) 21
2.4.3. Leakiness Index (LI) 22
2.5. Bio-geophysical Features 25
2.6. Leakiness at Different Image Scales 30

2.6.1. Scaling Patterns 30
2.6.2. Ecosystem Scaling 33
2.6.3. Scaling relations 38
2.6.4. Upscaling methods 39
2.7. Effect of Image Structure on Leakiness 40
2.7.1. Spatial scales 40
2.7.2. Spatial variation 41
2.7.3. Spatial patterns 44
2.8. Cover Position and Catchment Leakiness 45
2.8.1. Patchiness 45
2.8.2. Ground Cover 46
2.9. Conclusion 48

CHAPTER 3

RESEARCH METHODS

3.1. Introduction 49
3.2. Overview of processing and analysis 49
3.3. Study Area 50
3.4. Research Approach 55
3.5. Data Sources 55
3.5.1. Satellite imagery 55
3.5.2. Digital Elevation Models 57
3.5.3. Ground Truth Data 58
3.6. Experimental Design 60
3.7. Pre-processing 62
3.7.1. Imagery 62
3.7.2. DEMs 62
3.7.3. Analysis Masks 63
3.7.4. Ground Truth Data 63
3.8. Conclusion 63

CHAPTER 4

EFFECT OF IMAGE RESOLUTION AND VEGETATION COVER ONCATCHMENT LEAKINESS

4.1. Introduction 65
4.2. Methods 67
4.2.1. Data Requirements 69
4.2.1.1. Catchment DEM, Boundaries and Drainage Lines 69

4.2.1.2. Analysis Masks 71
4.2.1.3. Vegetation Cover Layers 73
Moving Standard Deviation Index (MSDI) 73
Normalised Difference Vegetation Index (NDVI) 74
Soil Adjusted Vegetation Index (SAVI) 75
Redness Index (RI) 75
Stress Related Vegetation Index 76
Corrected Vegetation Index (CORVI) 76
Perpendicular Distance Indices (PDI) 77
Soil and Atmosphere Resistant Vegetation Index (SARVI) 79
Ground Cover Index (GCI) 80
4.2.2. Leakiness Calculation 81
4.2.3. Adjusted Average Leakiness 81
4.3. Results 82
4.3.1. Catchment Leakiness 82
4.3.2. Variation in Catchment Cover and Leakiness 84
4.3.2.1. Variation in Cover 89
4.3.2.2. Variation in Leakiness 90
4.3.2.3. Adjusted Average Leakiness 92
4.3.3. Sub-catchment Leakiness 96
4.3.3.1. Ten Meter Resolution 96
Correlation between Indices 98
Leakiness response to amount and type of cover 99
4.3.3.2. Twenty Five Meter Resolution 100
Correlation between Indices 103
Leakiness Response to amount and type of cover 104
4.3.3.3. Two Hundred and Fifty Meter Resolution 105
Correlation between Indices 107
Leakiness response to amount and type of cover 108
4.3.4. Catchment Comparison 109
4.4. Discussion 110
4.4.1. Catchment Leakiness 110
4.4.2. Different Vegetation Cover Values 112
4.4.3. Adjusted Average Leakiness 114
4.4.4. Sub-catchment Responses 116
4.4.5. Response Relationships 117
4.5. Conclusion 118

CHAPTER 5

DEVELOPMENT OF LEAKINESS SCALING FUNCTIONS

5.1. Introduction 121
5.2. Scaling and Leakiness 121
5.3. Research Methods 124
5.3.1. Overview 124
5.3.2. Image and leakiness processing procedures 124
5.3.3. Statistical procedures 125
5.3.4. Scalogram derivation 126

5.4. Results 127
5.4.1. Stage of Upscaling 127
5.4.1.1. SAVI 128
5.4.1.2. STVI 129
5.4.1.3. PDrg 129
5.4.2. Resolution Scalograms for Calculated Leakiness 129
5.4.2.1. SAVI Cover 130
5.4.2.2. STVI Cover 132
5.4.2.3. PDrg Cover 133
5.4.3. Resolution Scalograms for Average Adjusted Leakiness 136
5.4.3.1. SAVI Cover 136
5.4.3.2. STVI Cover 137
5.4.3.3. PDrg Cover 137
5.4.4. Comparison of Scalograms 139
5.4.4.1. Coverage 139
5.4.4.2. Leakiness 139
Calculated Leakiness 140
High resolution calculated leakiness 142
Scale dependent relationships 143
Adjusted Average Leakiness 144
5.4.5. Variance Scalograms 144
5.4.5.1. SAVI and STVI 145
5.4.5.2. PDrg 146
5.4.5.3. Leakiness as a function of variance 146
5.4.6. Comparison between native and upscaled leakiness 147
5.5. Discussion 148
5.5.1. Comparison of upscaling procedures 148
5.5.2. Calculated Leakiness Scalograms 149
5.5.3. Adjusted Average Leakiness Scalograms 150
5.5.4. Resolution Scalogram Comparison 151
5.5.5. Variance Scalograms 152
5.5.6. Upscale and native leakiness comparison 153
5.5.7. Scale and feature relationships 153
5.6. Conclusion 154

CHAPTER 6

EFFECT OF UPSCALING ON IMAGE STRUCTURE

6.1. Introduction 155
6.1.1. Changing Scales 155
6.1.2. General application 158
6.1.3. Application to Leakiness 159
6.2. Research Methods 159
6.2.1. Data Sources 160
6.2.2. Variance Analysis 160
6.2.3. Correlation Analysis 161

6.3. Results 161
6.3.1. Native Images 162
6.3.1.1. Soil Adjusted Vegetation Index (SAVI) 162
Variance 162
Variogram Indices 164
Index correlation with leakiness 165
Summary of SAVI variograms index correlations 168
6.3.1.2. Stress Related Vegetation Index (STVI) 168
Variance 168
Variogram Indices 170
Index correlation with leakiness 171
Summary of STVI variogram index correlations 174
6.3.1.3. Perpendicular Distance (red/green) Index (PDrg) 174
Variance 174
Variogram indices 176
Index correlation with leakiness 176
Summary of PDrg variogram index correlations 180
6.3.1.4. Summary of all 3 native image variogram index correlations 180
6.3.1.5. DEM 180
Variance 180
Variogram indices 183
Index correlation with leakiness 183
Effect of resolution and lag 184
Sub-catchments 187
6.3.2. Upscaled Images 188
6.3.2.1. Soil Adjusted Vegetation Index (SAVI) 188
Variance 188
Variogram indices 191
Index correlation with leakiness 192
6.3.2.2. Stress Related Vegetation Index (STVI) 195
Variance 195
Variogram indices 198
Index correlation with leakiness 199
Sub-catchments 201
6.3.2.3. Perpendicular Distance Vegetation Index (PDrg) 203
Variance 203
Variogram indices 207
Index correlation with leakiness 207
6.3.2.4. DEM 211
Variance 211
Variogram indices 213
Effect of resolution and lag 213
6.3.3. Comparison between native and upscaled imagery 215
6.3.3.1. Soil Adjusted Vegetation Index comparison (SAVI) 215
Variance comparison 215
ContourComparison 217
6.3.3.2. SAVI cover images 218
Surface comparison 218
Index comparison 218
6.3.3.3. Stress Related Vegetation Index comparison (STVI) 219
Variance comparison 219
Contour comparison 221
Surface comparison 222
Index comparison 222
6.3.3.4. Perpendicular Distance (red over green) Index comparison (PDrg) 223
Variance comparison 223

Contour comparison....226
Surface comparison....226
Index comparison....227
6.3.3.5. Native DEM vs resampled DEM....228
6.4. Discussion....229
6.4.1. Image structure....230
6.4.1.1. Native scale images....230
6.4.1.2. Upscaled Images....232
6.4.2. DEM structure....235
6.4.3. Variance Surfaces....236
6.4.3.1. Native scale images....236
6.4.3.2. Upscale images....236
6.4.4. Correlation of image structure with leakiness....236
6.4.4.1. Native scale images....237
6.4.4.2. Upscaled images....237
6.5. Conclusion....239

CHAPTER 7

EFFECT OF VEGETATION COVER POSITION ON CATCHMENT LEAKINESS

7.1. Introduction....241
7.2. Methods....244
7.2.1. Zonal cover analysis plan....244
7.2.2. Zonal pixel adjustment procedure....245
7.2.3. No cover offset and Cover offset procedures....247
7.2.4. Morphological feature preparation and classification....247
7.2.4.1. Drainage Line Zones....247
7.2.4.2. Elevation zones....248
7.2.4.3. Slope zones....249
7.2.4.4. Aspect zones....250
7.2.4.5. Topographic zones....251
7.2.4.6. Cover zones....253
7.2.5. Analysis....254
7.3. Results....255
7.3.1. General Cover Increase....255
7.3.2. Drainage Distance Zones....256
7.3.2.1. SAVI Coverage....256
No cover offset....257
Cover offset....259
7.3.2.2. PDrg Coverage....260
No cover offset....261
Cover Offset....263
7.3.3. Elevation Zones....265
7.3.3.1. SAVI Coverage....265
No cover offset....266
Cover offset....268

7.3.3.2. PDrg Coverage 269
No cover offset 270
Cover Offset 272
7.3.4. Slope Zones 273
7.3.4.1. SAVI Coverage 274
No cover offset 274
Cover offset 276
7.3.5. Aspect Zones 278
7.3.5.1. SAVI Coverage 278
No cover offset 279
Cover offset 280
7.3.6. Topographic Zones 282
7.3.6.1. SAVI Coverage 283
No cover offset 284
Cover offset 286
7.3.6.2. PDrg Coverage 288
No Cover offset 289
Cover Offset 291
7.3.7. Cover Zones 292
7.1.1.1. SAVI Coverage 292
No cover offset 294
Cover offset 295
7.3.7.1. PDrg Coverage 297
No Cover Offset 298
Cover Offset 299
7.4. Discussion 301
7.4.1. Drainage Line Distance (DLD) Zones 301
7.4.2. Elevation Zones 303
7.4.3. Slope Zones 304
7.4.4. Aspect Zones 305
7.4.5. Topographic Zones 305
7.4.6. Cover Zones 307
7.4.7. Summary 308
7.5 Conclusion 312

CHAPTER 8

CONCLUSION

8.1. Introduction 313
8.2. Findings 313
8.2.1. Adjusted Average Leakiness Metric 313
8.2.2. Cover and Leakiness 314
8.2.3. Leakiness Scaling Functions 315
8.2.4. Scaling Effect on Image Structure 315
8.2.5. Position of Cover in Catchment 316
8.3. Future Research 317

REFERENCES.................................…………………319

APPENDICES ....…………………......331

TABLE OF FIGURES

CHAPTER 1

Figure 1.1 Landscape function measurement schemes. Analogue monitoring diagram. 7

CHAPTER 2

Figure 2.1. The diversity of Biogeographical Regions comprising the rangelands is shown by the coloured areas. Natural Resource Management Regions and Local Land Service regions (NSW only) are shown in initialled areas. 12
Figure 2.2 Trigger, Transfer, Reserve Pulse model of ecosystem function 16
Figure 2.3.The Leakiness Index for a rangeland monitoring site 200km north of Alice Springs, compared with mean levels of persistent vegetation from 1980 to 2002, (a) and Annual rainfall from 1979 to 2004 relative to the mean of 304 mm (b) 24
Figure 2.4.Examples of pattern scalograms for landscape metrics as a result of changing the resolution 31
Figure 2.5. Role of landscape scaling relations in influencing scaling functions and prediction of consequences 34
Figure 2.6 Patch to Interpatch differences in soil N in relation to patch size for small-scale local landscape vegetation-soil patches from 36
Figure 2.7 Apparent disjunction in scaling relationship for soil N accumulation between small local patches and large regional patches from 36
Figure 2.8 Effect of Isotropic Point Spread Function on pixel upwelling radiance... 41
Figure 2.9 Gaussian bounded variogram 42
Figure 2.10 Monotone semi-variogram after 44

CHAPTER 3

Figure 3.1 Chapter guide to the processing and analysis procedures 49
Figure 3.2 Location of experimental catchment 50
Figure 3.3 Remnant ecosystem coverage of experimental catchment 51
Figure 3.4 Relative amounts of each Remnant Ecosystem (ha) 51
Figure 3.5 Research Schema 55
Figure 3.6 Key reference points map 57
Figure 3.7 Ground truth field records 59
Figure 3.8 Experimental Analysis Path 60

CHAPTER 4

Figure 4.1 Ten-meter DEM catchment and sub-catchments 69
Figure 4.2 Twenty five meter DEM catchment and sub-catchments 70
Figure 4.3 Two hundred and fifty meter DEM catchment and sub-catchments 70
Figure 4.4 Ten meter scale catchment Analysis Masks 71
Figure 4.5 Twenty five meter scale Analysis Masks 72
Figure 4.6 Two hundred and fifty meter scale Analysis Masks 72
Figure 4.7 Example MSDI cover layers 74
Figure 4.8 Example NDVI cover layers 74
Figure 4.9 Example SAVI cover layers 75
Figure 4.10 Example RI Cover layers 75
Figure 4.11 Example STVI-4 Cover layers 76
Figure 4.12 Example CORVI Cover layers 77
Figure 4.13 Example PDrg Cover layers 78
Figure 4.14 Example PDrn Cover layers 78
Figure 4.15 Example PDrs Cover layers 79
Figure 4.16 Example SARVI Cover layers 79
Figure 4.17 Example GCI cover layer. 80
Figure 4.18 Vegetation Cover at three resolution 83
Figure 4.19 Leakiness at three resolutions 83
Figure 4.20 Response of Leakiness to Average Cover (multiple indices) 84
Figure 4.21 Vegetation cover distribution by cover index at 10m resolution 85
Figure 4.22 Vegetation cover distribution by cover index at 25m resolution 86
Figure 4.23 Vegetation cover distribution by cover index at 250m resolution 88
Figure 4.24 Variation in Average Cover by Cover Index and resolution 89
Figure 4.25 Leakiness at different resolutions for different cover indices. 90
Figure 4.26 Leakiness Sensitivity 91
Figure 4.27 Change in Leakiness Sensitivity to Cover 92
Figure 4.28 Adjusted Average Leakiness values 93
Figure 4.29 Adjusted Average Leakiness response to resolution 93
Figure 4.30 Adjusted Average Leakiness response to amount of cover. 94
Figure 4.31 Adjusted Average Leakiness Sensitivity 95
Figure 4.32 Change in AAL Sensitivity to Cover 95
Figure 4.33 Average Cover (%) for each sub-catchment (10m) 97
Figure 4.34 Leakiness of each sub-catchment by cover index (10m) 98
Figure 4.35 Clustering of Leakiness and Average Cover in data space (10m) 99
Figure 4.36 Average Cover for each sub-catchment (25m) 101
Figure 4.37 Adjusted Average Leakiness for each sub-catchment (25m) 102
Figure 4.38 Clustering of AA Leakiness and Average Cover in data space (25m) 104
Figure 4.39 Details of Band Ratio AA Leakiness and Average Cover in data space (25m) 104
Figure 4.40 Average Cover for each sub-catchment (250m) 106
Figure 4.41 Adjusted Average Leakiness for each sub-catchment (250m) 107

Figure 4.42 Clustering of AA leakiness and Average Cover in data space (250m) 108
Figure 4.43 Aggregate-of-sub-catchments ... 109
Figure 4.44 Whole-of-catchment ... 109

CHAPTER 5

Figure 5.1. Soil loss as a function of average vegetation cover. ... 122
Figure 5.2 Mean levels of ground cover (Botanal %) and catchment leakiness (LI) calculated from PD_{54} coverage of 5m resampled Quickbird imagery. 123
Figure 5.3 Mean levels of ground cover (Botanal %) and catchment leakiness (LI) calculated from the GCI coverage of 25m resampled Landsat imagery 123
Figure 5.4 Process Overview ... 124
Figure 5.5 Procedure used to upscale files and calculate leakiness ... 125
Figure 5.6 Statistical analysis test procedures used in development of scaling equations... 126
Figure 5.7 Scalogram development procedure... 127
Figure 5.8 Difference in Average Cover and Calculated Leakiness from upscaling the image versus upscaling the cover layer. ... 128
Figure 5.9 Comparison of Cover and Leakiness from upscaling the image versus upscaling the thematic cover layer ... 129
Figure 5.10 Relationship of Lcalc, Cover (SAVI) and Cell Count with Resolution 130
Figure 5.11 Distribution of Lcalc transformed (SAVI) against resolution ... 131
Figure 5.12 Comparison of Lcalc expt. against Lcalc pred. ... 131
Figure 5.13 Relationship of Leakiness, Cover (STVI) and cell count with Resolution ... 132
Figure 5.14 Distribution of transformed Leakiness (STVI) against resolution ... 132
Figure 5.15 Comparison of experimental Leakiness against predicted Leakiness (STVI). ... 133
Figure 5.16 Relationship of Leakiness, Cover (PDrg) and Cell Count with Resolution ... 134
Figure 5.17 Distribution of transformed Lcalc (PDrg) against resolution ... 134
Figure 5.18 Residuals for linear and cubic fits ... 134
Figure 5.19 Comparison of Cubic and Linear solutions to PDrg Lcalc predictive equations... 136
Figure 5.20 Relationship of AAL, Cover (SAVI) and Cell Count with Resolution 136
Figure 5.21 Relationship of AAL, Cover (STVI) and Cell Count with Resolution 137
Figure 5.22 Relationship of AAL, Cover (PDrg) and Cell Count with Resolution. 138
Figure 5.23 Effect of upscaling on Coverage ... 139
Figure 5.24 Calculated Leakiness response to change in resolution... 139
Figure 5.25 Adjusted Average Leakiness (AAL) response to change in resolution 140
Figure 5.26 Comparison of response of transformed Lcalc with resolution... 140
Figure 5.27 Projected leakiness response to change in resolution ... 141
Figure 5.28 Absolute difference between experimental and projected leakiness values ... 142

Figure 5.29 Fine scale projected and experimental leakiness 142
Figure 5.30 Separation of transformed leakiness at the 80m resolution break point143
Figure 5.31 AAL and Semivariance dependence on Resolution for upscaled SAVI cover images 145
Figure 5.32 AAL and Semivariance dependence on Resolution for upscaled STVI cover images 145
Figure 5.33. AAL and Semivariance dependence on Resolution for upscaled PDrg image 146
Figure 5.34 Variance scalograms for upscaled SAVI, STVI and PDrg cover images 146
Figure 5.35. Comparison of native and upscaled leakiness for SAVI, STVI and PDrg coverages 148

CHAPTER 6

Figure 6.1 Plot of First Range (a_o) against Nugget and Sill Variance ($c+c_o$) 157
Figure 6.2 Semi Natural log plot of areal resolution against Nugget and Sill Variance ($c+c_o$) for unscaled and upscaled NDVI images, ... 158
Figure 6.3 Variance analysis flow sequence 160
Figure 6.4 SAVI semivariance 162
Figure 6.5 SAVI native semivariance contours 163
Figure 6.6 SAVI native semivariance surface 163
Figure 6.7 SAVI native semivariance model 164
Figure 6.8 Native SAVI semivariance values as a function of resolution. 166
Figure 6.9 Native SAVI semivariance values as a function of cell number 167
Figure 6.10 Native SAVI semivariance values and Lcalc 167
Figure 6.11 Native SAVI semivariance values and AAL 167
Figure 6.12 STVI semivariance variograms 168
Figure 6.13 STVI native semivariance contours 169
Figure 6.14 STVI native semivariance surface 169
Figure 6.15 STVI native semivariance model 170
Figure 6.16 Native STVI semivariance index response to resolution. 172
Figure 6.17 Native STVI semivariance index response to catchment cell number. 172
Figure 6.18 Native SAVI semivariance index response to average cover. 173
Figure 6.19 Native STVI semivariance index response to Lcalc 173
Figure 6.20 Native STVI semivariance index response to AAL 173
Figure 6.21 PDrg semivariance variograms 174
Figure 6.22 PDrg native semivariance contours 175
Figure 6.23 PDrg native semivariance surface 175
Figure 6.24 PDrg native semivariance model 176
Figure 6.25 Native PDrg semivariance indices as a function of resolution. 178
Figure 6.26 Native PDrg semivariance indices as a function of catchment cell No.178
Figure 6.27 Native PDrg semivariance indices as a function of average cover 179
Figure 6.28 Native PDrg semivariance indices response to Lcalc. 179

Figure 6.29 Native PDrg semivariance indices` response to AAL 179
Figure 6.30 Semivariance of whole-of-catchment DEMs....................................... 181
Figure 6.31 Raw DEM semivariance contours 181
Figure 6.32 Native DEM semivariance surface 182
Figure 6.33 Native DEM semivariance model.. 182
Figure 6.34 DEM semivariance values as a function of resolution 184
Figure 6.35 DEM semivariance values as a function of catchment cell number..... 184
Figure 6.36 Lag Semivariance relationship with resolution (DEM, native)............ 184
Figure 6.37 Native DEM semivariance contour pattern 185
Figure 6.38 Relationship of native DEM semivariance to lag and resolution 186
Figure 6.39 Revised native DEM semivariance model... 186
Figure 6.40 Comparison of raw DEM semivariance (left) with modelled DEM semivariance (right)... 187
Figure 6.41 Semivariance of sub-catchments in the 10m DEM 187
Figure 6.42 Semivariance of sub-catchments in the 25m DEM 188
Figure 6.43 Semivariance of sub-catchments in the 250m DEM 188
Figure 6.44 Semivariance of resampled SAVI (10m - 30m) 189
Figure 6.45 Semivariance of resampled SAVI (50-250m) 189
Figure 6.46 Contour plot upscaled SAVI semivariance (5-30m) 190
Figure 6.47 Contour plot upscaled SAVI semivariance (5-250m) 190
Figure 6.48 SAVI upscaled semivariance... 191
Figure 6.49 SAVI upscale semivariance model.. 191
Figure 6.50 SAVI upscale semivariance values as a function of resolution............ 193
Figure 6.51 SAVI upscale semivariance values as a function of cell number......... 194
Figure 6.52 SAVI upscale semivariance relationship with Average Cover............. 194
Figure 6.53 SAVI upscale semivariance values relationship with Lcalc................. 194
Figure 6.54 SAVI upscale semivariance values relationship with AAL 195
Figure 6.55 Semivariance of resampled STVI (10-30m).. 195
Figure 6.56 Semivariance of resampled STVI (50-250m)...................................... 196
Figure 6.57 Contour plot STVI semivariance (5-30m)... 196
Figure 6.58 Contour plot SVI semivariance (5-250m) 197
Figure 6.59 STVI upscaled semivariance 197
Figure 6.60 STVI upscale semivariance model 198
Figure 6.61 STVI semivariance values as a function of resolution 199
Figure 6.62 STVI semivariance values as a function of cell number 200
Figure 6.63 STVI semivariance values relationship with Lcalc 200
Figure 6.64 STVI semivariance values relationship with AAL............................... 201
Figure 6.65 Semivariance of STVI in 10 sub-catchments (10m resolution)............ 201
Figure 6.66 Semivariance of STVI in 10 sub-catchments (25m resolution)............ 202
Figure 6.67 Semivariance of STVI in 10 sub-catchments (50m resolution)............ 202
Figure 6.68 Semivariance of STVI in 10 sub-catchments (100m resolution).......... 202
Figure 6.69 Semivariance of STVI in 10 sub-catchments (200m resolution).......... 203
Figure 6.70 Semivariance of STVI in 10 sub-catchments (250m resolution).......... 203
Figure 6.71 Semivariance of resampled PDrg (10-30m) 204

Figure 6.72 Semivariance of resampled PDrg (50-250m) 204
Figure 6.73 Contour plot PDrg semivariance (5-30m) 205
Figure 6.74 Contour plot PDrg semivariance (5-250m) 205
Figure 6.75 PDrg upscaled semivariance surface 205
Figure 6.76 PDrg upscale variance quadratic model 206
Figure 6.77 PDrg upscale variance 3rd power polynomial model 206
Figure 6.78 PDrg upscale semivariance values as a function of resolution 208
Figure 6.79 PDrg upscale conventional semivariance values as a function of cell number 209
Figure 6.80 PDrg upscale UPV semivariance values as a function of cell number . 209
Figure 6.81 PDrg upscale semivariance values as a function of average cover 210
Figure 6.82 PDrg upscale conventional semivariance values as a function of leakiness 210
Figure 6.83 PDrg upscale UPV semivariance values as a function of leakiness 211
Figure 6.84 Semivariance of whole-of-catchment DEMs resampled from 5m to 250m 211
Figure 6.85 Upscaled DEM semivariance contours 212
Figure 6.86 Upscaled DEM semivariance surface 212
Figure 6.87 DEM upscale semivariance model 213
Figure 6.88 Semivariance of resampled DEMs) 213
Figure 6.89 Contour plot of semivariance of resampled 5m AP DEM 214
Figure 6.90 Relationship of revised upscaled DEM semivariance to lag and resolution 215
Figure 6.91 Native Scale SAVI variograms 215
Figure 6.92 Upscale SAVI variograms. 216
Figure 6.93 Overlay of native and upscaled SAVI image variograms 217
Figure 6.94 Comparison of variance contours for native (left) and upscaled (right) 217
Figure 6.95 Comparison of SAVI semivariance models 218
Figure 6.96 Native scale STVI variograms 220
Figure 6.97 Upscaled STVI variograms 220
Figure 6.98 Overlay of native and upscaled STVI image variograms 221
Figure 6.99 Comparison of variance contours for native (left) and upscaled (right) STVI cover images 221
Figure 6.100 Comparison of STVI semivariance models 222
Figure 6.101 Native scale PDrg image variograms 224
Figure 6.102 Upscale PDrg image variograms 224
Figure 6.103 Comparison of PDrg native image variances with upscaled image variances 225
Figure 6.104 Comparison of variance contours for native (left) and upscaled (right) PDrg cover images 226
Figure 6.105 Comparison of PDrg semivariance models 226
Figure 6.106 Comparison of upscaled DEMs with native DEMs 228

Figure 6.107 Semivariance of whole of catchment DEMs resampled from 5m to 250m 228
Figure 6.108 Semivariance of resampled DEMs (solid lines) relative to the semivariance of native DEMs (dashed lines) 229
Figure 6.109 Variogram Index correlation relationships with Leakiness (Lcalc) ... 238

CHAPTER 7

Figure 7.1 General processing schema for applying cover treatments 245
Figure 7.2 Procedure for preparing the drainage line distance zones 248
Figure 7.3 Drainage line distance zones 248
Figure 7.4 Procedure for preparing the elevation zones 249
Figure 7.5 Elevation zones 249
Figure 7.6 Procedure for preparing the slope zones 250
Figure 7.7 Slope zones 250
Figure 7.8 Procedure for preparing the aspect zones 251
Figure 7.9 Aspect zones 251
Figure 7.10 Procedure for preparing the topographic zones 252
Figure 7.11 Topographic zones 252
Figure 7.12 Procedure for preparing the cover zones 253
Figure 7.13 SAVI cover zones 253
Figure 7.14 PDrg cover zones 254
Figure 7.15 Leakiness response to increase in SAVI coverage 255
Figure 7.16 Cover, slope and elevation of the DLD zones 256
Figure 7.17 Leakiness due to increase in SAVI cover at different distances from the drainage lines. (net increase in catchment cover) 257
Figure 7.18 Change in Leakiness due to increase in SAVI cover at different distances from the drainage lines. (net increase in catchment cover) 258
Figure 7.19 Response of leakiness to addition of SAVI cover by distance from drainage lines. (net increase in catchment cover) 258
Figure 7.20 Leakiness due to increase in SAVI cover at different distances from the drainage lines. (no net increase in catchment cover) 259
Figure 7.21 Change in Leakiness due to increase in SAVI cover at different distances from the drainage lines. (no net increase in catchment cover). 259
Figure 7.22 Response of leakiness to addition of SAVI cover by distance from drainage lines. (no net increase in catchment cover) 260
Figure 7.23 Leakiness due to increase in PDrg cover at different distances from the drainage lines (net increase in catchment cover) 262
Figure 7.24 Change in Leakiness due to increase in PDrg cover at different distances from the drainage lines (net increase in catchment cover) 262
Figure 7.25 Response of leakiness to addition of PDrg cover by distance from drainage lines (net increase in catchment cover). 263
Figure 7.26 Amount of leakiness due to change of PDrg cover by drainage line distance zone (no net increase in catchment cover). 263

Figure 7.27 Change in leakiness due to change in PDrg cover by drainage line distance zones (no net increase in catchment cover). 264
Figure 7.28 Response of leakiness to addition of PDrg cover by distance from drainage lines (no net increase in catchment cover). 264
Figure 7.29 Cover, slope and elevation of the elevation zones 265
Figure 7.30 Amount of leakiness due to increase in SAVI cover by elevation (net increase in catchment cover). 266
Figure 7.31 Change in Leakiness due to increase in SAVI cover by elevation zone (net increase in catchment cover). 267
Figure 7.32 Response of catchment leakiness to increase in SAVI cover by elevation (net increase in catchment cover). 267
Figure 7.33 Amount of leakiness due to change of SAVI cover by elevation (no net increase in catchment cover) 268
Figure 7.34 Change in Leakiness due to change of SAVI cover by elevation (no net increase in catchment cover). 268
Figure 7.35 Response of catchment leakiness to change of cover by elevation. (no net increase in catchment cover) 269
Figure 7.36 Amount of leakiness due to change of PDrg cover by elevation zone (net increase in catchment cover). 270
Figure 7.37 Change in leakiness due to change in PDrg cover by elevation zone (net increase in catchment cover). 271
Figure 7.38 Response of leakiness to addition of PDrg cover by elevation zone (net increase in catchment cover). 271
Figure 7.39 Amount of leakiness due to change of PDrg cover by elevation zone (no net increase in catchment cover). 272
Figure 7.40 Change in leakiness due to change in PDrg cover by elevation zone 272
Figure 7.41 Response of catchment leakiness to addition of PDrg cover by elevation zone. (no net increase in catchment cover 273
Figure 7.42 Cover, slope and elevation of the slope zones 273
Figure 7.43 Amount of leakiness due to increase in SAVI cover by slope (net increase in catchment cover). 275
Figure 7.44 Change in Leakiness due to increase in SAVI cover by slope (net increase in catchment cover). 275
Figure 7.45 Response of leakiness to addition of SAVI cover by slope (net increase in catchment cover) 276
Figure 7.46 Amount of leakiness due to change of SAVI cover by slope (no net increase in catchment cover) 276
Figure 7.47 Change in Catchment Leakiness due to change of cover by slope (no net increase in catchment cover) 277
Figure 7.48 Response of catchment leakiness to change of cover by slope (no net increase in catchment cover) 277
Figure 7.49 Cover, slope and elevation of the aspect zones 278
Figure 7.50 Amount of leakiness due to increase in cover by aspect (net increase in catchment cover) 279

Figure 7.51 Change in Leakiness due to increase in cover by aspect(net increase in catchment cover) 280
Figure 7.52 Response of leakiness to addition of cover by aspect(net increase in catchment cover) 280
Figure 7.53 Amount of leakiness due to change of cover by aspect zone (no net increase in catchment cover) 281
Figure 7.54 Change in leakiness due to change in cover by aspect (no net increase in catchment cover) 281
Figure 7.55 Response of catchment leakiness to change of cover by aspect (no net increase in catchment cover) 282
Figure 7.56 Cover, slope and elevation of the land form zones.............................. 283
Figure 7.57 Absolute effect on leakiness of increasing SAVI cover in each landform zone (net cover increase scenario) 285
Figure 7.58 Relative effect of increasing SAVI cover in each landform zone on leakiness (net cover increase scenario) 285
Figure 7.59 Leakiness response to addition of SAVI cover by landform zone (net cover increase scenario). 286
Figure 7.60 Effect if increasing SAVI cover on landform zones on catchment leakiness (no net increase scenario) 287
Figure 7.61 Relative effect of increasing SAVI cover in each landform zone on leakiness (no net increase scenario) 287
Figure 7.62 Leakiness response to addition of SAVI cover by landform zone. 288
Figure 7.63 Absolute effect on leakiness of increasing PDrg cover in each landform zone (net cover increase scenario) 289
Figure 7.64 Relative effect on catchment leakiness of increasing PDrg cover in each land form zone (net cover increase scenario)....................................... 290
Figure 7.65 Leakiness response to addition of PDrg cover by landform zone (net cover increase scenario) 290
Figure 7.66 Effect of increasing PDrg cover on landform zones on catchment leakiness (no net increase scenario) 291
Figure 7.67 Relative effect of increasing PDrg cover on landform zones on catchment leakiness (no net increase scenario)................................... 291
Figure 7.68 Leakiness response to addition of PDrg cover by landform zone (no net increase scenario). 292
Figure 7.69 Cover, slope and elevation of the SAVI cover zones 292
Figure 7.70 Amount of Catchment leakiness due to increase in cover in different original SAVI cover zones (net increase in catchment cover). 294
Figure 7.71 Change in Catchment Leakiness due to increase in cover in different original SAVI cover zones (net increase in catchment cover). 294
Figure 7.72 Response of catchment leakiness to addition of SAVI cover by original cover zones (net increase in catchment cover)..................................... 295
Figure 7.73 Amount of catchment leakiness due to increase in cover in each original SAVI cover zone (no net increase in cover). 295

Figure 7.74 Change in Catchment leakiness due to increase in cover in different original cover zones (no net increase in catchment cover).................... 296
Figure 7.75 Response of catchment leakiness to addition 296
Figure 7.76 Cover, slope and elevation of the PDrg cover zones 297
Figure 7.77 Amount of catchment leakiness due to increase in PDrg cover in different original PDrg cover zones (net increase in catchment cover). 298
Figure 7.78 Change in catchment leakiness due to change in PDrg cover of original PDrg cover zones (net increase in catchment cover). 299
Figure 7.79 Response of catchment leakiness to addition of PDrg cover of original PDrg cover zone (net increase in catchment cover). 299
Figure 7.80 Amount of catchment leakiness due to change of PDrg cover by original PDrg cover zone 300
Figure 7.81 Change in catchment leakiness due to change of PDrg cover by original PDrg cover zone 300
Figure 7.82 Response of catchment leakiness to addition of PDrg cover by original PDrg cover zone 301

LIST OF TABLES

CHAPTER 2

Table 2-1 PATCHKEY parameter codes 15
Table 2-2 LFA Indicators for Manual Field Assessment (Tongway and Hindley, 2004b) 17
Table 2-3. Comparison of Landscape Function Indices for Leakiness 19
Table 2-4 Performance of selected vegetation indices in estimating vegetation on two arid land systems in South Australia (R^2) (Jafari and Lewis *et al.* 2007) 26
Table 2-5 Comparison of accuracy in assessing arid vegetation in central New Mexico by SMA and Regression (from Xiao and Moody (2005)) 28
Table 2-6. Scalogram equations for Figure 2.4 (Wu and Shen *et al.* 2002) 32
Table 2-7 Conventional variogram Indices (from (Lloyd 2010)) 43
Table 2-8 UPV Indices (partial list from Balaguer and Ruiz *et al.* (2010)) 43

CHAPTER 3

Table 3-1 Catchment summary statistics 51
Table 3-2 Source imagery 56
Table 3-3 Rearrangement of MODIS bands for consistency with SPOT and Landsat spectral windows 56
Table 3-4 DEM Overview details 57
Table 3-5 Accuracy comparison for 9 GCPt DTM against field elevation values and SRTM 1s DTM 58
Table 3-6 Spectral bands in each images used to calculate vegetation cover indices 61

CHAPTER 4

Table 4-1 Vegetation Cover and Leakiness of the Experimental Catchment 82
Table 4-2 Correlation between Average Cover and Leakiness 84
Table 4-3 Variation in catchment average cover across 3 resolutions. 90
Table 4-4 Sensitivity of Leakiness to type of Vegetation Cover Index 91
Table 4-5 Adjusted Average Leakiness values 92
Table 4-6 Sensitivity of AAL to Vegetation Cover Index 94
Table 4-7 Amount of Average Cover (%) in each sub-catchment (10m) 96
Table 4-8 Amount of Leakiness for each sub-catchment (10m) 97
Table 4-9 Coefficients of Determination for Average Cover correlation (10m) 98
Table 4-10 Coefficients of Determination for Adjusted Average Leakiness correlation (10m) 99
Table 4-11 Correlation between Average Cover and AAL (10m) 100

Table 4-12 Amount of Average Cover in each sub-catchment (25m) 100
Table 4-13 Amount of Adjusted Average Leakiness for each sub-catchment (25m) 101
Table 4-14 Coefficients of Determination for Average Cover correlation (25m) ... 103
Table 4-15 Coefficients of Determination for Adjusted Average Leakiness correlation (25m) 103
Table 4-16 Correlation between Average Cover and AA leakiness (25m) 105
Table 4-17 Amount of Average Cover in each sub-catchment (250m) 105
Table 4-18 Amount of Leakiness for each sub-catchment (250m) 105
Table 4-19 Coefficients of Determination for Average Cover correlation (250m) . 107
Table 4-20 Coefficients of Determination for Adjusted Average Leakiness correlation (250m) 108
Table 4-21 Correlation between Average Cover and AA Leakiness (250m) 109
Table 4-22 Summary of correlation of AAL with cover 110
Table 4-23 Consistency response pattern 115

CHAPTER 5

Table 5-1 Paired samples test for SAVI cover from upscaling image versus cover layer 128
Table 5-2 Wilcoxon Signed Rank test results for SAVI coverage leakiness 128
Table 5-3 Goodness of fit for PDrg Leakiness transformed 135
Table 5-4 Significance tests for linear and cubic AAL scalograms 138
Table 5-5 Significance levels for fine scale projected leakiness 143
Table 5-6 Comparison of Best Fit equations and their CoD (R^2) values. 144

CHAPTER 6

Table 6-1 Equation 6-1 fit parameters 164
Table 6-2 Conventional Variogram indices for SAVI cover images 164
Table 6-3 UPV Variogram Indices for SAVI cover images 165
Table 6-4 Correlation (R^2) between SAVI native scale image variables and variogram indices 165
Table 6-5 Correlation (R^2) between SAVI native scale variogram indices 166
Table 6-6 Equation 6-2 fit parameters 170
Table 6-7 Conventional Variogram indices for STVI cover images 170
Table 6-8 UPV Variogram Indices for STVI cover images 170
Table 6-9 Correlation (R^2) between STVI native scale Image variables and all variables 171
Table 6-10 Correlation (R^2) between STVI native scale variogram indices 171
Table 6-11 Equation 6-3 fit parameters 175
Table 6-12 Conventional Variogram indices for PDrg cover images 176
Table 6-13 UPV Variogram Indices for PDrg cover images 176

Table 6-14 Correlation between PDrg native scale image variables and all variables (R^2) 177
Table 6-15 Correlation (R^2) between PDrg native scale variogram indices and all variables 177
Table 6-16 Equation 6-4 fit parameters 182
Table 6-17 UPV Variogram Indices for catchment DEM 183
Table 6-18 Correlation (R^2) of DEM variables 183
Table 6-19 Semivariance resolution expressions for native DEMs 185
Table 6-20 Equation 6-5 fit parameters 186
Table 6-21 Equation 6-6 fit parameters 191
Table 6-22 Conventional SAVI semivariogram indices for upscaled images 192
Table 6-23 UPV SAVI semivariogram indices for sub-catchments 192
Table 6-24 Correlation between SAVI upscale image variables and all variables (R^2) 193
Table 6-25 Equation 6-7 fit parameters 197
Table 6-26 STVI Conventional semivariogram indices 198
Table 6-27 STVI UPV semivariogram indices 198
Table 6-28 Correlation (R^2) between STVI upscale image variables and all variables (R^2) 199
Table 6-29 Equations 6-8 and 6-9 fit parameters 206
Table 6-30 PDrg Conventional semivariogram indices 207
Table 6-31 STVI UPV semivariogram indices 207
Table 6-32 Correlation (R^2) between PDrg upscale image variables 208
Table 6-33 Correlation between PDrg variogram indices (R^2) 208
Table 6-34 Equation 6-10 fit parameters 212
Table 6-35 Semivariance resolution expressions for resampled DEMs 214
Table 6-36 Comparison of native and upscaled SAVI variogram expressions 216
Table 6-37 Variables for native scale and upscaled SAVI semivariance models 218
Table 6-38 Correlation (R^2) of SAVI variance indices for native and upscaled images with leakiness 219
Table 6-39 Comparison of native and upscaled STVI variogram expressions 220
Table 6-40 Variables for native scale and upscaled STVI semivariances 222
Table 6-41 Correlation of STVI variance variables for native and upscaled images. 223
Table 6-42 Comparison of native and upscaled PDrg variogram expressions 224
Table 6-43 PDrg model variable values 227
Table 6-44 Correlation between PDrg variables for native and upscaled images (R^2) 227
Table 6-45 Relationship between “native” scale DEMs and resampled AP DEM 229
Table 6-46 Key native image structural values (repeated from Table 6-2, Table 6-7, and Table 6-12 for convenience) 230
Table 6-47 Key upscale image structural values (from Table 6-22, Table 6-26 and Table 6-30 for convenience) 233

Table 6-48 Significant native image variogram correlations (from Table 6-9 and Table 6-14). 237
Table 6-49 Significant upscaled image variogram correlations (From Table 6-24, Table 6-28 and Table 6-32) 237

CHAPTER 7

Table 7-1 Analysis Plan for effect of Cover Location on Catchment leakiness 244
Table 7-2 Pro-forma calculation of pixel adjustment values for No offset and Offset scenarios 246
Table 7-3 Adjustment of SAVI average cover and Leakiness results 255
Table 7-4 SAVI drainage distance zone adjustment values 257
Table 7-5 PDrg drainage line distance zone adjustment values 261
Table 7-6 SAVI cover elevation zone adjustment values (continued) 265
Table 7-7 PDrg cover elevation zone adjustment values (continued) 269
Table 7-8 SAVI cover slope zone adjustment values 274
Table 7-9 SAVI cover aspect zone adjustment values (continued) 278
Table 7-10 Land form zone cover adjustments for SAVI (continued). 283
Table 7-11 Land form zone analysis results for SAVI cover 284
Table 7-12 Land form zone analysis results for SAVI cover 286
Table 7-13 Land form zone cover adjustments for PDrg (c0ontinued). 288
Table 7-14 Land form zone analysis results for PDrg cover 289
Table 7-15 Land form zone analysis results for PDrg cover 291
Table 7-16 SAVI Cover zone adjustment values (continued) 293
Table 7-17 PDrg Cover zone adjustment values (continued) 297
Table 7-18 Summary of zones in which cover is most effective in reducing catchment leakiness 308
Table 7-19 Overall Summary of Response of Leakiness to cover added by feature zones 310

PHOTOGRAPHS

Photograph 2-1 Aerial views of vegetation patterns in the experimental catchment, Patchy (left) and Banded (right). ... 11
Photograph 3-1 Savannah grass lands ... 52
Photograph 3-2 Iron Bark woodland ... 52
Photograph 3-3 Blue Gum creek flat ... 53
Photograph 3-4 Mixed Iron Bark and Blue Gum woodland ... 53
Photograph 3-5 Break-away gully in duplex savannah Sodosol soil ... 54
Photograph 3-6 Gravel ridge line lacking vegetative cover ... 54
Photograph 4-1 Resource leaky area ... 68
Photograph 4-2 Resource conserving area ... 68

APPENDICES

Appendix 1 Sub-catchment details at 3 resolutions 331
Appendix 2: Stereo Aerial Photo details 332
Appendix 3: Data Dictionary for GCP and PSM data collection 333
Appendix 4: Trimble Nomad and ProXH used for field data collection 334
Appendix 5. Elevation comparison between Geoid (WGS 84) and Ellipsoid (GRS 1980) 335
Appendix 6 Field Ground Reference Point Records 336
Appendix 7 Additional modifications made to PDI 340
Appendix 8. Effect of upscaling the image versus upscaling the SAVI thematic cover layer 341
Appendix 9. Effect of upscaling the image versus upscaling the STVI thematic cover layer 342
Appendix 10.Transformed and Predicted values 343
Appendix 11.Transformed and predicted values 344
Appendix 12 PDrg calculated Leakiness values 345
Appendix 13 Comparison of experimental and predicted 346
Appendix 14 Comparison of experimental and predicted 347
Appendix 15 Comparison of experimental and predicted PDrg AAL values 348
Appendix 16 Effect of upscaling on percent cover 349
Appendix 17 Calculated and Adjusted Average Leakiness 350
Appendix 18 Normalised calculated Leakiness values 351
Appendix 19 Comparison of experimental and projected leakiness values 352
Appendix 20 Fine upscale cover and leakiness values 353
Appendix 21. Leakiness and semivariance 354
Appendix 22. Leakiness and semivariance 355
Appendix 23. Native DEM semivariance matrix 356
Appendix 24 Reconstructed DEM semivariance matrix 356
Appendix 25. LC Settings 357

ABBREVIATIONS

AAL…………	Adjusted Average Leakiness
ABCD……….	Natural pasture condition categories
AFM………...	Area between the First lag and the First Maximum
APs………….	Aerial Photographs
ARVI………..	Atmospherically Resistance Vegetation Index
ASTER……...	Advanced Spaceborne Thermal Emission and Reflectiuon Radiometer
ATE………....	Advanced Terrain Extraction
AVG………...	Non-overlapping Averaging interpolation resampling
BIL…………..	Bilinear interpolation resampling
BOTANAL….	Pasture yield estimating procedure
CAI……….….	Cellulose Absorption Index
CASI………...	Canadian AeroSpace Institute
CC…………...	Cubic Convolution resampling
CDLI………...	Cover based Directional Leakiness Index
CEC………….	Cation Exchange Capacity
CoD……….….	Coefficient of Determination (R^2)
CORVI……....	Corrected Vegetation Index
CSI…………..	Cross Scale Interaction
DEM…………	Digital Elevation Model
DLI…………..	Directional Leakiness Index
DN…………...	Digital Number
DTM…………	Digital Terrain Model
EO-1…………	Observer 1 satellite
EROS………..	Earth Resources Observation Center
ETM+………..	Enhanced Thematic Mapper plus
FCI…………..	Fractional Cover Index
FDO…………	First Derivative near the Origin
FETEX………	Feature Extraction software
FML…………	First Maximum Lag
FPC………….	Foliage Projective Cover
FR……………	First Range
FSV…………..	First Sill semi-Variance
GC………….	Ground Cover
GCI…………..	Ground Cover Index
GCPs………...	Ground Control Points
GloVis……..	USGS Global Visualisation Viewer

GPS…………. Global Positioning System
GRPs………... Ground Reference Points
GRS…………. Geodetic Reference Spheroid
HJ-1…………. Name of Chinese satellite
HRVIR……… High Resoultion Visible Infra-Red
HIS………….. Hyper Spectral Imager
IR……………. Infra-Red
LC…………... Leakiness calculator
Lcalc………… Leakiness calculated
LFI…………... Landscape Function Index
LI……………. Leakiness Index
LISEM………. Limburg Soil Erosion Model
LPS………….. Leica Photogrammetry Suite
M……………. Majority resampling
MAE………... Mean Average Error
MAUP………. Modifiable Areal Unit Problem
MCSMA……. Monte Carlo Spectral Mixture Analysis
MDLI……….. Modified Directional Leakiness Index
MERIS……… Medium Resolution Imaging Spectrometer
MFM………... Mean of the semivariogram up to the First Maximum
MGA………... Map Grid of Australia
MODIS……… Moderate Resoultion Imaging Spectrometer
MRBGI……… Multiple Regression Bare Ground Index
MSDI……….. Moving Standard Deviation Index
MSS………… Multi Spectral Scanner
MTF………… Multi-Scale Transfer Function
NDVI……….. Normalised Difference Vegetation Index
NIR…………. Near Infra-Red
NLWRA…….. National Land and Water Resources Audit
NN…………... Nearest Neighbour interpolation Resampling
NPV…………. Non-Photosynthetic Vegetation
NQ DTNRMB. North Queensland Dry Tropics Natural Resources Management Body
NSCVR…….. Nugget to Spatially Correlated Variance Ratio
NSVR………. Nugget to Sill Variance Ratio
NV………….. Nugget Variance
ORIMA……... Leica Orientation Management software
PATCHKEY.. A native pasture analysis procedure
PD_{54}………… Perpendicular Distance of band 5 over band 4
PD_{57}………… Perpendicular Distance of band 5 over band 7
PDIs………… Perpendicular Distance Indices

PD_{rg} ………...	Perpendicular Distance of red band over green band
PD_{rn} …………	Perpendicular Distance of the red band over the NIR band
PD_{rs}………….	Perpendicular Distance of the red band over the SWIR band
PMF …………	Pixel Modular Transfer Function
ProXH………	A brand of Trimble GNSS antennae
PS …………...	Point Support
PSF………….	Point Spread Function
PSMs………..	Permanent Survey Marker
PV…………...	Photosynthetic Vegetation
PVI-3………...	Perpendicular Vegetation Index number
QDERM……..	Queensland Department of Environment and Resource Management
Q-GRAZE…...	A proprietary pasture quality assessment software
QNRGC……..	Queensland Natural Resources Groups Cooperative
R…………….	Range
RGB…………	Red Green Blue
RI……………	Redness Index (vegetation cover)
RMS…………	Root Mean Squared
RSF………….	Ratio of Second to First lags
RUP…………	Round Kernel Variance Weighted Upscaling resampling
RVF…………	Ratio Variance at First lag
SAGA……….	System for Automated Geoscientific Analysis
SARVI………	Soil and Atmospherically Resistance Vegetation Index
SAVI………...	Soil Adjusted Vegetation Index
SCV…………	Spatially Correlated Variance
SD……………	Standard Deviation
SLATS………	Statewide Landuse and Trees Study
SMA…………	Spectral Mixture Analysis
SR……………	Second Range
SRTM 1s…….	Shuttle Radar Topography Mission one second resolution
SRTM3………	Shuttle Radar Topography Mission three second resolution
SSC………….	Soil Surface Conditions
STVI-4………	Stress related Vegetation Index #4
SUP………….	Square Kernel Variance Weighted Upscaling resampling
SV……………	Sill Variamce
SWIR………...	Shorth Wavelength Infra Red
TERN………..	Terrestrial Ecosystem Research Network
TEXTNN……	Textural Neural Network
THREDDS…..	A proprietary data server operated by Unidata
TM…………..	Thermatic Mapper
TRAPS………	Transect Recording and Processing System

TTRP……….. Trigger Transfer Reserve Pulse
UPV………… Universidad Politecnica de Valencia
VAST……….. Vegetation Assetts, States and Transition
VC………….. Vegetative Cover
VLS………… Variance Leakiness Scalograms
VW…………. Variance Weighted resampling
WGS……….. World Geodetic System

CHAPTER 1

INTRODUCTION

1.1. Introduction

Australian rangelands include the arid, semi-arid and savannah grazing lands as well as moister temperate and tropical grazing lands. They occupy 81% of the Australian continent yet to many Australians they are ‘out of sight and out of mind’. Their biodiversity has continued to decline since European settlement (Bastin 2008). The ecosystems of thirty six percent of the rangelands were degraded as of 1996 and 27.5% were considered too degraded to be economically recoverable (Industry Commission 1998, p. 373).

Their continued decline is due to many causes that collectively have decreased their capacity to retain pre-existing levels of scarce environmental resources (top soil, water, nutrients and organic matter) (Ludwig and Tongway *et al.* 2004). The spatial organisation of landscape features such as bands of vegetation, cryptogrammic crusts, dead and decaying cellulosic matter and topographic features has a major influence on the processes responsible for retaining or losing environmental resources (Ludwig and Tongway 1995). Measuring how landscape elements are organised provides a functional way of assessing the condition of rangelands (Ludwig and Bastin *et al.* 2000).

Measuring changes in landscape structure (the patchwork pattern of landscape elements) overtime is difficult because of the difficulty in finding reference benchmarks. Functional landscapes change all the time, so indices rather than absolute measurements of change are the preferred metric to assess their status. Structural indices have been used extensively to measure the patchiness of landscapes (Leitao and Miller *et al.* 2006, Ch. 1.4). While they work well in measuring man-made changes, these indices correlate poorly with changes in ecosystem condition (capacity to retain and recycling environmental resources) (Bastin and Ludwig *et al.* 2002). Indices related to factors that indicate ecosystem condition are preferred for monitoring rangelands (Tongway, D and N Hindley 2004).

Satellite imagery offers the opportunity to collect data over large areas of rangelands in a repetitive and cost effective manner (Ludwig and Tongway *et al.* 2004, p. 108). This makes it a potentially suitable source of information for land managers and policy makers about landscape condition. Temporal sequences of medium and coarse spatial scale images (e.g. Landsat, MODIS and MERIS) show changes in landscape features over time. High spatial resolution imagery (e.g. SPOT 5, Ikonos, Quickbird and WorldView II) has become more available in the past decade. It can be used to identify and quantify the patchiness of landscape elements and their changes over time.

Changing the scale of spatial observation changes the features that can be recognised from an image because of expression or regularisation of the image features due to autocorrelation (Lloyd 2010). This makes the comparison of landscape indices from images with different spatial resolutions difficult. Each resolution is effectively "seeing" a different view of the same area. However, this can be addressed by investigating how the structure of the image changes with change in resolution and how the structural changes permit expression or regularisation of bio-geographical features used to analyse the landscape.

The main structural feature of interest in assessing the ecosystem condition of the landscape is ground cover of which the various categories of vegetation cover are major components. Other components include bare ground areas, water bodies, drainage lines and topographic features such as pits, saddles and ridges.

To obtain maximum expression of a feature, the spatial scale should match the minimum spatial scale of the landscape element (Bradshaw and Fortin 2000). However, landscape elements such as vegetation cover may be organised at multiple spatial scales thus requiring different resolutions for optimal expression. Comparison of a landscape scene based on imagery at different resolutions is effectively comparing dissimilar features because different features are expressed at different resolutions. Wu (2004) recommended that multi-scale information should be used to identify landscape features that affect ecosystem function. Different features can become apparent at different resolutions and this affects the analysis of ecosystem function.

The conundrum that arises is that as it becomes increasingly important to measure and monitor landscape function, the landscape elements continue to reorganise over time and thus similar resolution imagery of a given area at differen times captures different features with greater or lesser accuracy (Bradshaw and Fortin 2000). Our ability to make temporal comparisons depends on the rate of change of the features and their size relative to the observation scale. This is compounded further by the advent of new image sensors with different spectral and spatial resolutions allowing the capture of new generations of landscape features. The challenge then is to interpret what landscape indices mean when derived from different temporal, spectral and spatial resolutions of the same area.

1.2. Statement of the Problem

This in turn depends on the spectral and spatial parameters of the image sensors. For a given scene and spectral bands, decreased spatial resolution is generally accompanied by decreased spatial variability and increased spatial dependence (Chen and Henebry 2009)**.** Vegetation cover features, such as the Normalised Difference Vegetation Index (NDVI) have been assumed to rescale accurately with change in image resolution; however, Goodin and Henebry (2002) showed that NDVI images of orthogonal corn plots (plots of corn in which the rows are planted at right angles to each other) rescaled from 0.625m to 3.125m did not correspond with directly observed data. Lausch and Pause *et al.* (2013) confirmed that upscaled and downscaled NDVI patterns did not correspond directly with observed raw image data in the range of 0.5m to 3m for a range of landscape surface structures. Each bio-geophysical element in the landscape was shown to have a different pattern of variance as evidenced by different forms of its variogram. As a consequence, the evidence of Lausch and Pause *et al.* (2013) suggests that in heterogeneous landscapes rescaling may have a non-linear effect because different landscape structures have different patterns of variance (different variogram forms). Differences between observed and rescaled images thus have the potential to affect the reliability of bio-geophysical data extracted from the images.

Testing of 5 different upscaling techniques for their ability to duplicate 4 different observation scales (1.5m to 10m) using CASI (Canadian Aeronautics and Space Institute) forest images, showed that no upscaling method produced the same results as the coarser observation scale (Hay and Niernann *et al.* 1997). The results varied by forest class, the amount of upscaling and the method of upscaling. Decrease in spatial resolution was accompanied by decrease in scene variance. The Variance Weighted (VW) upscaling technique produced a generalised upscaled spectral response that was closer to the coarse observation scale image than upscaling by Nearest Neighbour, Bilinear Interpolation or Cubic Convolution. The VW technique produced an image that more accurately identified forest classes than the coarser scale observation image, a function attributed to the inclusion of high-resolution detail in the upscaled image that was not present in the coarser observation scale image.

Greater persistence of spatial structure in upscaled images (0.187m – 1.0m) of orthogonal corn plots was also found compared to observation scale images (Chen and Henebry 2009). This was expressed as reduced variation in both spatial dependence and spatial heterogeneity due to reduced blurring by the Pixel Modular Transfer Function (PMTF) in the upscaled imagery. This suggests that the capacity of upscaling to simulate coarser scale observation images is a balance between the amount of upscaling, the resampling technique and the PMTF effect. If the amount of upscaling is low (<5 fold), the scene variance is high and the resampling method conserves variance; the upscaled image can have less variance and spatial heterogeneity than would be caused by the PMTF. If these conditions do not apply, the upscaled image may have more variance and greater spatial heterogeneity than the coarser scale observation image. No comparisons of image structure for SPOT, Landsat and MODIS satellite images between 10m and 250m appear to have been reported in the literature.

Vegetation cover indices are a major bio-geophysical input for calculating the Leakiness Landscape Function Index (LFI). The findings from the limited number of high resolution image rescaling comparisons on retrieval of bio-geophysical features serves as a strong caution of potential pitfalls in calculating vegetation cover indices.

LFIs are a potentially very useful source of information for managing rangelands and for informing policy development because they can be processed quickly for large areas and they encapsulate the aggregate effect of ecosystem function in the landscape over these areas. There is also a 40 year historical record of such imagery. However, ecosystem functions operate at different spatial scales (Ludwig and Wiens *et al.* 2000) meaning that the LFIs may not mean the same thing across broad scale image scenes (Bradshaw and Fortin 2000). This makes it potentially difficult to compare them across large areas when using a standard observation window (e.g. 30m for most Landsat images). Thus, it is desirable to know how LFIs change with change in detection of landscape features caused by type of vegetation cover measurement and resolution in order to use them reliably and accurately for landscape management.

Knowing the effect of image resolution and type of analysis of vegetation cover on LFI values may allow selection of the most cost effective scale of imagery for LFI analysis for the area of interest. Three aspects of this were investigated; i) the most suitable image resolution for analysis of the features of most significance to the functioning of a particular area, ii) the limitations of archival imagery of a set resolution for a particular landscape and iii) the effect of different image resolutions on LFIs. These issues were addressed by investigating the following specific questions.

A. How spatial scale (image resolution) affects the measurement of Landscape Function Indices?
    1. Can similar landscape features be extracted from the same scene at different observation scales?
    2. Can similar landscape features be extracted from the same scene at different upscale resolutions?
    3. How should LFIs from images at different resolutions be compared?
    4. Are there limits to the differences in resolution at which LFIs can be compared?
    5. Can LFIs be compared with each other when measured at upscale resolutions that match observations scales?

B. How spatial scale affects the interpretation of the Leakiness Landscape Function Index?
    1. What spatial scales are most suitable for measuring the landscape Leakiness Index?
    2. Does spatial scale effect on-ground interpretation of the landscape Leakiness Index?

Finally a practical application of the effect of changing the amount of vegetation cover on the Landscape Leakiness of a catchment was tested.

1.3. Aim

The aim of the research was to determine the effect of change in spatial scale of imagery on the measurement and interpretation of the Leakiness Landscape Function Index for assessing catchment condition.

1.4. Objectives

A. To determine how change in spatial scale affects the measurement and interpretation of the Leakiness Landscape Function Index. This was done in three subsections:
    1. Investigation of how image resolution affects measurement of vegetation cover and Leakiness.
    2. Comparison of Leakiness at different observation and upscale resolutions.
    3. Analysis of the relationship between image scale, image structure and change in Leakiness.

B. To evaluate options for improving the measurement of LFIs.

C. To evaluate a practical application of using the Leakiness LFI for measuring change in catchment Leakiness.

1.5. Significance of this Research

The broad scale loss of nutrients and soil along with increased water run-off is acknowledged as the root cause of decline in vegetation condition, decrease in biodiversity and reduced productive capacity of the Australian rangelands.This has led to development of different methods to monitor their condition such as by using Bio-Condition, (Eyre and Kelly *et al.* 2006), VAST (Thackway and Lesslie 2006), NLWAF (Whitehead 2001) and PATCHKEY (Corfield and Abbott *et al.* 2006). The

Landscape Function Analysis procedure (LFA) was developed by CSIRO to assess the:

> *“biogeochemical functioning of landscapes at the hillslope scale” (Tongway, D and N Hindley 2004, p. 11). “It measures the intactness of natural vegetation assemblages and soil structural patterns and the processes that maintain these patterns”(Ludwig and Tongway et al. 2004, p. 108).*

It began as a manual site-based method that found extensive use in measuring how rangelands accumulate and loose environmental resources in response to wind and water movement. Based on the Trigger, Transfer, Response, Pulse model (TTRP) of ecosystem behaviour (Ludwig and Wilcox *et al.* 2005), it was shown to provide good correlation with changes in vegetation cover (Ludwig, J. and G. N. Bastin *et al.* 2007, p. 8). However the labour intensity of this approach limits its application for large areas.

Satellite imagery has been used to compare temporal changes in land condition based on changes in index values such as the Foliage Projective Cover (FPC) (Armston and Denham *et al.* 2009; Danaher and Armston *et al.* 2004; Goulevitch and Danaher *et al.* 2007), Ground Cover Index (GCI) (Scarth and Byrne *et al.* 2008; Schmidt and Denham *et al.* 2010) and a range of vegetation cover indices (Jafari and Lewis *et al.* 2007; Sheffield 2009). It is procedurally difficult to assess the overall change in the landscape condition of a catchment from pixel-to-pixel comparisons although Karfs (2002) developed a trend summary image analysis procedure that encapsulated 18 years of change in landuse condition in the Victoria River Downs area of the Northern Territory.

A flow accumulation approach that measures the capacity of a catchment to leak resources (Leakiness Index (LI)) following rainfall, was developed by Ludwig and Eager *et al.* (2002). The LI is an example of a LFI that provides a simple numerical rating of the environmental functioning of an entire catchment. It is correlated negatively with the amount of ground cover in the catchment and the soil surface condition and positively with catchment slope (Ludwig, J. and G. N. Bastin *et al.* 2007).

The context in which the LFI was developed is shown in Figure 1.1.

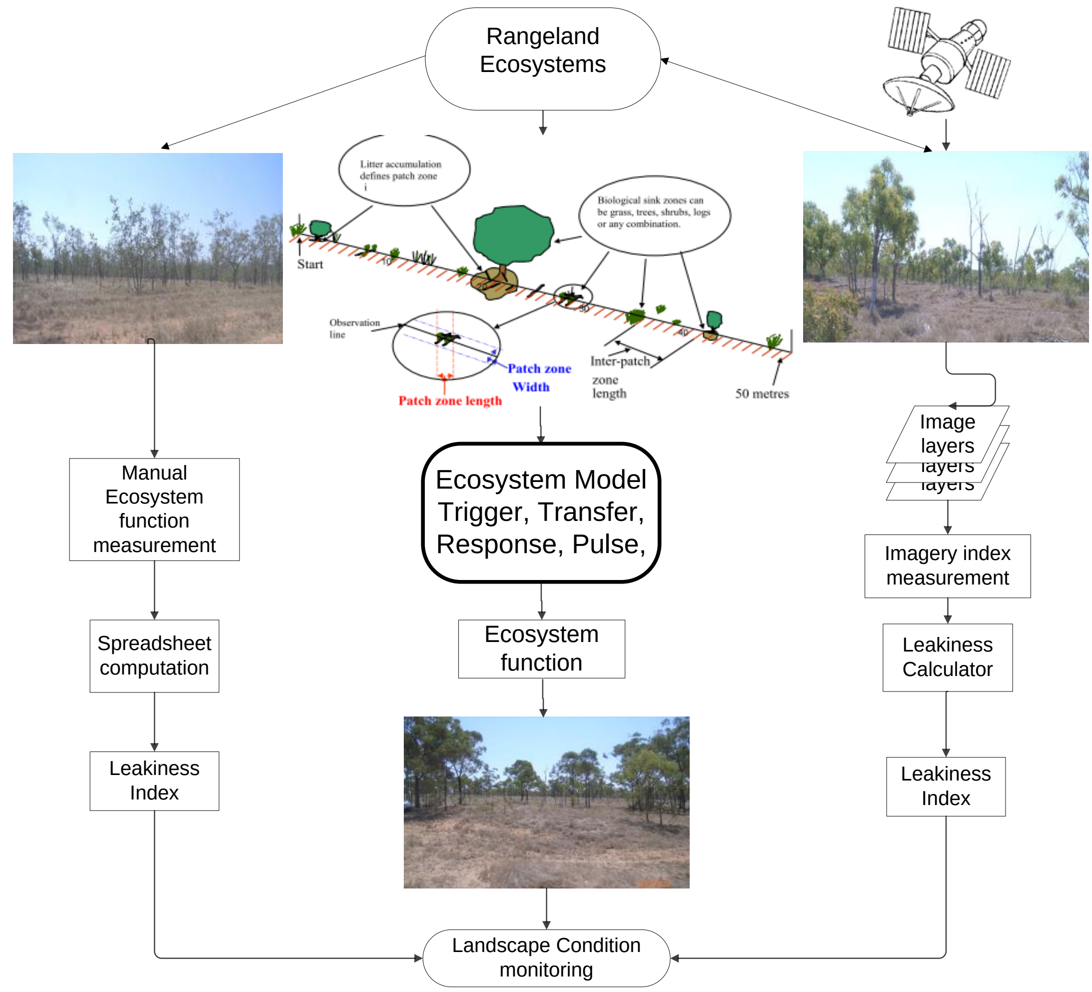

Figure 1.1 Landscape function measurement schemes.
Analogue monitoring diagram (Tongway, D and N Hindley 2004) **.**

Ecosystem function can be measured manually in the field (Tongway, D and N Hindley 2004) or assessed from satellite imagery (Ludwig and Eager *et al.* 2002). Both procedures result in a LFI. This value potentially can be used to monitor the condition of landscapes over time and to guide management changes. The following problems need to be resolved before LFIs from imagery can be used reliably for these purposes. They include:

- The effects of different vegetation cover indices on the measurement of LFIs.
- The effect of variation in size of landscape feature on accuracy of LFI calculation.
- The effect of different image observation scales on identification of landscape features and calculation of LFIs.
- The effect of change in amount, type and position of vegetation in a catchment on the Leakiness LFI.

This research investigates how changes in spatial scale of the source imagery affect the Leakiness Landscape Function Index. The purpose is to develop an improved understanding of what spatial scales should be used to measure different types of

LFIs. There is currently no information on LFIs calculated from different observation scale images of the same area collected at the same time. The effect of image scale on LFIs, through the resolution dependent expression of landscape features, needs to be known if LFIs are to be used as a reliable measure of landscape function. This information will allow LFIs, measured at different spatial scale, to be compared and used to inform managers about management strategies.

1.6. Limitations of the Study

Detailed findings from this research are only applicable to rangelands in the study area and are limited by the assumptions underlying the Leakiness Calculator algorithms (Ludwig and Eager *et al.* 2006). However, the general findings should apply to other rangelands with a Trigger, Transfer, Response, Pulse method of resource accumulation and response. The empirical exponents in the Landscape Leakiness Calculator software need to be selected carefully so as to reflect local conditions before calculating Leakiness Indices for other areas (Ludwig, J. and G. N. Bastin *et al.* 2007). Experience with imagery from prospective study areas is also necessary in selecting types of land-cover indices for use in the Leakiness Calculator.

Because the study relied on historical time series imagery, it was difficult to find good quality ground-truth data that provided an accurate record of the attributes of interest at the time the imagery was capture. The quality of the ground truth data is important in order to verify the accuracy of the classification of the land cover indices and to validate the calculated LFIs. This was overcome, firstly by selecting a study area in which the vegetation remained undisturbed (except for normal cattle grazing) between the time of capture of the satellite images and the date of field recording. Secondly, the images were collected and the fieldwork was done in the same season (early summer months before monsoonal rains occurred).

There are no freely available sources of high-resolution satellite imagery suitable for vegetation cover analysis in Queensland. Selection of the study area was limited depended on the availability of SPOT 5 (HRVIR) data from the Queensland Natural Resources Groups Cooperative QNRGC). Image data was available for 2005 and 2009 from which an image of the experimental catchment was found that was temporally and spatially coincident with a cloud free portion of a MODIS image. The closest "same season" Landsat image (TM 5) of the research area was captured 33 days earlier. This difference in dates is not considered significant as close inspection of the 3 images showed no "vegetation greening" effect between the image dates.

Landscape Leakiness Indices (LIs) used in this research were generated with the Leakiness Calculator (LC) software developed by CSIRO (Ludwig and Eager *et al.* 2006). It is still experimental software and only available for use by approved researchers. Its results have been reported in two peer reviewed publications (Bastin and Abbott *et al.* 2008; Ludwig, J. and G. N. Bastin *et al.* 2007). Field observations in these studies were consistent with calculated LI results. However, the developers of the LC acknowledged that its present algorithms do not i) include a patch size scale response function and ii) the soil surface condition (SSC) term is not pixel specific.

The first algorithm limitation means that the LI values do not respond to the effect of scale of different patch sizes in images of different resolutions. This may lead to the leakiness not accurately reflecting changes in patch sizes that occur in images at different resolutions. The same SSC value was used for each image resolution because it was of the same area. This should have no adverse effect on the analysis of Leakiness at different resolutions.

1.7. Conclusion

This section has outlined the broad nature of the challenge in monitoring rangeland condition in Australia and highlighted the potential role of Landscape Function Indices in this monitoring. While Landscape Function Indices derived from manual techniques are well established, their development and application from satellite imagery has begun only recently. Many aspects underpinning the application of LFIs from imagery are unresolved, especially the use of imagery at different scales. This research addresses key aspects of comparing Landscape Function Indices from imagery at different scales using the Leakiness Index.

The following sections of the thesis are organised along customary lines of first a general review of the literature about analysing landscape features and landscape function indices from remote imagery, Chapter 2, followed by the general research methods in Chapter 3. A more detailed review of specific literature, research methods, results and discussion applicable to each area of inquiry follows in Chapter 4, Effect of Image Resolution and Vegetation Cover on Catchment Leakiness, Chapter 5, Development of Leakiness Scaling Functions, Chapter 6, Effect of Upscaling on Image Structure and Chapter 7, Effect of Vegetation Cover Position on Catchment Leakiness. Chapter 8, Conclusions, provides a synthesis of the findings and recommendations for future research

.

CHAPTER 2

LITERATURE REVIEW

2.1. Overview

Rangelands cover over 80% of the Australian continent and encompass a wide range of climatic conditions and types of soil and vegetation. They extend from cool temperate to tropical zones and from very arid to seasonally high rainfall areas. Seventy per cent of the area is defined as arid with an average annual rainfall of less than 250mm (DOE 2014).

Rangeland ecosystems are fragile because of the paucity of environmental resources (water and nutrients) leading to a delicate balance between accumulation and depletion zones (Tongway and Valentin *et al.* 2012). This is illustrated by their frequently patchy or banded nature (Photograph 2-1**)**.

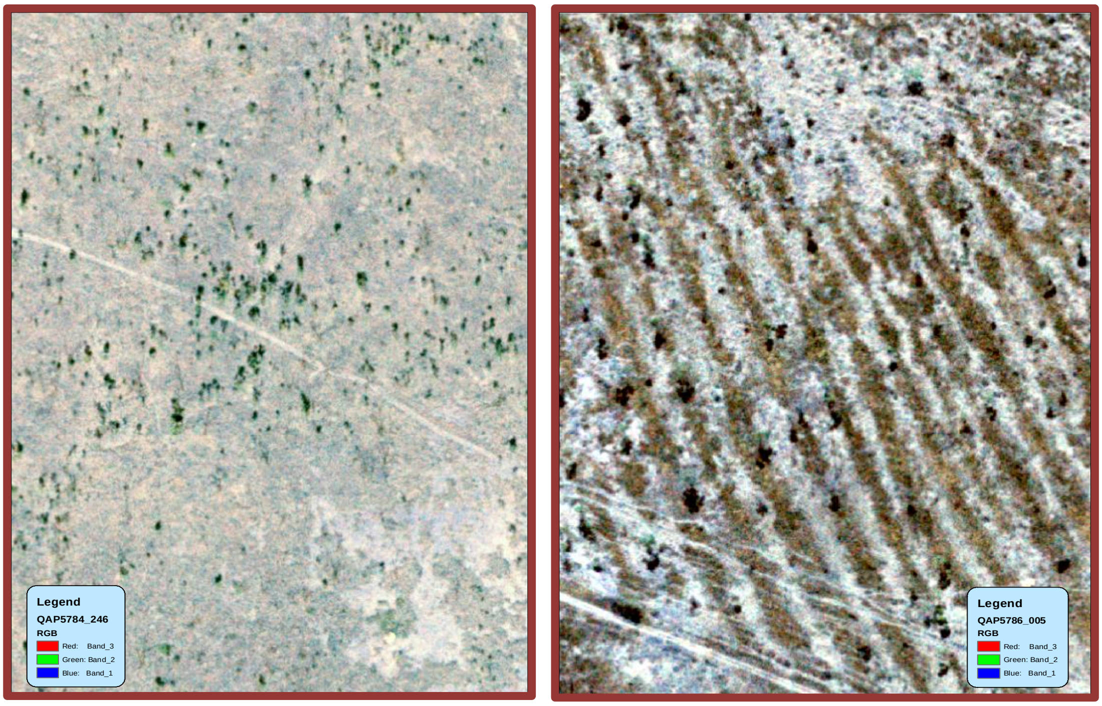

Photograph 2-1 Aerial views of vegetation patterns in the experimental catchment, Patchy (left) and Banded (right).

Management of the Australian rangelands since the time of European settlement has been one of using the seemingly abundant grazing resources only to realise the frailty of the ecosystems that underpin the resources after the resources declined dramatically. Policy settings that reflected populist solutions have exacerbated their decline. These include decisions such as the government land use designation of "grazing" for broad areas of non-tillable land, a permanent Torrens Title tenurial system versus nomadic tenures and leasehold land subdivision policies (Martin and Verbeek 2002), exceptional circumstance provisions for drought assistance, drought fodder transport subsidies (Industry Commission 1998), introduced animals (Woinarski and Fensham *et al.* 2000) and watering point expense taxation deductions (Landsberg and James *et al.* 1997) amongst others. Each apparent solution to a particular aspect of rangeland decline has sown the seeds for future problems. The challenge is to find management solutions that are robust enough to respond to the present problems and development challenges without creating future problems.

The rangelands are economically very important to Australia. Tourism and grazing generate more than $4.4 B in sustainable annual income (Bastin 2008). They also encompass a very large range of ecological communities and biological diversity as reflected by their encompassing 53 of Australia's 83 Biogeographical Regions (Figure 2.1). However, thirty six per cent of the rangelands were designated degraded as of 1999 and 27.5% of the rangelands, or ¾ of the degraded area was considered "economically unrecoverable" (Industry Commission 1998).

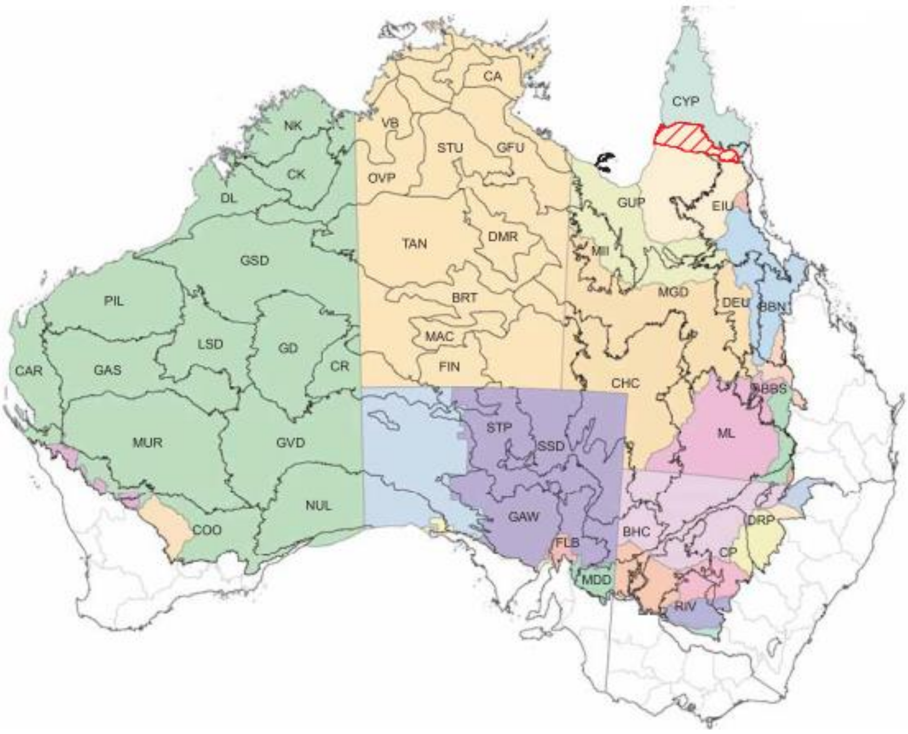

Figure 2.1. The diversity of Biogeographical Regions comprising the rangelands is shown by the coloured areas. Natural Resource Management Regions and Local Land Service regions (NSW only) are hown in initialled areas. (Ref: Cwlth. Dept. of Envir. Water, Heritage and the Arts, 2009)[1]

[1] This map has been included to provide an overview perspective of the location of the rangelands and their Biogeographical regions, not for identification of specific regions

Research to address these problems has remained fragmented between State departments of agriculture and natural resources and multiple Federal Government agencies. Most research has focused on restoring and maintaining pastoral values for sheep and cattle production (Landsberg and Crowley 2004) without recognizing that loss of such values was symptomatic of a system-wide decline in the unique biological resources of the rangelands (Woinarski and Fensham *et al.* 2000).

The Industry Commission “Inquiry into Ecologically Sustainable Land Management” recommended measures to “protect the public good” provided by the natural capital of the nation’s land resources (Industry Commission 1998). Foremost amongst these were changes to protect the environmental values and ecological services provided by agricultural lands including the rangelands. The Productivity Commission reported that there was poor coordination and a lack of clear priorities between Federal Government departments for implementing ecologically sustainable development and there was an increased need to recognise the “public good” from rehabilitating native vegetation and biodiversity and protecting endangered ecosystems (Productivity Commission 1999). There is no recent broadscale assessment of resource extraction impacts on the rangelands however, the legacy of unreclaimed disturbed lands is widely considered to be increasing due to these activities.

The need to monitor how landscapes function rather than how they are used was recognised by the National Land and Water Resources Advisory Council in 2001 (N L W R A 2001). Landscape Function formally became a major theme (1 of 9) for monitoring the condition of rangelands in 2005 (Bastin 2008, p. 7). Changes in landscape function of pastoral areas were found to be very varied across Australia from 1992-2005 with some areas improving and other areas declining. Landscape function for most areas in Queensland declined during this period, except for the Mt Isa Inlier Bio-geographical Region (Bastin 2008, p. 39).

Landscape Function Analysis (LFA) involves measurement of a suite of parameters that are surrogates for ecosystem function. The following sections explain how the need for these measurements arose, their usefulness in monitoring the status of the rangeland environment, their evolution into management and decision-making tools and technical difficulties in their application.

2.2. Rangeland Condition Monitoring

Most systems for monitoring rangelands are designed to measure their pastoral values (Landsberg and Crowley 2004). Such systems include QGRAZE (QGRAZE 1992), Grass Check (Pegler 1997) and Aussie GRASS (Hall and Bruget *et al.* 2001). The Transect Recording and Processing System (TRAPS) program covers 84 fixed sites in Queensland and records both herbaceous and woody cover (Bastin 2008, p. 212). The State-wide Land cover and Trees Study (SLATS) estimates woody vegetation cover from Landsat TM imagery rather than pasture values. It is validated using ground truth data from the TRAPS program. By focusing on forage and woody material production, these programs overlook a wider range of biodiversity values.

Assessment programs that incorporate biodiversity values include Habitat Hectares (Parkes and Newell *et al.* 2003), Biodiversity Benefits Index (Oliver 2003) and Bio-Condition (Eyre and Kelly *et al.* 2006). The expediency of rapid site-based assessments belies their shortcomings of interpreter bias, geographic selection, lack of specific biodiversity assessment and site-specific threats. The recently released 'Biodiversity Monitoring Program for Australian Rangelands was designed to overcome this shortcoming by providing a comprehensive approach to rangeland biodiversity monitoring (Kutt and Eyre *et al.* 2009).

Ecosystem function is the foundation of landscape condition. Monitoring of surrogates for ecosystem function offers the opportunity to look at the fundamental processes occurring in the landscape and to make predictions about the trajectory of its condition. Ideally, these should be interpreted according to a predictive framework (Gibbons and Freudenberger 2006, p. S11; Landsberg and Crowley 2004). Such frameworks may include classical succession (Westboy and Walker *et al.* 1989), state and transition (Gibbons and Freudenberger 2006), resilience (Pickup and Bastin *et al.* 1994), Trigger, Transfer, Reserve, Pulse (TTRP) (Ludwig and Tongway 1997) and Reference Condition (Landres and Morgan *et al.* 1999).

The interpretative model determines the attributes to monitor. Ideally they should meet the conditions of being; i) ecologically based, ii) widely applicable, iii) sensitive in response, iv) cost effective, v) robust, vi) interpretative and vii) repeatable (McElhinny and Gibbons *et al.* 2005). Scoring of attributes should reflect their contribution to the condition of the site by being either additive, multiplicative or statistically based (Gibbons and Freudenberger 2006, pp. S13-5).

The choice of indicators for monitoring rangeland condition should also recognize that many rangeland ecological processes are geographically and temporally discontinuous and function in a non-linear way (Eiswerth and Haney 2001). Change in predominant plant species may not be a good indicator of the effect of climate change or of herbivores and it may only provide an indirect indication of wildlife changes. While both plants and animals are affected by the underlying ecosystem processes, careful selection of indicator species remains the preferred approach.

Landscape Function Analysis (LFA) began as a manual field-based method for analysing and recording parameters about landscape features in a way that could be consistently analysed to derive reliable indices that indicated ecosystem condition (Tongway, D and N Hindley 2004). New techniques using satellite imagery to monitor surrogates of ecosystem condition are progressively replacing field based measurements (Bastin and Ludwig *et al.* 2002). These include measurements of the abundance, condition and relative position of landscape features as well as their changes over time.

PATCHKEY is a relatively new field land cover classification system designed to link features (Table 2-1) that describe the Queensland Department of Primary Industries and Fishery's ABCD land condition framework with observations of features that affect the hydrological function of the landscape (Corfield and Abbott *et al.* 2006).

Table 2-1 PATCHKEY parameter codes

Criteria	Description
Basal %	% basal area of tussock grasses
Functional Gps	
3P	Native perennial tussock grasses
INPG	Increaser native Perennial Grasses
EXPG	Exotic perennial grasses
ANNG	Annual Grasses and Forbes
LEGS	Native and introduced Legumes
Folia	% folia cover estimate
Litter	% litter cover estimate
Bare	% bare ground estimate
Yield	Estimate of dry biomass of standing grass in kg/ha
Burnt	Has patch been burnt recently, Y/N
Shrub	Do shrubs make up a high proportion of close to ground cover
Graze %	Estimate of % of plant grazed on whole patch
Soil hard	Soil hardness test, use LFA pen test
Ero Type	Type of erosion
Ero ext	Extent of erosion
Dep ext	Extent of deposition
Patch	Estimate of final patch type, from key

Testing at seven sites in the Burdekin Catchment yielded good correlation between land condition (ABCD) and classified high resolution satellite imagery (Quickbird 0.6m) (Abbott and Corfield undated). This correlation suggests its potential use in calibrating classified imagery for Leakiness Index calculations and for measuring landscape function over large areas.

Image resolution affects how landscape features are recorded. Ecosystem function varies with the size of the landscape patches (Ludwig and Wiens *et al.* 2000, pp. 90-1) and this compounds the interpretation of landscape function from imagery. Most imagery based LFA measurements have been based on Landsat imagery with pixel sizes ranging from 25m to 80m. To be able to analyse changes in rangeland condition over extended periods it is important to know how change in imagery resolution affects the correlation between LFIs and ecosystem function. Such knowledge would also allow comparison with results from new high-resolution imagery.

The following section discusses measurement of indicators of ecosystem condition and their linkages to ecological processes.

2.3. Ecosystem Condition Monitoring

The existence of banded vegetation patterns had been reported in central and western arid zones by various investigators (Mabutt and Fanning 1987) however, their significance remained unrecognized. A similar pattern of groves of trees interspersed between patches of bare soil and grass patches was also observed as a common theme in eastern Australian rangeland vegetation. This patterning was shown to be related to topography and landscape hydrological processes (Tongway and Ludwig 1990). Systematic transect analyses confirmed this vegetation patterning was associated with variations in levels of available nitrogen and phosphorus (Ludwig and Tongway 1995). The Trigger, Transfer, Reserve Pulse conceptual model (Figure 2.2) of rangeland function provides a framework for explaining how the natural features of wind, water and landscape elements (biotic and abiotic) combined to conserve and utilize resources (Ludwig and Tongway 1997).

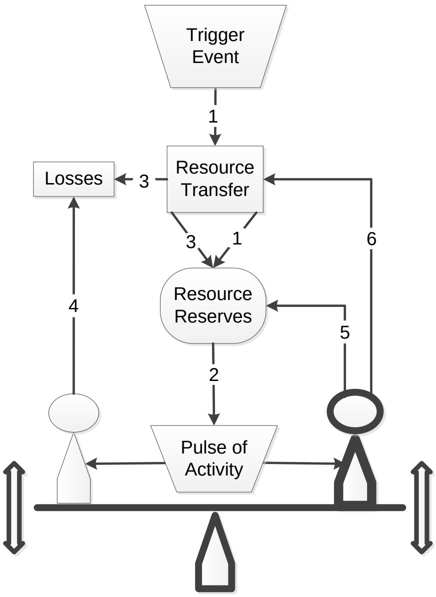

No.	Process
1	➢ Run-on ➢ Infiltration storage & capture ➢ Deposition ➢ Saltation capture
2	➢ Plant germination, growth ➢ Nutrient mineralization ➢ Uptake processes
3	➢ Run- off into streams ➢ Rill flow and erosion ➢ Sheet erosion out of system ➢ Wind erosion out of system
4	➢ Herbivory ➢ Fire ➢ Harvesting ➢ Deep drainage
5	➢ Seed pool replenishment ➢ Organic matter cycling/decomposition ➢ Harvesting ➢ Concentration by soil microfauna
6	➢ Physical obstruction ➢ Absorption processes

Figure 2.2 Trigger, Transfer, Reserve Pulse model of ecosystem function
(Ludwig and Tongway 1997)

The climatically driven redistribution processes are shown in Figure 2.2 They operate in both banded and non-banded landscapes (Wilcox and Breshears *et al.* 2003). Redistribution may be interrupted by man-made events such as fire, grazing and biomass removal. While the eco-hydrological processes occur over time, the important feature of this model is that the processes are also three dimensional spatial processes (Ludwig and Wilcox *et al.* 2005, p. 290). They occur at large horizontal spatial scales where there are distinct belts of trees and grassland and as well at smaller spatial scales such as between individual trees, shrubs, tussocks of grass and bare soil. They also occur vertically where they depend on the type of soil, its horizons and the types of biotic processes acting on it.

The processes are initiated by any event that changes the distribution of resources, the Trigger events, such as rainfall or windstorms (1) or Transfer events of water and nutrients (1), until their movement is blocked. At this point, a reserve accumulates and biotic processes (2) respond to the increase in available resources by producing a Pulse in plant and animal growth. This leads to a positive feedback loop resulting in the accumulation of more resources following subsequent Trigger events. Positive feedback (5, 6) is offset by events that reduce resources such as erosion, fire, grazing or harvesting (3, 4). When the rate of loss of resources from the system exceeds the rate of accumulation the condition of the ecosystem declines and vice versa (Ludwig and Wilcox *et al.* 2005). The density and type of features and their spatial distribution in the landscape have been found to be good surrogates for ecosystem function (Ludwig and Bastin *et al.* 2000).

Vegetation patches in a wide range of landscapes decrease run-off and sediment loss and enhance their storage. The increased water retained within patches results in greater biomass production per unit area. Macro-invertebrates increase in vegetation patches compared to inter-patch areas and their activity leads to increased soil permeability. Reducing the amount of surface obstruction on sloping areas increases the amount of sediment loss. This is accompanied by lower biomass production (Ludwig and Wilcox *et al.* 2005, pp. 291-4). These field findings confirm the concepts underlying the TTRP model. They also indicate the types of landscape features that can be used to assess temporal changes in ecosystem function.

The manual LFA procedure is based on simple, visually observable indicators closely related to the chemical and biological processes occurring in the ecosystem. They can be quickly recorded in a systematic way in the field (Table 2-2) (Tongway, D and N Hindley 2004).

Table 2-2 LFA Indicators for Manual Field Assessment (Tongway and Hindley, 2004b)

Stage	Indicator measured
I .Landscape Organisation	• Patch type (grass, log, shrub, tree, bare ground etc.) • Patch number • Patch size • Interpatch (fetch) length
II. Soil Type Condition	• Soil cover • Perennial grass butt cover and canopy cover of trees and shrubs • Litter cover • Soil surface crust brokenness • Lichen and moss cover • Form of erosion • Loose and mobile material • Surface nature • Surface roughness • Slake test

This procedure is applicable at both “hillslope” and “patch” landscape scales. Detailed spreadsheet procedures may be used to calculate Landscape Function Indices (LFIs) for Soil Stability, Infiltration and Nutrient Cycling. Change in LFI over time indicates whether the condition of the landscape is improving, detiorating or staying the same. LFIs can also be used for comparison within a dynamic range defined by reference sites for the best available site and for heavily degraded conditions or for identifying missing processes (Tongway, D and N Hindley 2004).

Measurement of the indicators listed in Table 2-2 is time consuming and costly for large areas (Herrick, J. E. and Wander, M. M. as cited in Ludwig and Tongway *et al.* 2004, p. 109) and this limits their adoption. The indicators also exist across a continuum of scales ranging from fine scale hillslopes to entire watersheds. This makes it desirable to identify simple indicators that can be used to monitor both small and large areas. Such indicators need to be sensitive to landscape function processes, easy to measure, calculate, and produce consistent results when used by different operators. They should also relate to a conceptual monitoring framework and have a predictive value (Ludwig and Tongway *et al.* 2004, p. 104).

Analysis of the pattern of PD54 indices (Pickup and Chewings *et al.* 1993) and the Landsat MSS Band 2 reflectances (Karfs 2002) for sites at different distances from stock watering points showed a strong correlation with associated land condition measurements such as sensitive plant species and the number of birds, small mammals and reptiles. These observations were confirmed by high resolution imagery and field surveys (Ludwig and Tongway *et al.* 2004, p. 112). A similar pattern of land condition was also observed at the coarser catchment scale (Ludwig and Tongway *et al.* 2004, pp. 114-5). These studies showed a consistent correlation between the quantity and quality of vegetation in patches, and with land condition at both coarse and fine scales. This suggested the measurement of intactness of ground cover (per cent cover) and greenness of patches (quality of cover) as surrogates for the condition of the landscape. Use of satellite imagery to record these attributes over large areas offers the opportunity for increased use of LFA in land management assessment and policy setting (Ludwig and Tongway *et al.* 2004, p. 115).

2.4. Landscape Function Indices (LFI)

The previous section described the development of Landscape Function Indices as tools to aggregate information about natural vegetation and soil condition at both the hillslope and watershed scales. The quantity and quality of patches was shown to correlate strongly with biodiversity and eco-hydrological processes in the Australian rangelands. This section discusses the development of a group of leakiness indices each of which was designed to measure the extent to which an area loses water after rainfall. Table 2-3 provides an overview of these leakiness indices.

Table 2-3. Comparison of Landscape Function Indices for Leakiness

Category	Leakiness Index Version		
	Directional Leakiness Index (DLI)	**Cover based Directional Leakiness Index (CDLI)**	**Leakiness Index (LI)**
Input data	a. Boundary file, rectangular b. Classified raster i. Binary Patch/Fetch	a. Boundary file, rectangular b. Indexed raster i. Vegetation cover % ii. DEM	a. Boundary file, any shape b. Indexed raster i. Vegetation cover % ii. DEM
Computation method	Flow distribution	Flow accumulation	Distributed flow accumulation
Key Index formulae	$DLI = 1 - \left[\frac{(L_{max} - L_{obs})}{(L_{max} - L_{min})}\right]^{\mathrm{k}}$	$DLI = 1 - \left[\frac{(L_{max} - L_{calc})}{(L_{max} - L_{min})}\right]^{\mathrm{k}}$	$DLI = 1 - \left[\frac{(L_{max} - calc)}{(L_{max} - L_{min})}\right]^{\mathrm{k}}$
Components	$L_{min} = 0$	$L_{min} = 0$	$L_{min} = 0$
	$L_{obs} = Distributon\ Equation$ (see text)	$L_{obs} = Progressive\ accumulation$ $L_{obs} = \sum_{i}^{j} (p_{i-1,j} + 1) l_{i,j}$	$L_{obs} = Distributon\ and$ $progressive\ accumulation$ $equation$ (see text)
	$L_{max} = i^2 \times j$	L_{max}=3500 or > if L_{calc} $inflection > 35\ pixel$	$L_{max} = \frac{L_{calc}}{\left[1 - \sqrt[3]{1 - LI}\right]}$
Application	Small areas, Gentle slope, Down column resource flows	Cover index handles moderate scale resolution images	Cover index handles moderate scale resolution images. Complex terrain
Limitations	Requires imagery at scale of patches and fetches. Suited for small regular down-slope areas	Suited for small regular down-slope areas. Cover index suitability for landscape conditions	DEM accuracy may limit application to areas of low relief. Cover index suitability for landscape conditions
Reference	(Ludwig and Eager *et al.* 2002)	(Ludwig and Eager *et al.* 2006)	(Ludwig, J. and G. N. Bastin *et al.* 2007)

2.4.1. Directional Leakiness Index (DLI)

The Directional Leakiness Index (DLI) was formulated to measure the lack of obstruction to flow of a particle moving through a network of patches and inter-patch zones (Ludwig and Eager *et al.* 2002). A DLI of one reflects no obstruction to flow and a DLI of zero reflects complete obstruction to flow of the particle. It provides a relative measure of how patches obstruct wind and water induced flow of soil or nutrients through a landscape. The key relationships are defined as follows:

$$DLI = 1 - R^k \tag{2-1}$$

where

$$R = \frac{(L_{max} - L_{obs})}{(L_{max} - L_{min})} \tag{2-2}$$

and

$$L_{obs} = \sum_j \left[(h_s/h_j) \cdot \left(\sum_i dp_{i,j}^2\right) + \left((h_s/h_j) - 1\right) \cdot \left(\left(dt_j + db_j\right)^2\right) + \left(dt_j^2 - db_j^2\right) \right] . (w_s/w_m) \cdot (pd) \tag{2-3}$$

$$\text{where: } L_{max} = i^2 \times j \tag{2-4}$$
$$\text{and } \quad L_{min} = 0 \tag{2-5}$$

R =	Retention factor	d =	Distance in m
L =	Leakiness	t =	Top of area
h =	Height in pixels	b =	Bottom of area
w =	Width in pixels	pd =	Pixel dimension in m
k =	Decay curve steepness,(=7)	i =	Number of columns
		j =	Number of rows

Equation 2-3 is a summation of unimpeded flow distances (inter-patches) scaled for the length and width of the sample area to the whole area. Where there are no obstructions $dp = 0$ and $dt = db$ so $L_{obs} = L_{max}$.

This relationship measures the relative ease of flow through a binary classified raster (obstructing and non-obstructing). Water always flows down slope while wind may flow in any direction. The authors recommend that separate calculations be done for wind and water driven movements because obstructions are classified differently for wind and water, and the results averaged. A Modified Directional Leakiness Index (MDLI) can be used in situations where flow direction is unknown (Ludwig and Eager *et al.* 2002). This involves calculating the leakiness in one direction (down the rows) and then reorienting the raster by 90° and recalculating the leakiness as though the water were flowing down the columns and then averaging the results as follows.

$$MDLI = {(DLI_r + DLI_c)}/{2} \tag{2-6}$$

where: r = row and c = columns

Testing of the DLI relationship on simulated rasters (Ludwig and Eager *et al.* 2002, pp. 161-9) established that the Index value:

- Decreased as patch cover increased.
- Is more sensitive to changes at low patch cover percentages.
- Decreased as the number of patches increased for a given level of coverage.
- Decreased as patches were more dispersed for a given level of coverage.
- Decreased as the shape and orientation of patches formed greater obstructions to the direction of flow, and
- Banded patches produced lower Index values than square patches.

Testing on classified high resolution images (pixel size = 0.2m) of landscapes oriented in different directions confirmed that the DLI values reflected the landscape condition. A limitation of this approach is that the imagery has to be of fine enough scale to detect non-flow obstructing inter-patches and that the flows are in a fairly straight-line direction. Both constraints limit its practical application.

2.4.2. Cover-based Directional Leakiness Index (CDLI)

The Cover-based Directional Leakiness Index (CDLI) was developed to overcome the size limitation of the DLI of only processing a small number of pixels. (Ludwig and Eager *et al.* 2006). It is based on calculating the amount of cover (as a %) for each pixel in an image, a resource loss term for each pixel (based on the amount of cover of the pixel) and accumulating the product of these values in a down-slope loss accumulation function according to the following relationships.

$$CDLI = 1 - R^k \tag{2-7}$$

$$R = \frac{(L_{max} - L_{calc})}{(L_{max} - L_{min})} \tag{2-8}$$

$$L_{calc} = \sum_i^j (p_{i-1,j} + 1) l_{i,j} \tag{2-9}$$

where: $l_{i,j} = 1 - \frac{c_{i,j}}{100}$,
and c = percent cover
k = decay function = 3

The L_{calc} expression progressively accumulates resources from pixel to pixel rather than distributing them as occurs in the L_{obs} expression (Equation 2-3). The decay function of k=3 was found to provide a better fit for the loss accumulation function compared to k = 7 for the distribution function (Ludwig and Eager *et al.* 2006, p. 331).

L_{max} is set for a "bare ground" situation so the loss multiplier $l_{i,j}$ = 1 and L_{max} = pixel number. This potentially can result in a very large L_{max} for large catchments. It is suggested that L_{max} be set for the number of rows for the initial "zero effect" to be effectively dissipated, usually 35 rows. In this case $L_{max} = 35 \times p_j$ (Ludwig and Eager *et al.* 2006).

L_{min} occurs when the loss multiplier $l_{ij} = 0$. This would be the case if all the area had 100% cover but it has been found that such areas still leak some resources. It is recommended that $L_{min} = \sum_i^{3500} \times c$ for a reference site of the type being evaluated. If this is done, then the CDLI value is relative to the reference site and is not an absolute value.

Testing the CDLI showed that the Index value:

- Decreased as the cover (per cent) increased.
- Is sensitive to the location of areas of higher amounts of cover.
- Is affected by differences in soil and vegetation type reflectances, and
- Is sensitive to the dispersion of the cover. This is a similar response to the DLI, which is sensitive to clumping and disaggregating of patches.

This procedure has three limitations. First, there is an initial zero value effect on the first group of pixels in each down-slope column. This can be overcome by using areas with greater than 35 rows of pixels. A sufficient width is also required for replication. The second limitation is the use of a continuous vegetation cover index as a surrogate for obstruction to flow. It may be more responsive to the flow of water than the flow of wind. The third limitation is that the progressive accumulation function continues to rely on a linear down-slope accumulation. This occurs infrequently in nature.

2.4.3. Leakiness Index (LI)

The Leakiness Index (LI) was developed to overcome limitations of the DLI and CDLI by incorporating elevation data along with cover data (Ludwig, J. and G. N. Bastin *et al.* 2007). The basic index relationship remains the same as Equations 2-7 and 2-8, however L_{calc} and L_{max} are calculated differently so as to incorporate accumulation and distribution to and from neighbouring pixels as shown in Equation 2-10.

$$L_{calc} = \sum_i^j p = \begin{bmatrix} (p_{i-1,j} \times s_{i-1,j}|e\&E) + (p_{i,j-1} \times s_{i,j-1}|e\&E) + \\ (p_{i,j+1} \times s_{i,j+1}|e\&E) + (p_{i+1,j} \times s_{i+1,j}|e\&E) + 1 \end{bmatrix} \times l_{i,j} \text{(2-10).}$$

where: $l_{i,j} = e^{-b \times c_{i,j}}$
and: p = progressive value
c = pixel cover index value (as a %).
b = -0.065, representing the steepness of the decline in soil loss with increasing cover (depends on soil type).

This expression shows the accumulation from four neighbouring pixels according to their relative elevation to each other. This is achieved by the use of the scalar function, $s_{i-1,j}|e\&E$. The full Leakiness Index calculation in the Leakiness Calculator (LC) (Ludwig, J. and G. N. Bastin *et al.* 2007, p. 10) incorporates the accumulation and losses from all eight neighbouring pixels, not just the 4 shown in Equation 2-10. The end result is that all flow within a boundary catchment (L_{calc}) is the accumulated exit flow at the lowest pixel (pour point) in the sample area such that.

$L_{max} = L_{calc}$
when $c_{i,j} = 0$
and thus $L_{max} = \sum_i^j p$.

This is for all the pixels in a mapped area and can become very large thus diminishing the sensitivity of LI. An interpolation procedure is recommended for setting L_{max} as follows (Ludwig, J. and G. N. Bastin *et al.* 2007, p. 11).

$$L_{max} = \frac{L_{calc}}{\left[1-\sqrt[3]{(1-LI)}\right]}. \tag{2-11}$$

followed by rounding up to the next 100

L_{max} must always be greater than L_{calc} for the LI ratio to fall within the bounds of 0 to 1. All other terms are as defined for Equation. 2-3.

The LI relationship provided consistent and verifiable results when tested on a rangeland site 200km north of Alice Springs (Purvis 2004). The site consisted of moderately sloping undulating terrain for which the grazing history management was well documented. Analysis using PD_{54} vegetation cover index values (Pickup and Chewings *et al.* 1993) derived from Landsat images for 1980, 1988. 1994 and 2002 and SRTM3 DEM values yielded progressively declining LI values with time (Figure 2.3 (a)).

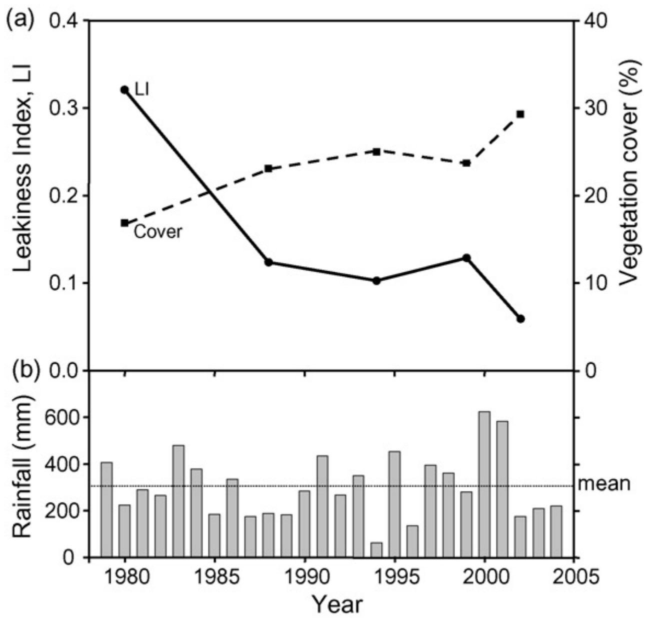

Figure 2.3.The Leakiness Index for a rangeland monitoring site 200km north of Alice Springs, compared with mean levels of persistent vegetation from 1980 to 2002, (a) and Annual rainfall from 1979 to 2004 relative to the mean of 304 mm (b)
(Ludwig, J. and G. N. Bastin *et al.* 2007)

Figure 2.3 (a) illustrates the steady improvement in the LI value (decrease) corresponding to the increase in vegetative cover over the 55 km^2 site. This response can be seen to be independent of the rainfall during the 24-year period (Figure 2-3 (b)).The advantages of this approach are that it can accommodate multiple drainage networks in moderately sloping undulating terrain and uses continuous cover indices as a surrogate for land condition. It does this within an irregularly shaped boundary file. This makes it potentially useful for comparing the LI of sub-catchments within a larger catchment for monitoring or management purposes.

However, the procedure has limitations that arise from the inputs that are required. The DEM provides the values used by the scalar distribution function, $s_{i-1,j}|e\&E$, to distribute flow to neighbouring pixels. The vertical accuracy of the DEM may limit the accuracy of the results in the flatter terrain that characterises much of the Australian rangeland. This sensitivity necessitates particular attention to DEM processing for such areas to remove sinks and ridges. The CDLI may be more suited to calculating the leakiness in such situations.

It remains for the LI to be tested and correlated more precisely with actual runoff from landscapes after rainfall events and with known changes in landscape function. The relationship between the type of vegetation cover index and change in landscape function also remains to be tested. For example, FPC a measure of perennial woody vegetation is unlikely to accurately indicate soil surface conditions for retaining resources while the GCI, the inverse of the BGI (Scarth and Byrne *et al.* 2008), may be expected to more accurately indicate potential for retaining resources.

The following sub-sections discuss the effect of change in image scale on selection and analysis of cover values used in the calculation of the Leakiness Index.

2.5. Bio-geophysical Features

Imagery has to be classified into bio-geophysical features before it can be used for landscape function analysis. Ground cover features, especially the vegetation component, are of particular concern for impeding the flow of water and air borne sediment. The patchwork way in which they are arranged relative to drainage and air current paths has a big effect on resource retention. Characterising how different measures of cover affect leakiness was a necessary first step to selecting particular cover indices for upscaling, variance and location analysis.

Assessment of the amount and type of ground cover, can be done in many ways (Bannari and Morin *et al.* 2009; Jafari and Lewis *et al.* 2007; Jensen 2007; Scarth and Byrne *et al.* 2008; Sheffield 2009). Traditionally vegetation cover has been assessed using a band ratio index approach with the analysis centred on the green and near infrared reflectance bands and thus based on the presence or absence of chlorophyll pigment in the vegetative material. As a group, these indices are easy and quick to calculate but become less effective as the chlorophyll is masked or decays.

The best known of these indices are perhaps the Normalised Difference Vegetation Index (NDVI) (Rouse, J. and R. Haas *et al.* 1974) and the Soil Adjusted Vegetation Index (SAVI) (Huete 1988). The NDVI is widely used because of its simple formulation, early development, wide use under conducive northern hemisphere conditions, utility for measuring seasonal and inter-annual changes in vegetation growth and minimising multiplicative atmospheric noise due to the nature of its ratio formulation. However, it has significant limitations for vegetative measurement, including its non-linear response to vegetation due to the additive effect of atmospheric path radiance and the effect of soil that may be visible through canopies. Its good correlation with leaf area (LA) breaks down due to saturation when LA is very high (Jensen 2007, p. 388-386). Arid and semi-arid zone plants have numerous xeric adaptations that change their response to NDVI measurements. This is illustrated in Table 2-4 where the NDVI correlations with perennial arid zone plant matter were low at 0.03 and 0.36 for two different land systems.

Table 2-4 Performance of selected vegetation indices in estimating vegetation on two arid land systems in South Australia (R^2) (Jafari and Lewis *et al.* 2007)

Index Type	Gina Land System			Buckshot Land System		
	Perennial Plants	Total Vegetation (PV)	Total Vegetation, Litter and Cryptograms (PV & NPV)	Perennial Plants	Total Vegetation (PV)	Total Vegetation, Litter and Cryptograms (PV & NPV)
NDVI	0.03	0.58	0.26	0.36	0.64	0.10
SAVI	0.01	0.57	0.24	0.36	0.64	0.12
PVI-3	0.71	0.78	0.61	0.49	0.61	0.47
PD_{54}	0.61	0.72	0.62	0.40	0.54	0.54
STVI-4	0.71	0.78	0.62	0.51	0.66	0.41

SAVI is considered an improvement on the NDVI that is achieved by the addition of a canopy background adjustment factor (L). This factor is designed to account for the differential red and near infra-red extinction through the canopy (Qi and Cabot *et al.* 1995). L values of around 0.5 were found to minimise soil brightness and reduce the need to calibrate the index for different soils (Huete and Justice *et al.* 1994). Table 2-4 shows that SAVI did not estimate arid vegetation any better than did NDVI.

Because of the inherent difficulties in accurately sensing arid zone vegetation from imagery, Jafari *et al.* (2007) systematically compared the accuracy of a series of indices (band ratio, distance based, orthogonal and plant water sensitive) for estimating vegetation on arid lands. While their accuracy varied across different land systems, there was a significant and repeatable difference in the estimate of perennial plants, total green vegetation (equivalent to PV and total plant matter including litter and cryptograms vegetation (equivalent to PV and NPV). Selective results from Jafari *et al.* (2007) are reproduced in Table 2-4 because of their relevance to the selection of ground cover indices for this research.

The values in Table 2-4 are Coefficients of Determination (CoD) of correlation between the image-derived estimates of the area covered by different categories of vegetation versus field assessment of the same area. They are not quantitative estimates of the amount of vegetation per se. There was no separate data for correlation with only NPV. It was assumed that the higher correlation with PV and NPV combined, also included a higher correlation with NPV. This data shows that, in the arid land study sites the PVI-3, PD_{54} and STVI-4 indices significantly outperformed the more often used NDVI and SAVI indices.

Earlier work by Pickup *et al.* (1994) in investigating a range of perpendicular distance indices showed that the PD_{54} index produced “the best separation between soil, rock or stone and vegetated surfaces”. In particular, the PD_{54} separation for

NPV was better than the more traditionally used PD_{57} separation[2]. The PD_{54}[3] index showed better results than the PVI-3 index for which reason it was included in this research. In addition to classifying the image based on the separation between the red (x axis) and green (y axis) bands, it was also decided to evaluate perpendicular distance cover classification based on red versus near infra-red (called PD_{rn}) and red versus short wave intra-red (called PD_{rs}).

The STVI-4 index was included in this research because it showed a much better estimation of PV and NPV than did NDVI and SAVI (Table 2-4). A new index called the Corrected stress Vegetation Index (CORVI), created by correcting STVI-4 with the Redness Index (RI) (Jafari and Lewis *et al.* 2007) was also included along with the Redness Index (RI) as a stand-alone index. A variation on the Redness Index approach, in areas where the background soils have a red hue, is to rescale the red band (Landsat TM 3) DN values to between 0-100 or part thereof and invert them (high red value = high soil reflectance = low vegetation cover and vice versa). The inverted values can then be used in the LC (Bastin and Abbott *et al.* 2007).

Another approach to reducing atmospheric effects in the red reflectance band is to normalise the red band radiation by the difference between the red and blue bands as is done in the Atmospherically Resistant Vegetation Index (ARVI) (Kaufman and Tanre 1992). This approach was combined by (Huete and Liu *et al.* 1997) with the SAVI formulation to create yet another vegetation index, the Soil and Atmospherically Resistant Vegetation Index (SARVI) which was included in this research.

In addition to using spectral differences in the green to near infra-red wavelengths to discriminate PV, NPV and BG, spectral differences in the shortwave infra-red (SWIR) region between 2,000-2,500nm can also be used to discriminate between vegetation and bare ground. This is due to the selective absorption of 2,200nm radiation by the OH^- ions on clay particles and of 2,100 and 2,300nm radiation by cellulose and lignin respectively. Imagery with these wavelengths is available from ASTER (Advanced Spaceborne Thermal Emission and Reflection Radiometer) imagery, EO-1 Hyperion (Earth Observer One) imagery and the AVIRIS (Airborne Visible Infrared Imaging Spectrometer) imaging spectrometer. Data from these sources was not used in this research due to it being either unavailable or because it lacked appropriate native scale resolution.

Gill *et al.* (2008) reported on the poor level of estimation of NPV compared to the generally good level of estimation of PV using existing band ratio techniques. The absence of a uniformly reliable way of estimating ground cover (PV and NPV)

[2] The subscript in these indices refers to the Landsat Multi-Spectral Scanner (MSS) band numbers as used on Landsat missions 1-3.
[3] The PD_{54} index was renamed the PDrg index to acknowledge the Landsat TM and ETM+ band names, red and green.

across a range of soil types (colours and textures) and climatic zones from band ratio equations lead to the investigation of two additional approaches, i) regression based bare ground prediction (Scarth and Byrne *et al.* 2006), and ii) spectral mixture analysis (SMA) (Gill and Phinn 2008; Schmidt and Scarth 2009). Both approaches yielded useful estimates of bare ground with mean average errors (MAE) ranging from 10.1% to 11.5% (Schmidt and Scarth 2009). The performance of both procedures was compared for accuracy in measuring fractional green vegetation cover (2 end members: bare soil and green vegetation) over an arid region in central New Mexico, USA from Landsat ETM+ imagery (Xiao and Moody 2005). They found that the regression approach gave results comparable to constrained 3 and 4 end member SMA models and both constrained (C) and unconstrained (U) 5 end member SMA models as shown in Table 2-5.

Table 2-5 Comparison of accuracy in assessing arid vegetation in central New Mexico by SMA and Regression (from Xiao and Moody (2005))

Parameter	SMA3		SMA4		NDVI		SMA5	
	U	C	U	C	NDVI regression	NDVI SMA	U	C
R^2	0.71	0.89	0.72	0.85	0.87	0.88	0.88	0.86
RMSE	0.159	0.099	0.150	0.123	0.105	0.106	0.100	0.118

Building on the success of Danaher *et al.* (2004) in developing a multiple regression procedure for estimating foliage projective cover (FPC) in Queensland, Scarth *et al.* (2006) developed a multiple regression, generalised cover index (GCI, also known as the Ground Cover Index). This was based on Landsat TM bands 3, 5 and 7 and utilised 431 field ground cover calibration sites. These were available from amongst over 2000 SLATS (State-wide Land Trees Study) sites used in the FPC research. They developed a Bare Ground Index (BGI), the inverse of which is the GCI. Testing of the model against Aussie Grass records yielded an $R^2 = 0.98$ (Scarth and Byrne *et al.* 2006, Fig. 8) and a RMS prediction error of 12.9%. However, Bastin *et al.* (2007, p. 24) reported that the GCI might be overestimating ground cover based on results from their study area at Virginia Park station in the Fanning River catchment in North Queensland. The BGI was available for Landsat imagery when this thesis research was initiated and it has been included in the 25 m resolution analysis work for reference and comparison purposes.

SMA is a hard classification approach that depends on determining the spectral properties of a number of pure components in the image, either based on known pure samples within the image, spectroradiometer spectra for the samples from the field or from a library of standard spectra. The maximum number of end-members (n), and thus the classes, that can be identified is limited by the number of data dimensions (spectral bands) available where n= (number of bands-1) (Jones and Vaughan 2010, p. 193). In images with limited data dimensions (such as SPOT or RGB imagery), this can be increased by the generation of additional data dimensions such as an NDVI or SAVI image. Hyperspectral imagery such as that collected by the Hyperion instrument on the EO-1 satellite or the Hyper Spectral Imager (HIS) on the HJ-1 satellite have more spectral bands and thus are more useful in this approach. However, early measurement of land cover changes in the Amazon River basin were successfully done using SMA with Landsat TM imagery (6 data bands) (Adams and Sabol *et al.* 1995).

SMA has been used to estimate PV, NPV and BG in Queensland using both green-near infrared end members as well as SWIR end members. Schmidt and Scarth (2009) analysed PV, NPV and BG from Landsat imagery of a black soil rangeland area near Clermont, Queensland using 4 and 5 end member models. They viewed the data as “promising” with many Coefficients of Determination between 0.78 – 0.69. The critical factor in such analyses is accurate identification of end members.

On a national scale, SMA based on NDVI and the cellulose absorption index (CAI) data dimensions generated from the EO-1 Hyperion hyperspectral sensor (includes both visible and SWIR wavelengths) has been used successfully to estimate different fractions of PV, NPV and BG in Australia’s tropical savannah zone (Guerschman and Hill *et al.* 2009). This approach was also used on the visible and shortwave infrared MODIS bands to generate 16-day composite estimates of PV, NPV and BG. These estimates compared well with grass curing estimates for the same site. Gill and Phinn (2008) showed that a Monte Carlo SMA (MCSMA) applied to ASTER SWIR rangeland imagery produced estimates of PV, NPV and BG that agreed well with field measurements. They were better than 3 end member SMA of Landsat and Ikonos imagery of similar areas and were comparable to results from airborne hyperspectral imagery (AVIRIS) (Gill and Phinn 2009).

An alternative SMA approach was developed by Zhang *et al.* (2012) for classifying a mixed agricultural area in China’s Xinjiang Uygar Autonomous Region. They developed a dual partition SMA model (dimidiate model) by developing “NDVI like” data dimensions from a large number of narrow (4.32nm) spectral bands for “pure vegetation” and “pure soil” end members. This was done using HSI imagery. Three hundred and thirty combinations of the 115 HSI bands were considered in pair-wise combinations to locate the 900nm and 682 nm bands that gave the optimal solution for the 2 end members. The “NDVI like” data dimensions were used in the SMA model to calculate the percentage of each pixel (100m x 100m) that was soil or vegetation. They reported a correlation with field data of $R^2 = 0.856$ and a RMSE of 10.92%. No information was presented about the NPV fraction.

In Australia, the AusCover web site maintained by the Terrestrial Ecosystem Research Network (TERN), hosts annual (dry season) Fractional Cover data for Australia derived from Landsat imagery (25m resolution). It contains 4 data bands at 25m resolution; i) Bare ground, ii). Green vegetation, iii). Non-green vegetation and iv) a Mask layer. These are available in NetCDF format from the THREDDS Server maintained by the National Science Foundation (Trevithick 2013). This data source constitutes an invaluable source of information about the PV, NPV and BG fractions at one resolution. However, the design of this research required landscape cover data at three resolutions so the AusCover fractional data was not used.

2.6. Leakiness at Different Image Scales

All ecosystem processes operate at different scales (Atkinson and Tate 2000, p. 607). As landscapes can be observed at different scales, it is essential to understand how the scale of observation affects the measurement of these processes. In the following discussion the area of interest is called the Support (Atkinson and Tate 2000) and it depends on the resolution at which it is observed. As the Support changes, so the spatial variation changes. This is due to the phenomenon known as the Modifiable Areal Unit Problem (MAUP). It is caused by the effect of change in the size and shape of the sample units on the statistics of the Support (Lloyd 2010, pp. 60-3). The effect is that as a Support is aggregated and disaggregated its inherent spatial variation is either expressed or regularized due to autocorrelation. The result depends on the type of resampling method used to change the resolution (Hay and Nieman 1996). Thus, measuring the amount of autocorrelation in a Support provides a measure of the spatial variation in the area of interest. This in turn may be able to be used to provide a measure of changes in Landscape Function Indices at different spatial resolutions.

Bradshaw and Fortin (2000) and Wu (2004) emphasised that environmental monitoring requires analysis of natural resource processes at multiple spatial and temporal scales . Frequently analyses are done with imagery selected because of its price and/or availability with scant regard for the impact of the scale of the image (resolution) on the natural resource signal and the ecological processes being analysed. The careful attention given to analytic procedures so as to extract maximum information can be lost if the scale of the ground truth data and the resolution of the imagery are not carefully considered relative to the pattern and process to be studied. However, identification of the scales of ecological patterns and processes is also a vexed issue making the selection of existing imagery of a suitable resolution challenging. Changing the scale of an image is one potential way to overcome this problem.

2.6.1. Scaling Patterns

This section discusses findings on the effect of image scaling on patterns in the landscape and the development of explanatory scalograms as a way of relating metrics at one scale to metrics at another scale. Wu *et al.*(2002) reported that most landscape studies considered only a few metrics and then only for a narrow range of scales. They reasoned that this approach failed to put the metrics in the larger context of a wider range of scales, image types and image extents. Thus while the scale of the event was reported it was often not positioned in its broader context.

Patches are aggregations of like cells and classes are aggregations of like patches (Leitao and Miller *et al.* 2006). Each is characterised by manifesting similar processes. Using the hierarchy of landscape, class (group of patches), patch and cell (pixel) used by Leitao and Miller *et al.* (2006).Wu and Shen *et al.* (2002) and Wu (2004) analysed the behaviour of 17 landscape metrics from 6 different types of landscapes at different scales and extents and identified repeatable types of behaviour for different metrics. Type I metrics responded in a predictable manner such as linear negative or positive or exponential negative or positive with scale, Type II metrics responded in a stair case manner (either positive or negative) with scale and for which there was no simple scaling relationship and Type III metrics responded erratically to change in scale and had no general scaling relations. Wu *et al.* (2002, 2004) systematised these types of behaviour by developing scalograms for each pattern as illustrated in Figure 2.4. The scalogram equations are given in Table 2-6. Spatial statistics supporting these patterns of behaviour have not been presented to date.

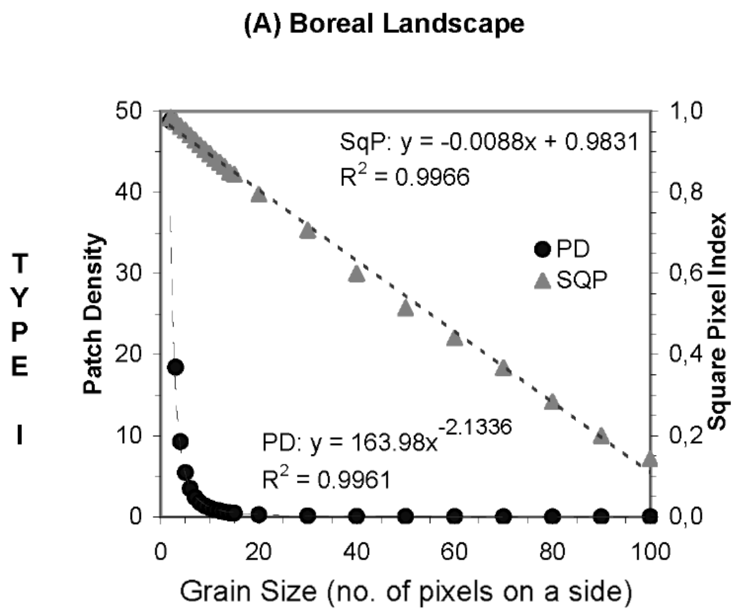

Figure 2.4.Examples of pattern scalograms for landscape metrics as a result of changing the resolution continued,(Boreal forest example, from Wu and Shen *et al.* (2002)

TYPE II

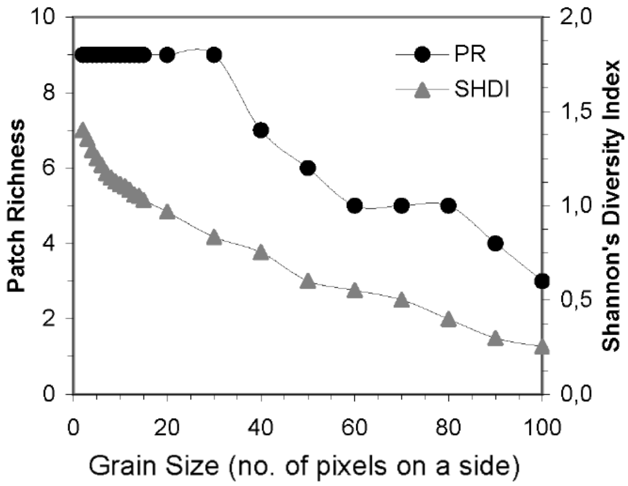

TYPE III

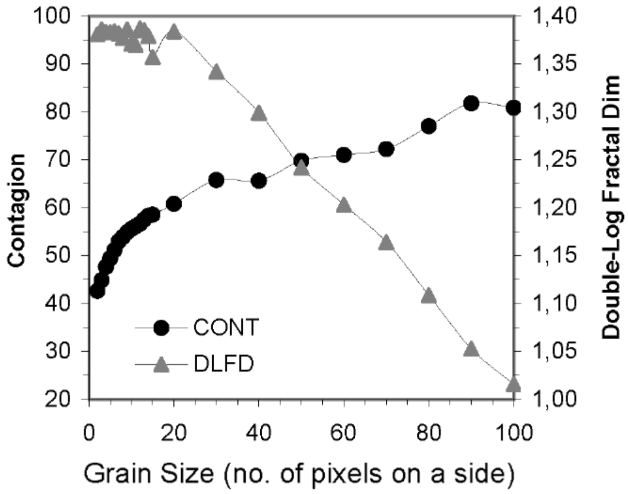

Table 2.4 (continyed)Examples of pattern scalograms for landscape metrics as a result of changing the resolution (Boreal forest example, from Wu and Shen *et al.* (2002)

Table 2-6. Scalogram equations for Figure 2.4 (Wu and Shen *et al.* 2002)

Landscape Metric	Scaling Relation
Patch Density (PD)	A decreasing power function Yg = a xgB, a > 0, B < 0, and xg ≥ 1
Square Pixel Index (Sq. P)	A declining linear function Y =a x + b, a < 0, b > 0, and xg ≥ 1
Patch Richness (PR)	The value of the metric declines in a step down staircase fashion as resolution decreases
Shannon's Diversity Index (SDI)	Yg = a log xg + b, where a < 0, b > 0 and xg ≥1
Contagion (Cont.)	No consistent scaling relationship between different landscapes
Landscape Fractal Dimensions (LFD)	The response curves may take various forms

Spatial patterns can be generated by pixel-based classifiers or increasingly by object classifiers. Mas and Gao *et al.* (2010) investigated the differences between these 2 classification approaches. Based on a study of 85 landscape metrics extracted from a

Landsat ETM+ scene of a mountainous area in the State of Michoacan in Mexico, all metrics showed variability due to classification and post processing methods, especially the core metrics. They suggested caution be used when comparing metric values from images with different dates of capture and different processing methods, especially classification involving segmentation, sieving, clumping and filtering methods.

It is thus reasonable to expect that ecological processes tend to reflect the scale at which they are analysed. The following section reviews findings on how scale affects ecosystem processes.

2.6.2. Ecosystem Scaling

Studies of ecosystem processes showed that their responses may be stable within limited ‘domains’ of scale but the relationship may change abruptly between ‘domains’ (Krummel and Gardner *et al.* 1987; Wiens 1989; Wu 2004). This is an application of Tobler’s First law of Geography (as cited by Atkinson and Tate 2000, p. 612):

> “*Observations closer in space are more alike than those that are further apart”.*

It may therefore be desirable to measure ecosystem responses at scales above and below the particular scale of interest in order to ‘bound’ the Scaling Function. The position at which these processes shift their scaling relationship may also vary by type of ecosystem process (Ludwig and Wiens *et al.* 2000).

Scale affects landscape indices at three levels. Firstly, environmental processes occur at different scales ranging from fine to coarse. For example, large patches of trees have a greater water infiltration rate than small patches of trees. Secondly, organisms respond to the accumulation of resources, temperature and space in a scale dependent way. The combination of these two scaling effects defines the ecosystem Scaling Function (Ludwig and Wiens *et al.* 2000, pp. 84-6). This establishes the scale at which it is most suitable to make observations for ecological purposes.

At the observation level, both physical landscape features and their spatial variation are measured. This image window may be at a different scale to the scale needed to measure the ecosystem scaling functions and this will affect what patterns and processes are observed. It may need to be adjusted to “see” the functions of interest. This adjustment (up-scaling or down scaling) involves aggregating or disaggregating the data and this results in regularising it. The spatial variation, which is critical to measuring landscape functionality, is lost by regularising. This is the problem at the center of a number of common landscape function scaling practices:

- Use of small samples (transect samples in m^2) to validate large Supports (many km^2),

- Effect of pan sharpening on shifting the scale of the spatial variance in the direction of small scale variance.
- Use of imagery at spatial resolutions inappropriate to detect the variance required by the landscape function for which it is being analysed.
- Calculation of Landscape Function Indices from Supports without considering the effect and amount of regularized variance.
- Changing the resolution of imagery by different resampling methods.

Figure 2.5 shows the interaction of landscape processes and patterns at environmental scales. Ludwig *et al.*(2000) defined Ecological Scaling Functions as:

> *"Integrat(ing) the scale dependency of patterns and processes in landscapes with the ways that organisms scale their responses to these patterns and processes"*

The scheme shown in Figure 2.5 is a modification of the findings of Wu *et al.*(2004) and Ludwig *et al.*(2000) combined with a framework in which to present the results of this research.

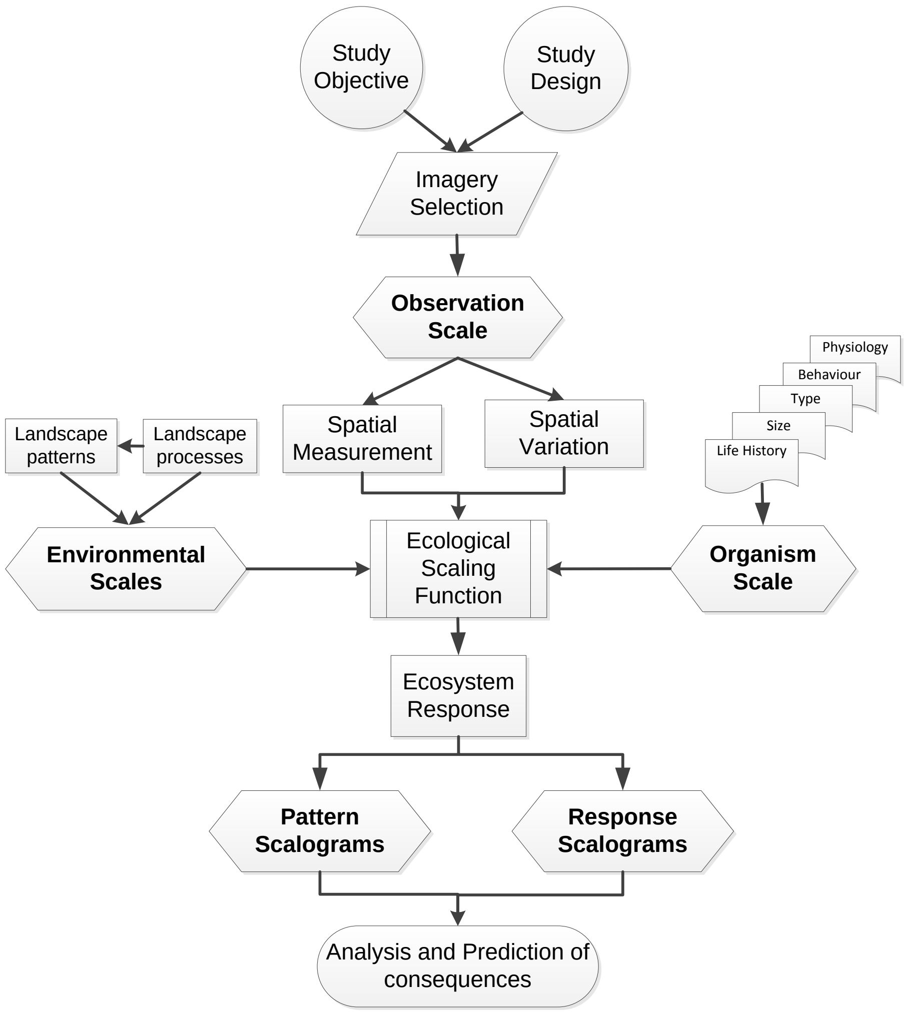

Figure 2.5. Role of landscape scaling relations in influencing scaling functions and prediction of consequences (after Ludwig and Wiens *et al.* 2000)

The results of scaling functions are observed and measured in terms of ecosystem responses. Their spatial heterogeneity and the scale at which they are observed determine what is seen and measured. By observing the responses at different scales, Response Scalograms can be calculated.

Observations of physical features, such as groups of trees or patches of bare soil can be tested by adjusting the scale and assessing whether the feature can still be observed (example of Pattern Scalograms). However, most ecosystem processes such as water infiltration, nutrient leaching and biological activity are not amenable to direct visual observation. Instead, they are evaluated by measuring surrogates such as soil types, run-on areas and patch cover and patch size (example of Response Scalograms). This does not provide assurance that the scale at which the surrogates are being measured is the appropriate scale for the purpose for which the data is to be used.

The appearance of heterogeneity or similarity in a landscape depends on the scale at which it is observed. Landscape patches that appear as isolated groups of large patches at a low resolution may subsequently classify as multiple smaller patches when viewed at a higher resolution. The issue that arises is what observational scale captures the spatial variation relevant to the processes for which the observation is to be used (Ludwig and Wiens *et al.* 2000, p. 87). Intuition suggests it may be different for different processes (e.g. wind versus water redistribution), different resource materials (e.g. fine dust versus heavier particles) and different loading rates (e.g. concentrated versus dilute). Field observations led Ludwig *et al.* (2000, p. 88) to propose a patch-resource scaling rule: "The concentration of resources into patches becomes increasingly greater as patch size increases", where patch size is based on area. This implies a non-linear increase in the capacity of patches to accumulate resources as they increase in size and vice versa.

This association was investigated through an exhaustive study of the relative concentration of soil nitrogen at 11 sites along a 1,000 km rainfall gradient in the savannah woodlands of the Northern Territory, Australia. Samples were taken from 0-5 cm depth soil from two types of patches, small perennial grass clumps and from larger woody patches, as well as from interpatch areas, which had no grass or trees covering them. The results exhibited a curvilinear relationship for Nitrogen accumulation with change in patch size according to the power function $[Y_N] = 0.565X^{0.615}$ (R2 = 0.96) where X = patch size (Figure 2.6). The authors interpreted this as showing the scale dependent nature of the runoff/run-on processes at a fine observational scale that produced an increased concentration of soil N in the patches as patch size increased. This supports the hypothesis that patch generation is a self-reinforcing process where positive feedback creates self-organising patterns in landscapes.

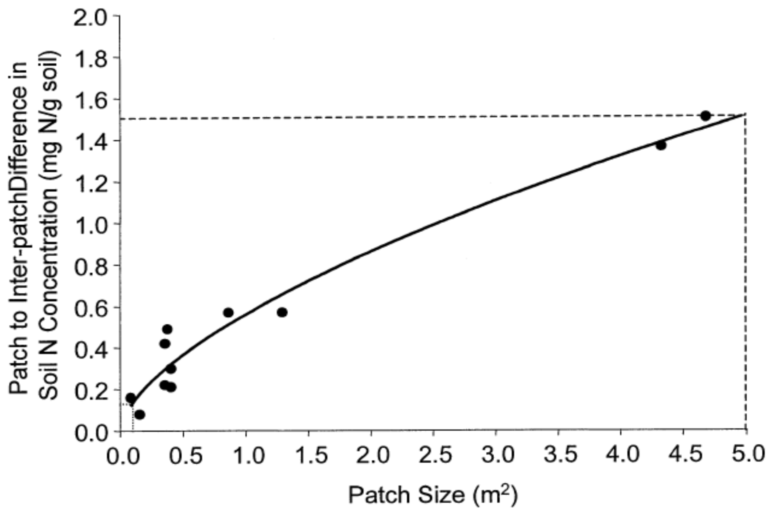

Figure 2.6 Patch to Interpatch differences in soil N in relation to patch size for small-scale local landscape vegetation-soil patches from (Ludwig and Wiens *et al.* 2000).

Analysis of published results for small and large patches showed evidence of a disjunction in resource accumulation capacity based on patch size when patch to inter-patch differences were taken into account as shown in Figure 2.7.

They interpreted these results as providing further support for the soil nitrogen patch scaling rule. Irrespective of whether the soil nitrogen level is high or low, the significant measure is the relative concentration in a patch versus its concentration in neighbouring interpatch areas. This difference can be plotted as a function of patch size (Figure 2.7). The sudden change in scaling relations evident in Figure 2.7 was viewed as evidence of the difference between local scale and regional scale landscape processes.

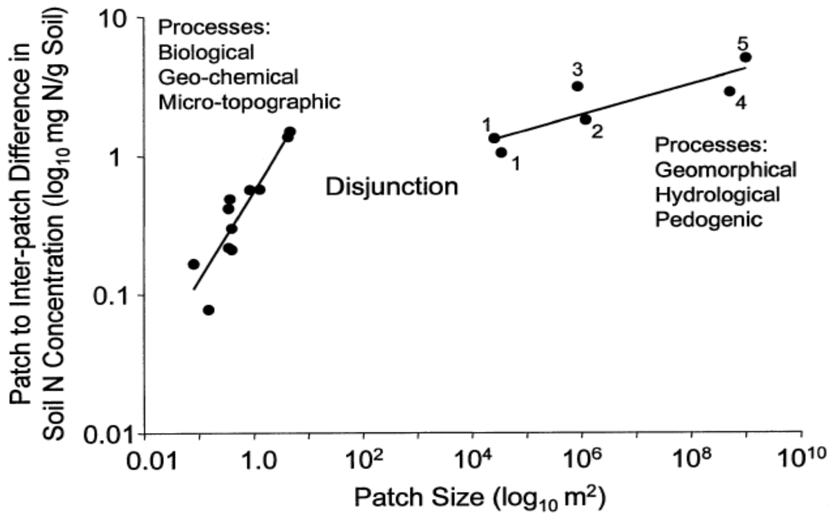

Figure 2.7 Apparent disjunction in scaling relationship for soil N accumulation between small local patches and large regional patches from (Ludwig and Wiens *et al.* 2000).

In studies of hillslope erosion in the Weaney creek watershed (near Charters Towers, North Queensland) Bartley and Toth *et al.* (2006) found that the spatial distribution of patches and their interaction with soil characteristics was necessary to explain differences in runoff and sediment yield. The location of high and low cover patches was found to be more important than the average condition of the landscape. It is generally accepted that sediment yield declines with increase in patch size (Schumm 1977).Bartley and Toth *et al.* (2006) found that:

> *"--- the spatial arrangement of vegetation may in some cases, override the effects of increasing spatial scale ---because severely disturbed small areas could form large bare patches and even rills and gullies, resulting in much higher sediment losses per unit area than a larger sized plot with a high cover".*

This is an inverse relationship between sediment generation and scale of patch, a phenomenon that has been observed previously (Wilcox and Breshears *et al.* 2003). This finding further highlights the need for accurate identification of patch size and type (amount of cover) for reliable application of scaling functions to calculate sediment loss in tropical savannahs. Bartley and Toth *et al.* (2006) concluded that in tropical savannahs the mosaic of vegetation and soil patches and their interactions predominated over the value of "average cover" when it came to correlation with sediment loss.

The influence of the structure of the mosaic of vegetation and soil patches on runoff and sedimentation was also modelled in a Mediterranean landscape setting using the LISEM (Limburg Soil Erosion Model) with field parameters from Rambla Honda, Spain (Boer and Puigdefabregas 2005). Vegetation cover was held constant throughout. Overall, they found that the landscapes behaved dynamically, with varying runoff and soil loss depending on the intensity and duration of precipitation, the autocorrelation distance of the vegetation and the gradient of the slope.

The spatial organisation of bare and vegetated patches was found to have a substantial impact on both sediment and water fluxes. Hillslopes on which the vegetation cover was spatially structured (defined autocorrelation levels) produced more runoff and soil loss than hillslopes where the vegetation cover was more uniformly distributed. Coarsely aggregated vegetation cover (longer auto correlation distance) also resulted in more runoff and soil sedimentation than finely aggregated vegetation, irrespective of amount of rainfall or slope gradient. Also, steep slopes behaved differently from gentle slopes in generating soil loss. Finely aggregated vegetation on gentle slopes resulted in more soil loss then coarsely aggregated vegetation whereas on steep slopes coarsely aggregated vegetation lead to more soil loss than finely aggregated vegetation. No studies on the structure of savannah vegetation on soil loss and erosion appear to have been reported.

In summary, while the amount and type of vegetation cover has a major influence on sediment and runoff from sparsely vegetated landscapes, there is a growing body of evidence that the structure of the landscape features (patch shape, size, location and autocorrelation distance, slope gradient and soil surface condition) play a major, albeit yet incompletely defined role in savannah hillslope runoff and sedimentation (Bartley and Toth *et al.* 2006, p. 3330).

In summary, these studies have shown that the observation scale of the patches affects the Scaling Function that applies to them. It raises the question as to the appropriate observation scale at which to measure land cover for calculation of landscape leakiness.

2.6.3. Scaling relations

Ecological process analysis requires accurate analysis of landscapefeatures from which the processes emanate. Optimal landscape feature identification requires three scales to be matched; i) spatial heterogeneity, ii) ecological process and iii) spatial and temporal image resolutions. These scales and the potential interaction between them need to be explicitly considered when measuring ecological processes (Bradshaw and Fortin 2000, p. 61). It is inevitable that these processes vary in both time and space. For example patch density changes over time subject to management and climatic factors as well as differing from one point to another at any given time (Leitao and Miller *et al.* 2006). It is generally agreed that the most suitable imagery for analysis of landscape features and ecological processes is one in which the resolution corresponds to or is finer than the size of the feature or process being analysed (Csillag and Fortin *et al.* 2000).

Landscapes are naturally spatially heterogeneous and consist of a number of patches of different sizes that cannot be matched by a single image resolution. It is thus necessary to agree on the predominant patch scale of interest and use imagery with a resolution that matches it or is finer than it is. In Section 4.1.2 for example, the effect of patchiness at different image scales on leakiness at Virginia Park Station was discussed based on the work of Bastin *et al.*(2008). However, if the analysis also includes concurrent use of larger patches ideally requiring use of lower resolution (larger scale) imagery, upscaling the higher resolution imagery may be an option. However, the resampled imagery will have neither the same pixel values nor the same structure as the lower resolution native image. This is the dilemma that lies at the core of rescaling imagery so as to correspond to the scale of original landscape features and which gives rise to the need for scalograms (Wu and Shen *et al.* 2002).

Errors in both value and structure of the image get introduced through processes such as; i) resampling to a different scale, and ii) “cleaning up” images through smoothing. Where patches are extracted from images in the form of polygons through classification, errors are introduced by rendering of data from ground truth information. The magnitude of these errors depends on the interaction between the landscape integrity and the scale of sampling. Errors generated in creating landscape patches propagate to errors in processes.

Thus to calculate ecological processes (e.g. leakiness) from images accurately and reliably, it is essential to understand both the process and the way in which it is represented by the image scale. Temporal comparisons therefore require consideration of change in patterns over time such that the same image scale may not be appropriate for measuring the same process over the same area at different times. For example, the patchiness of a degraded grazing catchment (e.g. during or after a period of severe drought) might be accurately measured using 30m resolution imagery (e.g. Landsat TM or ETM+) while the same catchment once rejuvenated might be more accurately measured using higher resolution imagery (e.g. SPOT or Ikonos).

Often a priori decisions have to be made about the scale of spatial auto-correlation in a landscape in order to select the most suitable image scale. Bradshaw and Fortin (2000) recommended that data be collected at multiple scales and at different times over the same area to minimising the effect of spatio-temporal changes on processes. They further recommended that where there is less information available about processes and rates of change, more reliance should be given to finer spatial scale information.

2.6.4. Upscaling methods

Upscaling refers to changing the resolution of an image to a coarser scale or lower resolution (Ludwig, J. and G. Bastin *et al.* 2007). It is done by resampling finer scale pixels to create coarser scale pixels. Most conventional GIS software offer three or four resampling algorithms, namely Nearest Neighbour (NN), Majority (M), Bilinear (BIL) and Cubic Convolution (CC) (Lillesand and Keifer *et al.* 2008, pp 487-489).

All upscaling methods affect the upscaled pixel values which in turn changes the patterns recognisable at different scales (Hay and Nieman 1996). This occurs because spectral variations captured by sensors change non-linearly with scaling trajectory (Turner and O'Neill *et al.* 1989). As a result, when data at different scales and/or from different sources are integrated, substantial errors can occur (King 1991).

Hay *et al.* (1996) evaluate the performance of three conventional upscaling methods plus three additional methods for maintaining feature accuracy. The additional methods were Non-overlapping Averaging (AVG), and Square (SUP) and Round (RUP) Kernel Variance Weighted Upscaling. When evaluated over the range from 1.5m to 10m resolution using Canadian Aeronautics and Space Institute imagery (CASI) of forest areas, they found that the SUP and RUP techniques produced superior results most of the time followed in declining order by AVG, BIL, NN and CC resampling methods.

2.7. Effect of Image Structure on Leakiness

This Section provides a review of the literature on how the scale of imagery affects the leakiness analysis of catchments. Particular emphasis is placed on spatial scale, its change with resolution and its relationship to landscape features. There are two types of spatial scale in images, scale of measurement and scale of variation in the measured data. As well, images also exist within a temporal scale as reflected by their date of capture. Spatial data are the result of sampling at a particular measurement scale (interval and support) and contain within them the spatial variation associated with that scale of measurement. They are thus only a filtered view of reality and inextricably link the scale of variation to the scale at which it was measured.

2.7.1. Spatial scales

Scale of measurement can affect the measurement of landscape processes through the use of temporal and spatial resolutions different from the ecological features driving the environmental processes (Bradshaw and Fortin 2000). Leakiness measurement relies on the type and location of cover features in a catchment (Ludwig, J. and G. Bastin *et al.* 2007). The scale of measurement determines the cover or bare ground features and their spatial variation as recorded in an image. These change with change in resolution due to scale dependent autocorrelation within the image. For example larger minimum mapping units imply the underestimation of landscape diversity and fragmentations (Saura 2002). What may appear as homogeneous features at one scale can become heterogeneous at another scale.

The amount of autocorrelation in a scene provides a measure of the spatial structure of the image. This can be used to measure how features are expressed or regularised by different native resolutions or by resampling techniques. This raises the question of which measurement scale is “best” for the landscape function processes being investigated.

To address this issue it is necessary to consider two aspects of image formation, Point Spread Function (PSF) (Mather 2004, p. 29) and Pixel Support (PS). PSF refers to the blurring and degradation due to the effect of relatively light or dark objects within a pixel’s IFOV (Instantaneous Field Of View), and noise and distortions when the radiance is transmitted through an optical filter to a sensor (Figure 2.8 after (Sakurambo 2009)). PS refers to the Support area (Atkinson and Tate 2000, p. 611) from which an image derives its PSF (X x Y in Figure 2.8). This shows that spatial variation in the center of the support receives more weight than towards the edges.

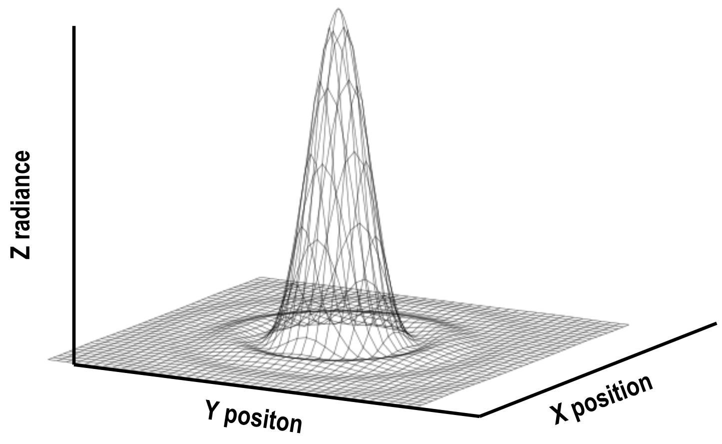

Figure 2.8 Effect of Isotropic Point Spread Function on pixel upwelling radiance

The image sampling framework defines the scale of measurement and thus the PSF and PS. To address these factors it is necessary to consider the support that accompanies each measurement scale and the relationship of the Support to the environmental features being measured. The value (DN) recorded by the sensor's charge coupled device is the quantised analogue electrical signal resulting from the averaged photon input for each Support as modified by the PSF applicable to each pixel.

2.7.2. Spatial variation

Spatial variation is defined by both first and second order properties of the image. These include the mean or average value (first order) and the variance of the values and their covariance function (second order). Second order properties measure relationships between data and this allows detection of structural shifts in images, which, while retaining similar first order properties, may be fundamentally different from each other. Spatial structure and spatial variability are both able to be quantified from the semi-variance and the variogram model for a scene (Garrigues and Allard *et al.* 2008).

The spatial structure of an image is measured by the difference in value between any two points compared to the average difference between all points in the area of interest. The extent to which points differ, based on how far apart they are, is a measure of their autocorrelation and it can be measured by calculating the image variogram. Variograms for images are estimated by calculating ½ of the squared difference between all available paired observations at given distances (called Lags) from each other. This is done for all the point separation distances in the area of interest (Lloyd 2010). The result is a plot of the semivariance (½ of the sum of the variances is used because the variance of each distance interval is calculated twice) against distance interval. Semi-variance is given by Equation 2-12 (after Lloyd 2010)

$$\gamma(l) = \frac{1}{2p(l)} \sum_{i=1}^{p(l)} \{z(x_1) - z(x_1 + l\}^2 \qquad (2\text{-}12)$$

where γ = semivariance
l = lag
p = paired observations

The distances between points can be calculated in all directions (omnidirectional) or in a particular direction (unidirectional) to detect anisotropy. Because the variogram characterises the amount of difference in values at different distances it provides a measure of the spatial structure of the image (or data). A ‘typical’ ascending bounded variogram is shown in Figure 2.9 with the major features identified. The key features are; i) Nugget Variance (NV) which represents the unresolved variation, ii) Sill Variance (SV) which is the total variance at the Sill, iii) Spatially Correlated Variance (SCV) or the variance of the structural component of the image, and iv) Range (R) which represents the scale or frequency of the spatial variation. There may be multiple scales of features in which case there will be multiple ranges called First Range (FR), Second Range (SR) et cetera. Unbounded variograms have no Range, which indicates that the variance continues to increase with lag and there is thus no autocorrelation between values. From these features various indices (UPV Indices (partial list from Balaguer and Ruiz *et al.* (2010))) have been developed. One of the most frequently used indices is the Nugget to Sill Variance Ratio (NSVR) which measures the proportion of total observed variation that cannot be explained by observed spatial dependence of the feature (Kravchenko 2003).

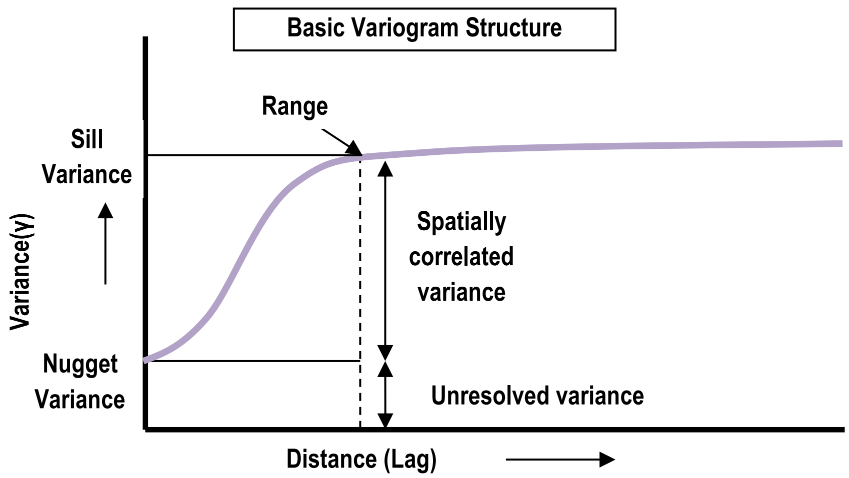

Figure 2.9 Gaussian bounded variogram

Bounded variograms provide a wealth of information about the structure of the image. Variance between images can be compared and analysed using indices. They are organised in two groups for convenience; i) conventional indices (Lloyd 2010) and ii) UPV indices as summarised in Table 2-7 and Table 2-8. Both approaches were used in investigating research Objective A3.

Table 2-7 Conventional variogram Indices (from (Lloyd 2010))

NV (Nugget Variance) = Unresolved Variation (Variation at Lag 1)

FR (First Range) = Scale of spatial variation,

- Short ranges = high frequency of spatial variation (e.g. 10m and 25m),
- Long ranges = low frequency of spatial variation (e.g. 250m)

SV (Sill Variance) = Variation at the Range (∑ Unresolved Variation + Structural Variation)

SCV (Spatially Correlated Variance) = Sill Variance - Unresolved Variance. (A measure of the structural variance)

NSVR (Nugget to Sill Variance Ratio) = Unresolved Variance/ Sill Variance. This measures the relative amount of variance captured by the scale of measurement.

NSCVR (Nugget to Spatially Correlated Variance Ratio) =Unresolved Variance/ (Sill Variance – Unresolved Variance)

(See Figure 2.9 for identification of terms in definitions).

Table 2-8 UPV Indices (partial list from Balaguer and Ruiz *et al.* (2010))

RVF (Ratio Variance First lag) =Total Variance/First Lag Variance

- High = high variation at long distances, or Low variation at short distances
- Low = Vice versa

RSF (Ratio Second First lags) = Second lag variance/ First lag variance.

FDO (First Derivative near the Origin) = ($\gamma_{1-}\gamma_2$)/h, where h= lag distance. This is effectively the slope of the variogram between the first two lags.

FML (First Maximum Lag) = First Range of semi-variogram. Equivalent to the Sill Variance.

MFM (Mean of semi-variogram up to First Maximum) = $\frac{1}{Max_{-1}}\sum_{i=1}^{Max_{-1}}\gamma_1$. This represents an average of the semivariance values between the first lag and the first maximum

AFM (Area between the First lag and the first Maximum) =
$\frac{h}{2}\left(\gamma_1 + 2\left(\sum_{i=2}^{\max\_1-1}\gamma_1\right) + \gamma_{\max_1}\right) - \left(\gamma_1\left(h_{\max_1} - h_a\right)\right)$

(See Figure 2.10 for identification of definition terms).

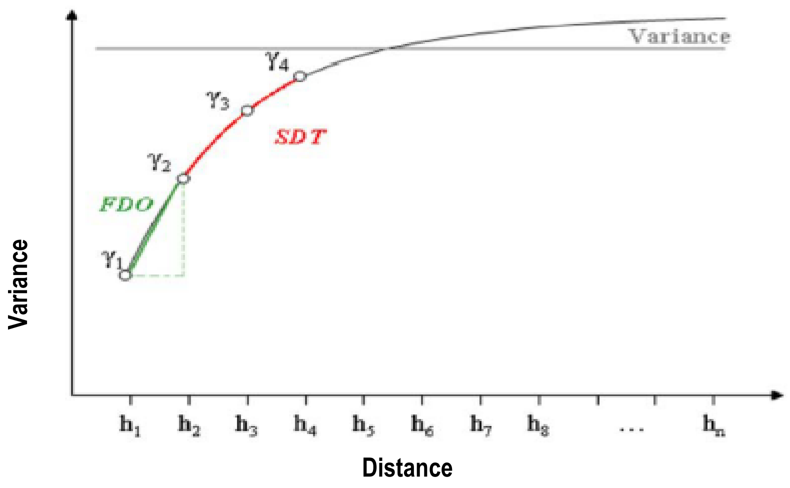

Figure 2.10 Monotone semi-variogram after (Balaguer and Ruiz *et al.* 2010)

2.7.3. Spatial patterns

Turner and O'Neill *et al.* (1989) showed that clumped landscape features were retained when resolution was decreased while features that were dispersed were rapidly lost. In studies of bare-ground patches in semi-arid ecosystems 2010) found the segmentation level whose regression predictions had a spatial dependence closest to the spatial organisation of the field samples showed the highest predicted-to-observed correlation. They suggested that a range of “best” analysis scales might exist depending on the attributes being measured along with a need for methods to identify scales that perform best for specific analysis purposes.

Image classifications minimizes the MAUP effect because data are aggregated with respect to patterns in the original image (Karl and Maurer 2010, p. 199). Selection of measurement scale that minimises the sill variance of features is a way to minimise the MAUP effect. This may offer a procedure to increase accuracy in measurement of cover features on which leakiness depends and in turn increase the accuracy of landscape leakiness calculations. This scale is likely to be different for different variables (Addink and deJong *et al.* 2007). Karl and Maurer (2010) demonstrated the use of regression techniques applied to spatial correlation between objects to accurately predict their occurrence at different scales. This approach supports the concept of scaling domains referred to earlier (Wu 2004). Within a scaling domain, the relationship between variance and scale stays the same because the underlying landscape patterns are governed by the same processes. Image segmentation (through object oriented analysis) was found to give better results than square pixel aggregation techniques (Karl and Maurer 2010).

Object oriented image classification, an alternative to pixel based classification, has gained favour because it uses contextual information, (second order information) and results in more accurate maps. However, it also introduces biases into landscape patterns, firstly through the MAUP effect and secondly through change caused by inherent variance differences in multi-date coincident images (Mas and Gao *et al.*

2010). The effect of the biases depends on the use of the classified image. Qi and Wu (1996) showed that there is a spatial scale of landscape features beyond which resolution effects don't have any measurable affect.

2.8. Cover Position and Catchment Leakiness

Until recently, the effect on landscape function of adding or removing cover has been little considered. Trees are often planted to "improve" or "restore" catchments. Typically, grasses and herbs are "controlled" to reduce competition and allow faster growth of the trees. However, neither process necessarily has regard for:

a. The type of "improvement" required in the catchment,
b. The most suitable type of vegetation to achieve the sought after "improvement" or
c. The morphological features on which the vegetation is to be located

This aspect of the research investigated the effect on catchment leakiness of systematically revegetating selected morphological features of the catchment using the "perennial tall tussock grasses" cover type (e.g. *Heteropogon contortus*) function in the LC.

2.8.1. Patchiness

The importance of morphological features in initiating the dynamic erosion-transfer-sink geomorphic system responsible for the banded vegetation patterns in central Australia was recognised by Mabutt and Fanning (1987). The vegetation grove-intergrove patterning characteristic of semi-arid eastern Australia was documented by Tongway and Ludwig (1990). They described the grove-intergrove pattern as being strongly influenced by the topography where there were repeating patterns of gently sloping water run-off zones (fetches) above an interception zone, which stored the water it received, followed by a run-on zone, which stored more water than it received. This sequence had the effect of slowing down the movement of resources from upland areas as it moved to the drainage channels. Physical separation of the areas allowed soil sampling of these areas and analysis showed consistent differences in water holding capacity, nutrient levels, cation exchange capacity (CEC) and soluble salt levels between the 3 zones.

Ludwig and Tongway (1995) postulated that long-lived patches favour landscape stability through self-reinforcing feedback processes. Small changes in topography can alter the hydrologic functioning of these systems such as caused by intensive grazing. Further studies on 3 land-systems in eastern Australia's semi-arid woodlands confirmed this pattern at 3 different scales (Ludwig and Tongway 1995). They found that each land-system was highly organised with distinctive resource rich patches separated by open, resource-poor areas. At the larger scale, the zones were separated by inter-groves while at the finer scale the components were more closely spaced across the landscape. Soil tests confirmed the patches were acting as sinks for nutrients lost from source areas. They concluded that such an overall network of patches was conserving the limited resources in the landscape.

Creating artificial accumulation areas, interspersed with run-on areas was successful in rehabilitating degraded semi-arid areas where mechanical treatments had failed (Ludwig and Tongway 1996; Tongway and Ludwig 1996). Piles of shrubs and branches were arranged across the landscape and after 3 years, they had increased organic nitrogen, organic carbon, CEC and exchangeable potassium and calcium in the surface layers. As well, the patches accumulated soil, increased water infiltration, increased biological activity and had higher respiration rates.

Loss of structured patchiness was found to have a large influence on the ability of landscapes to capture and store rainfall and soil (Ludwig and Tongway *et al.* 1999). Once the structured patchiness was lost, they found the landscape quickly lost its ability to capture, store and recycle new materials from upslope run-off areas and became “dysfunctional”. They concluded that the main cause of “dysfunctional” landscapes was overgrazing and that such landscapes could only be rehabilitated by rebuilding patchiness to trap and store resources. They suggested that this be done by relocating branches and groundcover into piles arranged on the contour in areas where rehabilitation was needed.

2.8.2. Ground Cover

Ground cover is often measured as “average cover” representing the percent of the overall area covered by biomass. It can be measured in many ways, sometimes directly as a percent of the area covered by organic matter or as the mass of material per unit area and sometimes indirectly by the use of photographic indices such as the Normalised Difference Vegetation Index (NDVI) (Rouse, J. W. and R. H. Haas *et al.* 1974), Perpendicular Distance Indices (PDIs) (Pickup and Chewings *et al.* 1993) or the Ground Cover Index (GCI), the inverse of the Multiple Regression Bare Ground Index (MRBGI) (Schmidt and Tindall *et al.* 2010) or other similar methods. These methods estimate field cover with a spatial resolution determined by the sampling window. “Average cover” values do not express patch scale information. GIS classification permits analysis of the spatial distribution of classes of cover and thus the identification of patches with different levels of cover.

Schumm (1977) first showed that soil erosion was not influenced by the amount of vegetation cover when the levels were under 15%. Abrahams *et al.* (1988) also found no correlation between runoff and vegetation when the cover was less than 10%. Boer and Puigdefabregas (2005 p. 150) reported that vegetation cover alone was insufficient to explain leakiness processes in catchments with patchy cover. Bartley and Toth *et al.* (2006 p. 3319) found that “average cover” measurements do not consider the spatial distribution pattern of the covered and bare areas. Boer and

Puigdefabregas showed that spatial organisation of bare and vegetated surfaces had a substantial impact on runoff and erosion (See Section 2.6.2).

Resource limited landscapes are initially characterised by having patchy cover. Patchiness of savannah landscapes is influenced by grazing pressure, soil type and forage palatability. Bartley and Toth *et al.* (2006 p. 3318) reported that there had been little investigation on how the geographical patchiness of "average cover" hillslopes affected runoff and sediment yield. Their research, based on 3 flumed field sites in the Weaney Creek catchment in the northern dry tropics area of Queensland, over a number of years found that:

(a) "Average cover" values do not explain the differences in runoff and sediment yield at the hillslope scale.
(b) The spatial distribution of patches and their soil characteristics need to be considered when interpreting runoff and sediment yield.
(c) Hillslope topography strongly affects hillslope hydrology.
(d) Antecedent soil surface conditions (SSC), surface scaling, type of clay, sub-surface flows, depth of the A-horizon and biological activity also affect hillslope runoff.
(e) While bare patches contribute to excess runoff and soil particle mobilisation, the position of the patches relative to down slope grassed patches ultimately determines whether the mobilised materials enter drainage lines (i.e. the coarser particles are filtered out)
(f) The suspended sediment proportion of total soil movement increases as cover increases.
(g) Runoff and sediment mobilisation during the "first flush" period are different from average annual runoff and sediment yields meaning that the spatial arrangement of cover at the beginning of the rainy season is of particular importance to catchment leakiness.
(h) Fine cover patches close to drainage lines trapped and stored sediment preventing it from entering watercourses.

They concluded that; (i) the spatial arrangement of cover can override the effect of increase in scale on reduction of sediment yield so that large scale areas can yield more sediment loss per unit area than small scale areas depending on the arrangement of the vegetation patches, (ii) the interaction of covered and uncovered patches at the hillslope scale can override results based on "average cover", (iii) bioturbation and soil surface condition are better predictors of runoff and sediment yield at the hillslope scale than cover, and (iv) the position of low and high cover patches is more important than the "average cover" of the catchment.

In further work, Ludwig and Bartley *et al.* (2007 p. 839) showed that loss of sediment from runoff areas depended on the scale of the patch configuration. Coarse grained hillslopes had 2.5 times the sediment loss of fine grained hillslopes with the same "average cover". This indicates the role of the scale of the patchiness in determining the amount of sediment loss, and by inference, the amount of nutrient loss. The authors suggested that the non-linearity's in the erosion process were due to different scales of bare areas amplifying sediment loss because the absence of a finer patch pattern did not slow down the runoff and retain the sediment before it entered the watercourse. They suggested that the non-linear response of erosion and runoff across scales (cross scale interaction (CSI)) is induced by grazing effects that create the patterns of coarse scale bare patches. By contrast, erosion from fine grained hillslopes scaled up linearly. The implications for grazing management are that more uniform cover (finer scale patches) on lower slopes and areas bordering riparian zones across which water flows to drainage channels is important to reduce the loss of sediment and nutrients to streams and ultimately to the marine environment.

The concept of sensitivity of whole of catchment leakiness to geomorphic location of vegetation cover is the basis for the leakiness testing investigated in Chapter 7.

2.9. Conclusion

The continuing poor ecological condition of the nation's rangelands, despite the above average rainfall in 2010-2012, and the increasing human pressure on them has increased the need for wide scale frequent monitoring of their condition. Monitoring of effects rather than of usage has been found to be more effective. Landscape Function Analysis has a sound theoretical basis. Its track record as a means of land condition monitoring is developing.

Use of satellite imagery for calculating Landscape Function Indices (LFIs) offers the opportunity for rapid assessment of large areas on a repetitive basis. The areas can be compared in an historical context using archival imagery. However, this approach is constrained by the dichotomy of scale. Calculation of LFIs depends on detecting spatial variance. Images with different resolutions have different variances because changing the spatial scale of an image also changes the variance by regularization.

The challenge to making greater use of satellite imagery for Landscape Functionality Analysis is two-fold: i) to find spatial resolutions that match the dimensions of the ecosystem Scaling Functions they are being used to detect, and ii) to find a way of preserving spatial variance as spatial resolution changes. This research addresses these issues. The foregoing discussion highlights the possibility of using semi-variogram analyses to calculate new Lags for lower resolution Supports (images) from higher resolution samples as a way of calculating comparable resolution scaling factors to solve the problem. The overall method is outlined in the following section and detailed approaches are described in Chapters 4, 5, 6 and 7.

CHAPTER 3

RESEARCH METHODS

3.1. Introduction

This section describes the research approach used to investigate the effect of different image resolutions on the measurement of Landscape Function Indices (LFIs). The LFI used in this study was the Leakiness Index (LI). The research investigated how changes in spatial scale affect the LI. Methods for comparing leakiness at different scales were developed. This enabled the development of Scalograms for converting leakiness at one scale to leakiness at another scale based on either change in image resolution or change in image variance. The effect of changing spatial scale on image structure was investigated to explain the changes in leakiness values.

3.2. Overview of processing and analysis

The study required that data be collected and pre-processed in such a way that comparisons of cover indices, leakiness and image structure could be compared at different resolutions with minimal processing artefacts. These procedures are covered in the balance of this chapter.

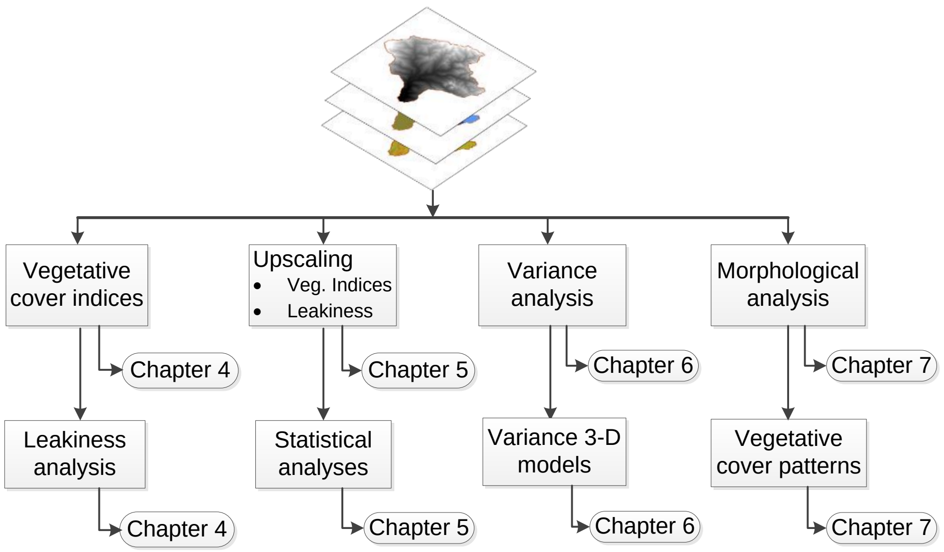

Figure 3.1 Chapter guide to the processing and analysis procedures

The detailed processing and analysis steps are different for each area of the study and are described in the Research Methods sections of their respective Chapters. Figure 3.1 provides a guide to the type of processing and analysis to be found in each chapter.

3.3. Study Area

A suitable study area was identified to meet the following research design criteria:

a. Savannah grazing catchment
b. Moderate size, about 6,000 ha
c. Mostly natural vegetation, as indicated by a high percentage of Remnant Ecosystem vegetation
d. Near to Permanent Survey Markers (PSMs)
e. Identifiable ground reference points (GRPs)
f. Contain or be near to SLATS (State-wide Land and Trees Study) reference sites
g. Cooperative landowners allowing access to their properties
h. Availability of stereo aerial imagery
i. Coincident cloud free satellite imagery at multiple scales

The experimental catchment is a savannah grazing catchment of 5,800 ha, 20 km SW of Charters Towers in North. Queensland (Figure 3.2).

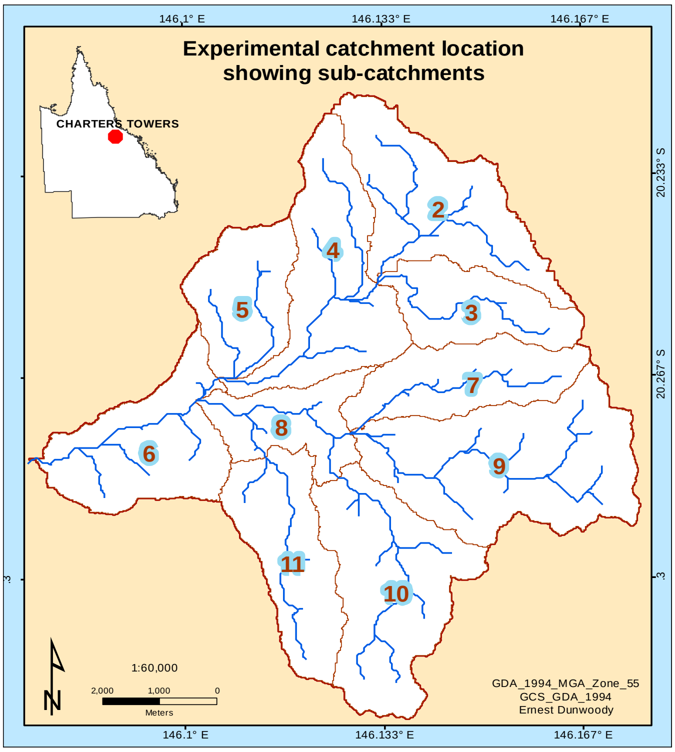

Figure 3.2 Location of experimental catchment

It was analysed at three resolutions and the attributes of the catchment at each resolution are shown in Table 3-1. Summary statistics for the sub catchments are shown in Appendix 1.

Table 3-1 Catchment summary statistics

Catchment	Perim_km	Area_ha	Slope_avg (%)
10m	53.51	5898.80	3.719
25m	49.90	5890.50	2.565
250m	35.74	5754.31	1.214

The catchment is comprised predominantly of River Red Gum (*Eucalyptus camaldulensis*) and Blue Gum (*E. tereticornis*) woodlands (Qld RE 9.5.3a) along the streams and Iron Bark woodlands (*E. crebra, E. xanthoclada*, and *E. drepanophylla*) (Qld RE 9.3.1) away from the streams (Figure 3.3). The relative amounts of each primary RE are shown in Figure 3.4.

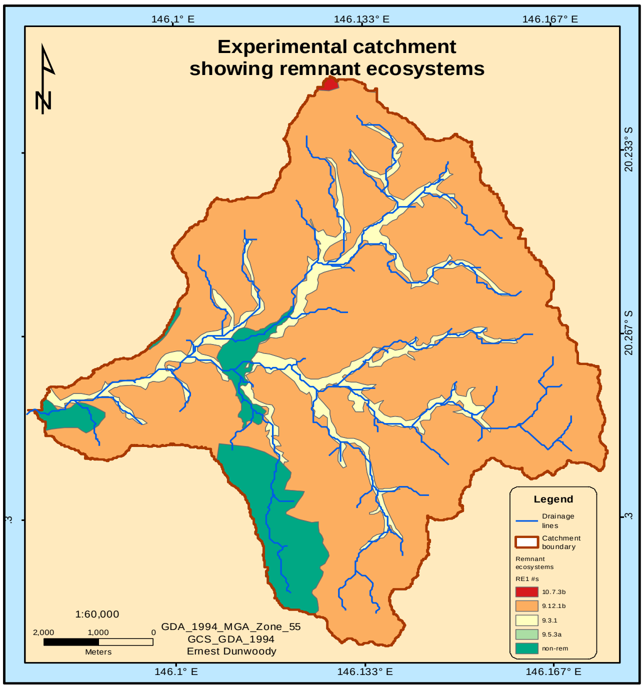

Figure 3.3 Remnant ecosystem coverage of experimental catchment

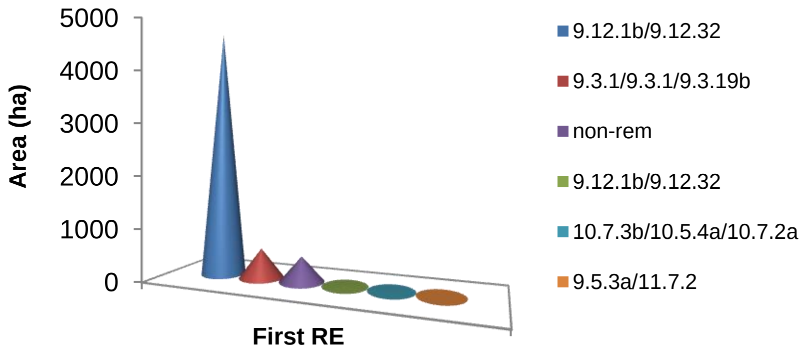

Figure 3.4 Relative amounts of each Remnant Ecosystem (ha)

In the late dry season of 2011 the catchment showed a range of vegetative cover conditions varying from well vegetated to sparse and minimal vegetation, break-away gullies and un-vegetated ridges as illustrated by Photographs 3-1 to 3-6.

Photograph 3-1 Savannah grass lands

Photograph 3-2 Iron Bark woodland

Photograph 3-3 Blue Gum creek flat

Photograph 3-4 Mixed Iron Bark and Blue Gum woodland

Photograph 3-5 Break-away gully in duplex savannah Sodosol soil

Photograph 3-6 Gravel ridge line lacking vegetative cover

3.4. Research Approach

The research approach involved a standardized analytical processing path in which combinations of different variables could be processed depending on the research question being tested. The schema for this is shown in Figure 3.5.

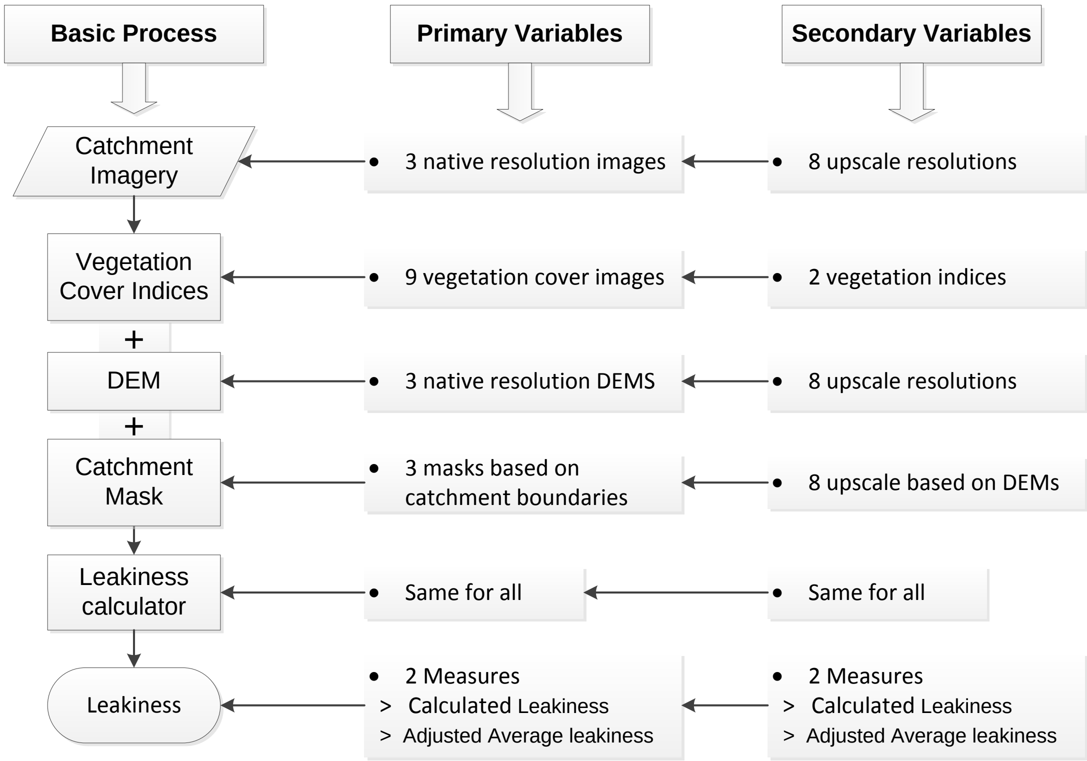

Figure 3.5 Research Schema

The left column shows the common processing path used for imagery at all scales. Different combinations of primary and secondary variables (columns 2 and 3) were applied depending on the experimental requirements. These are outlined further in Chapters 4, 5, 6 and 7. The sources of data for the variables are described in the next section.

3.5. Data Sources

3.5.1. Satellite imagery

Concurrent satellite imagery of the experimental catchment was needed to calculate the vegetation cover indices for use in the Leakiness Calculator. Table 3-2 summarizes the sources of the satellite imagery used for this.

Table 3-2 Source imagery

Satellite sensor	Image number	Capture date	Capture resolution	Image Source
SPOT 5 HRVIR	372_391_291205	29 Dec 2005	10m	North Queensland Dry Tropics NRM Body (NQ DTNRMB)
Landsat TM 5	l5095074_07420051126	26 Nov 2005	30m	GloVis (USDOI 2012a)
MODIS				
250m	mod02qkm.a2005363.0025.005.2010166234014	29 Dec 2005	250m	LP DAAC (USDOI 2012b)
500m	mod02hkm.a2005363.0025.005.2010166234014	29 Dec 2005	500m	

SPOT 5 HRVIR data was selected for the high resolution imagery because of its 10m resolution and its capture on the same date at which the MODIS image was captured and a month from the nearest Landsat image capture date. The chronologically closest Landsat image was from Landsat TM 5 captured on 26 November 2005, (path 095, row 074) approximately 1 month before the SPOT 5 and MODIS image capture dates. It was downloaded from the USGS Earth Resources Observation and Science (EROS) Center using GloVis (USGS 2014). Two MODIS images were used in order to obtain bands with spectral windows similar to the SPOT 5 and Landsat TM 5 spectral windows. They were downloaded from the Goddard Space Flight Center, Land Processes Distributed Active Archive Center (LPDAAC) (NASA 2014a).

Pixel dimensions and band configurations were adjusted in two of the images so that the vegetation cover indices could be calculated in a comparable manner from each image. The Landsat TM 5 image was resampled from 30m to 25m in ERDAS Imagine software using cubic convolution resampling. MODIS imagery at both 250m and 500m resolution was used to obtain spectral bands comparable to the SPOT 5 and Landsat TM 5 bands as shown in Table 3-3. Bands 3, 4 and 6 from the mod02hkm source image (500m pixels) were unstacked, resampled to 250m by cubic convolution and restacked with bands 1 and 2 from the mod02qkm image (250m pixels) to create the spectrally comparable rearranged MODIS image.

Table 3-3 Rearrangement of MODIS bands for consistency with SPOT and Landsat spectral windows

SPOT 5 (10m)		Landsat TM 5 (25m)		MODIS (250m) Source bands		MODIS (500m) Source bands		MODIS (250m) Rearranged bands	
B #	λ (μm)	B #	λ (μm)	B #	λ (μm)	B #	λ (μm)	B #	λ (μm)
		1	0.45-0.52			**3**	0.46-0.48	**1**	0.46-0.48
1	0.50-0.59	**2**	0.53-0.61			**4**	0.55-0.57	**2**	0.55-0.57
2	0.61-0.68	**3**	0.63-0.69	**1**	0.62-0.67			**3**	0.62-0.67
3	0.79-0.89	**4**	0.75-0.90	**2**	0.84-0.88			**4**	0.84-0.88
4	1.58-1.75	**5**	1.55-1.75			**6**	1.63-1.65	**5**	1.63-1.65

3.5.2. Digital Elevation Models

DEMs of the catchment, at the same resolution as the vegetation cover images, were needed to provide the hydraulic gradient values in the LC software. Table 3-4 provides an overview of the DEMs used for this research. They are described further below.

Table 3-4 DEM Overview details

DEM Type	As Received					Adjusted resolution	Adjustment method
	Format	Coord. Syst.	Datum	Resoln	Ht. Datum		
Aerial Photo	*.tiff	MGA 1994, Z 55	GDA94	5m	Grd. Ref. Pts.	10m	Cubic convol.
1sec SRTM-DEM-Sv1_0	ESRI GRID 32bit flt. pt	GCS	WGS 1984	1 sec	EGM 96	25m	Cubic convol.
GEODATA 9 sec DEMv3	*.ers 32 bit flt. pt.	GCS	GDA94	9 sec	AHD71	250m	Cubic convol.

Calibration of the DEMs began with a comparison of the GRS 1980 ellipsoid, on which the MGA 1994 projection is based, with the WGS 1984 Geoid on which the GPS data is based. GPS records from 5 First and Second Order Permanent Survey Marks (PSMs) were used for the comparison. The results showed an average vertical difference between the geoid and the ellipsoid in the Charters Towers area in favour of the ellipsoid of 56.175m. The XY differences were 0.159m and -0.344m. These results provided confidence in the accuracy of the field GPS records for ground truth data as described in the following section.

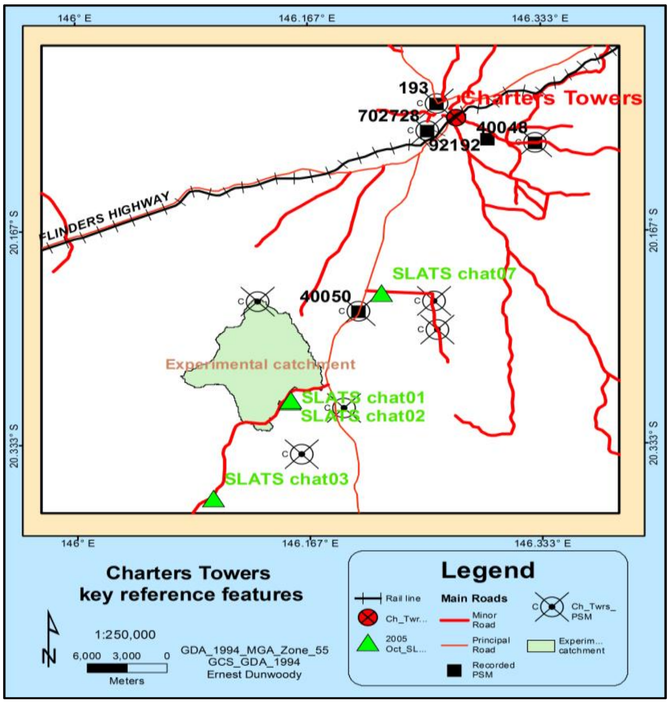

Figure 3.6 Key reference points map

Twenty six stereo aerial photographs (APs) (Appendix 2) were used to produce a high resolution DEM of the study area because no inexpensive high resolution DEM was available. A block file of the stereo images was created with ERDAS Leica Photogrammetry Suite (LPS) (Intergraph 2014) and then exported to Leica's Orientation Management Software (ORIMA) (Leica 2009) for creation of tie points in the 3-D model[4]. The model was geo-rectified using 9 post differentially corrected ground reference points (GRPs). The root mean squared (RMS) error of the final model was 0.2167 pixels. A DTM was extracted from the stereo model at a resolution of 5m using Intergraph's ERDAS Imagine Advanced Terrain Extraction (ATE) software (ERDAS 2006) in LPS using the convergence mode. The extracted DTM was resampled to 10m in ERDAS Imagine by cubic convolution and used as the high resolution DEM for this research.

The accuracy of the 10m DEM was tested against 71 field ground control points (GCPs) as well as the 1sec SRTM-DEM-Sv1_0 values (Table 3-5). The results show that the 9 GRPt DTM had an average vertical difference from the GCPs of -0.71m while the 1sec SRTM-DEM-Sv1_0 had an average vertical difference of -4.40 m. The Standard Deviation and Variance of the sample are also shown in Table 3-5. Both SD and Variance are higher for the 5m 9 GRPt DTM than the SRTM 1s DTM. This is expected because the higher resolution 9 GRPt DTM follows the ground contour more closely than the coarser 1sec SRTM-DEM-Sv1_0 and thus has a higher SD and Variance.

Table 3-5 Accuracy comparison for 9 GCPt DTM against field elevation values and SRTM 1s DTM

Comparison Criteria	9 GCPt DTM, ATE Extraction with convergence (5m pixels)	SRTM 1s DTM, (25 m pixels)
	Δ Z	Δ Z
Avg diff (m)	-0.71	-4.40
SD-s (m)	4.16	1.50
Var-s(m)	17.33	2.25

Further processing of the DEMs is described in the Section 3.7.2.

3.5.3. Ground Truth Data

A field campaign was conducted from 25 September to 6 October 2011 to collect GCPs, GRPs, Vegetative Cover (VC) values and to become familiar with the terrain of the catchment. All data was collected using pre-constructed data dictionaries

[4] The author is indebted to Mr Adrian Neal and Mr Mehedi Etemadi of the Queensland Department of Resources and Mines (as it then was) for assistance with creation of the 3-D model in ORIMA software

(Appendix 3) in a Trimble Nomad coupled by blue tooth with a ProXH pole mounted (2m) GPS antennae (Appendix 4).

Target GCPs were identified ahead of time from SPOT 5 and Landsat 5 imagery. Field records were collected up to 4 km outside the catchment boundary because of difficulty in accessibility to the interior of the catchment. These records were in the area covered by the stereo elevation model. Seventy one GCPs (Appendix 6) were located and recorded in the field for use in geo-referencing and calibrating the AP stereo model. Nine of these were used as GRPs for model georectification. GPS post differential correction was done for all field data using Trimble Path Finder Office software with base station reference files (*.dat) supplied by the Townsville City Council. The post differentially corrected products were exported in Shape file format (Figure 3.7).

Vegetative Cover data was collected using a modified, transect based, discrete point sampling method designed for pastoral environments (Muir and Schmidt *et al.* 2011). The VC records collected in September and October 2011, while indicative for the season, they were not suitable for calibrating vegetative cover indices from imagery captured in November and December 2005. They would however be useful for calibrating imagery captured closer to their date of collection if this opportunity subsequently arose. SLATS (State-wide Land and Trees Study) reference site locations are also shown in Figure 3.7 and ground cover records for those sites were available for 2005.

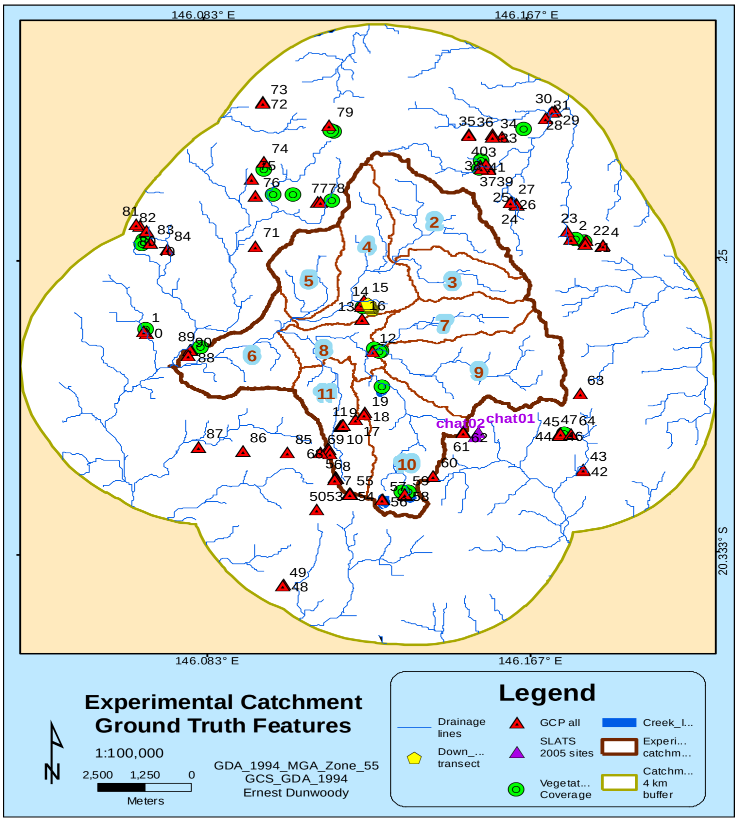

Figure 3.7 Ground truth field records

3.6. Experimental Design

The experiments were designed as a series of progressive analyses to eliminate alternatives as shown in

Figure 3.8.

This approach was used to:

a. find a path to a solution of how spatial scale affects the measurement and interpretation of the Leakiness Index,
b. find options for improving the measurement of Leakiness and
c. demonstrate a practical application of using leakiness measurement to improve landscape function.

Vegetation cover indices from which to calculate the leakiness were constrained by the type of vegetation (savannah) and the bands available in each satellite image. The selected indices and the spectral bands used to calculate them are shown in Table 3-6.

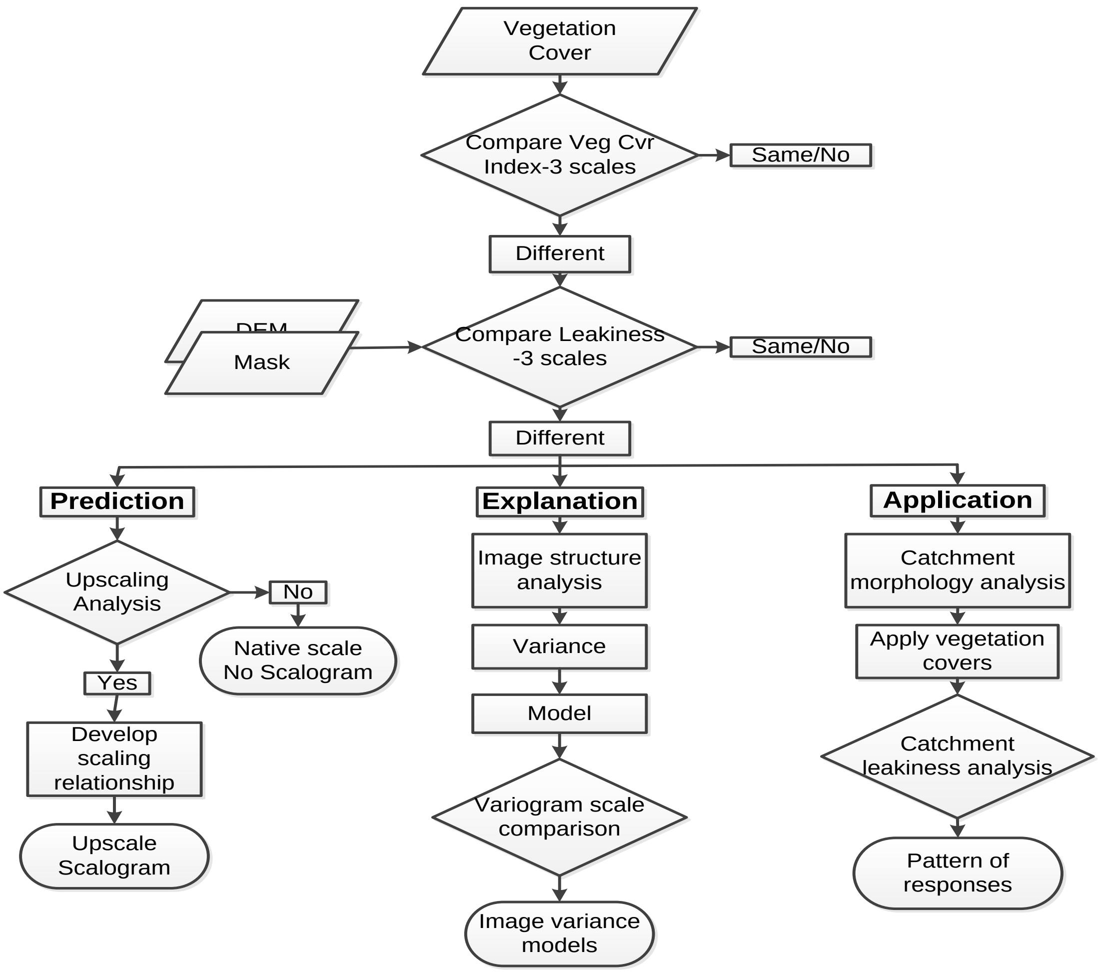

Figure 3.8 Experimental Analysis Path

Table 3-6 Spectral bands in each images used to calculate vegetation cover indices

Sensor	**SPOT 5**				**Landsat TM 5**							**MODIS (restacked 6 band)**					
Band #	1	2	3	4	1	2	3	4	5	6	7	1	2	3	4	5	6
Name	G	R	NIR	SWIR	B	G	R	NIR	MIR1	TIR	MIE2	B	G	R	NIR	NIR2	MIR
Vegetation Cover Index **Λ (nm)**	0.50-0.59	0.61-0.68	0.79-0.89	1.58-1.75	0.45-0.52	0.52-0.60	0.63-0.69	0.76-0.90	1.55-1.75	10.4-12.5	1.08-2.35	0.459-0.479	0.545-0.565	0.620-0.670	0.841-0.876	1.230 -1.256	1.628-1.652
MSDI		X					X							X			
NDVI		X	X				X	X						X	X		
SAVI		X	X				X	X						X	X		
RI	X	X				X	X						X	X			
STVI		X	X	X			X	X	X					X	X		X
CORVI	X	X	X	X		X	X	X	X				X	X	X		X
PDrn		X	X				X	X						X	X		
PDrg	X	X				X	X						X	X			
PDrs		X		X			X		X					X			X
SARVI					X		X	X				X		X	X		

The cover indices from each image were compared with each other and the General Cover Index (GCI) (Scarth and Byrne *et al.* 2008). Different resolutions and different indices produced different values. Leakiness was then calculated from them using the relevant DEM and catchment analysis mask and the pattern of responses was compared. A new measure of leakiness, the Adjusted Average Leakiness (AAL), was developed to overcome the influence of variable cell number on the results.

The pattern of leakiness while consistent with respect to the amount of cover was not consistent between cover index values or with image resolution. Two lines of inquiry were then followed, first to develop a predictive mechanism for leakiness between different scales and second to develop an explanation for the difference in behaviour of leakiness between different cover indices. The former led to the development of resolution based scalograms as a means of converting leakiness at one scale to leakiness at another scale. This was possible for upscaled images but not for comparison between images of different native scales. The second approach involved an investigation of structural changes in images due to different native and resampled scales. 3-D variance models were derived that explained the change in leakiness with change in resolution. This allowed the development of variance based leakiness scalograms.

This information was used to evaluate the effect on catchment leakiness of changing the location and amount of vegetation cover in a catchment. The approach was to classify different catchment morphologies and to impose controlled increases in vegetative cover on each morphological class one at a time. This was done for 2 scenarios: a constant-level-of-cover scenario and a net-increase-in-cover scenario. Measuring the change in overall catchment leakiness identified options that would both increase and decrease landscape leakiness.

3.7. Pre-processing

3.7.1. Imagery

The experimental catchment was contained within a single scene of each type of image (Table 3-2).The SPOT5 image was supplied by the North Queensland Dry Tropics Natural Resource Management Authority (NQ DTNRMB). It had previously been orthorectified by the Queensland Department of Resources and Mines (QDERM). The Landsat image was a Level 1T (Standard Terrain Correction image from the USGS) which had systematic radiometric and geometric accuracy from ground control points and topographic accuracy from the SRTM DEM applied to it (NASA 2014b).The MODIS images were MOD 02 images, which had Level 1B processing applied to them. This processing applies calibrated and geolocated at-aperture radiances (W/(m^2 μm sr) to each of the 36 bands from MODIS Level 1A sensor counts (MOD 01) (NASA 2010).

Because no scenes had to be merged and the experimental design did not involve any scene to scene comparison at the same resolution, no further atmospheric correction was applied to the images. The image DN values were used as received.

A standard sized rectangle containing the experimental catchment was extracted for each image for processing in the Leakiness Calculator.

3.7.2. DEMs

Extraction of the high resolution DEM from 26 stereo aerial images was described in Section 3.5.2. ArcHydro software (Maidment and Morehouse 2002) was used to define the drainage lines and catchment boundaries from the DEM at each resolution (Table 3-4). The difference in pixel resolution resulted in slightly different catchment outlines as shown in Chapter 4.

The Leakiness Calculator software automatically evaluates each DEM for sinks. It will not allow processing if it detects any sinks. The ArcGIS sink filling routine in the Hydrology geoprocessing toolbox in Spatial Analyst did not fill all the sinks. Instead the Planchon/Darboux algorithm available in the Terrain Analysis toolset in SAGA (System for Automated Geoscientific Analysis) (Cimmery 2010) was used because it filled all the sinks.

A rectangle containing the experimental catchment, of precisely the same size as the image rectangle, was extracted for each DEM for processing in the Leakiness Calculator. The lower left X and Y coordinates of both rectangles were adjusted to the same value to achieve precise coregistration by editing the coordinates in the flt.hdr sub-folder in MS Notepad.

3.7.3. Analysis Masks

Raster analysis masks are used in the Leakiness Calculator to define the processing extent. They were generated from the vector files of the catchment boundary at each of three analysis resolutions and positioned in a raster rectangle precisely to match the image and catchment DEM rectangles as described in the preceding section.

3.7.4. Ground Truth Data

Pre-processing of ground truth data for geo-referencing the AP DEM and testing the accuracy of the DEM was described in Sections 3.5.2 and 3.5.3.

3.8. Conclusion

This Chapter has covered the research methods common to each of the four areas of investigation. In addition to outlining the overall research approach, these include the sources of data and its pre-processing so that imagery at each resolution had similar spectral bands for calculating the vegetation cover indices. In addition, a matching DEM and analysis mask was prepared for each image resolution at both native scale and upscale resolutions.

The following Chapters discuss the literature relevant to each Chapter, the Research Methods for the specific topic covered in the Chapter, the Results and a Discussion of the findings.

CHAPTER 4

EFFECT OF IMAGE RESOLUTION AND VEGETATION COVER ON CATCHMENT LEAKINESS

4.1. Introduction

This section investigates the relationship between catchment cover and catchment leakiness through the use of a range of common vegetation indices and the bare ground cover index. Chapter 2 previously provided an overall description of the catchment leakiness calculation process and its dependence on the soil and cover factors.

The soil factor was held constant throughout this research because it was done all in the same catchment however, different methods for measuring vegetation cover were evaluated as discussed in Chapter 2. Both the type and location of photosynthetic vegetation (PV) and non -photosynthetic vegetation (NPV) were investigated for their effect on leakiness. This was done at three image resolutions (10m, 25m and 250m) to evaluate if; i) the type of cover affected the amount of leakiness at the same resolution, and ii) the change in pattern of cover between images of the same area, collected at different resolutions, affected the measure of leakiness.

It was hypothesised that if different vegetation cover indices measured different components of the vegetation, this would lead to both different amounts of cover and to different patterns of cover which in turn would be likely to lead to different catchment leakiness values as found by Ludwig and Eager *et al.* (2006). For example, it might be possible for a higher level of cover to lead to a higher level of leakiness rather than a lower level of leakiness that would otherwise be expected if the cover was located further away from the flow channels compared with closer to the channels.

The Leakiness Calculator algorithms were explained in Chapter 2. The LC software that implements these algorithms produces results in terms of Average Cover, Lmax values and Leakiness Index values for hydraulically sound catchments. The main unit used by prior researchers is the Leakiness Index (LI) a unit less number ranging between 0 - 1. LI declines asymmetrically and sigmoidally with increase in cover (Ludwig, J. and G. N. Bastin *et al.* 2007, p. 5). LI is also sensitive to the spatial patchiness of ground cover within a catchment (Bartley and Toth *et al.* 2006; Ludwig and Eager *et al.* 2006). Ludwig, J. and G. N. Bastin *et al.* (2007) showed that a catchment with a uniform vegetative grass cover of 43% yielded a LI of 0.06 while a non-uniformly grassed comparable catchment with a 54% average grass cover yielded a LI of 0.12. Grass cover was measured by the PD_{54} index (Pickup and Chewings *et al.* 1993) applied to 0.6m resolution orthorectified Quickbird imagery. These LI results matched field sediment runoff results which were low for the uniformly grassed site (0.003, 0.04 and 0.06 t/ha for 2003, 2004 and 2005) and higher for the patchy grassed site (3.10, 2.46 and 2.02 t/ha for 2003, 2004 and 2005).

The LC was tested on imagery of the Purvis Station, a property with a well-documented management record 200 km north of Alice Springs (Purvis 2004). PD54 cover indices from dry season Landsat imagery (MSS and TM) of a test site for 1980, 1988, 1994, 1999 and 2000 showed a steadily increasing trend of increase in cover, except for the year 2000. This matched the photographic and management records for the property. Calculated LI values were inversely related to the PD_{54} cover values for each time interval. Ludwig, J. and G. N. Bastin *et al.* (2007) interpreted this as good support for the usefulness of the LC to provide a measure of landscape function.

Leakiness studies on the Fanning River catchment and its sub-catchments in North Queensland using inverted and rescaled red band values from Landsat TM imagery collected during the dry seasons from 1986 to 2005 showed good correlation between leakiness (LI) and average cover. Two different settings in the LC were tested in this catchment, i) perennial tussock grasses and ii) stoloniferous mat forming grasses. The stoloniferous mat forming grass setting produced higher LI values than the perennial tussock grass settings. This indicated increased leakiness in areas with mat forming grasses as was expected. LI values of different sub catchments were calculated but could not be compared because each sub-catchment ‘had its own shape’. However, comparable cover data was available for like areas and it supported the direction of change in the LI results (Bastin and Abbott *et al.* 2007).

Subsequently, three levels (scales) of validation of the LI were reported by Bastin *et al.* (2008). At Virginia Park Station (NE of Charters Towers, QLD) ground cover data on $4m^2$ quadrats was collected using the BOTANAL technique (Tothill and Hargreaves *et al.* 1992) over extensive areas of 4 sub-catchments. The LI index was calculated at 5 m resolution using rescaled PD54 cover indices derived from resampled Quickbird 2.4m imagery. The BOTANAL records showed that litter was more than 50% of the ground cover in all sub-catchments and the mean total cover was marginally less than the remotely sensed cover (rescaled PD_{54} values). Leakiness (LI) calculated from total cover declined as the average level of ground cover (BOTANAL) increased (Bastin and Abbott *et al.* 2008, Fig. 10). However, when the

BOTANAL scores were converted to PATCHKEY scores (Corfield and Abbott *et al.* 2006) they found a better inverse correlation between LI and PATCHKEY than with BOTANAL scores (Bastin and Abbott *et al.* 2008, Fig. 13).

A comparison of Landsat derived GCI (25m) from both FPC masked and unmasked imagery of the same areas at Virginia park Station recorded much higher amounts of cover (%) than the rescaled PD_{54} index recorded and these were in turn higher than the BOTANAL records. After consideration of weather patterns and differences in data collection times, Bastin *et al.* (2008) concluded that: i) GCI was overestimating ground cover in this area, and ii) The rescaled PD_{54} index values appeared reliable for indicating pixel average cover in this part of the Burdekin River catchment. They also considered that the difference between PD_{54} Quickbird (2.4m) analyses and GCI Landsat analyses (25m) might be that the patch-interpatch discrimination possible at the higher resolution, is subsumed as mixtures within the lower resolution imagery because the physical nature of stoloniferous type grasses may not allow detection of the bare ground fraction thereby leading to a higher NPV component in the GCI analysis. It should be noted that this comparison was based on the linear regression GCI (Scarth and Byrne *et al.* 2008). No comparison has been reported with the fractional cover estimates of PV, NPV and BG developed using SMA procedures (Schmidt and Scarth 2009).

The same investigators found good negative correlation between the GCI from the Fanning River and Virginia Park sites with LI values. Bastin *et al.* (2008) noted that even if GCI over estimates cover and leads to lower LI values, that does not invalidate LI based trend analyses. No applications of the LC were found other than in Australia.

Coarser scale validation of the LI using both GCI and PATCHKEY measurements found that LI inversely correlated with GCI even at very low LI levels (Bastin and Abbott *et al.* 2008, Fig. 22). However, cross plots of LI with PATCHKEY values revealed no sensible relationship (Bastin and Abbott *et al.* 2008, Fig. 23).No applications of the LC were found for sites outside Australia.

The following section describes the methods used to calculate cover and leakiness for a range of cover indices at three different image scales of the experimental catchment and to compare the results.

4.2. Methods

Photograph 4-1 illustrates areas an area of the catchment that leaks resources and Photograph 4-2 shows an area that conserves resources.

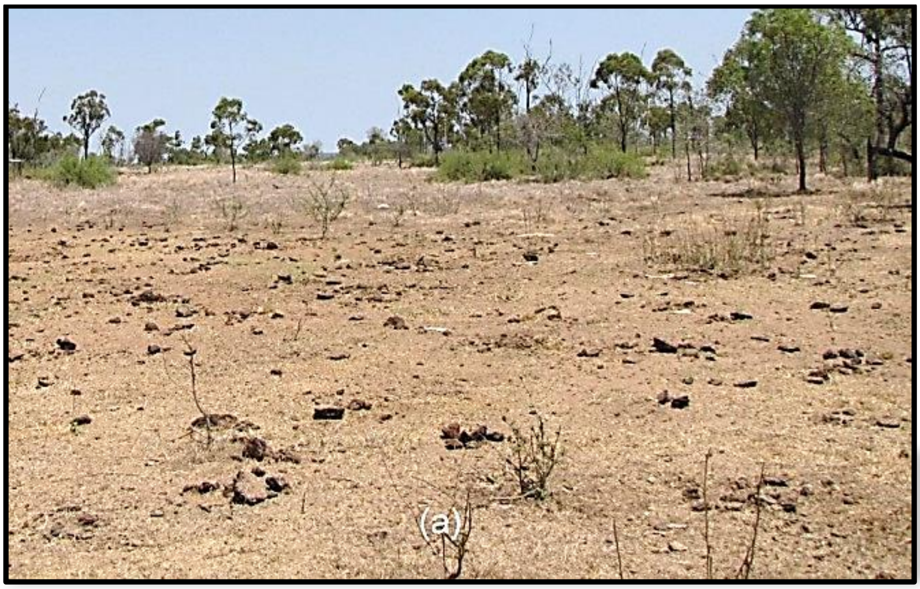

Photograph 4-1 Resource leaky area

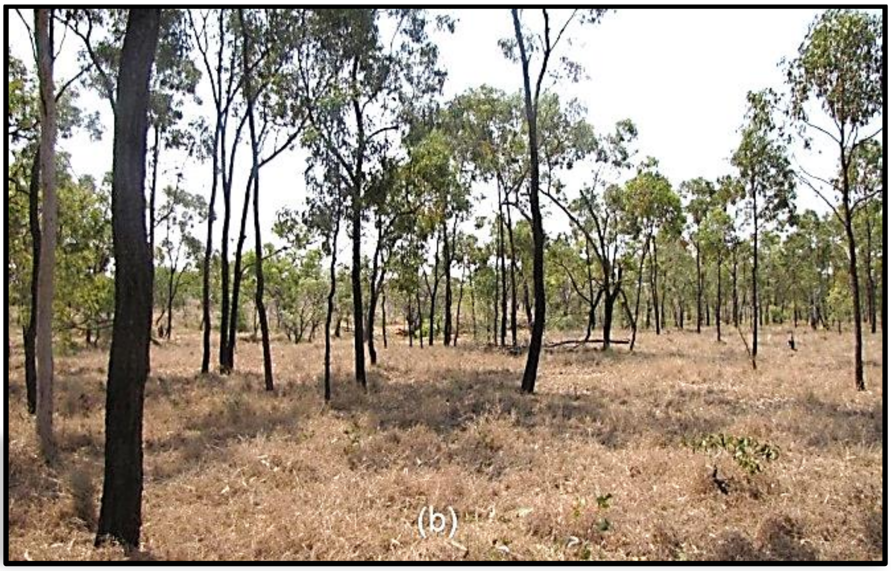

Photograph 4-2 Resource conserving area

These photographs illustrate that leakiness (a) is characterised by low levels of scattered ground cover while resource conserving areas (b) are characterised by high levels of more evenly spread ground cover. Measurement of the amount of ground cover and its spatial distribution can be used to determine the Leakiness of a catchment.

A comparison of the leakiness of the catchment at three different spatial scales requires the data sources used in the Leakiness Calculator (LC) to be consistent across scales. This section describes the procedures used to prepare the catchment DEMs, analysis masks and vegetation cover layers at each of three scales for use in the LC. It concludes with the procedure used to calculate the Adjusted Average Leakiness (AAL) values for each analysis.

4.2.1. Data Requirements

The LC requires three data sources, a DEM of the catchment, a mask of the analysis area, and a cover layer. The analysis masks may be either the whole catchment or a sub-catchment and the cover layers can be any measure of ground cover on a scale of 0 - 100. The original data sources and their pre-processing were described in Chapter 3. Each layer must be in raster format with cells of exactly the same size and geographically coincident. This section describes their preparation for use by the LC.

4.2.1.1. Catchment DEM, Boundaries and Drainage Lines

A DEM of the catchment is required at each resolution to drive the hydraulic flow calculation in the LC. The LC is particularly sensitive to any pits within the analysis DEM. Both the ArcHydro and ArcGIS Spatial Analyst Hydrology sink filling routines left many sinks unfilled. These were detected by the LC. Each of the four terrain processing sink filling routines in SAGA (Bock and Bohner *et al.* 2010) were found to fill all sinks.

The catchment and sub-catchment boundaries and drainage lines were analysed from each DEM using ArcHydro Tools (Maidment and Morehouse 2002). The results are shown in Figure 4.1, Figure 4.2 and Figure 4.3.

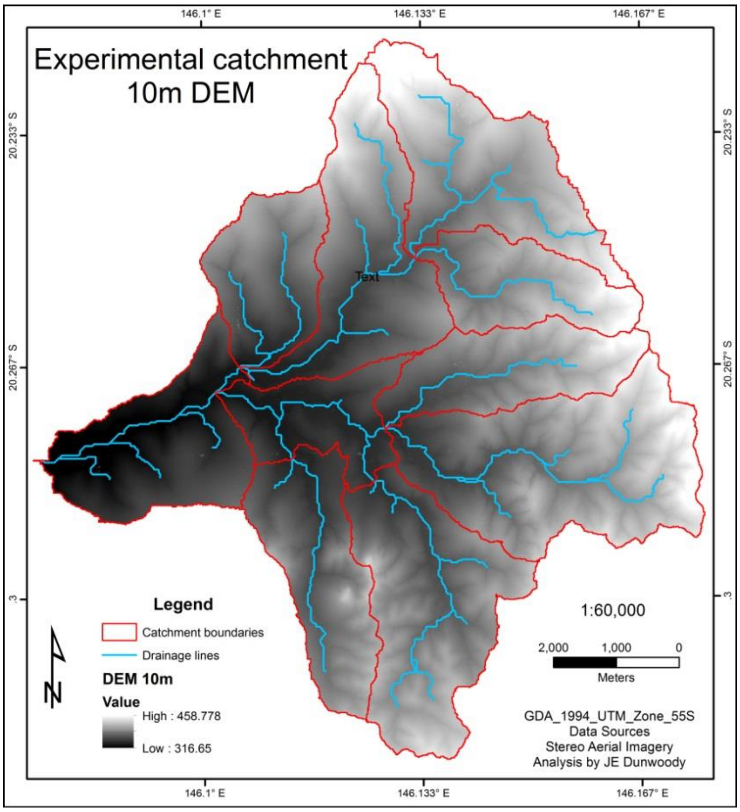

Figure 4.1 Ten-meter DEM catchment and sub-catchments

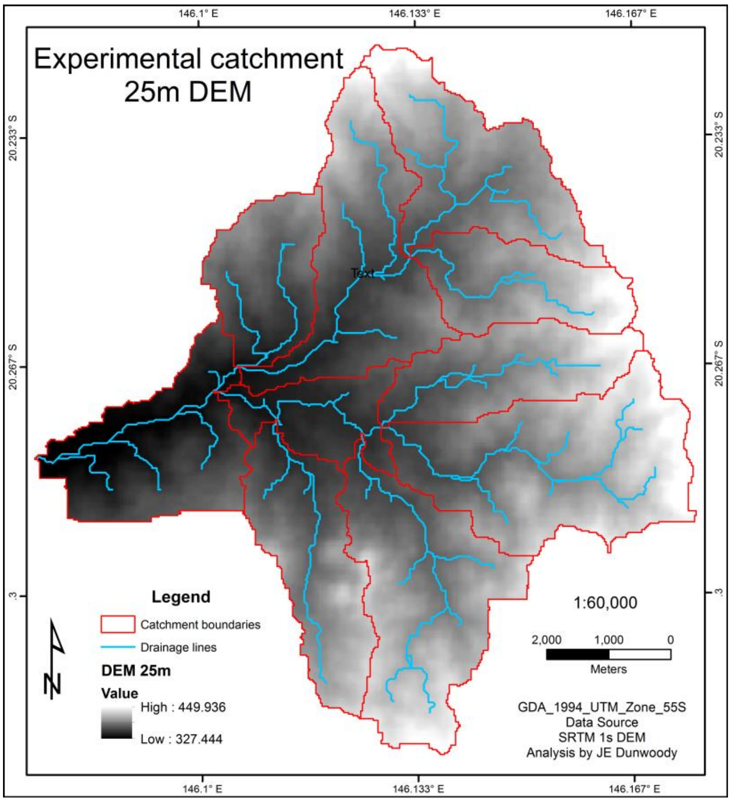

Figure 4.2 Twenty five meter DEM catchment and sub-catchments

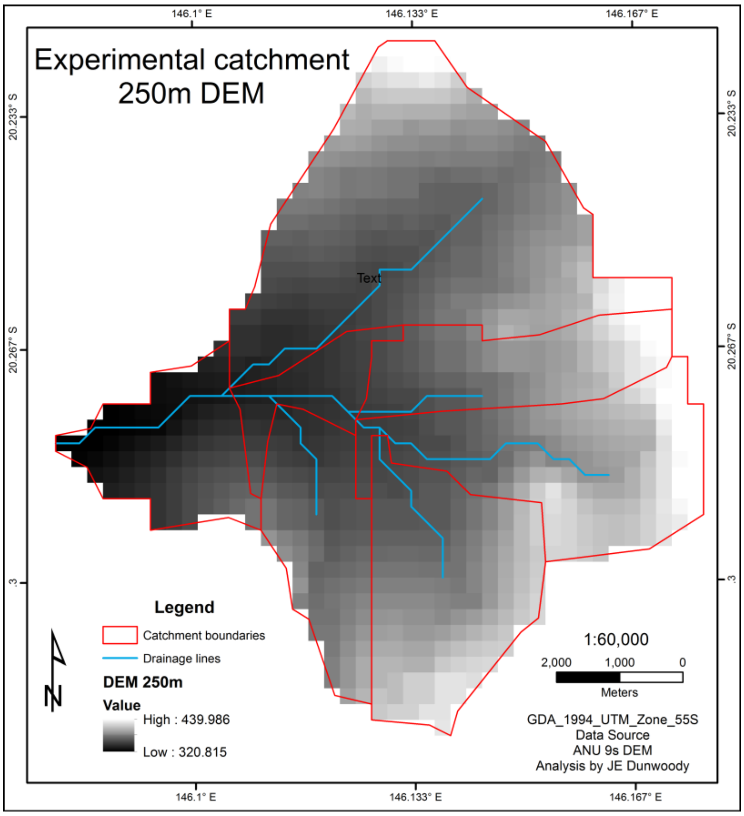

Figure 4.3 Two hundred and fifty meter DEM catchment and sub-catchments

The corresponding catchment statistics at each scale are given in summary form in Table 3-1 and in detail in Appendix 1.

4.2.1.2. Analysis Masks

Analysis masks are required by the LC to define the area(s) on which to perform the leakiness calculation. They can be the whole catchment or any sub-catchments within the whole catchment area that meet the following criteria:

- Defines an area that has a single pour point
- Has the same raster cell size as the DEM
- Has precisely the same geo-location as the DEM (same LLX and LLY values)
- Has a unique integer value
- Be in *.FLT format

Analysis masks for the catchments and sub-catchments at each resolution were created in ArcGIS by creating a Value field in the attribute table of the catchment shape files, assigning a unique value to each catchment or sub-catchment and then rasterising them with a cell value based on the shape file Value field. The respective analysis masks for each scale are shown in Figure 4.4, Figure 4.5 and Figure 4.6.

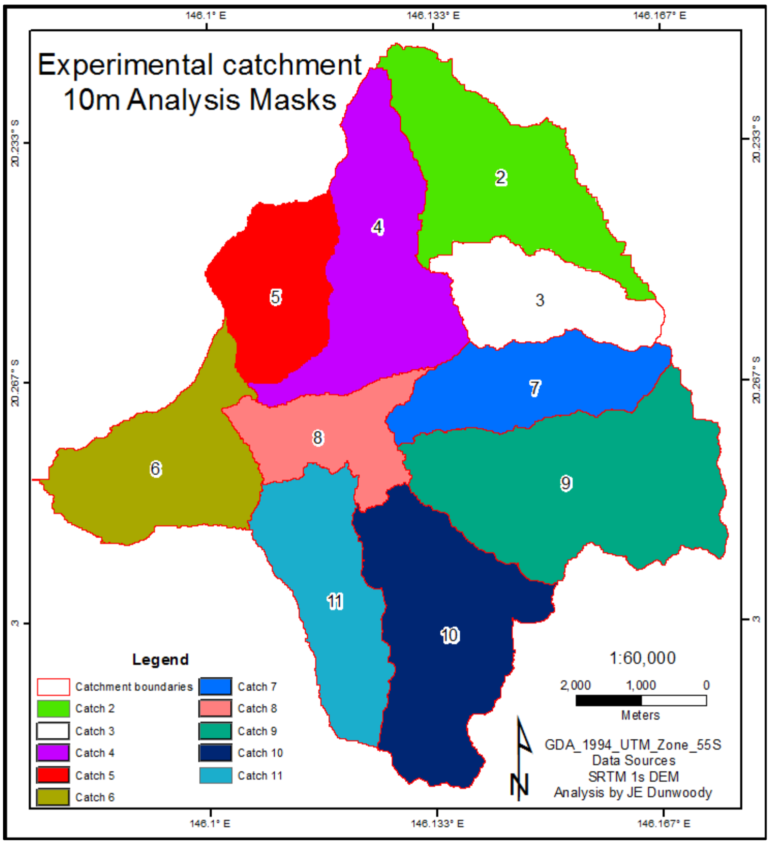

Figure 4.4 Ten meter scale catchment Analysis Masks

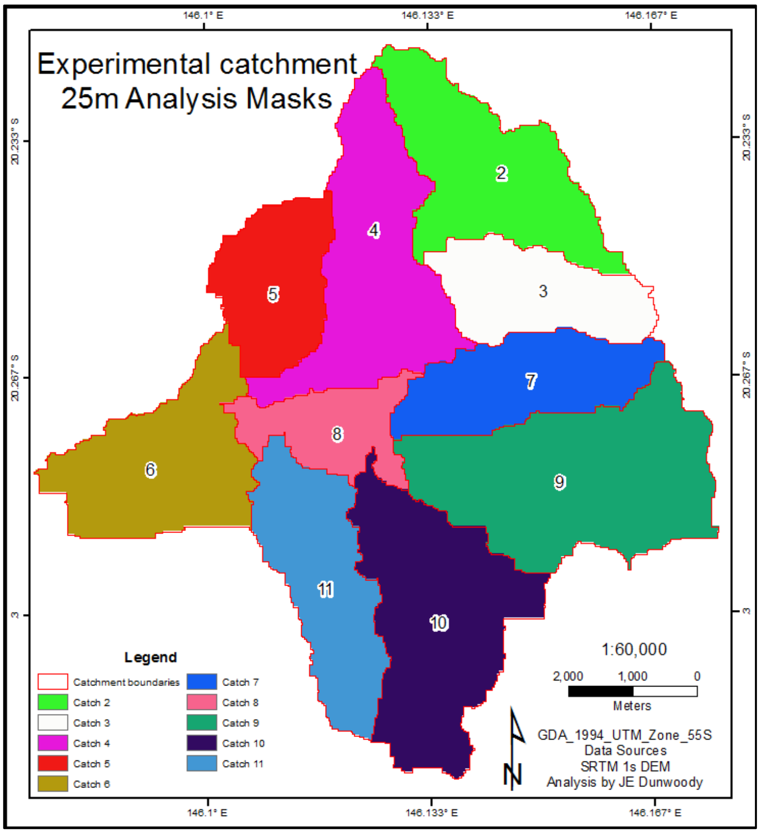

Figure 4.5 Twenty five meter scale Analysis Masks

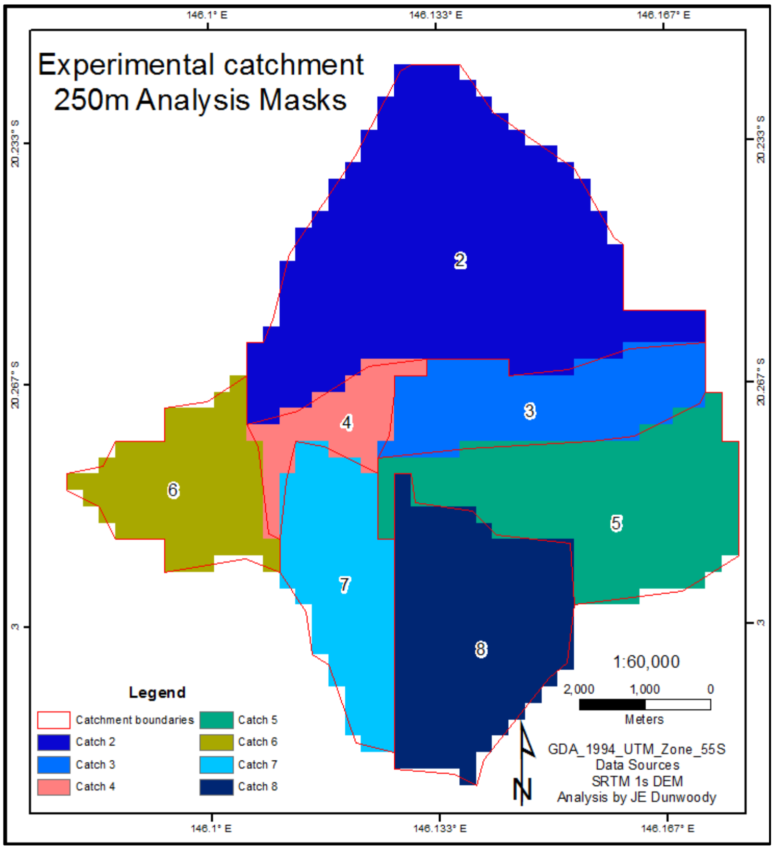

Figure 4.6 Two hundred and fifty meter scale Analysis Masks

4.2.1.3. Vegetation Cover Layers

The cover layers are essentially vegetation cover layers in which the type and extent of vegetation included in the layer depends on the particular characteristics of the image analysis technique. These layers provide the value for ***c*** in the leakiness loss term, Equation 4-1. (Ludwig, J. and G. N. Bastin *et al.* 2007).

$$l_{ij} = e^{-b \times c_{ij}} \tag{4-1}$$

where:
c = cover (in % for each pixel), and
b = 0.065, a decay constant for rate of loss of soil sediment

The range of cover analyses was limited to those that could be calculated comparably for each of the three types of images, namely; SPOT 5, Landsat TM and MODIS. The changes to the band order of these images to make them consistent for analyses at each scale are described in Chapter 3. The following sub-sections describe the processing procedure for each cover index.

Moving Standard Deviation Index (MSDI)

The MSDI is a textural classifier. It measures spatial variation in the landscape by passing a standard deviation filter over a selected band in the image (Lillesand and Keifer *et al.* 2008, p.570). The filter can be any size selected appropriate to the purpose of the analysis. For landscape classification purposes this is typically a 3x3 filter passed over the red band because of the bands sensitivity to the presence or absence of photosynthetic vegetation (Tanser and Palmer 2000). Degraded or unstable landscapes yield higher MSDI values than comparable but undisturbed or stable landscapes. There is significant correlation between the MSDI analyses and NDVI analyses (Tanser and Palmer 1999).

It was used to set the lower base line value for use in the LC. Generating LI values requires that an Lmax value be set (as an input to the LC calculation) that is close to the value of the maximum leakiness of the sample area. MSDI values at each resolution were used to estimate these Lmax values. Setting the Lmax value in this way ensured that all subsequent LI values were scaled between 0-1 (Ludwig, J. and G. N. Bastin *et al.* 2007, Appendix B). The MSDI was not used any further in this study beyond setting the initial Lmax values.

MSDIs for this research were generated for all three catchment images (SPOT 5, Landsat TM and MODIS) by using a 3x3 Focal Statistics Filter applied to the red band in ArcGIS Spatial Analyst. Pseudo coloured examples of the results are shown in Figure 4.7.

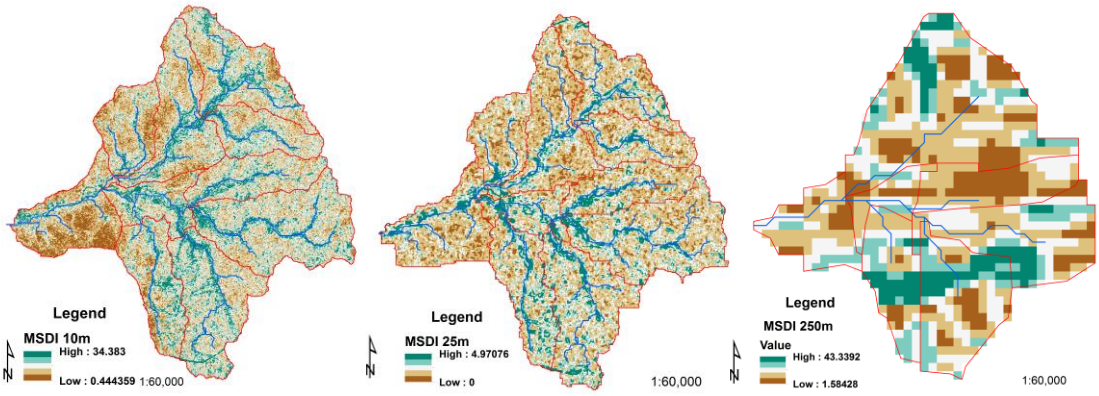

Figure 4.7 Example MSDI cover layers

Normalised Difference Vegetation Index (NDVI)

The NDVI (Rouse, J. and R. Haas *et al.* 1974) detects photosynthetically active vegetation (Equation 4-2).

$$NDVI = \frac{\rho_{nir} - \rho_{red}}{\rho_{nir} + \rho_{red}} \qquad (4\text{-}2)$$

The equation uses the ratio of the NIR reflectance minus the Red reflectance normalised by the sum of the NIR and Red reflectances. This reduces many forms of multiplicative noise in the reflectance values and allows monitoring of seasonal changes that stimulate or degrade chlorophyll pigment because of its strong absorption of visible red wavelength radiation. However, it has limitations such as, providing a non–linear measure of vegetation (stretching in low biomass environments and compressing in high biomass environments), being added to by atmospheric path radiance and by being influenced by background radiance (e.g. dark soils) (Jensen 2007, p 385-386).

NDVI thematic cover rasters were produced (Figure 4.8) using a simple ArcMap geoprocessing model.

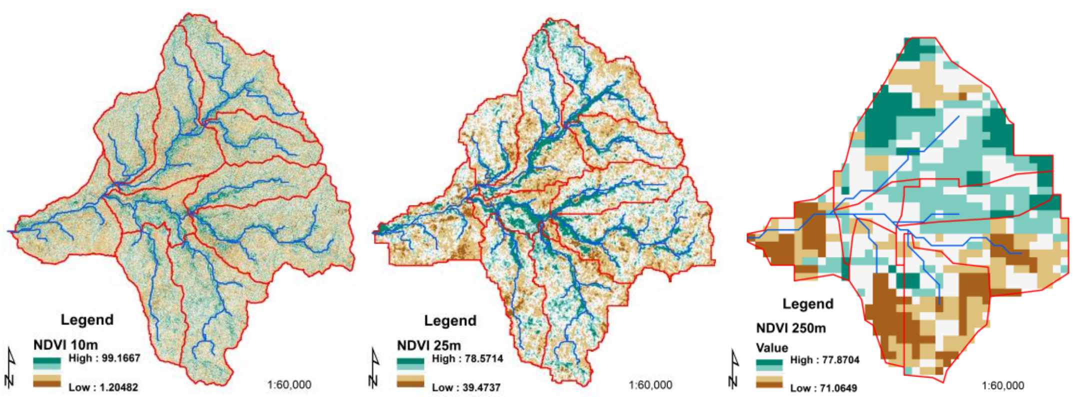

Figure 4.8 Example NDVI cover layers

Soil Adjusted Vegetation Index (SAVI)

SAVI is also a well-known band ratio relationship for detecting photosynthetically active vegetation first developed by Heute (1988) (Equation 4-3).

$$SAVI = \frac{(1+L)(\rho_{nir} - \rho_{red})}{\rho_{nir} + \rho_{red}} \tag{4-3}$$

The equation is very similar to the NDVI equation (Equation 4-2) except that it incorporates an adjustment factor L (= 0.5) to account for red and near -infrared reflectance extinction that occurs as it passes through the vegetation canopy. SAVI thematic cover rasters were produced (Figure 4.9) by applying the formulae in an ArcMap geoprocessing model.

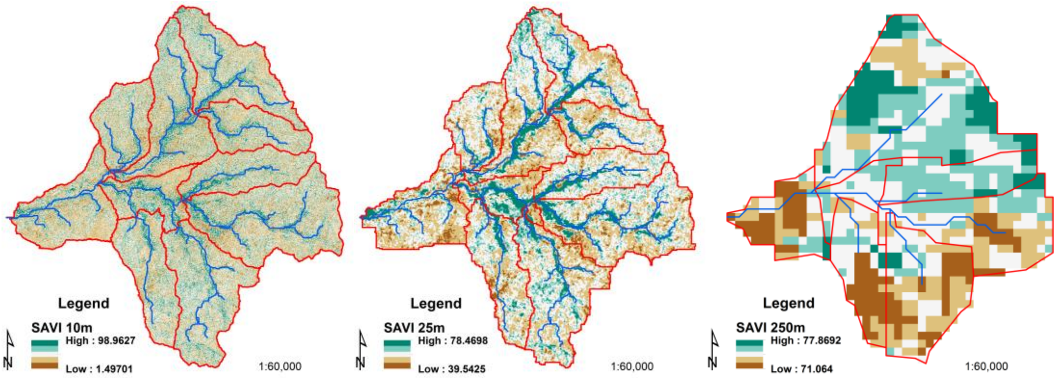

Figure 4.9 Example SAVI cover layers

Redness Index (RI)

The redness Index has been used to monitor vegetation condition where near infra-red reflectance band imagery is not available (Bannari and Morin *et al.* 2009) as shown in Equation 4-4.

$$RI = \frac{(\rho_{red} - \rho_{grn})}{\rho_{red} + \rho_{grn}} \tag{4-4}$$

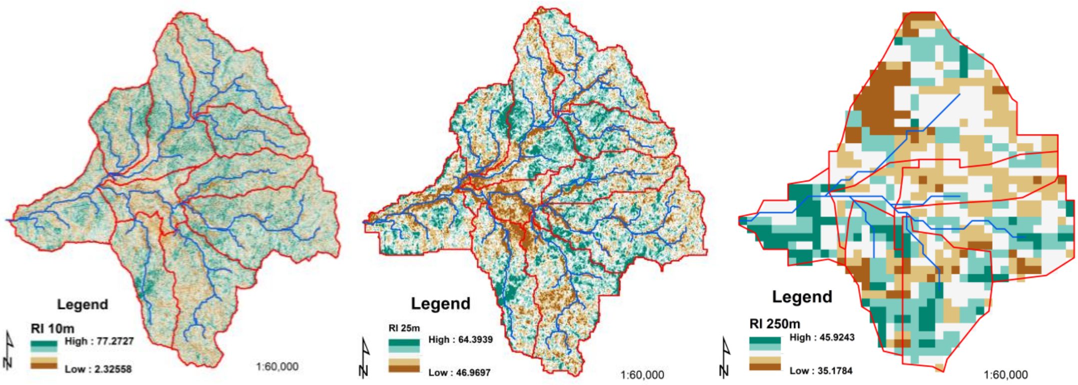

Figure 4.10 Example RI Cover layers

RI cover layers were generated by implementing the above formulae in ArcMap. Pseudo coloured examples of RI catchment layers are shown inFigure 4.10..

Stress Related Vegetation Index

The Stress Related Vegetation Indices were first proposed in 1994 by (Thenkabail and Ward *et al.* 1994). The STVI-1 index was found to give the best results on chenopod shrub lands out of a range of indices that were tested (O'Neil 1996). Evaluation of STVI-1and STVI-3 plus a new STVI-4 index in estimating vegetation in open semi-arid woodlands in South Australia found that STVI-4 gave the best overall results (Jafari and Lewis *et al.* 2007, p.45). It was used as the moisture stress vegetation index in this research and the formula is shown in Equation. 4-5.

$$STVI - 4 = \frac{(\rho_{nir} - (\rho_{red} x\, \rho_{mir}))}{(\rho_{nir} + \rho_{mir})} \qquad (4\text{-}5)$$

STVI-4 cover layers were created by implementing the above equation in a geoprocessing model in ArcMap. Pseudo coloured examples of STVI-4 catchment layers are shown in Figure 4.11.

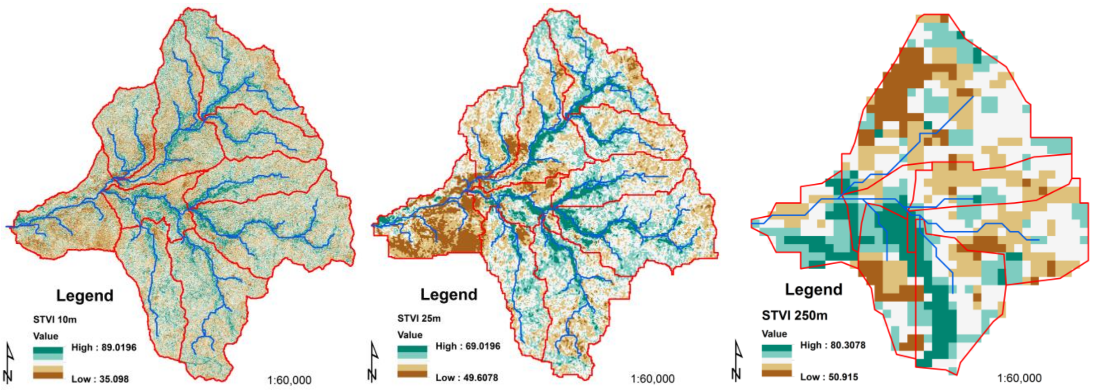

Figure 4.11 Example STVI-4 Cover layers

Corrected Vegetation Index (CORVI)

CORVI is a corrected modification of the SAVI-4 index (Jafari and Lewis *et al.* 2007, p. 43). In this modification, the RI is regressed against the respective STVI-4 index and the slope of the regression times the redness index is subtracted from the STVI-4 index to produce the CORVI as shown in Equation. 4-6.

$$CORVI = (STVI - 4) - (KxRI) \qquad (4\text{-}6)$$

where K = slope of RI over STVI-4

CORVI cover layers were created by implementing the above equation in a geoprocessing model in ArcMap. Pseudo coloured examples of CORVI catchment layers are shown in Figure 4.12.

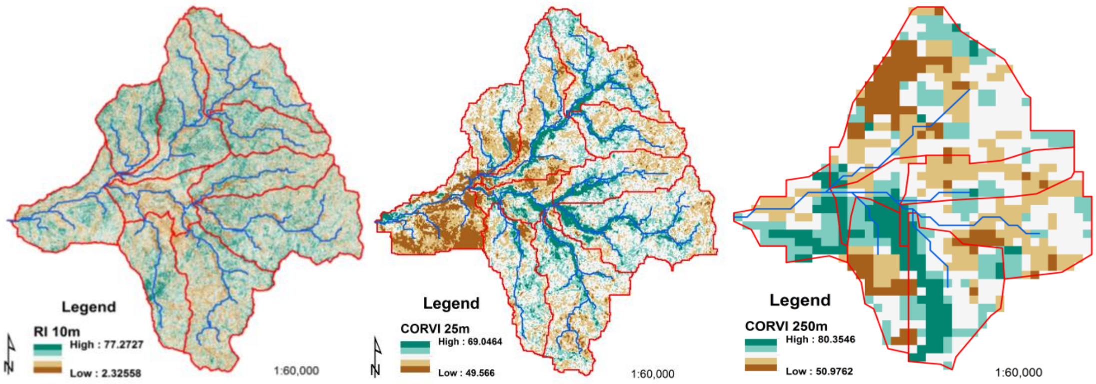

Figure 4.12 Example CORVI Cover layers

Perpendicular Distance Indices (PDI)

The PDI are a special application of the Perpendicular Vegetation Indices (PVI) first developed by Richardson and Weigand (1977) to improve the separation of vegetation from soil caused by a greater proportion of near infrared reaching the soil under high density canopy conditions. The PVI is measured as the vertical distance of the point of interest from the soil line defined by the lower bound of the scatter plot of the red reflectance (x) versus near infrared reflectance (y).

Pickup *et al.* (1993) found that a scatter plot of the green band (MSS, band 4) (x) against the red band (MSS, band 5) (y) which they termed PD_{54} showed a distinct soil line and provided a better separation of both dead and green vegetation from regolith materials. Although this index was first developed based on Landsat Multi-Spectral Scanner (MSS) sensor data, it has been modified for use with Landsat Thematic Mapper (TM) and Enhanced Thematic Mapper Plus (ETM+) sensor data by using pixel values from bands 2 and 3. Plots of PD_{54} values versus percent vegetation cover showed a strong positive correlation (Pickup and Chewings *et al.* 1993, p. 259, Fig. 4). This index depends on vegetation pixels (representing PV and NPV material) plotting separately in data space from soil pixels. Most rangeland soils in Australia are bright with a red hue. Because the soil line changes with change in the hue, value and chroma the soil line should be determined separately for each scene. In sites where the soil has a hue close to the hue of the PV or NPV material, the vegetation pixels may not plot separately from the soil line and this index may not be suitable for distinguishing vegetation cover.

In PDI plots as opposed to PVI plots, the upper bound of the scatter plot is the soil line and the lower bound the vegetation line with pixels with greatest PV vegetation clustering in the lower left of the scattergram. In this research, three PDIs were used. They varied by the band over which the red band of the image (y axis) was regressed (x axis) and are renamed accordingly:

- PDrg for red (y) over green (x),
- PDrn for red (y) over near infrared (x), and
- PDrs for red (y) over short wave infra-red (x).

The PDIs were calculated essentially according to the procedure outlined by Pickup *et al.* 1993 and as modified by Bastin and Chewings (2003) to reflect advances in computing software. The generalised formula for PDI calculation is shown in Equation. 4-7. The detailed changes are given in Appendix 7.

$$PD_{rz} = \left(\frac{abs((-V_1*(Band\ z*V_2))+Red\ Band-V_3)}{\sqrt{((V_2*V_2)}+1)}\right)*254/V_4 \qquad (4\text{-}7)$$

Where V1= 1
V2= slope of soil line
V3= intercept of soil line
V4= vertical distance between vegetation line
soil line
z = the band # plotted against the red band

seudo coloured examples of PDI catchment layers are shown in Figure 4.13, Figure 4.14 and Figure 4.15

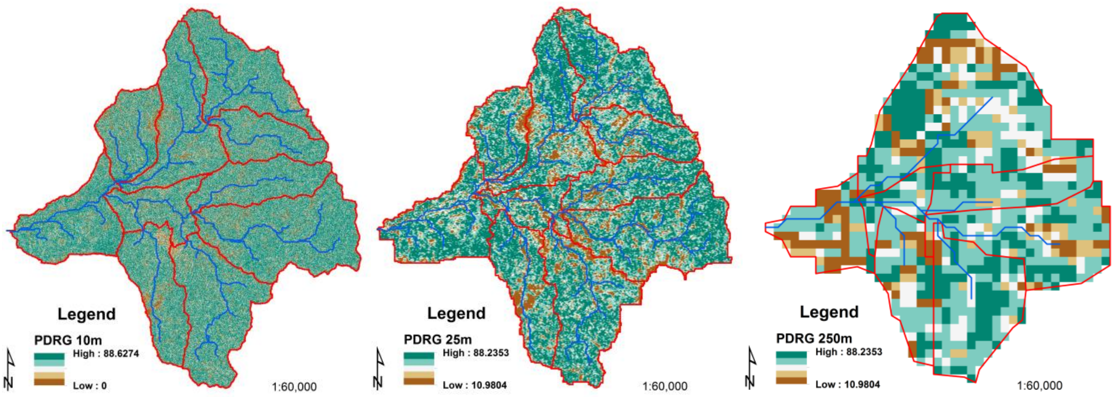

Figure 4.13 Example PDrg Cover layers

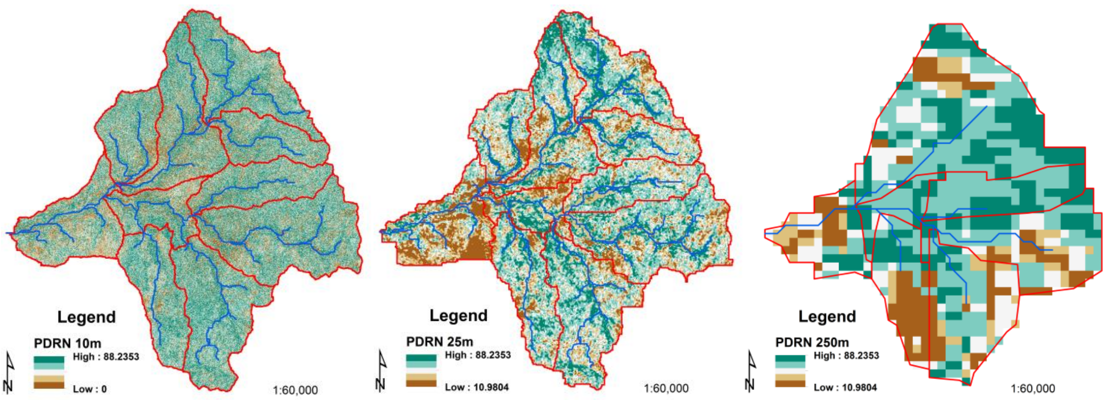

Figure 4.14 Example PDrn Cover layers

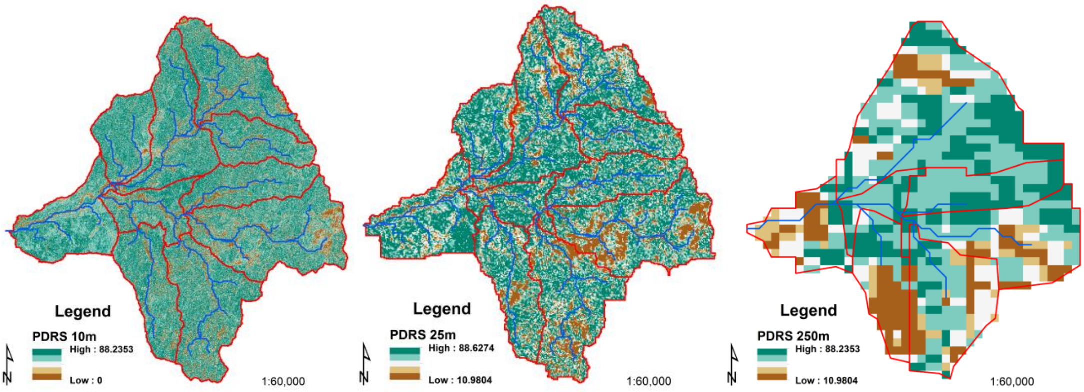

Figure 4.15 Example PDrs Cover layers

Soil and Atmosphere Resistant Vegetation Index (SARVI)

The SARVI was developed to compensate for the soil effects on the NDVI causing it to saturate over heavily vegetated sites and to reduce the effect of atmospheric contribution to NDVI. Huete *et al.* (1997) found that the SARVI did not saturate at high vegetation conditions and accurately followed variations in NIR reflectances. They also found it to be more sensitive to structural parameters such as leaf area index and leaf morphology. It is calculated according to Equation. 4-8.

$$SARVI = \frac{(1+L)(\rho_{nir}-\rho_{rb})}{\rho_{nir}+\rho_{rb}+L} \tag{4-8}$$

where $\rho_{rb} = \rho_r - \gamma(\rho_b - \rho_r)$
and L = 0. and $\gamma = 1$

SARVI cover layers were created by implementing the above equation in a geoprocessing model in ArcMap. Pseudo coloured examples of SARVI catchment layers are shown in Figure 4.16. A SARVI layer for the 10m resolution image was not calculated because of the absence of the blue layer (see ρ_{rb} *in* Equation 4-8).

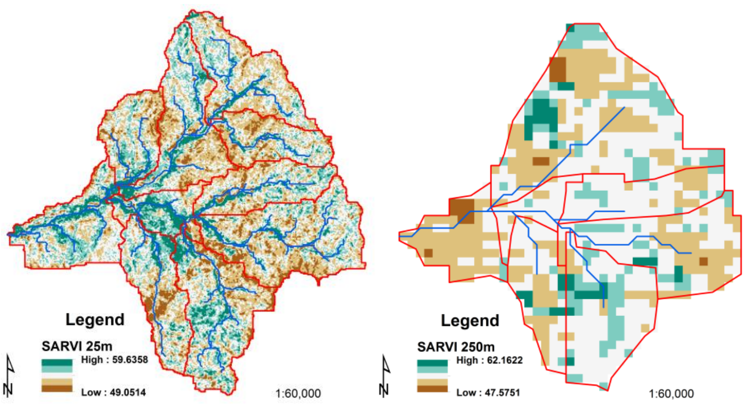

Figure 4.16 Example SARVI Cover layers

Ground Cover Index (GCI)

The aetiology of the terms Ground Cover Index (GCI), Bare Ground Index (BGI) and Fractional Cover Index (FCI) has changed as new image processing procedures have been developed and verified. Scarth *et al.* (2008) developed the Bare Ground Index by multi-regression modelling of corrected Landsat TM and ETM images using a large field site bare ground data base in Queensland, Australia. The initial GCI was developed from that work as the complement of the BGI according to the following relationship as used by Bastin *et al.* (2007, p.14).

$$GCI_{\%} = (100 - BGI_{\%}) \tag{4-9}$$

Subsequently, two improved vegetation cover procedures were developed (Schmidt and Trevithick 2010), the first based on multinomial regression (Scarth and Roder *et al.* 2011) and the second based on linear spectral unmixing (Schmidt and Denham *et al.* 2010). Both procedures predict three components, bare ground (BG), green vegetation (PV) and dry or senescent vegetation (NPV). These procedures generate reliable estimates of ground cover where there are low levels (<15%) of Foliage Projective Cover (FPC) although they have been applied across all areas (above and below 15% FPC). Schmidt and Scarth (2009) found that PV and NPV provided a better estimate of ground cover than was possible previously (Equation 4-9).

This research used GCI values for the experimental catchment from Equation 4-9 applied to BGI data generated according to Scarth *et al.* (2008) because this was the only data available at the time of this phase of the research. BGI values were not available for SPOT or MODIS imagery. Although the GCI values were only available for one resolution (Landsat resampled to 25m) and could not be included in any scaling comparisons at other resolutions, they were still included for purposes of reference for the other cover indices listed in the preceding sections. A pseudo-coloured example of the GCI catchment layer is shown in Figure 4.17.

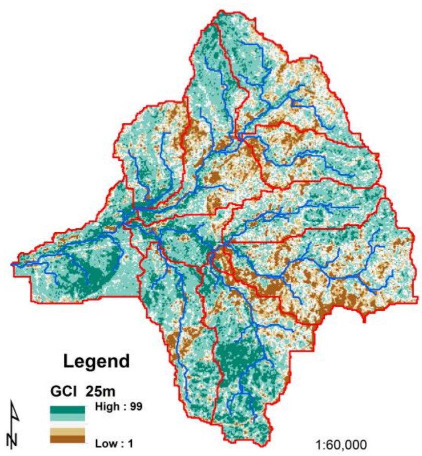

Figure 4.17 Example GCI cover layer.

4.2.2. Leakiness Calculation

The Leakiness Calculator (LC) (Liedloff 2007) was used to generate average cover and leakiness values in separate analyses of the 10, 25 and 250m resolution thematic cover images. The DEM and analysis mask inputs to the LC were the same for all analyses at each resolution. The different coverage layers were organised in ascending value of average cover for each resolution.

Different Lmax values do not affect the Lcalc values and accordingly the investigation was based on Lcalc leakiness values and subsequently AAL values. The AAL values provided a consistent measure of leakiness at different resolutions as explained in Section 4.2.3.

In this research in which the same catchment was being analysed at different resolutions (pixel sizes), it was found inconvenient to reset the Lmax value for different resolutions because this negated the comparability of the LI values. It was observed that the Lmax values did not affect the calculated Leakiness values (Lcalc). This lead to the development of a new metric for leakiness measurement as described in the following section.

4.2.3. Adjusted Average Leakiness

In order to progress the analysis of Leakiness between catchments at different resolutions (with different numbers of cells) and sub catchments of different areas (also with different numbers of cells), a new concept, the Adjusted Average Leakiness was developed. This was needed because Leakiness (Lcalc) is a progressive flow value determined by summing the contributions from all adjoining (8) pixels. By considering the pixels sequentially in descending order of elevation, all contributions to a pixel are considered (Ludwig and Eager *et al.* 2006, p. 10). This measure of the loss of resources by a catchment is proportional to the number of cells in the analysis area (see Section 4.4.1 for details).

In order to normalise this value by the number of cells in the catchment and thus develop a comparable measure of leakiness for a catchment with any number of cells an Average Leakiness value (AL) was defined as:

$$AL = \left({}^{Lcalc}/_{Nc} \right). \tag{4-10}$$

Where: Lcalc = calculated leakiness from the Leakiness Calculator,
Nc = Number of cells in the analysis mask per sub-catchment.

However, this can be an impractically small number so an adjustment (M) was made to define the Adjusted Average Leakiness (AAL) as follows:

$$AAL = \left({}^{Lcalc}/_{Nc} \right) \times M \tag{4-11}$$

where: $M = 10^x$, a user selected range scaling factor
x = power to base 10 of the number of cells in the catchment

The AAL provides a measure of the Leakiness on a unit cell basis for each analysis area.

4.3. Results

This section presents the results of analysing the amount of vegetation cover on the experimental catchment and sub-catchments and its calculated leakiness at three different image resolutions using eleven different measures of ground cover. The images used in the analysis were spatially congruent, had similar (but not identical) spectral bands and were captured at close to the same time (See Chapter 3).This is followed by an analysis of the correlation between ground cover and leakiness and resolution.

4.3.1. Catchment Leakiness

Table 4-1 summarises the amount of vegetation cover and the calculated leakiness (Lcalc) for eleven cover indices at three native image resolutions for the experimental catchment.

Table 4-1 Vegetation Cover and Leakiness of the Experimental Catchment

Vegetation Cover Index (VCI)	Average Cover (%)			Leakiness (Lcalc)		
	10m	25m	250m	10m	25m	250m
MSDI	5.27	0.735	14.654	1911.40	910.97	104.28
NDVI	44.80	54.656	74.515	86.63	12.564	0.997
SAVI	44.81	54.639	74.514	86.56	12.573	0.997
RI	56.16	58.186	40.639	34.01	8.759	9.388
STVI	56.43	56.608	65.895	37.02	10.440	1.780
CORVI	56.45	56.535	65.934	36.94	10.496	1.775
PDrn	61.73	54.056	63.354	68.90	49.783	5.098
PDrg	71.96	68.986	68.585	78.73	47.460	5.403
PDrs	72.62	65.706	57.732	32.21	24.177	7.308
SARVI	na	52.394	50.997	na	14.203	4.704
GCI	na	84.252	na	na	3.541	na

The effect of resolution on Average Cover and Leakiness for each of the vegetation cover indices is shown in Figures 4-25 and 4-26 respectively. The MSDI index values were used as a baseline reference level, pseudo-cover of the catchment (Tanser and Palmer 2000) in each image for the purpose of setting the Lmax value in the initial LC calculations (Ludwig, J. and G. N. Bastin *et al.* 2007). Their values have been scaled, as shown on the x axis label, in order to fit them in Figures 4-25 and 4-26. The following analysis focuses on the leakiness values derived from the vegetation cover values as measured by the respective vegetation cover indices.

Figure 4.18 shows that the relative amounts of vegetation cover vary by type of cover index and by resolution.

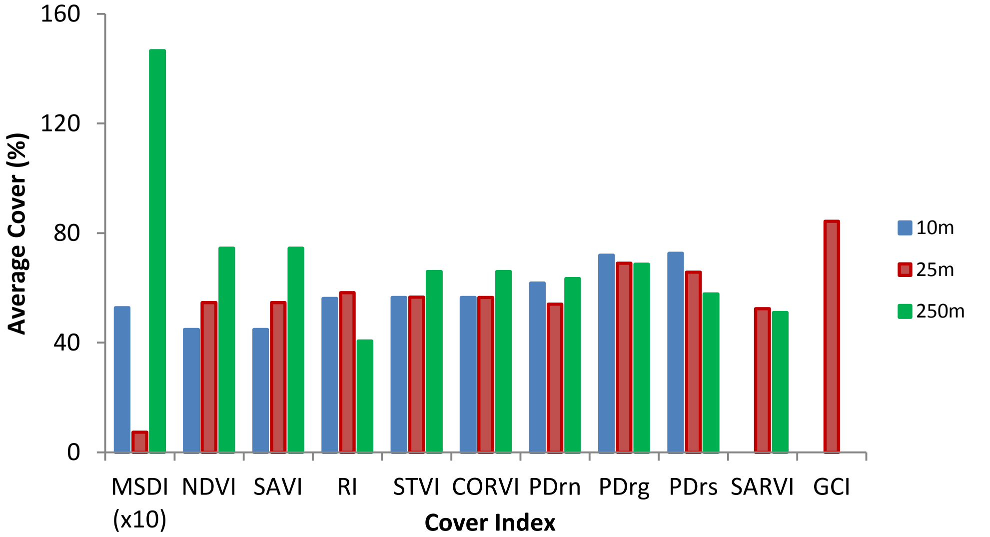

Figure 4.18 Vegetation Cover at three resolution

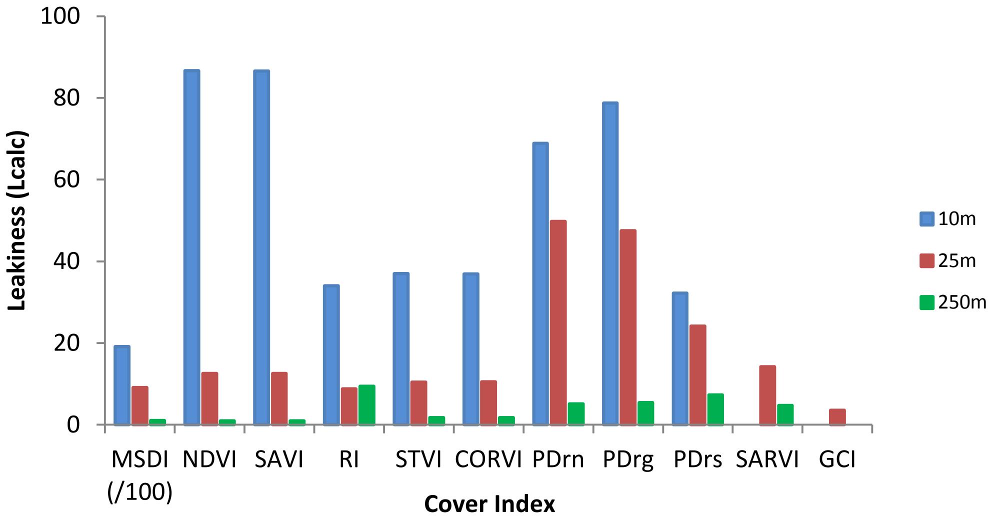

Figure 4.19 Leakiness at three resolutions

The relationship between Leakiness and Average Cover, as measured by different vegetation cover indices, was analysed for each resolution (Figure 4.20). An overall negative linear relationship between Leakiness and cover was expected based on the formulation of the leakiness index calculation and field experimental evidence (Ludwig and Eager *et al.* 2006, Fig 4). The general form of the association at each of the three resolutions is negative, but the correlation of Leakiness with 10m and 25m resolution Average Cover values is weak. The correlation of Leakiness with Average Cover at 250m resolution is more robust (R^2 = 0.68). These results are not unexpected because in this analysis, Average Cover is the percent of cover measured by different types of cover indices.

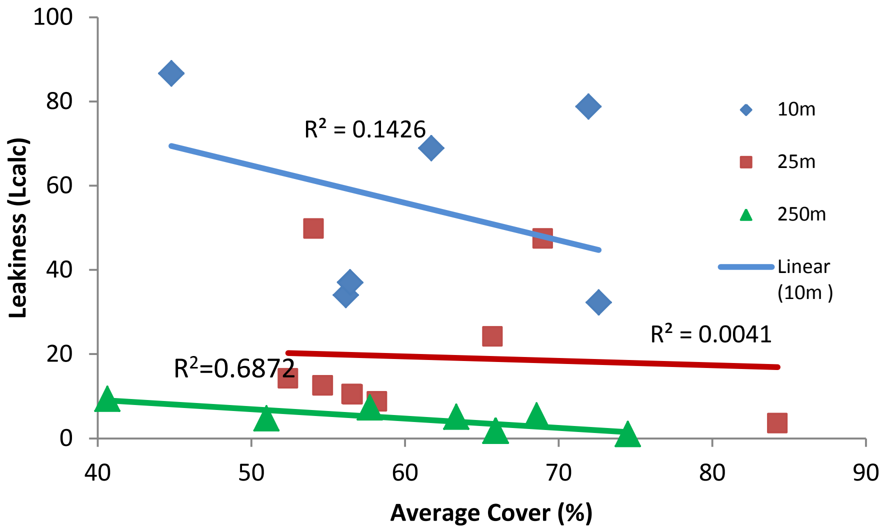

Figure 4.20 Response of Leakiness to Average Cover (multiple indices)

The statistical correlation between cover and leakiness at the 3 resolutions is shown in Figure 4.20 and given in Table 4-2. It is weak except at 250m.

Table 4-2 Correlation between Average Cover and Leakiness

Correlation	Resolution		
	10m	25m	250m
R	-0.378	-0.064	-0.829

4.3.2. Variation in Catchment Cover and Leakiness

The change in intensity of cover by location within the catchment for all cover indices at each resolution is shown in Figure 4.21, Figure 4.22 and Figure 4.23.

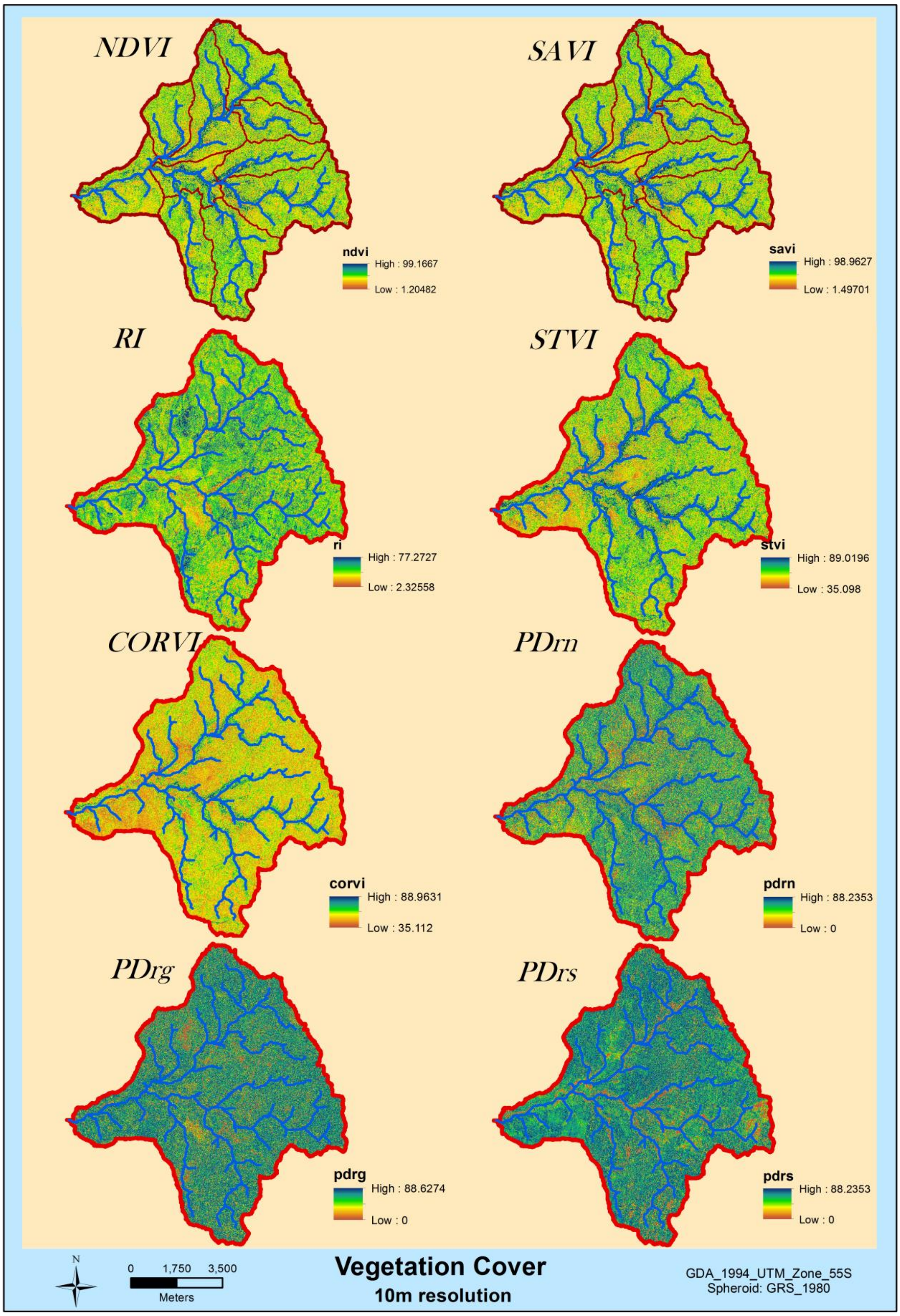

Figure 4.21 Vegetation cover distribution by cover index at 10m resolution

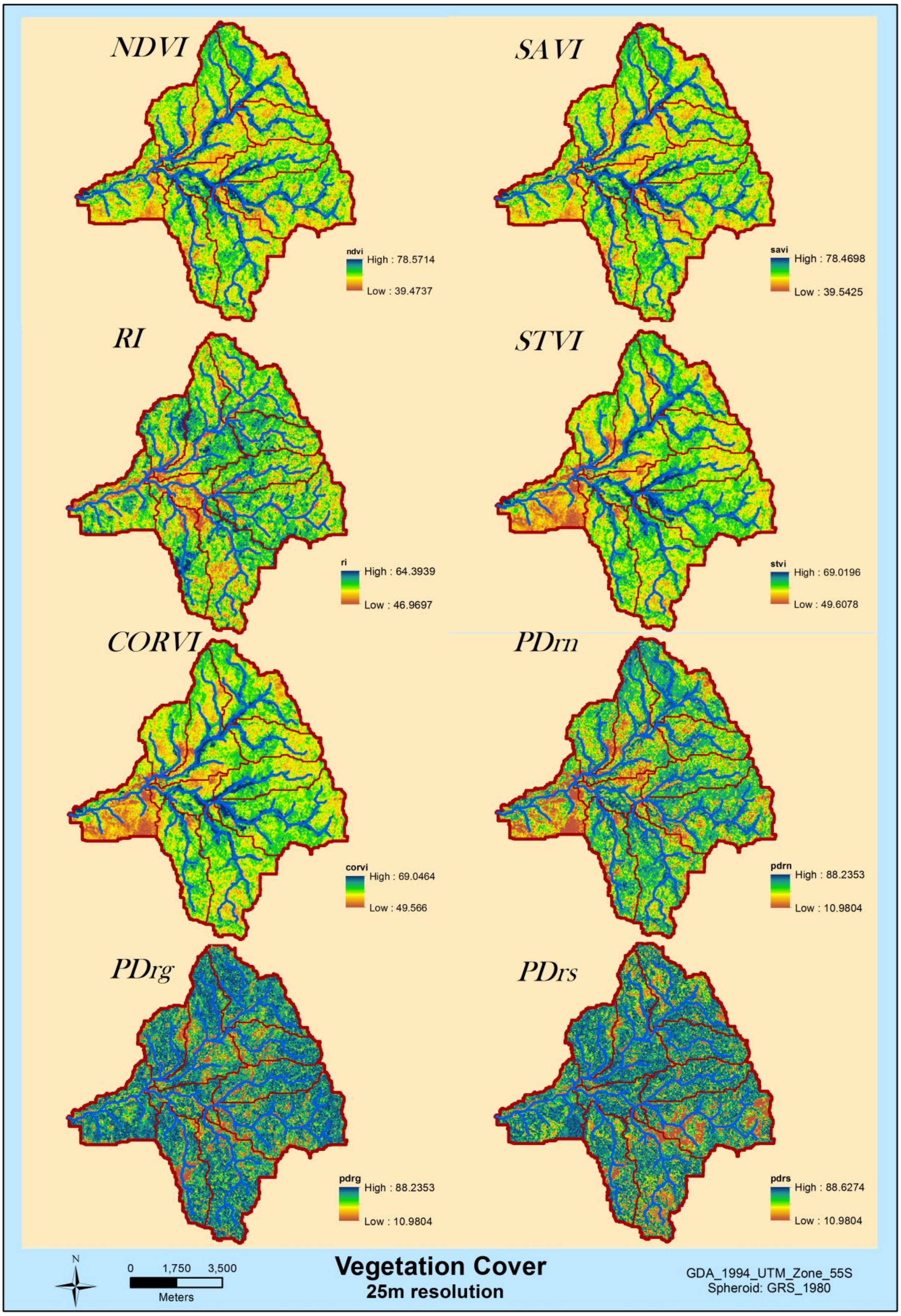

Figure 4.22 Vegetation cover distribution by cover index at 25m resolution

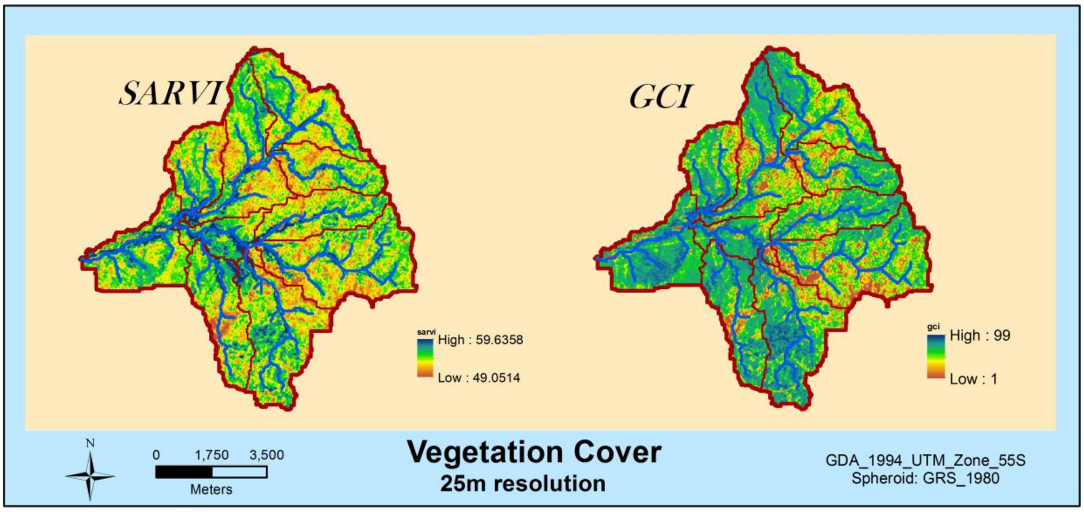

Figure 4-22 (continued) Vegetation cover distribution by cover index at 25m resolution

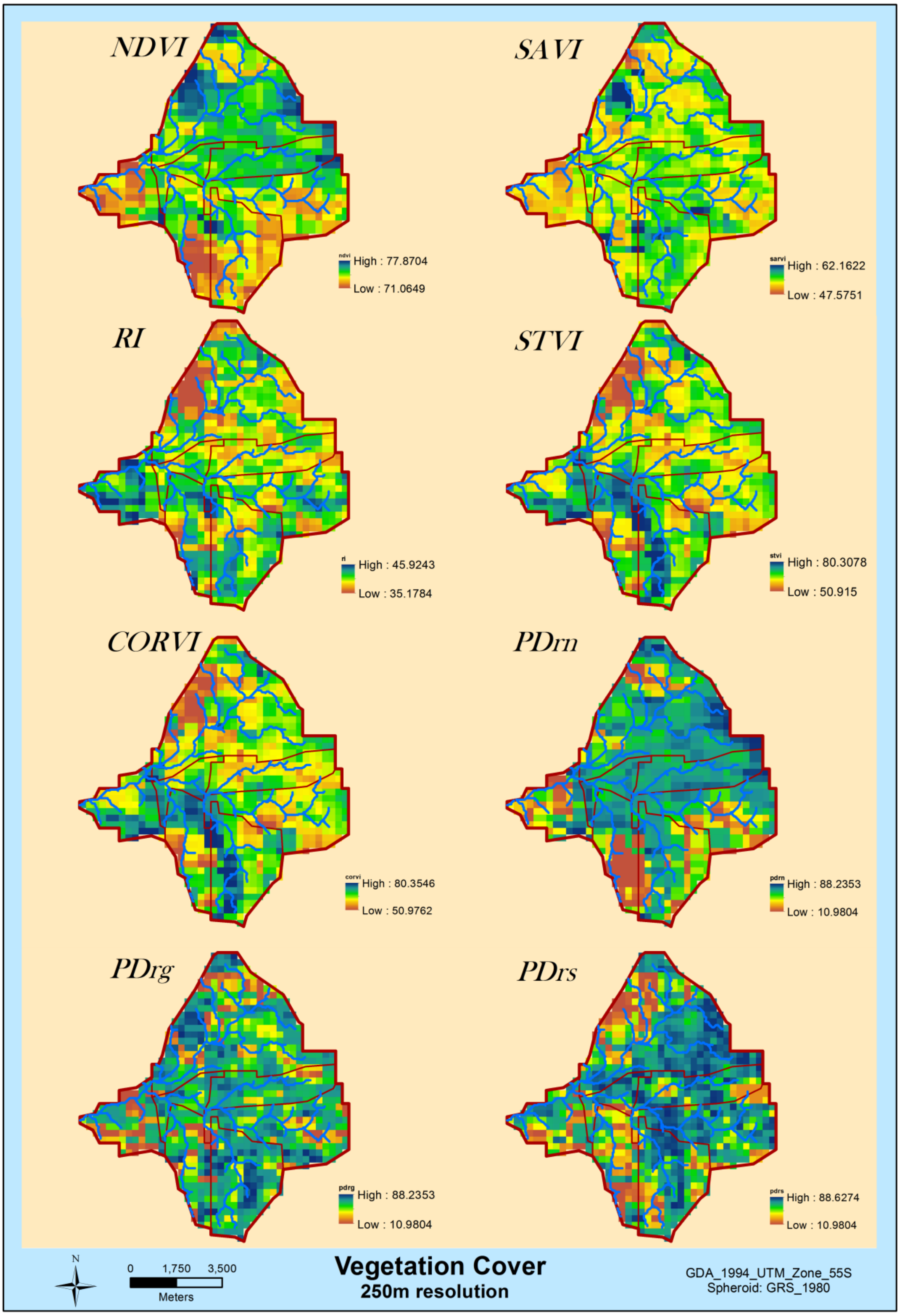

Figure 4.23 Vegetation cover distribution by cover index at 250m resolution

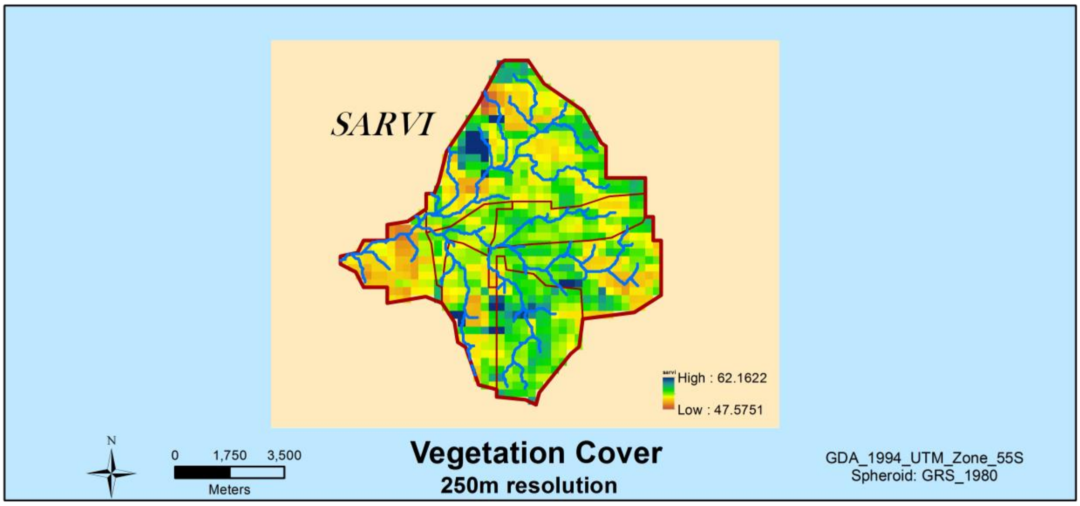

Figure 4-23 (continued) Vegetation cover distribution by cover index at 250m resolution

The difference in the images in Figure 4.21 to Figure 4.23 is due to the values behind the data in Table 4-1. Careful inspection of these images reveals that different vegetation indices not only have different values but also different patterns (variance).

4.3.2.1. Variation in Cover

The amount of Average Cover, measured by different vegetation cover indices, varied with resolution as shown in Figure 4.24. The Standard Deviation for the Cover Indices varied a lot (Table 4-3). PDrg had the lowest Std. Dev. (1.84) and NDVI and SAVI had the highest Std. Dev. (15.14 and 15.13).

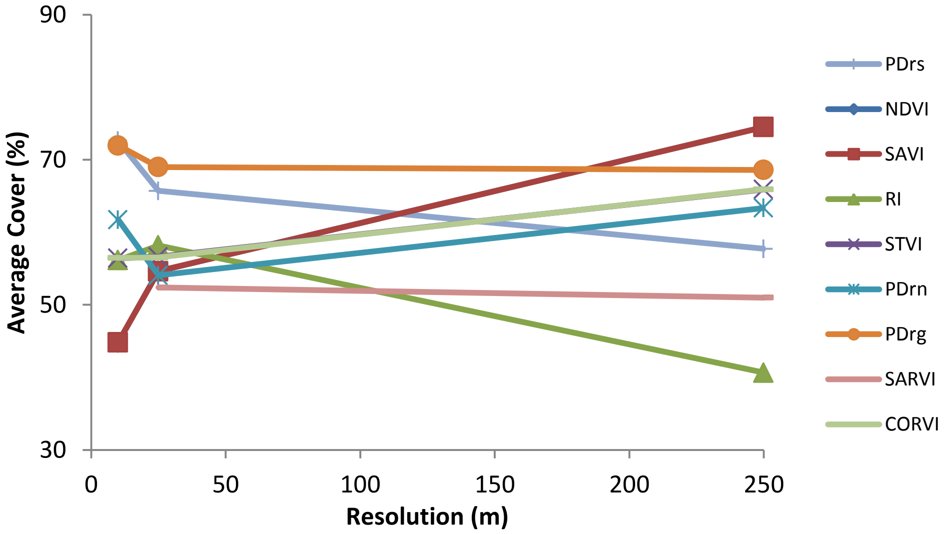

Figure 4.24 Variation in Average Cover by Cover Index and resolution

Table 4-3 Variation in catchment average cover across 3 resolutions.

Cover Index	Average Cover (%)			Std Dev
	10m	25m	250m	
MSDI	5.27	0.74	14.65	7.10
NDVI	44.80	54.66	74.52	15.14
SAVI	44.81	54.64	74.51	15.13
RI	56.16	58.19	40.64	9.60
STVI	56.43	56.61	65.90	5.41
CORVI	56.45	56.54	65.93	5.45
PDrn	61.73	54.06	63.35	4.97
PDrg	71.96	68.99	68.59	1.84
PDrs	72.62	65.71	57.73	7.45

4.3.2.2. Variation in Leakiness

The primary variable affecting the Leakiness of comparable catchments is the amount of vegetation cover (Ludwig and Eager *et al.* 2006). Irrespective of the amount of vegetation cover, the Leakiness declines as the resolution decreases (Figure 4.25). The reasons for this are covered in the next section. Figure 4.25 also shows that Leakiness varies by type of average cover.

The variability of the leakiness with resolution for each type of Cover Index was not calculated as it is clearly influenced by resolution and would lack meaningful interpretation.

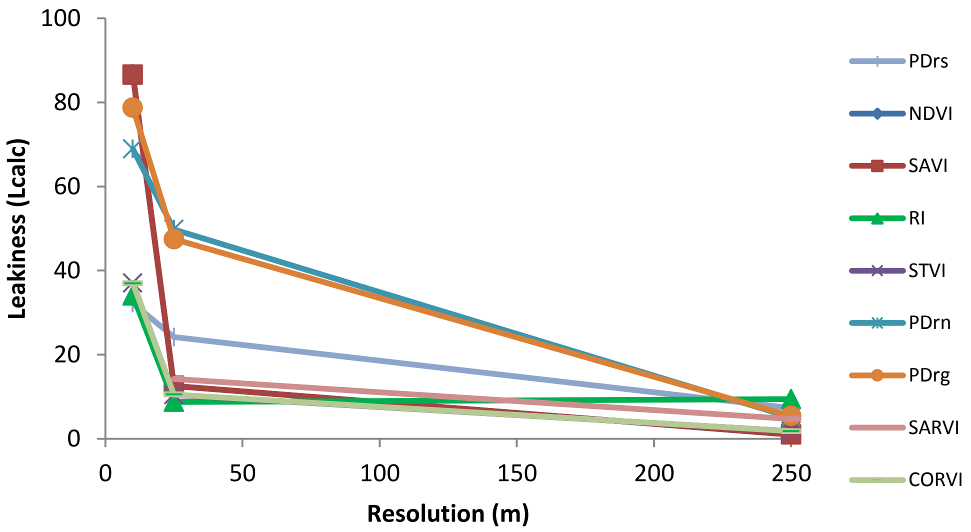

Figure 4.25 Leakiness at different resolutions for different cover indices.

The sensitivity of leakiness to type of vegetation cover is given in Table 4-4 and shown in Figure 4.26. This is a measure of how much the leakiness changes per unit change in average cover.

Table 4-4 Sensitivity of Leakiness to type of Vegetation Cover Index

Cover Index	Leakiness Sensitivity			Std. Dev.	Avg.
	10m	25m	250m		
NDVI	1.93	0.23	0.01	1.05	0.73
SAVI	1.93	0.23	0.01	1.05	0.73
RI	0.61	0.15	0.23	0.24	0.33
STVI	0.66	0.18	0.03	0.33	0.29
CORVI	0.65	0.19	0.03	0.33	0.29
PDrn	1.12	0.92	0.08	0.55	0.71
PDrg	1.09	0.69	0.08	0.51	0.62
PDrs	0.44	0.37	0.13	0.17	0.31
SARVI		0.27	0.09	0.13	0.18
GCI		0.04			

The cover indices, PDrs and RI have the lowest standard deviation across all resolutions while .

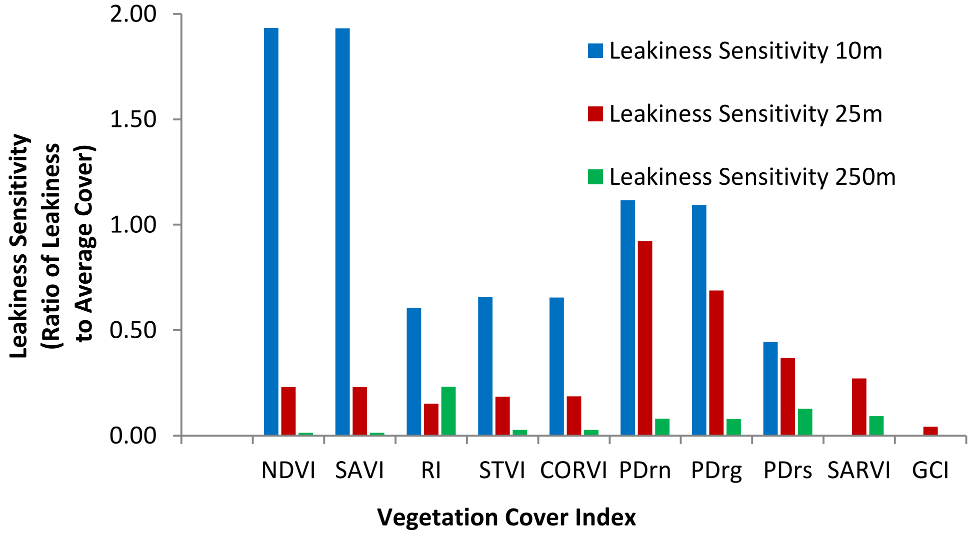

Figure 4.26 Leakiness Sensitivity

An analysis of the range of sensitivity of leakiness sensitivity to average cover (Figure 4.27) shows that it declines with increase in average cover.

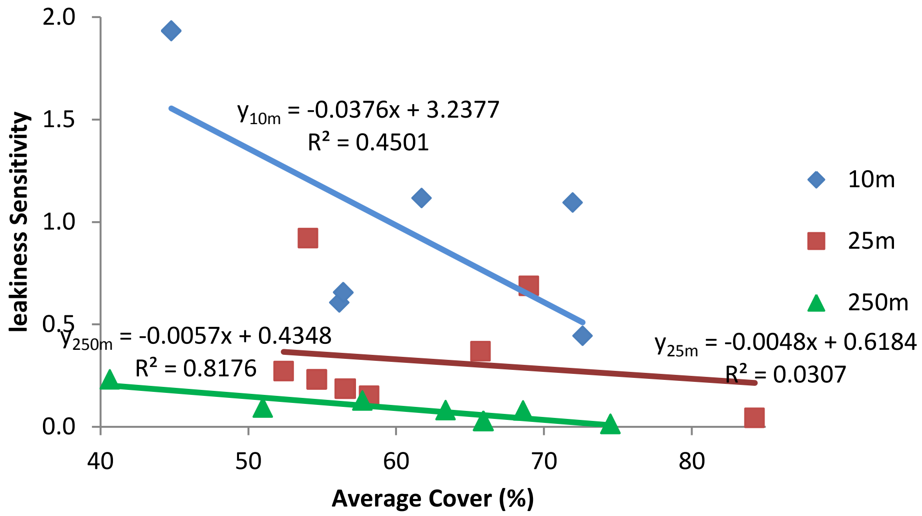

Figure 4.27 Change in Leakiness Sensitivity to Cover

4.3.2.3. Adjusted Average Leakiness

The development of the AAL was covered in sub-section 4.3. This section compares the results using the AAL values.

AAL values for each vegetation coverage and resolution are shown in Table 4-5 and graphed in Figure 4.28.

Table 4-5 Adjusted Average Leakiness values

Cover Index	Average Cover (%)			Adjusted Average Leakiness (AAL)		
	10m	25m	250m	10m	25m	250m
NDVI	44.80	54.66	74.52	14.69	13.33	5.59
SAVI	44.81	54.64	74.51	14.67	13.34	5.59
RI	56.16	58.19	40.64	5.77	9.29	52.62
STVI	56.43	56.61	65.90	6.28	11.08	9.98
CORVI	56.45	56.54	65.93	6.26	11.14	9.95
PDrn	61.73	54.06	63.35	11.68	52.82	28.58
PDrg	71.96	68.99	68.59	13.35	50.36	30.29
PDrs	72.62	65.71	57.73	5.46	25.65	40.96
SARVI		52.39	51.00		15.07	26.37
GCI		84.25			3.76	

Table 4-5 and Figure 4.28 show that AAL is not resolution dependent and varies with both cover and resolution. The subset graph within Figure 4.28 (upper right corner) provides a comparison of the Leakiness values for each cover index before conversion to AAL values.

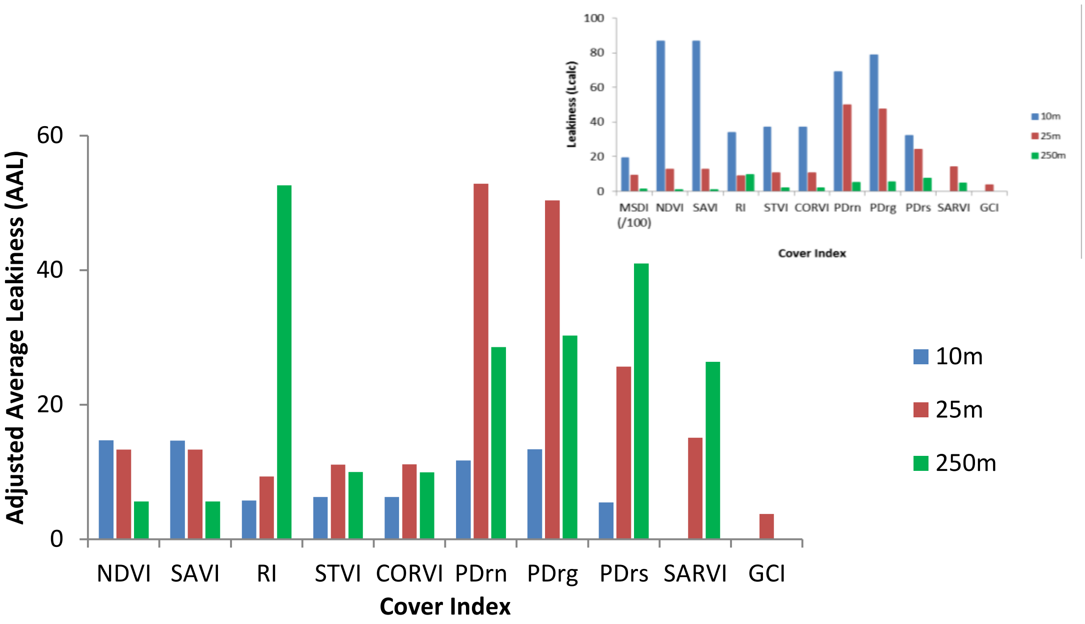

Figure 4.28 Adjusted Average Leakiness values

The AAL response to type of cover and resolution is shown in Figure 4.29 and the Leakiness vs Resolution graph is shown as a subset for comparison purposes. This shows that rather than decreasing with resolution, AAL, when measured on a unit cell basis, shows a general increase from 10m to 25m and then either a continued increase or decrease thereafter to 250m resolution. The reasons for this are discussed in Sections 4.4.

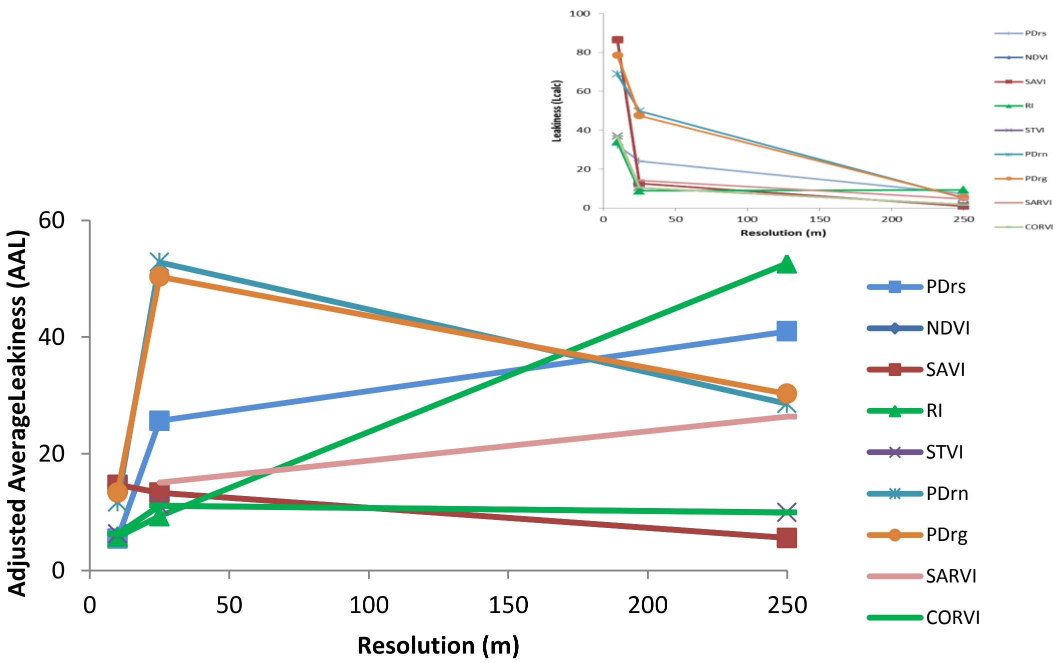

Figure 4.29 Adjusted Average Leakiness response to resolution

The relationship between AAL and Coverage is shown in Figure 4.30 with the previous relationship of leakiness with cover shown sub-setted in the upper right corner of the figure. AAL decreases as cover increases (expected) however, at 250m resolution the decrease in AL is steeper than it is for Leakiness.

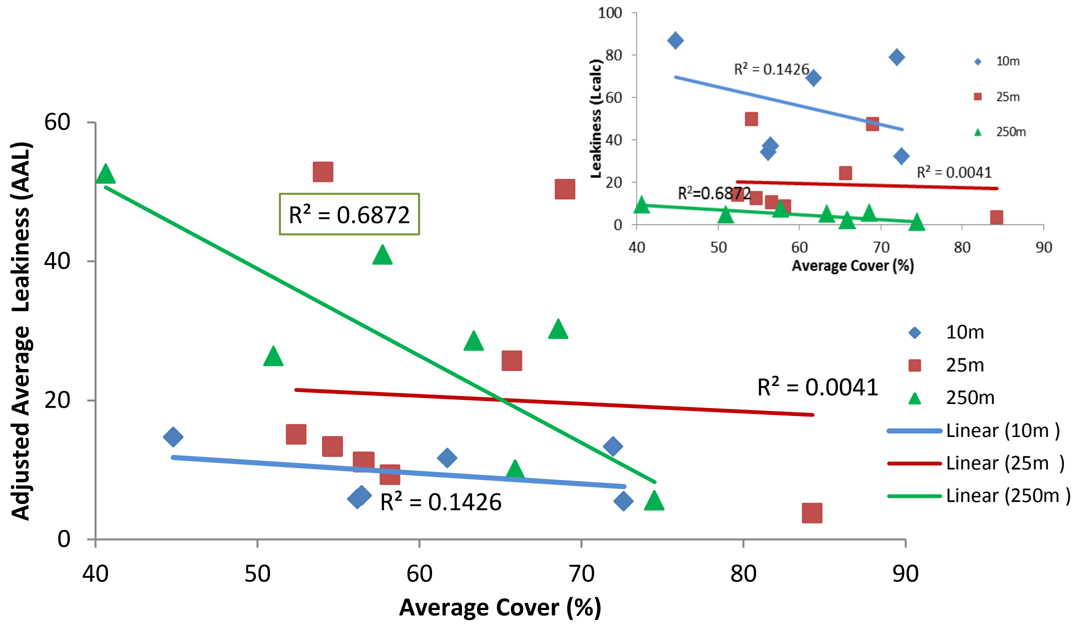

Figure 4.30 Adjusted Average Leakiness response to amount of cover.

AAL was also tested for its sensitivity to each type of vegetation cover (Table 4-6) with the results shown graphically in Figure 4.31 with the Leakiness sensitivity response shown in the subset figure. This provides a measure of how much the AAL changes for each unit of change in average cover.

Table 4-6 Sensitivity of AAL to Vegetation Cover Index

Cover Index	AAL Sensitivity		
	10m	25m	250m
NDVI	0.33	0.24	0.07
SAVI	0.33	0.24	0.08
RI	0.10	0.16	1.29
STVI	0.11	0.20	0.15
CORVI	0.11	0.20	0.15
PDrn	0.19	0.98	0.45
PDrg	0.19	0.73	0.44
PDrs	0.08	0.39	0.71
SARVI		0.29	0.52
GCI		0.04	

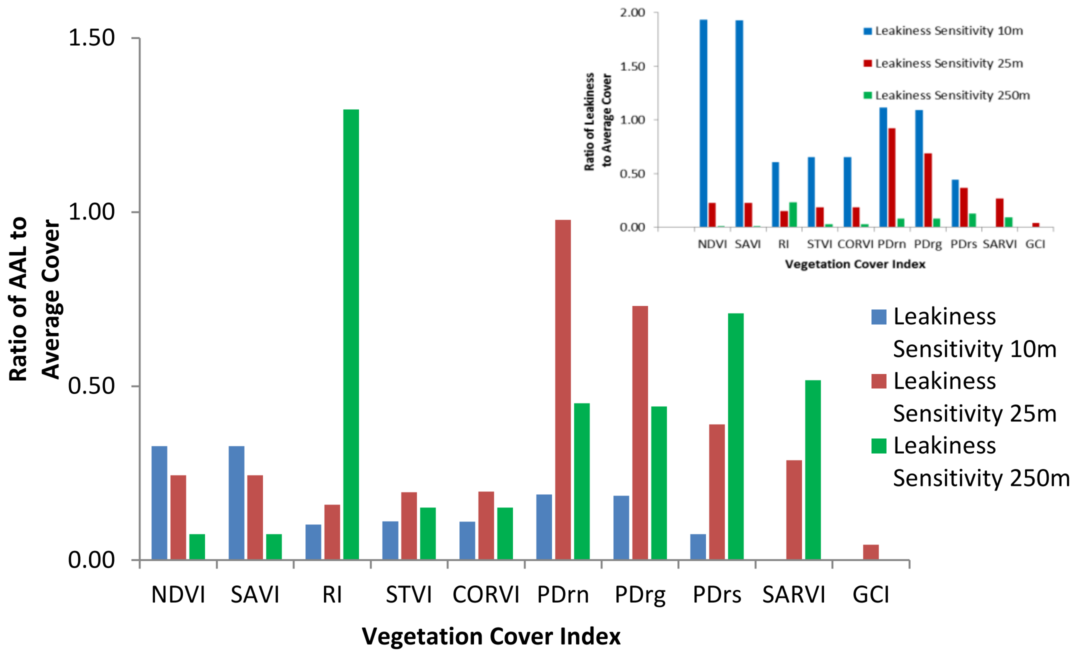

Figure 4.31 Adjusted Average Leakiness Sensitivity

Particular attention is drawn to the high sensitivity of AAL to RI cover at 250m resolution and the elevated sensitivities of AAL to PDI and SARVI cover at 25m and 250m resolution.

The sensitivity of the AAL to cover is shown as a function of cover in Figure 4.32. This shows that sensitivity of AAL to cover declines with increase in cover, which is a similar pattern for the sensitivity of Leakiness (Lcalc) to cover. While Leakiness was most sensitive to cover in 10m resolution imagery, AAL is most sensitive to cover in 250m resolution imagery.

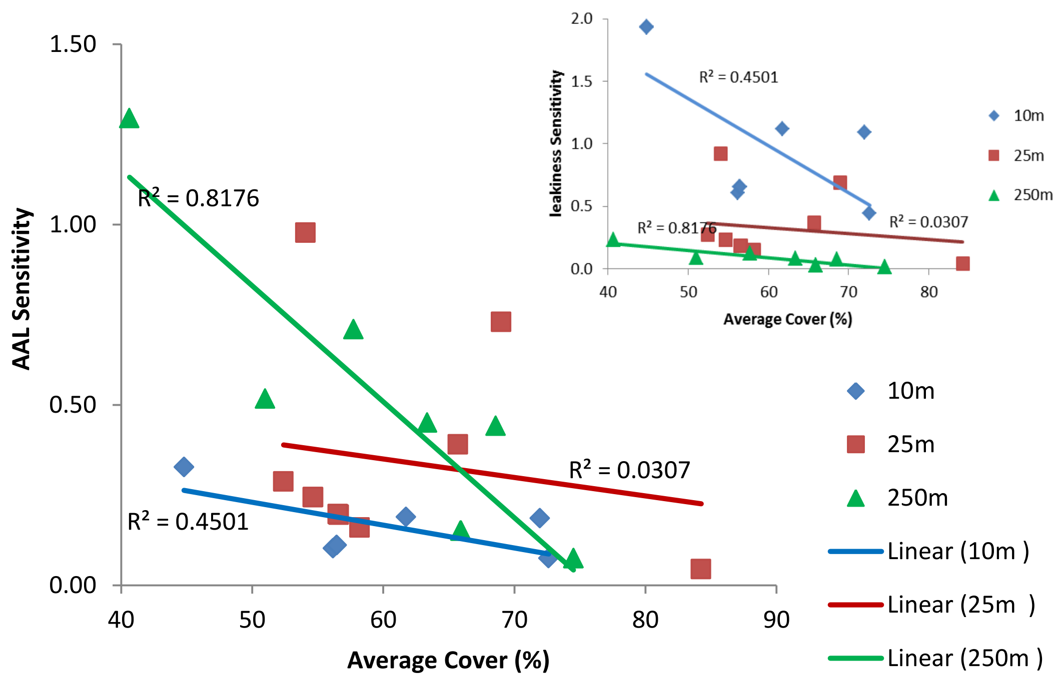

Figure 4.32 Change in AAL Sensitivity to Cover

4.3.3. Sub-catchment Leakiness

The following three sections provide a more in-depth analysis of the relationship between type of vegetation index and leakiness on a sub-catchment basis. The AAL was used in place of the calculated Leakiness (Lcalc) for the analysis of sub-catchments.

4.3.3.1. Ten Meter Resolution

The amount of Average Cover for each sub-catchment, at 10m resolution, is given in Table 4-7 and shown in Figure 4.33.

Table 4-7 Amount of Average Cover (%) in each sub-catchment (10m)

Sub-catchment	Area (ha)	Slope (%)	Average Vegetation Cover (%)							
			CORVI	NDVI	PDrg	PDrn	PDrs	RI	SAVI	STVI
2	696	3.6	56.7	45.1	73.3	64.2	73.1	56.2	45.1	56.7
3	392	3.8	56.4	44.7	71.7	61.6	73.4	56.6	44.7	56.4
4	710	3.1	56.4	44.8	71.4	60.2	73.9	56.3	44.9	56.4
5	410	3.0	56.1	44.4	69.1	60.8	74.9	56.6	44.4	56.1
6	590	2.5	55.3	44.1	73.3	57.5	74.0	56.1	44.1	55.3
7	451	3.8	56.7	45.1	72.3	62.1	72.8	56.2	45.1	56.7
8	336	2.2	56.9	45.7	71.1	59.8	70.5	55.0	45.7	56.9
9	1003	4.3	56.7	44.7	72.7	61.2	69.6	56.4	44.7	56.7
10	791	4.1	56.6	44.9	72.0	64.5	72.4	55.9	45.0	56.5
11	521	3.9	56.5	44.7	70.7	63.8	73.8	56.1	44.7	56.5
Avg.	590	3.4	56.44	44.82	71.75	61.57	72.83	56.13	44.83	56.42
Std. Dev.	210	0.69	0.46	0.45	1.30	2.20	1.64	0.45	0.45	0.46

Equation. 4-11 was used to remove the effect of catchment size and calculate the AAL for each sub-catchment given in Table 4-8.

The catchment wide average values and the amount of variation between sub-catchments are shown in the bottom two rows of each table. The average coverage for all sub-catchments concurs with the corresponding values in Table 4-1. The PDIs had higher amounts of Average Cover and their variation in Average Cover was greater than the other vegetation indices (Table 4-7). There is no comparable pattern in the AAL results (Table 4-8). NDVI and SAVI analyses yielded the lowest amounts of cover and the highest AAL values.

Table 4-8 Amount of Leakiness for each sub-catchment (10m)

Sub-catchment	Area (ha)	Slope (%)	Adjusted Average Leakiness (AAL)							
			CORVI	NDVI	PDRG	PDRN	PDRS	RI	SAVI	STVI
2	696	3.6	23.6	54.1	28.0	43.8	24.6	23.4	54.0	23.6
3	392	3.8	22.1	52.8	40.2	41.1	17.1	20.4	52.7	22.2
4	710	3.1	18.5	41.4	36.3	44.2	15.2	17.6	41.4	18.5
5	410	3.0	19.1	44.8	66.0	36.8	11.7	17.3	44.8	19.1
6	590	2.5	21.5	47.8	34.6	49.8	21.2	20.3	47.7	21.5
7	451	3.8	21.4	51.2	43.7	43.3	15.2	20.5	51.2	21.4
8	336	2.2	31.8	71.2	32.6	67.6	26.5	33.6	71.1	31.9
9	1003	4.3	13.7	33.2	26.8	32.5	9.8	12.1	33.1	13.7
10	791	4.1	17.0	40.6	45.9	31.1	13.9	15.7	40.6	17.1
11	521	3.9	23.6	54.4	32.1	37.0	13.3	24.1	54.4	23.6
Avg.	590	3.4	21.2	49.1	38.6	42.7	16.8	20.5	49.1	21.3
Std. Dev.	210	0.69	4.8	10.3	11.5	10.5	5.5	5.8	10.3	4.8

The inverse relationship between cover and leakiness exhibited by NDVI and SAVI based analyses confirmed expectations that low amounts of cover yield high levels of leakiness. However, this relationship was only weakly apparent for leakiness from the PDI cover analyses. High PDrg and PDrn Average Cover produced relatively high AAL values (lower values were expected) while high PDrs Average Cover resulted in very low Leakiness values (16.8 in Table 4-6). The result for PDrs is consistent with expectations of low leakiness from high average cover values (Bastin and Abbott *et al.* 2008, p. 22, Fig. 10; Ludwig, J. and G. N. Bastin *et al.* 2007).

Figure 4.33 and Figure 4.34 show the Average Cover and AAL values graphically for each 10m sub-catchment.

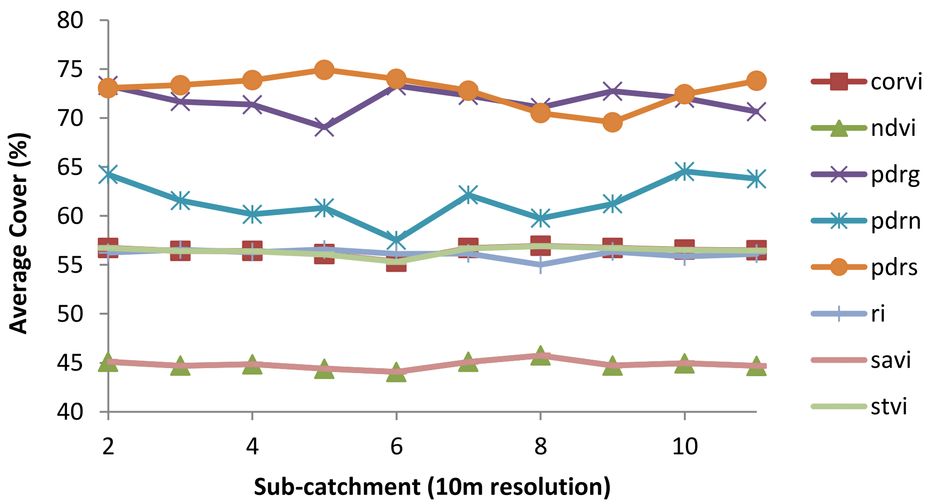

Figure 4.33 Average Cover (%) for each sub-catchment (10m)

Figure 4.33 shows that the PDI's are more sensitive to variations of cover within the catchment (Higher Std. Dev. values in Table 4-5) than the other indices. They also yielded the most variable AAL results (Figure 4.34) reflecting their high Std. Dev. values (Table 4-7).

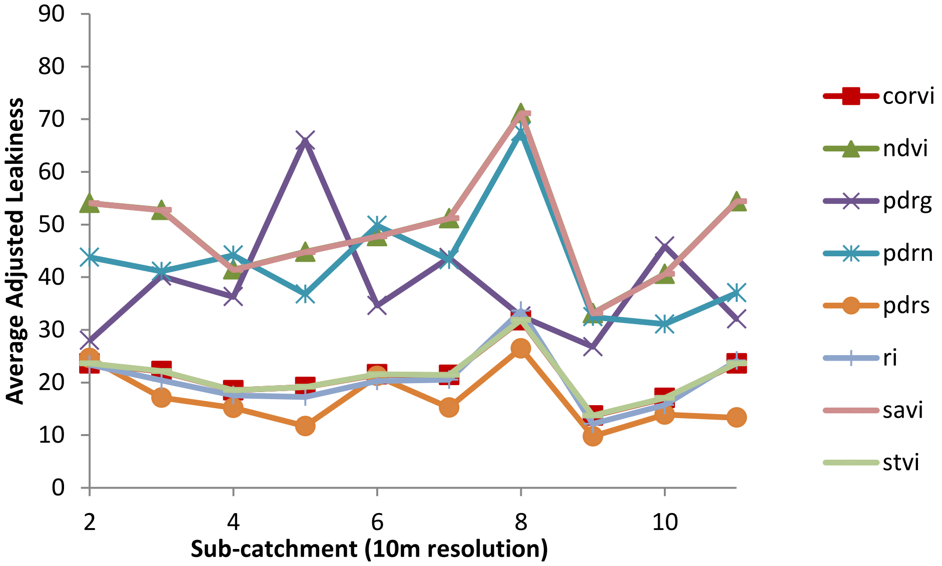

Figure 4.34 Leakiness of each sub-catchment by cover index (10m)

Correlation between Indices

Some vegetation cover indices have elements common to each other in their formulae. This can lead to results that are self-correlated. The strength of correlations between different Average Cover values and AAL values was tested by Pearson Correlation analysis (Salkind 2007). The results were converted to Coefficients of Determination (CoD) and these values are shown in Table 4-9 and Table 4-10 respectively.

Table 4-9 Coefficients of Determination for Average Cover correlation (10m)

	CoD								
	Slope	**CORVI**	**NDVI**	**PDrg**	**PDrn**	**PDrs**	**RI**	**SAVI**	**STVI**
Slope	1.00								
CORVI	0.15	1.00							
NDVI	0.00	0.74	1.00						
PDrg	0.03	0.00	0.00	1.00					
PDrn	0.55	0.33	0.09	0.00	1.00				
PDrs	0.04	0.38	0.32	0.12	0.00	1.00			
RI	0.22	0.12	0.51	0.00	0.01	0.25	1.00		
SAVI	0.00	0.74	1.00	0.00	0.09	0.32	0.51	1.00	
STVI	0.15	1.00	0.74	0.00	0.33	0.38	0.12	0.74	1.00

Table 4-10 Coefficients of Determination for Adjusted Average Leakiness correlation (10m)

	CoD								
	Slope	CORVI	NDVI	PDRG	PDRN	PDRS	RI	SAVI	STVI
Slope	1.00								
CORVI	0.38	1.00							
NDVI	0.29	0.99	1.00						
PDrg	0.01	0.04	0.03	1.00					
PDrn	0.69	0.73	0.65	0.07	1.00				
PDrs	0.41	0.65	0.59	0.14	0.69	1.00			
RI	0.35	0.99	0.97	0.06	0.71	0.63	1.00		
SAVI	0.29	0.99	1.00	0.03	0.65	0.59	0.97	1.00	
STVI	0.38	1.00	0.99	0.04	0.73	0.65	0.99	0.99	1.00

Coefficients of Determination reveal how much variation in one variable is explained by the other variable. Highly correlated interactions are shown in yellow. Neither Average Cover nor AAL showed any correlation with average catchment slope. Average Cover values generated using CORVI and STVI indices and NDVI and SAVI indices are highly correlated. This can be explained by the similarity of the formulae for each pair of indices (Section 4.2.1.3). Leakiness results show a wider pattern of correlation. All the band-ratio leakiness results were highly correlated, while the PDI results showed less correlation and the PDrg index showed the least correlation of all the cover indices.

Leakiness response to amount and type of cover

The response of AAL to cover is shown in Figure 4.35. The sub-catchment values cluster naturally by type of cover index when plotted in data space. Regression lines and R^2 values are shown for the three PDI data groups.

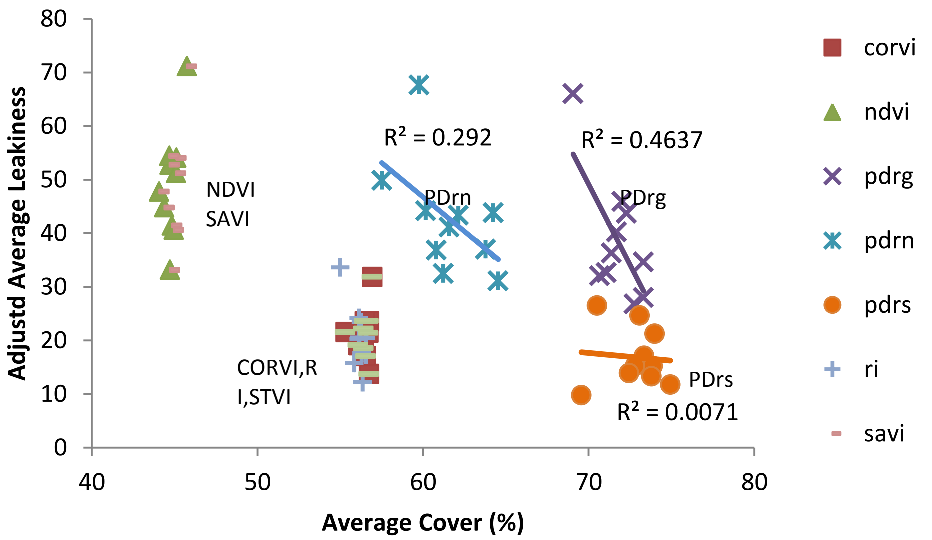

Figure 4.35 Clustering of Leakiness and Average Cover in data space (10m)

The PDI clusters reflect the combined effect of the variation (Std. Dev.) of the respective data (Average Cover and AAL, see Table 4-7 and Table 4-8) and the correlations between AAL values (Table 4-10). Clusters with high x and y values can be expected to be more sensitive to ground cover conditions and to yield more sensitive leakiness results than clusters with lower x and y values because they yield larger values for the same amount of image reflectance. The PDrg index has the highest overall x and y values for 10m resolution leakiness analysis.

The correlation between Average Cover and AAL across all sub-catchments at10m of resolution is shown in Table 4-11. PDrg, PDrn and RI show significant negative correlation between the Average Cover of a sub-catchment and it's AAL value. This is the expected direction of the correlation. SAVI and NDVI show a positive correlation and the other indices yield an indeterminate correlation. Both the positive and indeterminate correlations are unexpected.

Table 4-11 Correlation between Average Cover and AAL (10m)

Vegn. Index	CORVI	NDVI	PDrg	PDrn	PDrs	RI	SAVI	STVI
(R)	0.194	0.581	-0.681	-0.540	-0.084	-0.722	0.582	0.196

4.3.3.2. Twenty Five Meter Resolution

The amount of Average Cover for each sub-catchment at 25m resolution is shown in Table 4-12.

Table 4-12 Amount of Average Cover in each sub-catchment (25m)

Sub-catch-ment	Area (ha)	Slope (%)	Average Cover (%)									
			CORVI	GCI	NDVI	PDrg	PDrn	PDrs	RI	SARVI	SAVI	STVI
2	650	2.6	56.7	84.1	54.9	73.0	60.9	67.1	58.2	52.4	54.9	56.8
3	413	2.6	56.5	82.4	54.4	67.0	54.3	69.9	58.6	52.1	54.4	56.6
4	743	2.3	56.5	83.3	54.7	68.7	53.7	67.9	58.3	52.4	54.7	56.6
5	397	2.3	56.3	84.4	54.4	67.3	52.4	70.4	58.4	52.3	54.4	56.3
6	616	2.0	55.6	88.7	54.1	71.1	38.4	68.9	58.0	52.7	54.1	55.7
7	466	2.6	56.8	84.9	55.0	69.1	57.6	69.4	58.3	52.4	55.0	56.9
8	286	1.5	56.7	86.3	55.6	66.8	50.3	70.0	57.1	53.0	55.6	56.8
9	545	2.9	56.9	79.7	54.8	68.8	55.5	57.9	58.3	52.2	54.7	57.0
10	812	2.8	56.6	85.8	54.6	68.3	57.5	61.4	58.1	52.4	54.6	56.7
11	963	2.9	56.6	86.1	54.5	67.3	56.3	65.8	58.2	52.3	54.5	56.6
Avg.	589	2.4	56.5	84.6	54.7	68.7	53.7	66.9	58.2	52.4	54.7	56.6
Std. Dev.	209	0.5	0.37	2.43	0.41	1.98	6.13	4.15	0.39	0.26	0.41	0.37

Equation 4-11 was used to remove the effect of catchment size and calculate the AAL for each sub-catchment (Table 4-13).

Table 4-13 Amount of Adjusted Average Leakiness for each sub-catchment (25m)

Sub-catch-ment	Area (ha)	Slope (%)	Adjusted Average Leakiness									
			CORVI	GCI	NDVI	PDrg	PDrn	PDrs	RI	SARVI	SAVI	STVI
2	650	2.6	36.7	8.9	42.2	48	66	48.3	32.7	49.2	42.2	36.5
3	413	2.6	42.4	12.4	50.7	108	158	86.9	35.9	57.5	50.7	42.2
4	743	2.3	38.1	10.0	44.3	129	165	79.4	32.7	50.0	44.4	37.9
5	397	2.3	36.6	9.7	42.2	165	185	92.0	31.0	47.5	42.2	36.4
6	616	2.0	39.0	6.1	44.3	100	303	54.7	33.1	49.1	44.3	38.8
7	466	2.6	46.4	13.1	54.8	100	104	59.4	40.6	63.5	54.9	46.2
8	286	1.5	66.3	38.5	74.6	153	306	125	63.4	86.3	74.6	66.0
9	545	2.9	24.1	18.0	29.8	146	107	96.4	20.3	33.8	29.8	24.0
10	812	2.8	32.1	12.5	38.8	188	129	116	28.0	44.4	38.8	31.9
11	963	2.9	35.2	5.9	40.6	116	91	73.9	32.1	47.0	40.7	35.1
Avg.	589	2.4	39.7	13.5	46.2	125	161	83.2	35.0	52.8	46.3	39.5
Std. Dev.	209	0.5	11.08	9.46	11.99	40.1	83.69	25.37	11.3	14.1	12.0	11.04

The bottom two rows of each table show the catchment wide averages and the Standard Deviations between the sub-catchments. The average coverage for all sub-catchments agrees with the corresponding values in Table 4-1. The catchment wide Average Cover values lie between 50-60% except for the values for PDrg and PDrs and the GCI, which are higher. The AAL is highest for PDrn followed by PDrg and PDrs. This is unexpected based on the expected inverse relationship between average cover and leakiness. It is however consistent with the 10m leakiness results for PDrg and PDrn which yielded high leakiness values from high average cover values. Possible reasons for this are discussed further in Section 4.4.3. The high GCI Average Cover (84.6%) yielded a low AAL (13.5) as expected. Figure 4.36 shows the distribution of the Average Cover values across the sub-catchments.

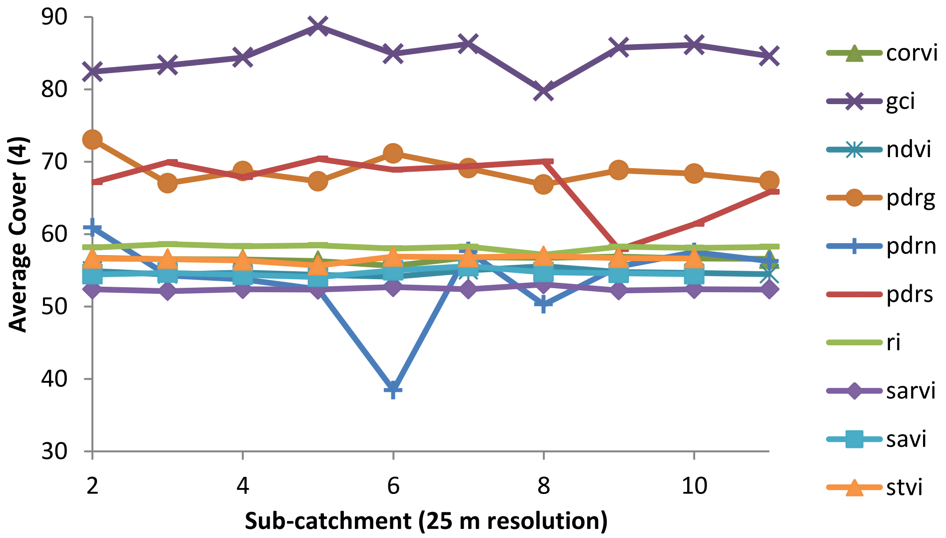

Figure 4.36 Average Cover for each sub-catchment (25m)

There are similarities between the amount of Average Cover by catchment at 10m and 25m resolution. Comparison of PDrn cover values in Figure 4.33 (10m) with Figure 4.36(25m) shows a distinctive low Average Cover in sub-catchment 6 at both resolutions. PDrg and PDrn yielded consistently higher cover measurements across all sub-catchments at both resolutions than the other cover indices. NDVI yielded consistent low values (45%) at 10m but its values grouped with the other index values in the 50-60% range at 25m resolution.

The GCI, which was only available at 25m resolution, was consistently high across all sub-catchments. It is included here because, although there are no comparable GCI values for 10 and 250m resolution images, it is of interest because of the Queensland-wide network of annual Bare Ground Index (BGI) analyses conducted by the (QDERM) (Scarth and Byrne *et al.* 2006). The GCI values for the experimental catchment were developed from Landsat TM imagery collected on 9 October 2005 while all the vegetation covers were generated from an image captured on the 26th of November 2005. The difference of almost two month in the time of between the GCI Landsat imagery and the imagery used in this research may have contributed to the large difference in values. This is considered further in Section 4.4.3.Figure 4.37 shows the distribution of AAL in each of the sub-catchments.

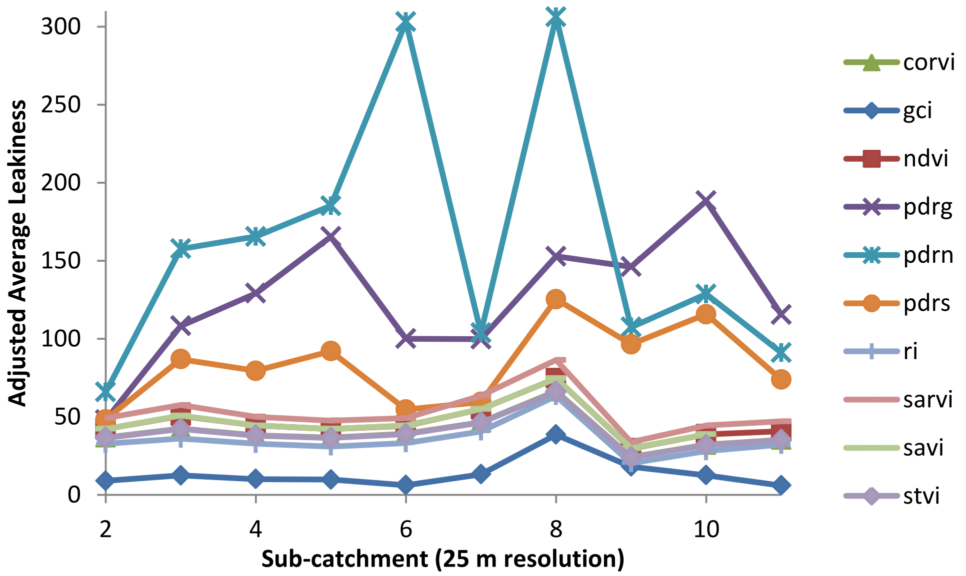

Figure 4.37 Adjusted Average Leakiness for each sub-catchment (25m)

The low leakiness response from high GCI cover values is clearly evident across the bottom of the graph including the positive inflection for sub-catchment 8. This corresponds with the negative inflection in the GCI for sub-catchment 8 evident in Figure 4.36. Leakiness from the PDI cover values group together in the high range, while leakiness from the remaining index cover values group together in a cohesive band around 50 AAL units. The spike in leakiness in sub-catchment 8 is evident for all coverages although there is no corresponding decrease in most cover values for this sub-catchment. The PDI leakiness values show high sub-catchment variability.

This may be due to their sensitivity to the location of different types of vegetation cover and to the soil background colour (Pickup and Chewings *et al.* 1993).

Correlation between Indices

Both the Average Cover and AAL results were tested for correlation between variables by use of Pearson Correlation analysis and the CoD values are shown in Table 4-14 and Table 4-15. Table 4-14 values indicating significant correlation are highlighted in yellow. These results show there is distinctly more correlation between Average Adjusted Leakiness from different cover indices than there is between Average Cover from different cover indices. The PDI exhibit the least correlation between values.

Table 4-14 Coefficients of Determination for Average Cover correlation (25m)

	CoD										
	Slope	**CORVI**	**GCI**	**NDVI**	**PDrg**	**PDrn**	**PDrs**	**RI**	**SARVI**	**SAVI**	**STVI**
Slope	1.00										
CORVI	0.13	1.00									
GCI	0.23	0.39	1.00								
NDVI	0.14	0.47	0.01	1.00							
PDrg	0.00	0.05	0.02	0.02	1.00						
PDrn	0.36	0.72	0.29	0.13	0.00	1.00					
PDrs	0.41	0.14	0.20	0.00	0.01	0.10	1.00				
RI	0.50	0.00	0.21	0.48	0.00	0.08	0.01	1.00			
SARVI	0.73	0.05	0.40	0.27	0.00	0.26	0.10	0.89	1.00		
SAVI	0.14	0.48	0.01	1.00	0.02	0.13	0.00	0.48	0.27	1.00	
STVI	0.14	1.00	0.40	0.47	0.05	0.72	0.14	0.00	0.05	0.47	1.00

Table 4-15 Coefficients of Determination for Adjusted Average Leakiness correlation (25m)

	CoD										
	Slope	**CORVI**	**GCI**	**NDVI**	**PDrg**	**PDrn**	**PDrs**	**RI**	**SARVI**	**SAVI**	**STVI**
Slope	1.00										
CORVI	0.02	1.00									
GCI	0.05	0.39	1.00								
NDVI	0.04	0.99	0.38	1.00							
PDrg	0.18	0.11	0.13	0.13	1.00						
PDrn	0.07	0.39	0.22	0.35	0.13	1.00					
PDrs	0.14	0.29	0.41	0.32	0.82	0.16	1.00				
RI	0.00	0.98	0.48	0.96	0.09	0.38	0.28	1.00			
SARVI	0.04	0.99	0.39	1.00	0.12	0.32	0.31	0.97	1.00		
SAVI	0.04	0.99	0.38	1.00	0.13	0.35	0.32	0.96	1.00	1.00	
STVI	0.02	1.00	0.39	0.99	0.11	0.39	0.29	0.98	0.99	0.99	1.00

Leakiness Response to amount and type of cover

The relationships between leakiness and cover, cluster in data space as shown in Figure 4.38. This figure shows the 10 clusters of Average Cover with AAL at 25m resolution. To the lower right is the GCI cluster while midway through the center of the graph are the three PDI clusters and to the lower center left is the group of band ratio index clusters. The band ratio clusters are shown in more detail in Figure 4.39.

This clustering reflects the combined effect of the variation (Std. Dev.) in values and their correlation (R^2) as shown earlier in Table 4-12 through Table 4-13. Clusters that show the highest Average Cover (x) and highest AAL (y) are the most sensitive to catchment leakiness conditions. The PDrg index has the highest overall ***x*** and ***y*** values for 25m resolution leakiness analysis. This pattern is similar to the pattern for 10m resolution clustering (Figure 4.35).

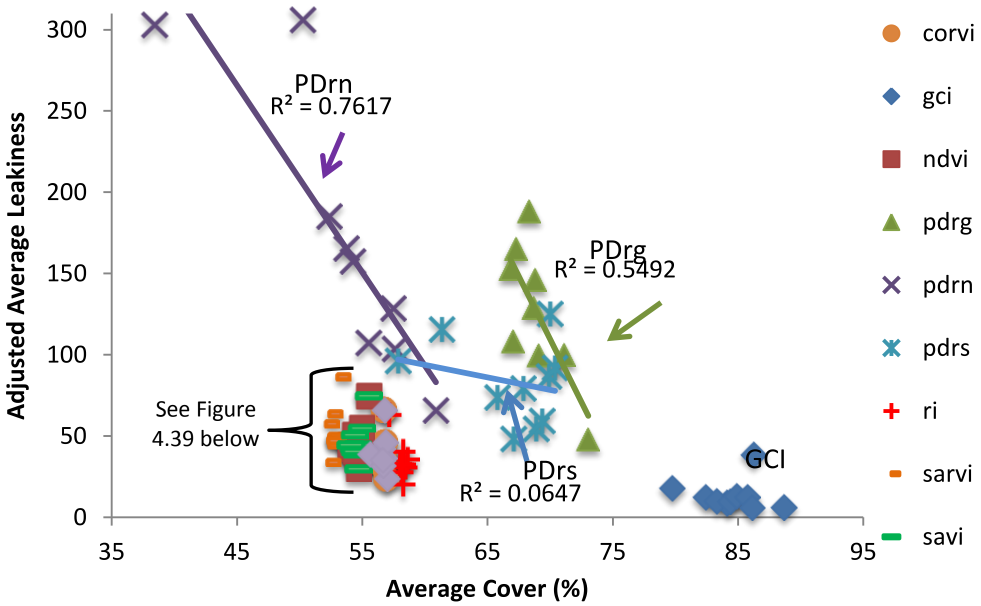

Figure 4.38 Clustering of AA Leakiness and Average Cover in data space (25m)

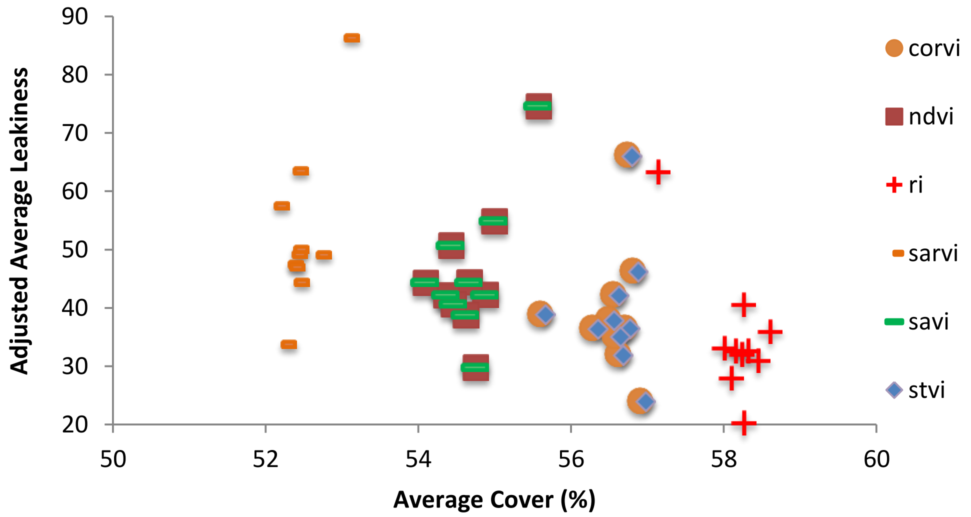

Figure 4.39 Details of Band Ratio AA Leakiness and Average Cover in data space (25m)

The correlation between Average Cover and Adjusted Average Leakiness for all sub-catchments at 25m resolution is shown in Table 4-16. PDrg, PDrn and RI show significant negative correlation between the Average Cover in a sub-catchment and its AAL, which is the expected direction of the correlation. SARVI, SAVI and NDVI show a positive correlation. The other index cover values have an indeterminate correlation. Both the positive and indeterminate correlations are unexpected and the reason for them is unknown. This pattern of correlation is a similar to the 10m resolution data in Figure 4.34 and is discussed further in Section 4.4.1.

Table 4-16 Correlation between Average Cover and AA leakiness (25m)

Vegn. Index	CORVI	GCI	NDVI	PDrg	PDrn	PDrs	RI	SARVI	SAVI	STVI
R	0.043	-0.065	0.660	-0.692	-0.868	-0.254	-0.761	0.714	0.659	0.037

4.3.3.3. Two Hundred and Fifty Meter Resolution

The amount of Average Cover for each sub-catchment at 250m resolution is shown in Table 4-17. Equation 4-11, was used to remove the effect of catchment size and calculate the AAL for each sub-catchment. These values are shown in Table 4-18.

Table 4-17 Amount of Average Cover in each sub-catchment (250m)

Sub-catchment	Area (ha)	Slope (%)	Average Cover (%)								
			CORVI	NDVI	PDrg	PDrn	PDrs	RI	SARVI	SAVI	STVI
2	1944	1.3	64.1	74.6	66.0	69.8	62.5	40.7	50.5	74.6	64.0
3	581	1.1	64.3	74.7	70.3	75.4	67.8	40.8	50.4	74.7	64.3
4	250	0.4	68.3	74.4	73.0	75.1	66.3	41.4	50.4	74.4	68.2
5	963	1.5	64.9	73.8	66.3	61.7	68.1	41.6	50.3	73.8	64.9
6	531	0.9	68.6	73.2	53.8	53.8	54.8	43.0	49.5	73.2	68.6
7	569	1.0	66.8	73.4	63.5	49.1	45.6	41.8	50.5	73.4	66.7
8	919	1.2	68.6	73.4	72.5	59.7	62.9	41.9	50.9	73.4	68.5
Avg.	822	1.1	66.5	73.9	66.5	63.5	61.1	41.6	50.4	73.9	66.5
Std. Dev.	551	0.33	2.04	0.64	6.64	10.30	8.23	0.78	0.43	0.64	2.05

Table 4-18 Amount of Leakiness for each sub-catchment (250m)

Sub-catchment	Area (ha)	Slope (%)	Adjusted Average Leakiness								
			CORVI	NDVI	PDrg	PDrn	PDrs	RI	SARVI	SAVI	STVI
2	1944	1.3	10.5	5.5	19.6	11.3	58.2	51.8	26.8	5.5	10.6
3	581	1.1	20.2	11.4	20.1	10.4	31.9	106.1	56.2	11.4	20.3
4	250	0.4	34.3	22.5	27.3	22.5	143.5	203.3	109.3	22.5	34.5
5	963	1.5	19.1	11.6	74.5	59.7	66.9	96.4	53.9	11.6	19.2
6	531	0.9	17.6	12.8	118.2	86.8	95.1	98.0	61.4	12.8	17.6
7	569	1.0	12.6	8.9	59.9	91.8	176.8	70.4	40.9	8.9	12.6
8	919	1.2	15.9	9.6	26.9	92.9	39.7	78.7	41.8	9.6	15.9
Avg.	822	1.1	18.6	11.7	49.5	53.6	87.4	100.7	55.8	11.7	18.7
Std. Dev.	551	0.33	7.71	5.31	37.03	38.22	54.51	48.92	26.31	5.31	7.79

The bottom two rows of each table show the catchment wide averages and the variation (Standard Deviation) in values between sub-catchments. The Average Cover values for all vegetation indices agree closely with the whole-of-catchment values in Table 4-1. These lie between 40-75%. The AAL is highest for the RI followed by the PDrs.The inverse relationship between high AAL and low RI Average Cover was expected, however a PDrs Average Cover value of 61.1% was expected to yield a much lower AAL than 87.4. Generally, high levels of band ratio index Average Cover values produced low AAL values. This is in line with expectations.

Figure 4.40 depicts the Average Cover values across the 7, 250m resolution sub-catchments (data from Table 4-17).

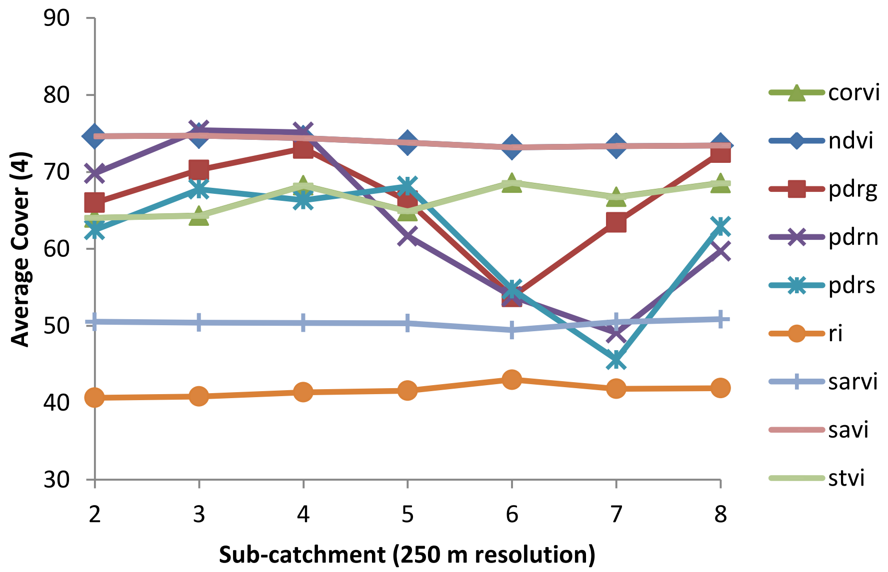

Figure 4.40 Average Cover for each sub-catchment (250m)

The 250m sub-catchment Average Cover values (Table 4-17 and Figure 4.40) cannot be compared directly with the 10m and 25m sub-catchment Average Cover values (Table 4-7 and 4-15 and Figure 4.33 and Figure 4.36) because of the different sub-catchment boundaries caused by the coarser DEM resolution when defining the sub catchments (see Figure, Figure 4.5 and Figure 4.6). The greater variation in the PDI cover values distinguishes them from the band ratio cover values that show less variation between sub-catchments.

Figure 4.41 shows the distribution of AAL in each of the 250m resolution sub-catchments (data from Table 4-18).

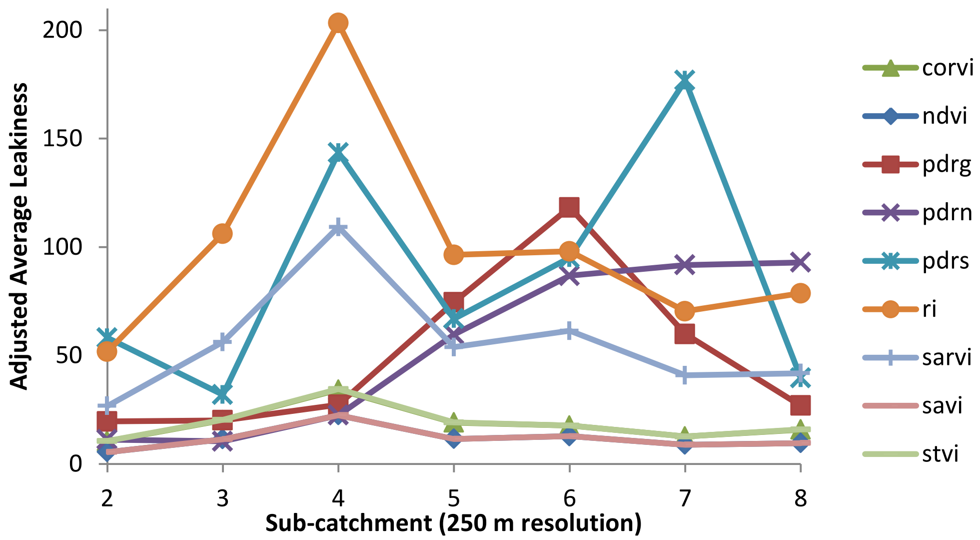

Figure 4.41 Adjusted Average Leakiness for each sub-catchment (250m)

The distinguishing feature in Figure 4.41 is the variable and high leakiness values due to RI vegetation cover. The PDI AAL values are larger and have a higher variation for most sub-catchments than the band ratio AAL values except for RI and SARVI.

Correlation between Indices

Both the Average Cover and AAL results were tested for correlation between variables by use of Pearson Correlation analysis and the CoD values are shown in Table 4-14 and Table 4-15.

Table 4-19 Coefficients of Determination for Average Cover correlation (250m)

	CoD									
	Slope	**CORVI**	**NDVI**	**PDrg**	**PDrn**	**PDrs**	**RI**	**SARVI**	**SAVI**	**STVI**
Slope	1.00									
CORVI	0.40	1.00								
NDVI	0.00	0.44	1.00							
PDrg	0.00	0.02	0.29	1.00						
PDrn	0.03	0.16	0.85	0.41	1.00					
PDrs	0.02	0.11	0.41	0.36	0.66	1.00				
RI	0.06	0.57	0.81	0.45	0.55	0.26	1.00			
SARVI	0.08	0.06	0.10	0.70	0.07	0.06	0.41	1.00		
SAVI	0.00	0.44	1.00	0.29	0.85	0.41	0.81	0.10	1.00	
STVI	0.40	1.00	0.44	0.02	0.16	0.11	0.57	0.06	0.44	1.00

Table 4-20 Coefficients of Determination for Adjusted Average Leakiness correlation (250m)

	CoD									
	Slope	CORVI	NDVI	PDrg	PDrn	PDrs	RI	SARVI	SAVI	STVI
Slope	1.00									
CORVI	0.04	1.00								
NDVI	0.09	0.96	1.00							
PDrg	0.00	0.00	0.01	1.00						
PDrn	0.02	0.04	0.01	0.38	1.00					
PDrs	0.09	0.10	0.19	0.08	0.09	1.00				
RI	0.11	0.98	0.98	0.00	0.05	0.15	1.00			
SARVI	0.11	0.96	0.99	0.01	0.02	0.18	0.98	1.00		
SAVI	0.09	0.96	1.00	0.01	0.01	0.19	0.98	0.99	1.00	
STVI	0.04	1.00	0.96	0.00	0.05	0.10	0.98	0.96	0.96	1.00

Values indicating significant correlation are highlighted in yellow. There is again distinctly more correlation between leakiness from different cover indices than there is between Average Cover from different cover indices. The PDI, as a group, exhibit the least correlation between values.

Leakiness response to amount and type of cover

The relationships between AAL and cover cluster in data space as shown in Figure 4.42.

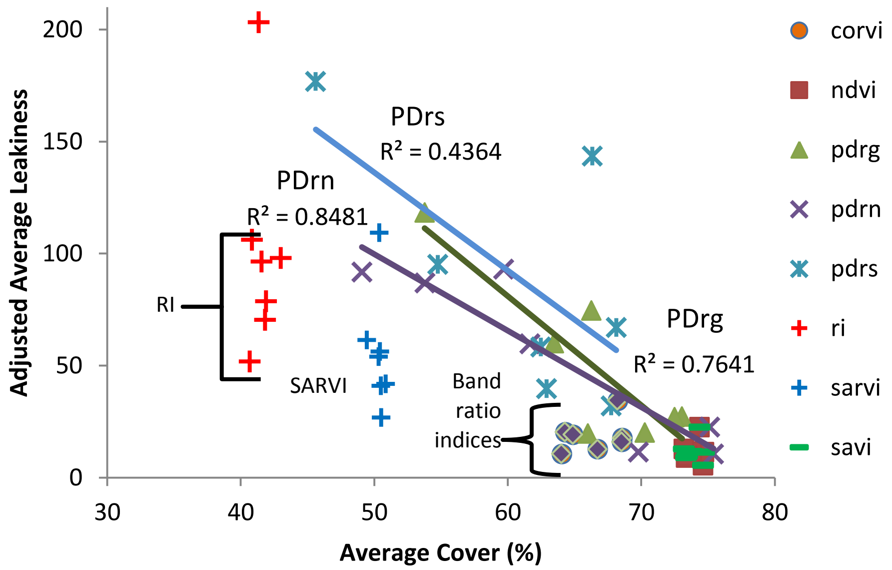

Figure 4.42 Clustering of AA leakiness and Average Cover in data space (250m)

The clustering in Figure 4.42 reflects the variance between sub-catchments and the correlation between AAL and average cover values. These results are different from the 10m and 25m resolution data space clustering results in that the RI and SARVI based data, cluster separately from the band ratio data with which they grouped previously. The results are similar to the 10 and 25m resolution data to the extent that the PDI index results show the most variation and generally have higher combined **x** and **y** values meaning they are more sensitive to variations in cover values.

The correlation between Average Cover and AAL, for all sub-catchments, at 250m resolution is shown in Table 4-21. The three PDI indices exhibit significant levels of expected negative correlation. RI Average Cover is not negatively correlated with AAL as it was at 10m and 25m resolution. NDVI and SAVI are not positively correlated with AAL as they were in the 10m and 25m analyses. None of the other index values are significantly correlated. The reason for the changes and the lack of negative correlation is not known.

Table 4-21 Correlation between Average Cover and AA Leakiness (250m)

Vegn. Index	CORVI	NDVI	PDrg	PDrn	PDrs	RI	SARVI	SAVI	STVI
R	0.355	0.099	-0.874	-0.921	-0.661	-0.003	-0.260	0.099	0.353

4.3.4. Catchment Comparison

The relationship between leakiness and cover can be compared between sub-catchments at each of the three resolutions and between an aggregate-of-sub-catchments and the whole-of-catchment basis. The aggregate-of-sub-catchment relationships between leakiness and cover are shown in Figure 4.43. They can be compared against the whole-of-catchment relationships shown in Figure 4-43 (same as previous Figure 4.27).

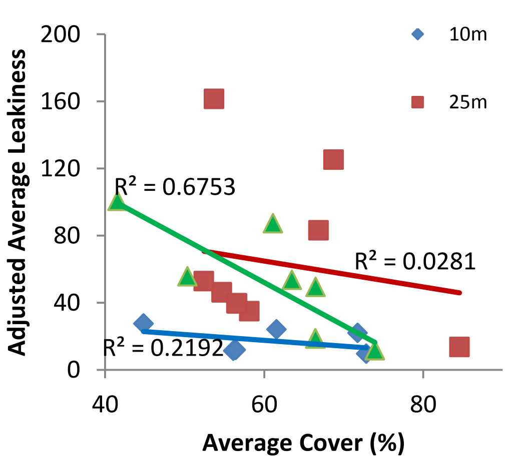

Figure 4.43 Aggregate-of-sub-catchments

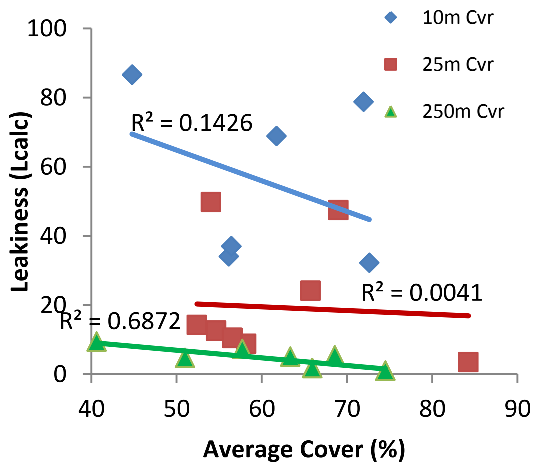

Figure 4.44 Whole-of-catchment

The feature to note about these figures is the numerical value of the R^2 correlations, not the position of the trend lines (because the AAL is subject to a range constant (M) that can be varied without changing the results). These results show a consistent correlation between AAL and average cover at all three resolutions because the R^2 values for each resolution are in general agreement with each other.

The correlation between average cover and leakiness values at three resolutions (from Table 4-11, Table 4-16 and Table 4-21) is summarised in Table 4-22. It shows the direction and consistency of correlation between AAL and cover. From inspection it can be seen that the three PDI indices and RI (except for RI at 250m) are negatively correlated (expected direction of correlation) while all other relationships are either positively correlated or show little correlation.

Table 4-22 Summary of correlation of AAL with cover

Resolution	Vegetation Indices (R)									
	CORVI	NDVI	PDrg	PDrn	PDrs	RI	SAVI	STVI	SARVI	GCI
10m	0.19	0.58	-0.68	-0.54	-0.08	-0.72	0.58	0.20	na	na
25m	0.04	0.66	-0.69	-0.87	-0.25	-0.76	0.71	0.66	0.04	0.04
250m	0.36	0.10	-0.87	-0.92	-0.66	0.00	0.10	0.35	-0.26	na

4.4. Discussion

The following section explains and interprets the effects of changing the scale of the image on leakiness in terms of the theory underlying the leakiness calculation and the field results from other investigators. These results and their possible explanations provide the background information for the chapters that follow on Variance, Upscaling and Location.

4.4.1. Catchment Leakiness

Table 4-1 listed the 11 cover indices initially used to analyse the experimental catchment. The formulae for these were covered in the respective subsections in Section 4.2.1.3. The MSDI is a simple structural classification index that measures the statistical heterogeneity in a landscape and has been used to map landscape degradation (Tanser and Palmer 1999). The filter used in this research was a 3x3 standard deviation filter applied to the red band. High MSDI values are indicative of degraded and disturbed landscapes. The values of 5.27, 0.74 and 14.65 (range of 0-100) are low and indicate low heterogeneity in the landscape. This is indicative of a natural (undisturbed) environment and is consistent with our physical observations of the experimental catchment (b).

The LC calculates leakiness values by a progressive flow equation (Ludwig, J. and G. N. Bastin *et al.* 2007, Appendix A; Ostendorf and Reynolds 1993) as explained in Section 4.2.3. The final leakiness (Lcalc) value for each catchment depends on the number of cells whose flow contributions have been progressively aggregated. There are more pixels (analysis cells) in the 10m resolution catchment than in the 25m resolution catchment with yet fewer cells in the 250m resolution catchment. This is the main reason contributing to the leakiness values (Lcalc) in Table 4-1 and Figure 4.19 being progressively smaller with decreasing resolution.

There is also a generally negative linear relationship between average cover and leakiness for each resolution as shown in Figure 4.19. The goodness of fit ranges from 0.004 (no correlation) for 25m resolution to 0.14 for 10m resolution and 0.68 for 250m resolution. The negative relationship between vegetation cover and leakiness is expected from the form of the progressive flow equation in which the L_{ij} term is a potential loss term reflecting reduced flow due to increased vegetation cover according to Equation 4-1. This is expected because Ludwig *et al.*(2007) showed that the theoretical cover leakiness relationship is asymmetric and negative sigmoidal in form.

This means that the greater the cover value, the higher the L_{ij} term and thus less water, soil and resources are available for flow to neighbouring pixels. The negative theoretical relationship between leakiness and cover was confirmed by Ludwig *et al.* (2007, p. 8) on field sites in the Northern Territory with a known grazing management record.

Ludwig *et al.* also recommended that users measure site specific soil-loss ratio data to calculate their own value of ***b***. The default value of ***b*** = - 0.065 was used for all analysis areas at each scale throughout this research. This means that the leakiness values may not fully reflect actual catchment soil loss conditions. There is also no cross-scale interaction term (Ludwig and Bartley *et al.* 2007) in Equation 4-1. Neither of these shortcomings is considered to affect the impact of image resolution on leakiness calculation because they were constant at all scales.

The low degree of correlation between cover and leakiness (Figure 4.27) is thought to be due to the leakiness values being generated from different types of cover values (different indices) which may lead to the cover values being distributed at different spatial locations in the catchment. The differences in cover distribution can be seen visually in Figure 4.21 to Figure 4.23. Ludwig and Eager *et al.* (2006, p.329) showed conceptually by Excel grid calculations that cover located in a flow network closer to the pour point of a catchment reduced the loss of resources more than an equivalent amount of cover located further away from the pour point. However, Bastin *et al.* found conflicting evidence that increased cover located further from the catchment pour point (i.e. at a higher elevation in the catchment) reduced leakiness more than if the increased cover was located lower in the catchment. Irrespective of which option is correct it is apparent that spatial location of cover affects the leakiness of the catchment.

Taken together, these findings mean that comparing the leakiness of catchments from imagery of different resolutions requires a metric that is independent of cell number. Also, while a generalised soil loss factor can be used for comparisons of the same catchment, if the leakiness of different catchments is to be compared catchment specific soil loss factors are strongly desirable. Because different cover indices measure different amounts of cover at a given location, they lead to different spatial distributions of cover. This means that it is essential that comparisons of leakiness between different catchments be based on similar measures of cover, however this creates a dilemma because the type of cover in different catchments may not be equally well measured by the same index.

4.4.2. Different Vegetation Cover Values

A range of different vegetation cover indices were used in the evaluation of leakiness response to change in image resolution so as to establish a profile of the catchment and to find if leakiness was more sensitive to different types of vegetation cover. More sensitive leakiness-cover relationships might be more sensitive to change in resolution. The merits of the different vegetation cover indices were discussed in Section 4.2.1.3.

Vegetation cover values for the 10m image (SPOT 5) range from 44.8% to 72.92% with the band ratio indices having the lower values (44.8% to 56.16%), the moisture stress indices having intermediate values (56.43% to 56.45%) and the PDI values (61.73$ to 72.62%) were the highest. At 25m resolution, (Landsat TM) the cover values ranged from 52.39% to 68.98%. Again, the band ratio values (52.3% to 58.19%) tended to be the lowest, the moisture stress index values (56.54% to 56.61%) were intermediate and the PDI values (54.06% to 68.99%) were in the higher range. The GCI at 84.252% was by far the highest average cover value. This is consistent with Bastin *et al.* (2008) findings that both masked and unmasked GCI values were consistently much higher than the corresponding PDrg values. However, their cover comparison was between imagery at different scales. The PDrg values were based on Quickbird 2.4 m pixels and the GCI values were from 30m Landsat pixels resampled to 25m. The cover data in this research (Table 4-1) shows PDrg cover values from like resolutions, namely10m (71.86%), 25m (68.99%) and 250m (68.59%).

The similarity between the profiles of cover values changed at 250m resolution where the band ratio values for NDVI and SAVI (74.51%) were the highest however the RI and SARVI values remained low (50% and 40.6%) as before. The STVI values were comparable (65.90% and 65.93%) to the PDI values (63.35% and 68.59%). PDrs was unexpectedly low at 57.73%.

The leakiness values for 10m and 25m resolutions correlated only weakly negatively with the average cover values (Table 4-2) however there was stronger negative correlation of leakiness with cover at 250m resolution (Table 4-2, $R^2 = 0.69$). This is the expected direction of correlation.

The PDrg index values (71.96%, 68.99% and 68.59%) were the values that were most consistently close to the GCI value of 84.25%. Bastin and Abbott *et al.* (2008)expressed the view that PDrg index values, in contrast to GCI values, “appeared reliable for indicating vegetation cover at Virginia Park”. This is consistent with the results obtained by (Pickup and Chewings *et al.* 1993).

The change in average cover of the catchment for each index at 10m, 25m and 250m is shown in Figure 4.18. The differences were unexpected because the 10m (SPOT) and 250m (MODIS) images were both captured on 29 Dec 2005 and the 25m (Landsat) image was captured 33 days earlier on 26 November 2005. There is very little difference in the band spectral windows of the three sensors (see Chapter 3) from which the different vegetation covers were calculated. The amount of variation between the cover indices for the three resolutions is indicated by the Standard Deviation shown in Table 4-3. NDVI and SAVI show the most variation (15.14 and 15.13) while PDrg shows the least variation (1.84).

As expected, leakiness declines with coarser resolutions due to there being fewer cells over which to aggregate the runoff (Figure 4.25). Ludwig, J. and G. N. Bastin *et al.* (2007 p.11) alluded to this when they pointed out the 1:1 linear relationship between Lmax and the number of pixels in the analysis area. Lmax represents the limiting value at the maximum for the leakiness (Lcalc) and thus it declines with decreasing resolution due to decrease in cell number.

The change in leakiness sensitivity with resolution is shown in Figure 4.26. Lower sensitivity values reflect a lower amount of leakiness, relative to the amount of cover. Thus, the expectation is that leakiness sensitivity will decline both with resolution and as the amount of cover increases. This is confirmed by the negative linear relationships for each resolution shown in Figure 4.27. PDrs and RI yield the least variable leakiness (Table 4-4, lowest Std. Dev.). This suggests that they might produce results that are more consistent across different resolutions.

However, the leakiness sensitivity for different indices responds differently as shown in Table 4-4 and Figure 4.26. The highest resolution is consistently the most sensitive. This is consistent with the reasoning of Bastin and Abbott *et al.* (2008) where they hypothesised that the larger resolution Landsat generated GCI may have failed to discriminate bare ground that that had been otherwise detected by the higher resolution Quickbird imagery (2.4m). The different sensitivity response with resolution may also be due to different vegetation indices identifying different concentrations of cover at different locations within the catchment leading to higher or lower leakiness.

In summary the pattern of vegetation cover values were consistent between 10m and 25m imagery but not with 250m imagery. However, the 10m and 250m imagery were collected on the same date while the 25m imagery was collected 33 days earlier. The small differences in band spectral windows between the SPOT and MODIS sensors are unlikely to be sufficient to account for these differences. GCI values were the highest cover values with PDrg cover being the next highest at all three resolutions. Overall, there was a consistent negative linear relationship between leakiness and both amount of cover and resolution. The highest resolution image also yielded the most sensitive leakiness values for each cover index.

4.4.3. Adjusted Average Leakiness

The LC generates both a Leakiness Index (LI) and a Calculated Leakiness (Lcalc). The relationship between LI and Lcalc is shown in Equation. 4-12 (Ludwig *et al.* 2007, p. 3).

$$LI = 1 - \left[\frac{Lmax - Lcalc}{Lmax - Lmin}\right]^k. \qquad (4\text{-}12)$$

$$where\ k = leakiness\ decay\ constant$$

For any given *k*, LI can be varied by changing Lmax. If *Lmax* = *Lcalc*, then *LI* = 1. Ludwig *et al.* recommended that *Lmax* be set to the largest *Lcalc* in the series of catchments being analysed so that all catchments will have an $LI \leq 1$. However, their recommendation assumes all analytic areas have the same size (same number of pixels). This is the case for time series analysis of catchments based on only one type of image. The analytic requirements for this research were different. The number of pixels in a given catchment changed when the resolution changed and as well, each sub-catchment covered a different area and thus included a different number of pixels. This change in pixel number made it impossible to use a standard Lmax setting for all analyses because if Lmax were to change between different sub-catchments and resolutions the LI values would not be comparable.

Different alternatives were considered in order to obtain a standard measure of leakiness both for catchments at different resolutions and for sub-catchments of different sizes. The concept of an Adjusted Average Leakiness (AAL), defined as the catchment leakiness/pixel (cell) was adopted as shown in Equation 4-11. Table 4-5 shows the leakiness values converted to AAL values. This allowed like–to-like comparison of the leakiness from catchments with different resolution imagery and sub-catchments of different sizes. Previously the requirement for similar catchment sizes and cell sizes has limited the use of the LC to temporal comparisons of the leakiness of the same catchment. This limitation was acknowledged by Bastin *et al.* (2007, p. 25). The AAL approach developed in this research allows comparison of different sized catchments with or without different cell sizes.

Table 4-5 and Figure 4.28 show that AAL values are not affected by resolution. RI, PDI and SARVI AAL values at 25m and 250m resolution are relatively much larger than their comparable Lcalc values, Table 4-1. This shift in magnitude of relative leakiness, when measured on a unit cell basis, is reflected in the sensitivity of AAL to cover (Figure 4.28). The AAL response to resolution shows a very different pattern from that of calculated leakiness (Figure 4.29). All AAL values increased from 10m to 25m resolution. The PDI AAL values decreased from 25m to 250m while all the other values either increased or stayed the same. The relationship between cover and AAL from one resolution to the next (e.g. 10m to 25m) is not consistent as shown in Table 4-23.

Table 4-23 Consistency response pattern

Cover index	Parameter	Shift direction		Pattern
		10>25m	25>250m	
PDrn	Cover	d	i	e/e
	AAL	i	d	
PDrg	Cover	d	d	e/u
	AAL	i	d	
PDrs	Cover	d	i	e/u
	AAL	i	i	
SAVI	Cover	i	i	e/e
	AAL	d	d	
NDVI	Cover	i	i	e/e
	AAL	d	d	
RI	Cover	i	d	u/e
	AAL	i	i	
STVI	Cover	i	i	u/e
	AAL	i	d	
CORVI	Cover	i	i	u/e
	AAL	i	d	
SARVI	Cover		d	_/e
	AAL		i	

where: i=increase, d=decrease
u=unexpected, e=expected

he relative sensitivity of AAL to average cover values (Figure 4.30) shows the same pattern as Lcalc to average cover (Figure 4.20). The AAL sensitivity also declines with increase in cover (Figure 4.32) as does Lcalc. However, while Lcalc, was most sensitive to cover at 10m resolution, AAL was most sensitive to cover at 250m resolution. This change reflects the effect of removing cell number from the calculation of catchment leakiness.

This section has shown that the AAL metric is not affected by resolution and thus provides a way to compare the leakiness of catchments with different resolution imagery and of different geographical sizes. It exhibits the same negative linear relationship with cover as Lcalc, however its response is not consistent with change in amount of cover between images of different resolutions (Table 4-23). Also AAL differed from Lcalc in that it was more sensitive to low resolution measures of cover than to high resolution measures.

4.4.4. Sub-catchment Responses

This section provides a replicated analysis of the average cover and leakiness responses by using the sub-catchments of the larger experimental catchment as replicates in order to test the stability of the relationships described in the previous sections. The size, and thus the number of pixels in each sub-catchment vary depending on precisely where the software (ArcHydro) located the sub-catchment break lines. The number of sub-catchments, their areas and average slopes are shown in the first three columns of Table 4-7 (10m), Table 4-12 (25m) and Table 4-17 (250m). The average vegetation cover values were generated by the LC. They cross check with the mean cover of the area covered by each sub-catchment mask and their aggregate average value agrees with the average cover shown in Table 4-1.

The 10m average cover and AAL results are shown graphically in Figure 4.33 and Figure 4.34. Figure 4.33 shows that all average cover values are relatively evenly distributed between the sub-catchments. The PDI cover values show more variation than the other vegetation cover indices. NDVI and SAVI show wide variation in leakiness values (S.D.=10.3) as do PDrg and PDrn (S.D.=11.5 and 10.5, Table 4-8).The other index AAL values are less variable and tend to change in concert with each other and PDrs. The difference in the way in which the AAL values vary by sub-catchment, relative to the lack of variation in the average cover, is thought to be due to the detection of different amounts of cover at different locations in each sub-catchment.(Abbott and Corfield undated) Ludwig, J. and G. N. Bastin *et al.* (2007) reported on LI values being sensitive to the spatial configuration of the cover at sites in North Queensland. Field data from flumes installed on hillslopes in a grazing catchment near Charters Towers established the importance of the distribution of vegetation cover, rather than just the average amount of cover, within a catchment on resource loss. Tests on catchments with the same average vegetation cover showed that there was 6-9 times more runoff and 60 times more sediment loss from hillslope catchments that contained bare ground patches than from catchments that didn’t contain bare ground (Bartley and Toth *et al.* 2006).

Analysis of the correlation between average cover and leakiness from the different vegetation cover indices on a sub-catchment scale showed no correlation with slope of the sub-catchment but a high degree of correlation between the leakiness from NDVI, SAVI, CORVI, RI and STVI covered catchments at 10m, 25m and 250m resolutions (Table 4-10, Table 4-15and Table 4-20). The areas highlighted in these tables show that there is more correlation between leakiness from different Cover indices than between average cover from different cover indices. The PDI based values exhibit the least correlation.

This is attributed to the similarity of the formulae for these vegetation cover indices (Section 4.2). Similar formulae mean that they are identifying closely similar concentrations of features at similar locations in the sub-catchments. Within this group, CORVI and STVI exhibit a higher leakiness correlation with each other (R^2 =

1.0) than with RI, NDVI and SAVI. This latter group of indices exhibit a second level of correlation with each other (R^2 = 0.97). The PDI produce leakiness values that have much less correlation. At 10m resolution (Table 4-10) PDrn and PDrs show weaker correlation with CORVI, NDVI, SAVI, STVI and RI (R^2 = 0.73 - 0.65, 0.65 - 0.59, 0.65 - 0.59, 0.73 - 0.65 and 0.71 - 0.63) and to each other (R^2 = 0.69). The PDrn and PDrs AAL correlations disappear at 25m (Table 4-15 and 250m (Table 4-20) resolution except only for a significant correlation between PDrg and PDrs (R^2 = 0.82) at 25m resolution. The PDrg leakiness is distinguished from all other leakiness values in showing no significant correlation with any other sources of leakiness except with PDrs at 25m (R^2 = 0.82). Because of this low amount of cross correlation PDrg appears to provide an estimate of leakiness that is distinctly separate from the other estimates.

Leakiness based on GCI estimates of cover also showed no correlation with any other sources of leakiness. GCI leakiness was only available at 25m resolution. The limitations on the GCI measure of cover were discussed in Section 4.4.2

The use of different sized sub-catchments within the overall catchment to replicate the analyses showed that leakiness was not correlated with catchment slope and that there was a high degree of correlation between the leakiness calculated from cover indices with similar formulae. Leakiness calculated from PDrg cover was distinguished by showing no significant correlation with any other cover except PDrs at 25m.

4.4.5. Response Relationships

The relationship between leakiness (AAL) and average cover is shown for each index at 10m, 25m and 250m resolution in Figure 4.35, Figure 4.38 and Figure 4.42. These Figures show that leakiness and average cover, group in different, but relatively consistent areas of data space. Across the three resolutions, leakiness from PDI has a negative linear relationship with average cover. The relationship between leakiness and the other sources of average cover is indistinct. This is not unexpected because the data are from different areas (sub-catchments).

Ludwig, J. and G. N. Bastin *et al.* (2007 Fig 1 (a)) showed that water driven sediment loss data collected by Carroll and Tucker (2000) and Lock (2000) declined exponentially with increasing vegetation cover when measured on pixel sized sample areas. Their LI values also decayed exponentially when calculated from catchments with fitted average cover that matched the pixel average cover and it provided a good fit with the experimental soil loss ratios. The AAL values used in this research were expected to behave in the same way as the LI values used by Ludwig, J. and G. N. Bastin *et al.* (2007) with respect to leakiness. A small difference is that the average cover values come from adjoining sub-catchments, not from the same catchment as they did in the Carroll and Waters *et al.* (2012) data.

The overall experimental catchment was considered homogeneous based on the small variation in average cover values for each sub-catchment (Table 4-7, Table 4-12 and Table 4-17). The range of cover values in the sub-catchments was less than the range of cover in the Carroll and Waters *et al.* (2012)(range 1% - 100%).

Comparison of the relationship between leakiness (AAL) and average cover (%) at each resolution on a whole-of-catchment basis and on an aggregate-of-sub-catchments basis (Figure 4.43) was made as a check on the consistency of the calculations. The significant feature to compare between these two figures is the CoD values of the trend lines for each resolution (not the position of the trend lines). The CoD values are similar for each resolution.

The correlation between leakiness (AAL) and average cover for each resolution is summarised in Table 4-22. PDrg and PDrn yield the most consistent leakiness values at all three resolutions. Their correlations are negative which is in the expected direction.

The results at the sub-catchment level confirm the earlier findings that PDrg cover yields the most consistent estimate of leakiness across all resolutions followed by PDrn. These findings are specific for the savannah type of cover in the experimental catchment.

4.5. Conclusion

Image based measurement of the environmental condition of savannah catchments can be a useful way to measure sustainable grazing productivity, biodiversity and catchment management condition. The CSIRO Leakiness Calculator is a tool that can be used to make these measurements to guide catchment management programs and to evaluate rangeland policy settings. To do these things it is necessary to compare catchments of different sizes and configurations using imagery collected by satellites with different sensor specifications, different resolutions and at different times.

This Chapter evaluated leakiness calculated from 8 different vegetation cover indices derived from satellite images with 3 different image resolutions and from sensors with similar but slightly different spectral windows. The results show that it is possible to make valid comparisons of catchment condition between different sized catchments using different resolution imagery provided adequate care is taken. This includes using the Adjusted Average Leakiness metric and the same vegetation cover analysis index. Changing the resolution affects the leakiness values, so the direction and quantum of the change should be determined ahead of making the comparisons. Finer resolution imagery appears to give more stable results than coarser resolution imagery.

The significance of these findings is that considerable care must be taken when using the Leakiness Calculator to assess the condition of different catchments from satellite imagery. This includes ensuring that the date of collection of imagery is comparable, the appropriate leakiness units are used to compare imagery of different resolutions and the type of coverage analysis is relevant to the type of soil and vegetation in the catchments and is the same for all comparative analyses. For assessments from imagery of the same native resolution, a number of vegetation indices were found to produce consistent results. However, the PDrg index was found to produce the most consistent estimates of leakiness from imagery of different native resolutions.

These findings have provided an overview of the range of leakiness responses from different types of cover measurements. This was necessary to select representative types of cover for analysing the effect of upscaling on leakiness and in preparing leakiness scalograms in the following Chapter.

CHAPTER 5

DEVELOPMENT OF LEAKINESS SCALING FUNCTIONS

5.1. Introduction

Increased use of higher spatial resolution air photos and satellite imagery raises the issue of how to compare the results from this imagery with the results from previously captured medium resolution imagery (e.g. Landsat MSS, TM and +ETM imagery) for which there is an established record. One option is to upscale the higher resolution imagery to the lower resolution historical imagery. While there are different ways of upscaling imagery, each of them has different effects on the structure of the image and thus the interpretations made from it. This section addresses the interaction between scale and identification of landscape patterns and ecological processes from imagery of different scales.

Environmental monitoring requires analysis of natural resource processes at multiple spatial and temporal scales (Bradshaw and Fortin 2000). Frequently analyses are done with imagery selected because of its cost and/or availability with scant regard for the impact of the scale of the image (resolution) on the natural resource signal and the ecological processes being analysed. The careful attention given to analytic procedures so as to extract maximum information can be lost if the scale of the ground truth data and the resolution of the imagery are not carefully considered relative to the pattern and process to be studied. However, identification of the scales of ecological patterns and processes is also a vexed issue making the selection of existing imagery of a suitable resolution challenging. Changing the scale of an image is one potential way to overcome this problem.

The theoretical aspects of the effect of changing scale on feature recognition through change to image structure were addressed in Chapter 2.

5.2. Scaling and Leakiness

Calculating leakiness from catchments at different resolutions incorporates the interactions of the Ecological Scale with the spatial heterogeneity of the cover image as seen through the Observation Scale window. Leakiness scaling functions (an example of a Response Scalogram) can therefore provide a combined result from multiple different scaling functions. Examples of ecological scaling functions were provided in Chapter 2. This section provides examples of pixel level scaling.

Ludwig, J. and G. Bastin *et al.* (2007) citing the work of Carroll and Tucker and of Loch, showed that soil loss from pixel sized plots occurred non-linearly with increasing vegetation cover as shown in Figure 5.1**.** Soil loss is defined by the loss function $L_{soil} = e^{-b}$ where b = - 0.065 (or other site specific value) is the exponential decay function for soil loss versus cover. This is a basic scaling function used in the leakiness calculation algorithm.

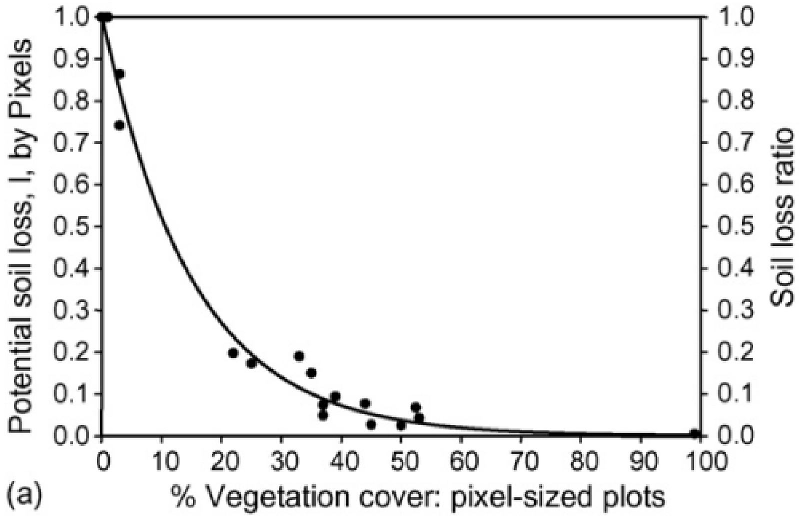

Figure 5.1. Soil loss as a function of average vegetation cover. (Ludwig, J. and G. N. Bastin *et al.* 2007, p. 445)

Only one field test of leakiness calculated at different scales has been reported. (Abbott and Corfield undated); Bastin and Abbott *et al.* (2008) compared the leakiness of different paddocks on Virginia Park Station (Charters Towers, Queensland) from 2.4m Quickbird imagery (captured December 2003) resampled to 5m and from Landsat imagery resampled from 30m to 25m. The Quickbird imagery was analysed as a PD_{54} coverage (Pickup and Chewings *et al.* 1993) while the Landsat imagery was analysed as the GCI coverage (Scarth and Byrne *et al.* 2006). Litter cover and total ground cover field data were collected from $4m^2$ quadrats using the BOTANAL technique (Tothill and Hargreaves *et al.* 1992) for both the Quickbird and Landsat image areas. While each image was of a different paddock at Virginia Park Station, the Leakiness Index values were found to parallel ground cover conditions at each resolution as shown in Figure 5.2 and Figure 5.3.

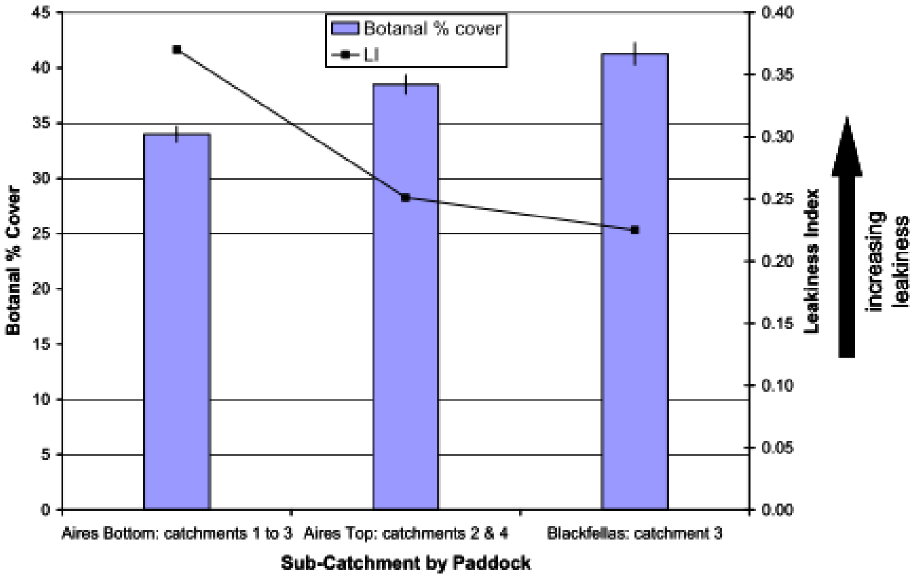

Figure 5.2 Mean levels of ground cover (Botanal %) and catchment leakiness (LI) calculated from PD_{54} coverage of 5m resampled Quickbird imagery.
(Bastin and Abbott *et al.* 2008, pp. 22, Figure 10,)

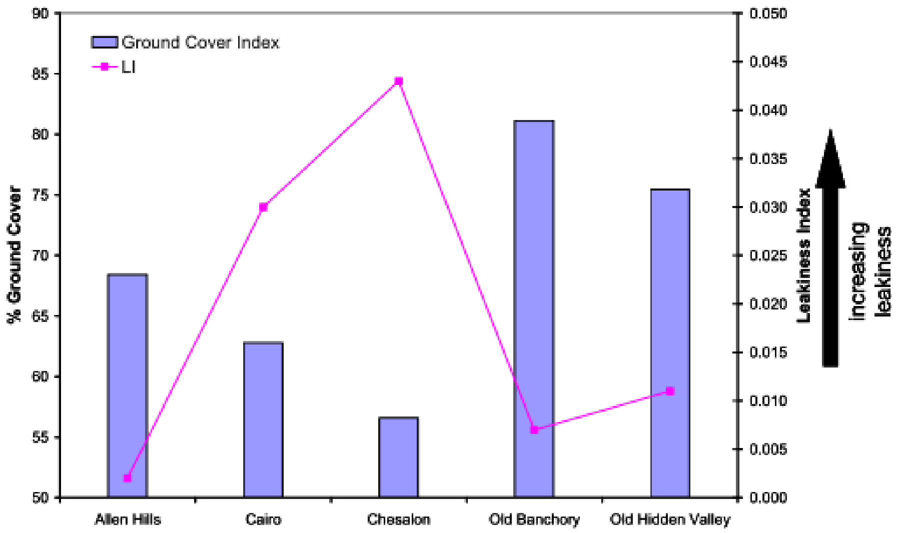

Figure 5.3 Mean levels of ground cover (Botanal %) and catchment leakiness (LI) calculated from the GCI coverage of 25m resampled Landsat imagery

The negative correlation between calculated LI values and cover in these figures is evidence that the LI is reflecting the effect of cover on leakiness. The data did not lend themselves to a scaling response calculation because they covered different geographical areas and were based on different indices of cover.

The next section describes the methods used to prepare leakiness scalograms at resolutions between 10m and 250m.

5.3. Research Methods

The following section describes the procedures used to upscale the SPOT image of the experimental catchment to coarser resolutions, to track the changes in each type of cover and in the respective leakiness values of the catchment and to develop scalograms for leakiness as a function of resolution and variance.

5.3.1. Overview

The 10m (SPOT) image of the catchment as described in Section 3 was used as the foundation image for upscaling. Upscaled images were analysed for SAVI, STVI and PDrg cover indices as described in Section 4.2.1.3. The 10m DEM (from Section 4.2.1.1) and Analysis Mask (from Section 4.2.1.2) were also upscaled at the same resolutions as the coverages for use in the LC. Leakiness was calculated using the LC in the same manner as described earlier in Section 4.2.2.

The subsequent procedures used in this section consisted of three major steps through which each leakiness calculation was processed to develop the respective Scalograms (Figure 5.4).

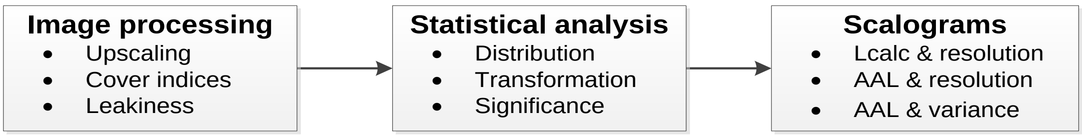

Figure 5.4 Process Overview

These three steps are explained in more detail in the following sections.

5.3.2. Image and leakiness processing procedures

The steps involved in processing the data files required by the LC (coverage, DEM and analysis mask) and calculating upscaled leakiness, both as Lcalc and as AAL, are shown in Figure 5.5 and described in more detail below.

The 10m SPOT image was adjusted to each coarser resolution in ArcGIS using the Cubic Convolution Resample geoprocessing tool. This method was selected over other methods because it is suitable for continuous data and the value of the new (resampled) cell is based on the 16 nearest input cell values producing a less distorted image than other conventional procedures (ERDAS 2010; ESRI 2014). The SAVI, STVI and PDrg indices were calculated from the upscaled images as described in Section 4.2.1.3. Before the thematic cover layers can be processed by the LC they have to be rescaled to 0-100%, converted to .FLT format and the llx and lly coordinates of each raster adjusted to precisely the same values as the DEM and the Analysis Mask. This was done as described by Liedloff (2007). Care was taken in the process of rescaling to maintain the full dynamic range inherent in the index calculation process. The Lcalc values from the LC *.OUT files were converted to AAL values using Equation 4-10.

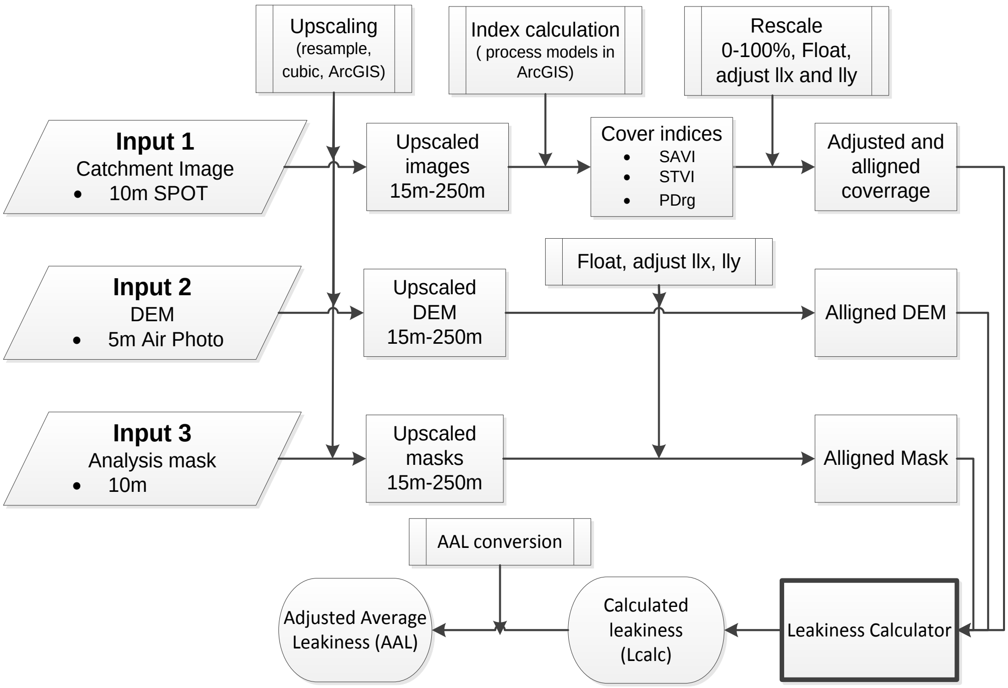

Figure 5.5 Procedure used to upscale files and calculate leakiness

5.3.3. Statistical procedures

Developing the scaling equations from the leakiness results often required various statistical tests. These were done with SPSS software, ver. 19 (IBM 2010). The general procedure that each leakiness analysis was subjected to and the type of test used is shown in Figure 5.6.

Each set of leakiness results were first inspected for normal distribution by graphing them. If there was any question as to their distribution normality, they were tested by the Kolmogorov-Smirnov test and the Shapiro-Wik test in SPSS. If these tests confirmed their lack of normality, transformations were developed, applied to the data and again tested by the above tests. This was repeated until a normal distribution was obtained. Either the raw leakiness data (if it was normally distributed) or the normalised leakiness data was graphically analysed in MS Excel to obtain the best fitting equation.

Where it was necessary to test for significant difference, as in the difference between experimental and projected data, the data was first tested for skewness. If it was not skewed, significance was tested using the 2 tailed “t” test and if it was skewed, it was tested for significance using either the nonparametric Wilcoxon Signed Rank test, or the Kruskal-Wallis test. Which of these 2 tests was used depended on whether the data sets were dependent or independent. As a general rule, a 2 σ significance level was applied.

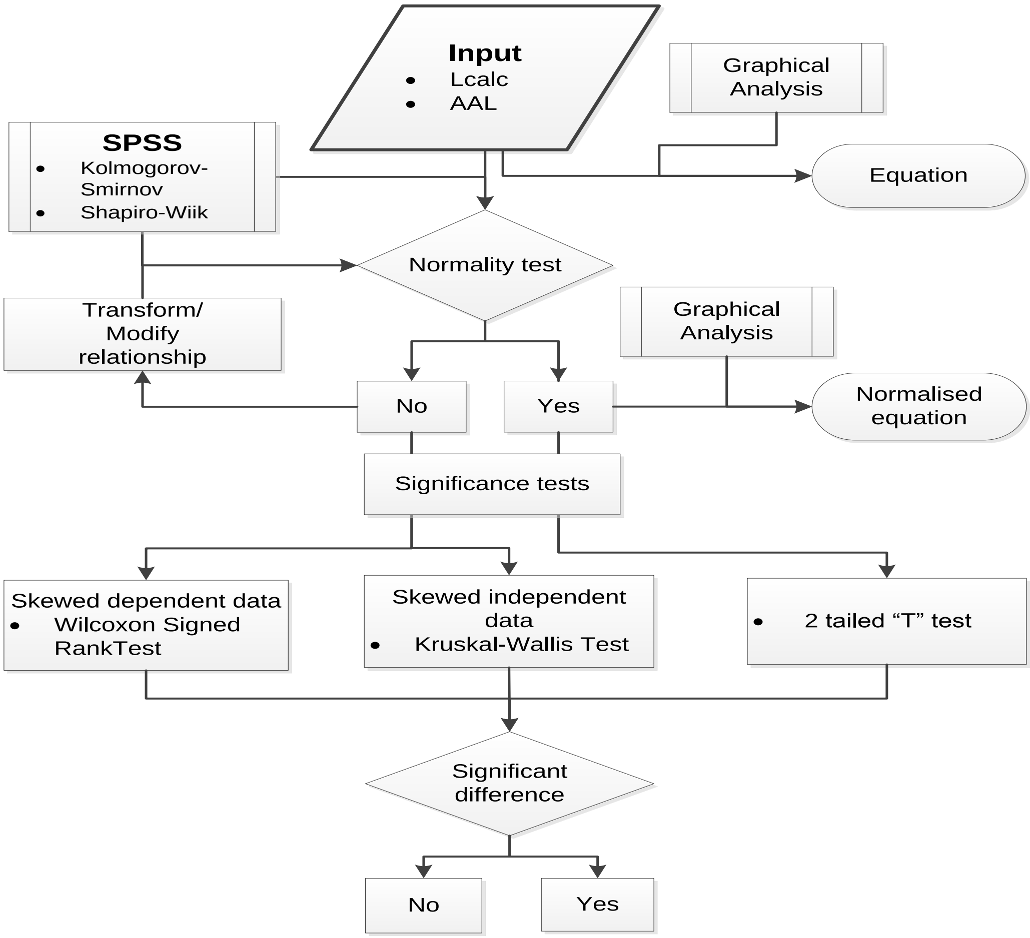

Figure 5.6 Statistical analysis test procedures used in development of scaling equations

5.3.4. Scalogram derivation

A standardised procedure for developing leakiness scalograms (scaling equations) was conceived as shown in Figure 5.7. Three types of scalograms were developed for each type of cover, SAVI, STVI and PDrg. Each type of scalogram required a slightly different procedure.

The Lcalc scalogram (Lcalc as a function of resolution, left hand column below) required normalisation of the leakiness before extracting the relationship. The normalised Lcalc function was then solved using the cell count and resolution function equations to yield the final scalogram. The AAL and resolution scalogram (middle column below) did not require normalisation and the scaling relationship could be extracted directly from the raw AAL data. AAL and variance scalogram (right hand column below) required substitution of the semivariance relationship with resolution, as derived in Chapter 6, to obtain leakiness as a function of variance. Each scalogram was tested for accuracy of prediction of leakiness and the results were statistically analysed for significant difference as outlined in Section 5.3.3.

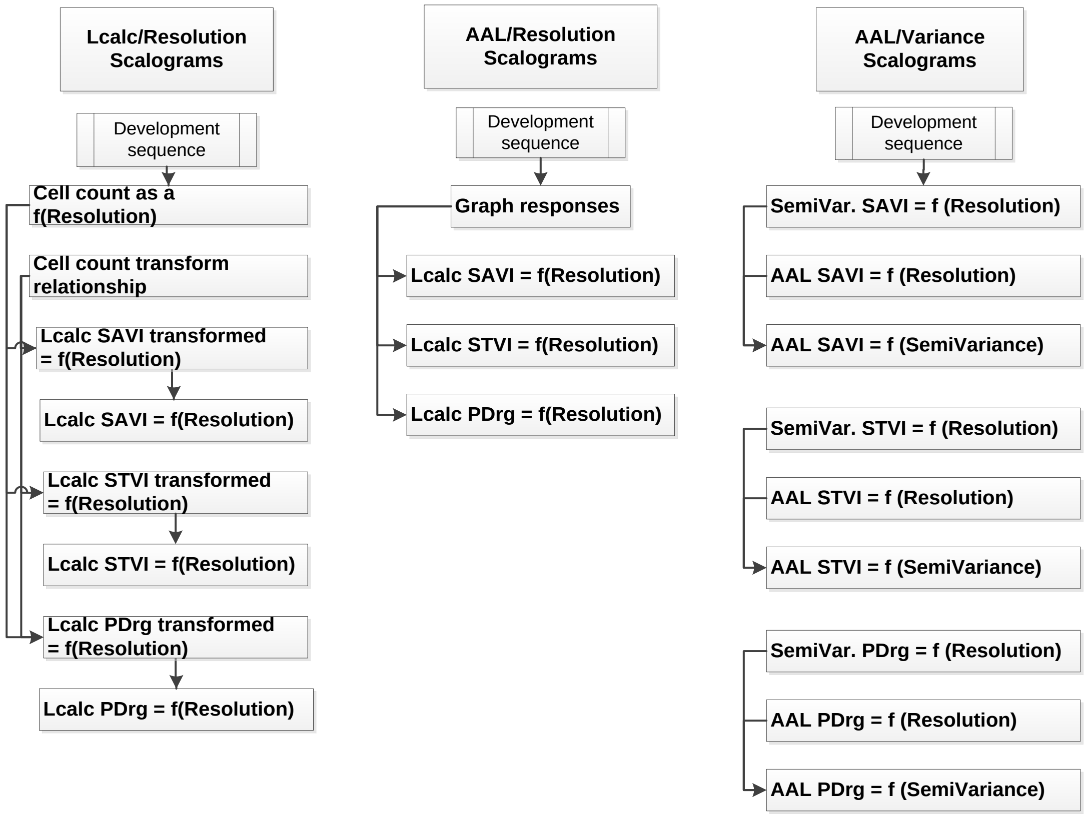

Figure 5.7 Scalogram development procedure.

5.4. Results

This section presents the results of the upscaling analysis for Leakiness of SAVI, STVI and PDrg vegetation covers of the experimental catchment. First, the experimental data are presented followed by the derivations of leakiness scalograms and finally an analysis of the goodness of fit between the experimental data and the values projected from the scalograms is presented.

5.4.1. Stage of Upscaling

Upscaling can occur before or after a thematic cover layer is generated. If it is done before the thematic cover layer is generated, the image is upscaled (all bands) and the subsequent steps as outlined in the Section 5.3.2 use the upscaled image to generate the leakiness. If it is done after the thematic cover layer is generated, the thematic cover layer at the same resolution as the source image is used as the foundation raster for upscaling. The stage at which the upscaling is done may affect the results as shown in the following subsections.

5.4.1.1. SAVI

A comparison of cover and leakiness results for SAVI cover upscaled before and after thematic cover raster generation is shown in Figure 5.8 .This shows the difference in distribution of Average Cover (a) and the Calculated Leakiness (Lcalc) (b) with resolution, depending on the stage at which upscaling is performed. The different averages and standard deviations are shown in the last two rows of.Appendix 8.

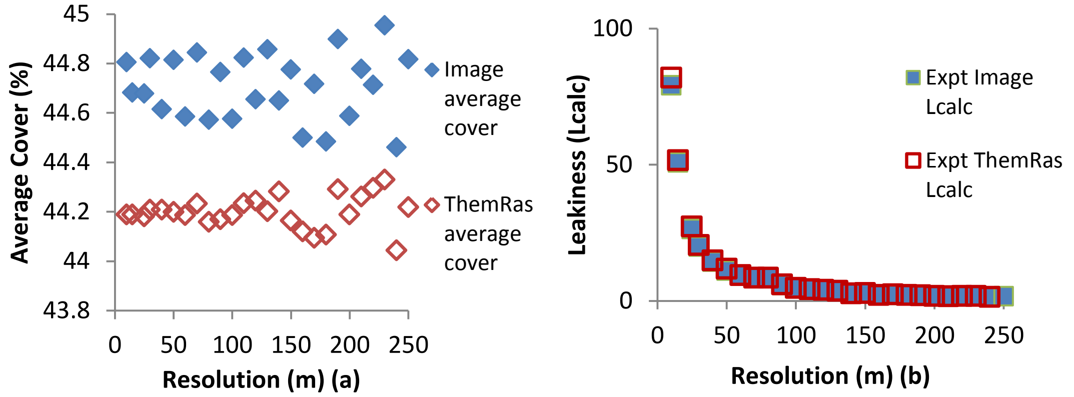

Figure 5.8 Difference in Average Cover and Calculated Leakiness from upscaling the image versus upscaling the cover layer.

These values were tested for significant difference. Both cover values were close to normal in distribution and a two tailed t test indicated the two cover samples were significantly different ($p < 0.05$) (Table 5-1).

Table 5-1 Paired samples test for SAVI cover from upscaling image versus cover layer

		Paired Differences					t	df	Sig. (2-tailed)
		Mean	Std. Deviation	Std. Error Mean	95% Confidence Interval of the Difference				
					Lower	Upper			
Pair 1	Cvr. Them resamp - Cvr. Image resamp	.509	.102	.020	-.550	-.469	25.831	26	.000

The Leakiness calculated from both scenarios was also tested for significant difference. These values were positively skewed and the non-parametric Wilcoxon Signed Rank Test was used. It showed that, despite their apparent closeness in value (Figure 5.8, b.) they were significantly different (Table 5-2).

Table 5-2 Wilcoxon Signed Rank test results for SAVI coverage leakiness

	Null Hypothesis	Test	Significance Level	Decision
1	The median of differences between Lcalc Thematic Resample and Lcalc Image Resample equals 0	Related Samples Wilcoxon Signed Rank Test	0.000	Reject the null hypothesis
Asymptotic significances are displayed		The significance level is 0.05		

5.4.1.2. STVI

In a manner similar to that presented in the previous sub-section, the effect of upscaling the image versus the thematic cover raster on Average Cover and Leakiness were analysed for STVI coverage. The results are shown in Figure 5.9 (data Appendix 9).

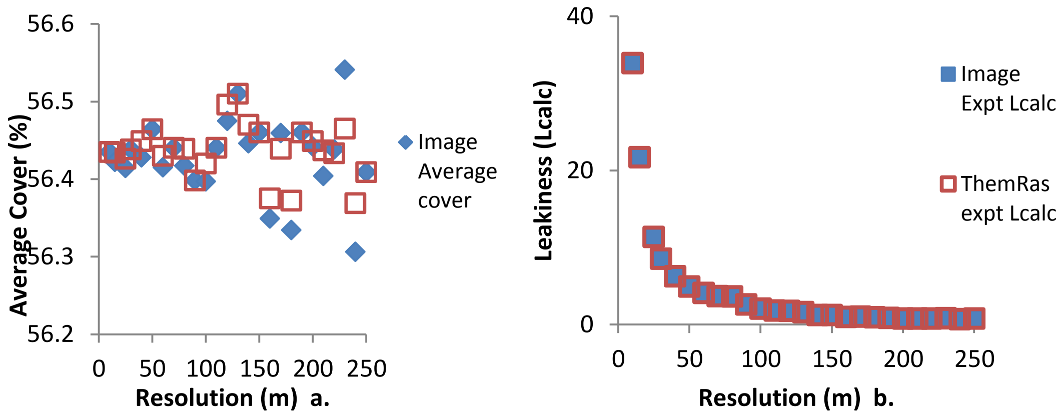

Figure 5.9 Comparison of Cover and Leakiness from upscaling the image versus upscaling the thematic cover layer

Inspection of the Averages and Standard Deviations for this data (Appendix 9) shows that the values are very close to each other. This is different from SAVI. Similar tests for significant difference were applied. A p-value of 0.058 indicated the samples were not significantly different; however, this p-value does not indicate strong similarity between the samples. The STVI Leakiness was tested for significant difference in the same manner as before. A p-value of 0.586 indicates that the samples are similar at the 95% probability level.

5.4.1.3. PDrg

PDrg upscaling was not done for the thematic PDrg raster because it was considered that the results from SAVI and STVI cover layers indicated that the upscaling should be done based on the image and not the thematic cover layers.

5.4.2. Resolution Scalograms for Calculated Leakiness

The previous Section showed that upscaling the image versus upscaling the cover layer led to different Cover and Leakiness values for SAVI coverage but similar values for STVI coverage. The results in the following sections are based on Leakiness calculated from upscaling the images before the cover layers were generated. This was done because i) this is the most likely situation in which the results of this research would find application, and ii) the finding of differences in leakiness results for SAVI between image upscaling and thematic raster upscaling suggests using the conservative approach of image upscaling.

However, this creates a related problem; that of rescaling the dynamic range of the layers to fall between 0 - 100 (required by the LC) without distorting the true range of values resulting from upscaling. This was overcome by using the theoretical limits of the cover values (e.g. SAVI = -1.497 to +1.497, STVI = -255 to +255) to set the rescaling limits rather than using the limiting values in individual resampled layers. Using individual sample limiting values (high and low) would distort the true range of the values as well as their relative position in the scale of from 0 to 100. The following sub-sections detail the development of the scalograms.

5.4.2.1. SAVI Cover

The upscaling results for calculated Leakiness based on SAVI cover (Figure 5.10) (Appendix 8) show that SAVI cover remains effectively constant with change in resolution while cell count and leakiness decline in a negative power relationship with change in resolution.

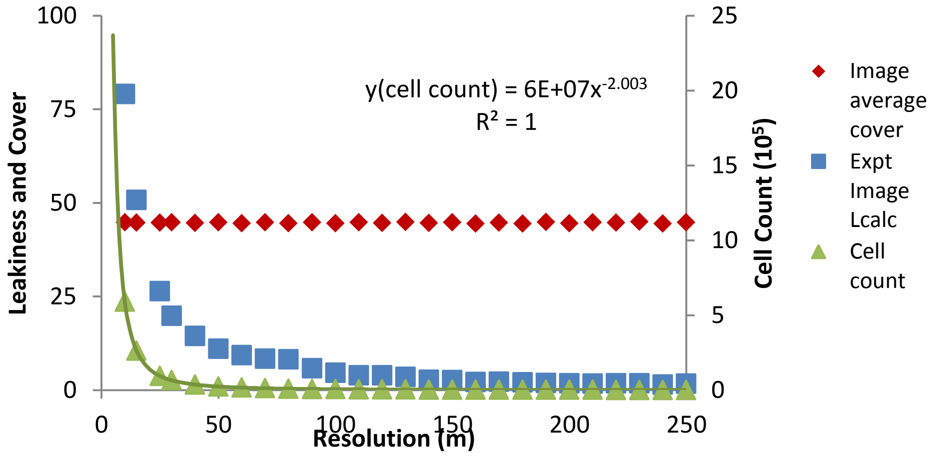

Figure 5.10 Relationship of Lcalc, Cover (SAVI) and Cell Count with Resolution

The relationship between Cell Count and Resolution, from Figure 5.10 is:

$$C = 6E + 07 \times R^{-2.003} \qquad (5\text{-}1)$$

where C = Number of pixels in image (column # x row #)
and R = Resolution in meters

Because the distribution of Lcalc is positively skewed, it is necessary to normalise these values so that an equation that gives equal balance to the full range of values can be developed. The following transformative relationship was developed by trial and error to normalise the Lcalc Leakiness results.

$$L_{c,t} = Lc \times \frac{Cmx/_{Cmn}}{C} \qquad (5\text{-}2)$$

where L = Leakiness, c = calculated, t = transformed
Cmx = maximum number of pixels (minimum resolution),
Cmn = minimum number of pixels (maximum resolution), and
C = as per Equation 5-1.

The transform values and the predicted Leakiness are shown in Figure 5.11 (Appendix 10). Statistical testing showed the transformed values had a distribution that was close to normal.

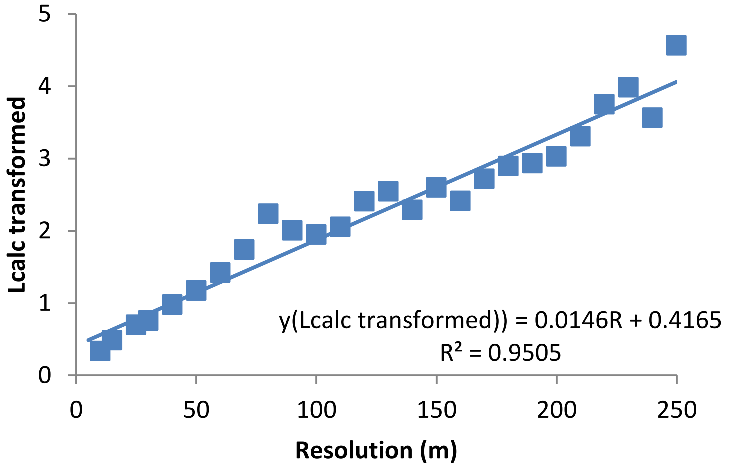

Figure 5.11 Distribution of Lcalc transformed (SAVI) against resolution

The relationship between the transformed Leakiness values and Resolution from Figure 5.11 is:

$$L_{ct,savi} = 0.0146R + 0.4165 \qquad (5\text{-}3)$$

Substituting Equations 5-1 and 5-2 in 5-3 and simplifying gives a predictive solution (scalogram) for Leakiness from SAVI coverage (Lc_{savi}) in terms of resolution.

$$Lc_{savi} = \frac{350.088R \quad +9987.09}{R^{2.003}} \qquad (5\text{-}4)$$

This scalogram can be used to predict the calculated Leakiness of the catchment (for SAVI cover) at any resolution within the calibration range once the slope and intercept of the normalised leakiness equation are known. Results from the scalogram (field 3 in Appendix 10) were tested for goodness of fit against the experimental Lcalc values as shown in Figure 5.12.

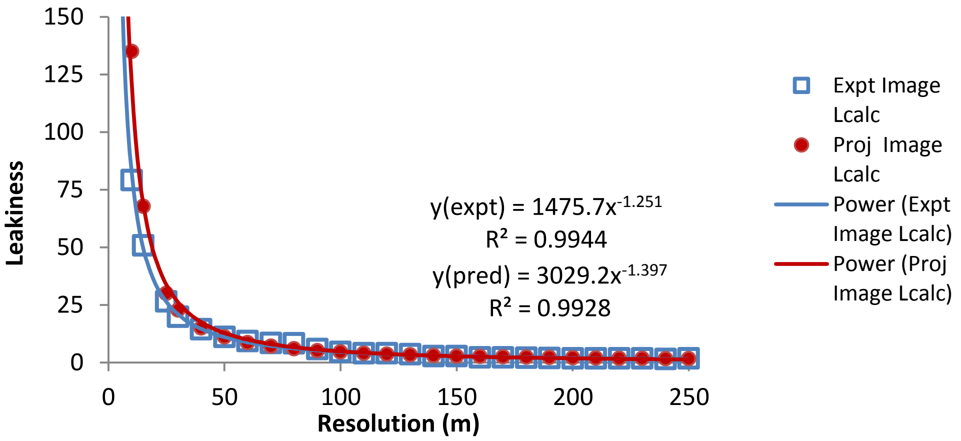

Figure 5.12 Comparison of Lcalc expt. against Lcalc pred.

The closeness of the results is apparent over most of the resolution range; however, there is increased discrepancy between the experimental and predicted values with increase in resolution (Figure 5.12). Statistical testing showed that both the results and their differences were not normally distributed. Accordingly, the goodness of fit between the scalogram values and the experimental leakiness values was tested and the results showed there was no significant difference between the samples (p = 0.186 > 0.05).

5.4.2.2. STVI Cover

The upscaling results for Leakiness based on STVI coverage are shown in Figure 5.13 (Appendix 9). They show a similar pattern of relationship between Cell Count, Cover and Leakiness with Resolution to that for SAVI cover (Figure 5.10).

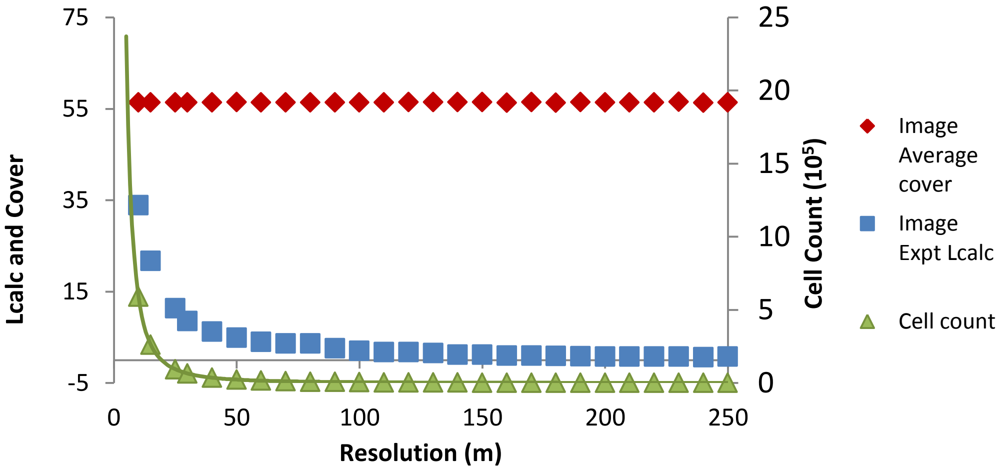

Figure 5.13 Relationship of Leakiness, Cover (STVI) and cell count with Resolution

The relationship between cell count and resolution are the same as derived previously (Equation 5-1).The distribution of Lcalc is again positively skewed. The same transformative relationship used with SAVI Lcalc (Equation 5-2) was used to transform the STVI Lcalc values into a 'normal' distribution as shown in Figure 5.14 (Appendix 10).

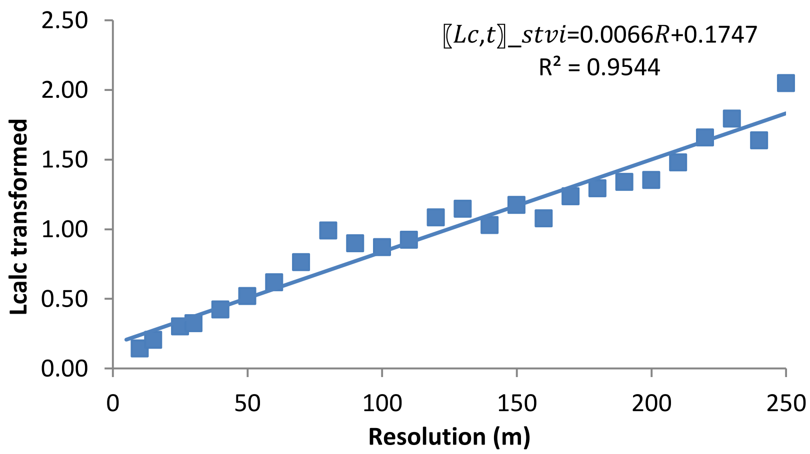

Figure 5.14 Distribution of transformed Leakiness (STVI) against resolution

The relationship between the transformed Leakiness values for STVI and resolution from Figure 5.14 is:

$$L_{ct.stvi} = 0.0066R + 0.1747 \qquad (5\text{-}5)$$

Simplifying as before results in a scalogram for STVI Leakiness (Lcalc,stvi) in terms of resolution (Equation 5-6).

$$Lc_{stvi} = \frac{158.259R \quad +4189.06}{R^{2.003}} \qquad (5\text{-}6)$$

The scalogram can be used to predict the Leakiness of a catchment (using STVI) at any new resolution, within the range for which it was calibrated, once the intercept and slope of the normalised leakiness equation are known. Results from the scalogram (Lcalc pred. field in) were tested for goodness of fit against the experimental Leakiness values as shown in Figure 5.15.

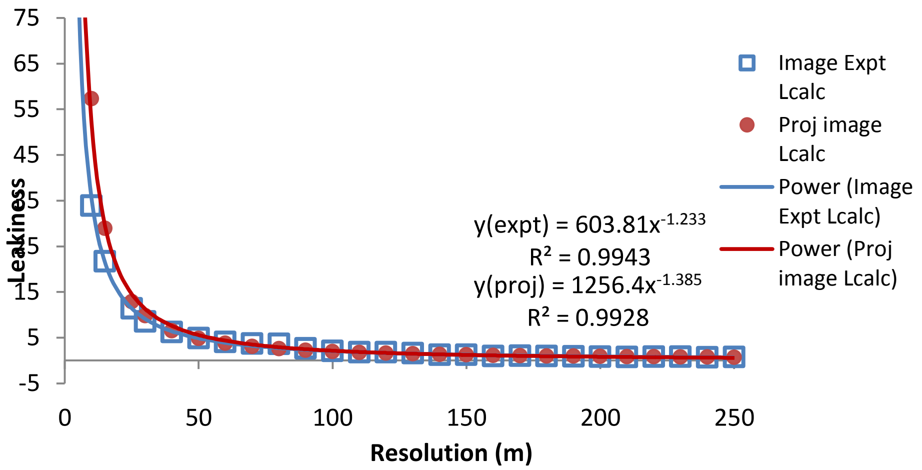

Figure 5.15 Comparison of experimental Leakiness against predicted Leakiness (STVI).

STVI comparative results have a similar pattern to the SAVI comparative results in that the predicted results are close to the experimental results over most of the range but diverge at high resolutions (low pixel dimensions). Statistical testing as before showed there was no significant difference between experimental and predicted STVI Leakiness values ($p = 0.461$ which is > 0.05) over the experimental range.

5.4.2.3. PDrg Cover

The upscaling results for Leakiness based on PDrg coverage shown in Figure 5.16 (data inAppendix 12) show that the relationship between Cell Count, Cover and Leakiness with resolution for PDrg is similar to the relationships for SAVI and STVI.

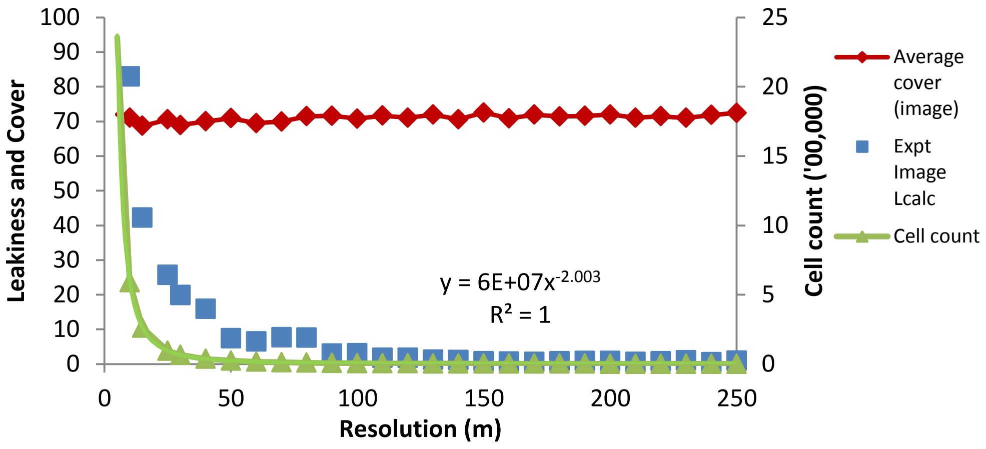

Figure 5.16 Relationship of Leakiness, Cover (PDrg) and Cell Count with Resolution

The Leakiness is skewed positively and was normalised as before. Cubic and linear relationships between the PDrg Lcalc transformed values and Resolution are shown in Figure 5.17 with the residuals shown in Figure 5.18. The cubic relationship provided the best fit with the experimental data for which a rational explanation could be developed. This is shown by the goodness of fit values for both relationships in Table 5-3.

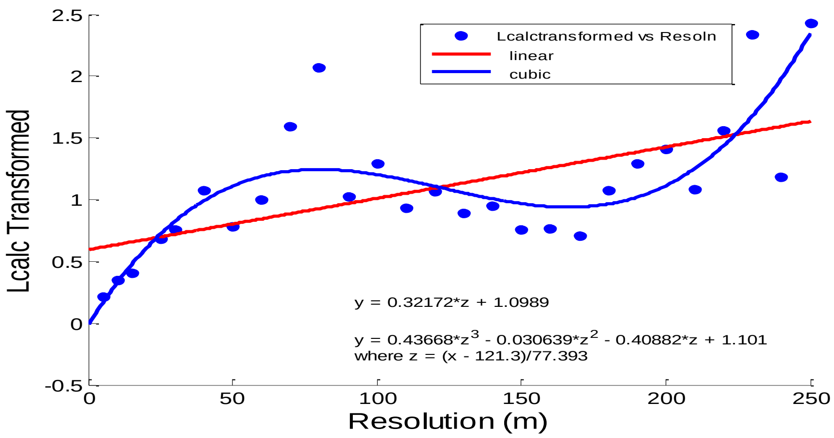

Figure 5.17 Distribution of transformed Lcalc (PDrg) against resolution

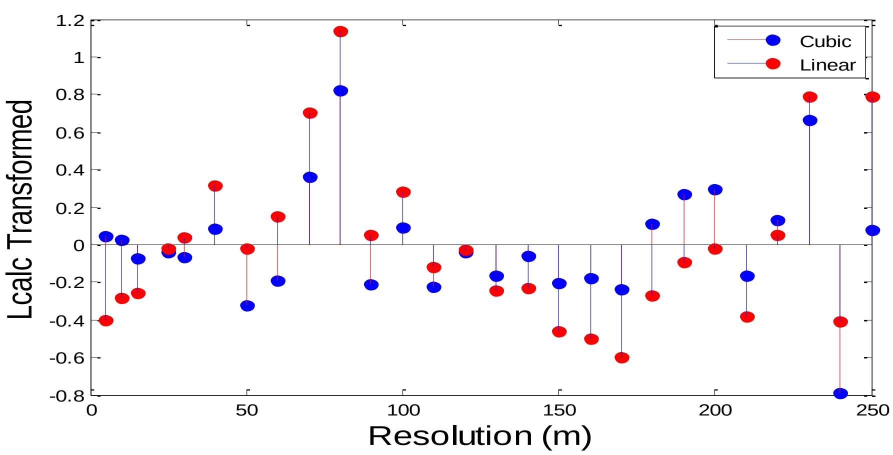

Figure 5.18 Residuals for linear and cubic fits

Table 5-3 Goodness of fit for PDrg Leakiness transformed

Parameter	Linear Fit	Cubic Fit
SSSE	4.898	2.523
R^2	0.355	0.668
Adjusted R^2	0.329	0.624
RMSE	0.443	0.331

The cubic relationship between PDrg normalised transformed Leakiness values and resolution from Figure 5.17 is:

$$Lc, t_{PDrg} = 9.420E - 7 \times X^3 - 3.479E - 4 \times X^2 + 3.754E - 2 \times X \quad - 1.466E - 2 \tag{5-7}$$

where $X = (\mathrm{R}^*\overline{R})/R_{SD}$ for which the values in this particular case were $\bar{R}$ = 121.3 and R_{SD} = 77.3

In this equation, Leakiness (Lc, t_{PDrg}) increases firstly as a linear function of resolution over which is imposed a response to the third power of the resolution. This is interpreted as firstly reflecting greater loss of resources between pixels of larger area being moderated by the reduced loss of resources within larger pixels of high coverage. The change in pixel size and value is the result of selected method of upscaling.

Higher order relationships with resolution gave higher degrees of fit to the experimental data but no rational explanation for such fit could be discerned.

Equation 5- 7 was solved for resolution as before resulting in the cubic solution scalogram:

$$Lc_{PDrg} = \frac{0.43668 \times X^3 - 3.0639E - 2 \times X^2 - 0.40882 \times X + 1.101}{4.17383E - 5 \times R^2} \tag{5-8}$$

The linear relationship between PDrg normalised transformed Leakiness values and resolution from Figure 5.17 is:

$$Lc, t_{PDrg} = 0.32172\,\mathrm{Z} + 1.0989 \tag{5-9}$$

where $Z = (R\text{-}121.3)/77.393$

Solving this produced the linear solution scalogram for calculating PDrg leakiness in terms of resolution (Equation 5-10):

$$Lc_{PDrg} = \frac{100.71R \quad +14255.28}{R^2} \tag{5-10}$$

Equation 5-8 was used to predict the cubic solution leakiness values and Equation 5-10 was used to predict the linear solution leakiness values (Appendix 12,fields 7 and 6 respectively). Figure 5.19 shows the difference between the predicted and experimental values. The cubic scalogram has the lowest error Standard Deviation as expected from the Goodness of Fit values. In a pattern that is similar to the SAVI and STVI leakiness predictions, the largest variance between the projected and experimental results occurs at the highest resolutions (Figure 5.19) (Appendix 12).

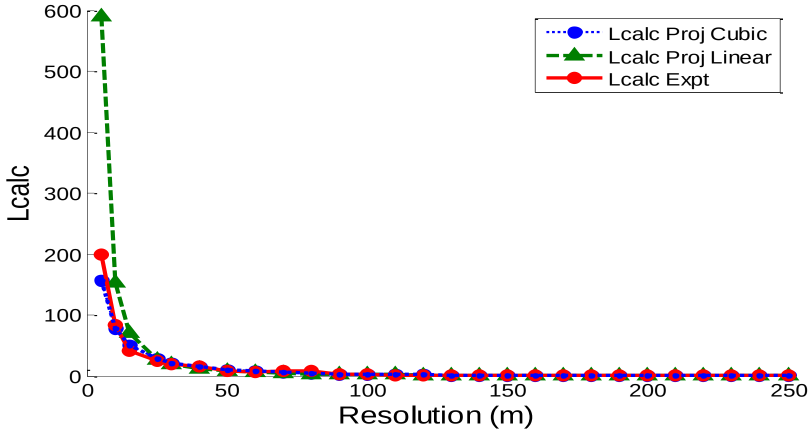

Figure 5.19 Comparison of Cubic and Linear solutions to PDrg Lcalc predictive equations.

5.4.3. Resolution Scalograms for Average Adjusted Leakiness

This section presents the development of scalograms for Average Adjusted Leakiness.

5.4.3.1. SAVI Cover

The upscaling results for AAL based on SAVI cover are shown in Figure 5.20 (data inAppendix 13). This shows that AAL values for SAVI cover are normally distributed and their relationship with resolution is linear ($R^2 = 0.95$).

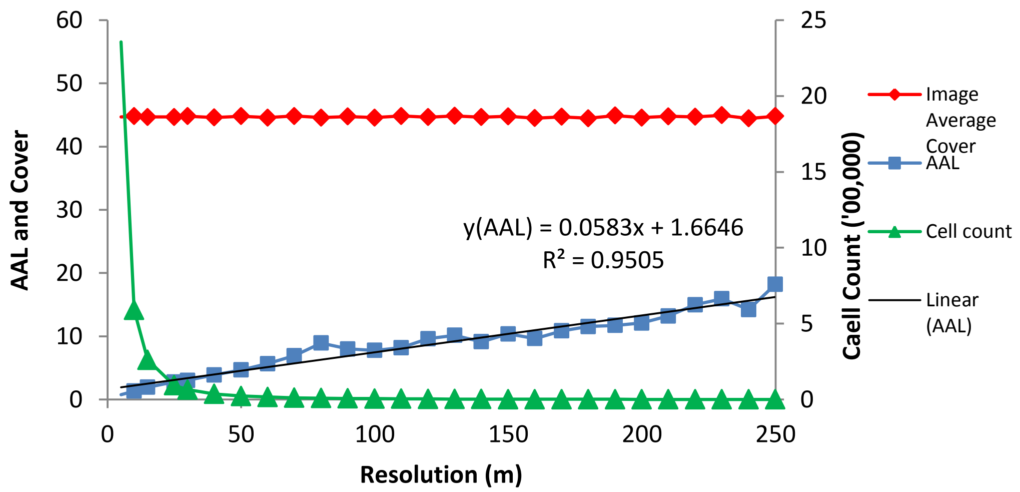

Figure 5.20 Relationship of AAL, Cover (SAVI) and Cell Count with Resolution

Cover and Cell count have the same relationships with resolution as given previously (Section 5.4.2.1). The normal distribution of AAL with resolution means that the trend line relationship can be used directly (without transformation) as the scalogram to predict the AAL of a catchment for imagery at any resolution within the range of analysis once the slope and intercept are known.

$$\mathrm{AAL_{SAVI}} = 0.0583\mathrm{R} + 1.6646 \quad (5\text{-}11)$$

This was tested and the numerical results are shown in Appendix 13..The validity of Equation 5-11 was confirmed because there was no significant difference between the experimental and predicted AAL values when tested by a Paired Samples t test. (p = 0.990)

5.4.3.2. STVI Cover

The upscaling results for AAL based on STVI cover are shown in Figure 5.21 (data inAppendix 14). This shows that AAL for STVI cover is normally distributed and its relationship with resolution is linear ($R^2 = 0.95$).

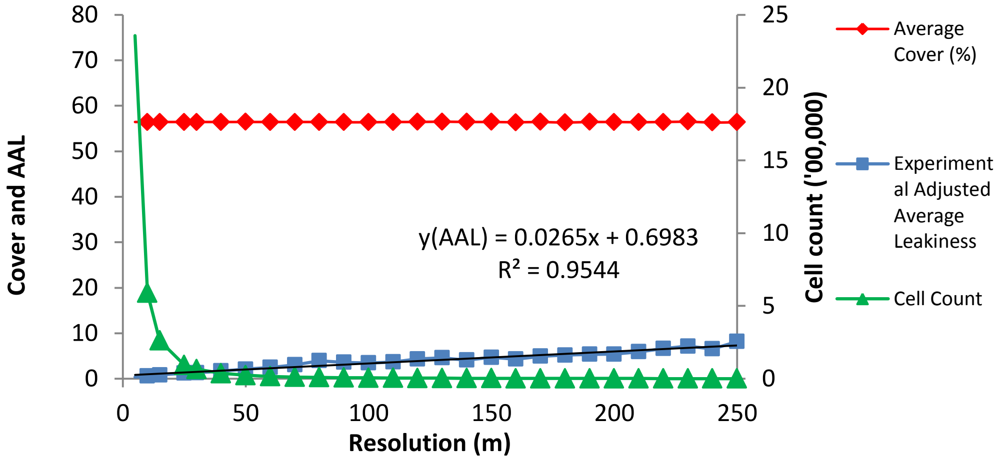

Figure 5.21 Relationship of AAL, Cover (STVI) and Cell Count with Resolution

The scalogram for AAL from STVI cover is

$$\mathrm{AAL_{STVI}} = 0.0265\mathrm{R} + 0.6983 \quad (5\text{-}12)$$

This was tested and the results are shown in Appendix 14.The validity of Equation 5-12 was confirmed because there was no significant difference between the experimental and predicted AAL values when tested by a Paired Samples t test, (p = 0.993 which is >0.05).

5.4.3.3. PDrg Cover

The upscaling results for AAL based on PDrg cover are shown in Figure 5.22 (data in Appendix 15). This shows that the AAL from PDrg cover is normally distributed and that there are two possible trend line solutions for the relationship of AAL with PDrg cover, linear (R^2= 0.35) and cubic (R^2= 0.67) are shown.

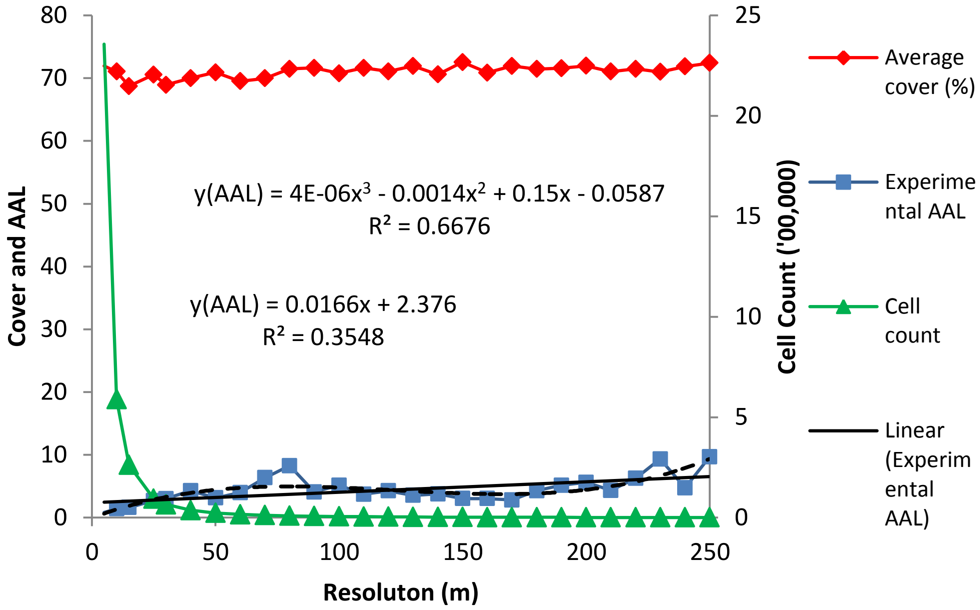

Figure 5.22 Relationship of AAL, Cover (PDrg) and Cell Count with Resolution

This analysis yielded two different scalograms.

$$AAL_{PDrg} = 0.0166R + 2.376 \quad (5\text{-}13)$$

$$AAL_{PDrgc} = 4E\text{-}06R^3 - 0.0014R^2 + 0.15R - 0.0587 \quad (5\text{-}14)$$

Statistical comparison of the linear and cubic scalograms (Equations 5-13 and 5-14), showed that they are significantly different (Table 5-4, Pair 1, $p = 0.028$, < 0.05) and that the cubic formulae produces results closer to the experimental results than the linear formulae (Table 5-4, Pair 2, $p = 0.023$, <0.05 versus Pair 3, $p = 0.995$, >0.05).

Table 5-4 Significance tests for linear and cubic AAL scalograms

Comparisons		Paired Differences					t	df	Sig. (2-tailed)
		Mean	Std. Deviation	Std. Error Mean	95% Confidence Interval of the Difference				
					Lower	Upper			
Pair 1	PredlinAAL - PredcubicAAL	-.724	1.619	.311	-1.364	-.084	-2.325	26	.028
Pair 2	ExptAALPDrg - PredcubicAAL	-.722	1.55	.299	-1.337	-.107	-2.413	26	.023
Pair 3	PredlinAAL - ExptAALPDrg	-.002	1.735	.334	-.689	.684	-.007	26	.995

These results show similarities to the calculated Leakiness scalogram results (Section 5.4.2.3) in which the cubic relationship between leakiness and resolution provided a more accurate estimate of Leakiness than did the linear relationship.

5.4.4. Comparison of Scalograms

This section provides a comparison of the effect of upscaling on cover and on leakiness scalograms for the three different types of coverages.

5.4.4.1. Coverage

Upscaling of the image has almost no effect on SAVI, STVI and PDrg coverage as shown in Figure 5.17 (data in Appendix 16). All Standard Deviations' were less than 1.0.

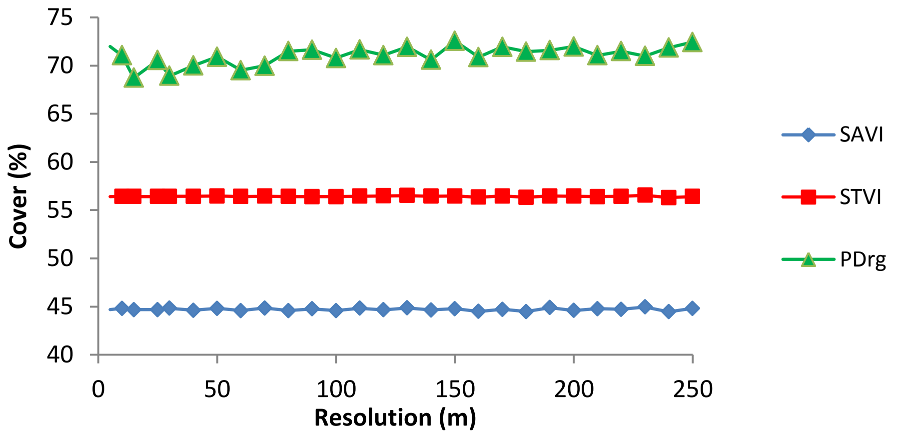

Figure 5.23 Effect of upscaling on Coverage

5.4.4.2. Leakiness

Upscaling had a pronounced effect on the levels of Calculated Leakiness and Adjusted Average Leakiness as shown in Figure 5.24 and Figure 5.25 (Appendix 17). Calculated Leakiness declines as the negative power of the resolution for each type of cover. The response to change in resolution is a similar negative power function for each type of cover with the decay exponents varying from -1.239 to -1.597.

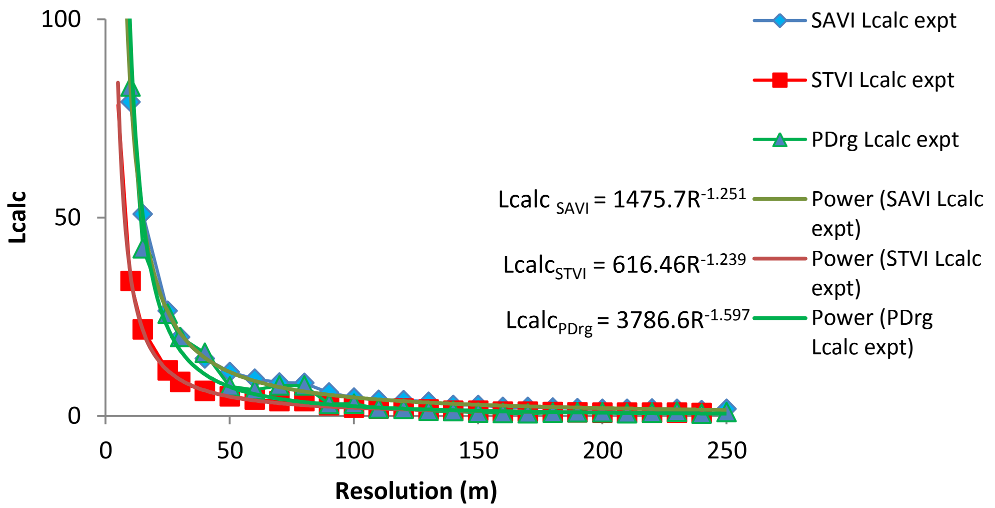

Figure 5.24 Calculated Leakiness response to change in resolution

Adjusted Average Leakiness increased either linearly or in a cubic relationship with decrease in resolution as shown in Figure 5.25 (Appendix 17).

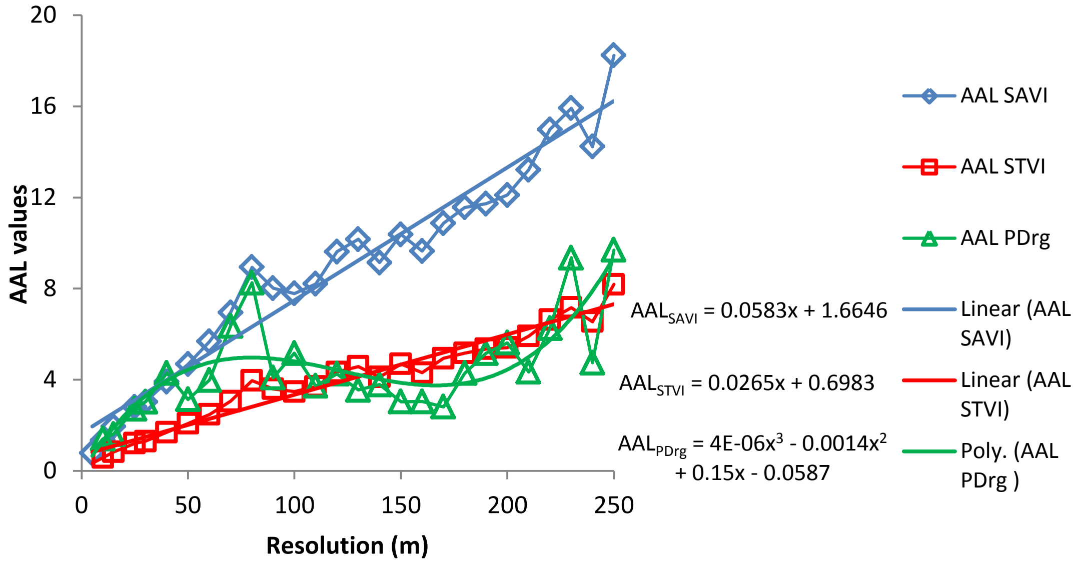

Figure 5.25 Adjusted Average Leakiness (AAL) response to change in resolution

Calculated Leakiness

To develop scalograms that would accurately estimate the response of Calculated Leakiness to change in resolution it was necessary to normalise Calculated Leakiness. This was done by transforming calculated leakiness values so as to have a normal distribution. The response of transformed calculated Leakiness to change in resolution is unique for each type of cover as shown in Figure 5.26 (Appendix 18).

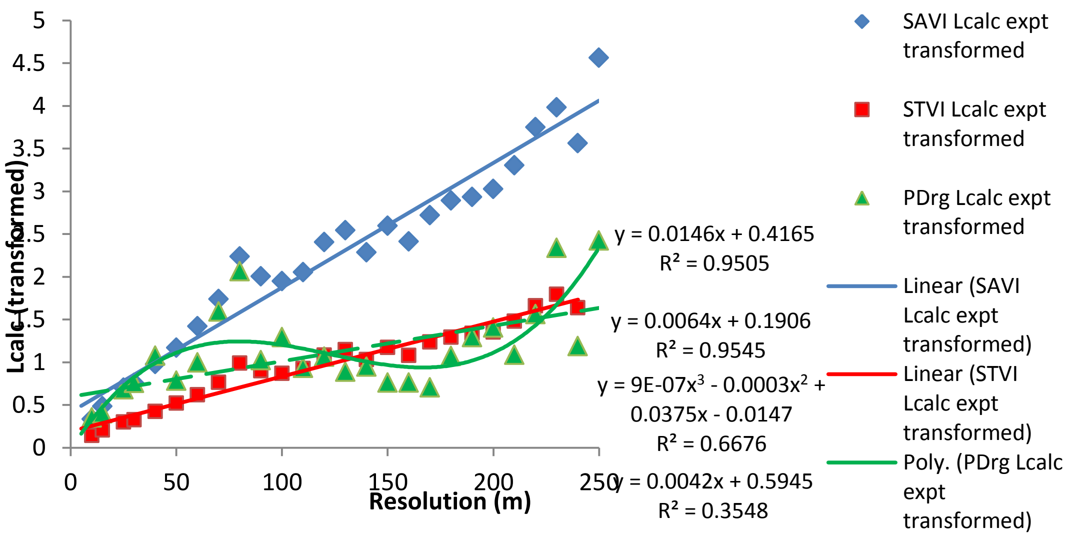

Figure 5.26 Comparison of response of transformed Lcalc with resolution

Transformed Calculated Leakiness responds in a similar manner to Adjusted Average Leakiness to change in resolution as shown by comparing Figure 5.25 and Figure 5.26. Transformed SAVI Leakiness decays more quickly with increase in resolution than transformed STVI leakiness, as indicated by the higher slope for SAVI leakiness than for STVI leakiness (0.0146 vs 0.0064). However, STVI has a higher level of cover in the experimental catchment compared to SAVI and thus has an overall lower base level of leakiness as shown in Figure 5.26. Both have a linear relationship between leakiness and cover.

Transformed PDrg leakiness can be modelled by either a linear (R^2 = 0.3548) or cubic (R^2 = 0.6676) relationship with resolution (Figure 5.26). Both relationships are shown here for comparison purposes but further work focused primarily on the cubic relationship because of its higher CoD (0.66 vs. 0.35). The implication of the cubic relationship is that the leakiness from PDrg varies (does not have a consistent slope) in its response to change in resolution over the range of 10m to 250m pixels.

The transformed response relationships were solved for resolution, to arrive at the scalogram equations given earlier. A comparison between the experimental and projected leakiness results is given in Figure 5.27 (data in Appendix 19).The results show a similar pattern of response to upscaling resolution for each type of cover with decay exponents for predicted leakiness ranging from -1.391 (SAVI) to -1.717 (PDrg (cubic) for AAL (Figure 5.24) versus -1.251 (SAVI) to -1.569 (PDrg (linear) for erimental leakiness (Figure 5.27).

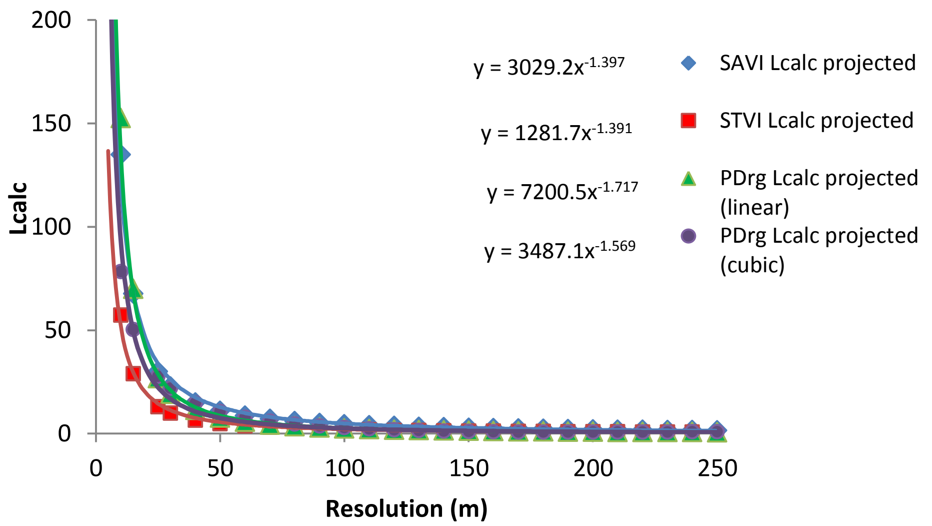

Figure 5.27 Projected leakiness response to change in resolution

The absolute differences between experimental and predicted leakiness values (Figure 5.28) are greater at higher resolutions (small pixel size) while there is more spread in the differences at low resolution.

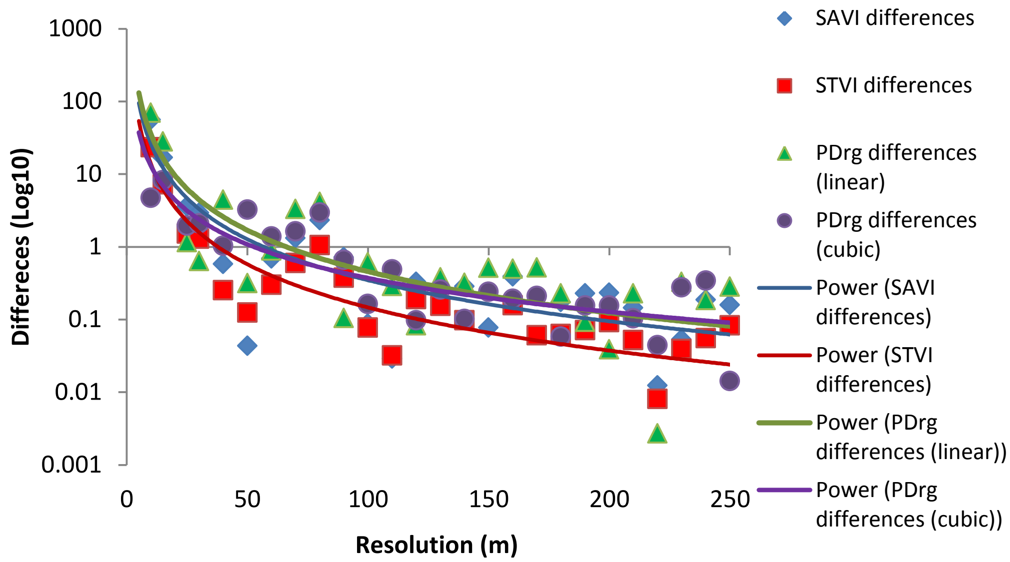

Figure 5.28 Absolute difference between experimental and projected leakiness values

High resolution calculated leakiness

The upscaling comparisons in the preceding sections encompassed the range from fine scale to broad scale comparisons (10-250m). This section analyses the fine upscale comparisons, which, for the purpose of this comparison, were defined as being from 10m to 30m. The upscaling experimental and projected data for the fine upscale range is shown in Figure 5.29 (Appendix 20).

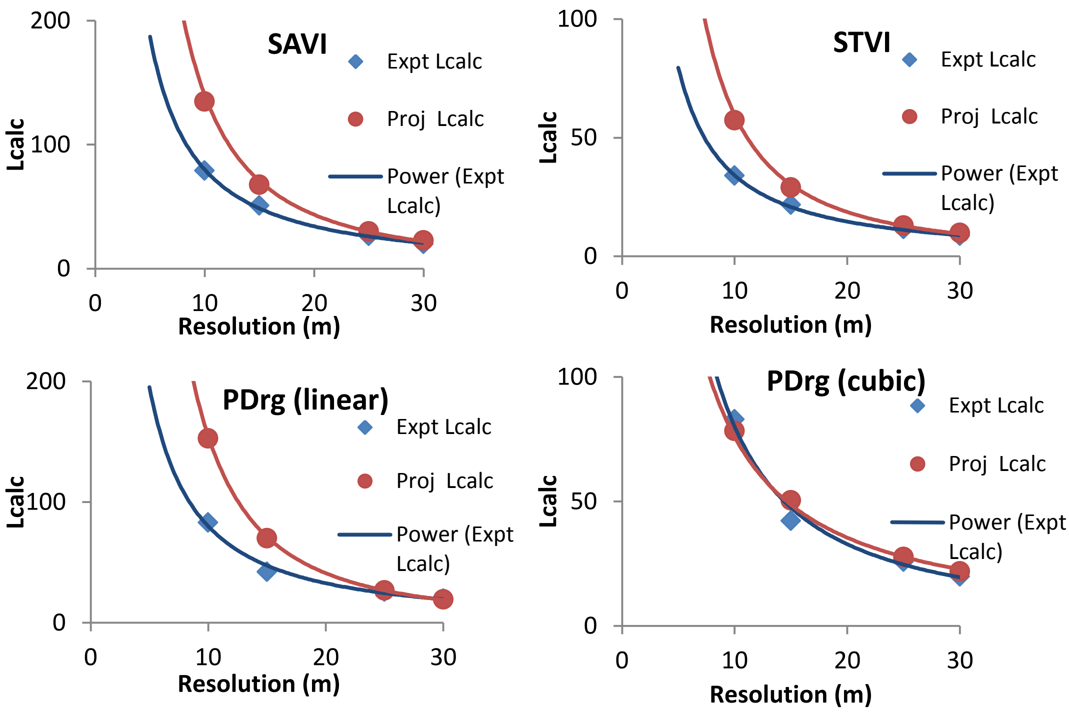

Figure 5.29 Fine scale projected and experimental leakiness

Testing for significant difference between the projected and experimental data, using the Wilcoxon Signed Rank Test for related data, showed there was a significant difference between the fine scale experimental and projected leakiness from SAVI and STVI at 2σ and from PDrg (linear) at 1σ as shown in Table 5-5.

Table 5-5 Significance levels for fine scale projected leakiness

Significance Level	Lcalc SAVI	Lcalc STVI	Lcalc PDrg (linear)	Lcalc PDrg (cubic)
95% (0.05)	Yes (0.043)	Yes (0.043)	No (0.08)	No (0.893)
68% (0.34)	na	na	Yes (0.08)	No (0.893)

Scale dependent relationships

The previous section provided evidence that there may be different relationships between leakiness and resolution at different scales. The existence of different relationships can be detected with the most sensitivity in the equations for "normal" relationships using the transformed leakiness data. This section investigates this possibility by analysing the transformed Lcalc versus resolution data at different resolution break points. First, the leakiness values were inspected and tested for 'best fit' at different break points in the range of 30-90m. Highest correlations for fitted trend lines were obtained when the data were segregated at the 80m break point. Second, the results are shown in Figure 5.30 and the respective 'best fit' equations are given in Table 5-6.

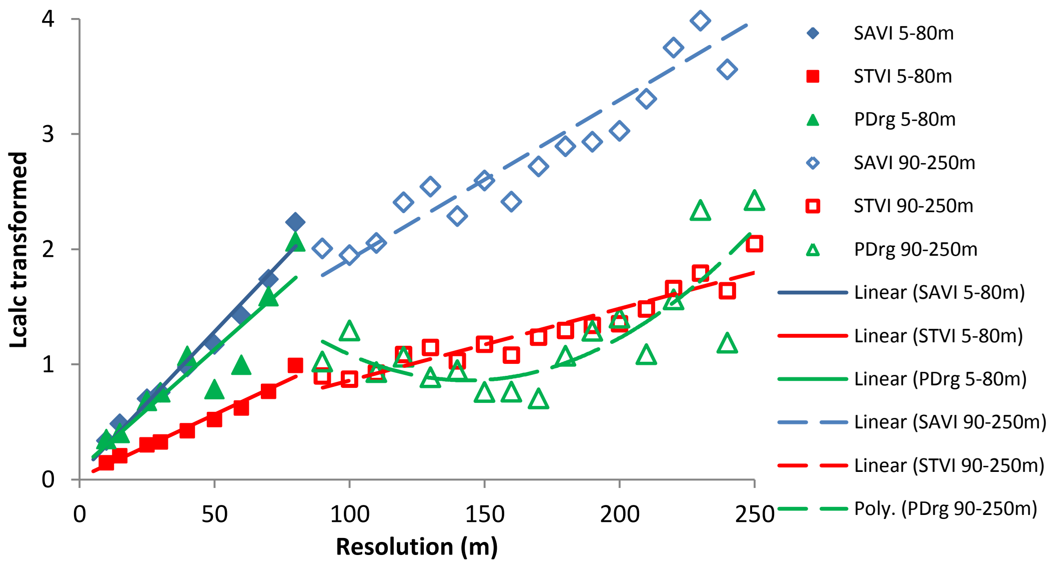

Figure 5.30 Separation of transformed leakiness at the 80m resolution break point

In Figure 5.30 the transformed Lcalc values for SAVI, STVI and PDrg have the same colour but different symbols indicate different resolution ranges as shown in the legend.

Table 5-6 Comparison of Best Fit equations and their CoD (R^2) values.

Cover Type	Resolution (10 – 80m)		Resolution (90-250m)		Resolution (10-250m)	
	Best Fit Expression	R^2	Best Fit Expression	R^2	Best Fit Expression	R^2
SAVI	y = 0.011x + 0.0149	0.977	y = 0.0138x + 0.5284	0.888	y=0.0146x + 0.4165	0.951
STVI	y = 0.0247x + 0.05	0.978	y = 0.0062x + 0.2351	0.895	y=0.0064 + 0.1906	0.955
PDrg	y = 0.0208x + 0.0919	0.876	$y = 0.0001x^2 - 0.0336x + 3.2789$	0.658	$y=9E\text{-}07x^3 - 0.0003x^2 + 0.0375x – 0.0147$	0.668

The slope of the ‘best fit’ equations for SAVI and STVI show little evidence in support of different relationships at different resolutions based on their R^2 values. However, the PDrg leakiness data suggest a linear relationship of leakiness with resolution from 10 to 80m followed by a quadratic relationship from 90 to 250m. The correlation of the quadratic relationship for the range 90-250m (Table 5-6, R^2=0.66) is less than the correlation of the overall cubic relationship (Table 5-6, R^2 = 0.67). The correlation of the linear relationship for transformed leakiness with resolution for PDrg in the range of 10 to 80m (R^2 = 0.88) is higher than the correlation of the cubic relationship. This suggests a linear scalogram would produce a more accurate projection for leakiness from PDrg in this range.

Adjusted Average Leakiness

AAL values for SAVI, STVI and PDrg were given in Figure 5.25. This data exhibited a normal distribution and was used in its present form for the AAL scalogram relationships (Equation 5-11, Equation 5-12 and Equation 5-14). The AAL scalograms for SAVI and STVI cover are linear (with different slopes) while the cubic scalogram for PDrg cover has a much higher CoD (0.67) than the linear scalogram (0.35).

Each relationship is unique indicating that AAL scalograms need to be developed for each way cover is measured. The catchment specificity of the scalograms was not evaluated because the experimental design did not include different catchments.

The evidence for AAL scale dependent relationships is similar to what was described for transformed leakiness data in the previous sub-section.

5.4.5. Variance Scalograms

The previous sections explored the nature and pattern of leakiness changes due to change in resolution and developed scaling equations that permit the estimation of leakiness at intermediate scales based on resolution. This section uses relationships between variance and resolution to investigate the effect of image variance on leakiness and to develop relationships that permit the estimation of leakiness from image variance. Two types of relationships are presented in Sections 5.4.5.1 and 5.4.5.2. The first category is a linear relationship between SAVI and STVI leakiness and upscaled image variance. The second category is a cubic relationship between PDrg leakiness and image variance.

5.4.5.1. SAVI and STVI

The semivariance of upscaled SAVI and STVI images varies with lag and resolution according to Equation 6-6 (from future Section 6.3.2.1) and Equation 6-9 (from future Section 6.3.2.2) as shown below.

$$V_{SAVIupsc} = 16.84 + 0.85*x - 0.0805*y - 0.016*x^2 - 0.0040*x*y + 0.002*y^2 \quad (5\text{-}15)$$

$$V_{STVI\ upsc} = 16.56 + 1.182*x + 0.140*y - 0.022*x^2 - 0.005*x*y + 0.002*y^2 \quad (5\text{-}16)$$

where V = semivariance, x = lag and y = resolution

The response of SAVI and STVI semivariance to resolution at any given lag was obtained by holding lag constant in each equation and evaluating its dependence on resolution. The values for AAL (from Equations 5-11 and 5-12 respectively) and for the semivariance at each upscaling resolution are shown in Figure 5.32 and Figure 5.33(data in Appendix 21). These figures show that AAL has a positive linear relationship with variance and a positive exponential relationship with resolution for SAVI and STVI.

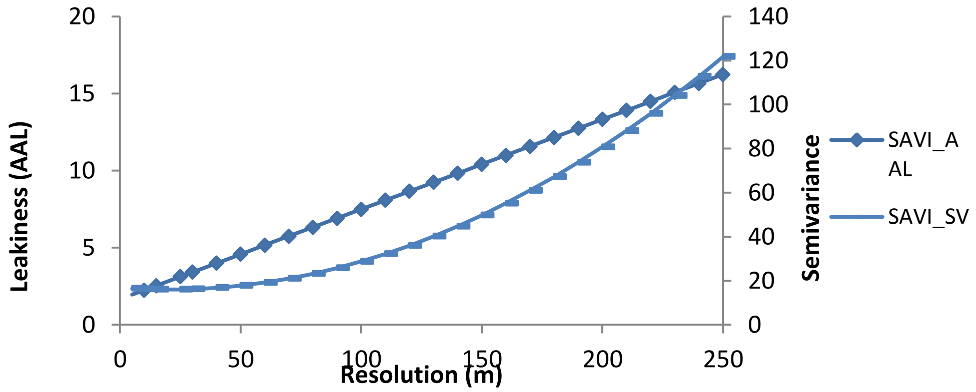

Figure 5.31 AAL and Semivariance dependence on Resolution for upscaled SAVI cover images

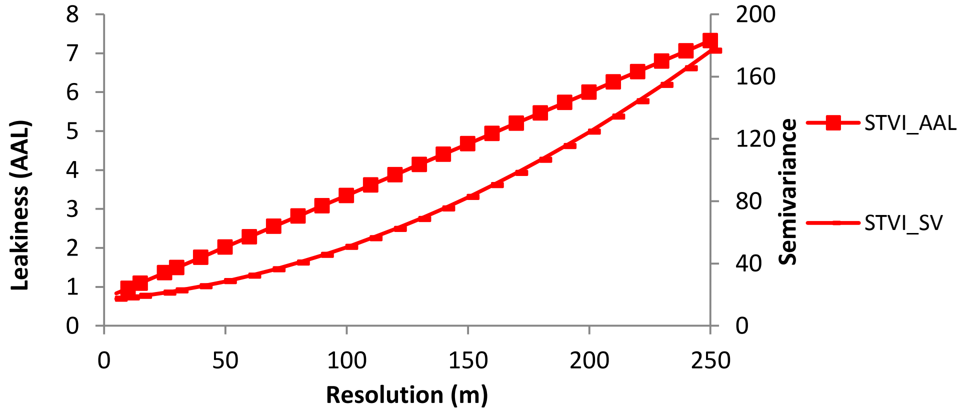

Figure 5.32 AAL and Semivariance dependence on Resolution for upscaled STVI cover images

5.4.5.2. PDrg

The semivariance of upscaled PDrg images also varies with lag and resolution according to Equation 6-11 (Section 6.3.2.3). The response of PDrg semivariance to resolution at any given lag was likewise obtained by holding lag constant and evaluating its dependence on resolution. The values for AAL (from Equation 5-14) and for the semivariance at each upscaling resolution are shown in Figure 5.33 (data in Appendix 22).

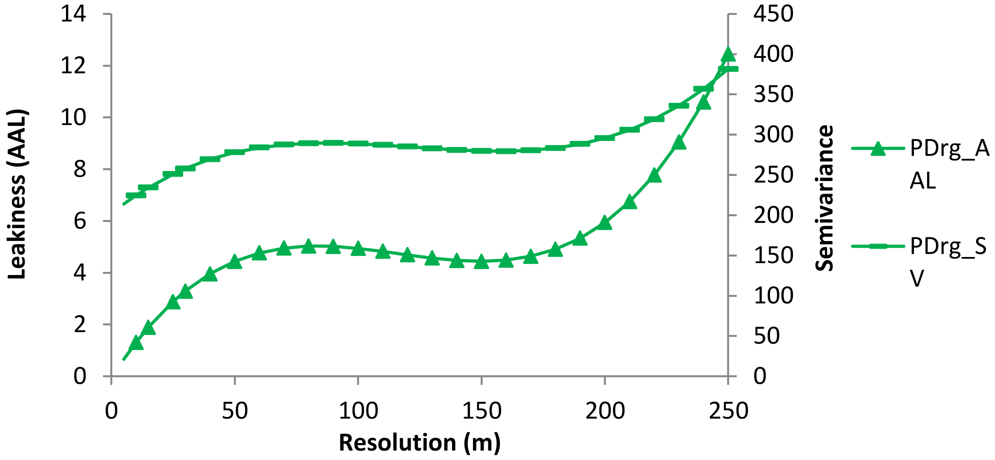

Figure 5.33. AAL and Semivariance dependence on Resolution for upscaled PDrg image

Figure 5.33 shows that AAL varies in the same direction as semivariance but at a different rate. Both dependent variables have a cubic relationship with image resolution. This is a function of the cubic relationship between Resolution and Leakiness in Equation 5-14.

5.4.5.3. Leakiness as a function of variance

Leakiness (AAL) can then be related to variance in each instance to yield the variance scalograms as shown in Figure 5.34.

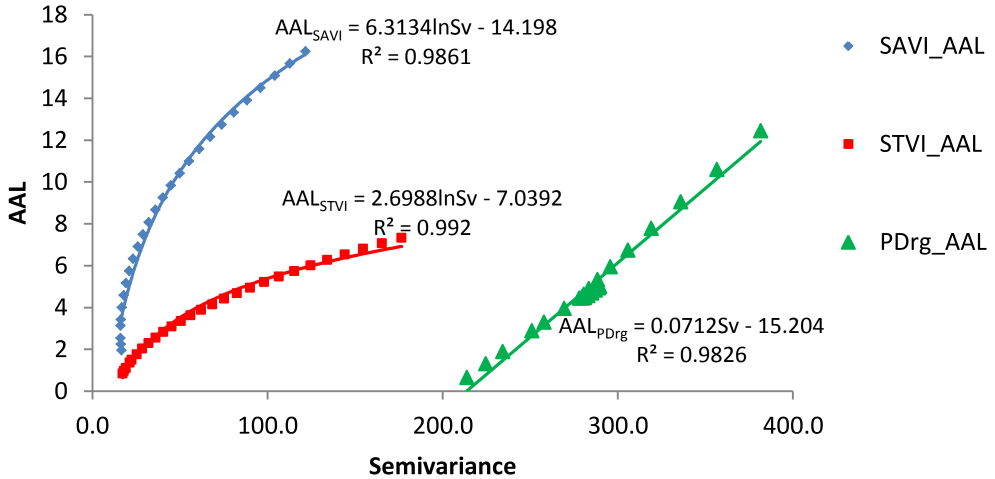

Figure 5.34 Variance scalograms for upscaled SAVI, STVI and PDrg cover images

The results show that SAVI and STVI AAL have scalograms that are a natural logarithmic relationship with variance as defined by Equations 5-15 and 5-16 and that PDrg AAL has a straight-line variance scalogram relationship as defined by Equation 5-17.

$$AAL_{SAVI} = 6.3134 \ln Sv - 14.198 \tag{5-17}$$

$$AAL_{STVI} = 2.6988 \ln Sv - 7.0392 \tag{5-18}$$

$$AAL_{PDrg} = 0.0712 Sv - 15.204 \tag{5-19}$$

where Sv = Semivariance

The SAVI and STVI scalograms show that initial increases in semivariance increase catchment leakiness more than subsequent increases in semivariance and that evenly distributed cover, at any level of cover, results in less leakiness than more variable cover at the same overall average level of cover. This is because the effect of semivariance on leakiness is positive logarithmic and because evenly distributed cover has a lower autocorrelation lag than more variably distributed cover. Figure 5.34 also shows that SAVI type cover changes leakiness more per unit of variance than STVI type cover. For example from inspection of Figure 5.34 it can be seen that 50γ of STVI semivariance changes the leakiness 3 units versus 50 γ of SAVI semivariance changes the leakiness 10 units.

PDrg cover variance has a much higher range than SAVI and STVI cover variance such that it cannot be compared numerically with SAVI and STVI (no X-axis overlap). Each unit of increase in PDrg cover variance increases leakiness by 7% (slope = 0.0712). The linear nature of the PDrg scalogram variance scalogram further suggests it as the preferred measure of cover for leakiness calculation in savannah landscapes with variable vegetation cover.

5.4.6. Comparison between native and upscaled leakiness

The native scale AAL values (Figure 4.28) were compared with the upscaled AAL values (Figure 5.20, Figure 5.21 and Figure 5.22) as shown in Figure 5.35.

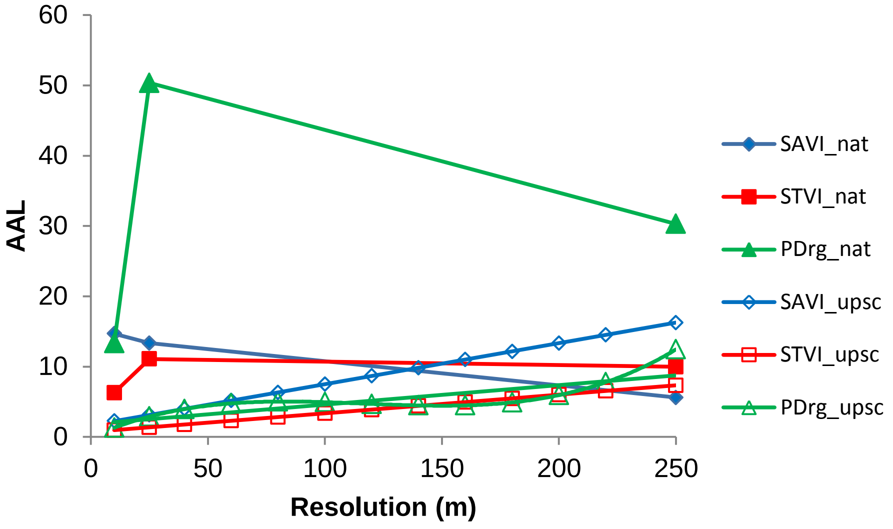

Figure 5.35. Comparison of native and upscaled leakiness for SAVI, STVI and PDrg coverages

This graph shows no evidence of correlation between leakiness calculated from upscaled imagery and from native scaled imagery. This means that it is not possible to upscale an image and get the same leakiness results as would be obtained from the raw image at the coarser scale. The reasons for this are investigated in the next chapter on image structure.

5.5. Discussion

The following sections provide an explanation of the upscaling procedures and derivation and use of the leakiness scalograms. The findings from this research are discussed in terms of previous research findings of the effects of upscaling imagery on object patterns.

5.5.1. Comparison of upscaling procedures

All upscaling was done using cubic convolution for the reasons given in Section 5.3.2. The leakiness results at upscaled resolutions from 10m to 250m (Appendix 8 and Appendix 9) were generated using the Leakiness Calculator (Ludwig and Eager *et al.* 2006). The Cell Counts correlate inversely with the Resolution, which is expected. They represent the number of cells in the experimental catchment included by the analysis mask for the leakiness calculation.

The difference in cover, caused by upscaling the image before calculation of cover, versus upscaling after cover was calculated is shown by comparing the amount of cover for both procedures (Figure 5.8 and Figure 5.9). The average cover for SAVI was 44.71% when calculated from the resampled image and 44.20% when calculated from the resampled cover raster. For STVI it was 56.43% from the image and 56.44% from the cover raster (Appendix 9). Small variations about the mean for each type of cover are due to the cubic convolution upscaling procedure. Statistical testing showed that the average cover values were different between the upscaled image and upscaled cover raster for SAVI cover but not for STVI cover. Comparison of the effect of upscaling before and after cover calculation was not done for PDrg cover because it was not practical to do it due to the procedure for calculating the PDrg index.

The experimental Leakiness (Lcalc) values are a measure of the aggregate leakiness of the catchment. Lcalc leakiness decreases as the number of pixels (cells) declines with decrease in resolution. It was previously shown (Section 4.4.1) that for catchments with a similar number of pixels, Lcalc decreased as the amount of cover in the catchment increased. This was because the leakiness calculation uses the cover values of each pixel to impose a resistance on the flow of resources from pixel to pixel. The results in Section 5.4 at first glance may appear to contradict the previous results on the effect of cover on leakiness. They are however consistent when one considers that the leakiness equation (Section 2) calculates the total leakiness as the sum of the individual leakiness values of each pixel. It follows that when there are fewer pixels there is less calculated leakiness. This is because the leakiness calculation is based on the absolute amount of flow between pixels and not on the flow flux (flow/unit area).

Statistical analysis showed that Lcalc from resampled images versus resampled cover rasters was different for SAVI coverages but similar for STVI coverages. Because of these findings, all subsequent analyses were based on leakiness calculated from resampled images rather than from resampled cover rasters.

5.5.2. Calculated Leakiness Scalograms

The nature of the upscaling process inherently skews the data positively because there are many more pixels in the same included area at higher resolutions. This necessitated transforming the data to get an approximately normal distribution to determine the relationship between the dependent leakiness variable, Lcalc with Resolution. A transform relationship was developed (Equation 5-2, p. 130) in terms of Cell Count. Because Cell Count can also be expressed as a function of Resolution (Equation 5-1) this allowed simplification of the resulting transformed Lcalc versus Resolution equations (Equation 5- 3, 5-5, 5-7 and 5-9) in terms of Resolution. This approach yielded the respective leakiness prediction relationships or Scalograms (Equations 5-4, 5-6, 5-8 and 5-10) in terms of only the Resolution variable.

Predicted Lcalc values for SAVI, STVI and PDrg were calculated using the respective scalograms (Equations 5-4, 5-6, 5-8 and 5-10). The differences between the experimental and predicted Leakiness values are given in Appendix 10, Appendix 11and Appendix 12. They provide a measure of the closeness of fit of the predicted values to the experimental values.

Goodness-of-fit for non-normally distributed leakiness data was tested using the Wilcoxon Signed Rank (WSR) test because each sample arises from the same level of the independent variable (Coakes and Steed *et al.* 2010, p. 178). The results showed no significant difference between the experimental and predicted values for SAVI, STVI and PDrg coverages at the 95% probability level.

However, tables of predicted values (Appendix 10,Appendix 11and Appendix 12) show increasingly larger differences with experimental values for leakiness in the range from 10-30m. This indicates the prediction relationships are not predicting values as correctly in this range as they are in the balance of the prediction range. This is probably because, as the normalised curves show (Figure 5.12, Figure 5.15 and Figure 5.19), the data in this range is not normalised as well as the balance of the data by the transform relationship (Equation 5-2). As a consequence, the Scalograms are less accurate in this resolution range. In practice the cell number changes rapidly (2^{nd} order) at high resolutions (low pixel size) and the relationship becomes asymptotic with the dependent variable resulting in very small changes in resolution causing large changes in predicted Lcalc values.

In summary, the results show that it is feasible to generate scalograms to predict calculated leakiness with 95% statistical accuracy in the resolution range from 25-250m. However, such leakiness scalograms become less accurate at resolutions above 25m. Comparison of leakiness at resolutions above 25m requires scalograms calibrated specifically for the higher resolution range.

5.5.3. Adjusted Average Leakiness Scalograms

AAL is the total amount of leakiness in a catchment averaged over the number of cells in the catchment, irrespective of the size of the cell. It increases as resolution decreases (larger cell size) although the average cover remains the same at all resolutions (Figure 5.20, Figure 5.21 and Figure 5.22). Inspection shows that AAL is cover-type specific and normally distributed. The normal distribution of AAL occurs because the AAL equation (Equation 4-10) divides the calculated leakiness by the number of cells in the analysis mask thereby neutralising the effect of resolution on cell count.

Because of this, AAL Scalograms are simply the AAL resolution prediction equations and require no further transformation. The differences between the experimental and predicted Leakiness values are given in

Appendix 13,

Appendix 14 and

Appendix 15. They were statistically compared as before with the experimental data. The results showed no significant difference at the 95% probability level for SAVI and STVI AAL. However, for PDrg the cubic scalogram produced results that had no significant difference (95% probability) to the experimental values but the linear scalogram predictions were significantly different to the experimental values as shown by the T test values in Table 5-4. There was no resolution dependent trend in the difference data for any of the three scalograms indicating equally valid prediction at all resolutions within the range.

In summary, the leakiness resolution relationship is the scalogram for AAL. This is a linear relationship for SAVI and STVI and a cubic relationship for PDrg and prediction is equally accurate at all resolutions in the analysis range.

5.5.4. Resolution Scalogram Comparison

Comparing the results at different resolutions (Section 5.4.4) showed that upscaling did not change catchment average cover but it did change catchment leakiness. This is illustrated by the difference in slopes of the AAL and transformed Leakiness responses to resolution (Figure 5.25 and Figure 5.26). Both AAL and transformed Leakiness for SAVI and STVI responded linearly to change in resolution with different slopes for each type of cover. Transformed Leakiness for PDrg cover was best explained by a cubic polynomial relationship with resolution (R^2 = 0.67). The linear PDrg relationship had a poorer fit to the experimental data (R^2 = 0.35).

The existence of different fits for each type of cover means that each type of cover has its own scaling relationship with change in resolution. There is no single relationship that can adequately explain how leakiness changes when images analysed for SAVI, STVI and PDrg cover are upscaled. The implications of this finding are that leakiness scalograms are likely to be different for other types of indices as well. Their slope and intercept will require determination for each type of cover used for leakiness assessment.

The tests for goodness of fit between the experimental and predicted calculated leakiness values over the range of 10-250m showed no statistically significant difference at the 95% probability level. However, their residuals were higher at higher resolutions (Appendix 10, Appendix 11and Appendix 12). Analysis of the goodness of fit between experimental and predicted values in the 10-30m range showed significant differences for SAVI and STVI leakiness and PDrg linear but not for PDrg cubic (Table 5-5). Linear predicted PDrg leakiness was significantly different from the experimental Lcalc at the 95% probability level but not at the 68% probability level. PDrg cubic projected leakiness was not significantly different at either probability level.

The difference in correlation with change in resolution means that in addition to using cover specific Scalograms, it may be necessary to use Scalograms specific for different ranges of resolution. For example, scaling relationships that apply to a particular type of cover from 10m to 80m may be substantially different from the scaling relationship for the same type of cover from 90m to 250m. The existence of resolution break points was investigated to see if prediction equations that treated leakiness differently at different resolutions might lead to more accurate predictions.

The results (Figure 5.30 and

Appendix 19) show that, while a break point exists between 80 – 90m resolution for SAVI, STVI and PDrg, the differences in slope and intercept values for SAVI and STVI scalograms before, and after the breakpoint, are small. CoD values of the equations for the full resolution range, while intermediate between the separate equation CoD values, remain high (SAVI R^2 = 0.9505, STVI R^2 = 0.9545).

The pattern is different for PDrg Lcalc. The cubic relationship for the 10-250m resolution range segregates into a straight-line relationship for the 10-80m segment and a quadratic relationship for the 90-250m segment. The straight-line relationship for the 10-80m segment has a CoD of 0.8764, which is substantially above the CoD of 0.6676 for the cubic relationship. This indicates it provides a better basis for leakiness prediction from PDrg in the range of 10-80m compared to the cubic-based prediction equation. This suggests that the user should carefully assess the behaviour of the prediction relationship for the range of resolutions in which it they are to be used.

These results show that leakiness scalograms are specific for each type of cover used for leakiness analysis and that they have limited ranges of resolution in which they can be applied. This range is set by the existence of breakpoints in the scalogram function. Scalograms provide more accurate prediction of leakiness if they are used within their breakpoint limits. The existence of breakpoints should be the subject of preliminary investigation before final scalograms are decided on for a project.

5.5.5. Variance Scalograms

This section applied the findings of a regular relationship between semivariance and resolution (Figure 6.49, Figure 6.60 and Figure 6.77) to the AAL scalograms to develop variance scalograms. Upscaling an image increases its sill semivariance but causes total semivariance to decrease over distance as shown by the form of the variograms in Figure 6.44, Figure 6.45, Figure 6.55, Figure 6.56, Figure 6.71and Figure 6.72. The generalised surface relationships for upscaled SAVI and STVI semivariance with resolution and lag are both two variable quadratic relationships (Figure 6.49 and Figure 6.60) which show a steady increase in variance with resolution. The PDrg semivariance relationship with resolution and lag (Figure 6.77) is a two variable cubic relationship. The effect of Resolution by itself (lag held constant) on both AAL and semivariance is shown in Figure 5.31, Figure 5.32 and Figure 5.33 (data in Appendix 21and Appendix 22). This shows that SAVI and STVI AAL depend on the natural log of the semivariance of the respective cover rasters and that PDrg AAL is a linear function of the semivariance of the cover raster(Figure 5.34). The semivariance Scalogram relationships from Figure 5.34 (Equations 5-15, 5-16 and 5-17) allow the determination of AAL from the semivariance of the upscaled image without recourse to its resolution.

These results show that leakiness (AAL) exhibits a precise and predictable relationship with upscaled image semivariance. The precise form of the relationship is different for different types of vegetation cover. As semivariance is a fundamental structural property of all images, this finding allows the generation of semivariance based scalograms for predicting leakiness from upscaled imagery without the need to know the changed resolution of the image.

5.5.6. Upscale and native leakiness comparison

Figure 5.35 shows that while there is a systematic change in leakiness with progressive upscaling there is no evident systematic change in native image leakiness with change in resolution. Further, upscaling the 10m image to 25m and 250m fails to yield leakiness values comparable with the native image leakiness at these same resolutions. The reasons for this are discussed in the following section.

5.5.7. Scale and feature relationships

Leakiness depends on the identification of features (in this case pixels) at a resolution that allows measurement of the amount of cover on the feature, e.g. bare ground, partially bare ground or fully covered ground. This is necessary so that when the cover value "*c*" is incorporated in the negative power term of the Leakiness equation (Equation 4-1) it imposes a restriction on resource flow relative to a value of zero. Dispersed high cover patches can be lost in the process of resampling (Turner and Gardner *et al.* 2001, pp. 103, Box 5.1) resulting in more low cover patches. As a consequence the results will reflect a higher leakiness due to progressive resampling (lower resolution). However, this does not appear to have occurred because the average cover remains constant during progressive resampling (Figure 5.10, Figure 5.13 and Figure 5.16)

This suggests that each coarser resolution has its own leakiness versus cover response curve (in negative exponential form) which stack progressively. As the cover remains constant the increase in leakiness is due to the progressive stacking of the response curves. The resulting observation of a linear increase in AAL with reduced resolution is in effect a vertical profile through these response curves at the X axis value corresponding to the respective amount of cover for either SAVI, STVI or PDrg. This may explain the progressive increase in AAL with decrease in resolution from upscaling. The different rates (slopes) of change between SAVI and STVI would then be due to differences in dispersion of cover patches and thus differences in rate of loss of dispersion during resampling.

PDrg cover clearly affects leakiness differently from SAVI and STVI cover. The cubic nature of the PDrg AAL Scalogram suggests two different spatial features are at play in this analysis, one at higher resolutions and one at lower resolutions. This is illustrated in Figure 5.30, which shows the higher agreement for 2-stage correlation analysis than for single stage (cubic) correlation analysis (PDrg row in Table 5-6).

5.6. Conclusion

Adjusted Average Leakiness (AAL) is a suitable metric for comparing the leakiness of catchments where there are different numbers of cells whereas the Leakiness Index (LI) is only suitable for comparing the results for catchments with the same number of pixels of the same size.

Resolution Scalograms were developed for both Calculated Leakiness and AAL. They accurately predicted the change in leakiness for SAVI, STVI and PDrg cover analyses. The Scalogram equations have coefficients that are different for each type of cover. They are accurate over a wide range of resolutions (30-250m) but separate Scalograms may be needed for calculating leakiness at high resolutions (10-30m) depending on the level of accuracy desired. The relationship between variance and resolution, established in Chapter 6, made it possible to derive Variance Scalograms. These allow the prediction of upscaled leakiness from variance without knowledge of the resolution.

The upscaled leakiness did not coincide with or relate systematically to the leakiness calculated from native scale imagery at 25m or at 250m. This finding reinforces the need for i) multi scale analyses of ecological processes and ii) the need to carefully consider the effects of changes in scale on analytic results. The reasons for this are investigated in the next chapter.

CHAPTER 6

EFFECT OF UPSCALING ON IMAGE STRUCTURE

6.1. Introduction

Chapters 4 and 5 covered the measurement of leakiness from three scales of native images of the experimental catchment using different physical cover indices as well as from upscaling the 10m resolution image through a series of intermediate resolutions to 250m. The results showed different cover indices produce different leakiness results both at the same scale and at different scales and that upscaling affects the leakiness for each cover index differently.

A review of the literature on image structure, its measurement at different spatial scales and its relationship to landscape process scales was provided in Chapter 2 (Section 2.7). This chapter investigates differences in native image structure and the effect of upscaling on image structure as a possible cause of the difference in leakiness results.

6.1.1. Changing Scales

Rescaling data in GIS is a fundamental operation that is easily and frequently done by many operators with little regard to its effect on the underlying structure of the data. Rescaling to larger supports requires interpolation to upscale the data so as to protect the native spatial variation. However, interpolation inevitably involves smoothing because of the influence of neighbouring pixels. Thus scaling induced regularisation can change the landscape process signal from what was originally observed. Optimal interpretation requires that the spatial and temporal resolution of the image record the spatial heterogeneity of the features at the ecological process scale. Thus large scale monitoring must consider the interaction between pattern and process to accurately assess ecological change (Bradshaw and Fortin 2000).

The variance of the native data is due to both the scale of original measurement as well as the support underlying the features. This information can be assessed from native image variograms and can be used to predict changes in the variable (feature of interest) with change in scale of measurement. For example, variograms of 10m images with a Range of 3 pixels (30m) and a SCVof 22.5γ when upscaled to 25m pixels yield a higher range and lower variance (6 pixels (150m) and 15 γ) indicate that the features are more like each other when measured at the lower resolution (25m). This pattern was reported by Atkinson and Tate (2000, pp. 618, Fig. 9). The effect of coarsening spatial resolution is to effectively remove the short-range variation from the image so that a lesser amount of long-range variation remains which decreases the semivariance. If on the other hand, semivariance is increased by decreasing the image scale it can indicate the higher resolution scale was not detecting the full range of features and that the features have a lower resolution than the resolution at which they were collected (imaged).

The amount of change depends on whether the aggregation is coarser or finer than the optimal autocorrelation range for the attributes of the parent image (Bian and Butler 1999). Collins and Woodcock (1999) showed that the regularised variogram provided an estimate of the resolution dependent variance and that this was independent of the spatial structure of the underlying scene. Atkinson and Tate (2000, p. 617) cited the relationship between the point semivariance and the regularised semivariance at any Lag (l) developed by Journel and Huijbregts (Equation. 6-1) as a way to increase the size of the support (resolution) without measuring the semivariance on the new support.

$$\gamma_{\mathrm{v}}(\mathrm{l}) = \bar{\gamma}(\mathrm{v}, \mathrm{v_l}) - \bar{\gamma}(\bar{\mathrm{v}}, \mathrm{v})\text{-} \qquad (6\text{-}1)$$

where γ_v = semivariance at support v
l = lag
$\bar{\gamma}(v, v_l)$ = point semivariance between two supports of size v separated by l

They showed that the method could be used to provide estimates of the regularised semivariance at larger lags without actually measuring it. This provides a way of rescaling spatial variation. The effect then of regularising spatial variation over the support is to remove small-scale variation in favour of large-scale variation. The amount removed depends on how much of the total SCV is due to small-scale support variance.

The accuracy with which features can be identified in upscaled images when compared to native images was tested and found to depend on the rescaling method (Hay and Nieman 1996). Variance weighted upscaling was found to produce superior results compared to the conventional methods of Nearest Neighbour (NN), Bilinear (BL) and Cubic Convolution (CC) upscaling while Non-overlapping Averaging (AVG) upscaling produced intermediate results. The effect of NN upscaling on high resolution NDVI images (0.625m to 3.125m) showed that it decreased the Standard Deviation and Coefficient of Variation of the upscaled image while they remained the same for coincident native images at the coarser scale (Goodin and Henebry 2002).

Variogram analyses of both types of images showed that as spatial resolution decreases, spatial dependence (FR) increased and the amount of spatially dependent variation (Sill and Nugget variance, SV) decreased in both native scale and upscaled images as previously reported by DeCola (1994). Upscaling inflated the intensity of both the SV and the FR more than in unscaled imagery as shown by plotting the ratio of the SV to FR (Figure 6.1). This is also consistent with DeCola's findings. In this instance the cost of NN rescaling was an overestimation of spatial structure that the authors concluded might hinder accurate retrieval of biophysical variables.

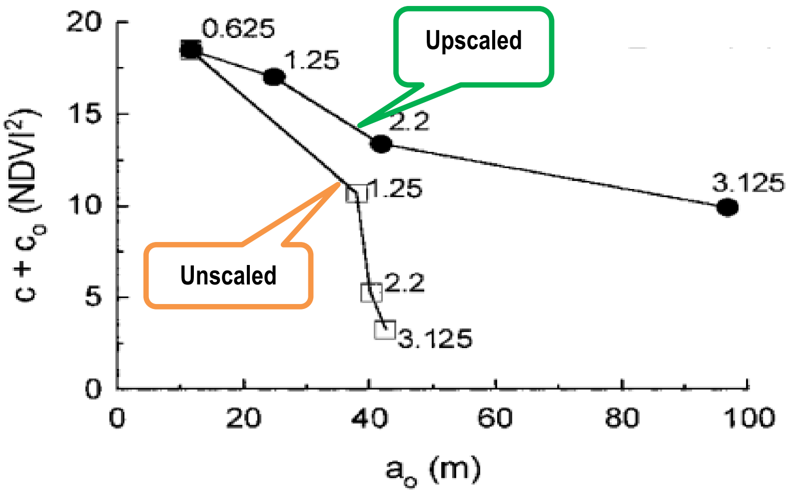

Figure 6.1 Plot of First Range (a_o) against Nugget and Sill Variance ($c+c_o$)
(Goodin and Henebry 2002)

The effect of rescaling images by simple block averaging (AVG) of NDVI images of high resolution (0.187m to 1.0m) of orthogonal corn plots showed the following changes in image structure (Chen and Henebry 2009):

a. The Means and the Coefficients of Variation were different between the unscaled images and the upscaled images.
b. The SV at a given lag decreased as the resolution decreased for both unscaled and upscaled images but the pattern of change was more regular for the upscaled images than for the unscaled images.
c. Rescaled images displayed a log-linear decay between the spatially dependent variance (SV) and range (FR) while unscaled images had a rapid initial decay and then a slower rate of decay to converge to similar values as the upscaled image as shown in Figure 6.2.
d. The upscaled images had a lower change in sill and nugget variance and range than the unscaled images.

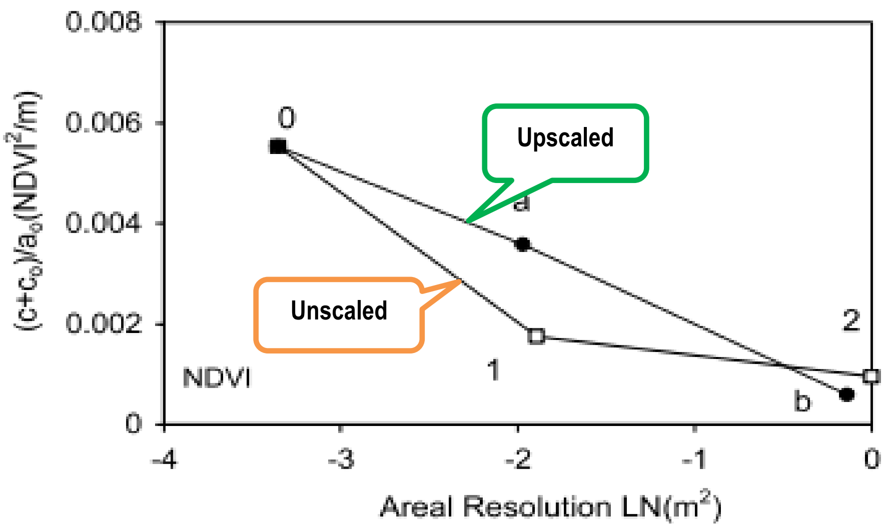

Figure 6.2 Semi Natural log plot of areal resolution against Nugget and Sill Variance ($c+c_o$) for unscaled and upscaled NDVI images,
(Chen and Henebry 2009)

They concluded that:

i. The loss of spatial structure caused a substantial loss in spatial variation, and
ii. Upscaling by simple block averaging does not accurately simulate the spatial effects of unscaled higher resolution images.

The effect of scaling (both up and down) high resolution (0.5 to 3m) NDVI imagery of natural areas using Nearest Neighbour, Bilinear, Cubic Convolution and simple Aggregation methods was tested by Lausch *et al.* (2013). They found that:

a. The rescaled imagery had a different spatial pattern from the unscaled imagery.
b. Different types of vegetation produced different patterns of response to rescaling as evidenced by their variograms.
c. Their rescaled images did not have $1/3^{rd}$ of the unscaled image variance reported by Goodin and Henebry (2002).
d. The rescaled imagery (between 1 and 3m) while different, had a spatial pattern similar to its source imagery.

These findings show that while a general trend of the effect of rescaling on imagery is emerging, there remain many unknown factors affecting the interpretation of scale-induced changes on image features. These include the type of scene being rescaled, the amount of rescaling, the direction of the rescaling (up or down) and the rescaling method.

6.1.2. General application

Both pattern and process play an important role in determining the scale at which to monitor ecosystems (Bradshaw and Fortin 2000). Spatial and temporal scales of the landscape features and the ecological processes must be considered when selecting the spectral, spatial and temporal resolution of imagery for landscape monitoring programs. Ludwig and Wiens *et al.* (2000) developed rules and equations for scaling functions to integrate scale dependent landscape patterns with the ecological processes associated with them. Their approach integrates the interdependency of measurement scale with ecological scale. The observation scale must allow detection of the ecologically significant landscape features from which the scaling relationships can then predict ecological behaviour. Ludwig and Wiens *et al.* (2000) illustrated this by proposing a rule for landscape patches, namely:

> *"The concentration of resources (per unit area) becomes increasingly greater as patch size increases".*

They also suggested the existence of a landscape patch rule for runoff. Further work established the importance of patch configuration on resource loss (Ludwig and Bartley *et al.* 2007).

6.1.3. Application to Leakiness

A primary tool for calculating rangeland condition and resource loss is the CSIRO Leakiness Calculator (See Section 2.4.3). The reasonableness of its predictions using ground cover data at 25m to 80m has been verified by a number of studies (Bastin and Abbott *et al.* 2008; Pickup and Chewings *et al.* 1993). Before this approach can be used more widely it is desirable to know how image scale affects leakiness measurements. This depends on the attributes detected by the scale of the image and the scale of the features in the area being analysed (Karl and Maurer 2010). The following section outlines the methods used to investigate and assess the effect of image scale on leakiness.

6.2. Research Methods

Fetex 2.0 software (Ruiz and Recio *et al.* 2011)was used to analyse the cover and DEM data for the catchment at each resolution to determine the catchment semivariance. The native and upscaled semivariance were analysed in Matlab to obtain their surface expressions. Indices were developed from the semivariance and tested for correlation with resolution and leakiness parameters as shown in Figure 6.3.

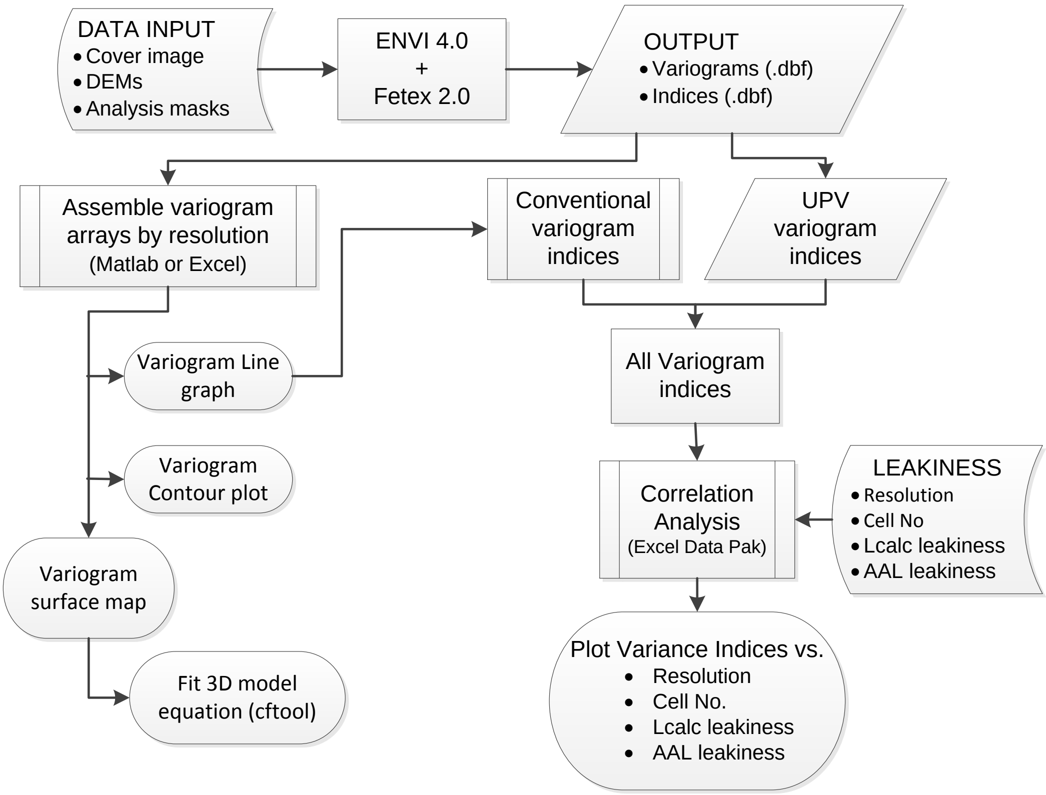

Figure 6.3 Variance analysis flow sequence

6.2.1. Data Sources

Analysis of the variance of cover layers and DEMs used similar data sources to those used in Chapters 4 and 5. Semivariance were calculated for SAVI, STVI and PDrg cover layers and for the DEMs at each scale for which the leakiness was calculated in Section 4.2 and 5.2.The original data sources and their pre-processing were described in Chapter 3. The following data were used as inputs to FETEX 2.0

- The same DEM files as used in the leakiness analysis (Section 4.2.1.1)
- The same analysis masks (converted to shape file format) used in the leakiness analysis (Section 4.2.1.2)
- The same vegetation cover files (SAVI, STVI and PDrg) used in the leakiness analysis (Section 4.2.1.3).
- Upscaled DEM and vegetation coverages were prepared as described in Section 5.3.

6.2.2. Variance Analysis

A number of alternative procedures were investigated for analysis of variance. The Geostatistical Analyst extension for ArcGIS 10.1 (ESRI 2012) was considered but rejected because it is designed for initial vector input rather than raster input. The Global Spatial Statistics tool (semivariance option) in ENVI 4.0 (Exelis 2012) was considered but also rejected because it did not provide a way of exporting the semivariance values. GSTAT (Edzer and Wesseling 1998) and TEXTNN (Leite and

Filho 2009) were also considered but not used because of the time required to set up the programs and become familiar with their operation. The feature extraction software for object based image analysis and classification, FETEX 2.0 (Ruiz and Recio *et al.* 2011) was selected because it, i) is designed to handle raster input data sets, ii) can be mounted as an add-in to ENVI IDL, iii) allows the use of masks to define areas of analysis, and iv) offers a variety of variance output products as discussed in the following section.

A demonstration copy of FETEX 2.0 was obtained and installed (Hermosilla 2013). Following successful operation, a fully functional licensed version of FETEX 2.0 was obtained under License from the Universidad Politecnica de Valencia (UPV) in Valencia Spain and installed as an add-on to the IDL module in ENVI 4.0 software.

All variograms produced in this analysis were omnidirectional. Conventional Variogram indices were manually extracted from the variograms using MS Excel. UPV indices were calculated automatically by Fetex 2.0 and exported as DBF files.

The change in variance of cover layers and DEMs was analysed in two ways, i) first by fitting expressions to their semivariograms and comparing the change in coefficients with change in scale and, ii) by assembling the values as arrays and interpolating them into a contour plot using the 'contour' function in Matlab software (Pratap 2010). The arrays were then plotted as 3D surfaces (Matlab 'surf' function) to which expressions were fitted using the Matlab Curve Fitting Tool box (cftools) to obtain the best practical fit to the surface. The change in surface expressions as a function of scale could then be compared.

6.2.3. Correlation Analysis

Correlation testing was done to find possible explanatory relationships between image scale, leakiness and variance parameters. The key parameters of each image, resolution, cell number, amount of cover, Lcalc and AAL were tested for correlation with both types of variogram indices. Additionally, the conventional indices were tested for correlation with the UPV indices. All testing was done in MS Excel using the Data Analysis add-in. Relationships were evaluated by plotting the results for visual inspection.

6.3. Results

The following sub-sections summarize the results for the analysis of change in variance of both native images (not resampled) at three resolutions and for images in which the resolution has been changed by resampling from 10m to 250m. These analyses are of single thematic bands for SAVI, STVI and PDrg vegetation cover for the experimental catchment. The change in variance of the DEM used in the leakiness calculation at each resolution was also analysed because it drives the hydraulic distribution function in the Leakiness Calculator.

6.3.1. Native Images

The following subsections present the results for the analysis of the SAVI, STVI and PDrg vegetation covers derived from SPOT, Landsat and MODIS and matching DEMs at 10, 25m and 250m resolution.

6.3.1.1. Soil Adjusted Vegetation Index (SAVI)

Each variance analysis result is shown in a similar manner in the following sections. First, the variograms of the images are presented followed by their interpolated contour plot followed by their three dimensional continuous surfaces. This approach was taken to help interpret how the information in the images changed with resolution. Two-variable models were fitted to the surfaces and compared.

Conventional and UPV indices were derived from the variograms and tested for correlation with the image parameters as a way of looking for relationships between variance, resolution and leakiness.

Variance

The semivariance of SAVI vegetation cover images, calculated at each of three resolutions are shown in Figure 6.4.

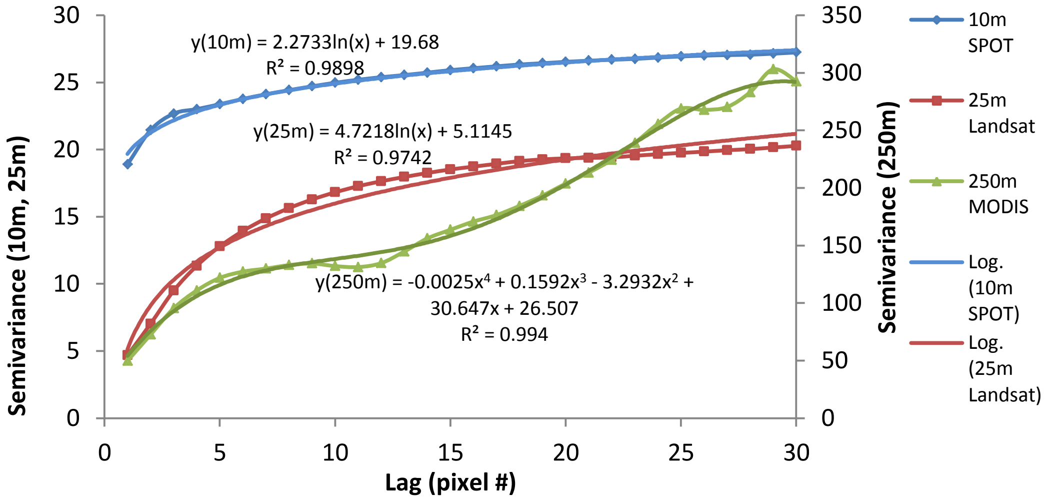

Figure 6.4 SAVI semivariance

The 10m and 25m images have natural log variograms while the 250m image has a quartic variogram.

The change in semivariance of SAVI vegetation cover with resolution was plotted as contours in Figure 6.5 and mapped as a surface in Figure 6.6. The contours provide a visual image of how the variance in the image changes with change in resolution and the distance between pixels (lag). For example, it can be seen that at any given resolution, say 100m, the variance between pixels 5 pixels a part is approximately 50 γ while the variance between 5 pixels at 150m resolution is approximately 75 γ. The greatest increase in variance occurs between pixels close to each other until the variance reaches an initial maximum at the Range. This variance tends to be repeated in other parts of the image. Areas of increased variance at greater distances between pixels show as elevations in the contour lines.

This can also be shown in 3 dimensions as a surface (Figure 6.7). Here the semivariance is plotted as a third axis to resolution and lag. This shows that at high resolution (e.g. 10m) the image has a low variance at all lags. However, as the Resolution decreases (e.g. 250m) and/or the distance between pixels (lag) increases the amount of variance increases but not at a uniform rate.

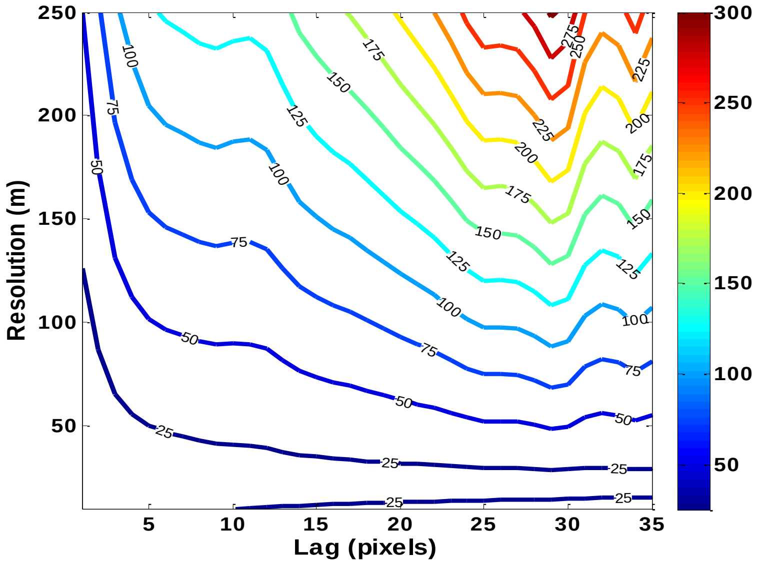

Figure 6.5 SAVI native semivariance contours

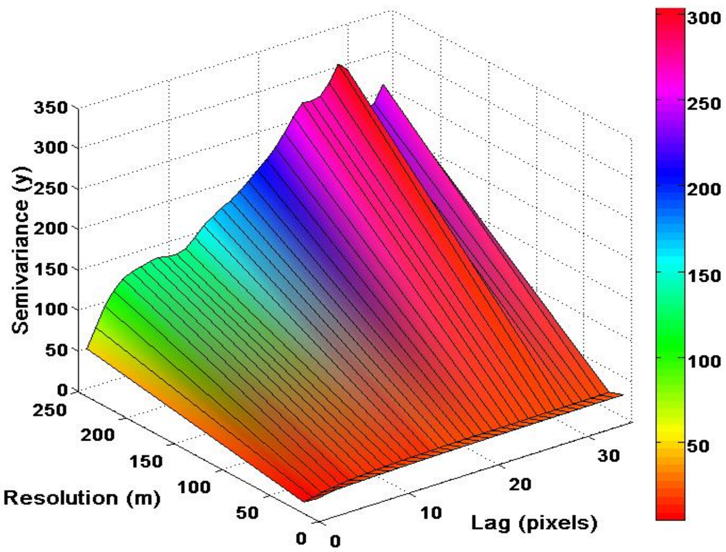

Figure 6.6 SAVI native semivariance surface

This surface was modelled as shown in Figure 6.7 by a 2-variable quadratic equation. This fitted the variance surface well as shown by the R^2 values in Table 6-1.

$$V_{SAVI\ native} = 25.73 + 1.47*x - 1.20*y - 0.05*x2 + 0.03*x*y + 0.01*y2 \qquad (6\text{-}1)$$

where V = semivariance, x = lag and y = resolution

Table 6-1 Equation 6-1 fit parameters

Fit parameters			
SSE	R^2	R^2adj	**RMSE**
17430.00	0.98	0.98	13.27

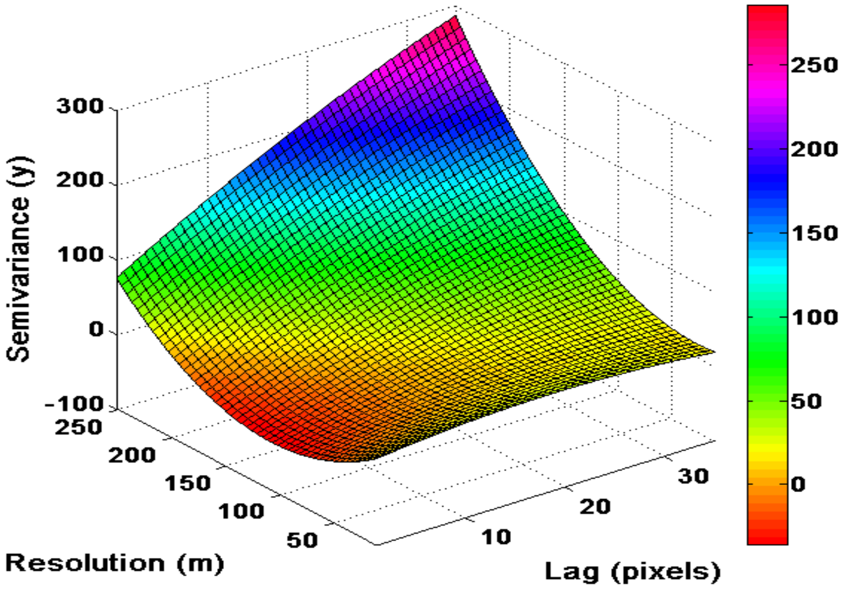

Figure 6.7 SAVI native semivariance model

Variogram Indices

Conventional and UPV indices (Table 6-2) were extracted as described in Section 6.2.2. The First Sill Semivariance (FSS) (Table 6-2) is a similar measure to the Mean up to the First Maximum (MFM) in Table 6-3. The values are close to each other. This parameter indicates the average of the semi-variogram values between the first lag and the first maximum. It measures the change in variability of the data. Further analysis of these indices is provided in Section 6.4.

Table 6-2 Conventional Variogram indices for SAVI cover images

Image resolution	Conventional variogram index values					
	Nugget Variance (NV)	First Range (FR) (m)	First Sill semi-Variance (FSV)	Spatial Correlated semi-Variance (SCV)	Nugget to Sill Variance Ratio (NSVR)	Nugget to Spat. Cor. Var. ratio (NSCVR)
10m	19.13	30	22.68	3.55	0.84	5.39
25m	1.92	150	15.64	13.72	0.12	0.14
250m	-10.27	1000	110.88	121.15	-0.09	-0.08

Table 6-3 UPV Variogram Indices for SAVI cover images

Image resolution	UPV variogram indices*.					
	RVF	RSF	FDO	FML	MFM	AFM
10m	1.45	1.13	2.55	41.00	25.91	302.01
25m	4.21	1.50	2.35	41.00	17.94	540.17
250m	3.40	1.46	22.81	9.00	108.33	534.47

* The abbreviations above are as per Balaguer (2010). Their full names and derivation are provided in Table 2-7 and Table 2-8.

Index correlation with leakiness

The correlation of these values with cover layer values, leakiness and with each other was analysed as described in Section 6.2.2. Significant correlations are shown in Table 6-4 and Table 6-5. Average cover is not included as there was no significant correlation with it. The significant correlations to note are FR, FSV and SCV that are correlated with both measures of leakiness (Lcalc and AAL). Likewise FDO, FML and MFM indices are correlated with leakiness. The FML is equivalent to the FSV and MFM measures a similar value to the SCV. FDO is different from the above and measures the rate at which the variance of the image changes up to the First Range.

Table 6-4 Correlation (R^2) between SAVI native scale image variables and variogram indices

All variables	Image Variables			
	Resoln	Cell #	Lcalc	AAL
Lcalc	0.98			
AAL	1.00		0.98	
Nugget Variance (NV)		0.98		
First Range (FR)	1.00		0.96	0.99
First Sill Variance (FSV)	0.99		1.00	0.99
Spatial Correl. Variance (SCV)	1.00		0.97	1.00
N/Sill var. Ratio (NSVR)		0.99		
NSCVR		0.93		
RVF		0.69		
RSF		0.84		
FDO	1.00		0.99	1.00
FML	1.00		0.99	1.00
MFM	0.98		1.00	0.99
AFM		0.90		

Table 6-5 Correlation (R^2) between SAVI native scale variogram indices

All Variables	Variogram Indices									
	Conventional indices						UPV indices			
	NV	FR	FSV	SCV	NSVR	NSCVR	RVF	RSF	FDO	FML
FSV		0.97								
SCV		1.00	0.98							
NSVR	0.96									
NSCVR	0.86				0.97					
RVF						0.90				
RSF					0.89	0.98	0.97			
FDO		0.99	1.00	0.99						
FML		0.99	1.00	0.99					1.00	
MFM		0.96	1.00	0.98					0.99	0.99
AFM	0.81				0.94	1.00	0.93	0.99		

Table 6-5 provides a cross check of the correlations listed above. The significant numbers to note are the high correlation between the FDO, FML and MFM indices and the FR, FSV and SCV.

The pattern of relationships for the four SAVI image variables (resolution, cell number, Lcalc and AAL) with the significantly correlated variance indices are shown in Figure 6.8, Figure 6.9, Figure 6.10 and Figure 6.11.

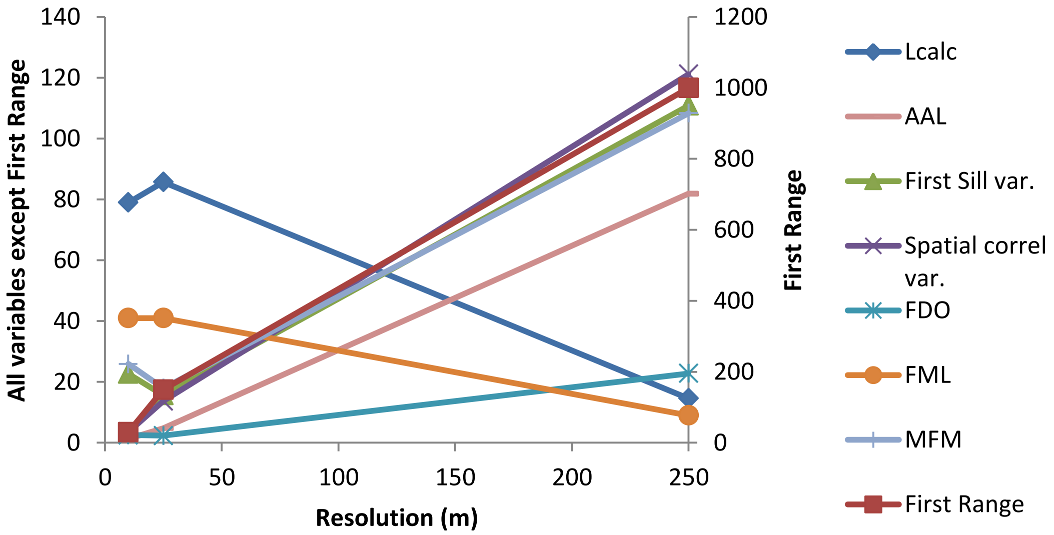

Figure 6.8 Native SAVI semivariance values as a function of resolution.

The FDO, FR and SCV increase consistently with decrease in resolution.

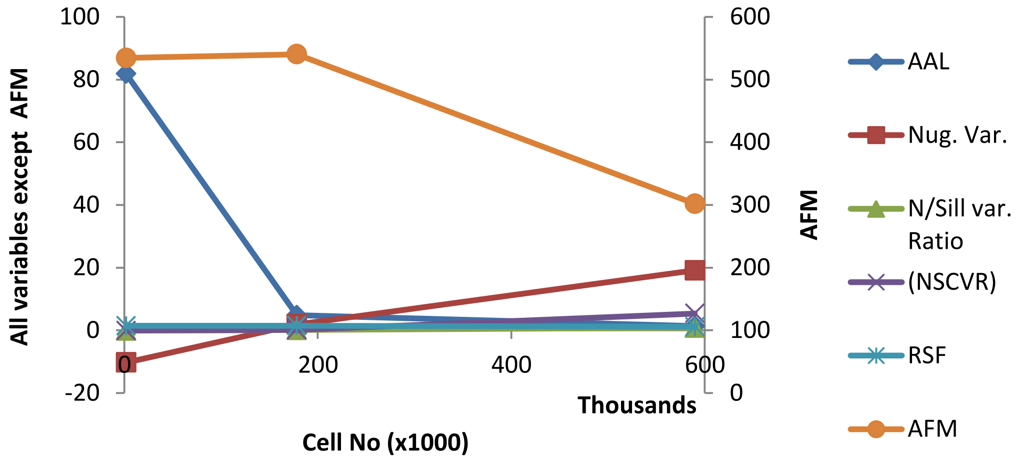

Figure 6.9 Native SAVI semivariance values as a function of cell number

The Nugget Variance increases steadily with cell number.

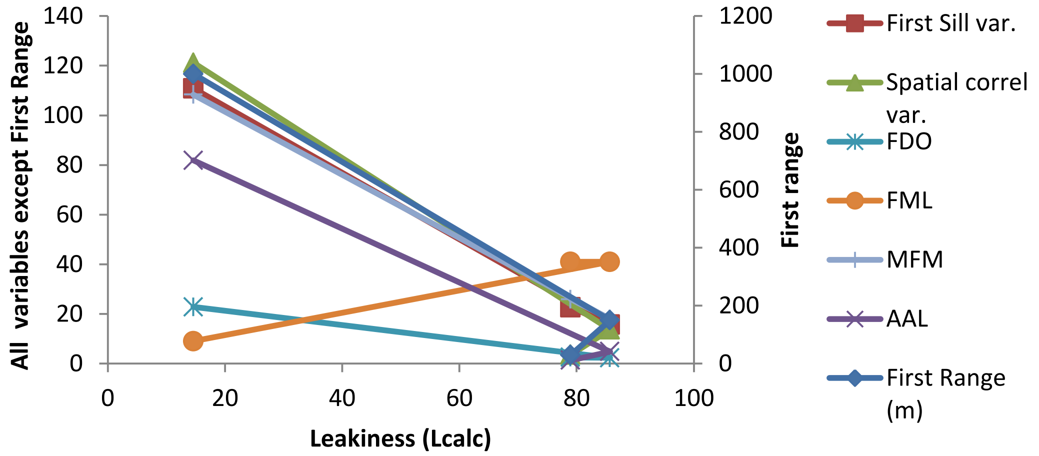

Figure 6.10 Native SAVI semivariance values and Lcalc

The FR and SV decreases with increase in Lcalc.

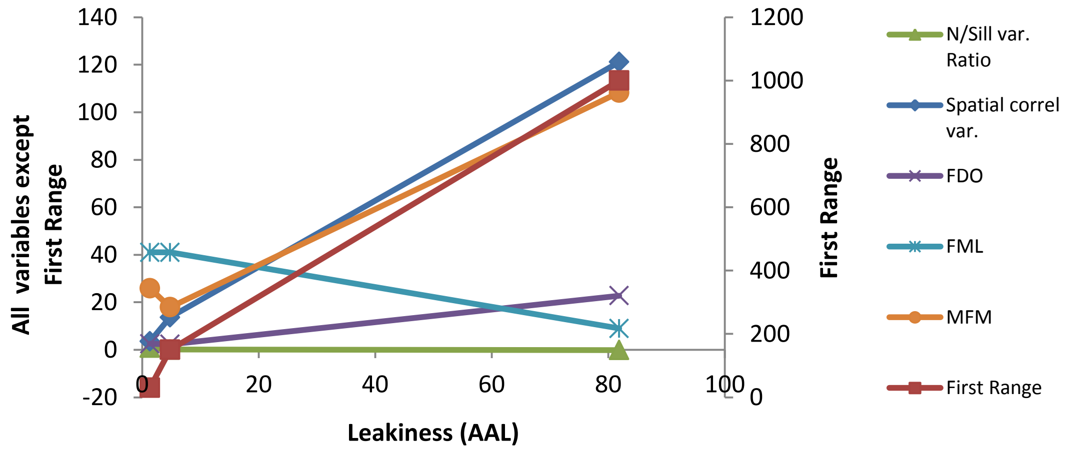

Figure 6.11 Native SAVI semivariance values and AAL

The FDO, FR and SCV increase with AAL. This is similar to their change with resolution.

Summary of SAVI variogram index correlations

The significant observation from these results is the correlation of FDO, FR and SCV with both resolution and AAL. FR provides a measure of the coarseness (range of pixels over which the variance is distributed) of the variance in the image as can be seen by inspection of Figure 2.9 and Figure 2.10. It directly influences the values for FDO and SCV. Both FDO and SCV are 2 similar measures of the slope of the variance before the First Range is reached and are expected to change as the resolution changes. The finding that AAL correlates with the change in these 3 indices indicate a dependency of AAL on the resolution of the image.

6.3.1.2. Stress Related Vegetation Index (STVI)

Variance

The semivariance of STVI vegetation cover images calculated at each of three resolutions over the catchment are shown in Figure 6.12.

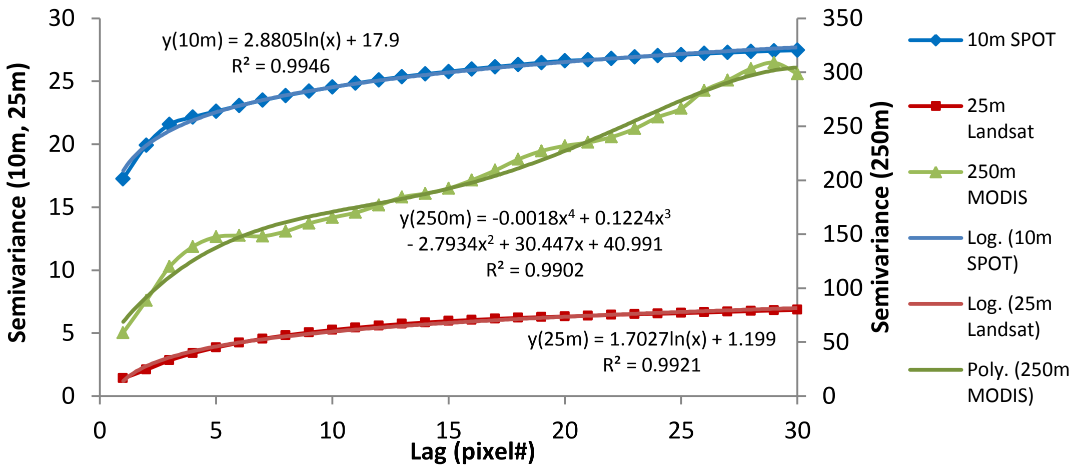

Figure 6.12 STVI semivariance variograms

Similar to the SAVI variogram the 10m and 25m STVI images have natural log variograms while the 250m STVI image has a quartic variogram. The STVI image variance behaves similar to SAVI image variance in that the 10m resolution images both have a FR at lag 3 and 22-23γ. The 25m STVI and SAVI images also have a similar FR at lag 8 but the amount of variance at lag 8 for SAVI is 16γ while for STVI it is much less at 5γ. Variance of the 250m STVI and SAVI images reveals three Ranges, the first at lag 4, the second at lag 29-30 and the third at lag 33-34. The magnitude of the semivariance at each lag is different. The significant difference between these patterns of variance is that 25m STVI has less variance at a given lag than the 250m image.

These differences are reflected in the plots of the interpolated semi-variance contours in Figure 6.13 and as mapped in Figure 6.14. They show the progressive change in the semivariance range values (points of maximum inflection) that accompany changes in image resolution.

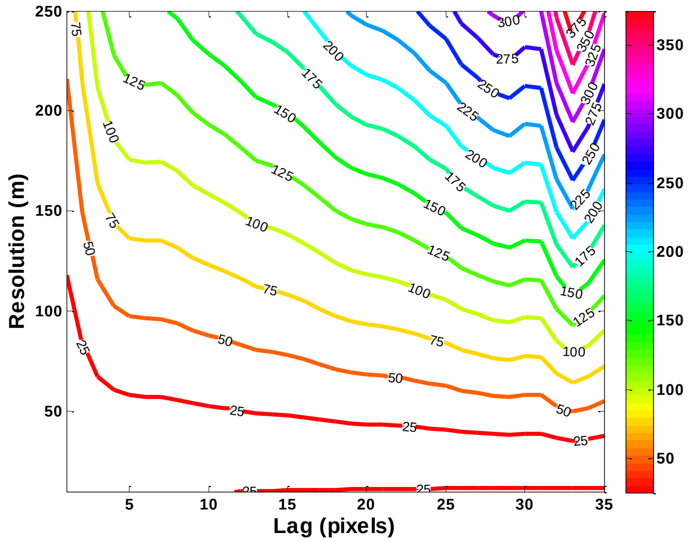

Figure 6.13 STVI native semivariance contours

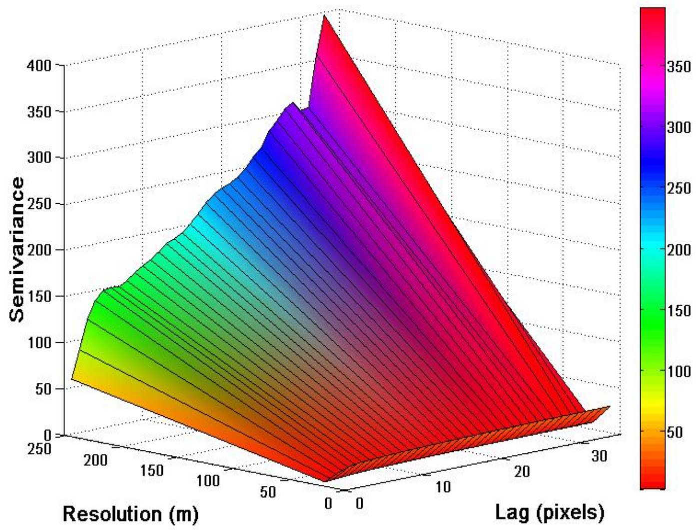

Figure 6.14 STVI native semivariance surface

This surface was modelled as shown in Figure 6.15 by a 2 variable quadratic equation (Equation 6-2). This fitted the variance surface well as shown by the R^2 values in Table 6-6.

$$V_{STVI\ native} = 49.71 - 0.68*x - 2.23*y - 0.01*x^2 + 0.03*x*y + 0.01*y^2 \qquad (6\text{-}2)$$

where V = semivariance, x = lag and y = resolution

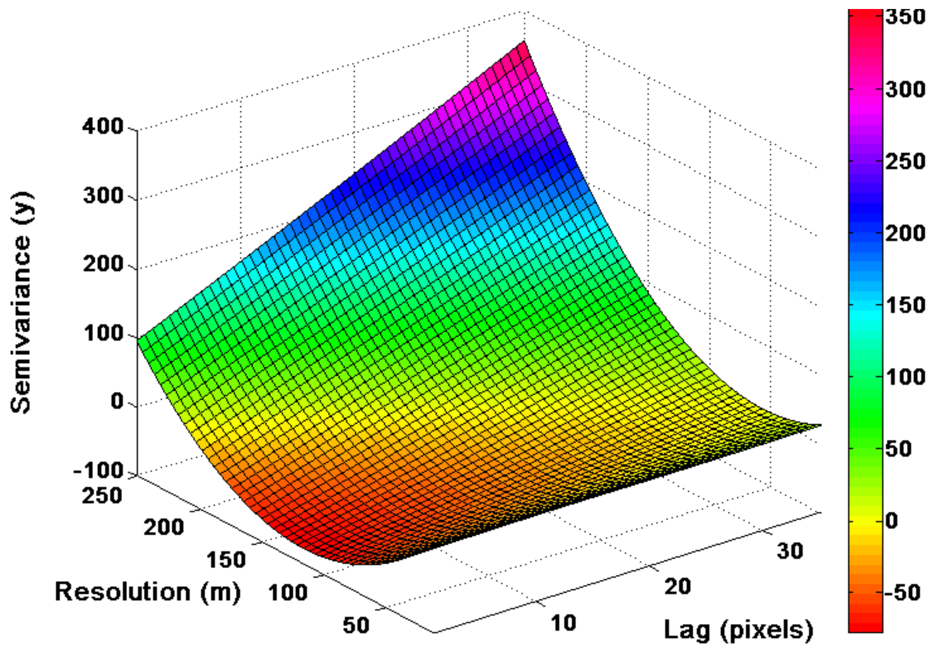

Figure 6.15 STVI native semivariance model

Table 6-6 Equation 6-2 fit parameters

Fit parameters			
SSE	R^2	R^2 Adj	RMSE
10580.00	0.99	0.99	10.34

Variogram Indices

The STVI semivariance contour plot (Figure 6.13) is generally similar to the SAVI semi-variance contour plot (Figure 6.5). Minor differences were detected in the conventional indices and UPV indices as shown in Table 6-7 and Table 6-8. The FSV values (Table 6-7) are similar to the MFM values (Table 6-8) as with SAVI. Further discussion of these indices is provided in Section 6.4).

Table 6-7 Conventional Variogram indices for STVI cover images

Image resolution	Conventional variogram index values					
	NV	FR (m)	FSV	SCV	NSVR	NSCVR
10m	15.44	40	22.15	6.71	0.70	2.30
25m	0.78	125	3.86	3.08	0.20	0.25
250m	23.43	1250	147.38	123.95	0.16	0.19

Table 6-8 UPV Variogram Indices for STVI cover images

Image resolution	UPV variogram indices.					
	RVF	RSF	FDO	FML	MFM	AFM
10m	1.65	1.15	2.66	41.00	25.79	361.93
25m	5.50	1.50	0.70	41.00	5.88	182.21
250m	3.26	1.51	29.97	29.00	198.64	3994.24

Index correlation with leakiness

The significant correlations between the variogram indices and image variables are shown in Table 6-9. The correlation of these values with cover layer values and with each other was again analysed as described in Section 6.2.2. Average cover was included as it showed significant correlation.

Table 6-9 Correlation (R^2) between STVI native scale Image variables and all variables

All Variables	Image Variables				
	Resoln	Cell #	Cover%	Lcalc	AAL
Cover	0.95				
Lcalc	0.95		1.00		
FR	1.00		0.95	0.94	
FSV	0.97		1.00	1.00	
SCV	0.99		0.98	0.98	
NSVR		0.95			
NSCVR		0.93			
RVF					0.99
RSF		0.93			
FDO	0.99		0.99	0.99	
FML	1.00		0.97	0.97	
MFM	0.98		1.00	0.99	
AFM	0.99		0.99	0.98	

Table 6-10 Correlation (R^2) between STVI native scale variogram indices

All Variables	Variogram Indices							
	Conventional Indices				UPV Indices			
	FR	FSV	SCV	NSVR	NSCVR	FDO	FML	MFM
FSV	0.97							
SCV	0.99	0.99						
NSCVR				1.00				
RSF				1.00	1.00			
FDO	0.98	1.00	1.00					
FML	1.00	0.99	1.00			1.00		
MFM	0.98	1.00	1.00			1.00	0.99	
AFM	0.99	0.99	1.00			1.00	1.00	1.00

FR, FSV and SCV are correlated with Lcalc, as they were for SAVI cover but not with AAL as they were for SAVI. However, they were correlated with the amount of cover, which they were not correlated with for SAVI cover. FDO, FML and MFM continued to show high correlation with Lcalc, but not AAL. They mirrored FR, FSV and SCV in that they had high correlation with amount of cover.Table 6-10 provides a cross check of the correlations listed above. The significant correlations to note are the FR, FSV and SCV with FDO, FML and MFM.

The patterns of relationship for the five STVI image variables (resolution, cell number, average cover Lcalc and AAL) with the significantly correlated variance indices are shown in Figure 6.16, Figure 6.17, Figure 6.18, Figure 6.19, and Figure 6.20.

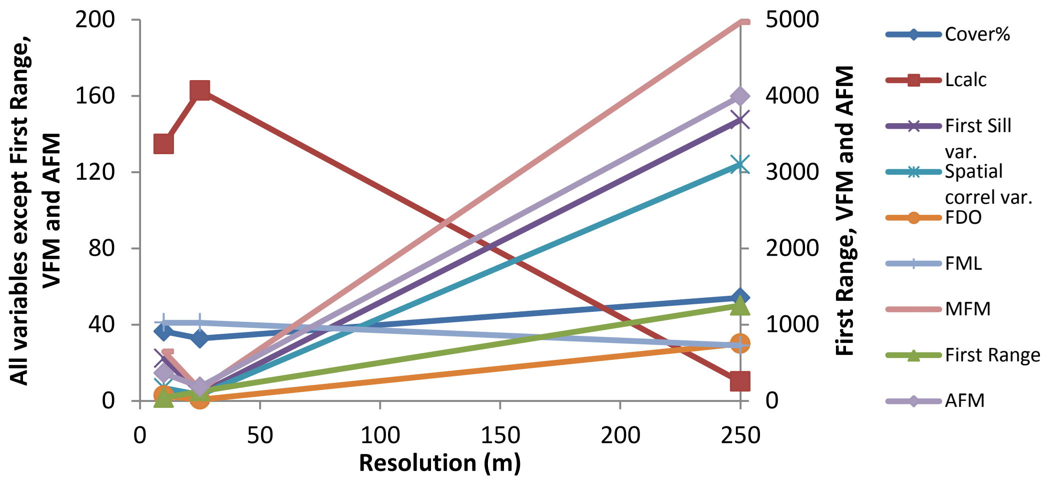

Figure 6.16 Native STVI semivariance index response to resolution.

The FDO, FR and SCV increase in a near linear manner with decrease in resolution as was the case with SAVI coverage.

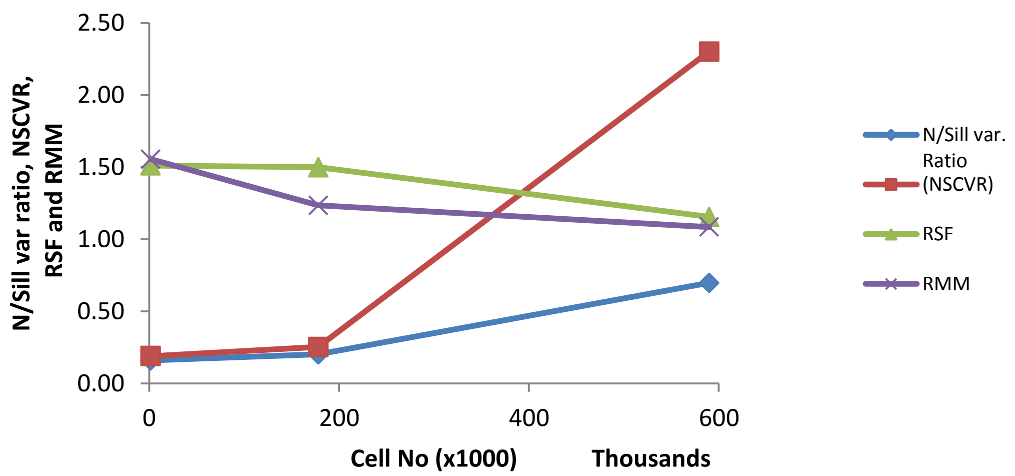

Figure 6.17 Native STVI semivariance index response to catchment cell number.

The NSVR increased generally linearly with Cell No while RSF and RMM decreased.

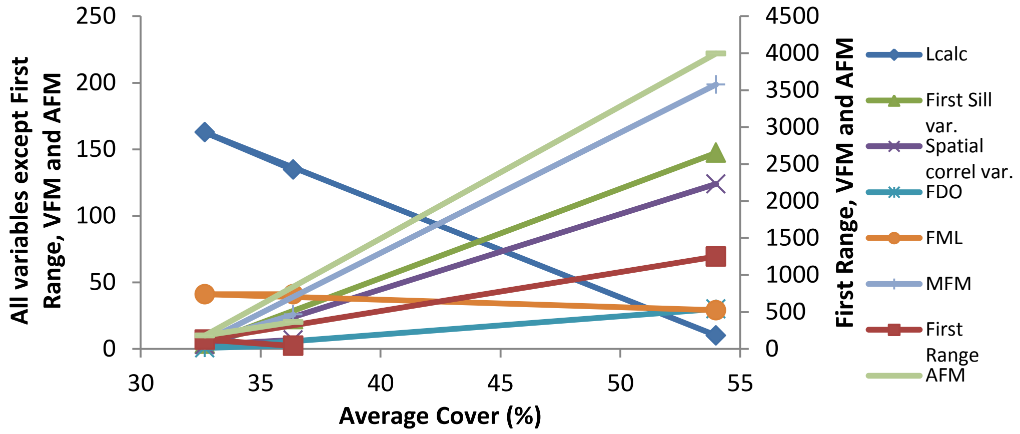

Figure 6.18 Native SAVI semivariance index response to average cover.

There is no clear pattern of relationships with Cover in this graph (The appearance of a number of linear relationships in the graph is misleading in that tabular data shows the values to be non-linear).

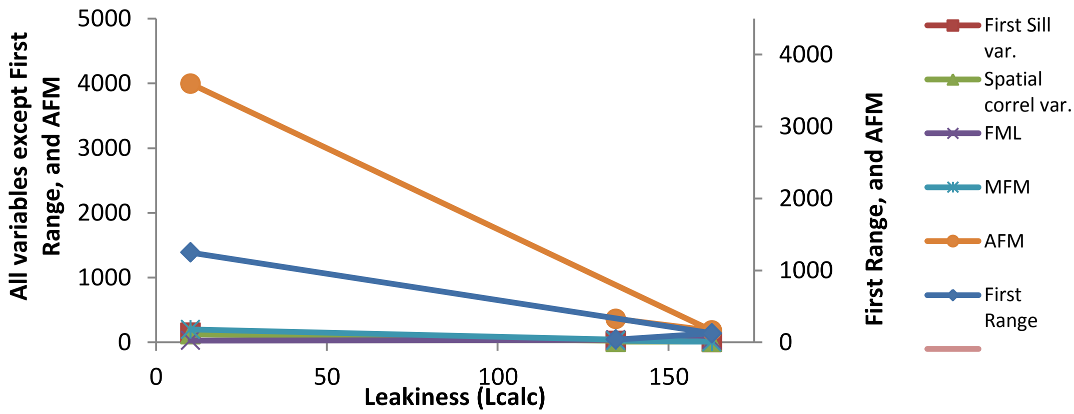

Figure 6.19 Native STVI semivariance index response to Lcalc

There is no clear pattern of relationships with Leakiness (Lcalc) in this graph (The appearance of a number of linear relationships in the graph is misleading in that tabular data shows the values to be non-linear).

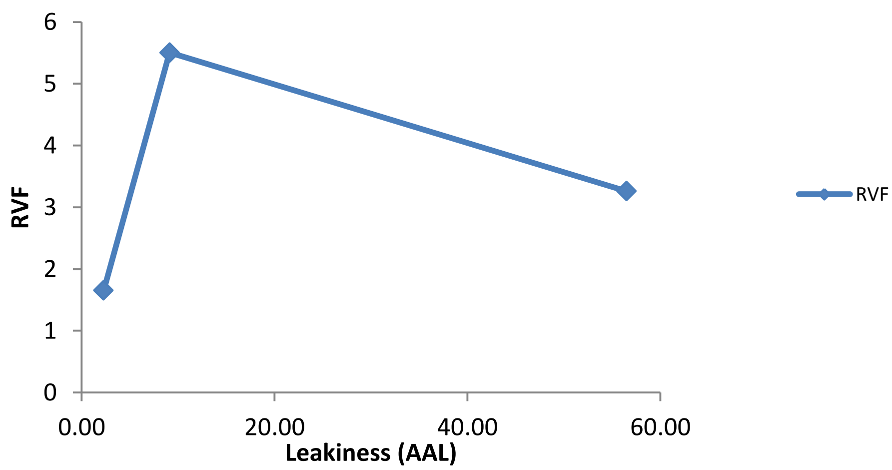

Figure 6.20 Native STVI semivariance index response to AAL

Summary of STVI variogram index correlations

STVI variance behaved differently from SAVI variance in that it did not exhibited any significant relationship between AAL and resolution. The correlation between Cover and Lcalc with Resolution was non-linear.

6.3.1.3. Perpendicular Distance (red/green) Index (PDrg)

Variance

The semivariance of PDrg vegetation cover images calculated at each of three resolutions over the catchment are shown in Figure 6.21.

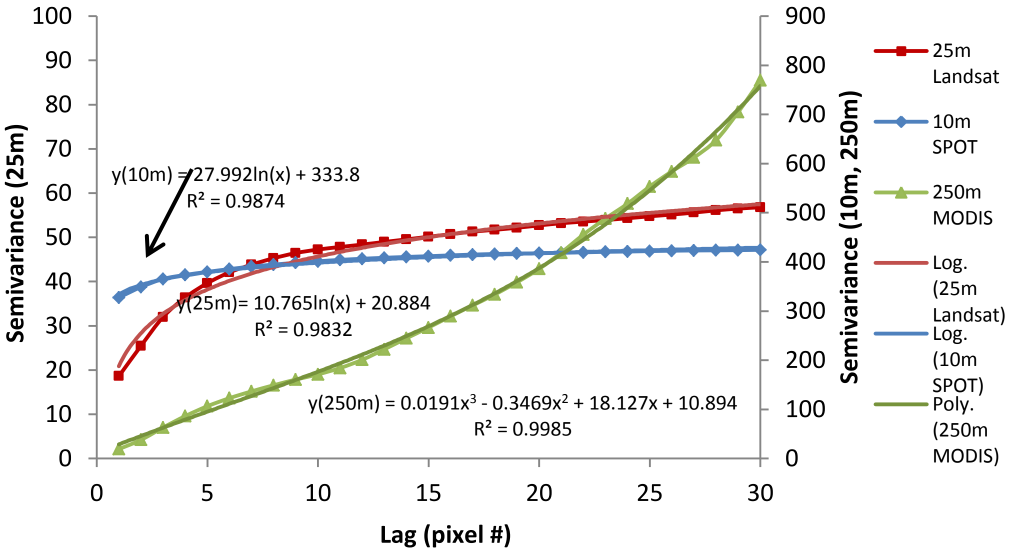

Figure 6.21 PDrg semivariance variograms

The 10m and 25m images have natural log variograms while the 250m image has a cubic variogram. The PDrg image variogram is very different in form from the SAVI and STVI image variograms. These differences include; i) the 10m and 25m resolution images have similar FR lags of 6 pixels with a semivariance of 45γ for both resolutions compared to the SAVI and STVI images which have different FR lags and semivariances for the 10m and 25m images, ii) the 250m PDrg variogram showed less distinction in Ranges than the SAVI and STVI images. The PDrg image was similar to the SAVI and STVI images in that the 250m resolution variance was much higher than the 10m and 25m resolution variance at all lags.

The PDrg vegetation cover variance was interpolated and plotted as contours in Figure 6.22 and mapped as a surface in Figure 6.23. This shows the change in semivariance ranges (points of maximum inflection) that accompany changes in image resolution.

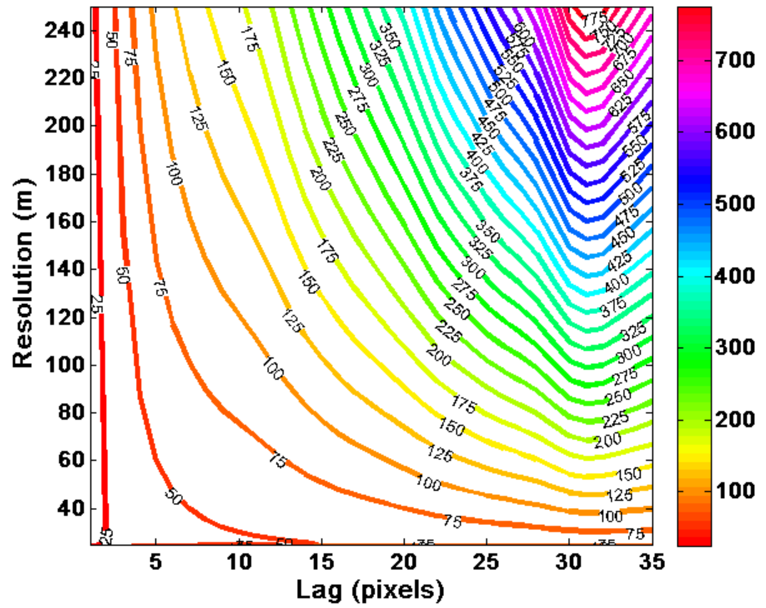

Figure 6.22 PDrg native semivariance contours

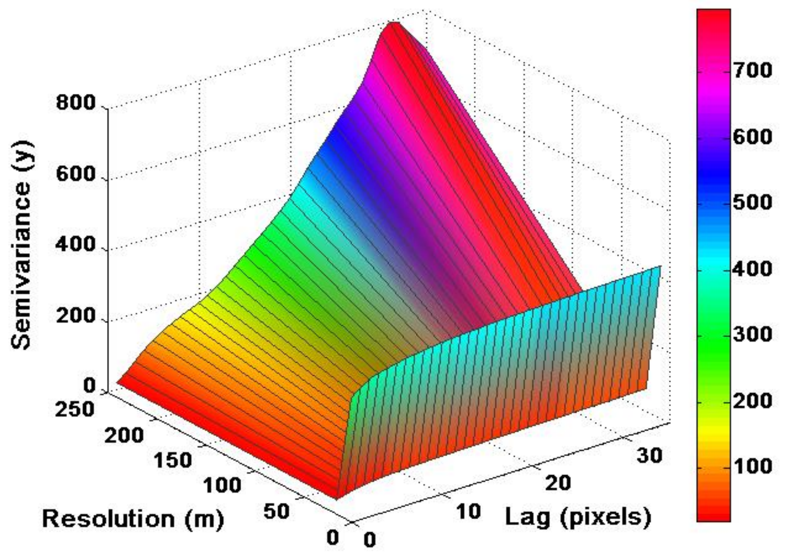

Figure 6.23 PDrg native semivariance surface

The model that fitted the variance surface the best was a 2-variable quadratic equation (Equation 6-3).

$$V_{\text{PDrg native}}=-994.30 + 89.88*x + 826*y + 2.48*x2 + 107.40*x*y + 1283*y2 \quad (6\text{-}3)$$

where V = semivariance, x = lag and y = resolution

Table 6-11 Equation 6-3 fit parameters

Fit parameters			
SSE	R^2	R^2 Adj	RMSE
89590.00	0.98	0.98	30.08

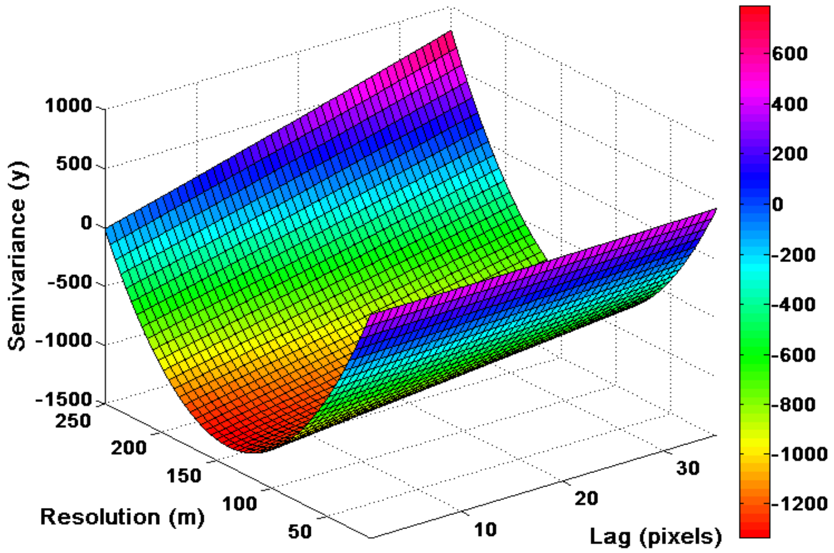

Figure 6.24 PDrg native semivariance model

Variogram indices

The difference in PDrg variograms from the SAVI and STVI variograms leads to different index values as shown in Table 6-12 and Table 6-13 (yellow highlighted values).

Table 6-12 Conventional Variogram indices for PDrg cover images

Image resolution	Conventional variogram index values					
	NV	FR (m)	FSV	SCV	NSVR	NSCVR
10m	314.63	40	373.53	58.90	0.84	5.34
25m	11.55	150	42.08	30.53	0.27	0.38
250m	15.20	1500	106.35	91.15	0.14	0.17

Table 6-13 UPV Variogram Indices for PDrg cover images

Image resolution	PDrg UPV variogram indices.								
	Varian	RVF	RSF	FDO	FML	MFM	VFM	AFM	RMM
10m	0.39	1.36	1.07	21.33	41.00	409.77	514.67	3649.49	1.05
25m	0.04	3.30	1.37	6.85	41.00	50.70	85.53	1312.86	1.19
250m	0.22	14.88	1.99	18.83	31.00	335.43	49184.70	9437.76	2.37

Index correlation with leakiness

Both groups of indices were analysed for correlation with resolution, catchment cell number, average cover, Lcalc and AAL as well as with each other. Significant correlations are highlighted in Table 6-14 and Table 6-15.

Table 6-14 Correlation between PDrg native scale image variables and all variables (R^2)

All Variables	Image variables				
	Resoln	Cell #	Cover%	Lcalc	AAL
Lcalc		0.85			
AAL	1.00				
NV		0.91		0.99	
FR	1.00				0.99
FSV				0.99	
SCV			1.00		
NSVR		0.99		0.92	
NSCVR		0.93		0.98	
RVF	0.99				0.98
RSF	0.93				0.89
FDO	0.09				
FML	1.00				1.00
AFM	0.89		0.94		0.93

The points to note from this table, by comparison with the similar tables for SAVI and STVI, are that FR and FML are the only indices that have a high correlation in common with either Lcalc or AAL between all 3 tables and thus all three types of cover. FML is comparable to SV at the FR (FSV) and this is common to Lcalc across all 3 types of cover. It represents the position at which the semivariogram stabilises or at which the granularity of the image is defined. This represents the average size of the principal structures or patterns of the image and their separation from each other (Balaguer and Ruiz *et al.* 2010).

Table 6-15 provides a cross check of the correlations listed above. The only significant correlation, common to the SAVI and STVI images is FR and FML as identified above.

Table 6-15 Correlation (R^2) between PDrg native scale variogram indices and all variables

All Variables	Image variables							
	NV	FR	FSV	SCV	NSVR	RVF	RSF	FML
FSV.	0.97							
NSVR	0.96		0.87					
NSCVR	1.00		0.95		0.98			
RVF		1.00						
RSF		0.93				0.96		
FDO								
FML		1.00				0.98	0.90	
MFM								
AFM		0.88		0.96		0.84		0.92

The patterns of relationship for the five PDrg image variables (resolution, cell number, average cover, Lcalc and AAL) with the significantly correlated variogram indices are shown in Figure 6.25, Figure 6.26, Figure 6.27, Figure 6.28 and Figure 6.29.

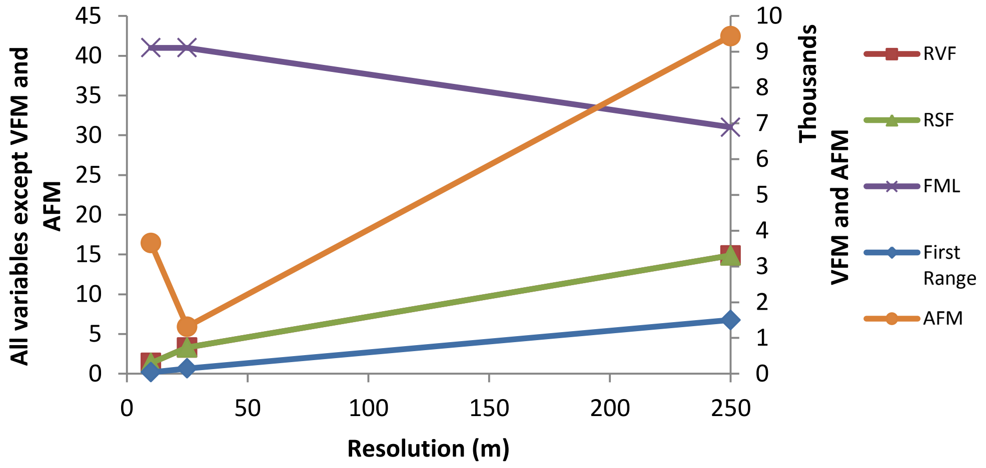

Figure 6.25 Native PDrg semivariance indices as a function of resolution.

The RSF, RVF and FR increase consistently with decrease in resolution. Only FR is common to the other cover images.

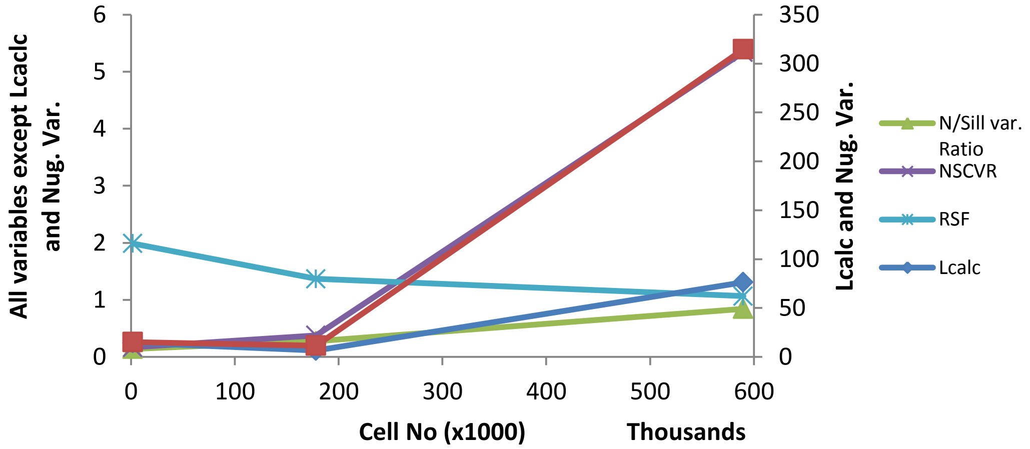

Figure 6.26 Native PDrg semivariance indices as a function of catchment cell No.

NSVR increases linearly with increase in cell number. This is common with STVI cover but not SAVI cover.

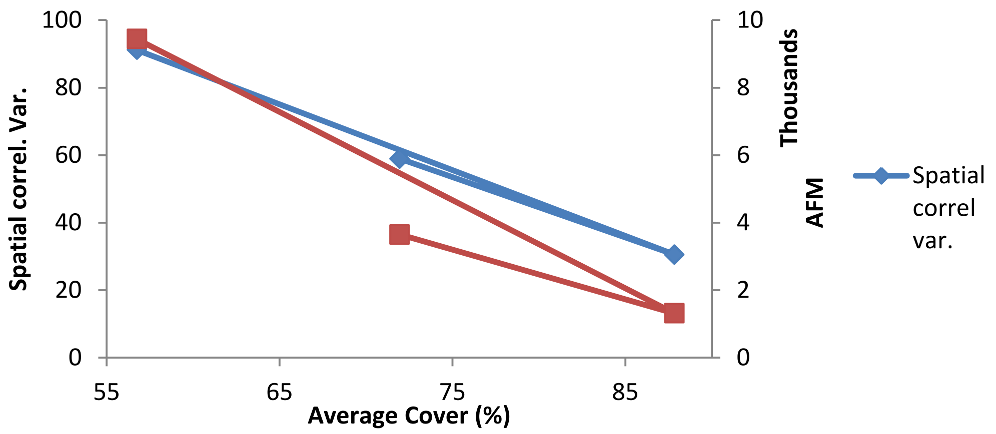

Figure 6.27 Native PDrg semivariance indices as a function of average cover

There is no clear pattern of relationship of either index with Cover in this graph.

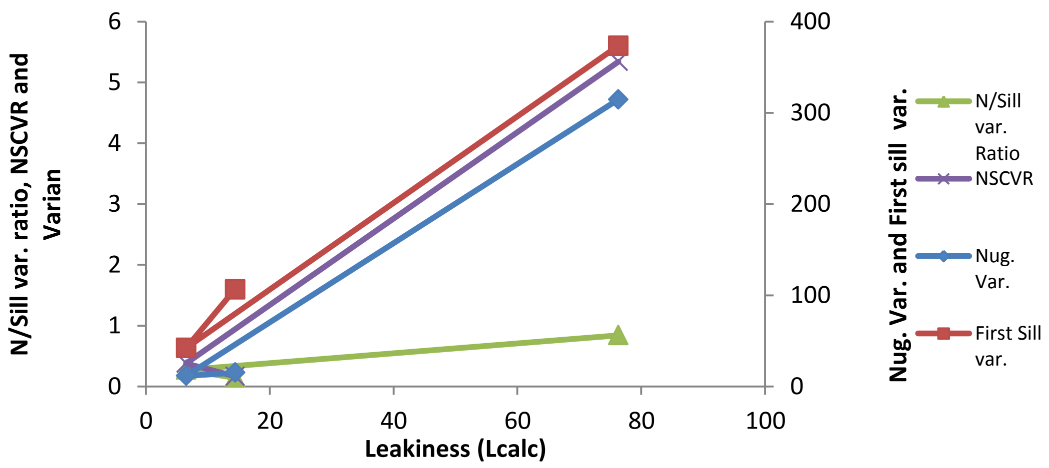

Figure 6.28 Native PDrg semivariance indices response to Lcalc.

Unlike SAVI and STVI, Lcalc increases with all 3 correlating PDrg indices whereas it decreased before. There is no clear correlation in this Figure.

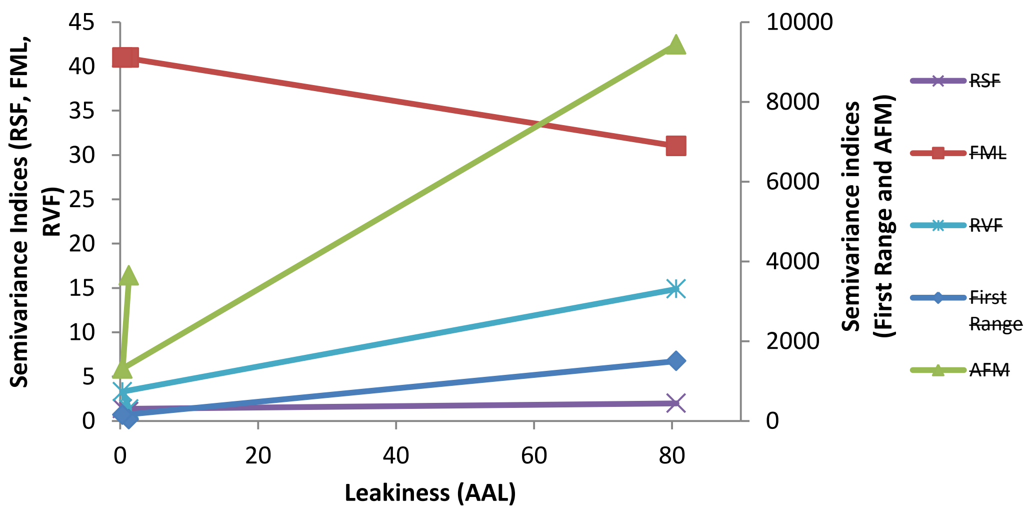

Figure 6.29 Native PDrg semivariance indices` response to AAL

FML and FR had a high correlation with AAL but did not show a consistent response with AAL. (The above graph lines for FML and FR are linear reflexive).

Summary of PDrg variogram index correlations

The FDO, FR and SCV indices did not correlate significantly with AAL as they did for SAVI cover

6.3.1.4. Summary of all 3 native image variogram index correlations

This analysis has failed to disclose any variogram indices that behave consistently across all three types of cover and all three resolutions. Particular indices have consistent relationships with resolution within a particular type of cover indicating consistent structural relationships across resolutions within a specific cover type. However, the way in which different vegetation indices analyse the cover in an image appears to preclude consistency of structural relationship across cover types.

6.3.1.5. DEMs

Variance

DEMs were included in the variance analysis because they provide the hydraulic head values for the flow aggregation equation in the Leakiness Calculator. The semivariance of the DEMs was calculated for the experimental catchment at three resolutions, 10m, 25m and 250m (Figure 6.30). The DEMs used for this analysis were the foundation DEMs used in the LI calculations (see Section 4.2.1.1).

DEMs are generated from point data and not from charged coupled devices that respond to aggregate radiance data from a support base. Because they do not have a support structure (the solid angle of the radiance), they exhibit a different spatial variance pattern from pixel-based images. This is reflected in the unbounded structure of their variograms. That is, their variance tends to increase linearly with distance from the origin for relatively small areas such as the experimental catchment.

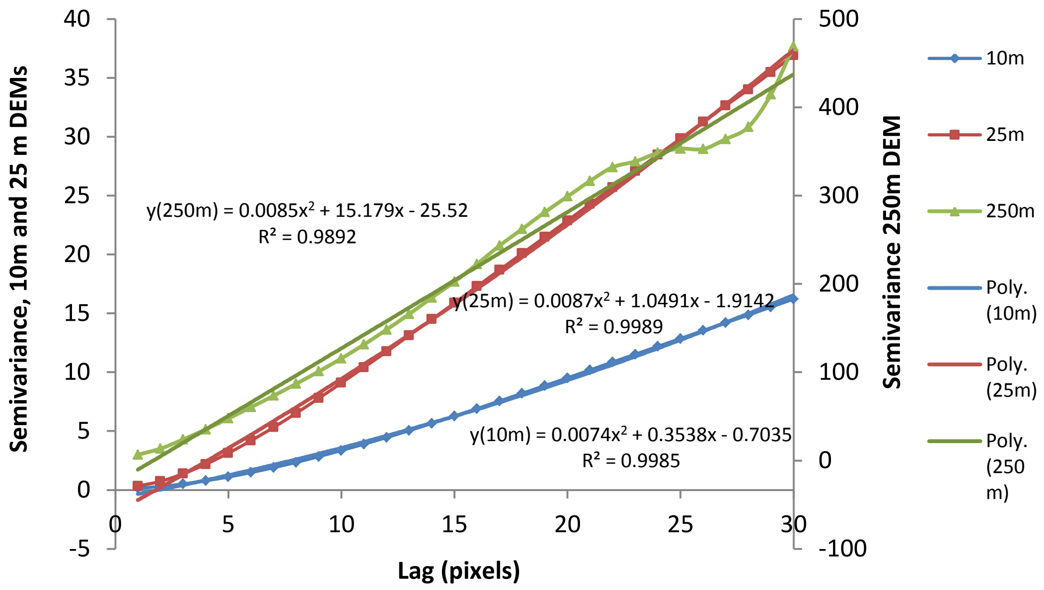

Figure 6.30 Semivariance of whole-of-catchment DEMs

The graph shows that DEM semivariance of the catchment increases with decrease in resolution for a given lag except at high lag values for the 250m DEM. This part of the pattern is similar to the pattern for cover images.

The semivariance contours for the DEM of the catchment are plotted in Figure 6.31 and the surface created by these is mapped in Figure 6.32.

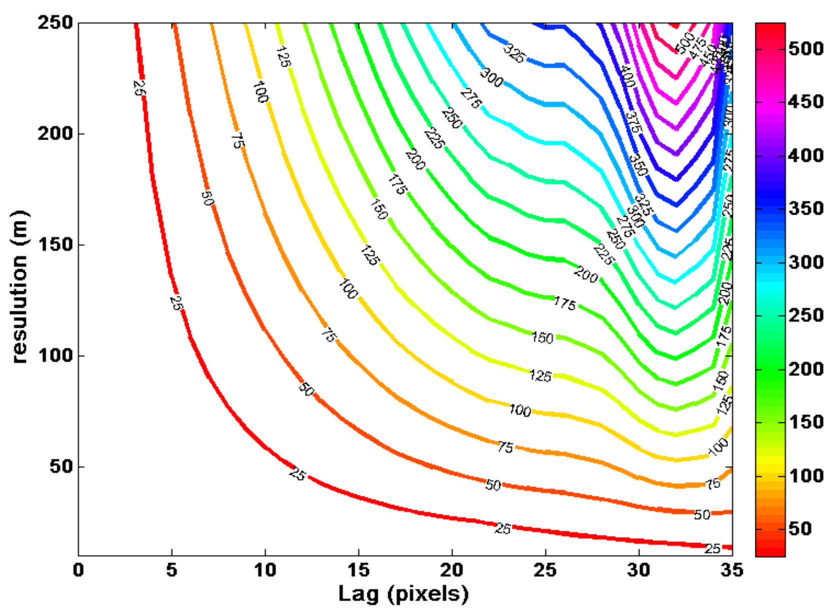

Figure 6.31 Raw DEM semivariance contours

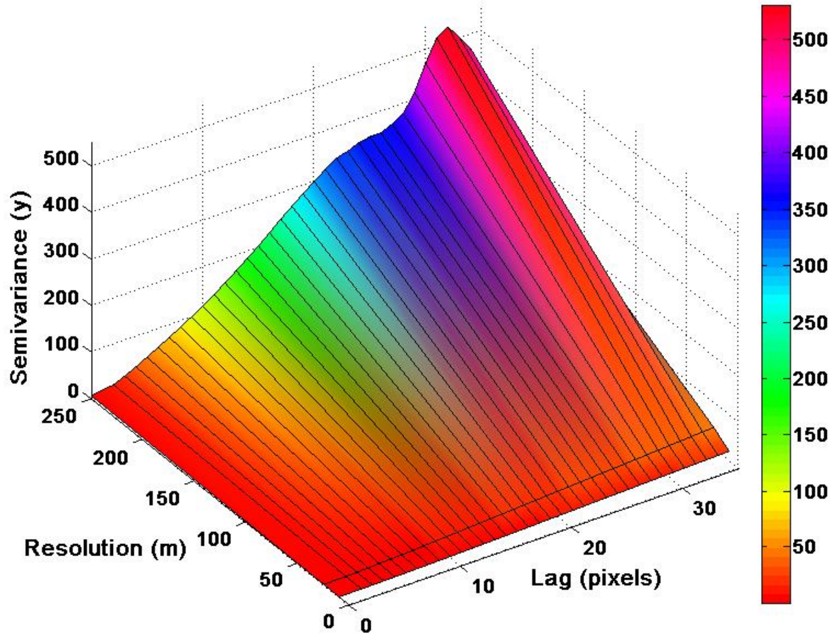

Figure 6.32 Native DEM semivariance surface

The surface was modelled, Figure 6.33, as a 2-variable quadratic equation (Equation 6-4). This fitted the variance surface well as shown by the R^2 values in Table 6-16.

$$V_{DEM\ native} = -1.15 + 0.53*x - 0.32*y - 0.02*x^2 + 0.06*x*y + 0.00*y^2 \qquad (6\text{-}4)$$

where V = semivariance, x = lag and y = resolution

Table 6-16 Equation 6-4 fit parameters

Fit parameters			
SSE	R^2	R^2 Adj	RMSE
44400.00	0.98	0.98	21.18

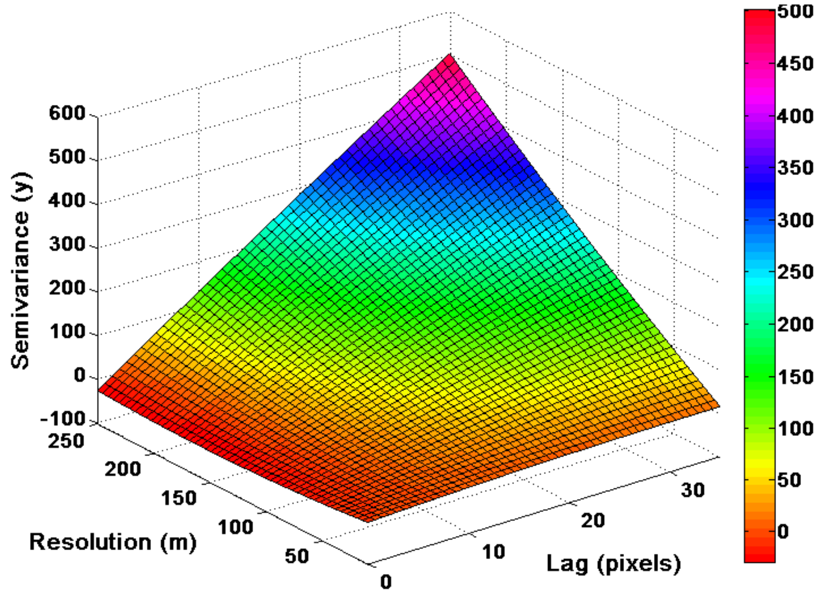

Figure 6.33 Native DEM semivariance model

Variogram indices

The DEM surface and semivariance contour plots (Figure 6.31 and Figure 6.33) differed from the surface and contour plots of image semivariograms because of the unbounded nature of the DEM semivariograms. Conventional indices cannot be calculated because of the unbounded nature of such semivariograms. The UPV indices generated by Fetex 2.0 are given in Table 6-17.

Table 6-17 UPV Variogram Indices for catchment DEM

Image resolution	DEM UPV variogram indices.								
	Varian	RVF	RSF	FDO	FML	MFM	VFM	AFM	RMM
10m	0.00	1974.08	1.88	0.14	41.00	10.60	53.26	416.88	2.19
25m	0.00	833.08	2.19	0.40	41.00	24.74	261.10	974.73	2.13
250m	0.00	30.34	2.08	7.02	32.00	231.80	22563.71	6953.58	2.29

Index correlation with leakiness

These indices were analysed for correlation with native resolution and catchment cell number of the DEMs. Significant correlations are shown in Table 6-18.

Table 6-18 Correlation (R^2) of DEM variables

All variables	DEM variables		Variogram indices			
	Resoln	Cell No.	FDO	FML	MFM	VFM
RVF		0.98				
FDO	1.00					
FML	1.00		1.00			
MFM	1.00		1.00	1.00		
VFM	1.00		1.00	1.00	1.00	
AFM	1.00		1.00	0.99	1.00	1.00
RMM	0.80		0.82	0.84	0.80	0.84

The patterns of relationship for the two DEM variables (resolution and cell number) with the significantly correlated variance indices are shown in Figure 6.34 and Figure 6.35.

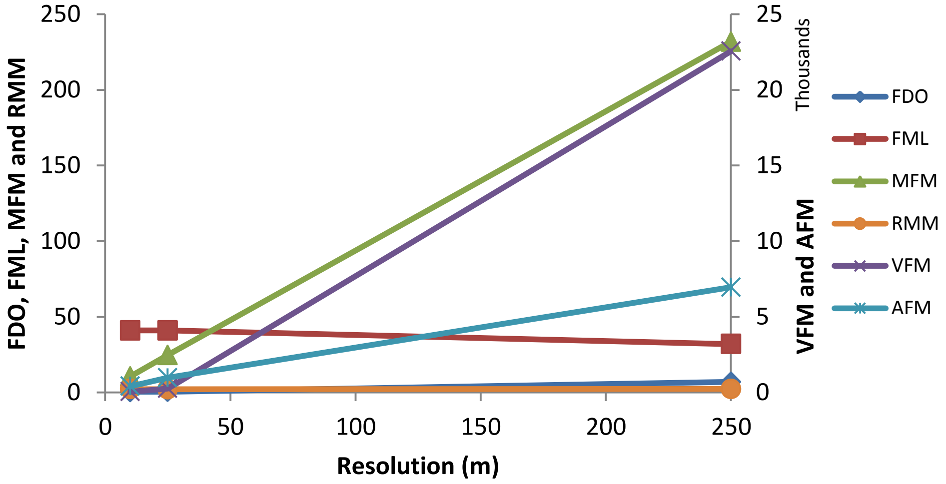

Figure 6.34 DEM semivariance values as a function of resolution

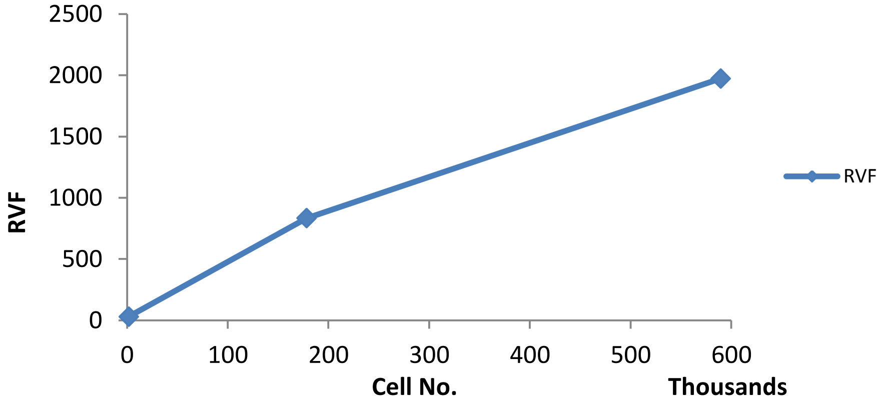

Figure 6.35 DEM semivariance values as a function of catchment cell number

Effect of resolution and lag

The relationship of the semivariance with resolution for 7 fixed Lag intervals is shown in Figure 6.36 (based on semivariance data underlying Figure 6.30. Lag 35 and Lag 40 have been omitted because at 250m resolution there were inadequate cells to compute the semivariance at 35 and 40 pixel intervals in all directions).

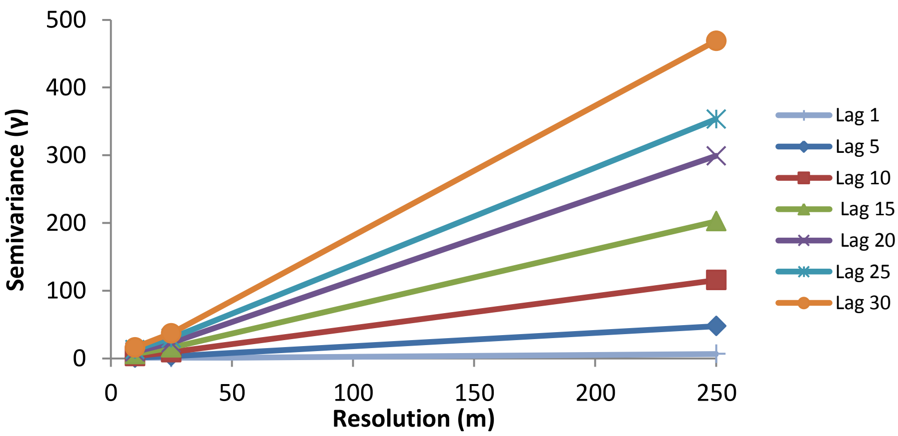

Figure 6.36 Lag Semivariance relationship with resolution (DEM, native)

The relationship of the lag semivariance as a function of resolution (Table 6-19) was recorded from the straight-line equations in Figure 6.36. They document the increase in slope with increase in lag.

Table 6-19 Semivariance resolution expressions for native DEMs

Lag #	Semivariance (γ)
1	y = 0.027x - 0.2228
5	y = 0.1956x - 1.2902
10	y = 0.4705x - 1.9897
15	y = 0.8226x - 3.2773
20	y = 1.2154x - 4.9931
25	y = 1.4265x - 3.537
30	y = 1.9012x - 6.577

where y = semivariance and

x = resolution in meters

The relationships in Table 6-19 represent a matrix for the native DEMs of the catchment that define in general how their elevation varies with change in lag and resolution (Appendix 23). This matrix is shown as a contour plot in Figure 6.37 and as a 3D surface map in Figure 6.38.

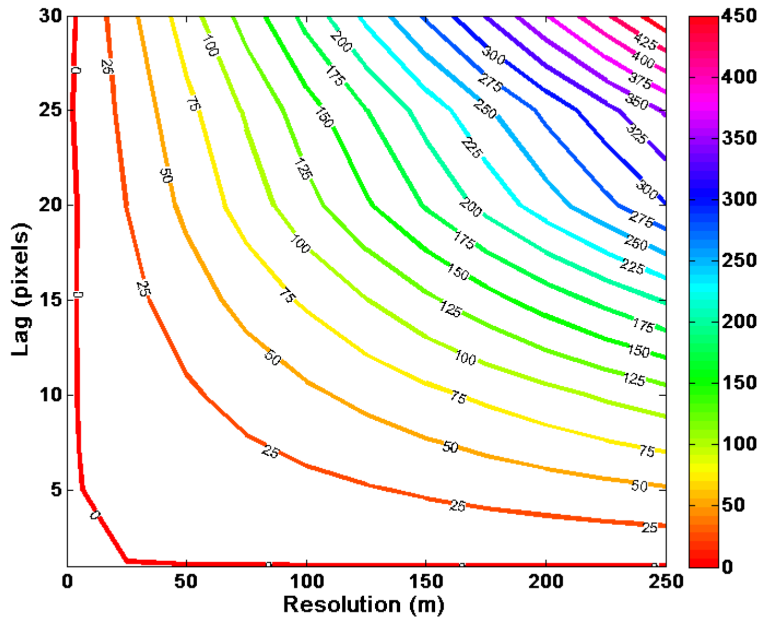

Figure 6.37 Native DEM semivariance contour pattern

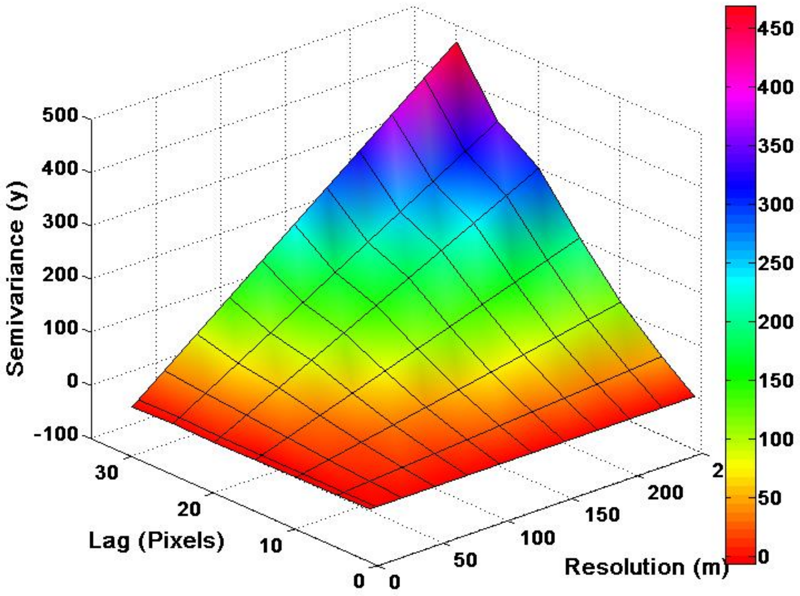

Figure 6.38 Relationship of native DEM semivariance to lag and resolution

The surface was modelled, Figure 6.39, as a 2-variable quadratic equation (Equation 6-5). This fitted the variance surface well as shown by the R^2 values in Table 6-20.

$$V_{\text{DEM native}} = 6.68 - 0.12*x - 1.69*y - 0.00*x^2 + 0.07*x*y + 0.05*y^2 \qquad (6\text{-}5)$$

where V = semivariance, x = lag and y = resolution

Table 6-20 Equation 6-5 fit parameters

Fit parameters			
SSE	R^2	R^2 Adj	RMSE
3086.00	1.00	1.00	6.29

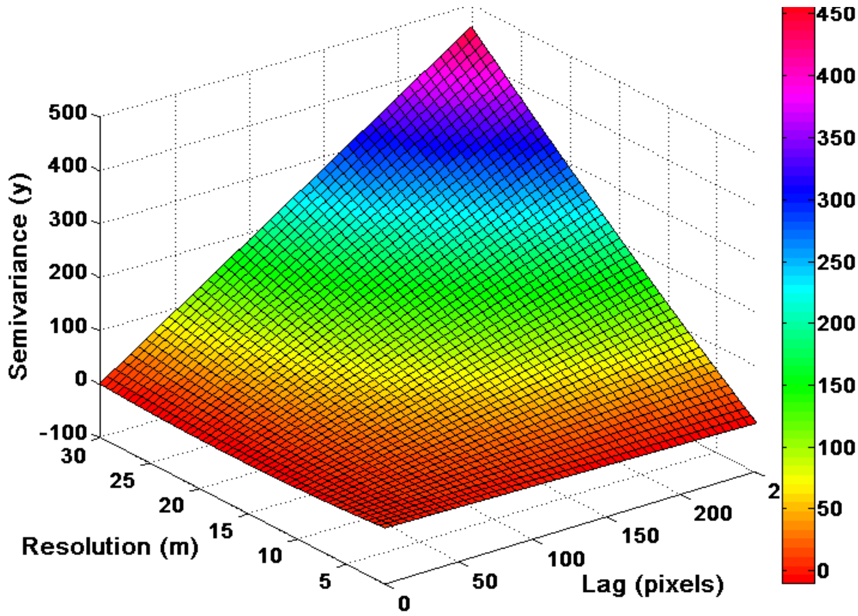

Figure 6.39 Revised native DEM semivariance model

The differences between the raw DEM and generalised DEM semivariance contour plots can be seen in a side-by-side comparison in Figure 6.40. The model smooths the effect of range on DEM variance.

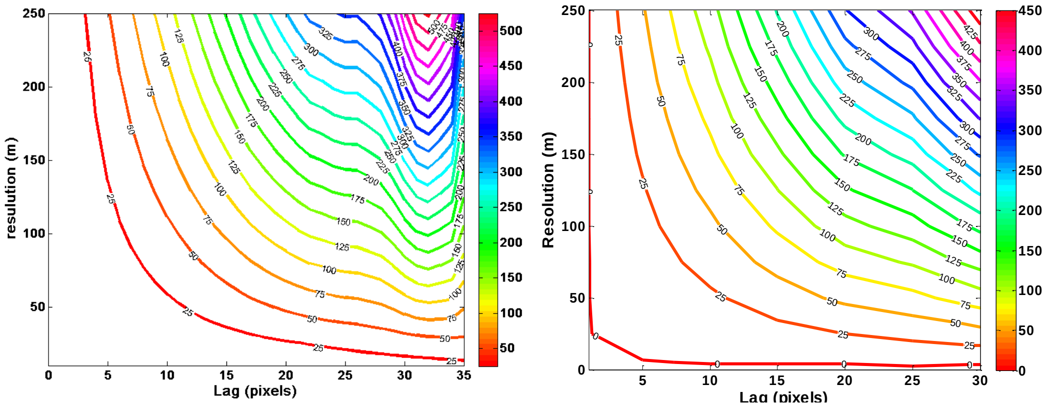

Figure 6.40 Comparison of raw DEM semivariance (left) with modelled DEM semivariance (right)

Sub-catchments

The semivariance for each of the sub-catchment DEMs at each resolution was investigated to confirm the behaviour of the whole-of-catchment variograms. These are shown in Figure 6.41, Figure 6.42 and Figure 6.43. They confirm the whole-of-catchment analysis pattern (unbounded) as shown in Figure 6.30. However, the elevation semivariance differs by catchment size and the sub-catchments rank differently for each resolution.

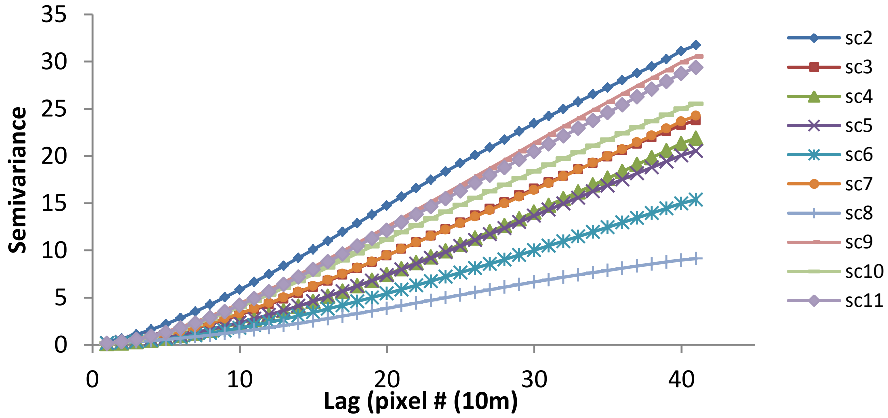

Figure 6.41 Semivariance of sub-catchments in the 10m DEM

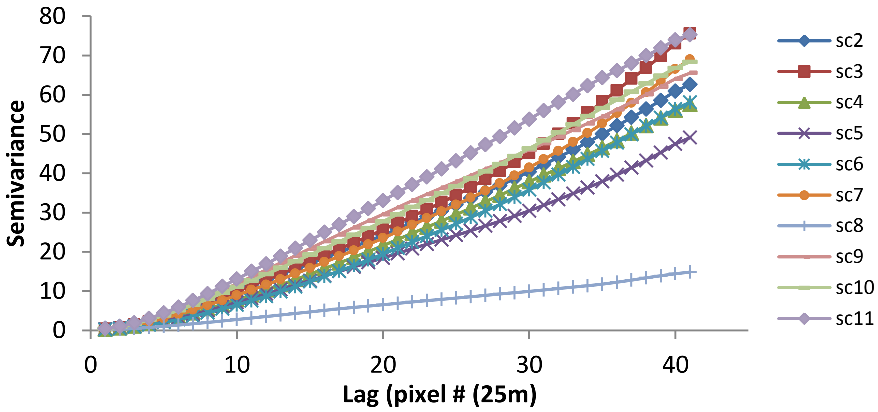

Figure 6.42 Semivariance of sub-catchments in the 25m DEM

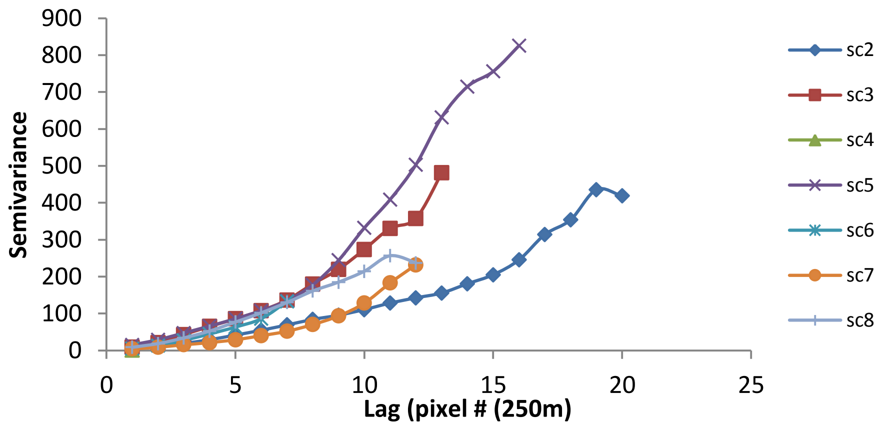

Figure 6.43 Semivariance of sub-catchments in the 250m DEM

Comparison of Figure 6.41, Figure 6.42 and Figure 6.43 shows that the sub-catchment DEMs rank in different variance order at different resolutions despite covering similar geographical areas. For example, sub-catchment 8 had the lowest variance (most even elevation) at both resolutions while sub-catchment 2 that had the highest variance at all lags at 10m resolution, an intermediate variance at 25 m resolution and had one of the lowest variances at 250m resolution.

6.3.2. Upscaled Images

The 10m resolution image of the experimental catchment was progressively resampled from 10m to 250m pixel resolution and then analysed to generate the thematic vegetation cover layers (SAVI, STVI and PDrg) and processed in preparation for analysis in the LC. The following sections present the results of the variance analysis of these images as used for catchment leakiness calculation.

6.3.2.1. Soil Adjusted Vegetation Index (SAVI)

Variance

The semivariance of the SAVI image, as used in the LC, was analysed using Fetex 2. (Section 6.2). The semivariograms for each resampled SAVI image for the whole catchment are shown in Figure 6.44 (10-30m resolution) and Figure 6.45 (50-250m resolution).

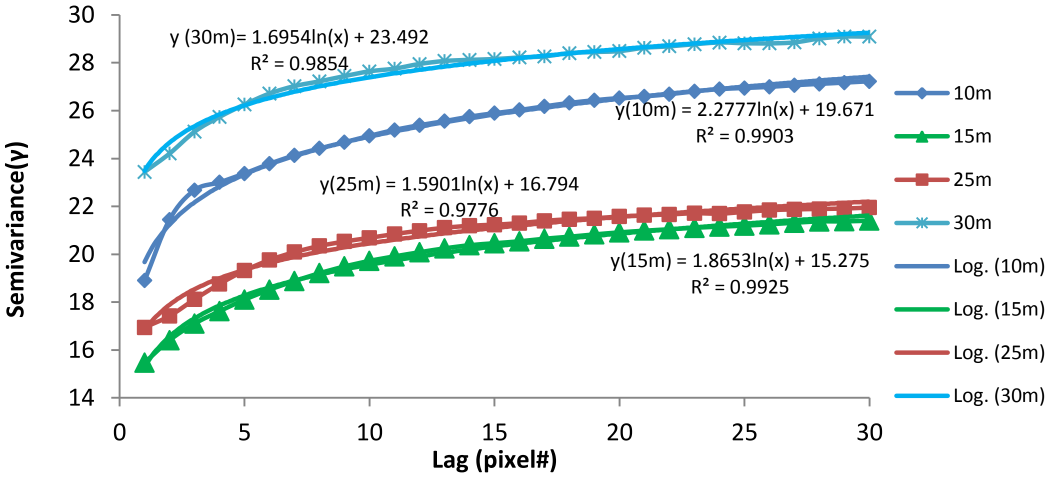

Figure 6.44 Semivariance of resampled SAVI (10m - 30m)

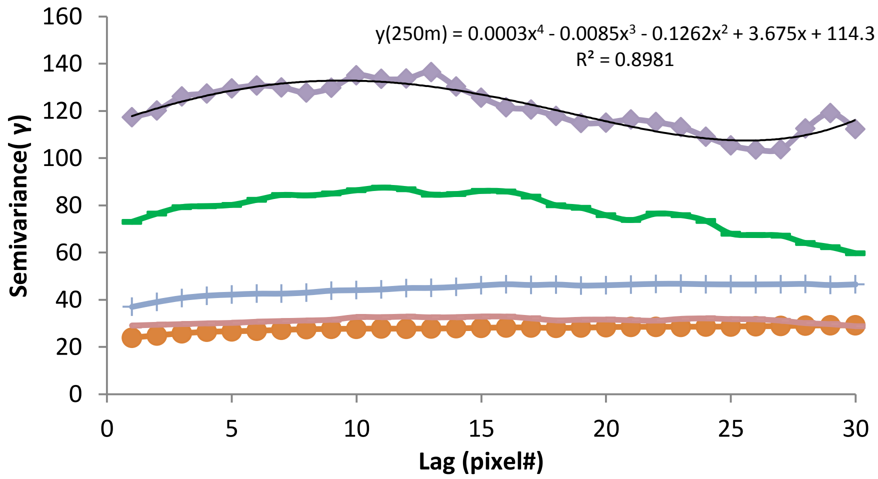

Figure 6.45 Semivariance of resampled SAVI (50-250m)

Variograms for less than 30m upscale images are all natural log variograms and the 250m upscale variogram has a quartic form (fourth degree polynomial) as shown in the above Figures. Quartic functions have infinite limits and can have multiple local maxima and minima (Gullberg 1997). The behaviour of the 250m variogram in Figure 6.45 is consistent with this in exhibiting both a maximum and minimum within the range of 0-30 pixels.

The form of the upscale variograms between 50-200m was not calculated, as there was no evidence of structure at these resolutions. Figure 6.44 and Figure 6.45 show that the semivariance initially decreases with resampling (from 10m to 15m resolution) and then increases with further decrease in resolution and the ordered structure of the image decays with progressive resampling from 3m to 250m resolution.

The change in semivariance of SAVI vegetation cover with progressive upscaling is interpolated and plotted as contours in Figure 6.46 and Figure 6.47 and mapped as a surface in Figure 6.48. This shows the change in semivariance ranges (points of maximum inflection) that accompany changes in image resolution.

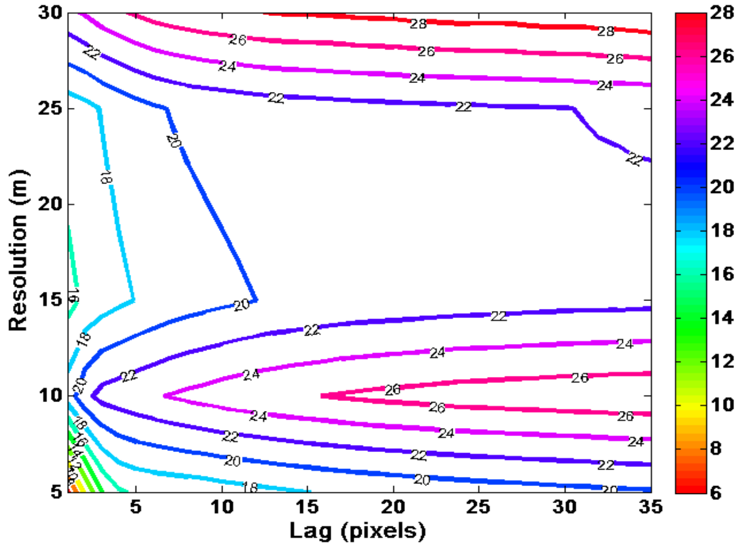

Figure 6.46 Contour plot upscaled SAVI semivariance (5-30m)

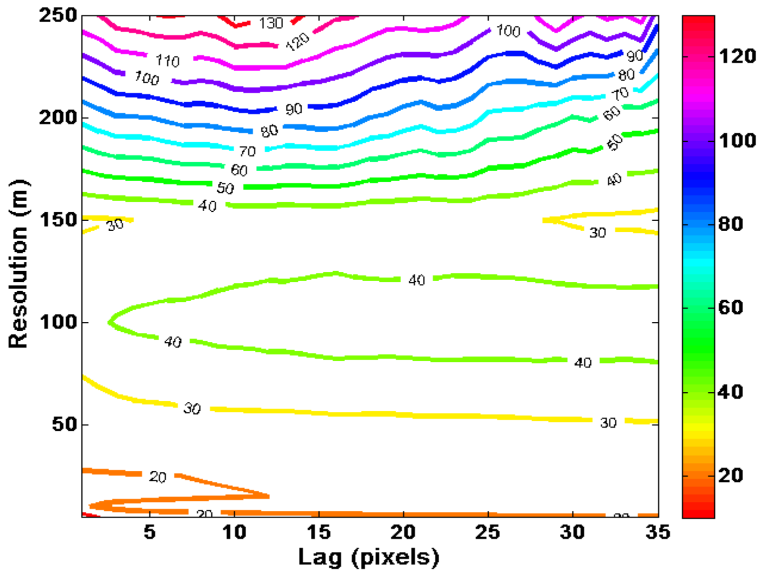

Figure 6.47 Contour plot upscaled SAVI semivariance (5-250m)

The surface was modelled (Figure 6.49) as a 2-variable quadratic equation (Equation 6-6). This provided a good fit to the variance surface as shown by the R^2 value in Table 6-21.

$$V_{SAVIupsc} = 16.84 + 0.85*x - 0.0805*y - 0.016*x^2 - 0.0040*x*y + 0.002*y^2 \quad (6\text{-}6)$$

where V = semivariance, x = lag and y = resolution

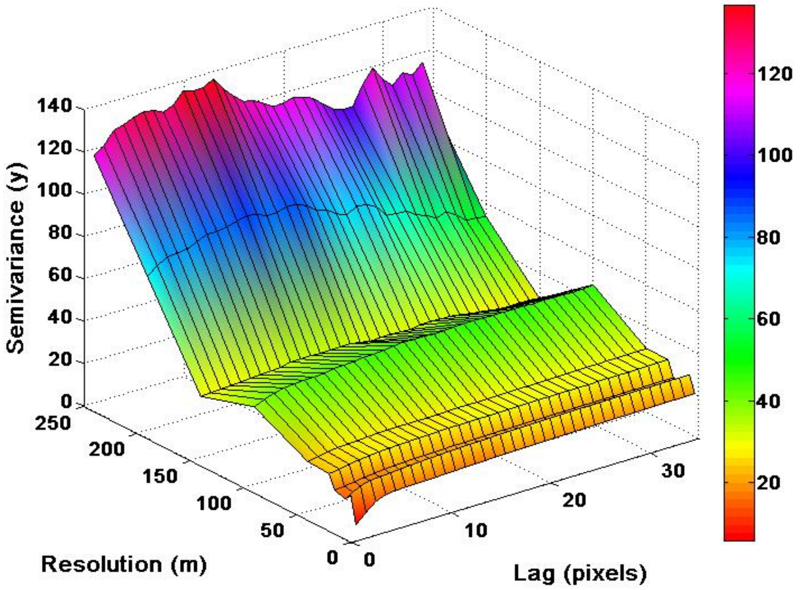

Figure 6.48 SAVI upscaled semivariance

Table 6-21 Equation 6-6 fit parameters

Fit parameters			
SSE	**R^2**	**R^2 Adj**	**RMSE**
2.67E+04	0.9204	0.9192	8.812

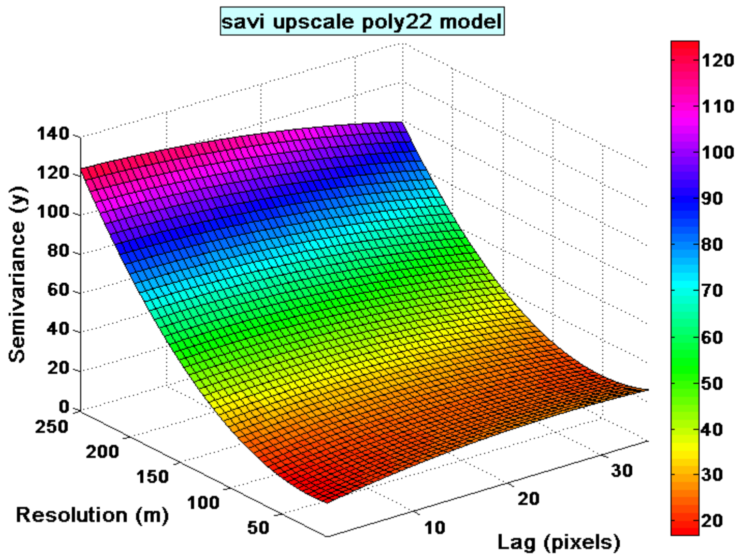

Figure 6.49 SAVI upscale semivariance model

Variogram indices

Conventional and UPV indices were extracted (as described in Section 6.2.2) and shown in Table 6-22 and Table 6-23.

Table 6-22 Conventional SAVI semivariogram indices for upscaled images

Image resolution (m)	SAVI conventional variogram indices					
	NV	FR (m)	FSV	SCV	NSRV	NSCVR
10	16.90	30	22.68	5.78	0.75	2.92
15	14.62	80	18.46	3.84	0.79	3.81
25	15.88	150	19.76	3.88	0.80	4.09
30	22.23	180	26.72	4.49	0.83	4.95
50	22.64	200	26.41	3.77	0.86	6.01
100	34.73	400	41.73	7.00	0.83	4.96
150	28.43	1500	32.67	4.24	0.87	6.71
200	70.44	1200	82.33	11.89	0.86	5.92
250	111.93	1500	130.71	18.78	0.86	5.96

Table 6-23 UPV SAVI semivariogram indices for sub-catchments

Image resolution (m)	SAVI UPV variogram indices.								
	Varian	RVF	RSF	FDO	FML	MFM	VFM	AFM	RMM
10	1.86	1.65	1.15	2.66	41.00	25.79	5.71	361.99	1.09
15	1.37	1.37	1.06	0.95	38.00	20.18	2.36	194.07	1.07
25	1.37	1.25	1.03	0.48	35.00	20.95	1.78	154.47	1.06
30	1.79	1.18	1.03	0.77	24.00	27.40	2.07	115.79	1.05
50	1.74	1.13	1.04	0.95	16.00	27.03	1.40	70.91	1.05
100	2.60	1.11	1.06	2.06	16.00	43.08	6.21	129.64	1.08
150	1.88	1.00	1.01	0.30	12.00	30.92	1.57	49.02	1.06
200	4.83	1.04	1.05	3.45	11.00	81.69	17.71	160.87	1.07
250	7.54	1.04	1.02	2.93	6.00	125.21	23.75	158.15	1.04

Index correlation with leakiness

Both groups of indices were analysed for correlation with upscaled catchment cell number, average cover and leakiness as well as with each other. Significant correlations are shown in Table 6-24.

Table 6-24 Correlation between SAVI upscale image variables and all variables (R^2)

All variables	Image Variables				Variogram Indices					
	Resoln (m)	Cell No	Avg. cover	Lcalc	AAL	NV	FSV	SCV	NSVR	RVF
Lcalc		0.97								
AAL	0.85		0.88							
NV	0.85				0.81					
FR	0.89									
FSV	0.83				0.82	0.99				
SCV		0.98		0.93						
NSVR		0.82		0.90						
RVF		1.00		0.97				0.99	0.84	
RSF		0.99		0.93				0.99		0.99
MFM	0.82				0.82	0.98	1.00			
AFM		0.81		0.87					0.87	0.80

The correlation between variogram indices is ascribed to them being based on a number of common measurement parameters. The pattern of relationships for the three SAVI image variables (resolution, cell number and leakiness) with the significantly correlated variance indices are shown in Figure 6.50, Figure 6.51, Figure 6.52, Figure 6.53 and Figure 6.54.

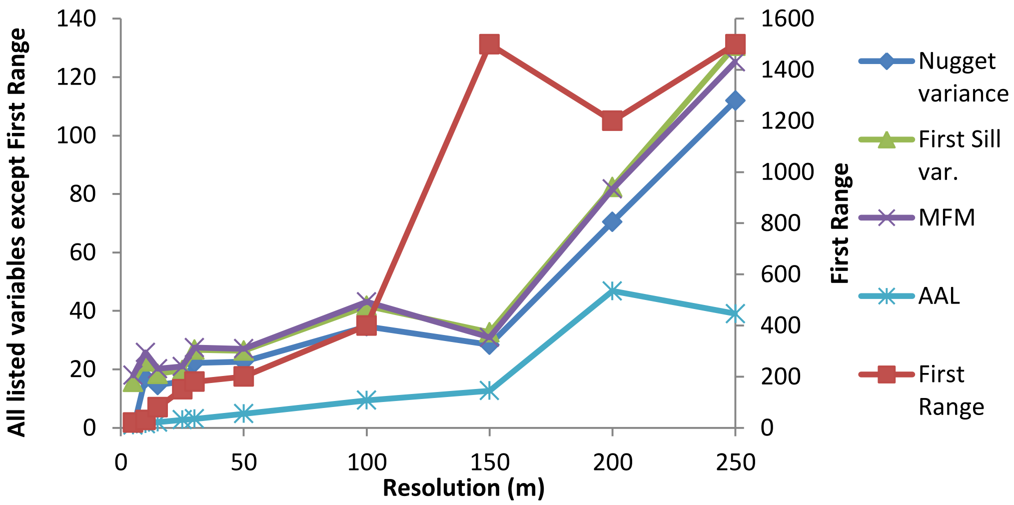

Figure 6.50 SAVI upscale semivariance values as a function of resolution

There is a general increase in the value of NV, FSV and MFM variogram indices as well as with AAL, with decrease in resolution however, it is not uniform. This may be due to features merging to different extents at different upscaling resolutions.

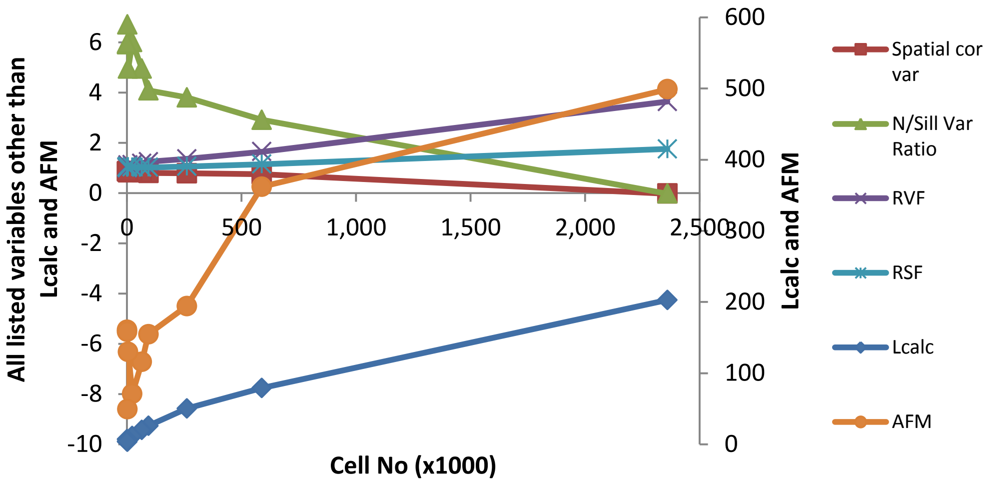

Figure 6.51 SAVI upscale semivariance values as a function of cell number

The main feature in this figure is the increase in Lcalc with increase in Cell No. as explained in Section 4.2.3.

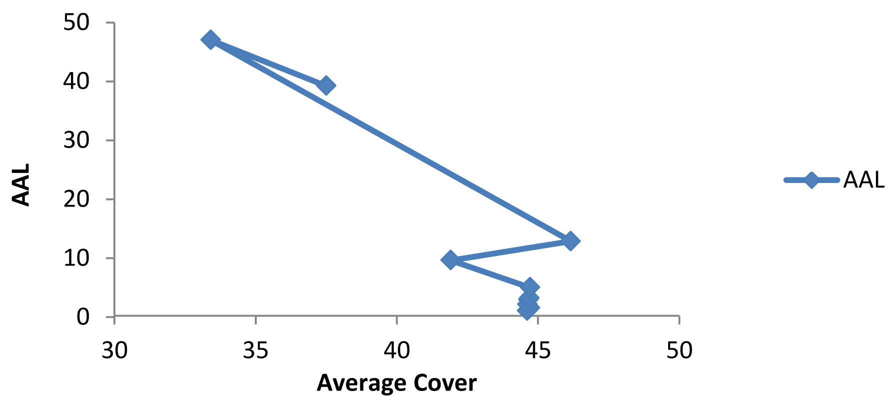

Figure 6.52 SAVI upscale semivariance relationship with Average Cover

As would be expected an increase in average cover was accompanied by a decrease in AAL, however it was not regular as would be expected. This irregularity is thought to be due to aggregation of cover in different spatial locations as resampling occurs relative to the flow paths in the catchment.

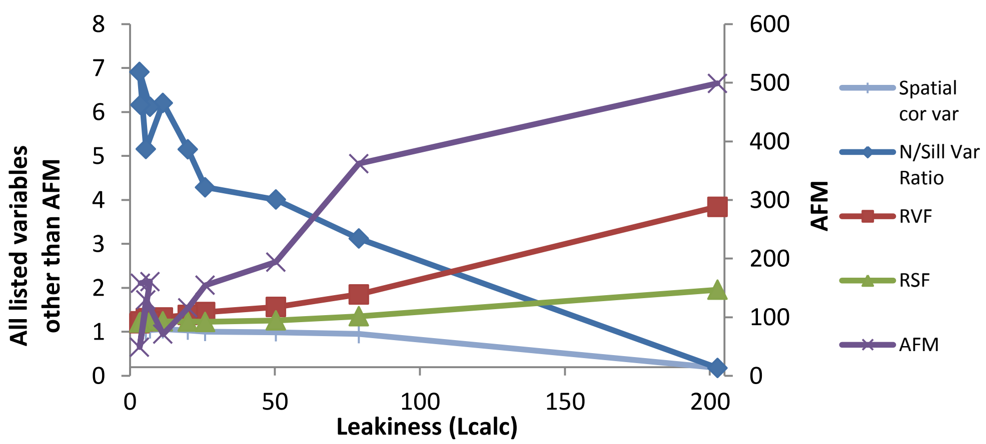

Figure 6.53 SAVI upscale semivariance values relationship with Lcalc

The NSVR decreased with increase in Lcalc in a generally linear manner but with irregularities. The RVF and RSF increased regularly as Lcalc increased while the SCV decreased regularly.

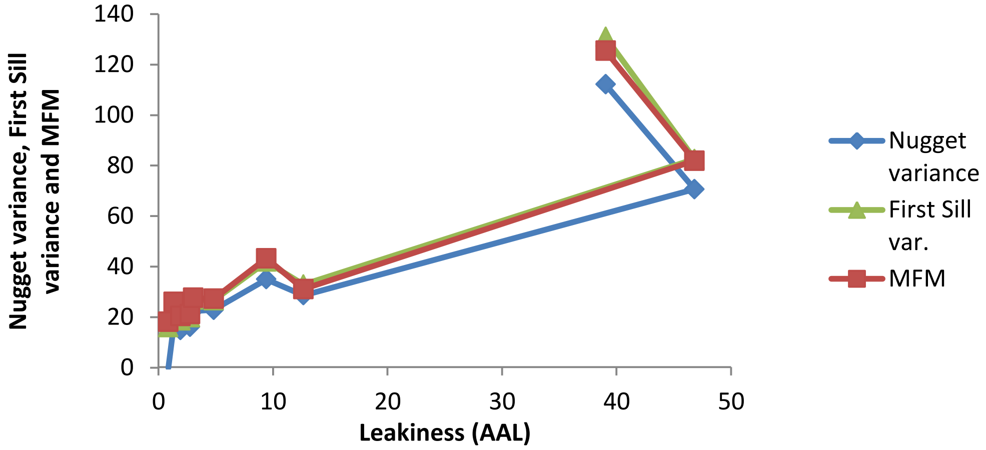

Figure 6.54 SAVI upscale semivariance values relationship with AAL

All three variogram indices increased with increased leakiness but the increase was irregular.

While each of the above relationships can be explained individually, there does not appear to be any overall unifying explanation. It is thought that this is due to the way in which the pixel support structure in the original image decays in the resampling process.

6.3.2.2. Stress Related Vegetation Index (STVI)

Variance

The semivariograms for each resampled STVI image for the whole catchment are shown in Figure 6.55 (10-30m resolution) and Figure 6.56 (50-250m resolution).

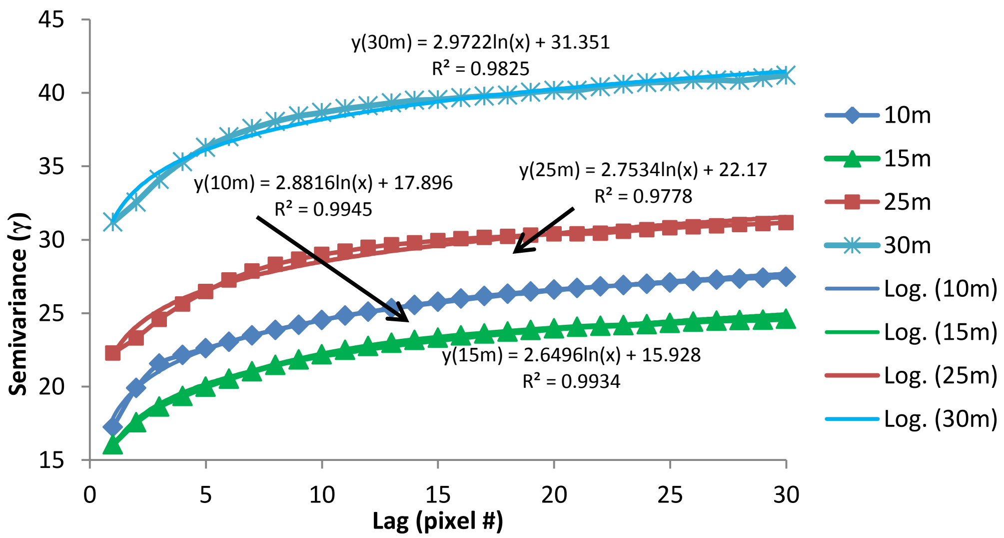

Figure 6.55 Semivariance of resampled STVI (10-30m)

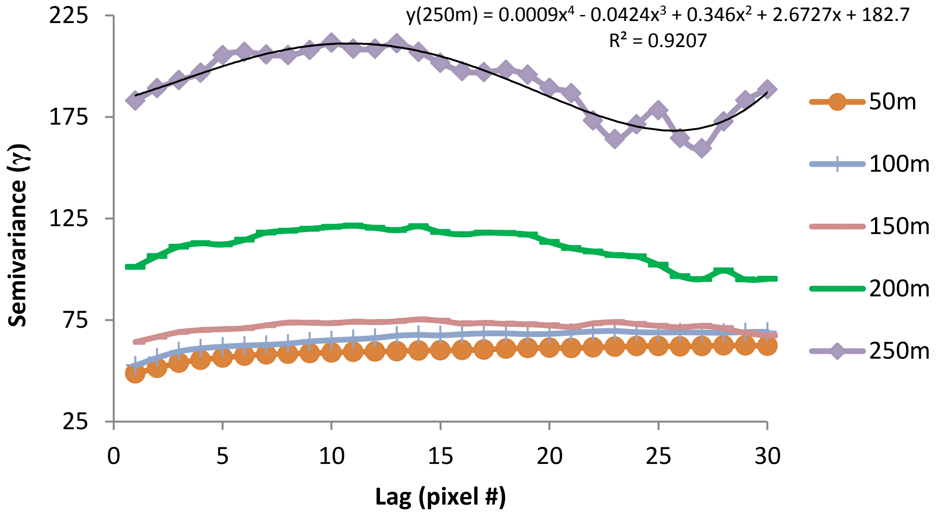

Figure 6.56 Semivariance of resampled STVI (50-250m)

This shows that the semivariance initially decreases with resampling (from 10m to 15m resolution) and then increases with further decrease in resolution to 250m. The ordered structure of the image also decays with progressive resampling from 15m to 250m resolution. This is similar to SAVI image variogram behaviour.

The change in semivariance of STVI vegetation cover with progressive upscaling is plotted as contours in Figure 6.57 and Figure 6.58 and mapped as a surface in Figure 6.59.

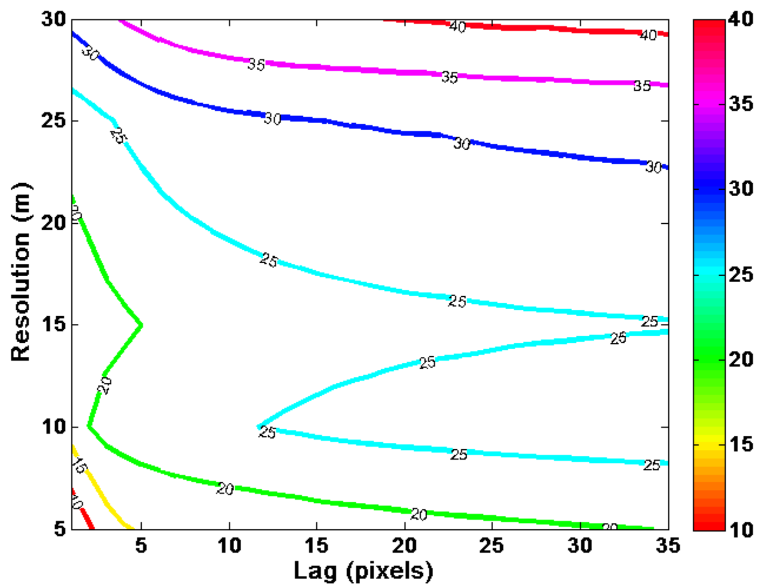

Figure 6.57 Contour plot STVI semivariance (5-30m)

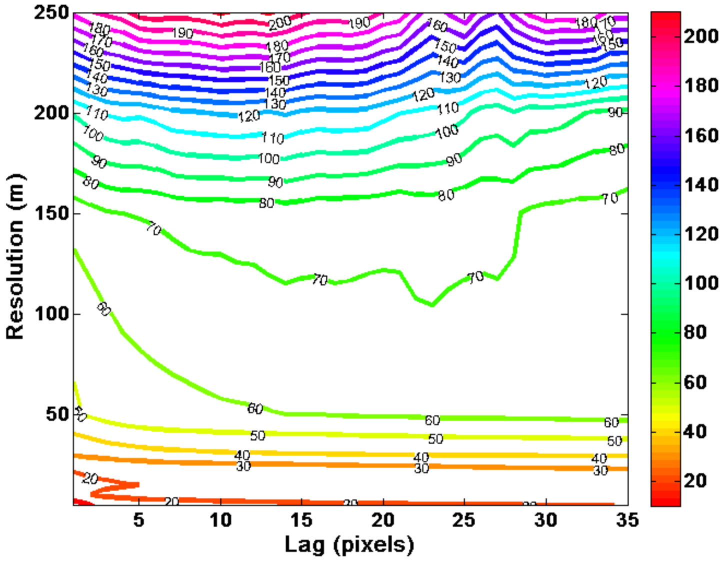

Figure 6.58 Contour plot SVI semivariance (5-250m)

The surface was again modelled (Figure 6.60) as a 2 variable quadratic equation (Equation 6-7). This fitted the variance surface well as shown by the R^2 values in Table 6-25.

$$V_{STVI\ upsc} = 16.56 + 1.182*x + 0.140*y - 0.022*x^2 - 0.005*x*y + 0.002*y^2 \quad (6\text{-}7)$$

where V = semivariance, x = lag and y = resolution

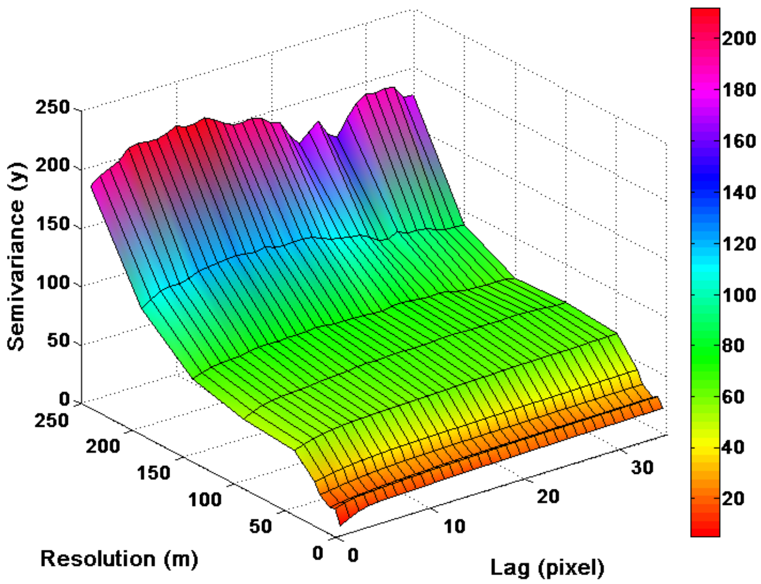

Figure 6.59 STVI upscaled semivariance

Table 6-25 Equation 6-7 fit parameters

Fit parameters			
SSE	R^2	R^2 Adj	RMSE
6.30E+04	0.0208	0.9288	13.53

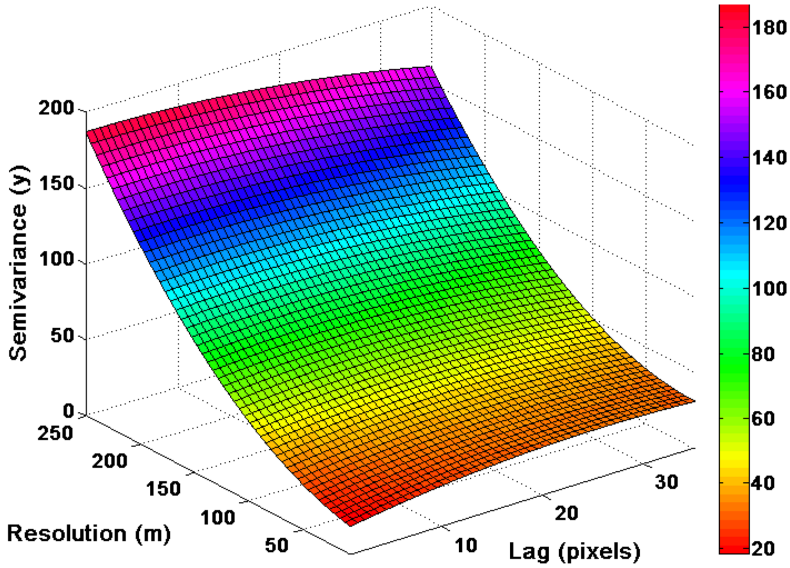

Figure 6.60 STVI upscale semivariance model

Variogram indices

Conventional and UPV indices were extracted (as described in Section 6.2.2) and are shown in Table 6-26 and Table 6-27.

Table 6-26 STVI Conventional semivariogram indices

Image resolution (m)	STVI conventional variogram values					
	NV	FR (m)	FSV	SCV	NSRV	NSCVR
10	14.85	40	22	7.16	0.67	2.07
15	14.91	95	20	5.59	0.73	2.67
25	20.70	150	29	8.30	0.71	2.49
30	29.57	210	38	8.43	0.78	3.51
50	45.55	250	55	9.45	0.83	4.82
100	48.52	400	60	11.49	0.81	4.22
150	61.24	600	70	8.76	0.87	6.99
200	95.62	800	120	24.38	0.80	3.92
250	168.90	1250	220	51.10	0.77	3.31

Table 6-27 STVI UPV semivariogram indices

Image resolution (m)	STVI UPV semivariogram Indices								
	Varian	RVF	RSF	FDO	FML	MFM	VFM	AFM	RMM
10	1.86	1.65	1.15	2.66	41	25.79	5.71	361.99	1.09
15	1.65	1.56	1.09	1.51	40	23.10	4.72	293.02	1.08
25	1.98	1.38	1.05	1.03	41	29.69	5.18	321.02	1.07
30	2.52	1.28	1.04	1.36	26	38.40	6.37	213.75	1.06
50	3.75	1.22	1.05	2.66	28	59.14	10.74	332.02	1.06
100	3.92	1.19	1.07	3.84	17	63.57	17.72	230.75	1.08
150	4.32	1.06	1.04	2.54	8	69.72	8.23	103.67	1.06
200	6.82	1.08	1.05	5.35	11	114.32	37.62	236.03	1.06
250	12.02	1.06	1.03	6.10	6	195.71	72.45	247.35	1.06

Index correlation with leakiness

Both groups of indices were analysed for cross correlations and the significant correlations are shown in Table 6-28.

Table 6-28 Correlation (R^2) between STVI upscale image variables and all variables (R^2)

All variables	Image variables				Variogram Indices					
	Resoln	Cell No	Lcalc	AAL	NV	FR	FSV	SCV	NSVR	RVF
Lcalc		0.94								
AAL										
NV	0.90			0.70						
FR	0.97			0.73	0.97					
FSV	0.87			0.71	0.99	0.95				
SCV					0.79		0.87			
NSVR		0.97	0.90							
RVF		0.99	0.91						0.98	
RSF		0.99	0.87						0.97	0.99
FDO										
FML	0.85									
MFM	0.89			0.71	0.99	0.96	1.00	0.84		
AFM			0.73							

There was no significant correlation with average cover. The correlation between semivariogram indices (right side of Table 6-28) is ascribed to the indices having common measurement parameters. The pattern of relationships for the three STVI image variables (resolution, cell number and leakiness) with significantly correlated indices is shown in Figure 6.61, Figure 6.62, Figure 6.63 and Figure 6.64.

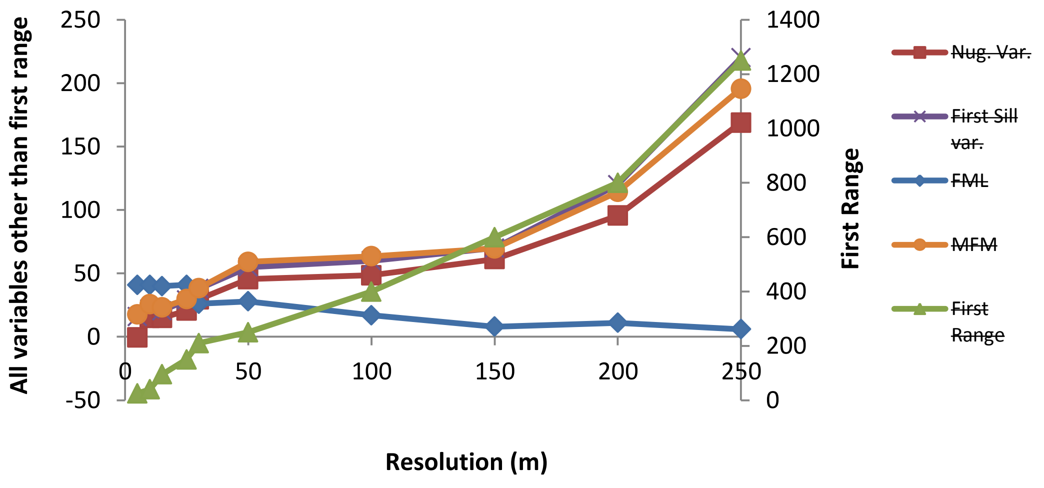

Figure 6.61 STVI semivariance values as a function of resolution

There is a general increase in NV, FSV, MFM and FR variogram indices with decrease in resolution. This is similar to the upscaled SAVI image but it is more uniform than with SAVI.

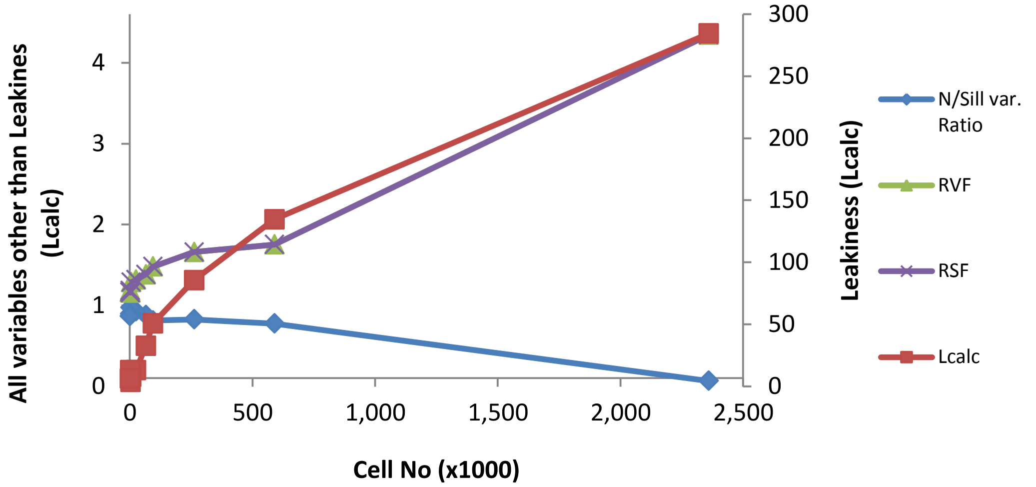

Figure 6.62 STVI semivariance values as a function of cell number

Lcalc increases with Cell No. as explained in Section 4.2.3. The NSVR decreased with increase in Cell No. as it did in the SAVI upscaled image. The other indices behaved differently in the STVI upscaled image compared to the upscaled SAVI image.

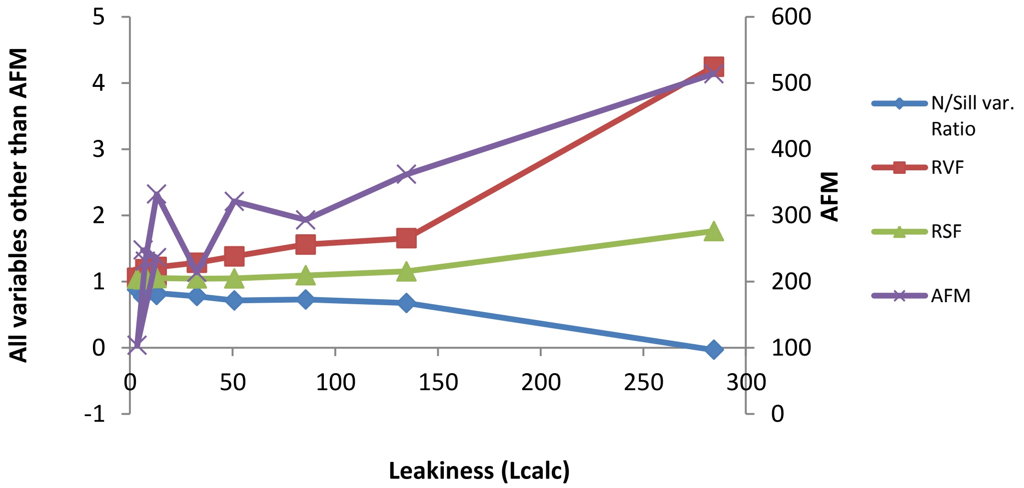

Figure 6.63 STVI semivariance values relationship with Lcalc

RVF and RSF behaved similarly in STVI upscaling to SAVI upscaling increasing linearly with increase in Lcalc. NSVR and AFM behaved differently between upscaled STVI and SAVI images

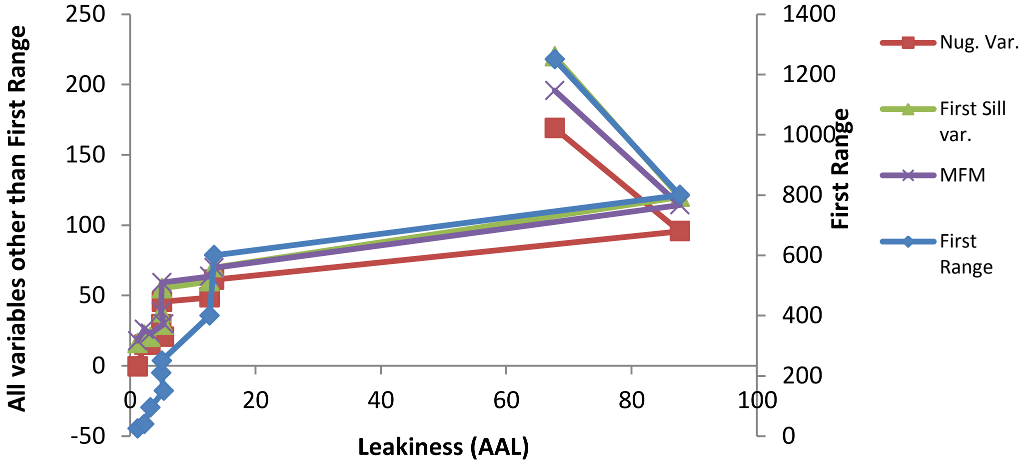

Figure 6.64 STVI semivariance values relationship with AAL

There was a similar pattern of general increase in NV, FSV and MFM in upscaled STVI to the pattern in upscaled SAVI images. Additionally FR behaved in the same manner.

Again, while each of the above relationships can be explained individually, there does not appear to be any overall unifying explanation. It continues to reinforce the thought that this is due to the way in which the pixel support structure of the original image decays as the resampling progresses.

Sub-catchments

Analysis of the STVI cover image for the sub-catchments of the resampled area yielded an initial pattern of bounded variograms that progressively decayed with further resampling to a condition of unstructured variance in the images as shown in Figure 6.65, Figure 6.66, Figure 6.67, Figure 6.68, Figure 6.69 and Figure 6.70.

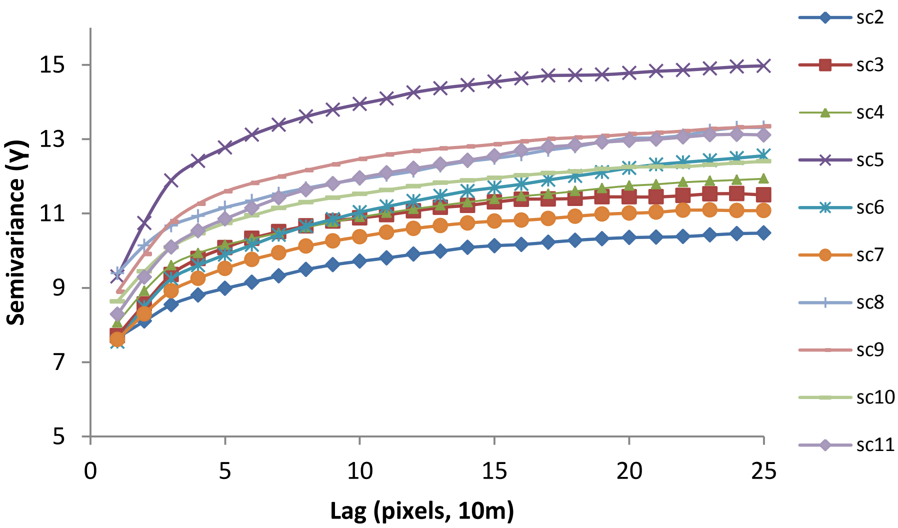

Figure 6.65 Semivariance of STVI in 10 sub-catchments (10m resolution)

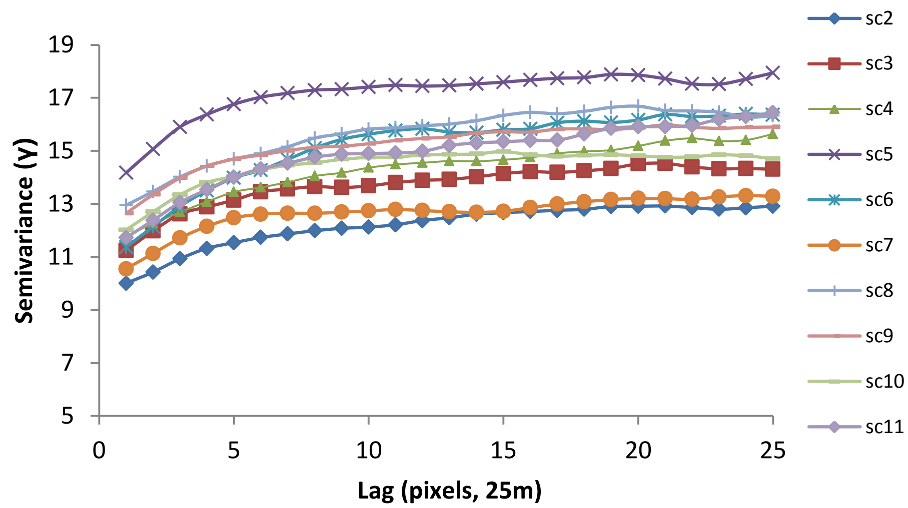

Figure 6.66 Semivariance of STVI in 10 sub-catchments (25m resolution)

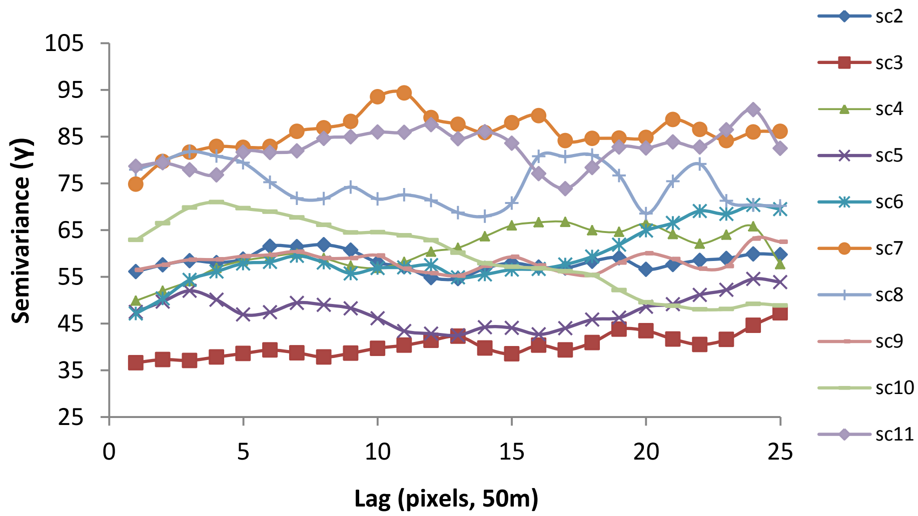

Figure 6.67 Semivariance of STVI in 10 sub-catchments (50m resolution)

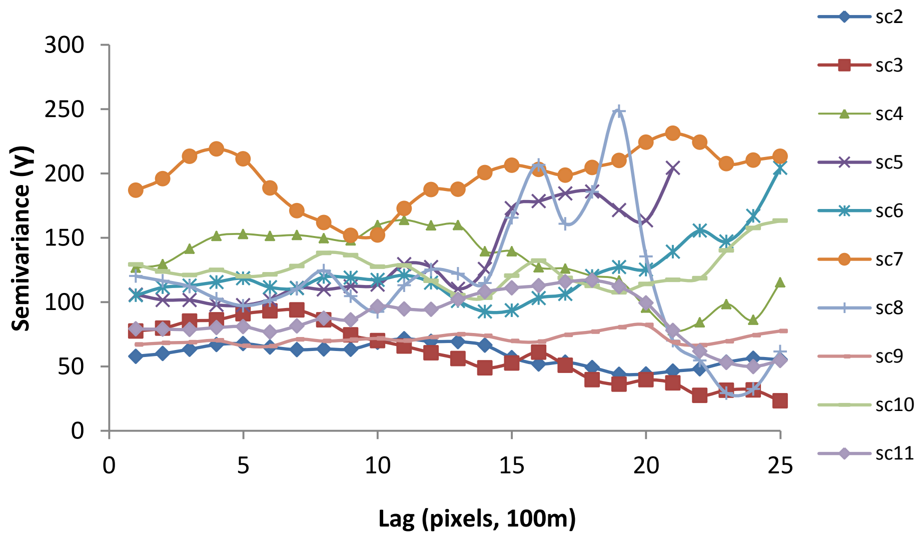

Figure 6.68 Semivariance of STVI in 10 sub-catchments (100m resolution)

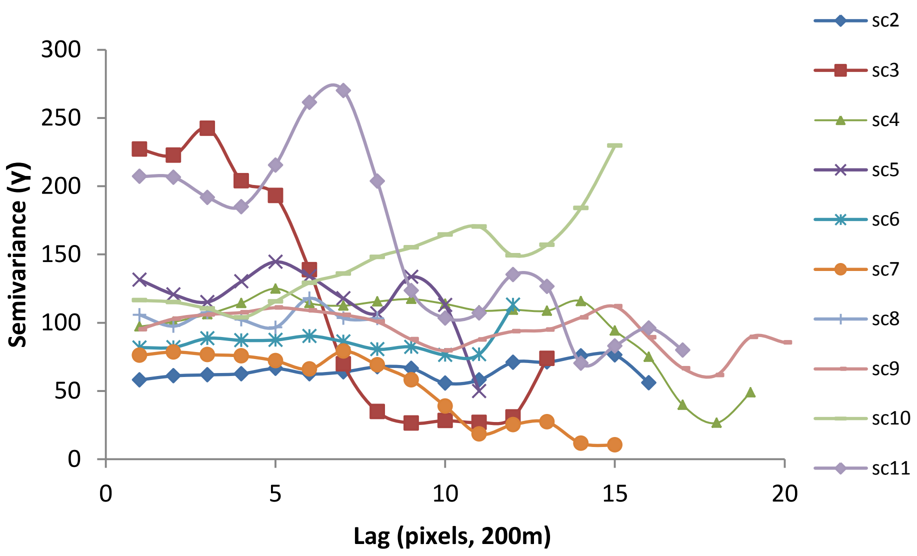

Figure 6.69 Semivariance of STVI in 10 sub-catchments (200m resolution)

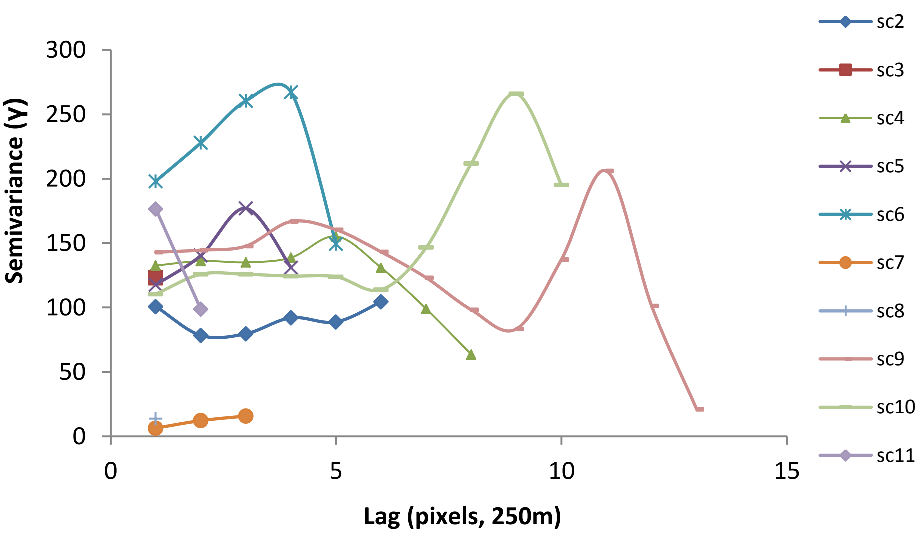

Figure 6.70 Semivariance of STVI in 10 sub-catchments (250m resolution)

The change in form of the sub-catchment variograms, from one of concise bounded behaviour at 10m resolution, to erratic unbounded behaviour at 250m resolution, confirms the behaviour of the overall catchment variograms for resampled STVI layers. This loss of variogram structure indicates loss of structure of the vegetation cover image caused by the resampling. It is consistent with the findings of Atkinson and Tate (2000).

6.3.2.3. Perpendicular Distance Vegetation Index (PDrg)

Variance

The semivariograms for each resampled PDrg image for the whole catchment are shown in Figure 6.71 (10-30m resolution) and Figure 6.72 (50-250m resolution).

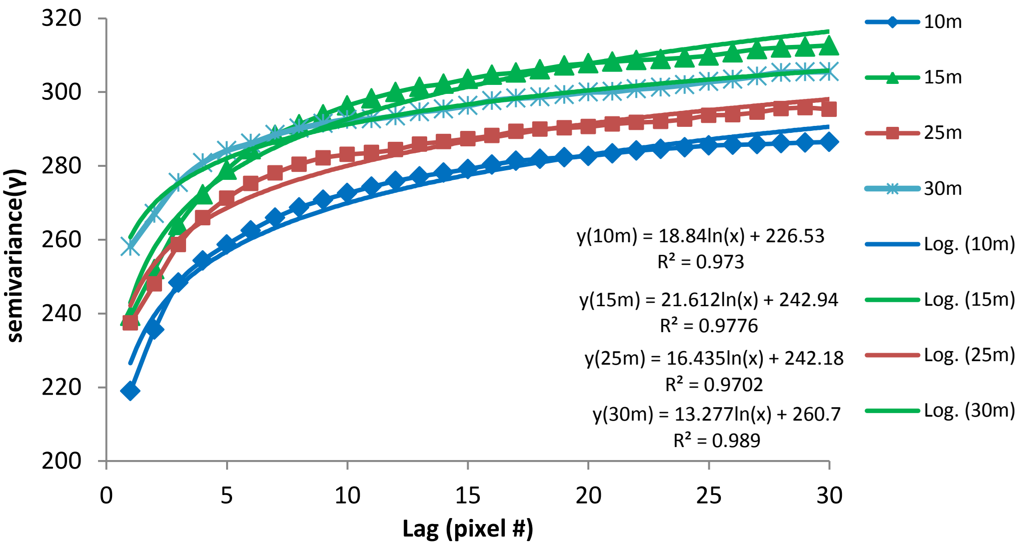

Figure 6.71 Semivariance of resampled PDrg (10-30m)

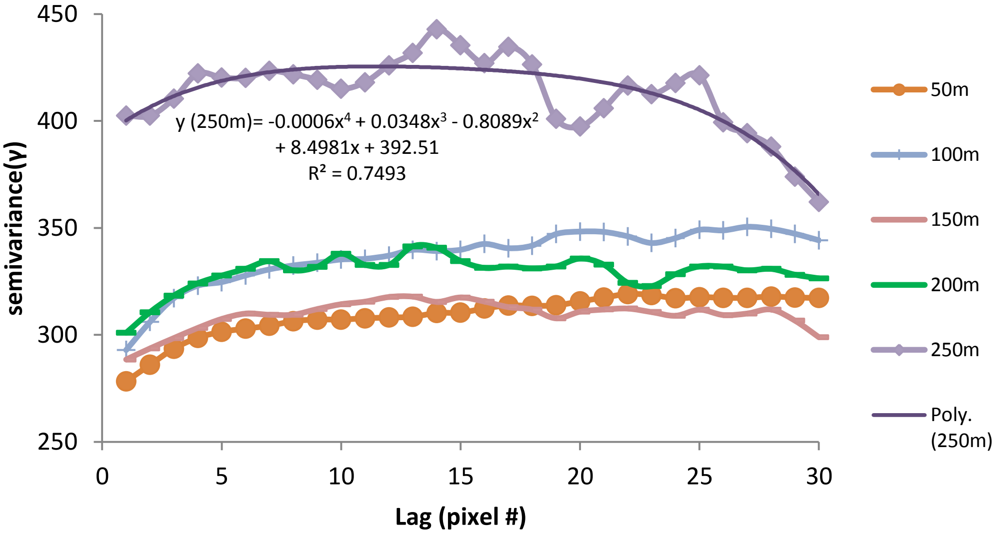

Figure 6.72 Semivariance of resampled PDrg (50-250m)

Figure 6.71 and Figure 6.72 show that the semivariance initially increases from 10 to 15 resolution, then decays at 25m resolution after which it continues to increase to 250m resolution. The ordered structure of the image decays with progressive resampling from 10m to 250m resolution.

The semivariance of PDrg vegetation accompanying progressive upscaling is plotted as contours in Figure 6.73 and Figure 6.74 and the surface profile is mapped in Figure 6.75.

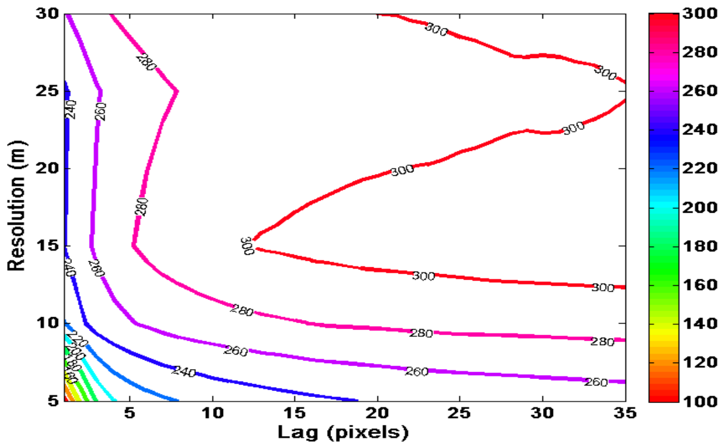

Figure 6.73 Contour plot PDrg semivariance (5-30m)

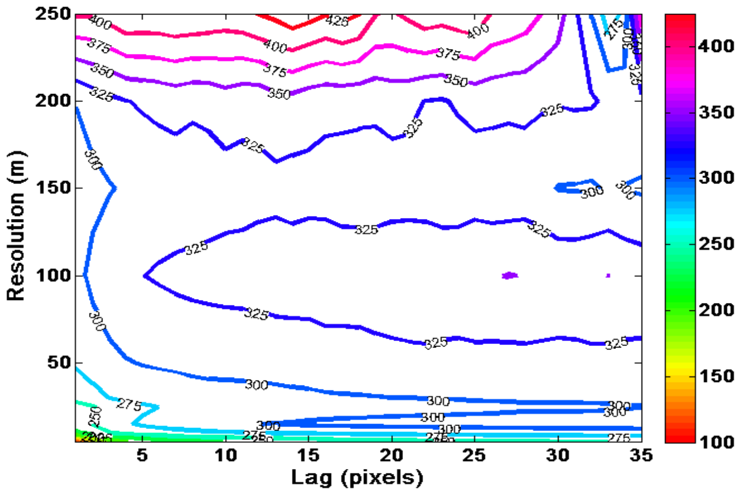

Figure 6.74 Contour plot PDrg semivariance (5-250m)

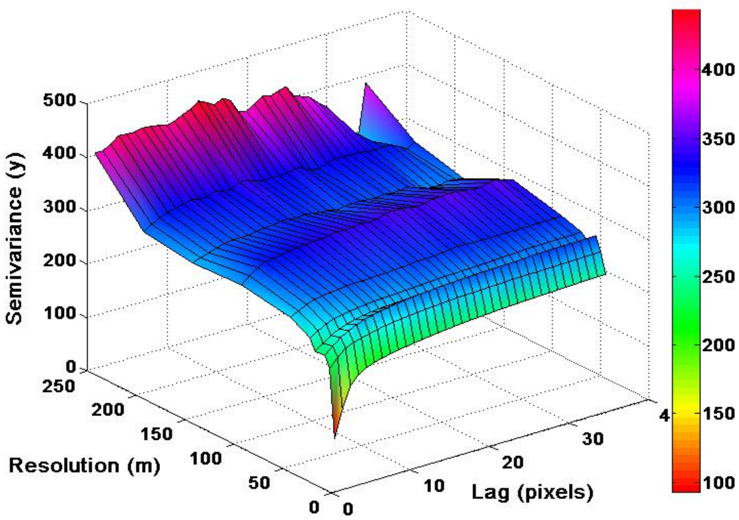

Figure 6.75 PDrg upscaled semivariance surface

This surface was modelled as both a 2-variable quadratic equation (Equation 6-8) (Figure 6.76) and as a 2-variable cubic equation (Equation 6-9) and (Figure 6.77). It was necessary to use a 3rd power polynomial fit due to the form of the variogram.

The fit of both equations is shown in Table 6-29. The quadratic expression did not produce a satisfactory fit ($R^2 = 0.68$) while the cubic expression produced a good fit with an R^2>0.9. This is illustrated in Figure 6.76 and Figure 6.77

$$V_{PDrg\ upsc} = 218.6 + 5.226*x + 0.665*y - 0.095*x^2 - 0.014*x*y + 0.000*y^2 \quad (6\text{-}8)$$

$$V_{PDrg\ upsc} = 202 + 5.178*x + 2.468*y - 0.226*x^2 + 0.007*x*y - 0.022*y^2\ 0.022*y^2 + 0.004x^3 - 0.0003x^2y + 0.00002\ xy^2 + 0.00006y \quad (6\text{-}9)$$

Table 6-29 Equations 6-8 and 6-9 fit parameters

Quadratic fit parameters				Cubic fit parameters			
SSE	R^2	R^2 Adj	RMSE	SSE	R^2	R^2 Adj	RMSE
2.5E+05	0.68	0.67	2.7E+01	2.3E+04	0.9701	0.9693	8.182

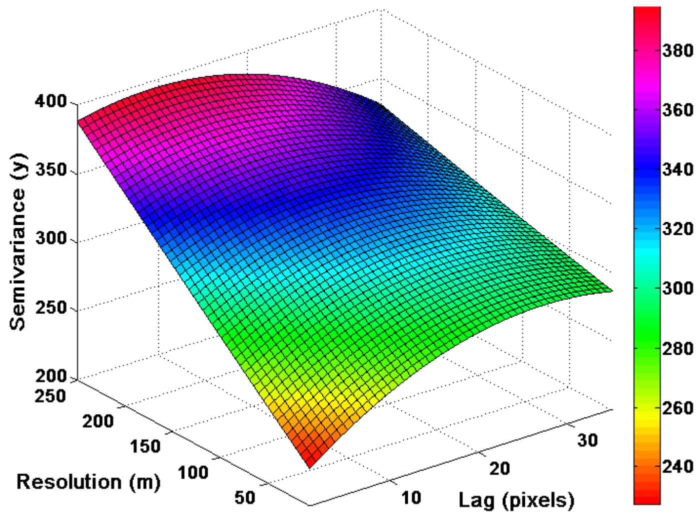

Figure 6.76 PDrg upscale variance quadratic model

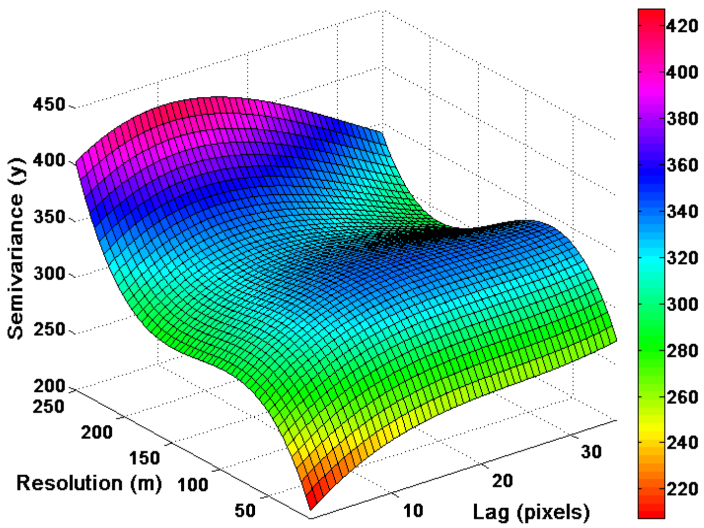

Figure 6.77 PDrg upscale variance 3rd power polynomial model

Variogram indices

Conventional and UPV indices were extracted from the variograms in Figure 6.71 and Figure 6.72 (see Section 6.2.2) and shown in Table 6-30 and.Table 6-31

Table 6-30 PDrg Conventional semivariogram indices

Image resolution (m)	PDrg conventional variogram values					
	NV	FR (m)	FSV	SCV	NSRV	NSCVR
10	192.65	50	258.67	66.02	0.74	2.92
15	224.78	75	278.94	54.16	0.81	4.15
25	223.87	125	271.20	47.33	0.83	4.73
30	245.40	150	284.11	38.71	0.86	6.34
50	266.51	200	298.67	32.16	0.89	8.29
100	274.33	400	322.99	48.66	0.85	5.64
150	278.64	600	303.23	24.59	0.92	11.33
200	283.89	800	324.09	40.20	0.88	7.06
250	383.17	1000	422.17	39.00	0.91	9.82

Table 6-31 STVI UPV semivariogram indices

Image resolution (m)	PDrg UPV semivariogram Indices								
	Varian	RVF	RSF	FDO	FML	MFM	VFM	AFM	RMM
10	18.18	1.37	1.08	16.58	41	277.36	229.25	2576.93	1.04
15	19.76	1.36	1.05	12.70	41	301.41	304.56	2746.95	1.05
25	18.50	1.28	1.04	10.60	29	282.66	196.02	1520.65	1.05
30	18.63	1.19	1.03	8.88	40	297.12	128.02	1791.32	1.04
50	18.99	1.13	1.03	7.78	22	306.19	94.56	873.16	1.04
100	20.47	1.16	1.04	13.17	16	328.58	170.34	839.11	1.04
150	18.31	1.05	1.02	5.19	6	300.19	56.64	348.16	1.03
200	19.83	1.08	1.03	9.65	7	321.01	121.24	424.58	1.04
250	25.37	1.04	1.00	-0.09	4	409.41	64.83	420.18	1.03

Index correlation with leakiness

Both groups of indices were analysed for cross correlations and the significant correlations (R^2) are shown in Table 6-32 and Table 6-33.The correlation between variogram indices (Table 6-33) occurs because they are based on a number of common measurements. The pattern of relationships for the three PDrg image variables (resolution, cell number and leakiness) with the significantly correlated variance indices are shown in Figure 6.78, Figure 6.79, Figure 6.80, Figure 6.81, Figure 6.82 and Figure 6.83.

Table 6-32 Correlation (R^2) between PDrg upscale image variables

All variables	Image variables			
	Resoln	Cell No	Cover	Lcalc
Lcalc		0.99		
NV		0.83		0.87
FR	1.00			
FSV			0.87	
SCV		0.98		0.95
NSVR		0.99		0.96
RVF		0.98		0.96
RSF		0.97		0.93
FDO		0.94		0.93
FML	0.85			
MFM			0.93	
AFM/10		0.86		0.92

Table 6-33 Correlation between PDrg variogram indices (R^2)

All Variables	Variogram indices							
	NV	FSV	SCV	NSVR	NSCVR	RVF	RSF	FDO
SCV	0.79							
NSVR	0.83			0.99				
NSCVR	0.72							
RVF	0.85			0.98	0.99			
RSF	0.81			0.98	0.99	0.99		
FDO	0.91			0.95	0.96	0.96	0.95	
FML		0.84						
MFM	0.81		0.98					
AFM/10	0.87			0.84		0.88	0.80	0.85

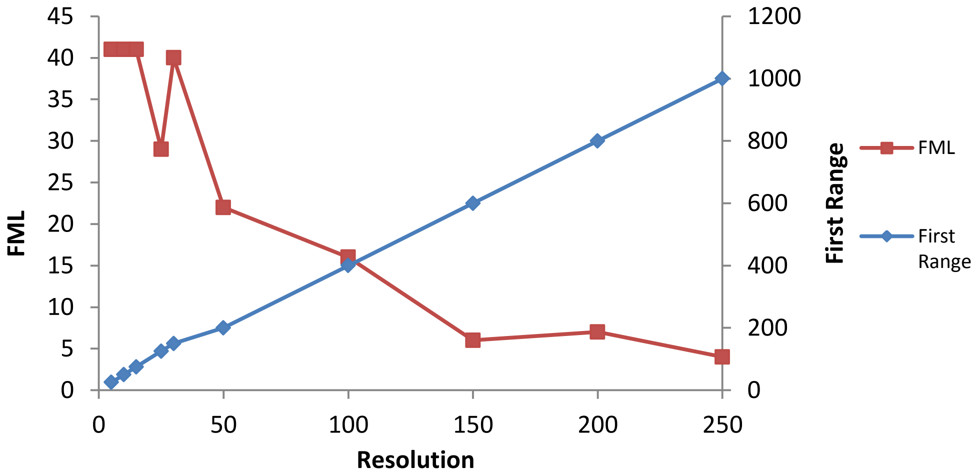

Figure 6.78 PDrg upscale semivariance values as a function of resolution

FR increased linearly and regularly with decrease in resolution while FML (Equiv. to FSV) decreased in an irregular manner. The FR increased in an irregular manner with decrease in SAVI resolution and in a regular manner with decrease in STVI resolution. This appears to be a similar pattern of response by different types of cover images upon upscaling.

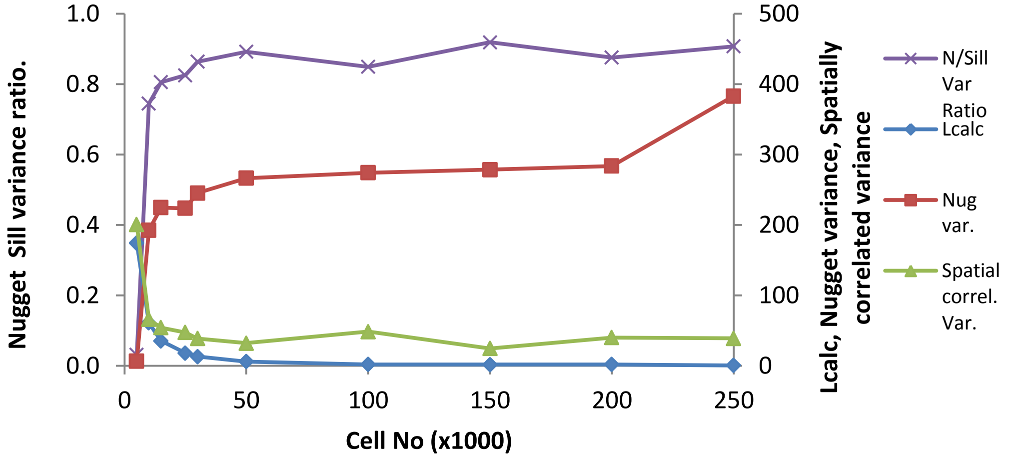

Figure 6.79 PDrg upscale conventional semivariance values as a function of cell number

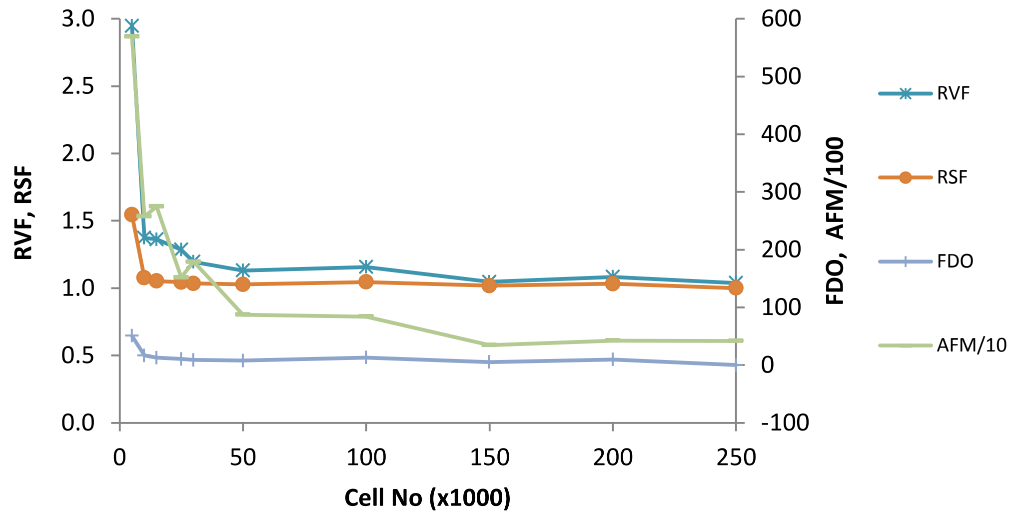

Figure 6.80 PDrg upscale UPV semivariance values as a function of cell number

Two figures, Figure 6.79 and Figure 6.80, were used to summarise the relationships with cell number. In Figure 6.79, Lcalc decreased exponentially to a low value with increase in cell number and then levelled out. This is different from both the SAVI and STVI images in which Lcalc increased steadily with cell number. The theory of the LC expression predicts that Lcalc should increase with cell number (Ludwig and Eager *et al.* 2006). SCV followed a similar pattern. NV and NSVR increased exponentially with increase in cell number to approximately 25,000 cells and then levelled out. In Figure 6.80 all the other vario gram indices decreased with increase in cell number.

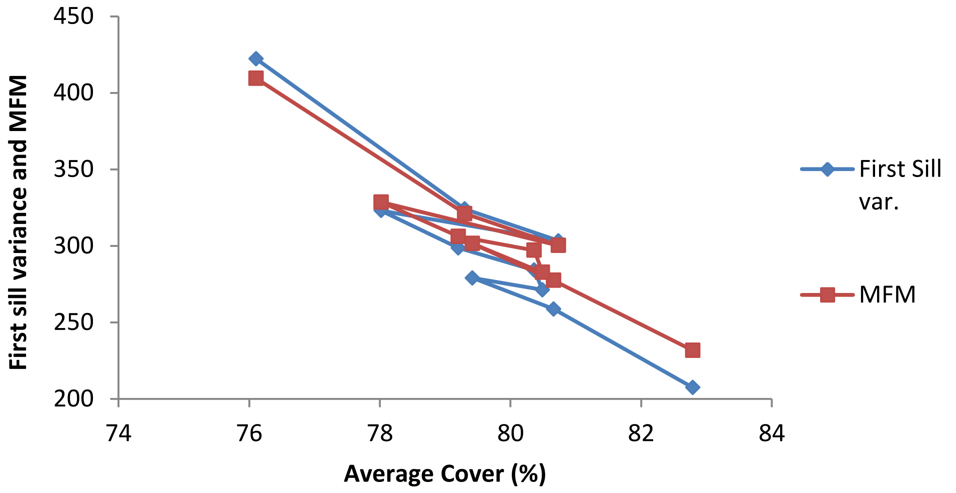

Figure 6.81 PDrg upscale semivariance values as a function of average cover

Both FSV and MFM indices decrease in an irregular linear manner with increase in average cover. There was no comparable pattern for SAVI and STVI indices.

Two figures, Figure 6.82 and Figure 6.83, summarise the relationships between Lcalc and the Variogram indice.

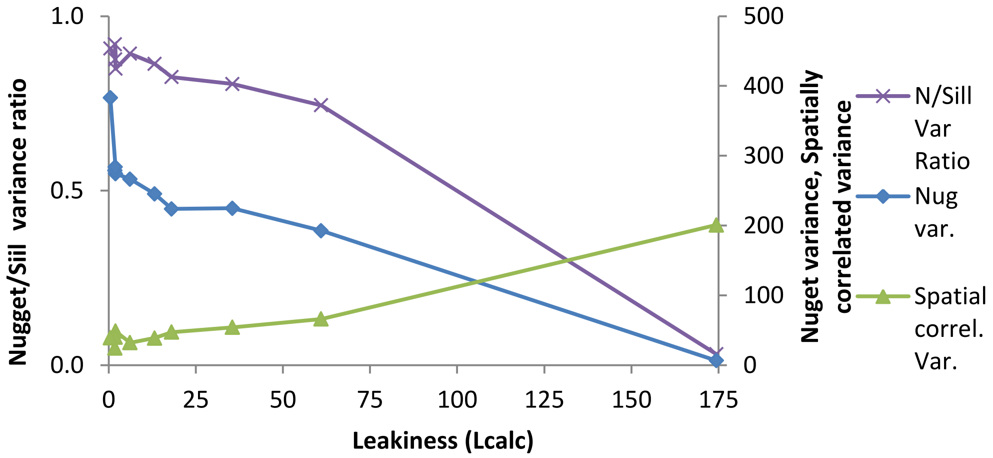

Figure 6.82 PDrg upscale conventional semivariance values as a function of leakiness

NSVR and NV decrease as Lcalc increases. This is similar to SAVI in which NSVR decreases with increase in Lcalc. SCV increased in PDrg but decreased with increase in Lcalc in SAVI. The RVF, RSF and AFM indices increased with increase in Lcalc for both PDrg and SAVI cover images.

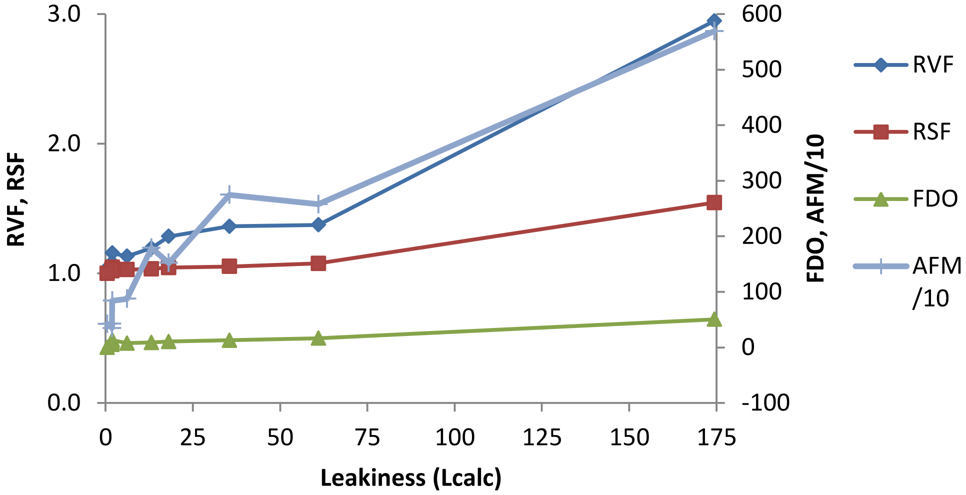

Figure 6.83 PDrg upscale UPV semivariance values as a function of leakiness

The pattern of variogram index behaviour again appears unique to change in resolution of PDrg cover except for the FR index that appears to increase in a generally linear manner with decrease in resolution across the 3 cover types.

6.3.2.4. DEM

Variance

The 5m DEM extracted from stereo aerial imagery was progressively resampled to 10m, 25m, 50m, 100m, 200m and 250m resolution. Semivariograms for each of these resampled DEMs are shown in Figure 6.84.

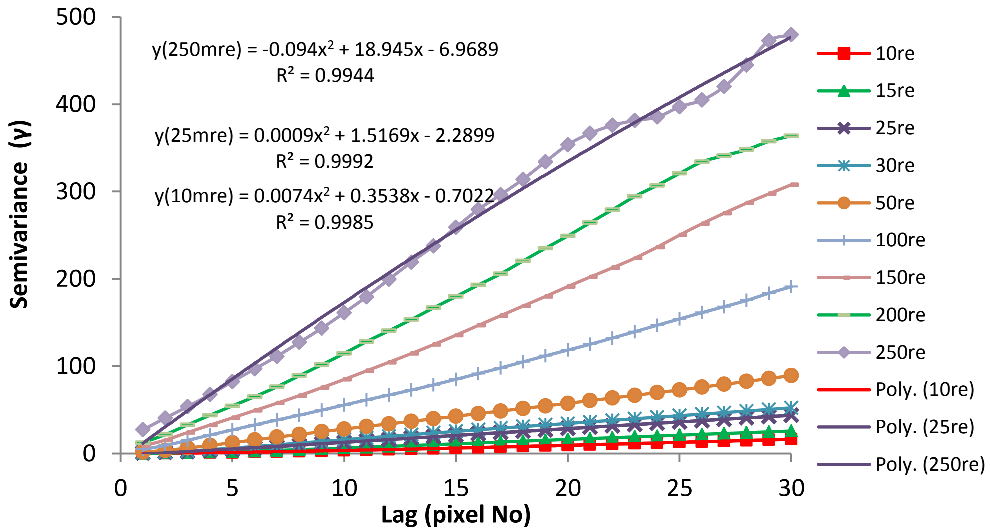

Figure 6.84 Semivariance of whole-of-catchment DEMs resampled from 5m to 250m

This shows that the highest resolution DEMs (10m) have the lowest variance at a given lag and vice versa. The semivariance of the upscaled DEM is plotted as contours in Figure 6.85 and the surface profile is mapped in Figure 6.86.

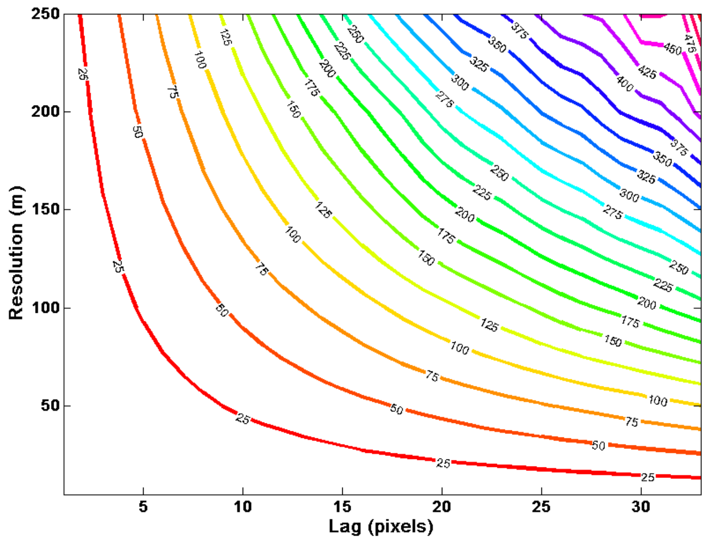

Figure 6.85 Upscaled DEM semivariance contours

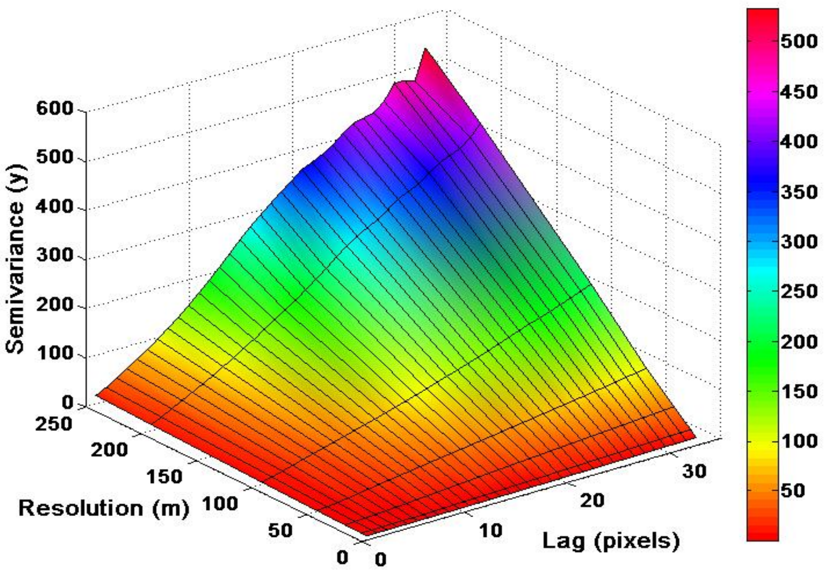

Figure 6.86 Upscaled DEM semivariance surface

The surface was modelled by a 2-variable quadratic equation, Equation 6-10 , as shown in Figure 6.87) The fit of Equation 6-10 to the variance surface is shown in Table 6-34.

$$V_{\text{DEM upscaled}} = -1.339 + 0.0096*x - 0.0871*y - 0.0031*x^2 + .0658*x*y + 0.00022*y^2 \tag{6-10}$$

Table 6-34 Equation 6-10 fit parameters

Fit parameters			
SSE	R^2	R^2 Adj	RMSE
8.76E+03	0.9976	0.9976	6.238

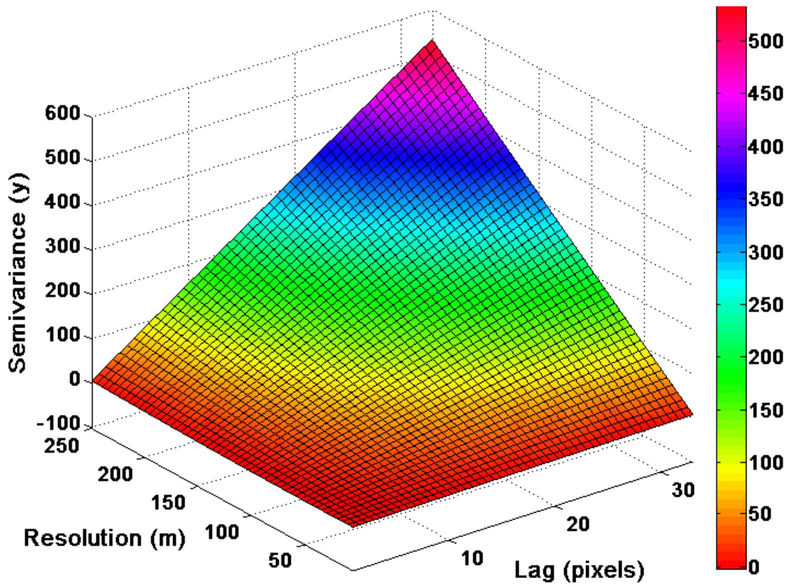

Figure 6.87 DEM upscale semivariance model

Variogram indices

Variogram indices were previously derived for the 10m, 25m and 250m DEMs. The profiles of the resampled DEM variograms are similar to the non-resampled DEM variograms. This indicates they would yield similar indices. These were not separately derived because they would not have added any new information about the effect of resampling on DEM variance.

Effect of resolution and lag

A similar analysis of semivariance with resample resolution was conducted as before (Section 6.3.1.5) based on Figure 6.84. The semivariance showed a simple linear relationship with distance for any given lag in the resampled DEM as shown in Figure 6.88.

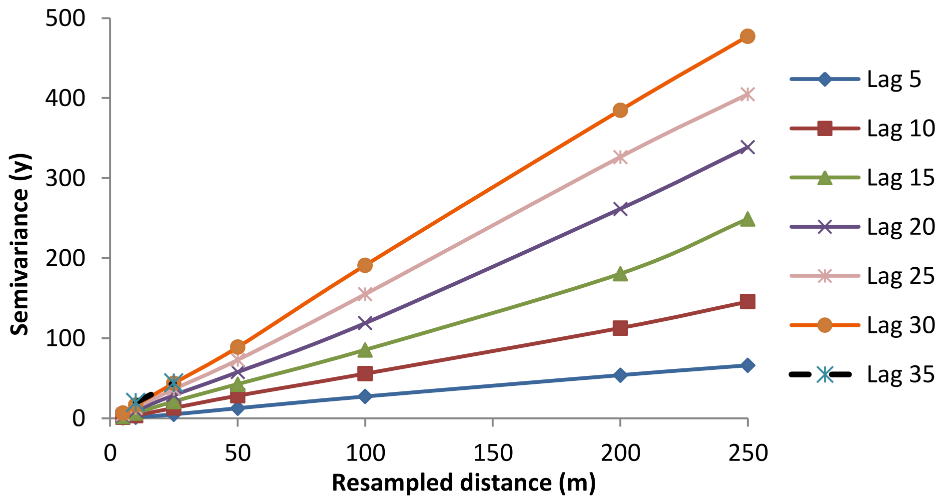

Figure 6.88 Semivariance of resampled DEMs)

The equations relating semivariance with resolution for given lag numbers for the resampled DEMs are given in Table 6-35. The slope of the variogram increases with lag.

Table 6-35 Semivariance resolution expressions for resampled DEMs

Curve	Lag Equation
Lag 5	y = 0.2724x - 1.2103
Lag 10	y = 0.5838x - 2.0357
Lag 15	y = 0.9781x - 5.5515
Lag 20	y = 1.3585x - 7.2929
Lag 25	y = 1.6437x - 5.5472
Lag 30	y = 1.9333x - 4.125

These relationships, which constitute a semivariance matrix for the resampled DEMs, define how the semivariance changes with both lag and resolution as shown in Appendix 6-2. The resulting semivariance contours are plotted in Figure 6.89 and mapped as a surface in Figure 6.90.

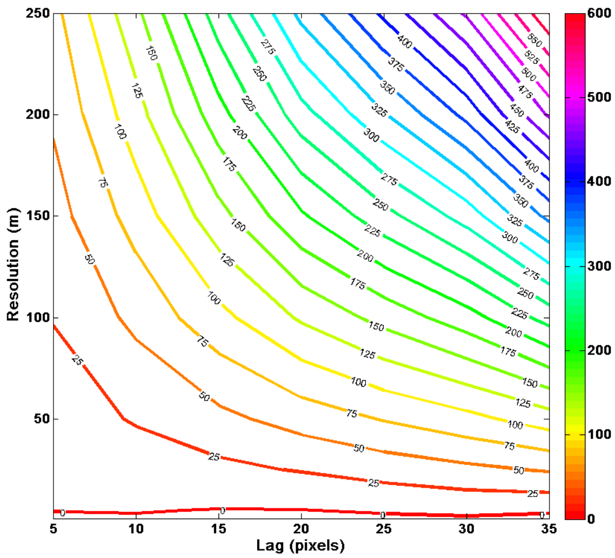

Figure 6.89 Contour plot of semivariance of resampled 5m AP DEM

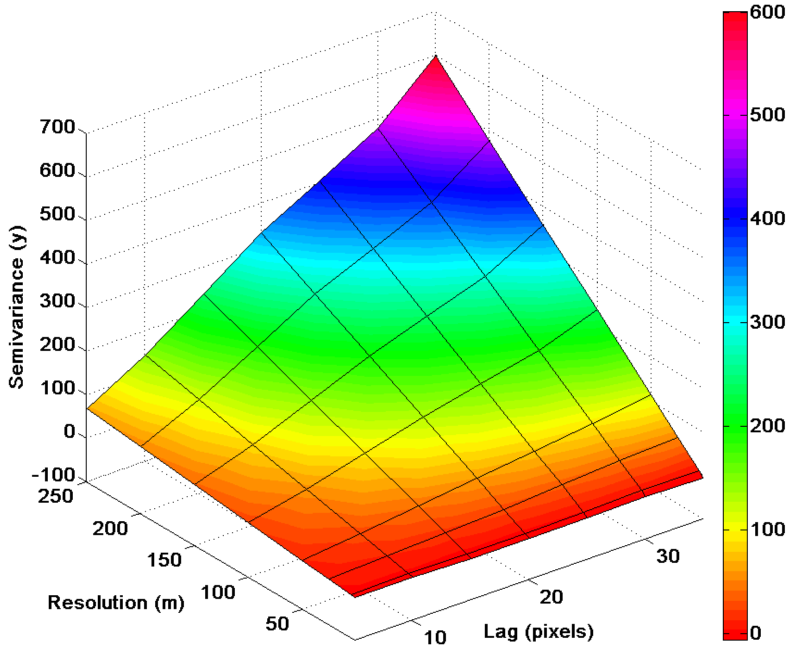

Figure 6.90 Relationship of revised upscaled DEM semivariance to lag and resolution

6.3.3. Comparison between native and upscaled imagery

The following subsections present a side-by-side comparison of the native image variances with the resampled image variances.

6.3.3.1. Soil Adjusted Vegetation Index comparison (SAVI)

Variance comparison

Figure 6.91 shows the variograms for 10m, 25m and 50m native scale SAVI coverages and Figure 6.92 shows the variograms for the upscaled SAVI coverages.

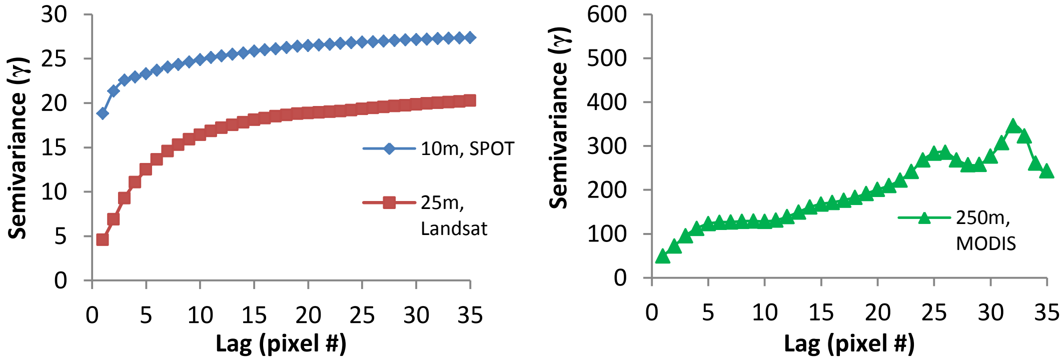

Figure 6.91 Native Scale SAVI variograms

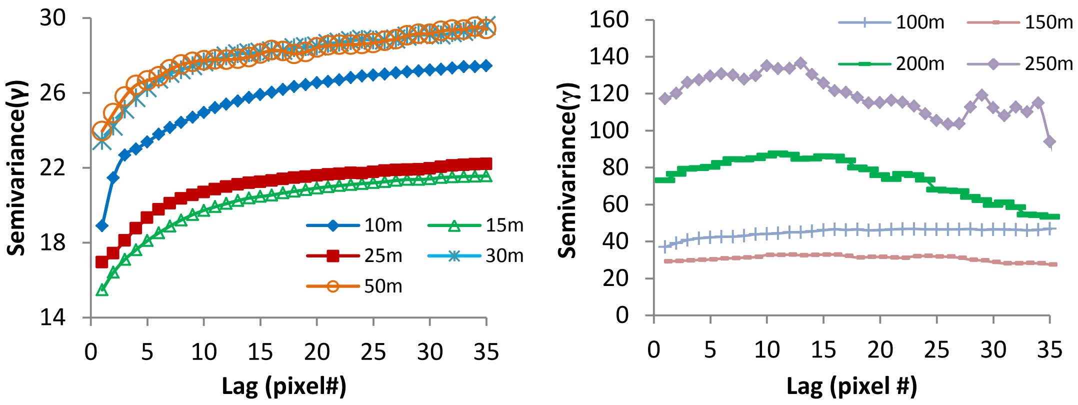

Figure 6.92 Upscale SAVI variograms.

The shape of the variograms indicates the structure of the image. It is a measure of the pattern of variance with distance from the origin. At 15 m and 25 m resampling, the upscaled variograms have essentially the same shape (bounded exponential) as the native variograms. At higher levels of upscaling the variogram shape degenerates, indicating a loss of image structure and spatially dependent variance. The quantitative differences in variogram between the native and upscaled images can be seen in the equations in Table 6-36.These differences are discussed in Section 6.4.

Table 6-36 Comparison of native and upscaled SAVI variogram expressions

Image Type	**Resolution**	**Native scale variograms** (y= Variance (γ), x= Lag (*l*))	**Upscaled variograms** (y= Variance (γ), x= Lag (*l*))
SAVI	**10m**	$y_{(10m)}$ = 2.2733ln(x) + 19.68	$y_{(10m)}$ = 2.2777ln(x) + 19.671
	15m	na	$y_{(15m)}$ = 1.8653ln(x) + 15.275
	25m	$y_{(25m)}$ = 4.7218ln(x) + 5.1145	$y_{(25m)}$ = 1.5901ln(x) + 16.794
	30m	na	$y_{(30m)}$ = 1.6954ln(x) + 23.492
	250m	$y_{(250m)} = -0.0025x^4 + 0.1592x^3 - 3.2932x^2 + 30.647x + 26.507$	$y_{(250m)} = 0.0003x^4 - 0.0085x^3 - 0.1262x^2 + 3.675x + 114.3$

Figure 6.93 provides a comparison in the same graph of the variance for the native SAVI cover image (solid symbols) compared to the variance of the upscaled SAVI image (hollow symbols).

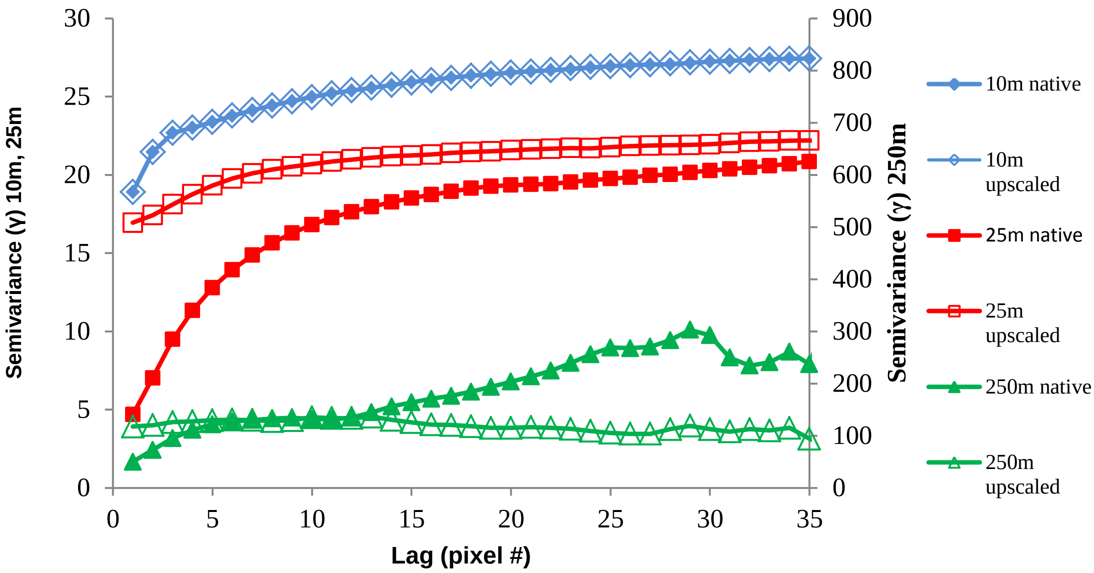

Figure 6.93 Overlay of native and upscaled SAVI image variograms

The 10m image variograms are identical as expected because they were not upscaled. The 25m upscaled image variance is greater than the 25m native image at the nugget and the sill. It has a similar FR lag and the total variance is the same. The 250m upscaled image variance has a larger nugget, a similar FR and SV but the variance declines below the original 250m image variance with further upscaling rather than approximating the same as the original 250m image variance. The 250 m ‘native’ image was derived from MODIS mod02qkm (250m) and mod02hkm (500m) images. The latter was downscale in the process of compiling the ‘parent’ image. This downscaling may have had an effect on the semivariance of the ‘native’ 250m image.

ContourComparison

A side-by-side comparison of the semivariance contours for native and upscaled SAVI cover images (Figure 6.94) illustrates the effect of upscaling on image variance.

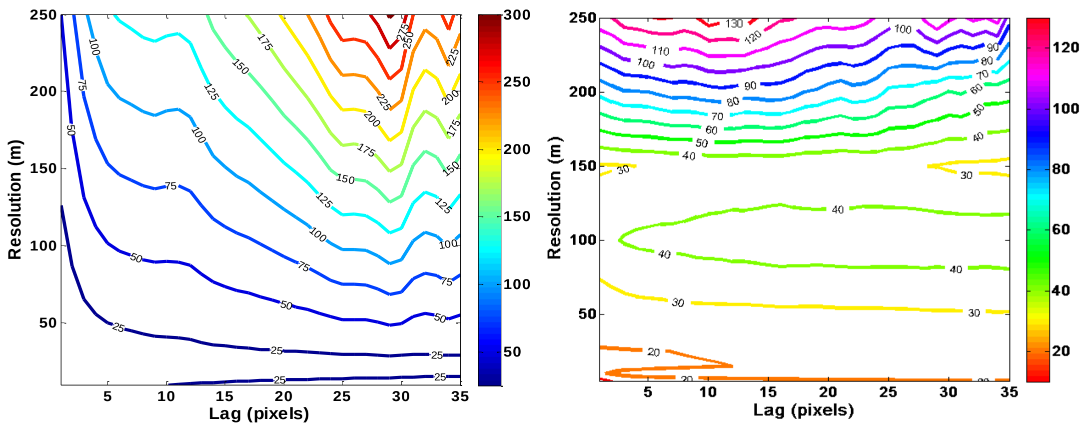

Figure 6.94 Comparison of variance contours for native (left) and upscaled (right)

6.3.3.2. SAVI cover images

Surface comparison

A side-by-side comparison of the semivariance surface models for native and upscaled SAVI cover images illustrates the effect of upscaling on image variance with lag and resolution (Figure 6.95). The much lower value of the variance at higher lag and resolution in the resampled image model can be seen compared to the native image model.

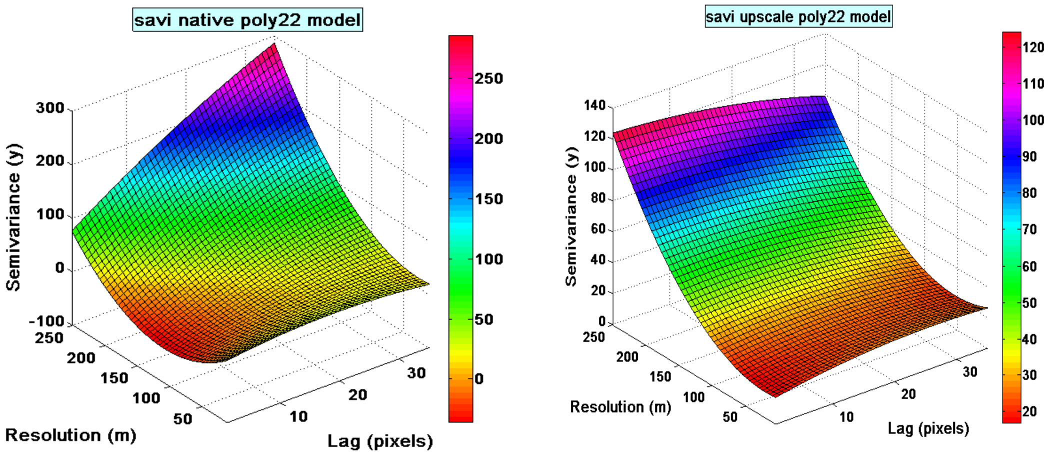

Figure 6.95 Comparison of SAVI semivariance models

Both models have the same 2-variable quadratic form as shown by Equations 6-3 and 6-8.The difference in variable values between the two models is shown in Table 6-37.

Table 6-37 Variables for native scale and upscaled SAVI semivariance models

Scale	Expression parameters					
	Intercept	x coefficient	y coefficient	x^2 coefficient	xy coefficient	y^2 coefficient
Native scale	25.73	1.47	-1.20	-0.05	0.03	0.01
Upscaled	16.8400	0.8502	-0.0805	-0.0159	-0.0040	0.0020

Index comparison

The more highly correlated semivariance variables are shown in Table 6-38 for both native scale and upscaled SAVI images (significant correlations highlighted).

Table 6-38 Correlation (R^2) of SAVI variance indices for native and upscaled images with leakiness

All variables	Native Image Variables				Upscaled Image Variables				
	Resoln	Cell No	Lcalc	AAL	Resoln	Cell No	Cover	Lcalc	AAL
Lcalc	0.98					0.97			
AAL	1.00		0.98		0.85		0.88		
NV		0.98			0.85				0.81
FR	1.00		0.96	0.99	0.89				
FSV	0.99		1.00	0.99	0.83				0.82
SCV	1.00		0.97	1.00		0.98		0.93	
NSVR		0.99				0.82		0.90	
NSCVR		0.93							
RVF		0.69				1.00		0.97	
RSF		0.84				0.99		0.93	
FDO	1.00		0.99	1.00					
FML	1.00		0.99	1.00					
MFM	0.98		1.00	0.99	0.82				0.82
AFM		0.90				0.81		0.87	

The FR and FML are 2 different measures of the Lag where the variogram reaches its first local maximum. This is considered a key indicator of image structure, being a measure of the "*average size of the principal structures or patterns in the image and their separation from each other*" (Balaguer and Ruiz *et al.* 2010 , p.234.). These values were significantly correlated with the leakiness (both AAL and Lcalc) in the native scale image but neither were significantly correlated with leakiness in the resampled image. This highlights the difference in image structure caused by the resampling.

AAL was correlated with resolution in both images but less so in the resampled image. This agrees with the expected pattern for AAL. The FSV and MFM (measure similar parameters) indices are correlated with AAL in both native and resampled images.

6.3.3.3. Stress Related Vegetation Index comparison (STVI)

Variance comparison

Figure 6.96 shows the variograms for 10m, 25m and 50m native scale STVI coverages and Figure 6.97 shows the variograms for the upscaled STVI coverages.

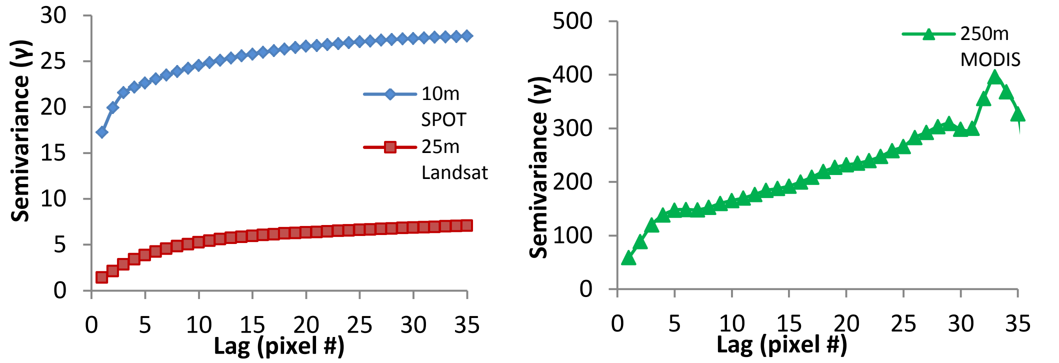

Figure 6.96 Native scale STVI variograms

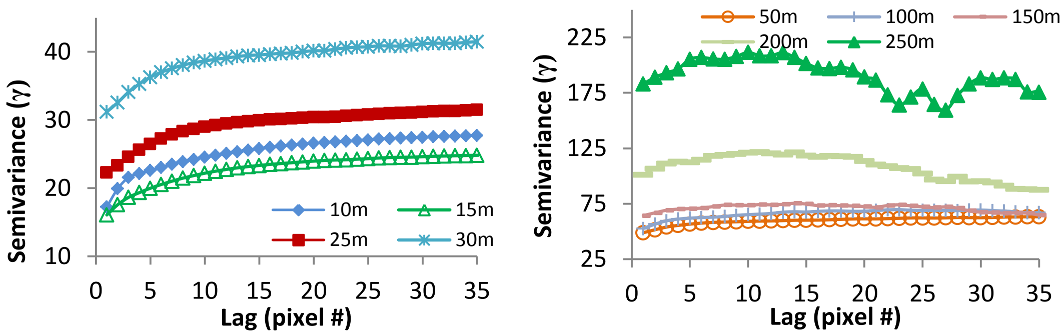

Figure 6.97 Upscaled STVI variograms

As stated previously (Section 6.3.3.1, Variance comparison) the shape of the variograms indicates the structure of the image. The quantitative differences in the variograms between the native and upscaled images can be seen in the equations in Table 6-39. These differences are discussed in Section 6.4.

Table 6-39 Comparison of native and upscaled STVI variogram expressions

Image Type	Resolution	Native scale Equation (y= Variance (γ), x= Lag (*l*))	Upscaled Equation (y= Variance (γ), x= Lag (*l*))
STVI	**10m**	$y_{(10m)}$ = 2.8805ln(x) + 17.9	$y_{(10m)}$ = 2.8816ln(x) + 17.896
	15m	na	$y_{(15m)}$ = 2.6496ln(x) + 15.928
	25m	$y_{(25m)}$ = 1.7027ln(x) + 1.199	$y_{(25m)}$ = 2.7534ln(x) + 22.17
	30m	na	$y_{(30m)}$ = 2.9722ln(x) + 31.351
	250m	$y_{(250m)} = -0.0018x^4 + 0.1224x^3 - 2.7934x^2 + 30.447x + 40.991$	$y_{(250m)} = 0.0009x^4 - 0.0424x^3 + 0.346x^2 + 2.6727x + 182.7$

Figure 6.98 provides a comparison of the variance for the native STVI cover images (solid symbols) compared with the upscaled STVI image variance (hollow symbols) overlaid on the same graph.

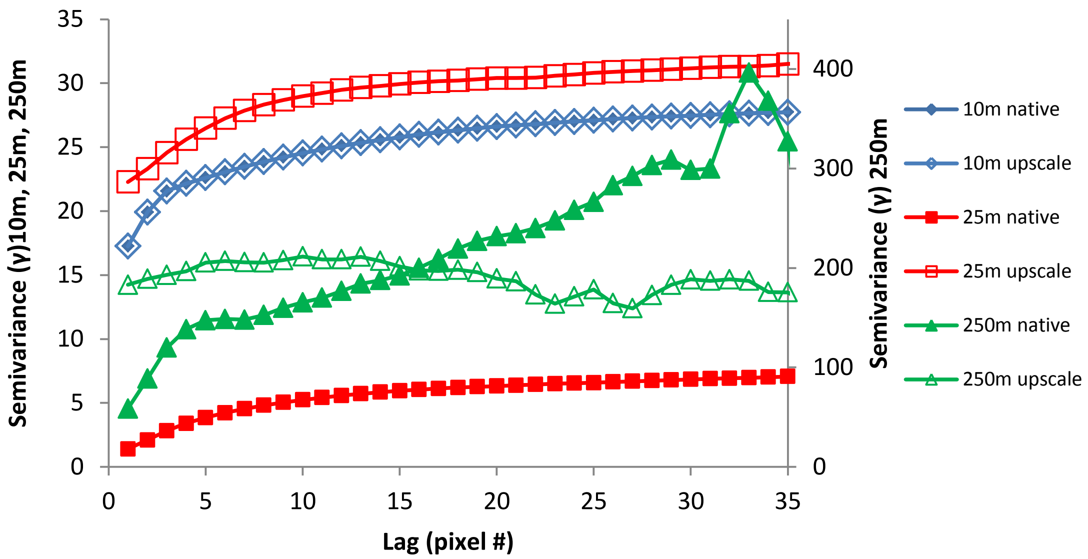

Figure 6.98 Overlay of native and upscaled STVI image variograms

In this figure, the 10m resolution variance plots are identical as expected because they were not upscaled. The 25m upscaled image variance is greater at all points than the 25m native image at all locations and is greater than the 10m native image variance. Unlike the SAVI image, the 25m upscaled image variance plateaus at much higher values than the native image, indicating that upscaling has increased the overall variance in the image. The native STVI image had a low SV of approximately 5γ while the SAVI image had a SV of 15γ. The 250m upscaled image variance is initially greater than the native image at the Sill, but it progressively declines, while the native image variance continues to increase with increased lag. This is a generally similar pattern of variance changes to the 250m SAVI image.ontour comparison

A side-by-side comparison of the semivariance contours for native and upscaled STVI cover images (Figure 6.99) illustrates the effect of upscaling on image variance.

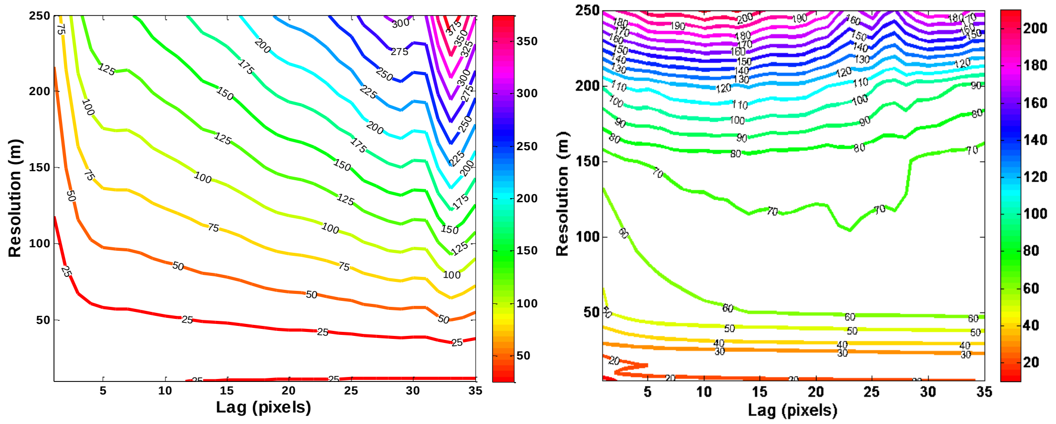

Figure 6.99 Comparison of variance contours for native (left) and upscaled (right) STVI cover images

This shows a similar pattern of change in variance to that shown for SAVI cover images in Figure 6.94.

Surface comparison

A comparison of the semivariance surface models for native scale and upscaled STVI cover images is shown in Figure 6.100.

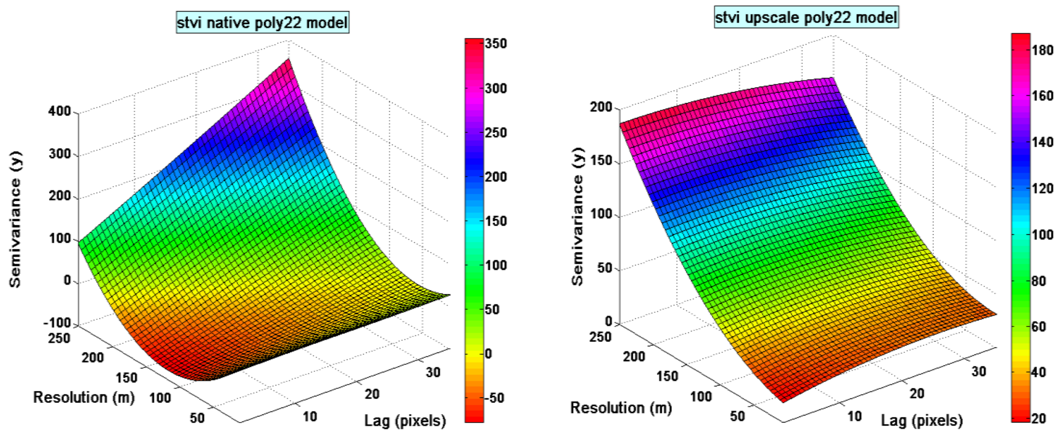

Figure 6.100 Comparison of STVI semivariance models

Both models have the same 2-variable quadratic form as shown by Equations 6-4 and 6-9. The difference in variable values between the two models is shown in Table 6-40.

Table 6-40 Variables for native scale and upscaled STVI semivariances

Scale	Expression parameters					
	Intercept	x coefficient	y coefficient	x^2 coefficient	xy coefficient	y^2 coefficient
Native scale	49.71	-0.68	-2.23	0.01	0.03	0.01
Resampled	16.560	1.182	0.140	-0.022	-0.005	0.002

The much lower value of the variance at higher lag and resolution in the upscaled image model compared to the native image model can be seen in Figure 6.100 and Table 6-40.

Index comparison

The more highly correlated semivariance variables are shown in Table 6-41 for the native scale and upscaled STVI images.

Table 6-41 Correlation of STVI variance variables for native and upscaled images.

All variables	Native Image Variables					Upscaled image variables			
	Resoln	Cell No.	Cover	Lcalc	AAL	Resoln	Cell No.	Lcalc	AAL
Cover	0.95								
Lcalc	0.95		1.00				0.94		
NV						0.90			0.70
FR	1.00		0.95	0.94		0.97			0.73
FSV	0.97		1.00	1.00		0.87			
SCV	0.99		0.98	0.98					
NSVR		0.95					0.97	0.90	
NSCVR		0.93							
RVF					0.99		0.99	0.91	
RSF		0.93					0.99	0.87	
FDO	0.99		0.99	0.99					
FML	1.00		0.97	0.97		0.85			
MFM	0.98		1.00	0.99		0.89			0.71
AFM	0.99		0.99	0.98					

The importance of FR and FML index values was discussed following Table 6-38. These values were significantly correlated with the Leakiness (Lcalc but not AAL) but in the resampled image, FR was correlated with AAL and not Lcalc (yellow highlighted cells in Table 6-41).

AAL was not correlated with resolution in either image as it was in SAVI. The FSV and MFM indices were correlated with Resolution and Lcalc in the native STVI image but not in the upscaled image. The pattern of correlations for other variance indices between the native scale and upscaled STVI images are also substantially different from the SAVI image pattern of correlation. This indicates dissimilar image structures and dissimilar responses to upscaling between SAVI and STVI images.

6.3.3.4. Perpendicular Distance (red over green) Index comparison (PDrg)

Variance comparison

Figure 6.101 shows the variograms for 10m, 25m and 250m native scale PDrg coverages and Figure 6.102 shows the variograms for the upscaled STVI coverages.

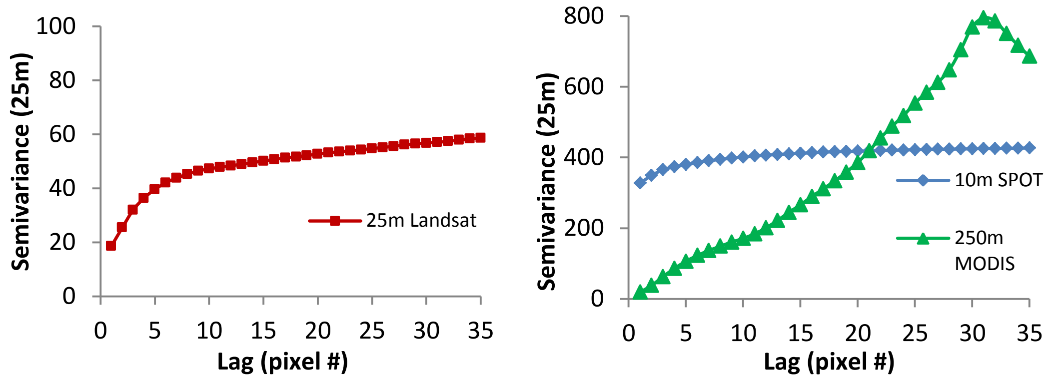

Figure 6.101 Native scale PDrg image variograms

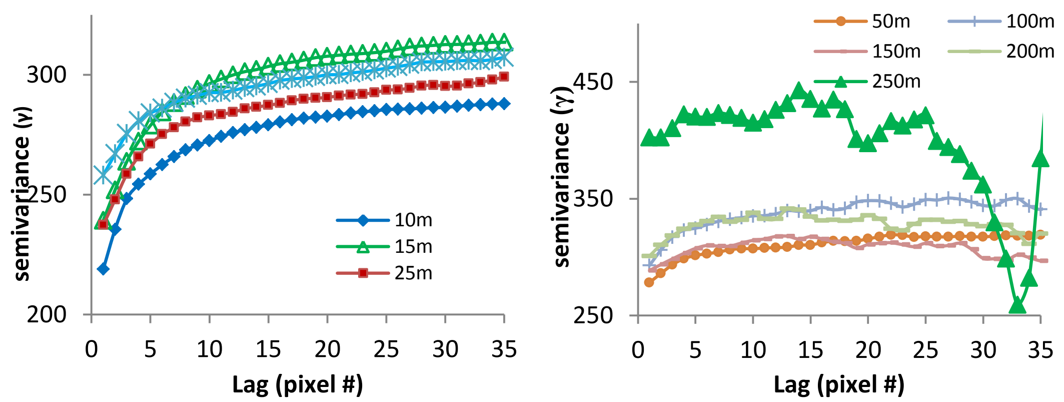

Figure 6.102 Upscale PDrg image variograms

The quantitative differences in the variograms between the native and upscaled images can be seen in the equations in Table 6-42. These differences are discussed in Section 6.4.

Table 6-42 Comparison of native and upscaled PDrg variogram expressions

Image Type	Resolution	Native scale Equations (y= Variance (γ), x= Lag (*l*))	Upscaled Equations (y= Variance (γ), x= Lag (*l*))
PDrg	10m	$y_{(10m)} = 27.992\ln(x) + 333.8$	$y_{(10m)} = 18.84\ln(x) + 226.53$
	15m	na	$y_{(15m)} = 21.612\ln(x) + 242.94$
	25m	$y_{(25m)} = 10.765\ln(x) + 20.884$	$y_{(25m)} = 16.435\ln(x) + 242.18$
	30m	na	$y_{(30m)} = 13.277\ln(x) + 260.7$
	250m	$y_{(250m)} = 0.0191x^3 - 0.3469x^2 + 18.127x + 10.894$	$y_{(250m)} = -0.0006x^4 + 0.0348x^3 - 0.8089x^2 + 8.4981x + 392.51$

In the native scale PDrg images, (Figure 6.101) the 25m resolution image has the lowest semivariance (same pattern as native STVI) with a sill of 42γ. This is followed by the 10m resolution image with a sill of 373γ (compared to 22.5γ for SAVI and STVI) and the 250m resolution image with a sill of 795γ (compared with 100 γ for SAVI and 150γ for STVI). The PDrg image has a very different pattern of variance when compared to SAVI and STVI at the same resolution. There is only slight evidence of nesting in the PDrg 250m variogram at a range of 6 pixels (1,5000m) which compared with the first range for SAVI and STVI variograms at 4 pixels (1000m). The first clearly defined range for the 250m PDrg variogram is at 32 pixels (7.75km). The NV, FR and FSV values for the PDrg native image show they have greater variance at all 3 resolutions than the native SAVI and STVI cover images.

In the upscaled image (Figure 6.102) the 25m image variogram has more variance than the 10m image variogram (same pattern as resampled STVI) and their SVs are 258γ and 271γ respectively. Further upscaling shows a progressive decay of the bounded exponential form of the variogram indicating loss of spatially dependent variance. The resampled PDrg SVs are consistently higher than the upscaled SAVI and STVI SVs confirming the higher variance in the upscaled PDrg images.

Figure 6.103 presents a comparison of the native and upscaled 10m, 25m and 250m variograms.

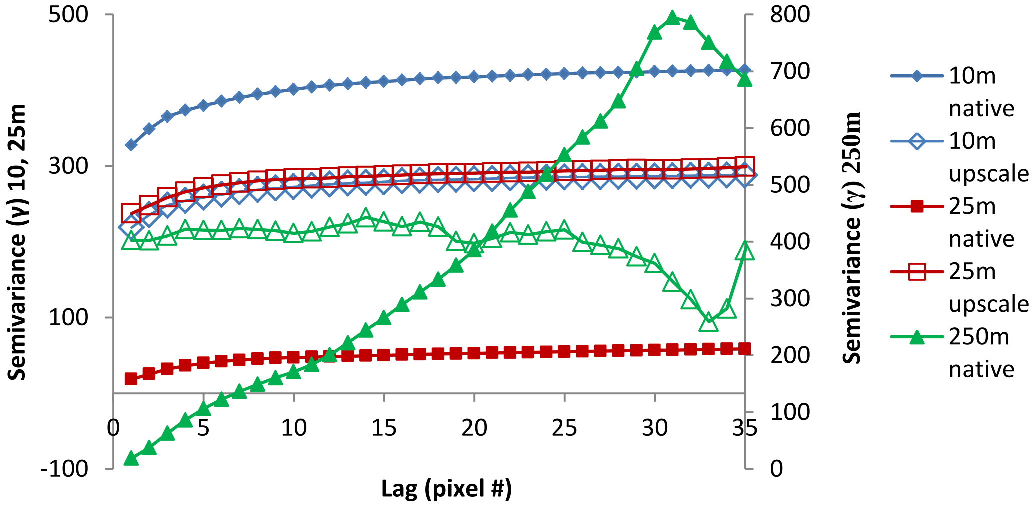

Figure 6.103 Comparison of PDrg native image variances with upscaled image variances

This figure shows that the upscaled 10m image has a lower variance than the native 10m image (these were upscaled from 5m to match the lowest resolution DEMs). The upscaled 25m image has a higher variance than the native 25m image than which is similar for both SAVI and STVI although the magnitude of variance is substantially different. The 250m upscaled image has a higher variance than the native 250m image at lags less than 20 (5km) however it continues to decrease at greater lags while the native image variance increases.

Contour comparison

A side-by-side comparison of the semivariance contours for native and upscaled PDrg cover images (Figure 6.104) shows the effect of upscaling on image variance.

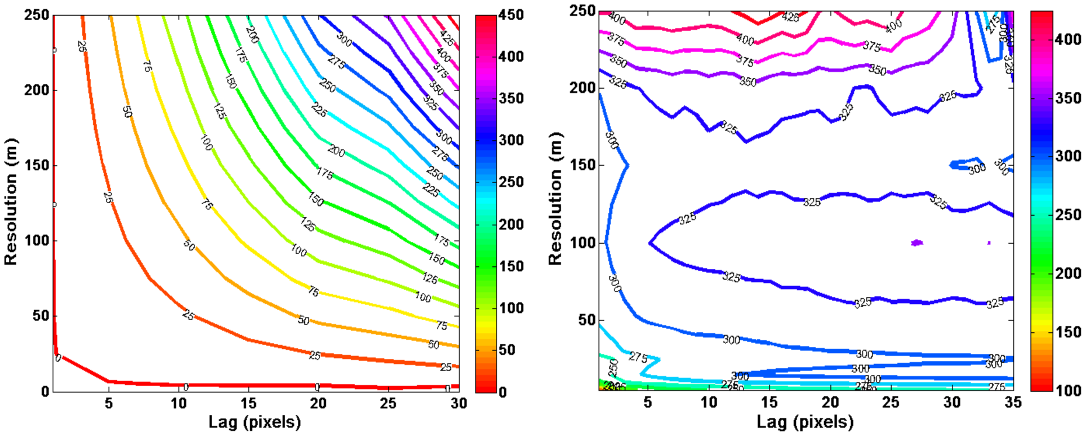

Figure 6.104 Comparison of variance contours for native (left) and upscaled (right) PDrg cover images

This shows a similar pattern of change in variance following upscaling to that shown for SAVI and STVI cover images in Figure 6.94 and Figure 6.99.

Surface comparison

A comparison of the semivariance surface models for native scale and upscaled PDrg cover images is shown in Figure 6.105.

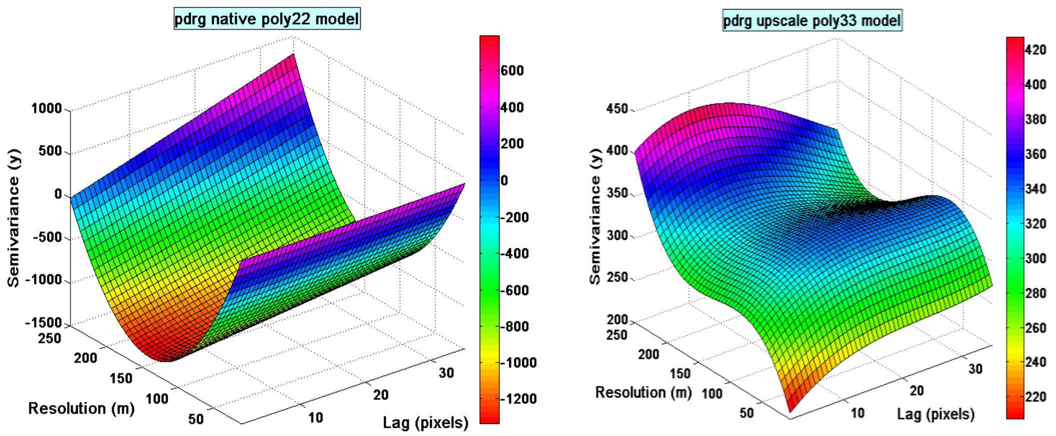

Figure 6.105 Comparison of PDrg semivariance models

These 2 models clearly have different forms. The PDrg native scale model can be modelled as a 2-variable quadratic equation while the PDrg upscaled image requires a 2-variable cubic expression to model it satisfactorily. The coefficients are shown in Table 6-43.

Table 6-43 PDrg model variable values

Scale	Inter-cept	x	y	x^2	xy	y^2	x^3	x^2y	xy^2	y^3
Native scale	-994.3	89.88	826.0	2.48	107.4	1283.0				
Up scaled	202.0	5.178	2.468	0.226	0.007	-0.022	0.004	-0.0003	0.00002	0.00006

The reasons for this difference can be seen in the reflex nature of the upscaled variance surface when compared with the concave nature of the native scale variance surface. The shape and position of the upscaled image variograms along with the increased complexity of the semivariance model clearly establish that the process of upscaling changes the image structure away from the structure of a native scale image of comparable resolution.

Index comparison

The more highly correlated semivariance variables are shown in Table 6-44 for the native scale and upscaled PDrg images.

Table 6-44 Correlation between PDrg variables for native and upscaled images (R^2)

All variables	Native Image variables					Upscaled image variables			
	Resoln	Cell No.	Cover	Lcalc	AAL	Resoln	Cell No.	Cover	Lcalc
Lcalc		0.85					0.99		
AAL	1.00								
NV		0.91		0.99			0.97		0.98
FR	1.00				0.99	1.00			
FSV				0.99				0.87	0.84
SCV			1.00				0.98		0.96
NSVR		0.99		0.92			0.99		0.96
NCSVR		0.93		0.98					
RVF	0.99				0.98		0.98		0.96
RSF	0.93	0.83			0.89		0.97		0.93
FDO							0.97		0.95
FML	1.00					0.86			
MFM					1.00			0.93	0.83
AFM	0.89		0.94		0.93		0.87		0.92

The FR and FML show significant correlation with resolution in both native and upscaled images but only FR shows significant correlation with AAL in the native scale images. The pattern of correlations of variance indices between the native scale and upscaled images is substantially different from each other and from the patterns in the SAVI and STVI images. This indicates dissimilar image structures both between the native and upscaled PDrg images and between the native and upscaled PDrg images and the SAVI and STVI mages as a group.

6.3.3.5. Native DEM vs resampled DEM

Figure 6.106 shows the position of the native DEM variograms relative to the resampled DEM variograms and highlights the relative position of the 2, 250m variograms.

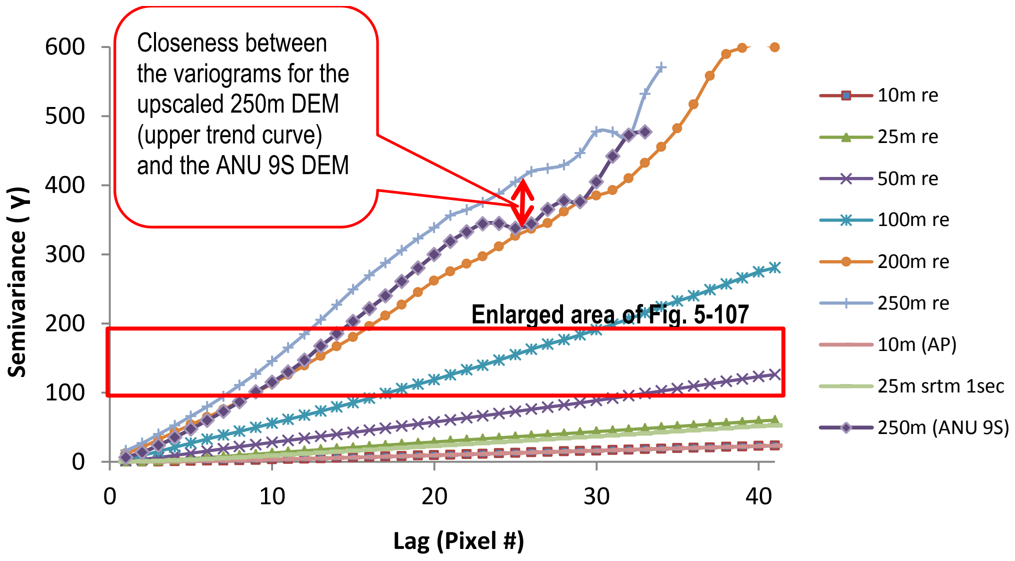

Figure 6.106 Comparison of upscaled DEMs with native DEMs

Figure 6.107 illustrates the finer detail in the 0-100 γ semivariance region of Figure 6.106. It also highlights the relative positions of the 25m native and resampled variograms. The 10m DEM resolution variograms overlap each other in Figure 6.107 because they are both developed from the 5m AP DEM.

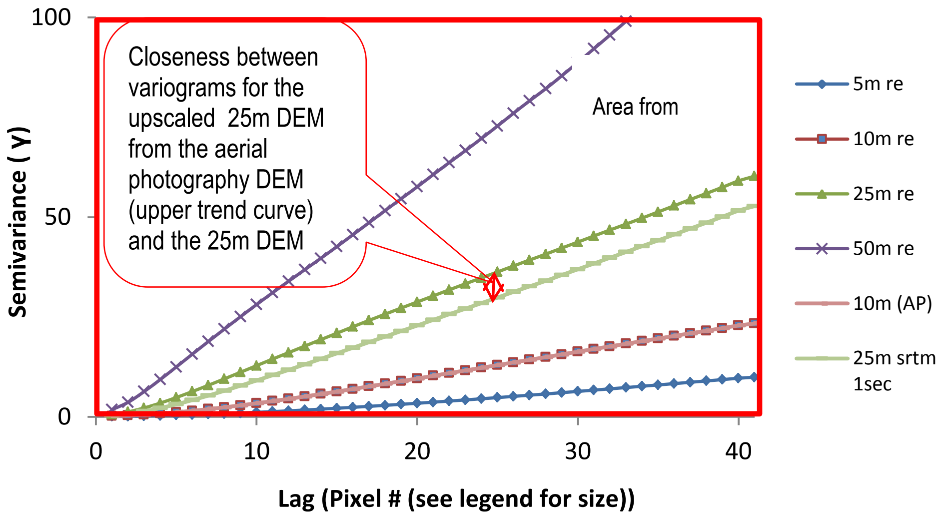

Figure 6.107 Semivariance of whole of catchment DEMs resampled from 5m to 250m

The 25m and 250m resampled DEMs exhibit a similar change in pattern of variance with resolution (increase in slope) when compared to the native 25m and 250m DEMs. This difference in slope is quantified by the equations in Table 6-45.

Table 6-45 Relationship between "native" scale DEMs and resampled AP DEM

Image Type	Resolution	Native scale Equations (y= Variance (γ), x= Lag (*l*))	Upscaled Equations (y= Variance (γ), x= Lag (*l*))
DEM	10m	$y_{(10m)} = 0.0074x^2 + 0.3538x - 0.7035$	$y_{(10mre)} = 0.0074x^2 + 0.3538x - 0.7022$
	25m	$y_{(25m)} = 0.0087x^2 + 1.0491x - 1.9142$	$y_{(25m)} = -0.0007x^2 + 1.5604x - 2.4248$
	250m	$y_{(250m)} = 0.0085x^2 + 15.179x - 25.52$	$y_{(250m)} = -0.0662x^2 + 18.57x - 20.347$

The semivariance of the resampled DEMs was compared with the native DEMs and found to behave similarly with lag. However, the semivariance of the resampled DEMs were consistently greater at each Lag than the native DEMs as shown by the solid lines (resampled DEM) which have a greater slope than the dashed lines in Figure 6.108.

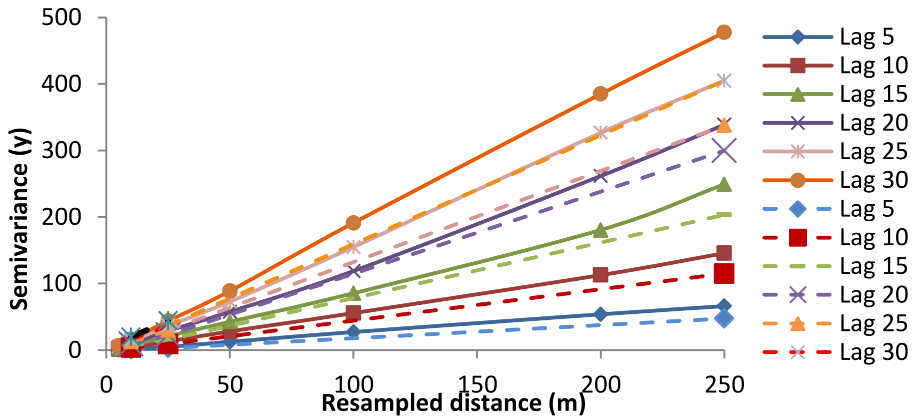

Figure 6.108 Semivariance of resampled DEMs (solid lines) relative to the semivariance of native DEMs (dashed lines)

The implication of this for Leakiness calculation from resampled imagery is higher leakiness values due to faster runoff than would be calculated from native scaled DEMs.

6.4. Discussion

The discussion section is first organised into structural observations about the images as indicated by their second order differences, namely variograms and variance surfaces. These are quite different measurements from the first order differences (covered in Chapter 4). This is then followed by a discussion of how the structures of the images change because of cubic convolution upscaling measured by second order image values. Finally, the implications of these results for leakiness calculation are discussed.

6.4.1. Image structure

6.4.1.1. Native scale images

Figure 6.4, Figure 6.12 and Figure 6.21 show the variance structure of each native image. All three images have natural logarithmic variograms at 10m and 25m resolution, while at 250m resolution their variograms are quartic except for PDrg, which is cubic. These are bounded variograms with a characteristic Nugget Variance (NV), Sill Variance (SV), First Range lag (FR), Spatially Correlated Variance (SCV) and a Nugget Sill Variance Ratio (NSVR) as shown in Table 6-46.

Table 6-46 Key native image structural values
(repeated from Table 6-2, Table 6-7, and Table 6-12 for convenience)

Variogram parameter	Native scale cover images								
	SAVI			STVI			PDrg		
	10m	25m	250m	10m	25m	250m	10m	25m	250m
FR (m)	30	175	1000	40	125	1250	40	150	1500
FR (pixels)	3	7	4	4	5	5	4	6	6
NV (γ)	19.7	5.1	26.5	17.9	1.2	41	333.8	20.9	10.9
SV (γ)	23	16	110	23	4	148	376	42	106
SCV (γ)	4	14	121	7	3	124	59	31	91
NSVR	0.86	0.38	0.24	0.78	0.3	0.28	0.89	0.50	0.10

In the SAVI 10m resolution image (Figure 6.4), there is a high degree of autocorrelation with most of the diversity captured within a FR lag of three pixels or 30m. It continues to rise, becoming asymptotic at 30 pixels or 300m. This indicates that most of the variance is exhausted by 30m and thereafter there is little additional variance or change in structure in the image. On the other hand when the catchment was measured at 25m resolution, a lot of the small scale diversity had disappeared (by aggregation) into the larger pixels, and these continue to differ from each other up to a FR lag of 7 pixels (175m) after which there is little additional variance or change in structure in the image. At 250m resolution the catchment has a SV of 110γ at a FR lag of 4 pixels (1000m).This is much greater than either the 10m or 25m resolution variances. It indicates this scale is identifying a different type of image feature from the 10m and 25m sampling scale and that this attribute has a much larger variation between feature elements. The additional shoulders in this variogram suggest two additional ranges at which further different features are identified at lags of 15 and 25 pixels respectively.

In the STVI images (Figure 6.12), the 10m resolution image captures most of the diversity in feature values within a FR lag of 4 pixels or 40m and a SV of 23γ. It continues to rise becoming asymptotic at 35 pixels or 350m. As before, this indicates that most of the variance is exhausted by 40m and there is little additional new information or change in structure in the image at greater distances. In a manner similar to SAVI, the 25m resolution image has a small FR lag of 5 pixels (125m) but a much smaller SV of 4γ. This shows much more removal of small-scale diversity at

25m resolution in STVI than in SAVI (more homogeneity in pixel values). After 5 pixels separation there is little additional variation in the image. Also, in a manner similar to SAVI, the 250m resolution variogram has a low FR lag of 5 pixels (1250m) with evidence of subsequent nesting (2^{nd} and 3^{rd} range lags at 17 pixels and 28 pixels). The SV of 148γ is similar to SAVI and indicates identification of different and more diverse feature elements from the 10 and 25m resolution SAVI images.

The PDrg images (Figure 6.21) have a very different pattern of variance in which the highest resolution imagery (10m) has the highest amount of SV (376.8 γ). This is due to very high NV (333.8 γ) (the unexplained variance in the image at a lag of one pixel). This SV occurs at a FR lag of 4 pixels, (40m) which means that the image is relatively homogeneous with a wide variation in the image feature values. As also occurred in the previous 2 images, the semivariance continues to rise, becoming asymptotic at 30 pixels or 300m. This indicates that most of the variance is exhausted by 40m and thereafter there is little additional structural change in the image. Also in a manner similar to SAVI and STVI, the 25m resolution image has a small FR lag of 6 pixels (150m) and a relatively much smaller SV of 42γ. This shows even more removal of the small-scale diversity at 25m resolution in PDrg images than in SAVI and STVI images and a large decrease in variance with change in scale from 10m pixels to 25m pixels thereby indicating that 25m is the scale closest to the image feature size for PDrg images. The 250m resolution PDrg image variogram is unbounded and continues to show increased variation up to 30 pixels (7,500m).

The Spatially Correlated Variances (SCVs), shown in the 5^{th} row of data in Table 6-46, can be a more significant measure of inherent image variance than SV. The SAVI 10m image has an SCV less than the 25m image, which indicates that 10m, is closer to the SAVI image feature size than 25 or 250m. STVI 25m imagery has less SCV than STVI 10m or 250m imagery indicating that 25m is the closest of the three resolutions to the image feature size for STVI images. The 250m SAVI and STVI images have similarly large variances. The pattern changes for PDrg where the 25m image has the lowest SCV of the 3 resolutions.

There is no data on which to know if this pattern applies to other catchments but it clearly indicates the very different structure of the different types of cover images at three different scales in the experimental catchment. From this information, it can be seen that the type of cover analysis can either detect or fail to detect image feature patterns depending on the scale at which they exist in the analysis area. This has large implications for the calculation of leakiness because it depends on the relative location of the features within a watershed and the amount of coverage of those features.The NSVR (6^{th} data row in Table 6-46) decreases with decrease in resolution for all images.

The preceding data provide a background against which to make comparisons with other investigators research findings. The behaviour of the native scale images at different resolutions is different from that previously reported by other investigators

(Chen and Henebry 2009; DeCola 1994; Goodin and Henebry 2002). These investigators reported that FR consistently increased and the SV decreased at lower resolutions. Table 6-46 shows that the FR remains about the same pixel value at all 3 scales while the SV decreases with decrease in resolution from 10 to 25m and then increases with further decrease in resolution to 250m. This pattern was consistent across all 3 types of images.

This response pattern changes a little when SCV is considered. It increases with decrease in resolution for SAVI and STVI images but remains “V” shaped for PDrg images. The change for SAVI and STVI does not correspond to previous reported findings while the change in PDrg SCV is only partially consistent with the previously reported findings. The difference in these results may be due to:

a. **Scaling Range.** All previously reported findings were based on analysis of very high-resolution images (sub-meter to meter pixel resolution) which for NDVI they used, is likely to be well below the image feature resolution threshold. Accordingly, the SV would be expected to decrease as such images were upscaled towards the image feature resolution. Evidence for this view exists in the pattern of SV shift in the upscaled images.
b. **Type of Feature.** The type of natural resource feature captured by the imagery may cause the different pattern of image variance response. Lausch *et al.* (2013) established, albeit with 1-3m resolution imagery, that images of different natural landscapes showed different patterns of variance as evidenced by their variogram characteristics.
c. **Type of Rescaling.** The previous investigators used Nearest Neighbour and Non-overlapping Averaging rescaling whereas this research used Cubic Convolution rescaling.

6.4.1.2. Upscaled Images

The following pairs of figures, Figure 6.44 and Figure 6.45, Figure 6.55 and Figure 6.56, and Figure 6.71 and Figure 6.72, show the variance structure of each series of upscaled images. All three series continue to have bounded natural logarithmic variograms when upscaled from 10m through 15m, 25m and 30m after which they show increasing loss of structure with progressive upscaling. For this reason the shape and characteristics of upscaled variograms at 50m, 100m, 150m and 200m resolution were not considered in further detail.

Table 6-47 Key upscale image structural values (from Table 6-22, Table 6-26 and Table 6-30 for convenience)

Variogram parameter	Upscale cover images								
	SAVI			STVI			PDrg		
	10m	25m	250m	10m	25m	250m	10m	25m	250m
FR (m)	30	175	1500	40	175	1250	50	125	1000
FR (Pixels)	3	7	6	4	7	5	5	5	4
NV (γ)	19.7	16.8	114.3	17.9	22.2	182.7	226.5	242.2	392.5
SV (γ)	23	20	131	22	29	220	259	271	422
SCV (γ)	6	4	19	7	8	51	66	47	39
NSVR	0.86	0.84	0.87	0.78	0.77	0.83	0.87	0.89	0.93

The SAVI image variance (Figure 6.44) decreases to a minimum at 15m then increases a little at 25 m and rises back above the 10m image when upscaled to 30m. This indicates that most variance is absorbed by the 15m pixels and the structural variance is exhausted by the FR lag of 7 pixels (105m). Thus 15m is a more optimal resolution at which to identify SAVI image features than either 10 or 25m, and based on theory, this resolution would be expected to yield a more accurate estimate of leakiness than either the 10 or 25m resolutions of the SPOT image. The upscaled 25m image has the same FR as the native image (lag 7) but is less homogeneous, i.e. higher variance, than the native image SV of 20γ versus 16γ. They merge at the asymptote as shown in Figure 6.93. The 30m image has a similar FR at lag 7 (210m) but a higher SV (27γ) indicating larger pixels are identifying features with greater variance. All subsequently larger pixels produce images with higher SV. The NVs also increased with upscaling. Image structure exhausts quickly with more upscaling as shown in Figure 6.45.

The STVI upscaled image variance behaved in a similar pattern to SAVI, but with different values. The image variance decreased as it was upscaled from 10m to 15m (Figure 6.55) indicating increased absorption of variation by 15 m pixels compared to 10 m pixels. However, the variance steadily increased with further upscaling so that the upscaled 25m image has more variance than the 10m image. (This is different from the SAVI image where the 25m upscaled image had less variance than the 10m image). All other upscaled STVI images had more variance which is consistent with the findings of Kerry and Oliver (2008). The FR lag is 4 for the native 10m STVI image but immediately increases to 7 for the 15m upscaled image and remains at 7 from 15m to 30m resolution. Upscaling above 30m exhausts image structure (high NSVR) as shown in Figure 6.56.

For the sub-catchments, the variograms (Figure 6.65 to Figure 6.70) show a close grouping of bounded natural logarithmic variograms at 10m and 25m resolution but the organised structure in the image disappears above 50m resolution. At 10m the FR lag varies between 3-4 pixels with a SV of from 8 to 12γ. At 25m the FR lag increases to 4-5 pixels and the SV increases to 11-16γ. At 50m resolution and above all sub-catchments show strong loss of structure. The sub-catchment image variograms behave consistently with gradual increase in FR and SV with decrease in resolution.

The PDrg image behaves differently from SAVI and STVI images upon upscaling. All levels of upscaling produce higher SV values. The FR lag remained stationary at 5 for all upscaling from 10 to 30m. Initial upscaling from 10m to15m increases the SV from 259γ to 279γ and then upscaling to 25m reduces the SV to 270γ while upscaling to 30m increases the SV to 282γ. It initially rises, then decreases and rises again with further upscaling. This indicates that 10m resolution (or less) is the optimal image feature scale for the PDrg image and that there is a second image feature scale close to 25m in PDrg images. Higher levels of upscaling (from 50m to 250m) produce progressive degradation in the image structure and higher amounts of variance.

The SCV for the upscaled images show that upscaling SAVI images decreased SCV at 25m and 250m when compared to the native images (5^{th} data row in Table 6-47). Upscaling STVI images increased SCV at 25m but decreased it at 250m and upscaling PDrg increased SCV at 25m but decreased it at 250m.

The scale that produces the lowest SCV is the most appropriate scale at which to measure the features of interest because, at this scale, the mixed pixel effect is the lowest. This will not necessarily appear as the most homogeneous image scale because of the compounding effect of the unresolved variance. The data from Figure 6.92 and Figure 6.97 suggest that 15m is the optimal scale at which to identify SAVI and STVI features and 10m is the optimal scale to identify PDrg features.

The NSVR (6^{th} data row in Table 6-47) remains relatively constant at each upscaled resolution and for each type of analysis. This contrasts with unscaled images where it decreased at lower resolutions. This is caused by persistent higher unexplained variance (NV) in the upscaled images (Table 6-47).

Comparing these findings against the findings of other investigators shows a number of differences. The FR lag remained between 3-7 pixels for upscaling from 10 to 250m while previous investigators found an increase in FR lag from both Nearest Neighbour and block Averaging upscaling (Chen and Henebry 2009; DeCola 1994; Goodin and Henebry 2002). The SV remained steady or increased as resolution decreased in these results, whereas SV decreased with decrease in resolution in the results reported in the 3 previous references. The SCV did not display any consistent pattern of change with decrease in resolution.

The differences between these results and the results reported by other investigators for upscaled images may be due to the reasons listed earlier, namely the range of change in resolution relative to the image feature scale, the type of natural resources imaged and the type of rescaling method.

The position of the upscaling variograms relative to each other differs for different cover analyses. The 10m variogram for SAVI (Figure 6.44) shifts downwards (lower SV) when upscaled to 15m and then moves up a little (but still below the original 10m variogram) when rescaled to 25m and only after upscaling to 30m does it remain above the original 10m variogram. The 10m variogram for STVI (Figure 6.55) has a lower SV when upscaled to 15m but then moves up above the original 10m variogram when upscaled to 25m and continues to have higher levels of SV at progressively lower resolutions. PDrg upscaling (Figure 6.71) exhibits yet another pattern of change in variance with upscaling. The original 10m variogram has the lowest variance. Upscaling it to 15m results in more image variance than upscaling it to 25m. The 15m variogram also intersects the 30m variogram at a lag of 6 pixels after which it has a higher variance than the 30m resolution image.

The analysis above has shown that analysing the variance of the cover images at different native scales and different coarser scales can shed light on the structure of the image and assist in identifying the best scale at which to analyse the feature of interest. The data suggest that the optimal resolution for SAVI and STVI image feature analysis is close to15 m while for PDrg it is 10m or less.

6.4.2. DEM structure

DEMs at each resolution yielded unbounded quadratic variograms for the catchment as shown in Figure 6.30. When the 10m DEM was upscaled it also yielded similar quadratic unbounded variograms. The highest resolution (largest scale) consistently had the lowest rate of increase in semivariance as shown graphically in Figure 6.84 and Figure 6.106 and as measured by the slope of the variogram expressions shown in Table 6-45.

The variances of the upscaled 25m and 250m DEMs were very similar to the native DEMs at the same resolution (Figure 6.106) except that they had slightly higher variances. The absence of structure in the original DEM (10m) led to there being no structure to degrade in the upscaling process. This would explain why the upscaled DEMs retained the same shape as the native DEMs at the lower resolutions. However, it does not explain the small but progressive increase in slope with decrease in resolution that was observed. This appears to be indicative of increased variance at smaller scales due to upscaling degrading residual structure in the DEM.

The quadratic structure of the DEM variograms is thought to be due to the relatively small size of the experimental catchment such that more and more features are captured at increasing ranges. This explains why the elevation variance continues to increase at all ranges within the relatively small catchment. It may require a larger catchment with this type of topography to capture all the features to display a bounded variogram.

6.4.3. Variance Surfaces

While the variance of an image at a single scale can be represented as a 2D variogram (lag versus semivariance), at multiple scales it can be represented in 3 dimensions; lag versus resolution versus semivariance. The 3 dimensions were portrayed first as contours, and then as surfaces to which model equations were fitted in order to quantify and compare the behaviour of the cover images and the effect of upscaling on them.

6.4.3.1. Native scale images

The native scale images have variance surfaces in the form of 2-variable quadratic expressions as shown by Equations 6-3, 6-4 and 6-5 (see Sections 6.3.1.1, 6.3.1.2 and 6.3.1.3). From inspection, the similarity between the SAVI and STVI image variance surfaces is evident. They both have positive intercepts while PDrg has a strong negative intercept. All PDrg coefficients are much larger than the SAVI and STVI coefficients indicating a much higher levels of variance. This is consistent with the larger SV and SCV values in Section 6.4.1.1.

6.4.3.2. Upscale images

The upscaled image variances were modelled in a similar manner and took the form of 2-variable quadratic expressions for SAVI and STVI and a 2-variable cubic expression for PDrg (see Sections 6.3.2.1, 6.3.2.2 and 6.3.2.3). Again, from inspection, the similarity between the SAVI and STVI upscaled image variance surfaces is evident. Coefficient values for all 2-variable quadratic terms are of a similar order and magnitude. However, the upscaled PDrg image variance surface is not fitted well by a 2-variable quadratic expression and instead requires a 2-variable cubic expression to achieve a satisfactory fit ($R^2 = 0.97$). This provides further evidence that the structure of the PDrg cover image is fundamentally different from the SAVI and STVI cover images. The cubic expression is clear indication of two different scales of features in this image and supports the inverted scale variogram order seen in Figure 6.102. This occurs when upscaling the resolution from 10m to 15m increases the SV followed by a decrease in SV when furthered upscaled to 25m and then followed by an increase in SV when further upscaled to 30m resolution and beyond (Figure 6.71).

6.4.4. Correlation of image structure with leakiness

The relationship between image structure and leakiness was explored through the use of variogram indices as explained in Sections 6.2.2 and 6.2.3.

6.4.4.1. Native scale images

To simplify discussion of these results, the significant correlations between variogram indices and leakiness for each cover image are collected together in Table 6-48. These results show that some correlations with leakiness are consistent across two types of cover images but not across all 3. This is interpreted as there being no consistent variance parameter that is related to leakiness in the three native scale images.

Table 6-48 Significant native image variogram correlations (from Table 6-9 and Table 6-14).

	All variogram indices	Image Cover					
		SAVI		STVI		PDrg	
		Lcalc	AAL	Lcalc	AAL	Lcalc	AAL
Conventional Indices	NV					0.99	
	FR	0.96	0.99	0.94			0.99
	FSV	1.00	0.99	1.00		0.99	
	SCV	0.97	1.00	0.98			0.79
	NSVR				0.68	0.92	
	NSCVR				0.72	0.98	
UPV indices	RVF				0.99		0.98
	RSF						0.89
	FDO	0.99	1.00	0.99			
	FML	0.99	1.00	0.97			1.00
	MFM	1.00	0.99	0.99			
	AFM			0.98			0.93

6.4.4.1. Upscaled images

In a manner similar to above the variogram indices that showed significant correlation to upscaled cover images were assembled in Table 6-49.

Table 6-49 Significant upscaled image variogram correlations (From Table 6-24, Table 6-28 and Table 6-32)

	All variogram indices	Image Cover					
		SAVI Upscale		STVI Upscale		PDrg Upscale	
		Lcalc	AAL	Lcalc	AAL	Lcalc	AAL
Conventional Indices	NV		0.81		0.70	0.87	
	FR				0.73		
	FSV		0.82		0.71		
	SCV	0.93				0.95	
	NSVR	0.90		0.90		0.96	
UPV indices	RVF	0.97		0.91		0.96	
	RSF	0.93		0.87		0.93	
	FDO					0.93	
	MFM		0.82		0.71		
	AFM	0.87		0.73		0.92	

NSVR, RVF, RSF and AFM are correlated with Lcalc leakiness in all three upscaled images (highlighted) but not with AAL leakiness. This suggests that the Lcalc leakiness of upscaled images may be related to or affected by the change in semivariance and therefore it might be possible to relate this measure of an image to the change in its Lcalc leakiness but not to its AAL leakiness.

To assist understanding of the correlation of variance with Lcalc leakiness, the 3 relevant graphical relationships (from Figure 6.53, Figure 6.63 and Figure 6.82) are re-presented here in Figure 6.109.

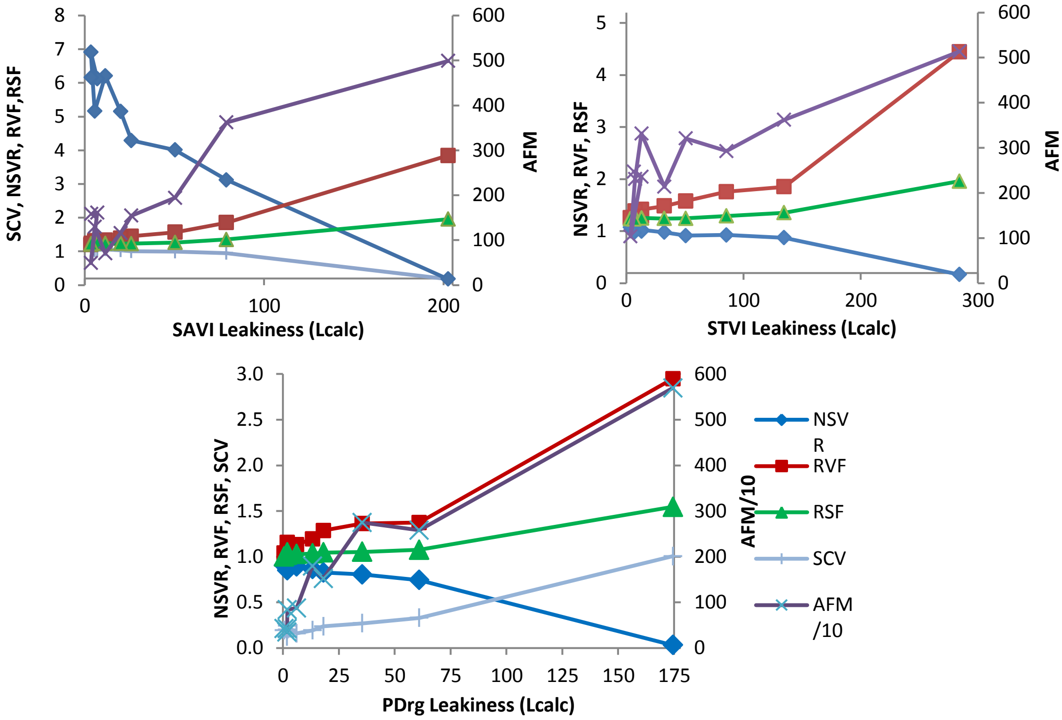

Figure 6.109 Variogram Index correlation relationships with Leakiness (Lcalc)

The following patterns of response are evident from Figure 6.109.

a. SCV (Spatially Correlated Variance) decreases linearly with SAVI leakiness, is not significantly correlated with STVI leakiness and increases linearly with PDrg leakiness. There is no consistent pattern of response.
b. NSVR (Nugget Sill Variance Ratio) decreases linearly with increase in leakiness in all images, but the rate of decrease is different for different images.
c. RVF (Total Variance/First Lag Variance) increases approximately linearly with increase in leakiness in all 3 images.
d. RSF (Second Lag Variance/First Lag Variance) increases linearly with increase in leakiness but the rate of increase is less than the RVF rate of increase.

e. AFM/10 (Area between the first lag and the first maximum ($1/10^{th}$)) increases with increase in leakiness, however there are marked irregularities in the pattern of increase.

These relationships may have potential for explaining how Lcalc leakiness changes in response to image upscaling. However, before proceeding to develop such relationships they should be tested on different catchments, upscaling ranges and rescaling methods. No correlations between AAL leakiness and variance were found. Correlations between variance and leakiness in upscaled images were not investigated any further in this research because the objective was to investigate the effects of image scale on leakiness and this necessitated the use of AAL leakiness for which no correlations were discovered.

6.5. Conclusion

All cover images at each resolution have a unique variance as defined by their variograms. At 10m and 25m resolution the variograms are natural logarithmic variograms while at 250m, the SAVI and STVI images have quartic variograms and the PDrg image has a cubic variogram. The FR remained essentially stationary, the SV always decreased from 10m to 25m resolution and then increased at 250m resolution, the SCV varied with decrease in resolution and the NSVR consistently decreased with reduced resolution. The form of the 3-D variance surface for all native scale images is dual quadratic.

The variance of all images decayed with progressive upscaling. The variogram structures remain natural logarithmic with upscaling from 15m to 30m but then progressively decayed to quartic at 250m. As the images were upscaled the FR increased and the SV either decreased or increased depending on the particular image, the amount of change in scale. The natural logarithmic form of the variogram decayed at higher levels of upscaling indicating loss of image structure. The NSVR stayed the same with progressive upscaling. This indicated loss of spatial structure as a result of upscaling where the unexplained variance remains high.

The initial increase or decrease in variance of the image following upscaling indicates the optimal scale at which to measure the image features. Based on minimal variance, SAVI features had a spatial resolution closer to 15m than 10m, STVI features had a spatial resolution closer to 15m than 25m and PDrg features had a spatial resolution close to 10m, the resolution at which they were measured.

Native images showed no scale dependent variance relationship with either Lcalc or AAL leakiness for all types of cover. Upscaled images have 4 variogram indices (NSVR, RVF, RSF and AFM) that show high scale dependent correlation with Lcalc leakiness but not with AAL leakiness. These indices are not useful for relating leakiness to image structure at different scales because leakiness at different scales has to be measured using AAL leakiness.

The native and upscaled images had different variance responses from previously reported work. The differences may be due to scaling range, scene structure and rescaling methods.

In conclusion, upscaling 10m images to 25m and 250m does not produce images with the same structure as either the 25m or 250m native images. The change in structure of the image means that it is not identifying the same image features as a native image at that resolution and thus it will have a different leakiness value. This is the core of the explanation as to why upscaled images do not have, and indeed cannot have, the same leakiness as similar resolution native images. However this does not prevent the use of scalograms to compare the leakiness between upscaled images with different resolutions and variances.

CHAPTER 7

EFFECT OF VEGETATION COVER POSITION ON CATCHMENT LEAKINESS

7.1. Introduction

Catchment condition is often expressed in terms of averages, such as the average amount of Bare Ground or the average amount of Ground Cover over the catchment. Such values, while useful as general indicators of catchment condition, overlook the importance of the location of the cover relative to morphological features of the catchment in determining how the catchment is functioning to retain or leak resources. The importance of cover location within a catchment is based on the work of many people but perhaps most notably in Australia the early works of Tongway, Pickup, Bastin and Ludwig who's various reports are cited in the following section. Their work shows that resource limited catchments are composed of alternating resource sinks and fetches (areas from which resources are lost). Resource sinks are characterised morphologically by resource accumulation areas such as pits, swales and tree lines, in and across the landscape, in which there is a higher concentration of nutrients, water and organic material than in fetch areas. These areas can be identified from visible and NIR wavelength satellite imagery as areas of increased cover. Cover as a general term is used to indicate a wide range of non-bare ground attributes related primarily to the presence of dead or living photosynthetic material.

In this Chapter, the effect of the location of added cover on the leakiness of resources was investigated. Methods, as described in Section 7.2, were used to segment the catchment according to different morphological features (slope, landform etc.) and increased levels of cover were applied to these areas in a systematic pattern. The leakiness of the modified catchments was then assessed using the LC and the results were analysed to identify the sensitivity of cover location on leakiness.

Satellite imagery is used to measure biomass cover values both directly (subject to ground truth verification) and indirectly to estimate many other parameters for which the presence or absence of biomass cover is a surrogate. These include direct values such as presence or absence of photosynthetic and non-photosynthetic material, indirect attributes such as habitat, soil protection, resource accumulation, infiltration and carbon sequestration and by analogy biodiversity and landscape function. The methods used to derive these values from image reflectance values should serve to caution the interpretations placed on them.

Conventional ways of changing cover include clearing trees, forage harvesting, grazing animals, burning crop residues or pastures, planting and growing crops and forests or natural area revegetation by destocking or intentional revegetation (Beeton and Buckley *et al.* 2006). These activities, which occur as part of customary land management practices, are usually done either in the course of producing revenue from land, for safety, environmental or aesthetic reasons. The objectives decide where the cover is added or removed. The effect of position within the catchment on catchment function is rarely a consideration.

Irrespective of the objective, the position in the catchment where the cover is changed affects the functioning of the catchment as an ecological unit. This effect may not be visible at first if the catchment is rich in resources. In resource limited catchments (Tongway and Ludwig 1990), interruption to natural resource flows quickly becomes apparent through changes in plant community composition, water quality changes and soil erosion. As catchments are managed to “work harder”, through the production of more goods and services for human use, resources of water, nutrients and carbon become more limited and the position of the catchment shifts along the resource spectrum from abundance to paucity. Resource gradients are a well-documented feature of working catchments (Niyogi and Koren *et al.* 2007). Gradients take the form of progressive changes in terrestrial and aquatic communities at distances from watering points, supplemental feeding points and anywhere animals concentrate (Landsberg and James *et al.* 1997; Pringle and Landsberg 2004). These visible changes reflect the changes in ecological processes that occur at the local scale within these gradients and more generally in catchments as a whole.

Cover-dependent landscape function elements such as water, nutrients and sediment move along hydrological gradients in a catchment, impeded by morphological and ecological processes. Elevation and cover are the primary determinants of this movement until ultimately the resources reach the marine environment. Human alteration of morphological landscape features and the removal of cover leading to adverse freshwater and marine impacts are worldwide phenomena (Wilkinson and Brodie 2011).

The following section discusses spatial location aspects of these phenomena by using the LC to measure catchment leakiness in the context of the broad range of variables affecting loss of catchment resources. A more complete discussion of the development and functioning of the CSIRO Leakiness Calculator software (LC) and the Leakiness Index (LI) are given in Chapter 2.

The previously reported findings of Bartley and Toth *et al.* (2006) and Boer and Puigdefabregas (2005) that loss of catchment resources depended on (i) the location of the cover in the hydrologic flow pattern, (ii) patch size, (iii) patch CSI (cross scale interaction) effects, and (iv) patch SSC (soil surface conditions) help define the parameters that ideally need assessment by a leakiness tool. Hydrologic location of cover can be determined by pixel position in a DEM. Patch size requires classification of cover and variance analysis of the patch classes through the use of semivariograms. CSI effects depend on patch size and SSC, and SSC depends on soil type and treatment. It is best measured by field ground truth studies.

The LC software and LI were developed by Ludwig *et al.* (Ludwig, J. and G. N. Bastin *et al.* 2007) based upon earlier development of the Directional Leakiness Index (DLI), Multi-Directional Leakiness Index (MDLI) (Ludwig and Eager *et al.* 2002) and the Cover based Directional Leakiness Index (CDLI) (Ludwig and Eager *et al.* 2006) as discussed in Chapter 2. The LI provides a quantitative measure (a unit less number) of the aggregate loss of soil from a catchment in a form that can be compared with losses under different management conditions and at different times (same cell size and number). By combining the amount of cover with position in the terrain and thus the hydrologic flow path, it gives cover location sensitivity to the calculation. Its limitations are that it does not include sensitivity to patch size nor to CSI effects. It has the capability to be sensitive to SSC by modification of the exponential power function b in the loss term $l_{i,j} = e^{-bxc_{ij}}$. The value of b defines the steepness of soil loss with change in cover (default b = -0.065) which is a measure of the SSC.

The LC can be used to evaluate the effect of change in the amount of cover at different positions by selective alteration of the input cover layers (See Section 7.2). The cover rasters can be changed so that they selectively increase cover in particular areas and either increase the “average cover” of the layer or keep the “average cover” the same by offsetting it in other areas of the catchment. The SSC value b can be changed or held constant however it applies to all pixels in the coverage. Because the LC has no variables for patch size or for CSI, the results are not sensitive to changes in these values. It will require new assessment techniques to incorporate the effect of patch size, CSI effects and SSC at the patch level on catchment leakiness. Boer and Puigdefabregas (2005) suggested using variance and autocorrelation techniques to measure the spatial variation of cover classes.

The following sections describe how the cover layers were changed, evaluated using the LC and analysed to determine which physical parts of the catchment were the most sensitive to the loss of resources. Confidence in the interpretation of these results should be tempered by the reservations discussed above.

7.2. Methods

7.2.1. Zonal cover analysis plan

Change in cover can be imposed on a catchment in a number of ways, either as a percentage increase of each pixel's cover value, as an absolute increase in each pixel's cover value or on a threshold basis whereby cover is allocated preferentially to the pixels with the lowest values in each zone until the available cover allocated to that zone is consumed. Additionally, the overall cover of the catchment can be increased by a standard amount for each analysis or it can be held constant. If overall catchment cover is held constant, then increases in cover in one area of the catchment have to be offset by reductions in other areas of the catchment. All analyses were done using previously generated DEMs, catchment masks and cover layers for SAVI and PDrg cover. Table 7-1summarizes the cover location analysis plan.

Table 7-1 Analysis Plan for effect of Cover Location on Catchment leakiness

Morphological feature	Name	Number of Zones	SAVI Cover	PDRG Cover	Number of Treatments	No Offset /Offset
Drainage Line	DDL	6	Y	Y	4	Y/Y
Elevation	Elevn.	6	Y	Y	4	Y/Y
Slope	Slope	6	Y	N	4	Y/Y
Aspect	Aspect	6	Y	N	4	Y/Y
Topographic feature	Topo.	6	Y	Y	4	Y/Y
Amount of cover	Cvr.	6	Y	Y	4	Y/Y

All morphological features were classified into 6 classes by the procedures described in the following subsections. SAVI coverage was analysed for all features however PDrg coverage was only analysed for 4 features as shown in Table 7-1. This was due to the limited available time and to the unremarkable results from SAVI analysis for the 2 feature classes that were omitted from PDrg coverage analysis (slope and aspect). Four increases in cover (treatments) were applied to each class and each treatment was imposed with and without offset. In all, 480 analyses were done.

The general procedure for modifying the catchment cover files so as to impose the treatments on each morphological feature is shown in Figure 7-1.

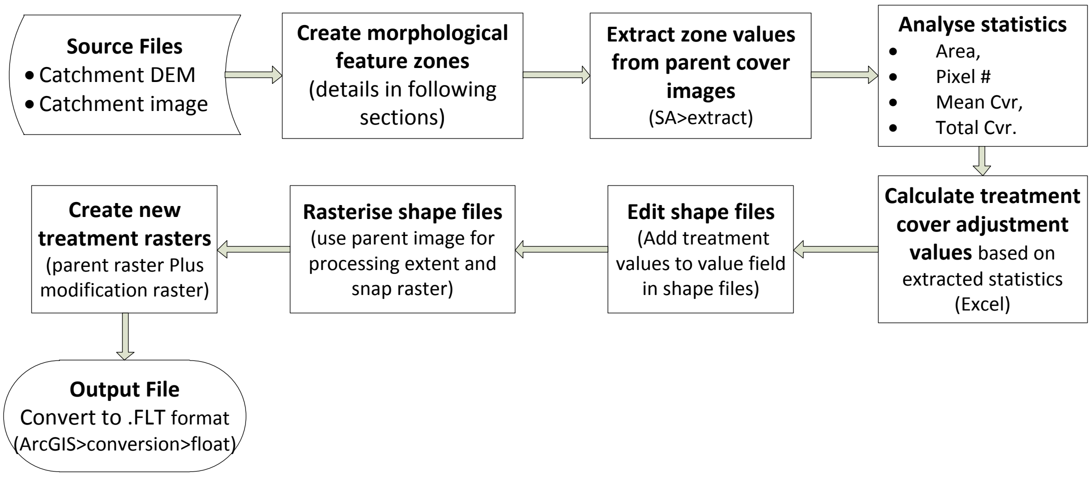

Figure 7.1 General processing schema for applying cover treatments

Either the DEM or the Cover image of the catchment was used as the starting point for identification of the zone shapes of the morphological features of interest. The procedures by which this was done differed for each feature and are described in Section7.2.4. Each feature class zone was then used to extract its respective cover layer characteristics from the SAVI and PDrg layers. The statistics in these layers were then used in the following procedure.

7.2.2. Zonal pixel adjustment procedure

The following procedure defines how the values of zones of pixels within a catchment can be adjusted up and down so as to impose a desired level of cover adjustment. This can be done either with or without offsetting the cover values on the rest of the catchment. This is a useful procedure to explore the effect of change in vegetation in selected areas of the catchment on overall catchment leakiness such as when investigating potential revegetation sites.

It is designed to work with zones created by any method such as distance from drainage lines, elevation, slope or existing cover. Currently the formulation is limited to changing one zone at a time and either distributing the balance of the change across all other zones or leaving the cover values of the other zones unchanged. Where it is desired to change the amount of vegetation cover in more than one zone at a time (such as when there are many finely classified zones) it is suggested that the catchment be rezoned so that the included area is in only one zone. The changes can be made in Excel or Matlab according to the following formulation.

$$Z_j = \sum_{i=1}^{n} X_{j,i} Y_{j,i} \tag{7-1}$$

where Z= Wtd. Value of all Cover

$$\text{Sum } Z = \sum_{j=1}^{m} Z_j = \sum_{j=1}^{m} \times \sum_{i=1}^{n} X_{j,i}\, Y_{j,i} \tag{7-2}$$

$$\text{Change in Z} = (1+\text{p})\, Z_1 = Z_1 + p\, Z_1 \tag{7-3}$$

where p = percent change and therefore

$$\text{Remaining Z} = Sum\ Z - Z_1\ = \sum_{j=1}^{m} \times \sum_{i=1}^{n} X_{j,i}\, Y_{j,i} - \sum_{i=1}^{n} X_{1,i} Y_{1,j} \qquad (7\text{-}4)$$

and so

$$\text{Residual Z} = \left(\sum_{j=1}^{m} \times \sum_{i=1}^{n} X_{j,i}\, Y_{j,i}\right) \text{-}(p \sum_{i=1}^{n} X_{1,i} Y_{1,i}) \qquad (7\text{-}5)$$

therefore

$$\text{Adj. Bal. \%} = \frac{(\text{Sum Z} - \text{Change Z})}{Sum\ Z - Z_1} = \frac{Residual\ Z}{Sum\ Z - Z_1} = \frac{\left(\sum_{j=1}^{m} \times \sum_{i=1}^{n} \boldsymbol{X_{j,i} Y_{j,i}}\right) - (\boldsymbol{p} \sum_{i=1}^{n} \boldsymbol{X_{1,i} Y_{1,i}})}{\sum_{j=1}^{m} \times \sum_{i=1}^{n} \boldsymbol{X_{j,i} Y_{j,i}} - \sum_{i=1}^{n} \boldsymbol{X_{1i,} Y_{1,j}}} \qquad (7\text{-}6)$$

where: in general:

X = pixel n = number of pixels
Y = pixel value m = number of zones
i=row
j=column

This procedure is illustrated by a pro-forma example (Table 7-2) where the no-cover offset (net increase in catchment cover) and cover offset (no net increase in catchment cover) values are calculated for a 10% - 40% increase (*p=0.10- 0.40*) in zone cover applied to 6 hypothetical catchment zones (Z_1-Z_6).

Table 7-2 Pro-forma calculation of pixel adjustment values for No offset and Offset scenarios

Zone	**Total**	**Z1**	**Z2**	**Z3**	**Z4**	**Z5**	**Z6**
Pixel No	94,254	11,996	22,197	20,037	17,030	12,272	10,722
∑ zone values	5,103,005	663,606	1,213,070	1,080,884	914,003	657,398	574,044
Mean value	54.14	55.32	54.65	53.94	53.67	53.57	53.54
No cover offset scenario							
Change (% of zone)		Absolute value of per pixel increase in a zone. (Either use percent or absolute value in ArcGIS/SA/Math/Times or Plus)					
10		5.53	5.47	5.39	5.37	5.36	5.35
20		11.06	10.93	10.79	10.73	10.71	10.71
30		16.60	16.40	16.18	16.10	16.07	16.06
40		22.13	21.86	21.58	21.47	21.43	21.42
Cover offset scenario							
Change (% of zone)		Absolute value of per pixel change (decrease) that has to be made to the balance of the pixels to offset the % increase in each zone.					
10		-0.81	-1.68	-1.46	-1.18	-0.80	-0.69
20		-1.61	-3.37	-2.91	-2.37	-1.60	-1.37
30		-2.42	-5.05	-4.37	-3.55	-2.41	-2.06
40		-3.23	-6.73	-5.83	-4.73	-3.21	-2.75

7.2.3. No cover offset and Cover offset procedures

For the No cover offset scenario (net-increase) the cover of each pixel in each zone was increased one zone at a time, by a set percentage of the total catchment cover (4 increments, e.g. 1.5%, 3%, 6% and 12% of the catchment or 10%, 20%, 30% and 40% of the zone) but the cover in the balance of the catchment was not reduced by a compensatory amount. This had the effect of increasing the total catchment cover by the amount of added cover.

For the Cover offset scenario (no net-increase) the cover of each pixel in each zone, was again increased one zone at a time, by the same percentages of the total catchment or zonal cover (as used in the No cover offset scenario) and the cover in the balance of the zones was reduced by a compensatory amount (Equation 6), so that the average catchment coverage remained the same. This approach eliminated the need for considering the curvilinear effect of coverage on leakiness (Figure 7.15) when considering change in zone cover on leakiness.

The morphological feature zones were approximately similar in size (as indicated by the number of pixels per zone) except for the topographic feature zones which were of substantially different sizes. For all morphological features, except the topographic features, the amount of cover change was calculated as a percent of the catchment (1.5%, 3%, 6% and 12%) and applied to each zone as described earlier. The difference in size between the topographic feature zones made this approach impractical. The topographic feature zone treatments were based on a percent of the zone cover (10%, 20%, 30% and 40%) rather than a percent of the catchment cover and the method of analysis was adjusted to reflect this (See Topographic Zones (Section 7.3.6).

7.2.4. Morphological feature preparation and classification

The following subsections provide details of the procedures used for preparation of the data files used in Figure 7.1 to prepare the modified rasters for analysis using the LC. All zone polygons were created from the conditioned srtm 1 s DEM for the catchment using processing methods specific to the type of zone being created.

7.2.4.1. Drainage Line Zones

The Drainage Line (DL) zone polygons were created using Arc Hydro to delineate the catchments and drainage lines followed by sequential buffering at 50m and 100m intervals around the drainage lines as described in Figure 7.2.

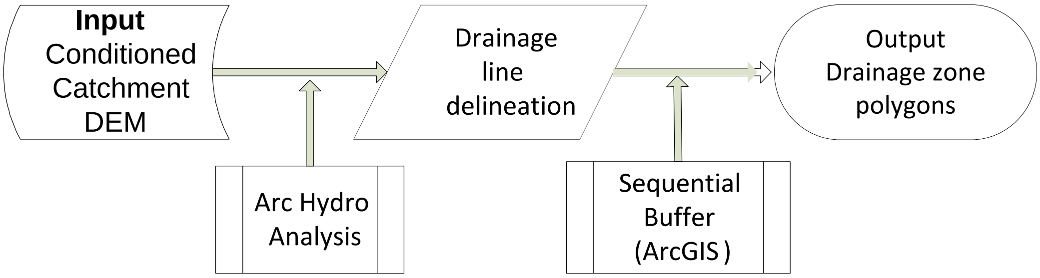

Figure 7.2 Procedure for preparing the drainage line distance zones

The resulting DDL zones are shown in Figure 7.3.

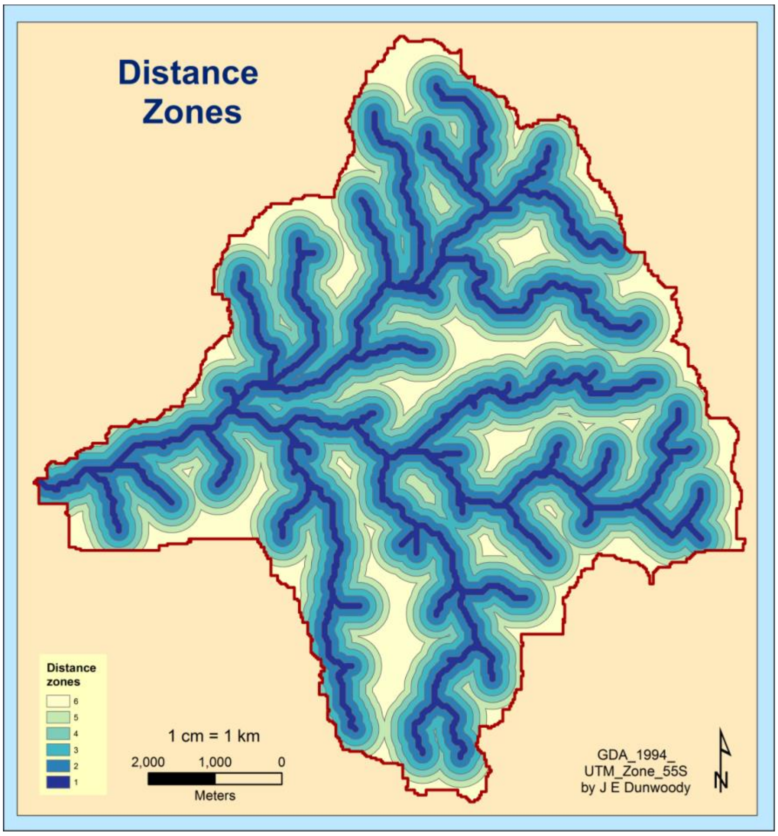

Figure 7.3 Drainage line distance zones

These DLD zones were used in step 3 in the procedure outlined in Figure 7.1 to generate the changed cover values for the new rasters used in the LC.

7.2.4.2. Elevation zones

The Elevation (Elevn.) zone polygons were created using ArcGIS Spatial Analyst to slice the DEM into 6 equal area zones based on elevation as described in Figure 7.4.

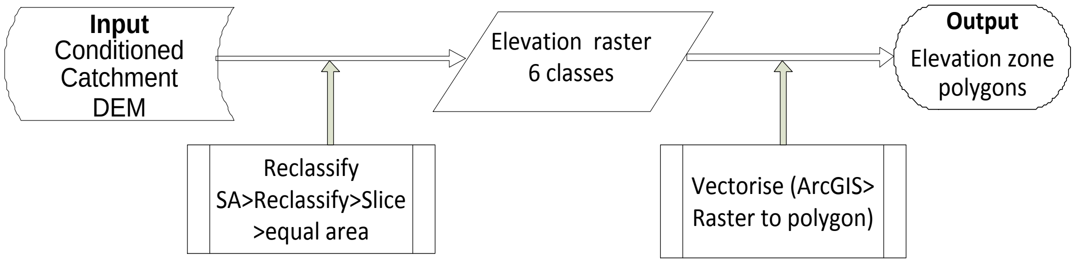

Figure 7.4 Procedure for preparing the elevation zones

The resulting elevation zones are shown in Figure 7.5.

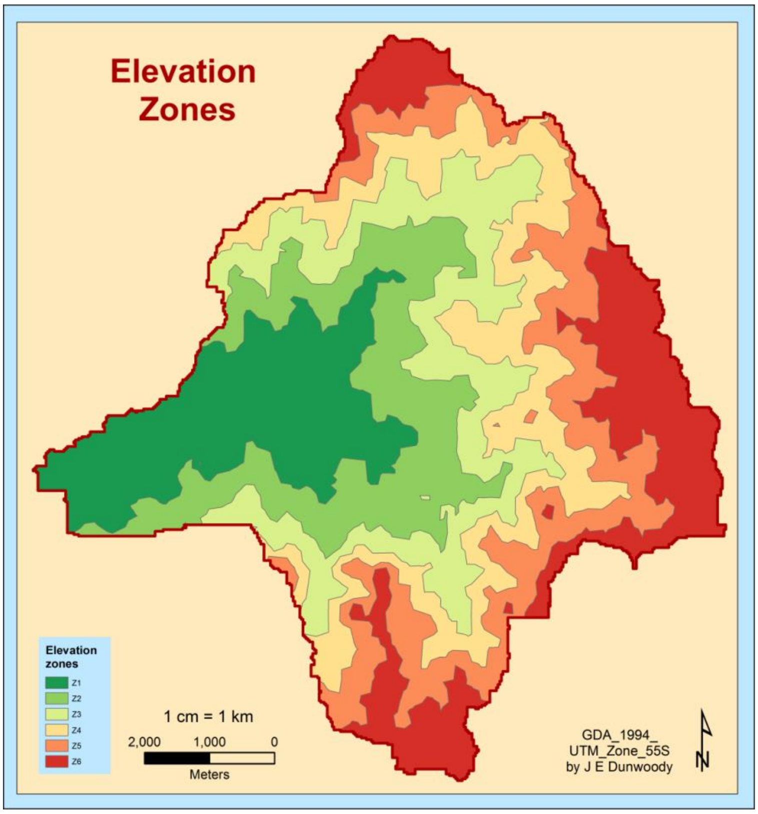

Figure 7.5 Elevation zones

The Elevation zones were used in step 3 in the procedure outlined in Figure 7.1 to generate the changed cover values for the new elevation zone rasters used in the LC. The changed cover values are given in Section 7.3.3.2 for SAVI and Section 7.3.2.2 for PDrg cover.

7.2.4.3. Slope zones

The Slope zone polygons were created using the Topographic Modelling geoprocessing module in the ENVI 5 software as shown in Figure 7.6. The kernel size used was 9 pixels.

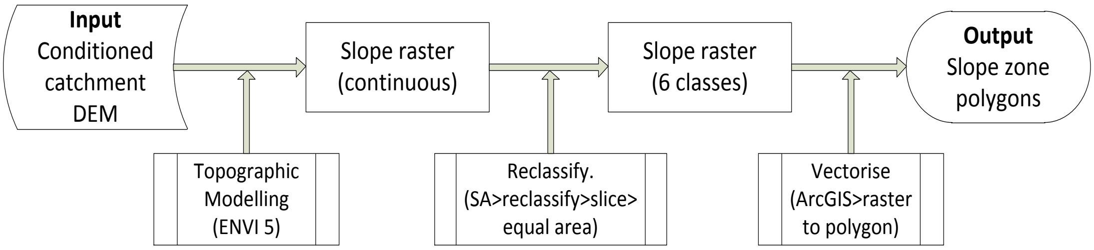

Figure 7.6 Procedure for preparing the slope zones

This was followed by slicing the slope zones into approximately equal areas using ArcGIS Spatial Analyst to reclassify the slope raster. The reclassified slope raster was vectorised to slope zone polygons. The resulting slope zones are shown in Figure 7-7.

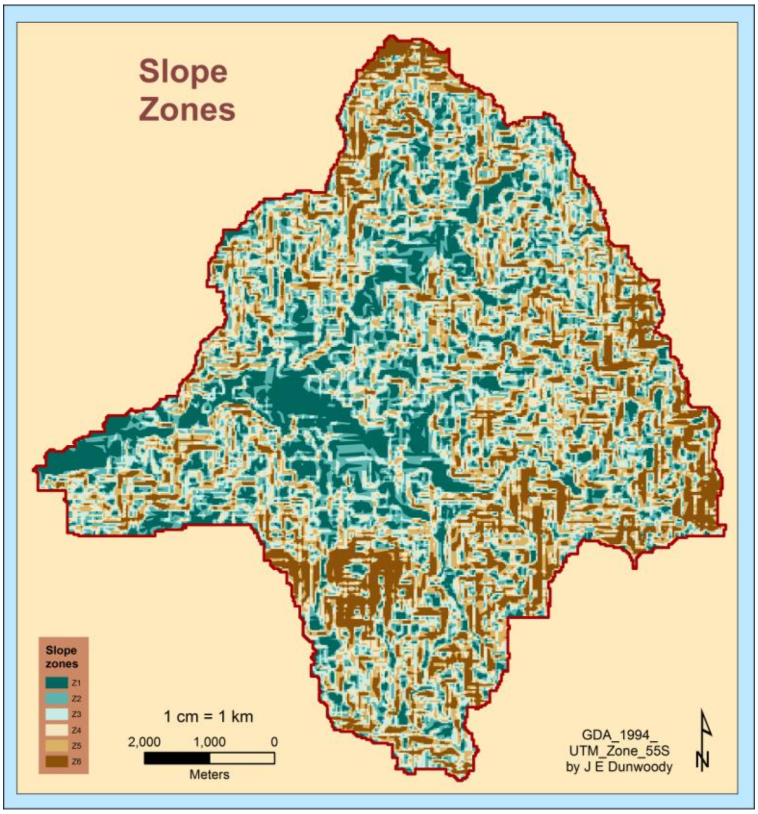

Figure 7.7 Slope zones

The Slope zones were used in step3 in the procedure outlined in Figure 7.1 to change cover values for the new elevation zone rasters used in the LC. The changed cover values are given in Section 7.3.4.1 for SAVI cover.

7.2.4.4. Aspect zones

The Aspect zone polygons were also created using the Topographic Modelling geoprocessing module in ENVI 5 software. The kernel size was 9 pixels and the elevation and azimuth were both set at 60°. The aspect raster was classified into 6 zones of approximately equal area by slicing using ArcGIS Spatial Analyst and the reclassified raster was vectorised into 6 aspect zone polygons as shown in Figure 7.8.

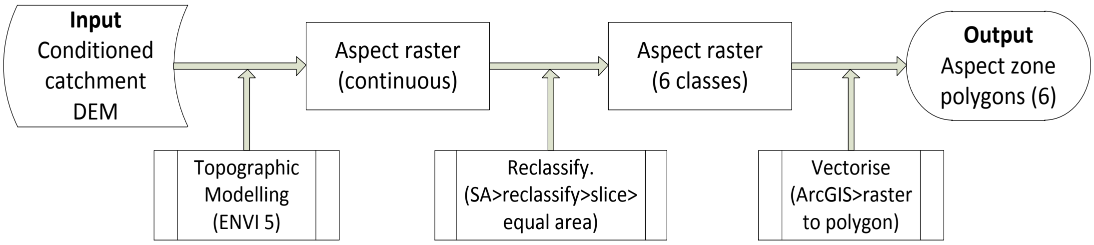

Figure 7.8 Procedure for preparing the aspect zones

The resulting aspect zones are shown in Figure 7.9.

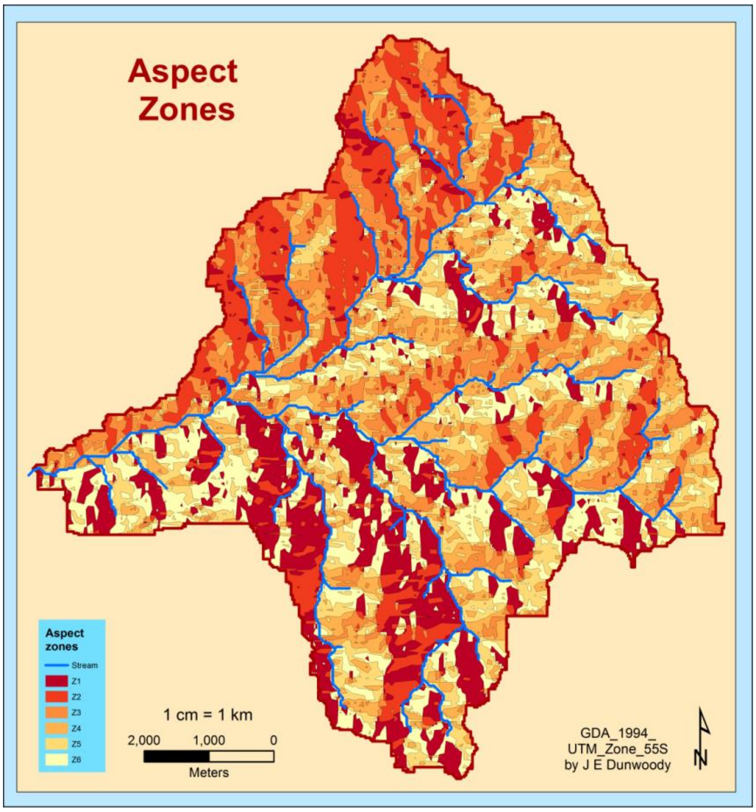

Figure 7.9 Aspect zones

The Aspect zones were used in step 3 in the procedure outlined in Figure 7.1 to generate the changed cover values for the new elevation zone rasters used in the LC. The changed cover values are given in Section 7.3.5.1 for SAVI cover.

7.2.4.5. Topographic zones

The topographic zone polygons, each representing a different landform, were created using the Topographic Features geoprocessing module in the ENVI 5 software. Key parameter settings were Kernel size 9 pixels, Slope Tolerance 7.5 and Curvature Tolerance 0.25. All 6 topographic landforms were selected. The processing first produced a multiband ENVI processing file (*.enp) which was converted to an ENVI vector file (*.evf) and this was exported to 6 polygon shape files, one for each land form, using the Export all Available Vectors function in Envi Classic (32 bit) software (Figure 7.10).

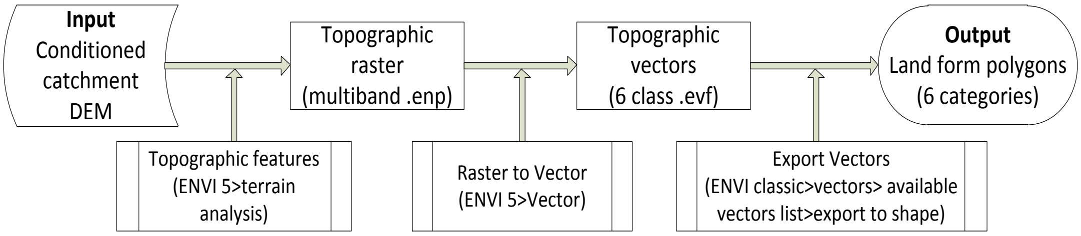

Figure 7.10 Procedure for preparing the topographic zones

The resulting topographic zones are shown in Figure 7.11.

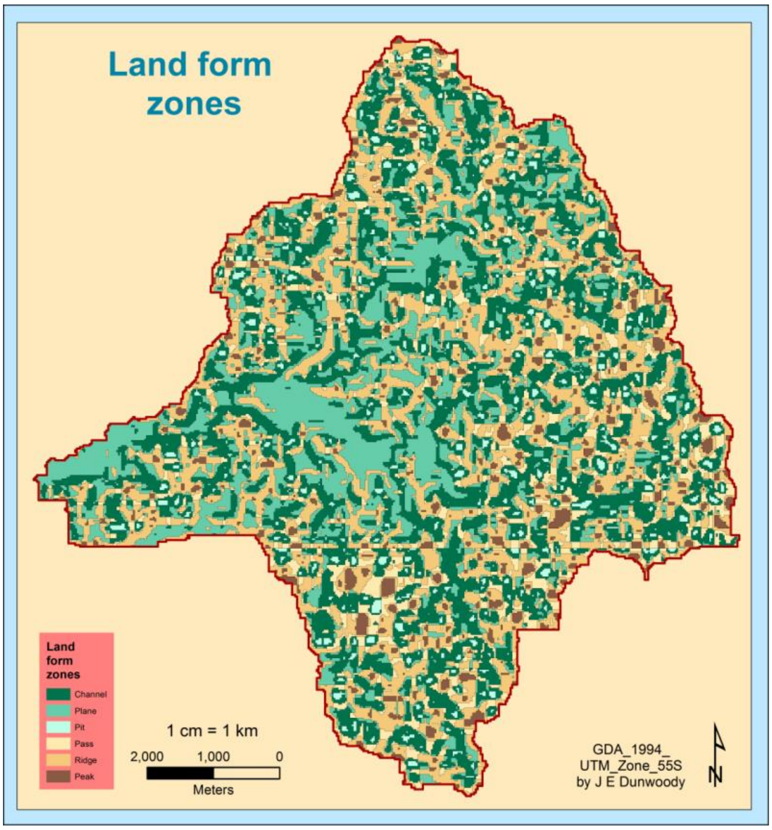

Figure 7.11 Topographic zones

The Topographic Zones, represented by the different landforms, were used in step 3 in the procedure outlined in Figure 7.1 to generate the changed cover values for the new elevation zone rasters used in the LC. The amount of change in cover was calculated differently for the topographic zones than for the other zones because the topographic zones covered widely different areas while the other zones contained approximately similar areas. The details of the different procedure and the changed cover values are given in Sections 7.3.6.1and 7.3.6.2 for SAVI and PDrg cover respectively.

7.2.4.6. Cover zones

The Cover zone polygons were created by slicing both the SAVI and PDrg cover rasters in to 6 approximately equal area classes and vectorising them as described in Figure 7.12.

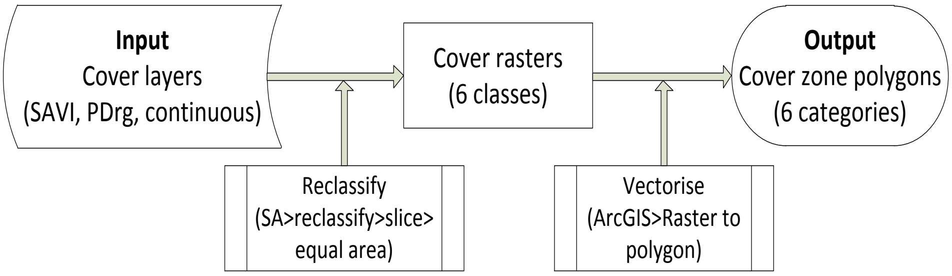

Figure 7.12 Procedure for preparing the cover zones

The resulting topographic zones are shown in Figure 7.13 and Figure 7.14 for SAVI and PDrg cover zones respectively.

The Cover zones were used in step 3 in the procedure outlined in Figure 7.1 to generate the changed cover values for the new elevation zone rasters used in the LC. The changed cover values are given in Section 7.1.1.1 and 7.3.7.1 for SAVI and PDrg cover respectively.

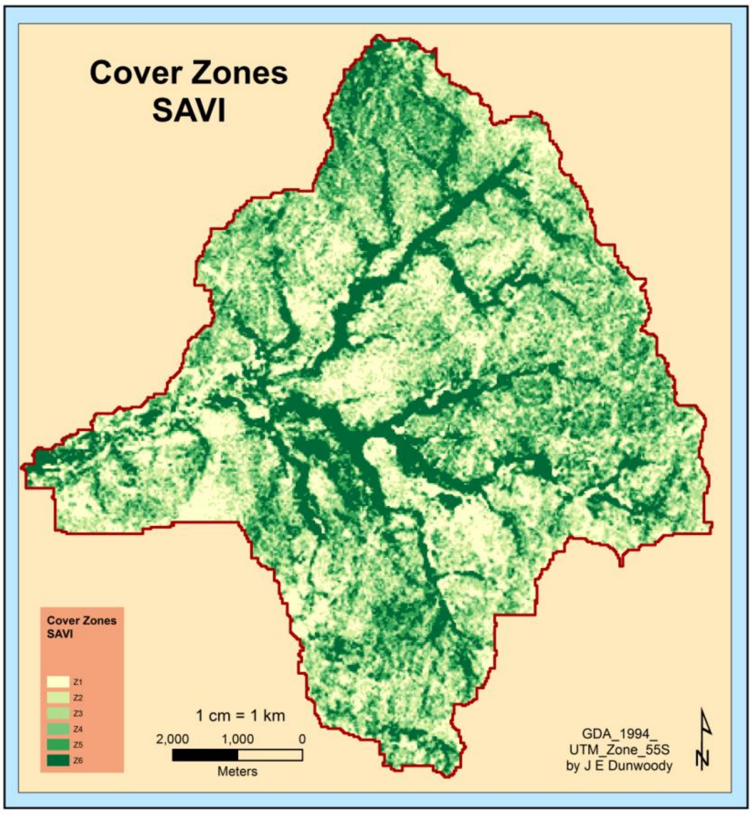

Figure 7.13 SAVI cover zones

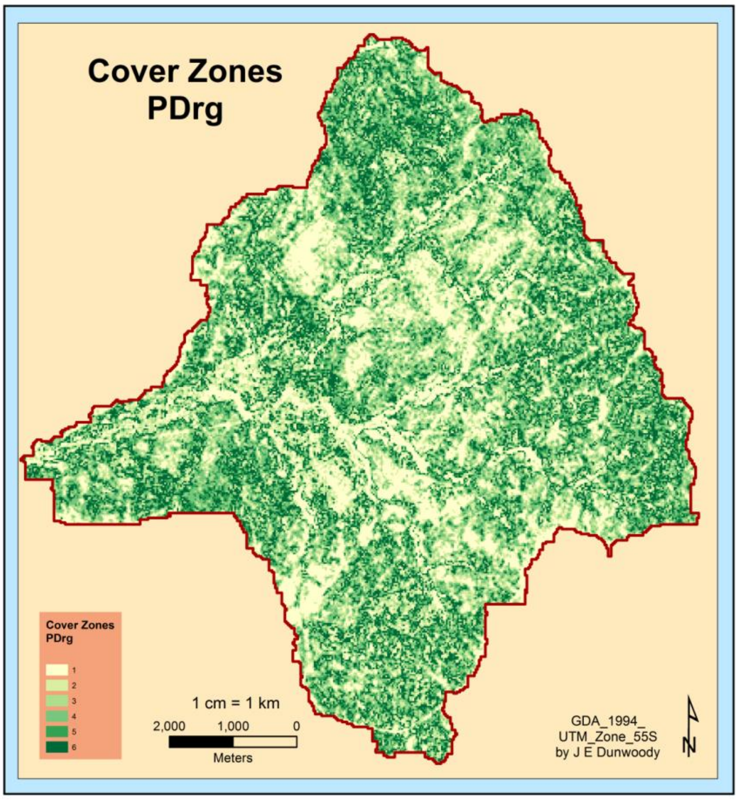

Figure 7.14 PDrg cover zones

7.2.5. Analysis

All analyses of the modified catchment covers were done using the CSIRO Leakiness Calculator. Details of the LC settings are given in Appendix 7A. The key elements of these settings are that all analyses used the tall tussock grass setting, Lmax was set at 200 and the soil loss constant was left at -0.065. While this latter value may not be the most appropriate value for each zone, it was necessary to use standard values for all analyses to get comparable results. These values best reflected the overall catchment conditions. All analyses were based on the Adjusted Average Leakiness (AAL) parameter as described in Chapter 5 rather than the LI.

The difference in cover treatment between the Topographic Zones (subsection 7.4.5) and the other 5 morphological cover treatments required a different analysis procedure. The AAL was used to compare the results for the 5 morphological features with similar sized zones while a normalised AAL was used to compare the effect of changing the amount of cover in different topographic zones. The normalisation corrected for the large difference in pixel count between topographic zones. The detailed calculation procedure is described in subsection 7.3.6.

7.3. Results

This section presents the results of changing the location of cover within a catchment on the overall leakiness of the catchment. Different locations within the catchment were analysed based on their morphological characteristics discernible from imagery (Table 7-1). This was done for SAVI and PDrg measures of cover because the previous research showed (Chapter 5) there were major differences between these two measures of cover. The findings have implications for catchment management policies, selection of areas for additional vegetation cover and the cost-effective amount of vegetation cover for different areas.

7.3.1. General Cover Increase

SAVI cover was used to test the response of the LC software to increasing cover on leakiness. Average catchment cover was adjusted by 5% increments using ArcGIS. The results are shown in Table 7-3 and Figure 7.15.

Table 7-3 Adjustment of SAVI average cover and Leakiness results

Average cover (%)	LI	Lcalc	AAL
54.64	0.80	10.41	1.10
59.64	0.74	9.05	0.96
64.64	0.60	6.52	0.69
69.64	0.47	4.70	0.50
74.64	0.35	3.39	0.36
84.64	0.20	1.77	0.19
94.64	0.11	0.92	0.10
104.64	0.06	0.48	0.05

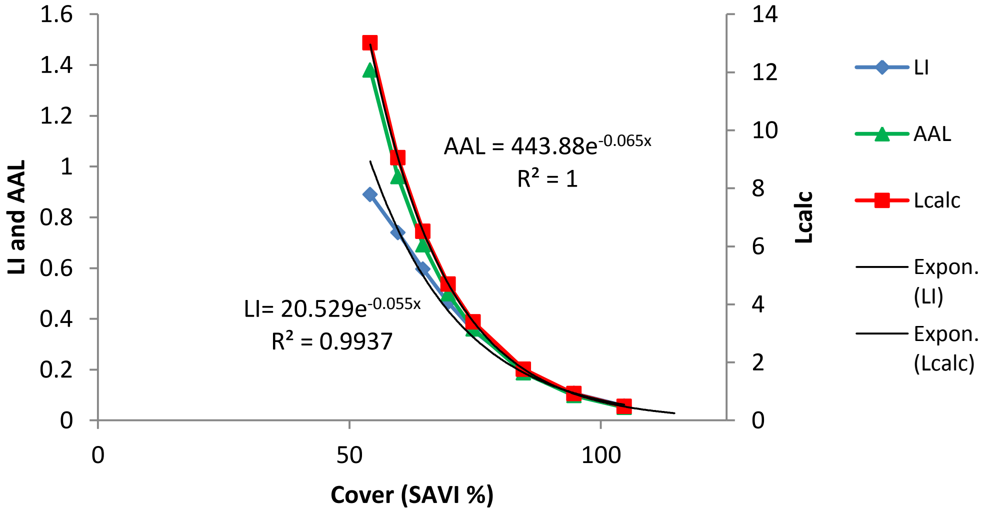

Figure 7.15 Leakiness response to increase in SAVI coverage

All three measures of leakiness decreased exponentially with increase in cover. This is consistent with the findings of Ludwig, J. and G. N. Bastin *et al.* (2007). It confirms that the LC is working as expected. AAL changed in concert with Lcalc. The LI results show a small difference in pattern from Lcalc and AAL. This is caused by the selection of the particular Lmax factor used in LI calculation.

7.3.2. Drainage Distance Zones

The effect of increasing the amount of cover, relative to the position of the drainage lines, was tested both with and without cover offset. Each method used the same drainage line zones as shown in Figure 7.3. The cover, slope and elevation values for these zones are shown relative to each other in Figure 7.16 and included in Table 7-4. The elevation increased steadily with distance from the drainage line (as expected) while there was only a small but consistent increase in slope. Both SAVI and PDrg cover remained relatively constant across all zones.

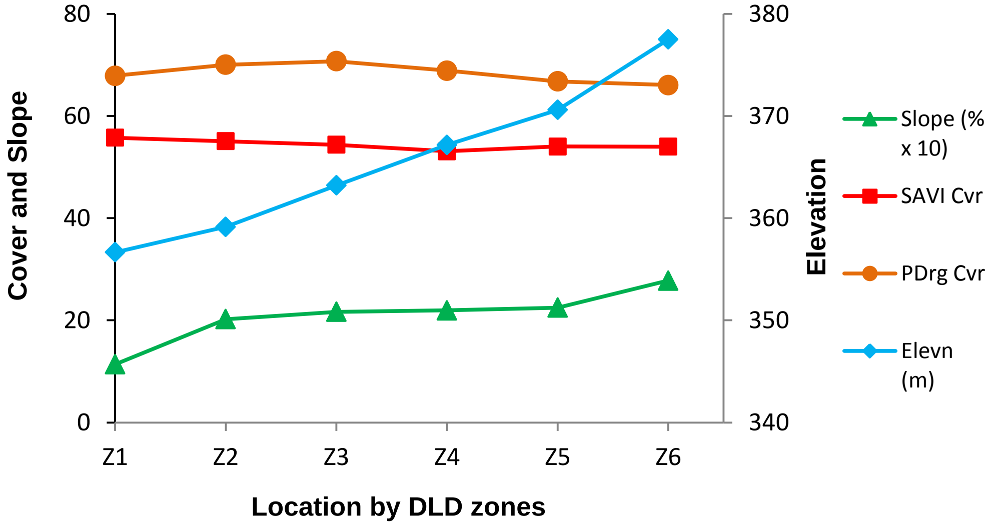

Figure 7.16 Cover, slope and elevation of the DLD zones

7.3.2.1. SAVI Coverage

Table 7-4 summarizes the zone characteristics and the values used to adjust the level of SAVI cover in each zone for both the no-offset and offset scenarios.

Table 7-4 SAVI drainage distance zone adjustment values

Category	Total	Z1	Z2	Z3	Z4	Z5	Z6
Dist. from Center Line (m)		0-50	50-150	150-250	250-350	350-450	>450
Area (ha)	5,887	750	1,390	1,250	1,060	768	669
Elevn (m)	364.6	356.7	359.2	363.2	367.2	370.6	377.5
Slope (%)	2.5	1.1	2.0	2.2	2.2	2.2	2.8
Pixel No.	94,247	11,989	22,197	20,037	17,030	12,272	10,722
∑ Zone Cover	5,142,044	668,529	1,222,600	1,089,822	921,771	663,231	579,102
Mean Cover (%)	54.6	55.7	55.1	54.4	53.1	54.0	54.1
Increase (% catchment)		No-offset (Increase in cover per pixel)					
1.5		6.43	3.47	3.85	4.53	6.29	7.19
3		12.87	6.95	7.70	9.06	12.57	14.39
6		25.73	13.90	15.40	18.12	25.14	28.77
12		51.47	27.80	30.80	36.23	50.28	57.55
Decrease (% catchment)		Offset scenario (Decrease in cover per pixel)					
1.5		-0.94	-1.07	-1.04	-1.00	-0.94	-0.92
3		-1.88	-2.14	-2.08	-2.00	-1.88	-1.85
6		-3.75	-4.28	-4.16	-4.00	-3.76	-3.69
12		-7.50	-8.56	-8.31	-7.99	-7.53	-7.39

No cover offset

Figure 7.17, Figure 7.18 and Figure 7.19 show the effect on catchment leakiness of increasing cover at different distances (zones) from the drainage lines without offsetting this increased cover elsewhere in the catchment. This results in a net increase in catchment average cover.

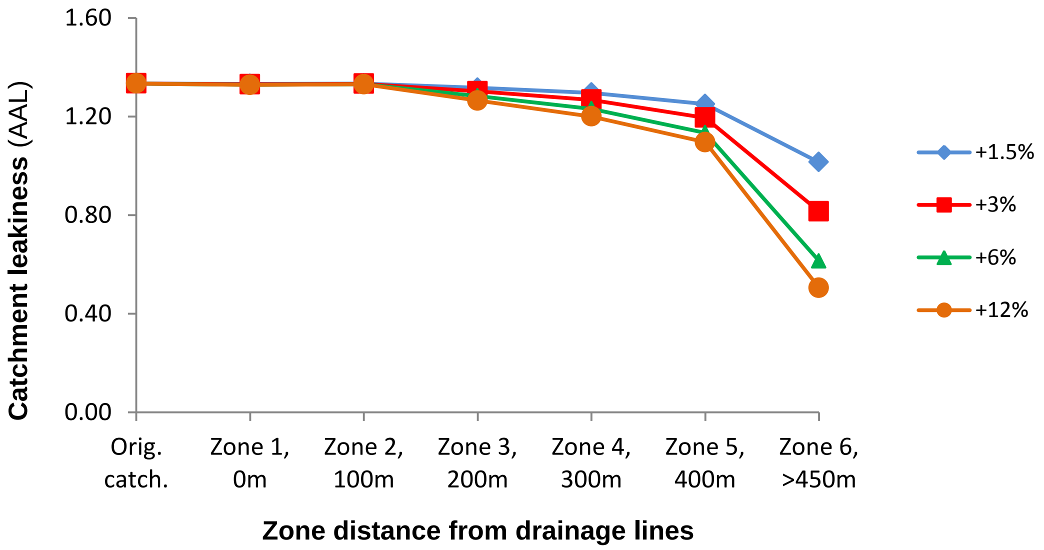

Figure 7.17 Leakiness due to increase in SAVI cover at different distances from the drainage lines. (net increase in catchment cover)

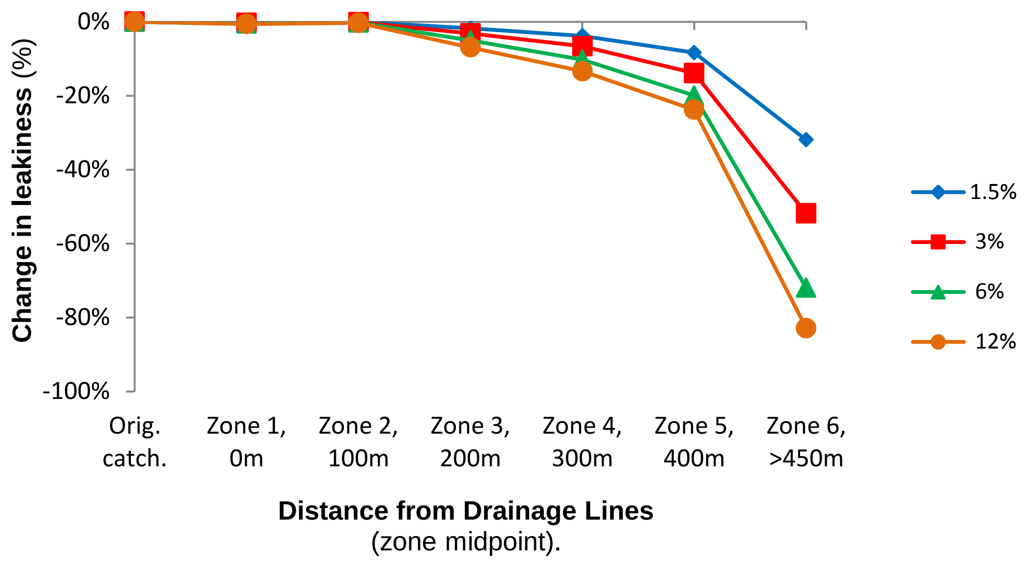

Figure 7.18 Change in Leakiness due to increase in SAVI cover at different distances from the drainage lines. (net increase in catchment cover)

Figure 7.17 and Figure 7.18 show that when cover was added to the experimental catchment it was more effective at reducing leakiness if the zone to which it was added was further from the drainage line. It is not known from this data whether this pattern is true for other catchments or not, but the response was consistent for each zone and for each level of added cover. These results were unexpected because conventional wisdom is that addition of cover to zones closer to drainage lines result in the most reduction in leakiness. The reasons for this are discussed in Section 7.4.

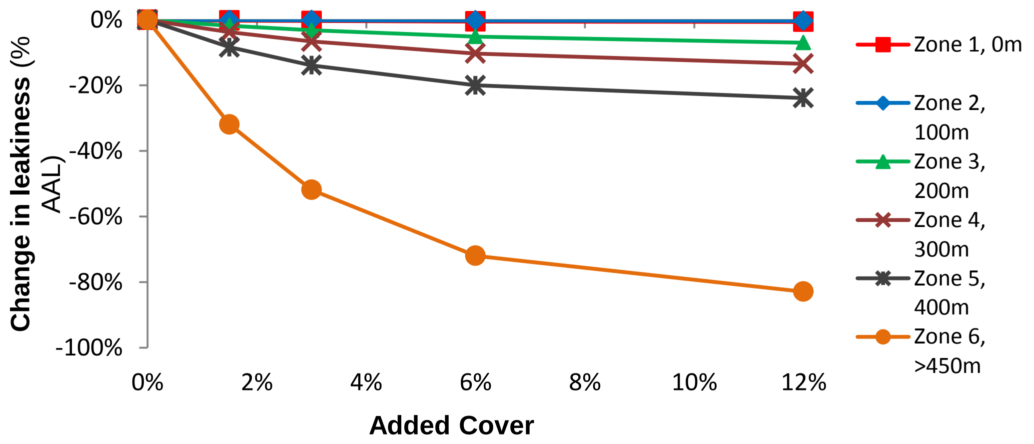

Figure 7.19 Response of leakiness to addition of SAVI cover by distance from drainage lines. (net increase in catchment cover)

Figure 7.19 shows the preceding results displayed on a zonal basis rather than on a percent cover basis. Addition of cover to zones 3-6 leads to reduced leakiness with the response being generally negative curvilinear. This is consistent with the leakiness response to change in cover exhibited in Figure 7.15. It also demonstrates that leakiness is reduced more by adding cover to the zone furthest from the drainage line to which it flows. The rate of response of leakiness to addition of cover is greater for small additions than for larger additions, i.e. the negative slope of the response curve decreases with increase in added cover.

Cover offset

Figure 7.20, Figure 7.21and Figure 7.22 show the effect on catchment leakiness of increasing the amount of cover at different distances from the drainage lines and offsetting this added cover proportionally over the rest of the catchment. (The effect of this is to hold the average catchment cover constant).

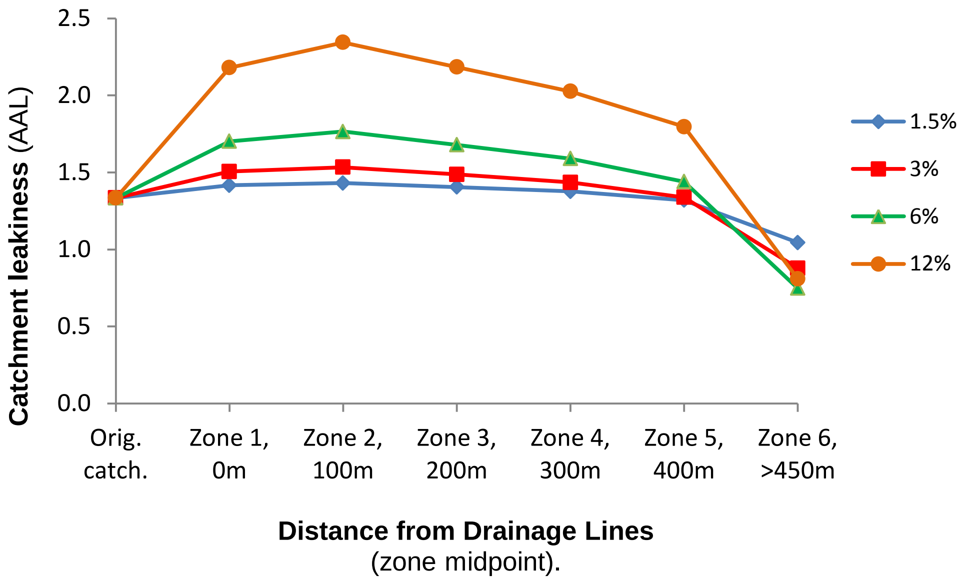

Figure 7.20 Leakiness due to increase in SAVI cover at different distances from the drainage lines. (no net increase in catchment cover)

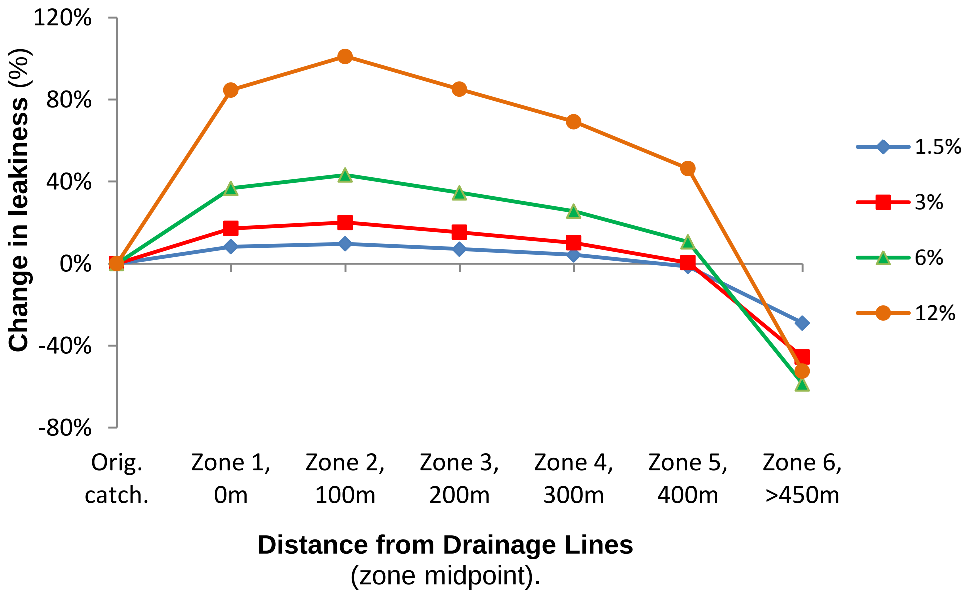

Figure 7.21 Change in Leakiness due to increase in SAVI cover at different distances from the drainage lines. (no net increase in catchment cover).

These results show that catchment leakiness increases when cover is added to all zones other than the most distant zone and the overall catchment cover is held constant. This occurred for all increases in cover that were tested and is unexpected. The amount of the increase in leakiness is potentially very high, exceeding 100%, when 12% of catchment cover is added to Zone 2. The mean distance from the drainage line for this zone is 100m. It was expected that the leakiness would decrease sufficiently to compensate for the more distant zone cover offsets when cover was added to zones that were close to the drainage line. The possible reasons for this are discussed in Section 7.4.Figure 7.22 shows the preceding results displayed on a zonal basis rather than on a percent cover basis.

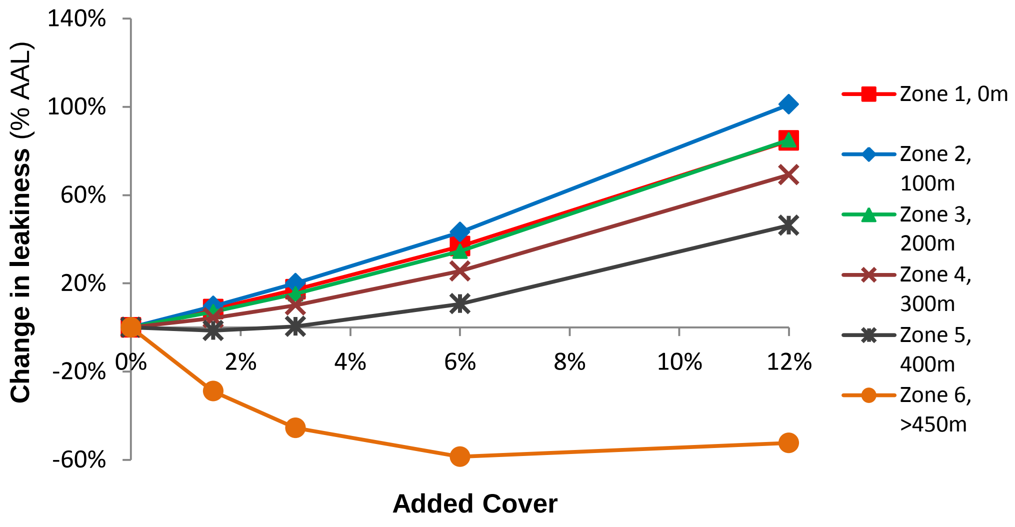

Figure 7.22 Response of leakiness to addition of SAVI cover by distance from drainage lines. (no net increase in catchment cover)

Increase in cover, when accompanied by offsetting decreases in cover proportionally across the catchment, increases overall catchment leakiness in all zones except when added to the zone most distant from the drainage lines (Zone 6). A maximum reduction in leakiness occurs by adding 6% of the catchment's cover to Zone 6. Additional cover added to Zone 6 (and offset by a reduction across the rest of the catchment) produced no further reduction in leakiness.

7.3.2.2. PDrg Coverage

Table 7-5 summarizes the values used to adjust the level of PDrg cover in each zone for both the no-offset and offset scenarios.

Table 7-5 PDrg drainage line distance zone adjustment values

Zone	Total	Z1	Z2	Z3	Z4	Z5	Z6
Distance from drainage center line (m)		0-50	50-150	150-250	250-350	350-450	>450
Area (ha)	5,887	750	1,390	1,250	1,060	768	669
Elevation (m)	364.6	356.7	359.2	363.2	367.2	370.6	377.5
Slope (%)	2.5	1.1	2.0	2.2	2.2	2.2	2.8
Pixel No.	94,247	11,989	22,197	20,037	17,030	12,272	10,722
∑ Zone Cover	6,489,081	814,044	1,554,875	1,417,904	1,173,575	820,045	708,837
Mean Cover (%)	68.8	67.9	70.1	70.8	68.9	66.8	66.1
Increase (% of catchment)		**No cover offset scenario (increase in cover per pixel)**					
1.5		8.12	4.39	4.86	5.72	7.93	9.08
3.0		16.24	8.77	9.72	11.43	15.86	18.16
6.0		32.48	17.54	19.43	22.86	31.73	36.31
12.0		64.95	35.08	38.86	45.72	63.45	72.63
Increase (% of catchment)		**Percent increase in cover by zone (%)**					
1.5		11.96	6.26	6.86	8.29	11.87	13.73
3.0		23.91	12.52	13.73	16.59	23.74	27.46
6.0		47.83	25.04	27.46	33.18	47.48	54.93
12.0		95.66	50.08	54.92	66.35	94.96	109.85
Decrease (% of catchment)		**Cover offset scenario (decrease in cover per pixel)**					
1.5		-1.18	-1.35	-1.31	-1.26	-1.19	-1.17
3.0		-2.37	-2.70	-2.62	-2.52	-2.37	-2.33
6.0		-4.73	-5.40	-5.25	-5.04	-4.75	-4.66
12.0		-9.47	-10.81	-10.49	-10.08	-9.50	-9.32
Decrease (% of catchment)		**Percent decrease in cover by zone (%)**					
1.5		-1.72	-1.97	-1.92	-1.83	-1.72	-1.68
3.0		-3.43	-3.95	-3.84	-3.66	-3.43	-3.37
6.0		-6.86	-7.89	-7.68	-7.32	-6.87	-6.74
12.0		-13.72	-15.78	-15.36	-14.65	-13.74	-13.47

No cover offset

Figure 7.23, Figure 7.24 and Figure 7.25 show the effect on catchment leakiness of increasing PDrg cover at different distances (zones) from the drainage lines without offsetting this elsewhere in the catchment (net cover increase).

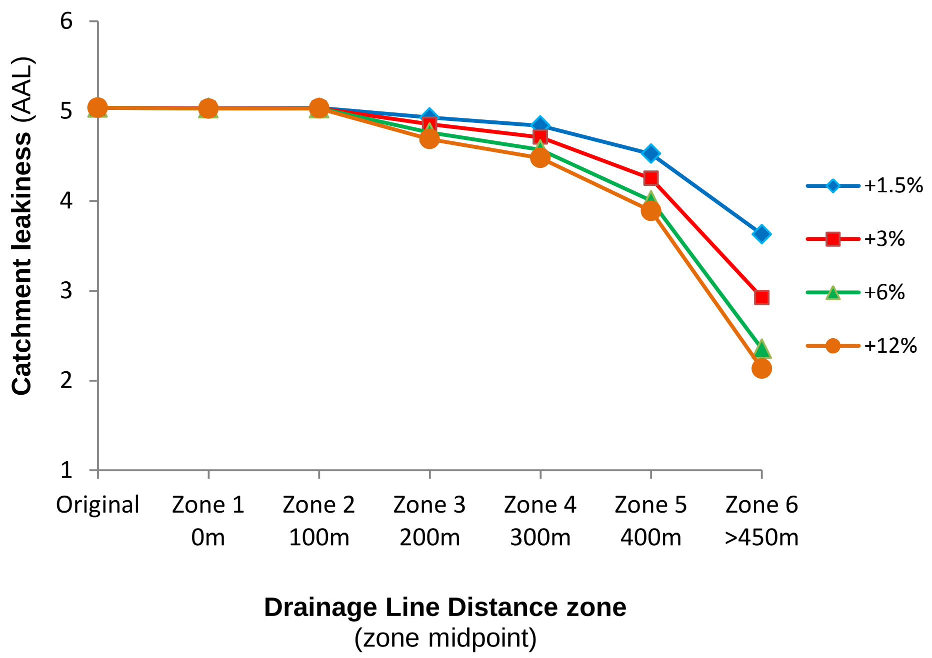

Figure 7.23 Leakiness due to increase in PDrg cover at different distances from the drainage lines (net increase in catchment cover)

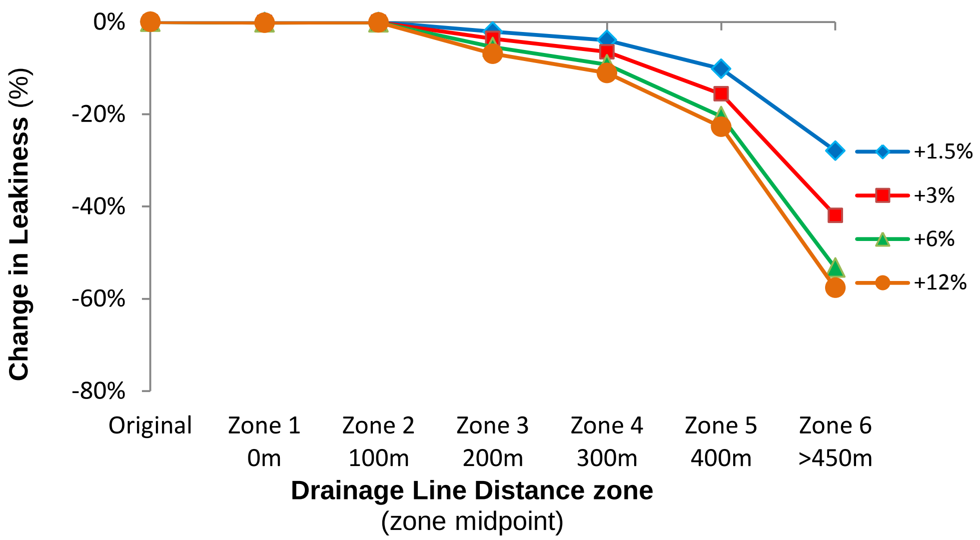

Figure 7.24 Change in Leakiness due to increase in PDrg cover at different distances from the drainage lines (net increase in catchment cover)

Figure 7.23 and Figure 7.24 show that PDrg cover is also most effective at reducing leakiness when added to areas furthest from the drainage lines. The response was consistent for each zone and for each level of added cover. This is similar to the pattern found for addition of SAVI cover and, as was the case for SAVI cover, the results are unexpected. The possible reasons for this are discussed in Section 7.4.

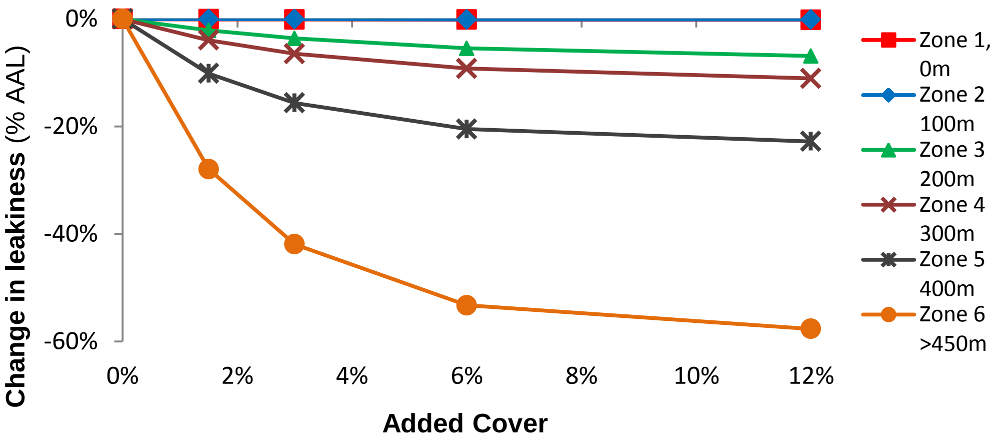

Figure 7.25 Response of leakiness to addition of PDrg cover by distance from drainage lines (net increase in catchment cover).

Figure 7.25 shows the preceding results displayed on a zonal basis, rather than on a percent cover basis. Addition of cover to zones 3-6 leads to reduced leakiness with the response being generally negative curvilinear. It is consistent with the leakiness response to change in cover exhibited in Figure 7.15. The most reduction in leakiness occurs if the zone to which the cover is added is further from the drainage line. The rate of response of leakiness to addition of cover is greater for small additions than for larger additions. This is a similar pattern to the response of SAVI cover by zone

Cover Offset

Figure 7.26, Figure 7.27 and Figure 7.28 show the effect on catchment leakiness of increasing the amount of PDrg cover at different distances (zones) from the drainage lines while holding the overall catchment cover constant.

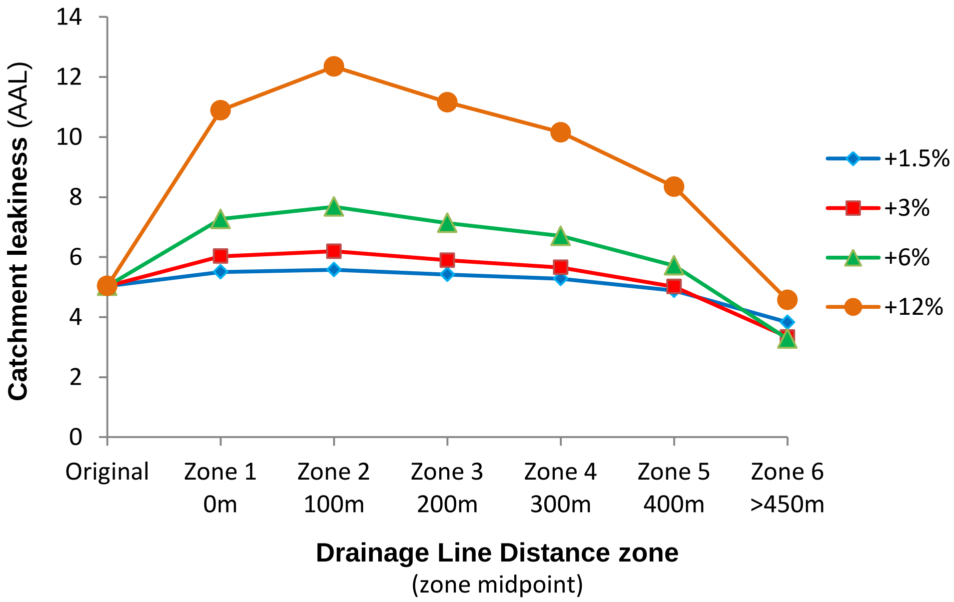

Figure 7.26 Amount of leakiness due to change of PDrg cover by drainage line distance zone (no net increase in catchment cover).

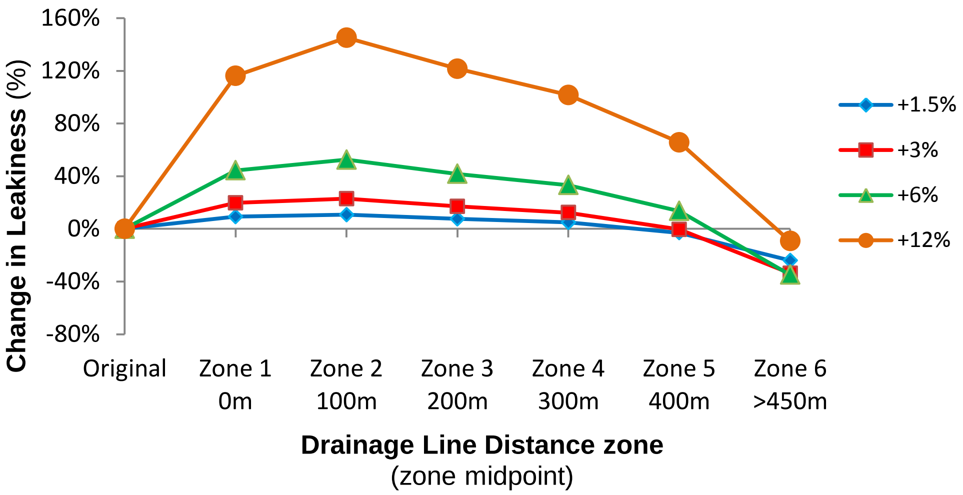

Figure 7.27 Change in leakiness due to change in PDrg cover by drainage line distance zones (no net increase in catchment cover).

The PDrg cover results show a similar pattern of catchment leakiness response to SAVI cover. The catchment leakiness increases when cover is added to all zones other than the most distant zone for all amounts of increase in cover that were tested. This is likewise unexpected. The amount of the increase in leakiness is potentially very high, exceeding 100%, when 12% of catchment cover is added to Zones 1 - 4. These zones are 0 - 300 m from the drainage line. It was expected that the leakiness would decrease sufficiently to compensate for the more distant zone cover offsets when cover was added to zones that were close to the drainage line. The possible reasons for this are discussed in Section 7.4. Analysis of these results by Zone is shown in Figure 7.28.

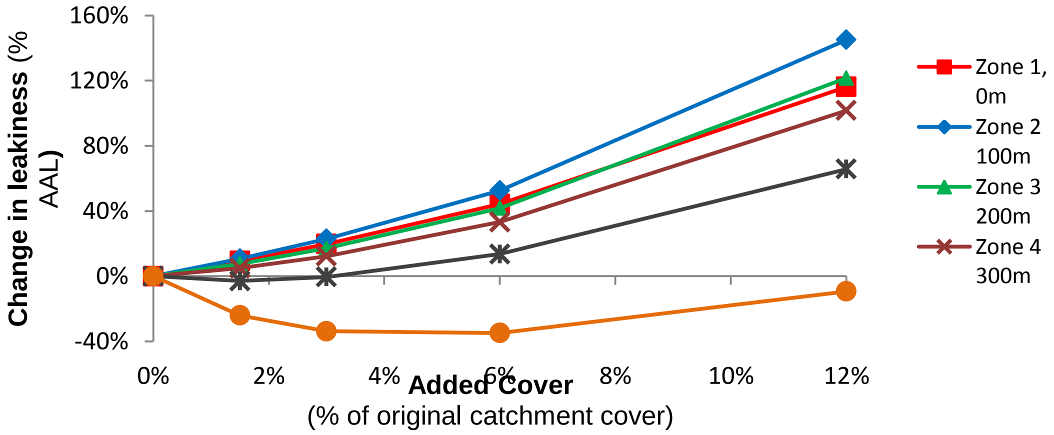

Figure 7.28 Response of leakiness to addition of PDrg cover by distance from drainage lines (no net increase in catchment cover).

Zone 6, the zone most distant from the drainage lines, again shows up as the only zone to which addition of cover under this scenario reduces catchment leakiness. Again, smaller additions of cover (1.5 – 6%) are more effective than larger additions at reducing leakiness.

7.3.3. Elevation Zones

The effect of increasing the amount of cover, relative to the position of the elevation zones, was tested both with and without cover offset. Each method used the elevation zones shown in Figure 7.5. The cover, slope and elevation values for these zones are shown relative to each other in Figure 7.29 and included in Table 7-6. The elevation increased steadily with each elevation zone while there was only a small but consistent increase in slope. Both SAVI and PDrg cover remained relatively constant across all elevation zones.

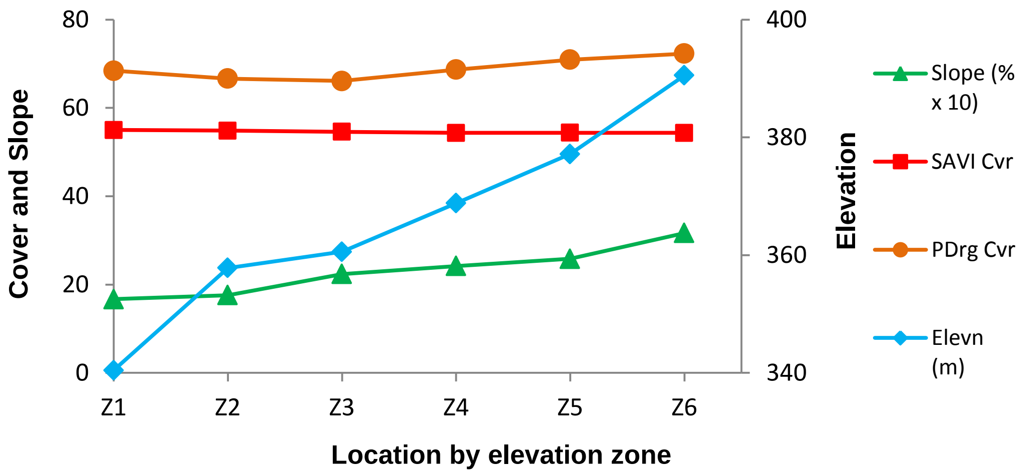

Figure 7.29 Cover, slope and elevation of the elevation zones

7.3.3.1. SAVI Coverage

Table 7-6 summarizes the values used to adjust the level of SAVI cover in each zone for both the no-offset and offset scenarios.

Table 7-6 SAVI cover elevation zone adjustment values (continued)

Zone	Total	Z1	Z2	Z3	Z4	Z5	Z6
Description		lowest	intermediate				highest
Area (ha)	5,890	992	983	976	989	970	980
Elevation (m)	364.6	340.4	357.8	360.5	368.8	377.2	390.5
Slope (%)	2.4	1.6	1.7	2.2	2.4	2.5	3.1
Pixel No.	94,247	15,860	15,736	15,614	15,817	15,522	15,698
∑ Zone Cover	5,145,345	872,144	863,084	852,838	859,789	844,370	853,120
Mean Cover (%)	54.6	55.0	54.9	54.6	54.4	54.40	54.4
Increase (% of catchment)		**No cover offset scenario (increase in cover per pixel)**					
1.5		4.86	4.90	4.94	4.88	4.97	4.91
3		9.73	9.80	9.88	9.75	9.94	9.83
6		19.46	19.61	19.77	19.51	19.88	19.66
12		38.93	39.23	39.54	39.03	39.77	39.33

Table 7-6 (continued) SAVI cover elevation zone adjustment values

Zone	Total	Z1	Z2	Z3	Z4	Z5	Z6
Increase (% of catchment)		**Percent increase in cover by zone (%)**					
1.5		8.85	8.94	9.05	8.98	9.14	9.05
3		17.70	17.88	18.10	17.95	18.28	18.09
6		35.40	35.77	36.20	35.91	36.56	36.19
12		70.80	71.54	72.40	71.81	73.12	72.37
Decrease (% of catchment)		**Cover offset scenario (decrease in cover per pixel)**					
1.5		-0.98	-0.98	-0.98	-0.98	-0.98	-0.98
3		-1.96	-1.96	-1.96	-1.96	-1.96	-1.96
6		-3.93	-3.93	-3.92	-3.93	-3.92	-3.93
12		-7.87	-7.86	-7.85	-7.87	-7.84	-7.86
Decrease (% of catchment)		**Percent decrease in cover by zone (%)**					
1.5		-1.81	-1.80	-1.80	-1.80	-1.79	-1.80
3		-3.61	-3.60	-3.60	-3.60	-3.59	-3.60
6		-7.22	-7.21	-7.19	-7.20	-7.18	-7.19
12		-14.45	-14.42	-14.38	-14.41	-14.36	-14.39

No cover offset

Figure 7.30, Figure 7.31 and Figure 7.32 show the effect on catchment leakiness of increasing SAVI cover in different elevation zones without offsetting this elsewhere in the catchment (net cover increase).

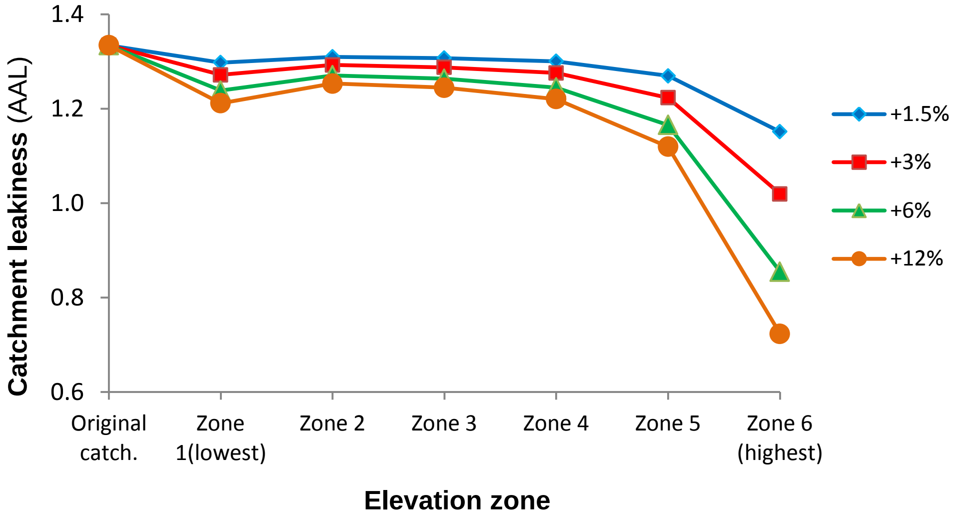

Figure 7.30 Amount of leakiness due to increase in SAVI cover by elevation (net increase in catchment cover).

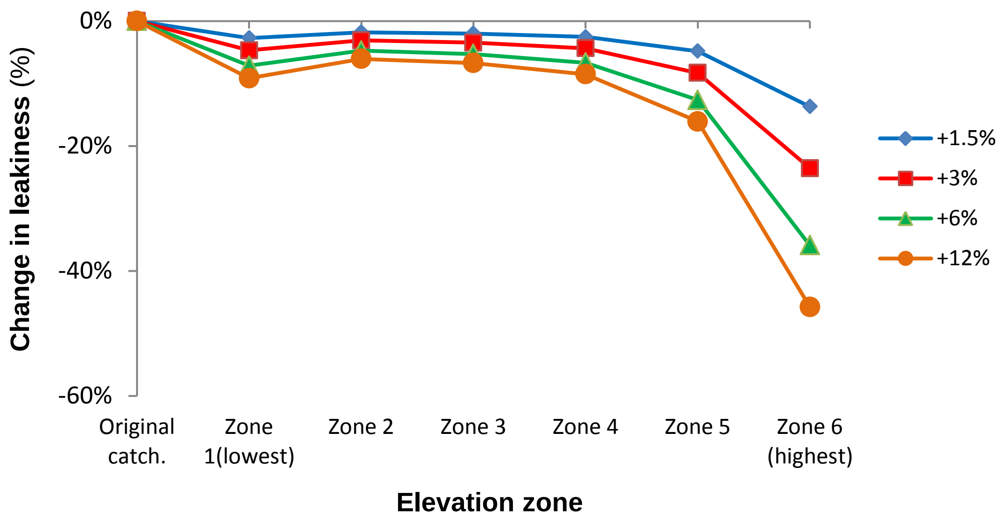

Figure 7.31 Change in Leakiness due to increase in SAVI cover by elevation zone (net increase in catchment cover).

These Figures show that when cover was added to the experimental catchment, it was more effective at reducing leakiness when added to the higher elevation zones. The response was consistent for each zone and for each level of added cover. These results, while unexpected, are consistent with the drainage distance zone results.

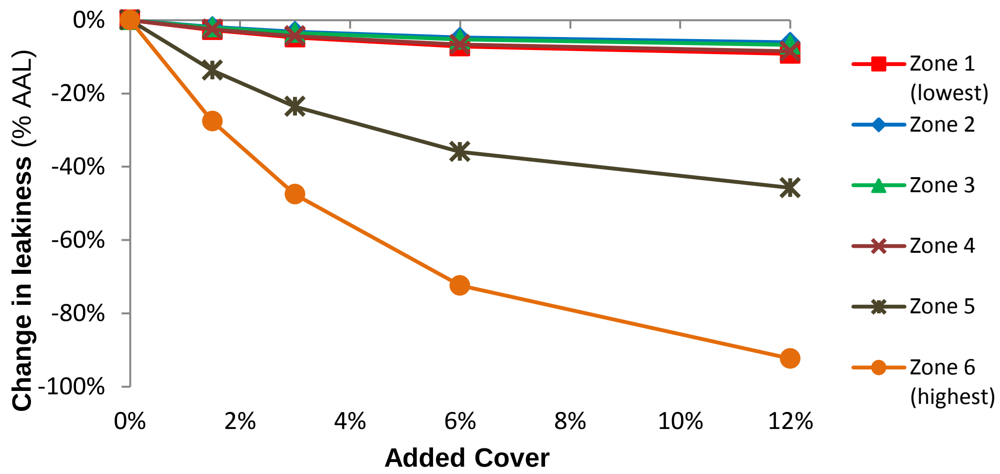

Figure 7.32 Response of catchment leakiness to increase in SAVI cover by elevation (net increase in catchment cover).

Figure 7.32 shows the preceding results displayed on a zonal basis rather than on a percent cover basis. Most reduction of leakiness occurs if cover is added to higher elevation zones, namely Zones 5 and 6 with the response being generally negative curvilinear. This is consistent with the leakiness response to change in cover exhibited in Figure 7.15. The rate of response of leakiness to addition of cover is similar to what was found before, namely it is greater per unit of cover for small additions than for larger additions.

Cover offset

Figure 7.33, Figure 7.34 and Figure 7.35 show the effect on catchment leakiness of increasing SAVI cover in different elevation zones and offsetting this additional cover by reducing cover across the rest of the catchment (no net cover increase).

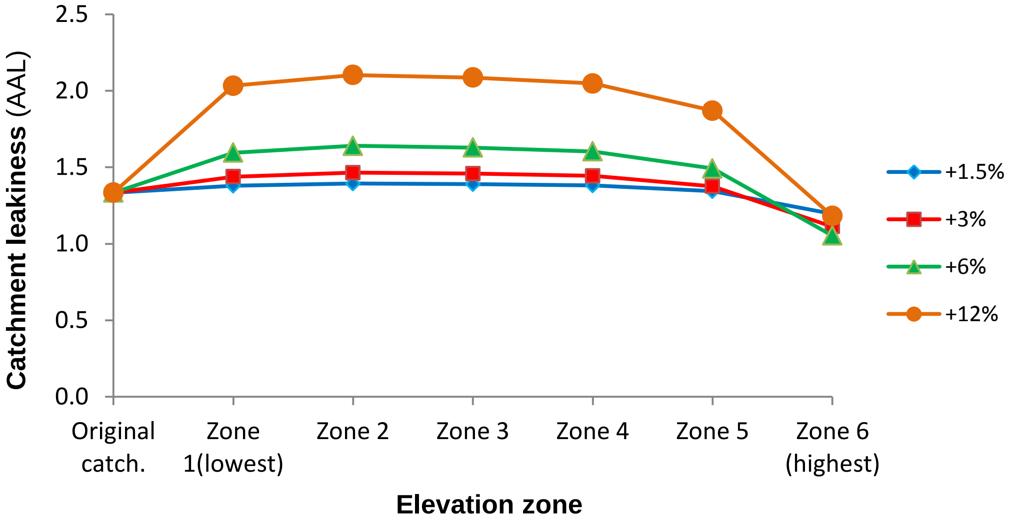

Figure 7.33 Amount of leakiness due to change of SAVI cover by elevation (no net increase in catchment cover)

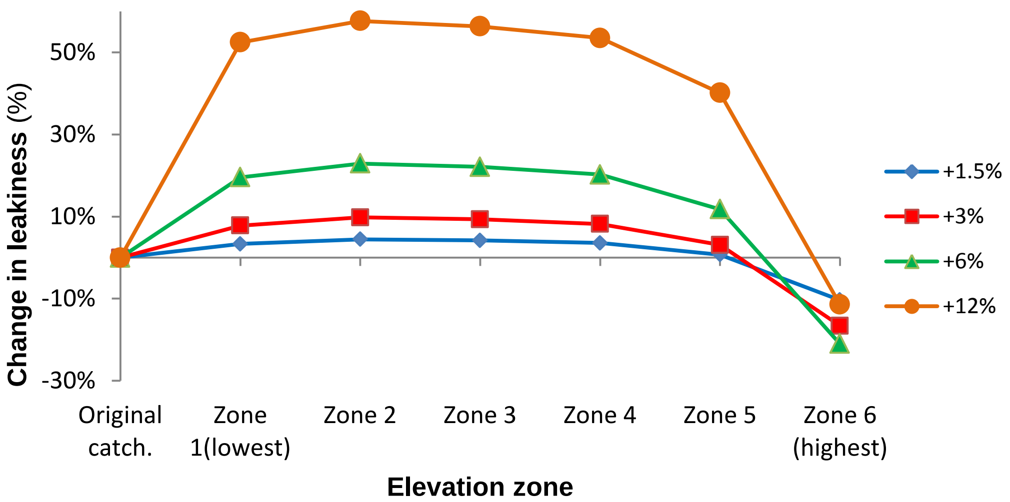

Figure 7.34 Change in Leakiness due to change of SAVI cover by elevation (no net increase in catchment cover).

These Figures show, that when cover was added to the catchment in one elevation zone and offset elsewhere in the catchment the leakiness increased except if the additional cover was added to the highest elevation zone (Zone 6). These results are consistent with the no-cover offset scenario for the drainage line distance results.

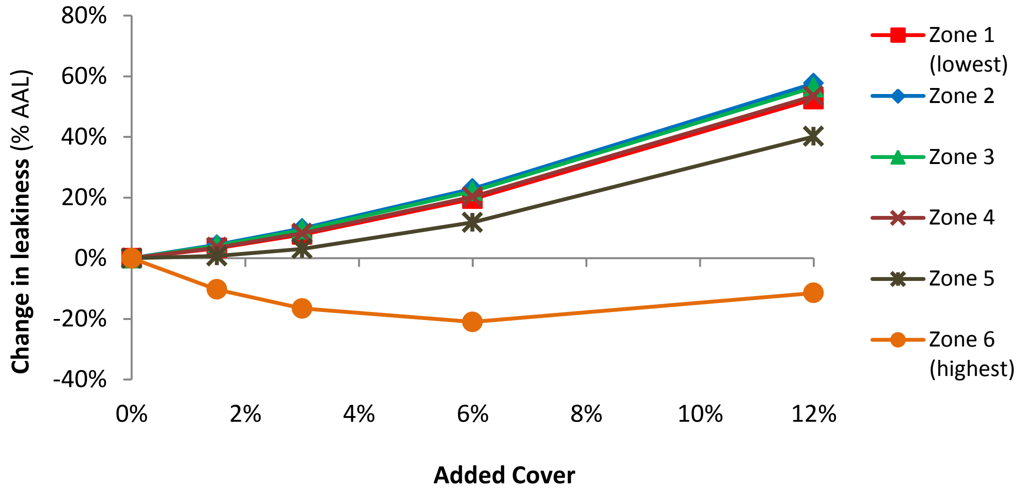

Figure 7.35 Response of catchment leakiness to change of cover by elevation. (no net increase in catchment cover)

Figure 7.35 shows the preceding results displayed on a zonal basis rather than on a percent cover basis. The highest elevation zone (zone 6) is the only zone to which the addition of cover that is offset elsewhere in the catchment results in reduced catchment leakiness.

7.3.3.2. PDrg Coverage

Table 7-7 summarizes the zone characteristics and the values used to adjust the level of PDrg cover in each zone for both the no-offset and offset scenarios

Table 7-7 PDrg cover elevation zone adjustment values (continued)

Zone	Total	Z1	Z2	Z3	Z4	Z5	Z6
Description		lowest	Intermediate				highest
Area (ha)	5889	983	979	982	982	981	979
Elevn (m)	364.6	340.4	357.8	360.5	368.8	377.2	390.5
Slope (%)	2.4	1.6	1.7	2.2	2.4	2.5	3.1
Pixel No.	94,247	15,860	15,736	15,614	15,817	15,522	15,698
∑ Zone Cover	6,489,081	1,085,621	1,048,619	1,032,458	1,086,541	1,100,921	1,134,922
Mean Cover (%)	68.9	68.5	66.6	66.1	68.7	70.9	72.3
Increase (% of catchment)		No cover offset (increase in cover per pixel)					
1.5		6.137	6.186	6.234	6.154	6.271	6.201
3.0		12.274	12.371	12.468	12.308	12.542	12.401
6.0		24.549	24.742	24.936	24.616	25.083	24.802
12.0		49.098	49.485	49.871	49.231	50.167	49.604

Table 7-7 (c0ntinued) PDrg cover elevation zone adjustment values (continued)

Zone	Total	Z1	Z2	Z3	Z4	Z5	Z6
Increase (% of catchment)		Percent increase in cover by zone					
1.5		8.97	9.28	9.43	8.96	8.84	8.58
3.0		17.93	18.56	18.86	17.92	17.68	17.15
6.0		35.86	37.13	37.71	35.83	35.37	34.31
12.0		71.73	74.26	75.42	71.67	70.73	68.61
Decrease (% of catchment)		Cover offset (decrease in cover per pixel)					
1.5		-1.242	-1.240	-1.238	-1.241	-1.236	-1.239
3.0		-2.483	-2.480	-2.476	-2.482	-2.473	-2.478
6.0		-4.967	-4.959	-4.951	-4.964	-4.946	-4.957
12.0		-9.934	-9.918	-9.903	-9.928	-9.891	-9.913
Decrease (% of catchment)		Percent decrease in cover by zone					
1.5		-1.80	-1.79	-1.78	-1.80	-1.81	-1.82
3.0		-3.60	-3.58	-3.57	-3.60	-3.61	-3.64
6.0		-7.21	-7.16	-7.14	-7.21	-7.23	-7.27
12.0		-14.41	-14.31	-14.27	-14.41	-14.45	-14.54

No cover offset

Figure 7.36, Figure 7.37 and Figure 7.38 show the effect on catchment leakiness of increasing PDrg cover in different elevation zones without offsetting this elsewhere in the catchment (net cover increase).

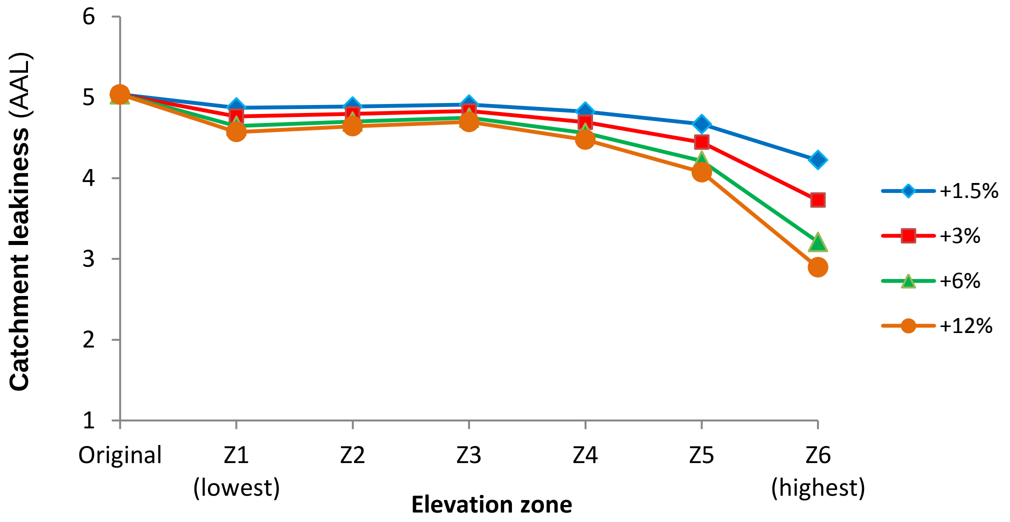

Figure 7.36 Amount of leakiness due to change of PDrg cover by elevation zone (net increase in catchment cover).

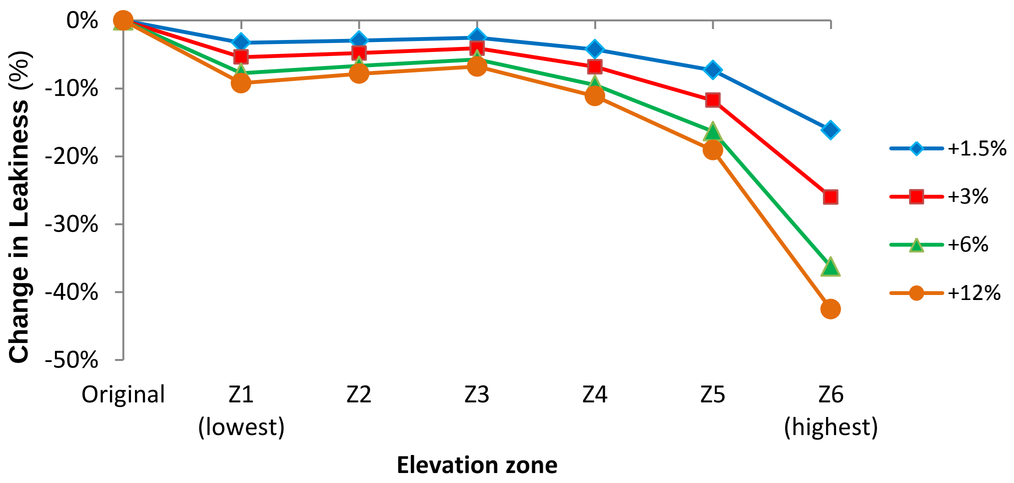

Figure 7.37 Change in leakiness due to change in PDrg cover by elevation zone (net increase in catchment cover).

These figures show that when PDrg cover was added to the catchment it was more effective at reducing leakiness when added to the higher elevation zones than when added to the lower elevation zones. The response was consistent for each zone and for each level of added cover. This result is similar to the result from adding SAVI cover.

Figure 7-38 shows the preceding results displayed on a zonal basis rather than on a percent cover basis.

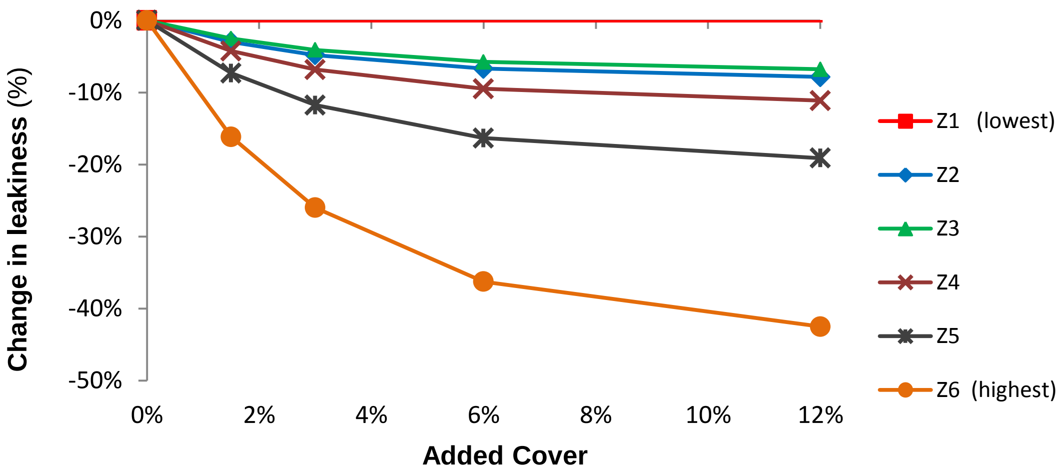

Figure 7.38 Response of leakiness to addition of PDrg cover by elevation zone (net increase in catchment cover).

Addition of cover to elevation zones 2-6 led to reduced leakiness with the response being generally negative curvilinear. This is consistent with the leakiness response to change in cover exhibited in Figure 7-15. Most reduction of leakiness occurs if cover is added to higher elevation zones, namely zones 4, 5 and 6. The rate of response of leakiness to addition of cover is similar to what was found before, namely it is greater per unit of cover for small additions than for larger additions.

Cover Offset

Figure 7.39, Figure 7.40 and Figure 7.41show the effect on catchment leakiness of increasing PDrg cover in different elevation zones while offsetting this additional cover by reducing cover across the rest of the catchment (no net cover increase).

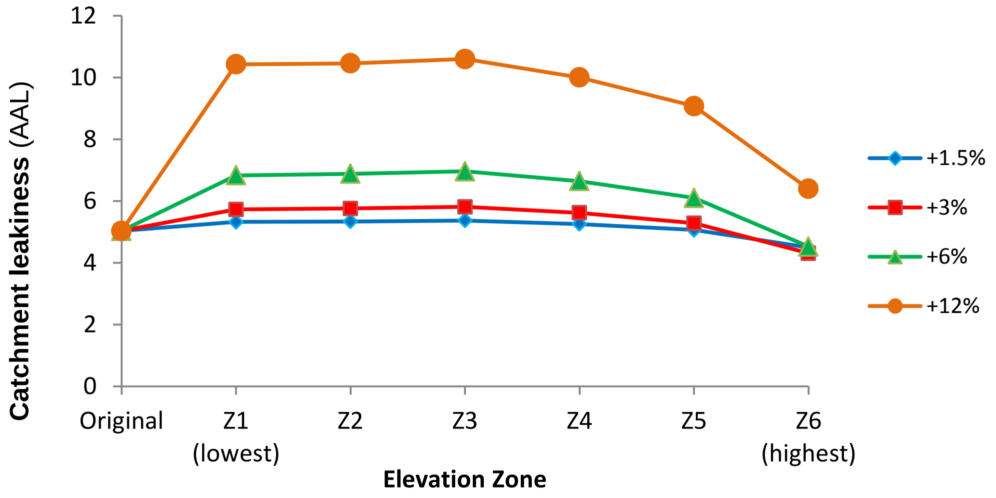

Figure 7.39 Amount of leakiness due to change of PDrg cover by elevation zone (no net increase in catchment cover).

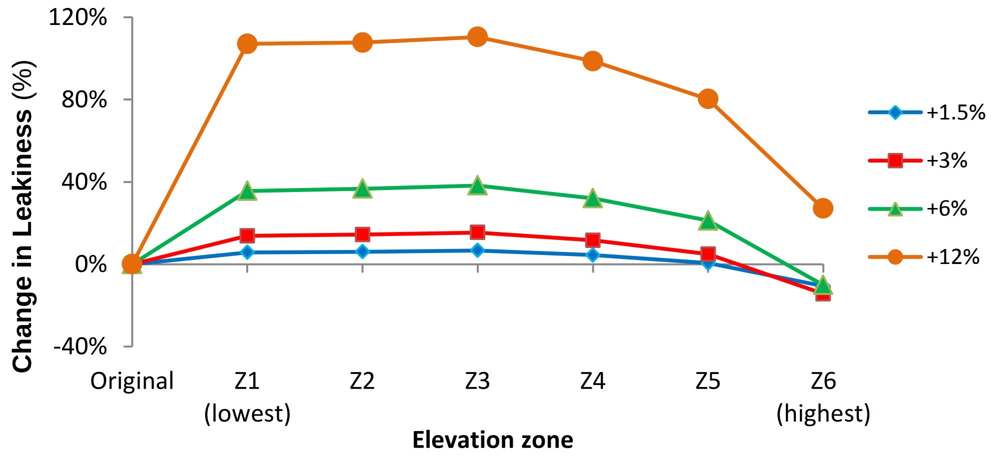

Figure 7.40 Change in leakiness due to change in PDrg cover by elevation zone (no net increase in catchment cover).

These Figures show, that when cover was added to the catchment in one elevation zone and offset elsewhere in the catchment the leakiness increased except if the additional cover was added to the highest elevation zone (Zone 6). These results are consistent with the no-cover offset scenario and the drainage line distance zone results.

Figure 7.41shows the preceding results displayed on a zonal basis rather than on a percent cover basis.

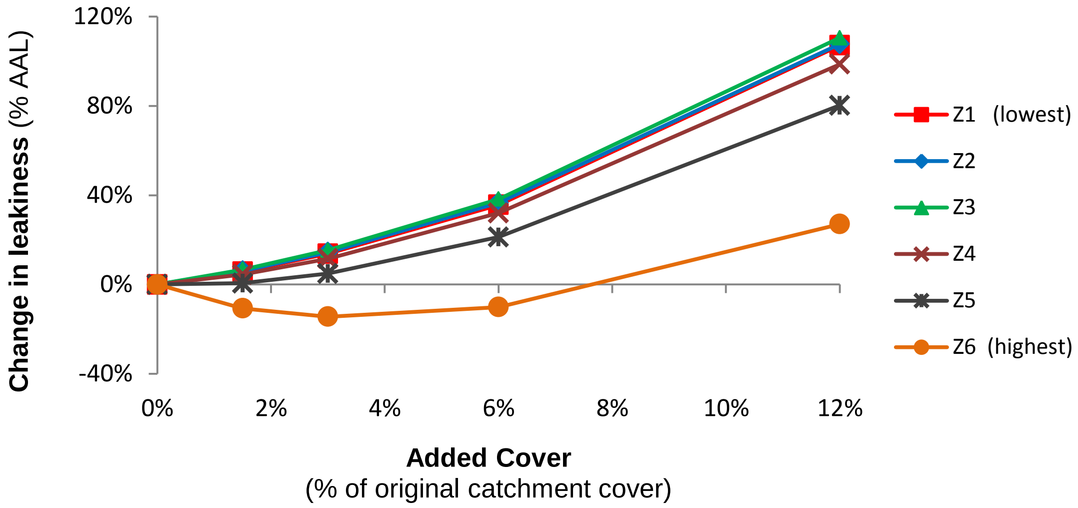

Figure 7.41 Response of catchment leakiness to addition of PDrg cover by elevation zone. (no net increase in catchment cover

The highest elevation zone is the only zone to which the addition of cover that is offset elsewhere in the catchment results in reduced catchment leakiness. Additions of more than 6% cover to zone 6 increases catchment leakiness.

7.3.4. Slope Zones

The effect of increasing the amount of cover, relative to the amount of slope, was tested both with and without cover offset. Each method used the slope zones as shown in Figure 7-7. The cover, slope and elevation values for these zones are shown relative to each other in Figure 7.42 and included in Table 7-8. The elevation increased steadily for each slope zone however there was a sharp increase in slope between the second last and last slope zones. Only the effect of SAVI cover on leakiness was assessed for slope zones and this was fairly constant across all slope intervals.

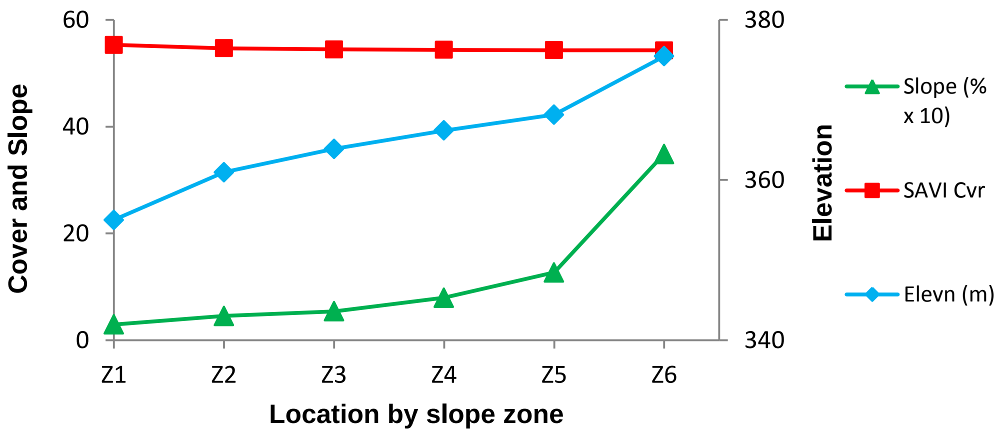

Figure 7.42 Cover, slope and elevation of the slope zones

7.3.4.1. SAVI Coverage

Table 7-8 summarizes the zone characteristics and the values used to adjust the level of SAVI cover in each zone for both the no-offset and offset scenarios.

Table 7-8 SAVI cover slope zone adjustment values

Zone	Total	Z1	Z2	Z3	Z4	Z5	Z6
Description		lowest	Intermediate				highest
Area (ha)	5,890	1,007	1,025	969	976	953	960
Elevn (m)	364.6	355.0	360.9	363.8	366.2	368.2	375.5
Slope (%)	2.5	0.3	0.5	0.5	0.8	1.3	3.5
Pixel No.	94,247	16,108	16,395	15,565	15,650	15,345	15,182
∑ Zone Cover	5,145,345	891,201	906,297	847,787	850,990	833,462	824,263
Mean Cover (%)	54.6	55.3	54.7	54.5	54.4	54.3	54.3
Increase (% of catchment)		**No cover offset (increase in cover per pixel)**					
1.5		4.79	4.70	4.95	4.93	5.03	5.08
3		9.58	9.41	9.91	9.86	10.05	10.16
6		19.16	18.83	19.83	19.72	20.11	20.33
12		38.33	37.66	39.66	39.45	40.23	40.66
Increase (% of catchment)		**Percent increase in cover by zone**					
1.5		8.66	8.52	9.10	9.07	9.26	9.36
3		17.32	17.03	18.21	18.14	18.52	18.73
6		34.64	34.06	36.41	36.28	37.04	37.45
12		69.28	68.13	72.83	72.56	74.08	74.91
Decrease (% of catchment)		**Cover offset (decrease in cover per pixel)**					
1.5		-0.98	-0.99	-0.98	-0.98	-0.97	-0.97
3		-1.97	-1.98	-1.96	-1.96	-1.95	-1.95
6		-3.95	-3.96	-3.92	-3.92	-3.91	-3.90
12		-7.90	-7.93	-7.84	-7.85	-7.82	-7.80
Decrease (% of catchment)		**Percent decrease in cover by zone**					
1.5		-1.81	-1.82	-1.80	-1.80	-1.79	-1.79
3		-3.63	-3.64	-3.59	-3.59	-3.58	-3.57
6		-7.26	-7.28	-7.18	-7.19	-7.16	-7.14
12		-14.51	-14.57	-14.37	-14.38	-14.32	-14.29

No cover offset

Figure 7.43, Figure 7.44 and Figure 7.45 show the effect on catchment leakiness of increasing PDrg cover in different slope zones without this being offset elsewhere in the catchment (net cover increase).

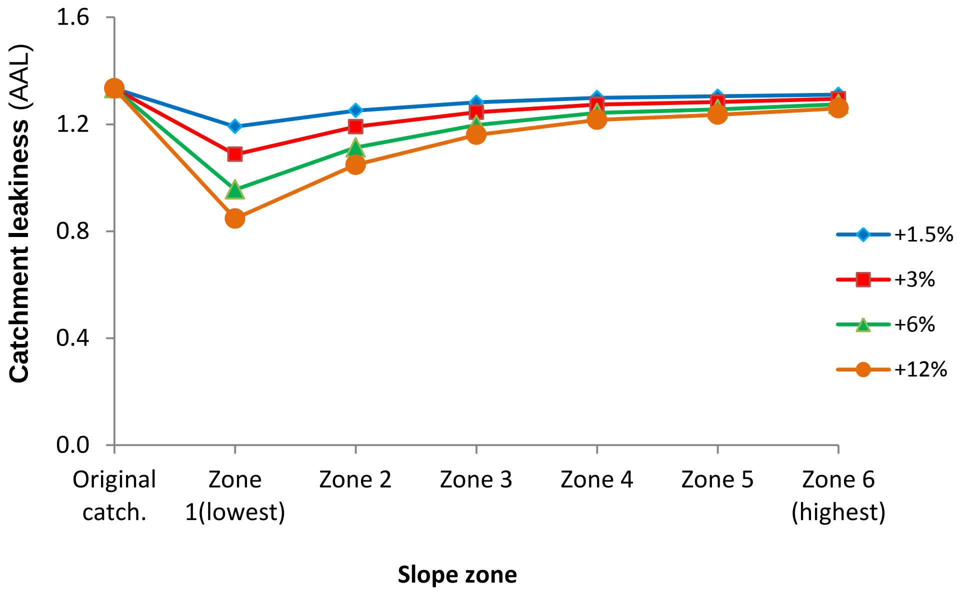

Figure 7.43 Amount of leakiness due to increase in SAVI cover by slope (net increase in catchment cover).

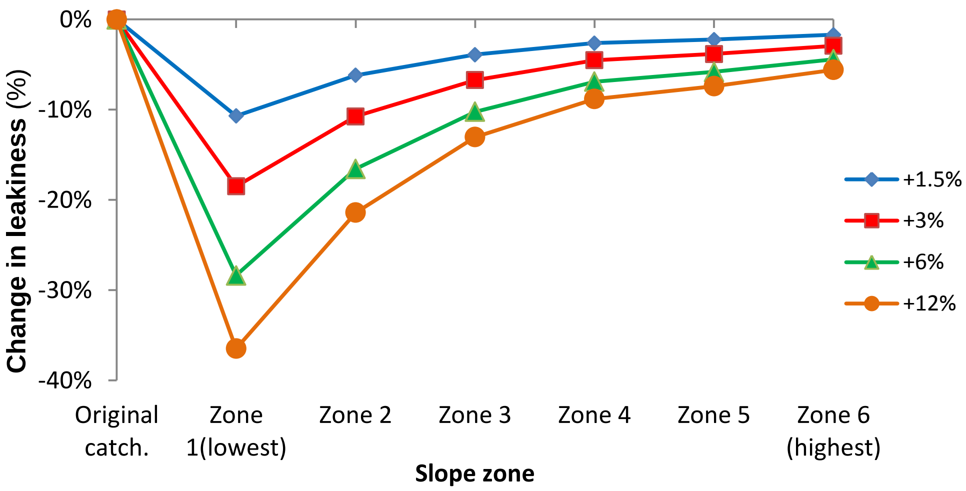

Figure 7.44 Change in Leakiness due to increase in SAVI cover by slope (net increase in catchment cover).

These figures show, that when SAVI cover was added to the catchment, it was more effective at reducing leakiness when added to the zones with the lowest slope with decreasing effect on reducing leakiness as the mean slope of the zone increased. The response was consistent for each zone and for each level of added cover. This result is not consistent with the results for drainage line distance zones and elevation zones that showed added cover decreased leakiness the most when added to the highest areas or areas furthest from the drainage lines that in general were the higher areas with higher slopes.

Figure 7.45 shows the preceding results displayed on a zonal basis rather than on a percent cover basis. Addition of SAVI cover reduces leakiness the most on the slowest sloping zones and the exponentially negative response is consistent with the leakiness response to change in cover exhibited in Figure 7-15. The rate of leakiness reduction is greater per unit of cover for small additions than for larger additions of cover.

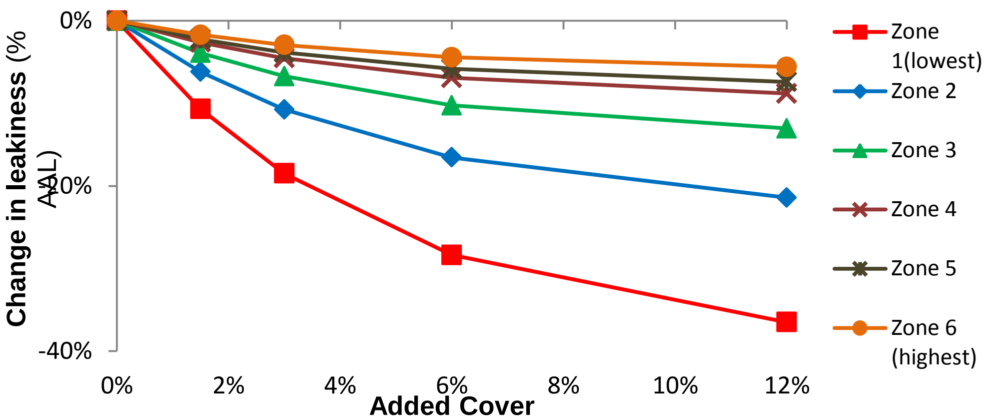

Figure 7.45 Response of leakiness to addition of SAVI cover by slope (net increase in catchment cover)

Cover offset

Figure 7.46, Figure 7.47 and Figure 7.48 show the effect on catchment leakiness of increasing SAVI cover in different slope zones without this being offset elsewhere in the catchment (net cover increase).

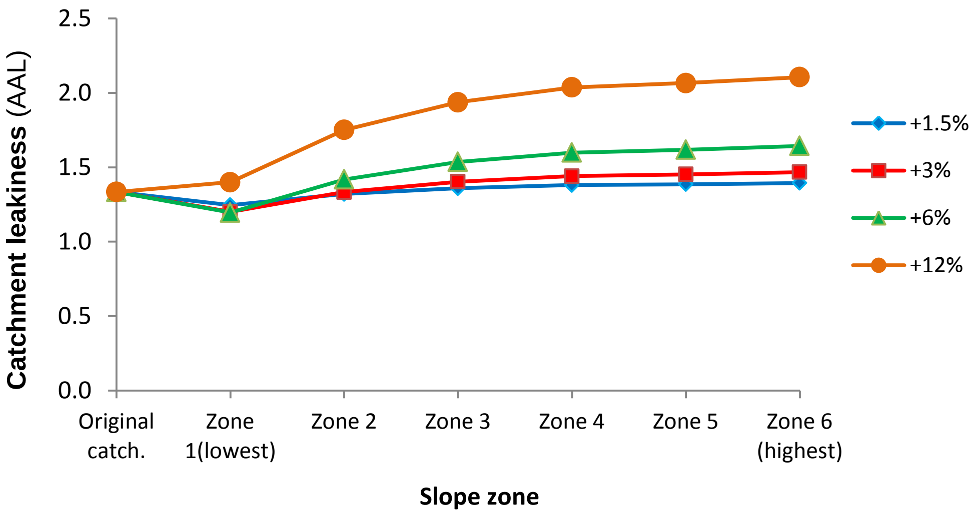

Figure 7.46 Amount of leakiness due to change of SAVI cover by slope (no net increase in catchment cover)

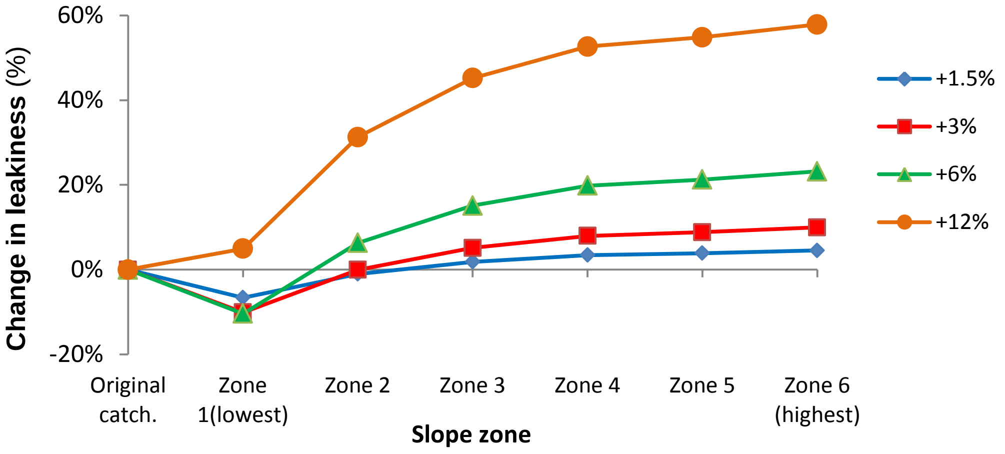

Figure 7.47 Change in Catchment Leakiness due to change of cover by slope (no net increase in catchment cover)

These figures show, that when cover was added to the catchment by slope zone, and offset elsewhere in the catchment, the leakiness increased except if added in small amounts (1.5-6%) to the zone with the lowest slope. This is consistent with the previous results for no-cover offset but inconsistent with the elevation and drainage line distance zone results as explained previously.

Figure 7.48 shows the preceding results displayed on a zonal basis rather than on a percent-added cover basis.

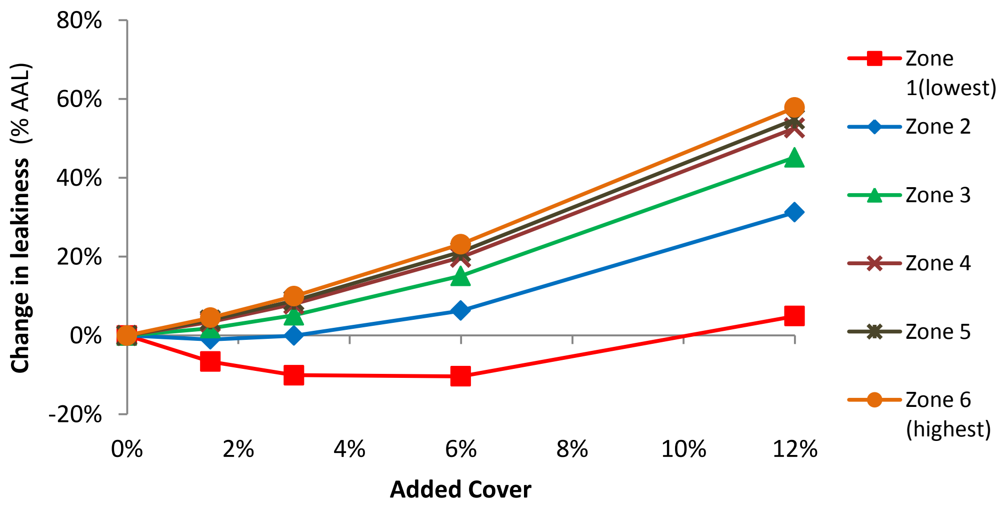

Figure 7.48 Response of catchment leakiness to change of cover by slope (no net increase in catchment cover)

The lowest elevation zone is the only zone to which the addition of cover, which is offset elsewhere in the catchment, results in reduced catchment leakiness. Addition of more than 10% cover to Zone 6 increased catchment leakiness.

7.3.5. Aspect Zones

The effect of increasing the amount of cover, relative to the position of the aspect zones, was tested both with and without cover offset. Each method used the same aspect zones as shown in Figure 7.9. The cover, slope and elevation values for these zones are shown relative to each other in Figure 7.49and included in Table 7-9. The elevation and slope were fairly constant for each aspect zone with the elevation declining for aspect Zone 6. SAVI cover was the same across all zones.

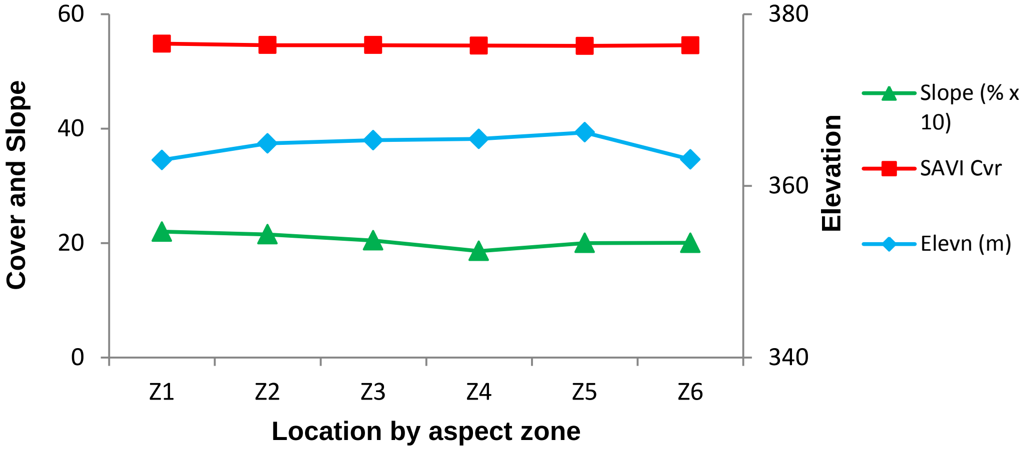

Figure 7.49 Cover, slope and elevation of the aspect zones

7.3.5.1. SAVI Coverage

Table 7-9 summarizes the zone characteristics and the values used to adjust the level of SAVI cover in each zone for both the no-offset and offset scenarios.

Table 7-9 SAVI cover aspect zone adjustment values (continued)

Zone	Total	Z1	Z2	Z3	Z4	Z5	Z6
Description		NE	E	SE	SW	W	NW
Area (ha)	5,889	984	980	983	982	981	979
Included Degrees (°)		0-82	82-164	164-221	221-267	267-307	308-360
Range (°)		82	82	57	46	40	52
Elevn (m)	364.6	363.0	364.9	365.3	365.4	366.2	363.1
Slope (%)	2.5	2.2	2.2	2.0	1.9	2.0	2.0
Pixel No.	94,247	15,755	15,673	15,727	15,760	15,663	15,665
∑ zone Cvr.	5,145,345	863,796	855,365	858,443	858,802	852,755	854,549
Mean Cvr.(%)	54.59	54.83	54.58	54.58	54.49	54.44	54.55
Increase (% of catchment)		No cover offset (increase in cover per pixel)					
1.5		4.90	4.92	4.91	4.90	4.930	4.93
3		9.80	9.85	9.82	9.79	9.86	9.85
6		19.60	19.70	19.63	19.59	19.71	19.71
12		39.19	39.40	39.26	39.18	39.42	39.42

Table 7-9 (continued) SAVI cover aspect zone adjustment values

Zone	Total	Z1	Z2	Z3	Z4	Z5	Z6
Increase (% of catchment)		**Increase in cover by zone (%)**					
1.5		8.93	9.02	8.99	8.99	9.05	9.03
3		17.87	18.05	17.98	17.97	18.10	18.06
6		35.74	36.09	35.96	35.95	36.20	36.13
12		71.48	72.18	71.93	71.90	72.41	72.25
Decrease (% of catchment)		**Cover offset (decrease in cover per pixel)**					
1.5		-0.98	-0.98	-0.98	-0.98	-0.98	-0.98
3		-1.97	-1.97	-1.97	-1.97	-1.96	-1.96
6		-3.93	-3.92	-3.93	-3.93	-3.93	-3.93
12		-7.87	-7.86	-7.86	-7.87	-7.86	-7.86
Decrease (% of catchment)		**Decrease in cover by zone (%)**					
1.5		-1.80	-1.80	-1.80	-1.80	-1.80	-1.80
3		-3.61	-3.60	-3.60	-3.60	-3.60	-3.60
6		-7.21	-7.20	-7.20	-7.20	-7.19	-7.19
12		-14.42%	-14.39	-14.40	-14.40	-14.38	-14.39

No cover offset

Figure 7.50, Figure 7.51and Figure 7.52 show the effect on catchment leakiness of increasing PDrg cover in different aspect zones without this being offset elsewhere in the catchment (net cover increase).

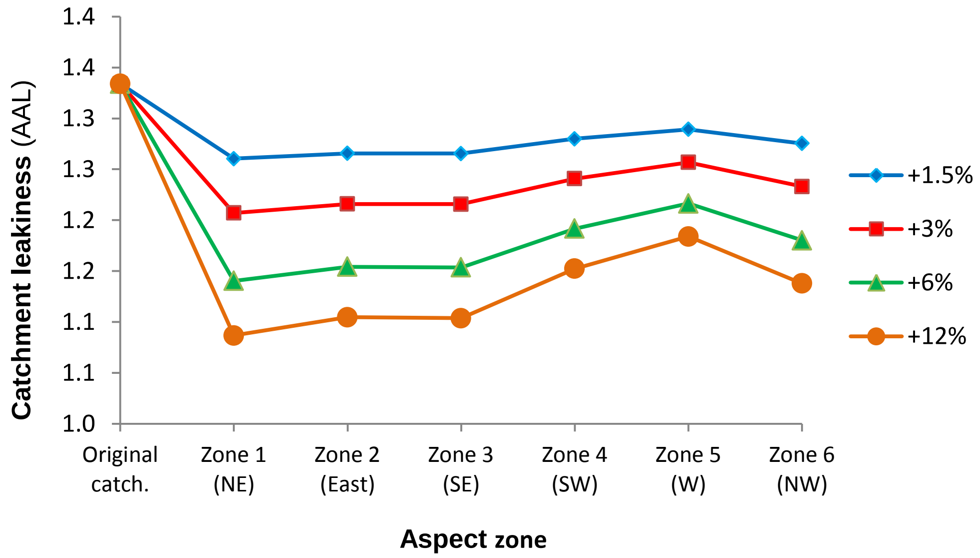

Figure 7.50 Amount of leakiness due to increase in cover by aspect (net increase in catchment cover)

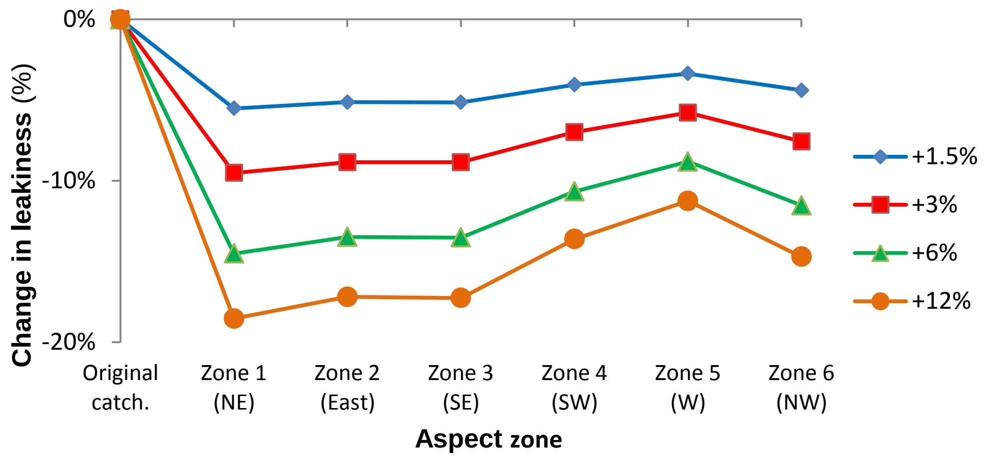

Figure 7.51 Change in Leakiness due to increase in cover by aspect(net increase in catchment cover)

These figures show that when SAVI cover was added to the catchment, it was close to equally effective at reducing the leakiness of all aspect zones when added in small amounts (+1.5%) but was more effective in the eastern aspect Zones 1-3 (0° to 221°) when added in larger amounts (+6 to +12%). The transition between aspect zones was gradual as shown in the figures above with aspect Zone 5 (267° – 307°) being the least responsive to added cover.

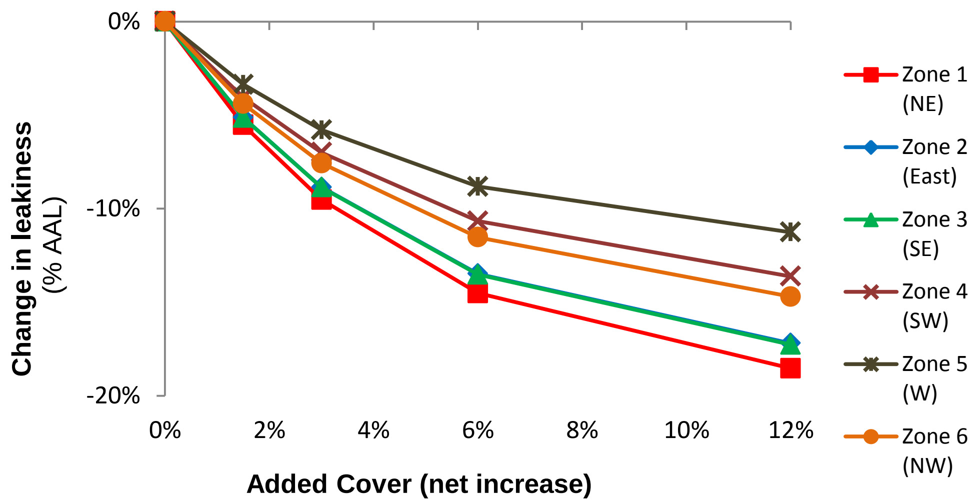

Figure 7.52 Response of leakiness to addition of cover by aspect(net increase in catchment cover)

Figure 7.52 shows the preceding results displayed on a zonal basis rather than on a percent cover basis. Addition of cover to all aspect zones reduces leakiness with the response being greatest for zones 1, 2 and 3 in declining order. The rate of response of leakiness to addition of cover is similar to what was found before, namely it is greater for small additions than for larger additions.

Cover offset

Figure 7.53, Figure 7.54 and Figure 7.55 show the effect on catchment leakiness of increasing SAVI cover in different aspect zones while offsetting this additional cover by reducing cover across the rest of the catchment.

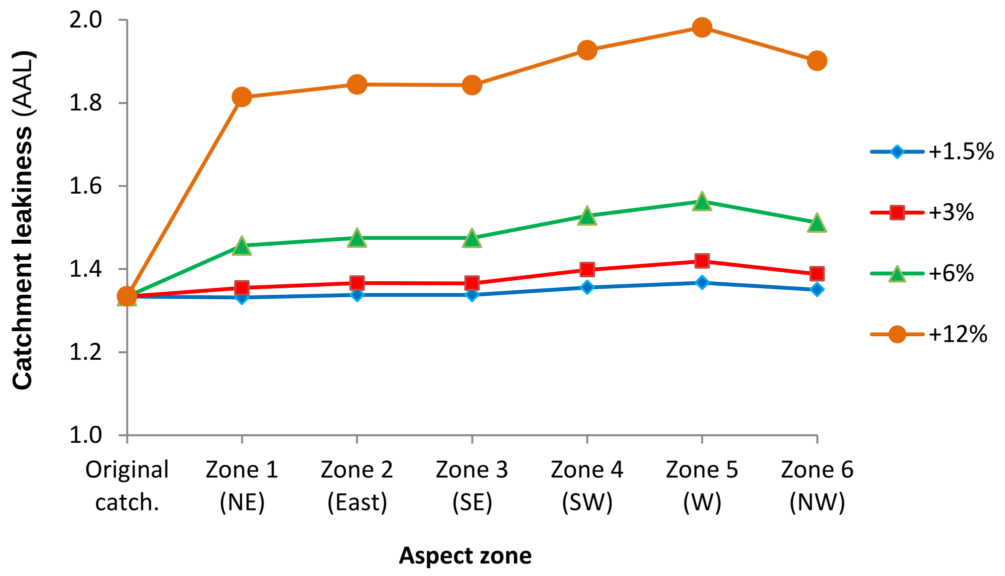

Figure 7.53 Amount of leakiness due to change of cover by aspect zone (no net increase in catchment cover)

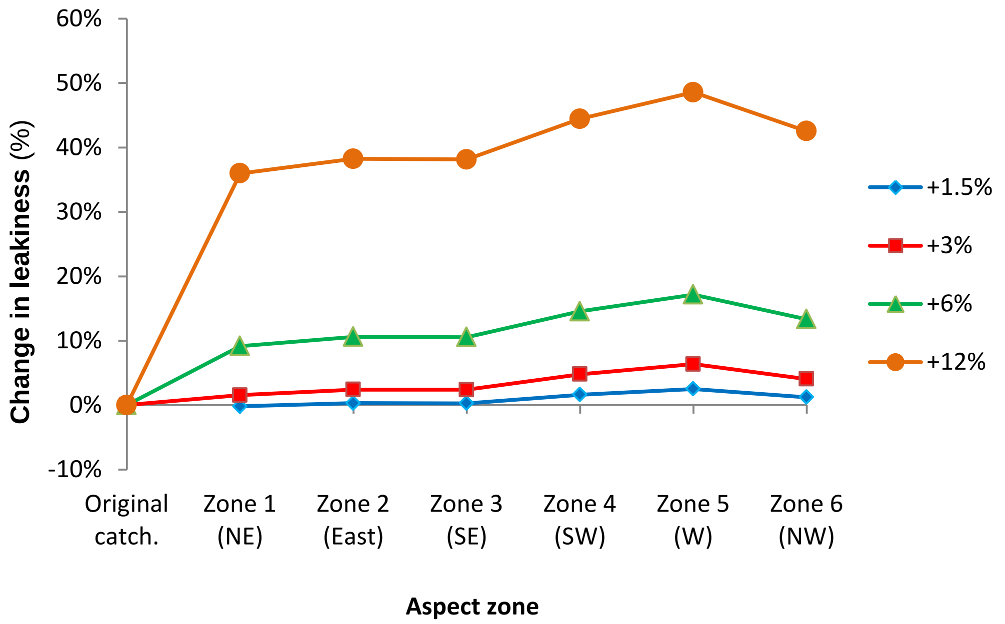

Figure 7.54 Change in leakiness due to change in cover by aspect (no net increase in catchment cover)

These figures show, that when cover was added to the catchment in one aspect zone and offset by decreasing it proportionally across the rest of the catchment, the leakiness increased. This effect was greatest when additional cover was added to Zone 5.

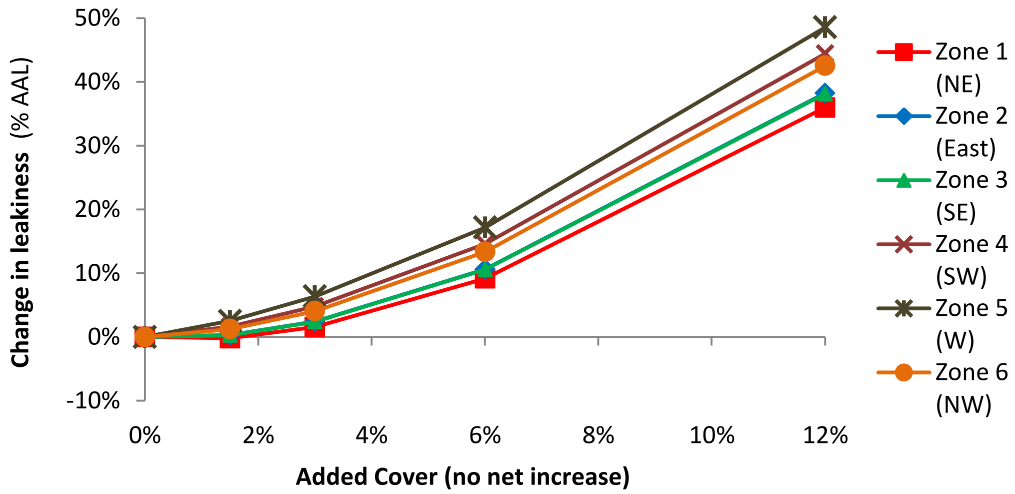

Figure 7.55 Response of catchment leakiness to change of cover by aspect (no net increase in catchment cover)

Figure 7.55 shows the preceding results displayed on a zonal basis rather than on a percent cover basis. Addition of cover to all aspect zones caused increased leakiness when it was offset by a decrease across the rest of the catchment.

7.3.6. Topographic Zones

The topographic zone analysis was based on 6 landforms; channels, passes, peaks, pits, planes and ridges as shown in Figure 7.11. (The terms ‘landform’ and ‘topographic zone’ refer to the same thing and are used interchangeably according to the context). Each landform had 4 cover treatments applied to it.

The landforms had substantially different areas (see cell count row in Table 7-10). This made it impractical to compare the effects of an increase in cover for each zone relative to the total cover of the catchment because some zonal covers would have exceeded 100% cover for even small percentage additions of catchment cover. Instead, the increase in cover for each landform zone was calculated as a percent of their existing cover and the effect this had on overall catchment cover was calculated (Catchment cover change section of Table 7-10). This allowed analysis of the sensitivity of changing the cover on each type of landform, on catchment leakiness.

The effect of increasing the amount of cover in each of the topographic zones was tested both with and without cover offset. Each method used the same outline for the landforms as shown in Table 7-10 and elevation values for these zones are shown relative to each other in Figure 7-56 and given in Table 7-10. In Figure 7-56 the landforms have been arranged on the X-axis in the same sequence that generated a steadily declining leakiness in Figure 7.57, Figure 7.58 and Figure 7.59. Plains and ridges are distinguished by abrupt changes in elevation in this sequence. Channel slope is the same height as for passes, ridges and peaks while pits and plains had lower slopes. SAVI cover was the same for all landforms but PDrg cover was highest in pit areas and became progressively lower as the landforms moved to peak areas.

The difference in behaviour of the PDrg cover index, relative to the SAVI cover index, for land form types indicates its greater sensitivity to the differences in cover that occur on different land forms.

7.3.6.1. SAVI Coverage

Table 7-10 summarizes the characteristics for the landform zones and the values used to adjust the level of SAVI cover on each landform for both the no-offset and offset scenarios.

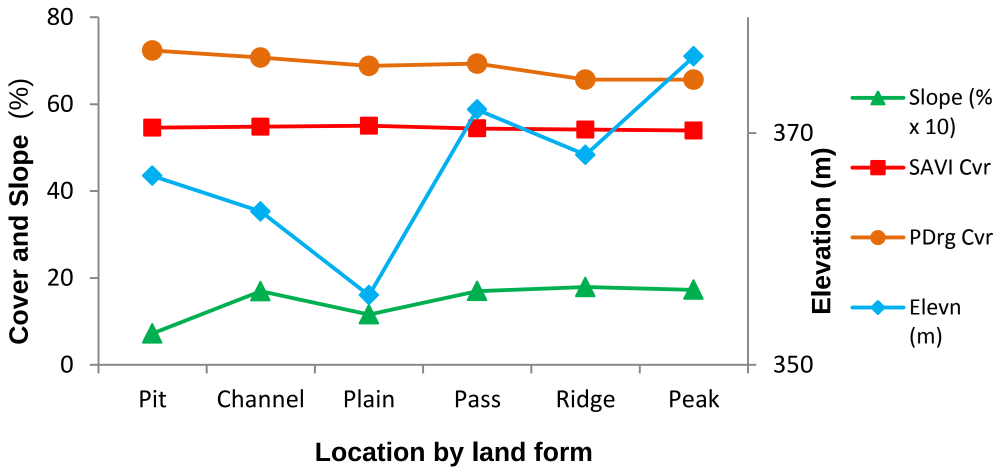

Figure 7.56 Cover, slope and elevation of the land form zones

Table 7-10 Land form zone cover adjustments for SAVI (continued).

Zones	Total	Z1	Z4	Z5	Z6	Z2	Z3
Description		Channel	Pass	Peak	Pit	Plain	Ridge
Area (ha)	5,965	1,844	669	257	183	1,321	1,690
Elevation (m)	364.6	363.2	372.0	376.6	366.3	356.0	368.1
Slope (%)	2.5	1.7	1.7	1.7	0.7	1.2	1.8
Pixel No.	94,220	29,135	10,567	4,067	2,899	20,847	26,705
∑ Zone Cover	5,143,500	1,596,455	575,047	219,325	158,236	1,148,776	1,445,662
Mean Cover (%)	54.6	54.8	54.4	53.9	54.6	55.0	54.1
Increase (% Zone)		No cover offset scenario (increase in cover per pixel)					
10		5.48	5.44	5.39	5.46	5.50	5.41
20		10.96	10.88	10.79	10.92	11.01	10.83
30		16.44	16.33	16.18	16.38	16.51	16.24
40		21.92	21.77	21.57	21.84	22.01	21.65
Increase (% Zone)		Percent increase in cover by zone (%)					
10		3.1	1.1	0.4	0.3	2.2	2.8
20		6.2	2.2	0.9	0.6	4.5	5.6
30		9.3	3.4	1.3	0.9	6.7	8.4
40		12.4	4.5	1.7	1.2	8.9	11.2

Table 7-10 (continued) Land form zone cover adjustments for SAVI

Zones	Total	Z1	Z4	Z5	Z6	Z2	Z3
Decrease (% Zone)		**Cover offset scenario (decrease in cover per pixel)**					
10		2.45	0.69	0.24	0.17	1.56	2.14
20		4.91	1.37	0.49	0.35	3.13	4.28
30		7.36	2.06	0.73	0.52	4.69	6.42
40		9.81	2.75	0.97	0.69	6.25	8.57
Decrease (% Zone)		**Percent decrease in cover by zone (%)**					
Same values as “Percent increase in cover by zone” values above							

As was done previously, two scenarios were tested, a net-increase scenario and a no-net-increase scenario. In the net-increase approach the cover in each zone was increased by 4 increments (10 – 40% of the zone cover) as shown in Table 7-10 with no compensatory reduction in cover in the balance of the catchment. This had the effect of increasing the total catchment cover by the amount added to each zone.

In the no-net-increase scenario, the cover in each zone was increased, one zone at a time, by the same amount as in the no-net-increase scenario however the cover in the balance of the catchment was reduced by a compensatory amount, so that the average catchment coverage remained the same.

No cover offset

In this analysis, the cover on each landform zone was increased, one zone at a time, while the cover on the rest of the topographic zones remained the same. This resulted in variable net increases in catchment average cover. Two factors affect the dependent variable Leakiness in this scenario, change in distribution of cover and total amount of cover. Table 7-11 shows the results of changing the cover on a zonal basis without comparing the effect on the total catchment because the comparison is on the basis of leakiness per unit of added cover.

Table 7-11 Land form zone analysis results for SAVI cover

Change in Zone Cover (%)	Leakiness change per unit cover ((AAL/unit cover) x 10^6)						
	No change	Pit	Channel	Plane	Pass	Ridge	Peak
10	0	0	-0.067	0.425	-1.194	-1.570	-2.056
20	0	0	-0.057	0.361	-1.016	-1.335	-1.754
30	0	0	-0.049	0.309	-0.872	-1.147	-1.508
40	0	0	-0.042	0.268	-0.757	-0.995	-1.309

To help understand these results they are also presented in a graphical format in Figures 7-57 and 7-58. These figures show the absolute and relative effects of changing (increasing) the amount of cover in each landform by 10%, 20%, 30% and 40% and leaving the balance of the cover in the catchment unchanged. The results have been normalised to accommodate for different sized zones.

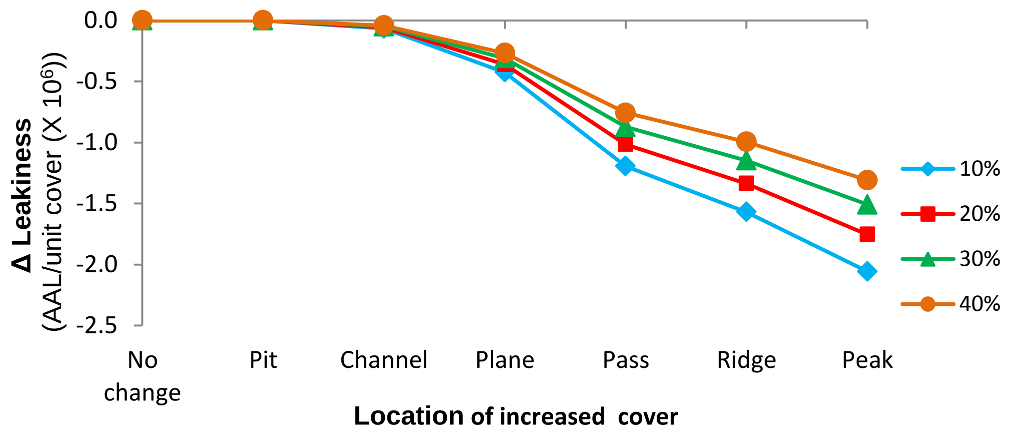

Figure 7.57 Absolute effect on leakiness of increasing SAVI cover in each landform zone (net cover increase scenario)

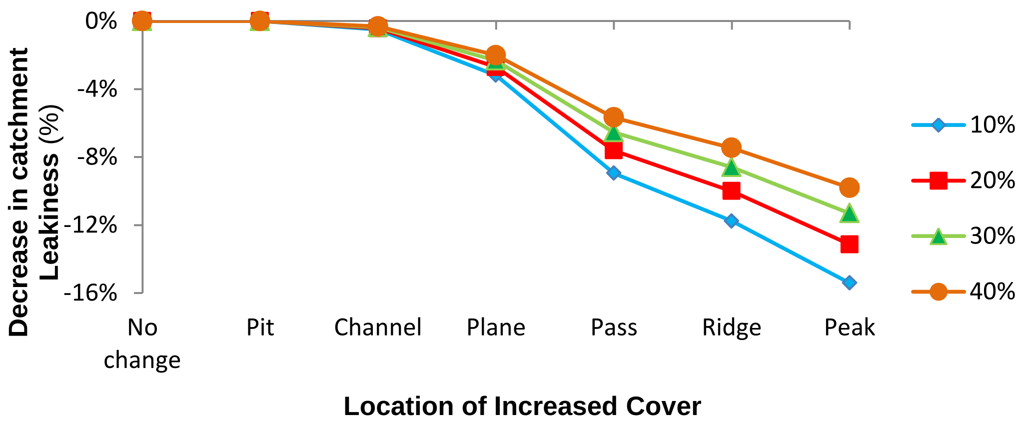

Figure 7.58 Relative effect of increasing SAVI cover in each landform zone on leakiness (net cover increase scenario)

These Figures show that cover was more effective at reducing leakiness if it was added to peak, ridge and pass land forms (in descending order) than if it was added to pit, channel or plain land forms (in increasing order). This is consistent with the results from the DLD zone cover analysis (Section 7.4.3) and elevation zone analysis (Section 7.4.4) where it was found that cover was most effective in reducing leakiness if it was added either to areas that were furthest from the drainage lines or at the highest elevations if it was added to areas closer to drainage lines or at lower elevations. In addition, decrease in leakiness per unit added cover was greater for smaller additions of cover than for larger additions of cover.

The response of catchment leakiness to increases in cover of each topographic feature was investigated and the results are shown in Figure 7-59.

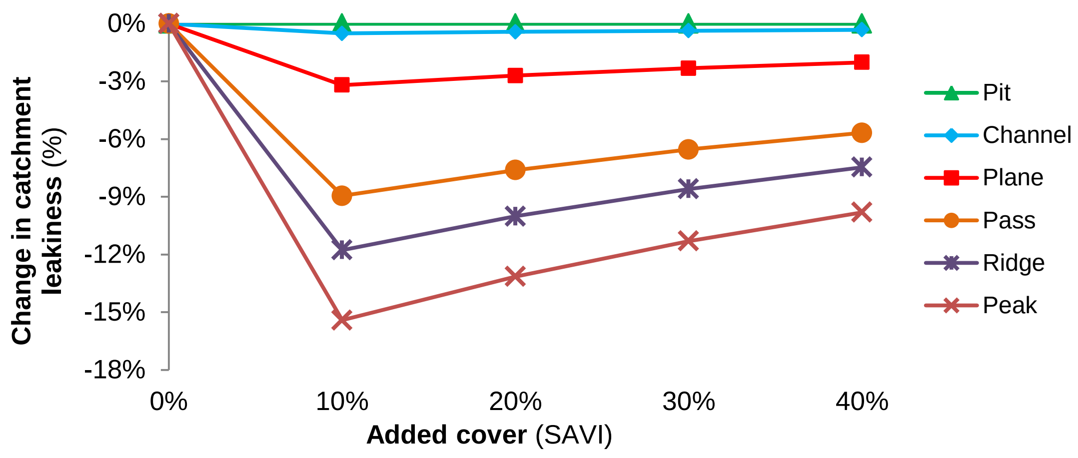

Figure 7.59 Leakiness response to addition of SAVI cover by landform zone (net cover increase scenario).

The results show that small additions of cover were more effective at reducing leakiness, per unit of added cover, than larger additions, in all topographic zones except for pits and channels where the addition of cover had no effect on leakiness (Figure 7.59). This occurs because there is no flow from pits and channels immediately precede the catchment discharge point.

Cover offset

Table 7-12 shows the results of changing the cover on a zonal basis and offsetting the increase by an equivalent reduction of cover over the rest of the catchment.

Table 7-12 Land form zone analysis results for SAVI cover

Change in Zone Cover (%)	Leakiness change per unit cover ((AAL/unit cover) x 10^6)						
	No change	Pit	Channel	Plane	Pass	Ridge	Peak
10	0	0.952	1.359	0.682	-0.301	-0.967	-1.200
20	0	0.986	1.500	0.811	-0.107	-0.687	-0.868
30	0	0.981	1.650	0.926	0.059	-0.449	-0.622
40	0	0.981	1.817	1.037	0.198	-0.240	-0.420

To assist in understand these results they are also presented in graphical form in Figure 7.60 and Figure 7.61. These show the absolute and relative effects on catchment leakiness of increasing cover on different topographic zones while reducing cover over the balance of the catchment proportionally to maintain the same overall level of catchment cover.

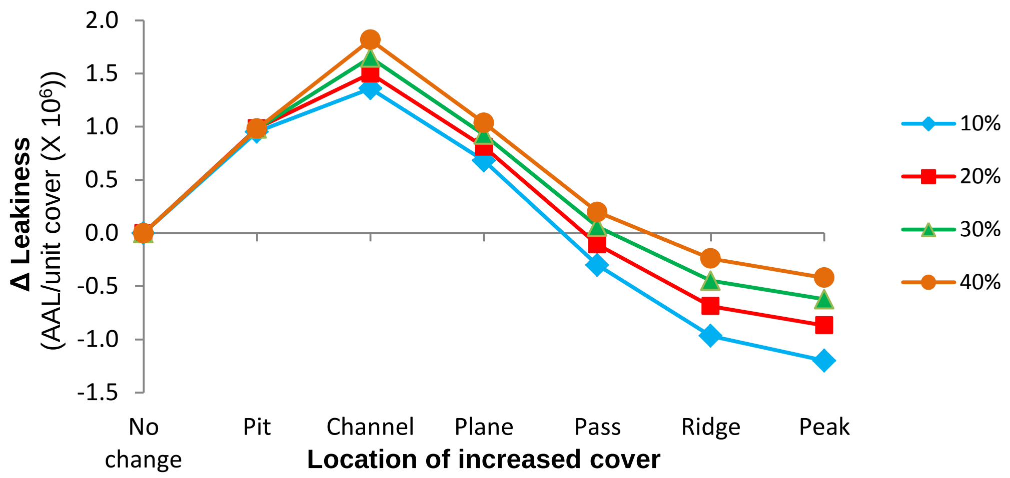

Figure 7.60 Effect if increasing SAVI cover on landform zones on catchment leakiness (no net increase scenario)

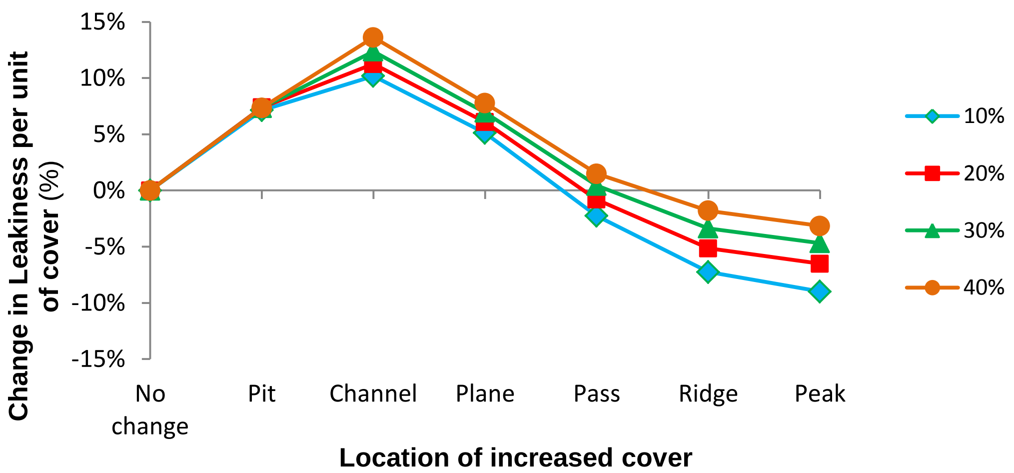

Figure 7.61 Relative effect of increasing SAVI cover in each landform zone on leakiness (no net increase scenario)

These two figures show that adding cover to different topographic zones, while offsetting the amount of added cover proportionally across the balance of the catchment, leads to an increase in leakiness if the cover is added to pits, channels and planes. Adding small amounts of cover to pass areas can decrease the catchments leakiness while adding larger amounts (≥ 30%) can increase leakiness. This is because the addition of cover in these areas is not very effective at reducing leakiness, while leakiness is increased (due to the offset effect) in areas where cover is reduced because these are areas where cover is more effective at reducing leakiness (ridges and peaks). This is consistent with the results from the previous No Cover Offset section and the Cover Offset results for the drainage distance zones.

The response of catchment leakiness to increases in cover of each topographic feature, while being offset across the rest of the catchment, was investigated. The results are shown in Figure 7.62.

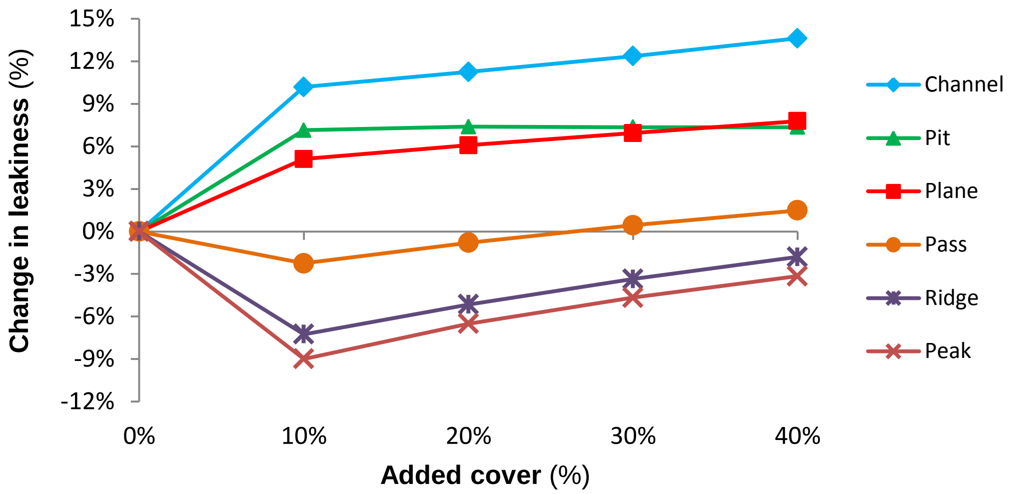

Figure 7.62 Leakiness response to addition of SAVI cover by landform zone.

This figure shows a similar pattern of change in catchment leakiness to that shown in Figure 7.59, only the reduction per unit of cover is less. While addition of cover to pits and channels had no effect on leakiness in the No Cover Offset scenario (Figure 7.59) addition of cover to channels reduced leakiness in the Cover Offset scenario. The effectiveness of cover in reducing leakiness declines with larger additions of cover.

7.3.6.2. PDrg Coverage

Table 7-13 summarizes the characteristics for the landform zones and the values used to adjust the level of PDrg cover in each landform for both the no-offset and offset scenarios. It shows the values used for testing both the No Cover Offset and the Cover Offset scenarios.

Table 7-13 Land form zone cover adjustments for PDrg (c0ontinued).

Zones	Total	Z1	Z4	Z5	Z6	Z2	Z3
Description		Channel	Pass	Peak	Pit	Plane	Ridge
Area (ha)	5,965	1,844	669	257	183	1,321	1,690
Elevation (m)	364.6	363.2	372.0	376.6	366.3	356.0	368.1
Slope (%)	2.5	1.7	1.7	1.7	0.7	1.2	1.8
Pixel No.	94,220	29,135	10,567	4,067	2,899	20,847	26,705
∑ Zone Cover	6,489,081	2,060,745	732,628	266,879	209,654	1,436,261	1,782,913
Mean Cover (%)	68.9	70.7	69.3	65.6	72.3	68.8	66.8
Increase (% Zone)		No cover offset scenario (increase in cover per pixel)					
10		7.07	6.93	6.56	7.23	6.88	6.68
20		14.15	13.87	13.12	14.46	13.76	13.35
30		21.22	20.80	19.69	21.70	20.64	20.03
40		28.29	27.73	26.25	28.93	27.52	26.70

Table 7-13 (continued) Land form zone cover adjustments for PDrg

Zones	Total	Z1	Z4	Z5	Z6	Z2	Z3
Increase (% Zone)		**Percent increase in cover by zone (%)**					
10		3.2	1.1	0.4	0.3	2.2	2.7
20		6.4	2.3	0.8	0.6	4.4	5.5
30		9.5	3.4	1.2	1.0	6.6	8.2
40		12.7	4.5	1.6	1.3	8.8	11.0
Decrease (% Zone)		**Cover offset scenario (decrease in cover per pixel)**					
10		-3.17	-0.88	-0.30	-0.23	-1.96	-2.64
20		-6.33	-1.75	-0.59	-0.46	-3.91	-5.28
30		-9.50	-2.63	-0.89	-0.69	-5.87	-7.92
40		-12.66	-3.50	-1.18	-0.92	-7.82	-10.56
Decrease (% Zone)		**Percent decrease in cover by zone (%)**					
Same values as "Percent increase in cover by zone" values above							

No Cover offset

The PDrg cover data were processed similarly to the SAVI cover data in Subsection 7.3.6.1. Table 7-14 shows the results of changing the cover on a zonal basis without considering the effect of total catchment cover change.

Table 7-14 Land form zone analysis results for PDrg cover

Change in Zone Cover (%)	Leakiness change (AAL/unit of cover x 10^6)						
	No change	Pit	Channel	Plane	Pass	Ridge	Peak
10	0	0	-0.064	-1.291	-3.344	-7.420	-7.848
20	0	0	-0.052	-1.042	-2.708	-5.917	-6.363
30	0	0	-0.043	-0.859	-2.238	-4.850	-5.269
40	0	0	-0.036	-0.722	-1.883	-4.063	-4.444

As before, these results are also presented graphically in Figure 7.63 and Figure 7.64.

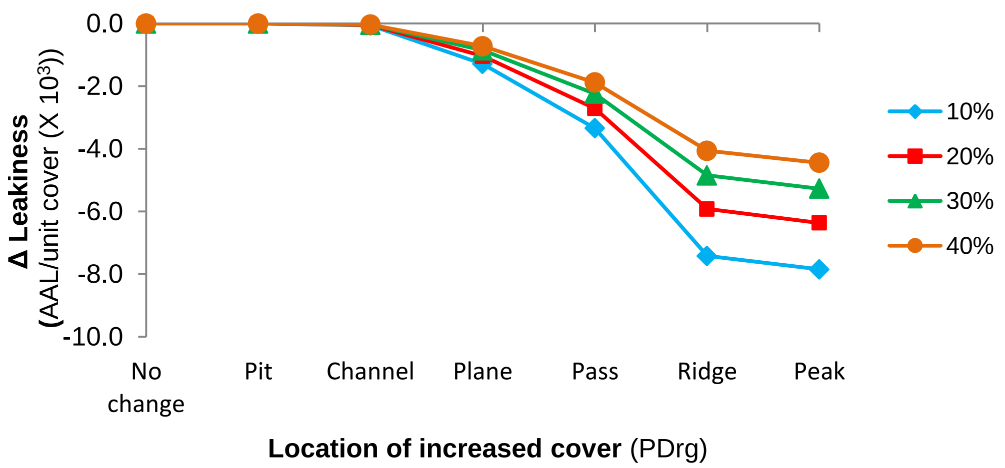

Figure 7.63 Absolute effect on leakiness of increasing PDrg cover in each landform zone (net cover increase scenario)

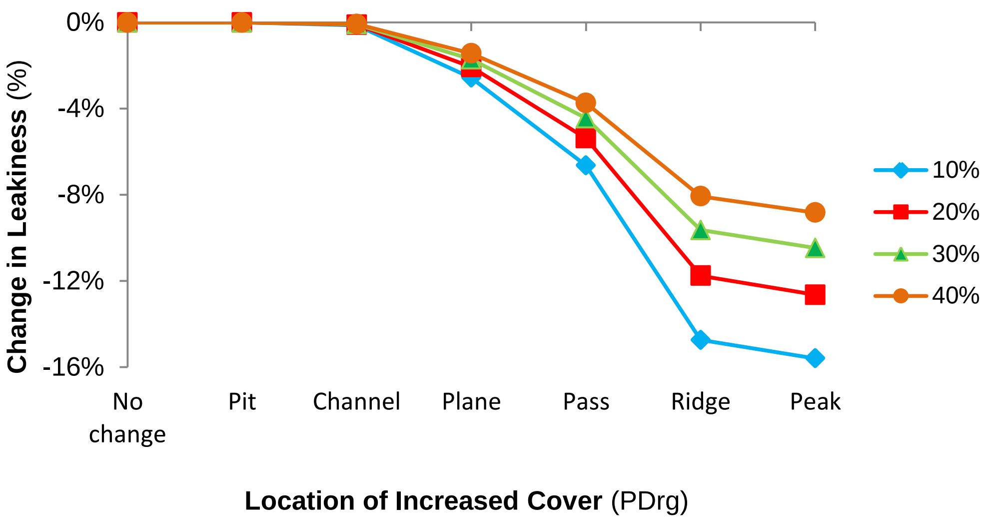

Figure 7.64 Relative effect on catchment leakiness of increasing PDrg cover in each land form zone (net cover increase scenario).

These figures show a similar effect to that found for adding SAVI cover to different landform zones (Subsection 7.3.6.1). PDrg cover was most effective at reducing leakiness when added to peak, ridge and pass landforms. This is also consistent with the results from the drainage line distance zone cover analysis (Section 7.3.2) where it was found that cover was most effective in reducing leakiness if it was added to areas that were more distant from the drainage lines than to areas closer to drainage lines. In addition, the unit decrease in leakiness was greater for smaller additions of cover than for larger additions of cover.

Increases in PDrg cover to each topographic feature yielded similar results to the addition of SAVI cover (Figure 7.65).

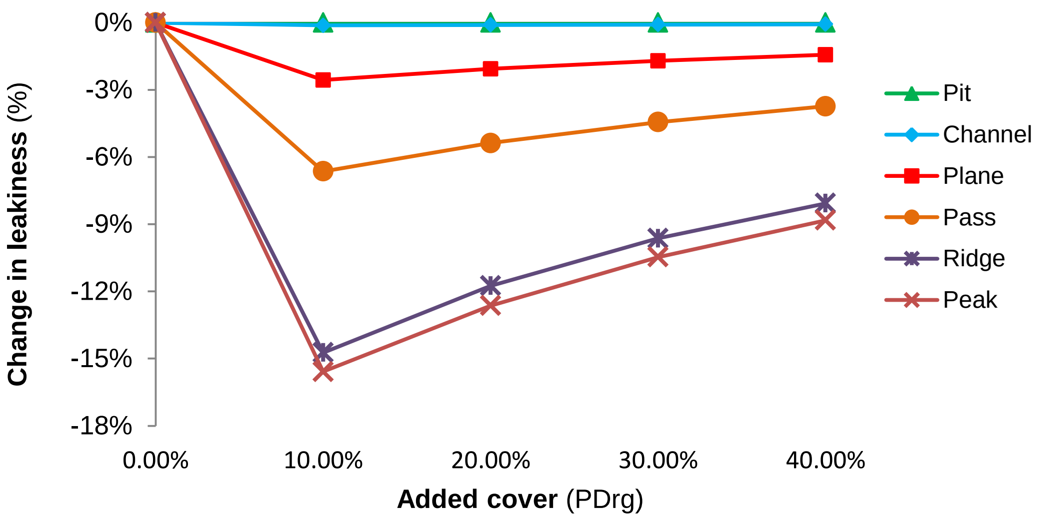

Figure 7.65 Leakiness response to addition of PDrg cover by landform zone (net cover increase scenario)

Cover Offset

Table 7-15 shows the results of changing the cover on a zonal basis and offsetting the increase by an equivalent reduction of cover over the rest of the catchment.

Table 7-15 Land form zone analysis results for PDrg cover

Change in Zone Cover (%)	Leakiness change per unit cover						
	No change	Pit	Channel	Plane	Pass	Ridge	Peak
10	-	4.206	6.630	3.814	0.797	-5.506	-4.059
20	-	4.238	7.816	4.539	1.589	-3.840	-2.539
30	-	4.285	9.432	5.289	2.229	-2.563	-1.403
40	-	4.326	9.690	6.108	2.772	-1.517	-0.533

The results are presented graphically in Figure 7.66 and Figure 7.67.

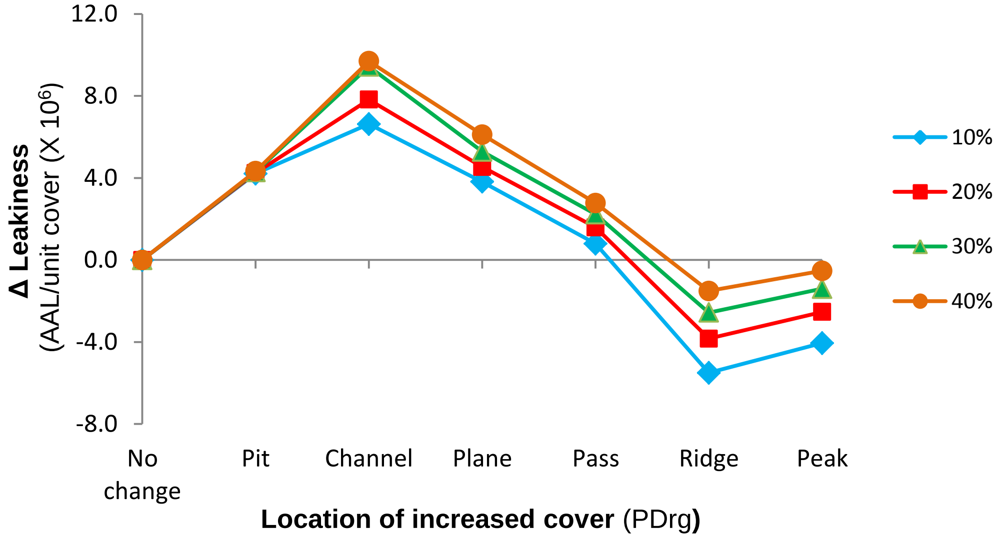

Figure 7.66 Effect of increasing PDrg cover on landform zones on catchment leakiness (no net increase scenario)

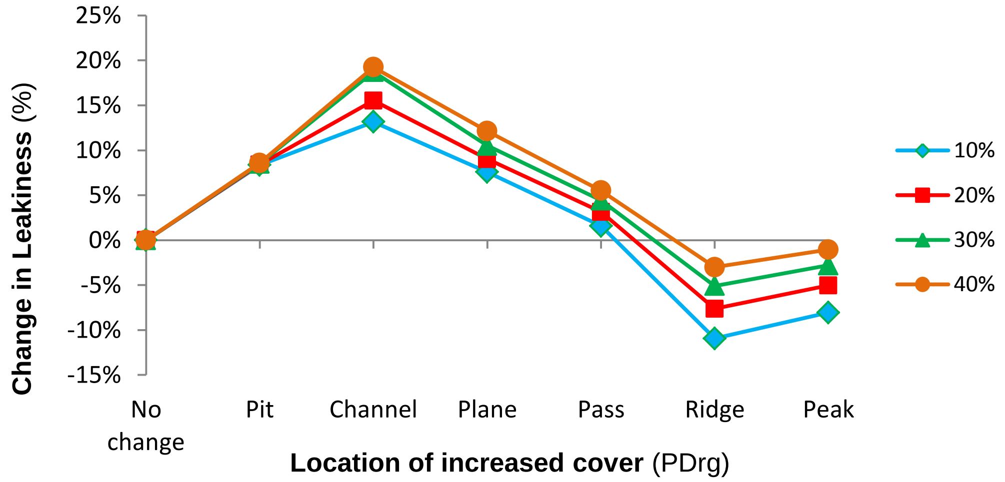

Figure 7.67 Relative effect of increasing PDrg cover on landform zones on catchment leakiness (no net increase scenario)

The preceding figures show that adding cover to different landform zones, while offsetting the amount of added cover proportionally across the balance of the catchment, leads to an increase in leakiness if the cover is added to pits, channels, planes and passes.

The response of catchment leakiness to increases in cover on each landform, while being offset across the rest of the catchment, is shown in Figure 7.68.

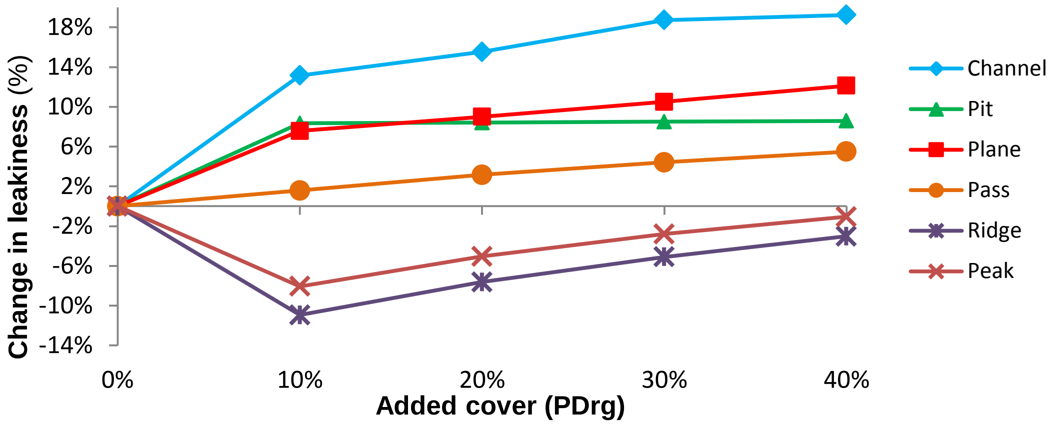

Figure 7.68 Leakiness response to addition of PDrg cover by landform zone (no net increase scenario).

7.3.7. Cover Zones

Cover zones are zones that depend on the type of cover analysis performed on the original satellite image. Thus SAVI cover zones have different boundaries from PDrg cover zones. The effect of increasing the amount of cover, on different cover zones, was tested both with and without cover offset. Cover zones specific for either SAVI cover or PDrg cover were used as shown in Figure 7.13 and Figure 7.14.

7.1.1.1. SAVI Coverage

The cover, slope and elevation values for the SAVI cover zones are shown relative to each other in Figure 7.69 and are included in Table 7-16.

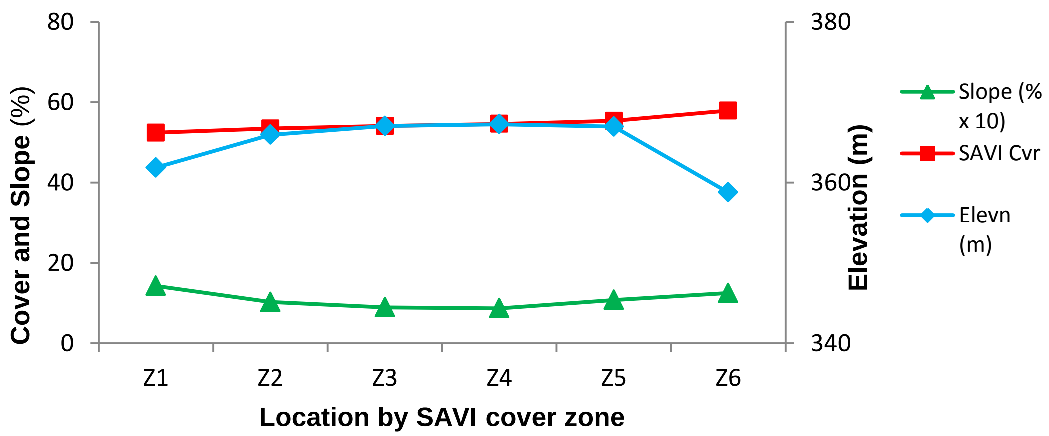

Figure 7.69 Cover, slope and elevation of the SAVI cover zones

Elevation was lowest in the areas that had the lowest and highest SAVI cover, despite the SAVI cover only varying a small amount across the catchment. The slope was the highest in both the lowest and highest SAVI cover zones.

Four levels of change in cover (treatments) were made to each of the cover zones. Table 7-16 shows both the zonal characteristics as well as the values used to adjust the level of cover in each zone for the Net- increase and No-net- increase scenarios.

Table 7-16 SAVI Cover zone adjustment values (continued)

Zones	Total	Z1	Z2	Z3	Z4	Z5	Z6
Description.	Whole	lowest	low medium	medium	above medium	high medium	highest
Area (ha)	5890.44	1034	994	925	1186	796	955
Elevation (m)	364.6	361.9	366.0	367.1	367.3	367.0	358.8
Slope (%)	2.5	1.4	1.0	0.9	0.9	1.1	1.3
Pixel No.	94,247	16,026	16,802	15,731	14,325	15,802	15,561
∑ Zone Cover	5,142,044	840,178	898,537	850,890	782,691	874,943	901,583
Mean Cover %	54.6	52.4	53.5	54.1	54.6	55.4	57.9
Cover Range %		39.5-53.1	53.1-53.8	53.8-54.4	54.4-54.9	54.9-55.9	55.9-78.5
Added Cover (units and %)		**No cover offset scenario (increase in cover per pixel)**					
80,000	1.6%	4.99	4.76	5.09	5.58	5.06	5.14
160,000	3.1%	9.98	9.52	10.17	11.17	10.13	10.28
320,000	6.2%	19.97	19.05	20.34	22.34	20.25	20.56
640,000	12.5%	39.94	38.09	40.68	44.68	40.50	41.13
Added Cover (%)		**Percent increase in cover by zone (%)**					
1.6		9.5	8.9	9.4	10.2	9.1	8.9
3.1		19.0	17.8	18.8	20.4	18.3	17.7
6.2		38.1	35.6	37.6	40.9	36.6	35.5
12.5		76.2	71.2	75.2	81.8	73.1	71.0
Reduced Cover (units and %)		**Cover offset scenario (decrease in cover per pixel)**					
80,000	1.6%	-1.02	-1.03	-1.02	-1.00	-1.02	-1.02
160,000	3.1%	-2.05	-2.07	-2.04	-2.00	-2.04	-2.03
320,000	6. 2%	-4.09	-4.13	-4.08	-4.00	-4.08	-4.07
640,000	12.5%	-8.18	-8.26	-8.15	-8.01	-8.16	-8.13
Decrease Cover (%)		**Percent decrease in cover by zone (%)**					
1.6		-2.0	-1.9	-1.9	-1.8	-1.8	-1.8
3.1		-3.9	-3.9	-3.8	-3.7	-3.7	-3.5
6.2		-7.8	-7.7	-7.5	-7.3	-7.4	-7.0
12.5		-15.6	-15.5	-15.1	-14.7	-14.7	-14.0

No cover offset

Figure 7.70, Figure 7.71 and Figure 7.72 show the effect on catchment leakiness of increasing SAVI cover in each cover zone by 1.5% to 12% of the catchment cover. The additional cover has not been offset by reduction in cover elsewhere in the catchment.

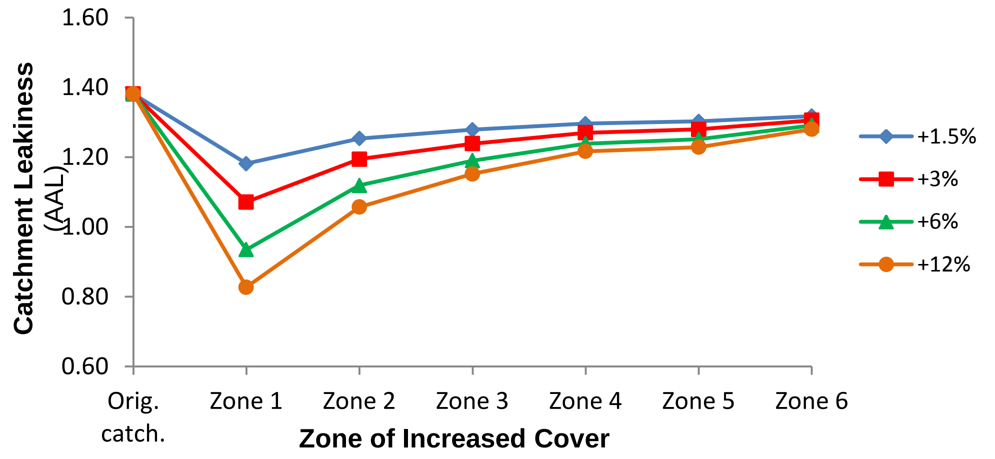

Figure 7.70 Amount of Catchment leakiness due to increase in cover in different original SAVI cover zones (net increase in catchment cover).

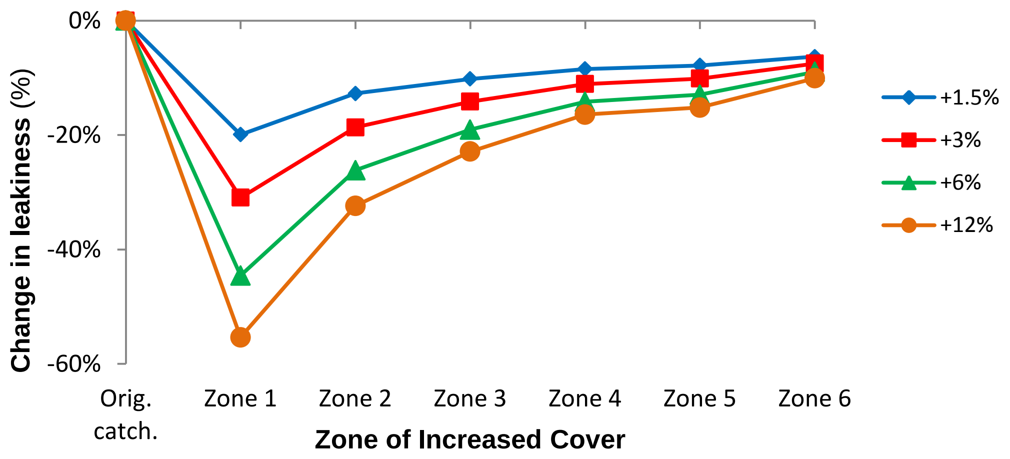

Figure 7.71 Change in Catchment Leakiness due to increase in cover in different original SAVI cover zones (net increase in catchment cover).

The preceding figures show that when cover was added to the catchment it was more effective at reducing leakiness if it was added to the cover zone with the least original cover (Zone1). The effectiveness of the added cover in reducing leakiness decreased as the zone's original level of cover increased. Figure 7.72 shows the preceding results displayed on a zonal basis rather than on a percent cover basis.

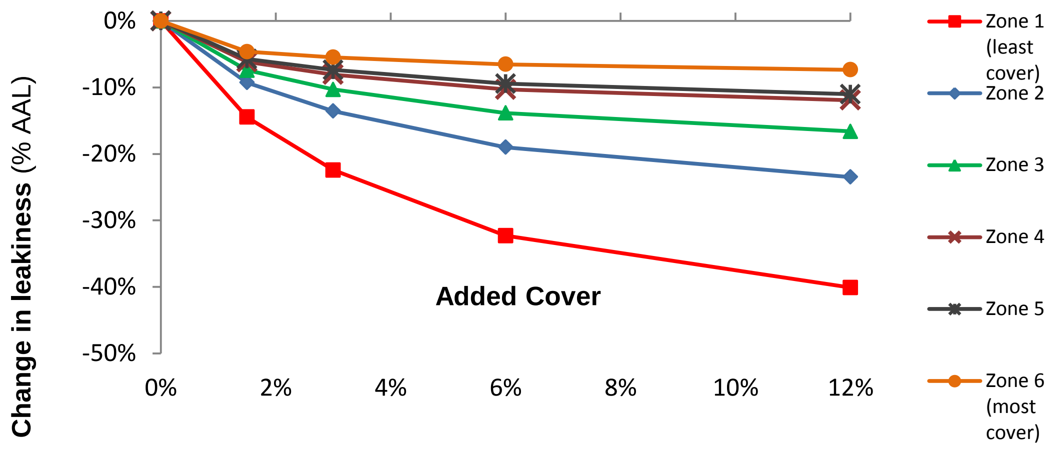

Figure 7.72 Response of catchment leakiness to addition of SAVI cover by original cover zones (net increase in catchment cover).

This shows that addition of cover to all cover zones reduces leakiness with the response being greater for zones with least original cover. The leakiness response to increased cover is negative exponential, which is consistent with the response exhibited in Figure 7.15. The rate of response of leakiness to addition of cover is greater for small additions than it is for large additions of cover, i.e. the negative slope of the response curve decreases with increase in added cover.

Cover offset

Figure 7.73 and Figure 7.74 show the effect on catchment leakiness of increasing cover in each SAVI cover zone by 1.5% to 12% of the catchment while holding the overall catchment cover constant.

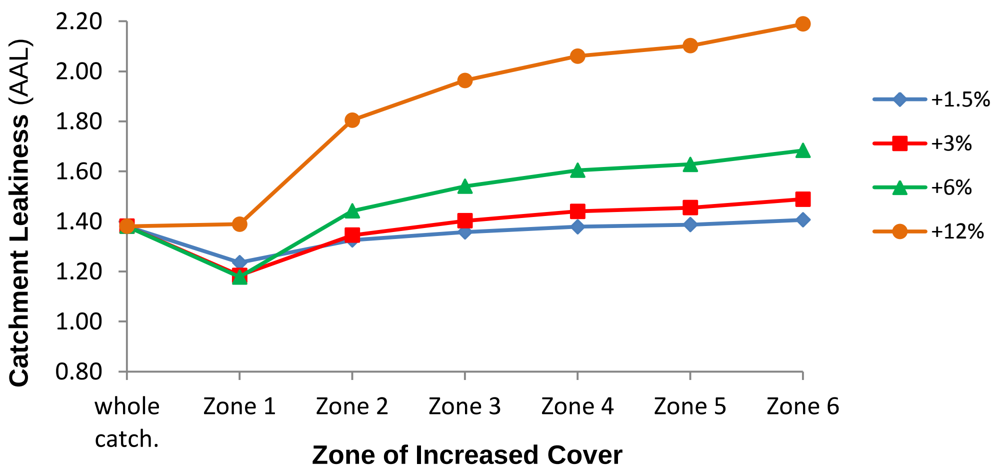

Figure 7.73 Amount of catchment leakiness due to increase in cover in each original SAVI cover zone (no net increase in cover).

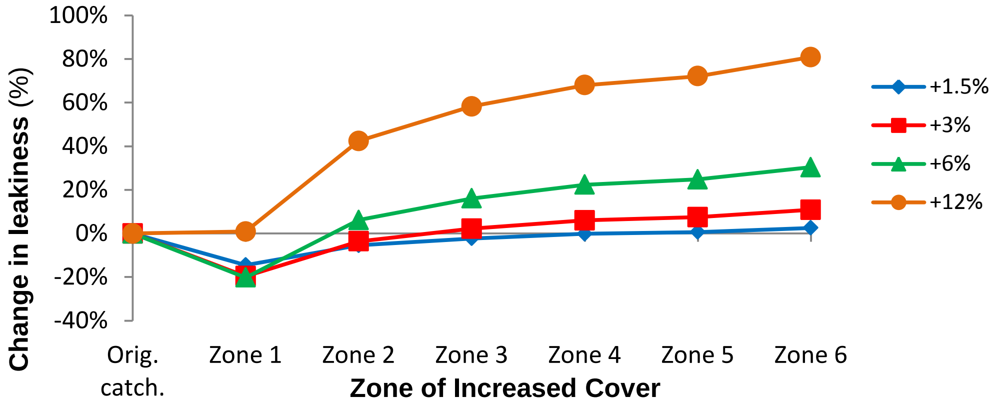

Figure 7.74 Change in Catchment leakiness due to increase in cover in different original cover zones (no net increase in catchment cover)

The results show that catchment leakiness decreases or stays the same when cover is added to the zone with the lowest original cover (Zone 1) when this additional cover is offset by reducing cover evenly across the rest of the catchment. However, when cover is added to any of the other cover zones, and the addition is offset proportionally across the remainder of the catchment, the leakiness increases except when small amounts of cover (1.5% and 3%) are added to Zone 2 (the zone with the second lowest amount of original cover) or 1.5% of catchment cover is added to Zone 3 (the zone with the third lowest amount of original cover).

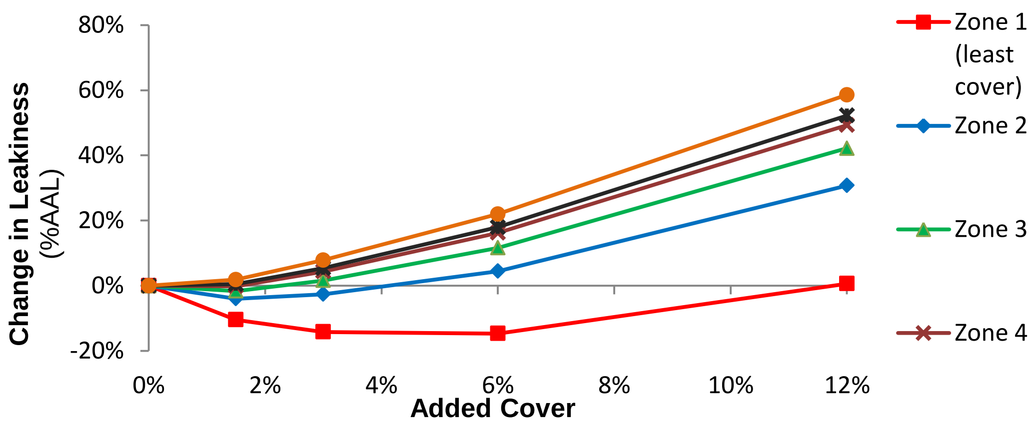

Figure 7.75 Response of catchment leakiness to addition of net cover by zone (no net increase in catchment cover).

Figure 7.75 shows the preceding results displayed on a zonal basis, rather than on a percent basis. It confirms that the biggest decrease occurs when cover is added to Zone 1 followed by lesser decreases when cover is added to the zones with more original cover (Zones 2 and 3 respectively). In all cases the cover added to one zone is offset by reduction in cover across the balance of the catchment so as to retain the same average catchment cover. Leakiness is reduced the most by the addition of 3-6% cover to Zone 1. The amount of cover reducing leakiness decreases before increasing with subsequent increase in amount of cover in the original zone.

7.3.7.1. PDrg Coverage

The cover, slope and elevation values for the PDrg cover zones are shown relative to each other in Figure 7.76 and included in Table 7-16.

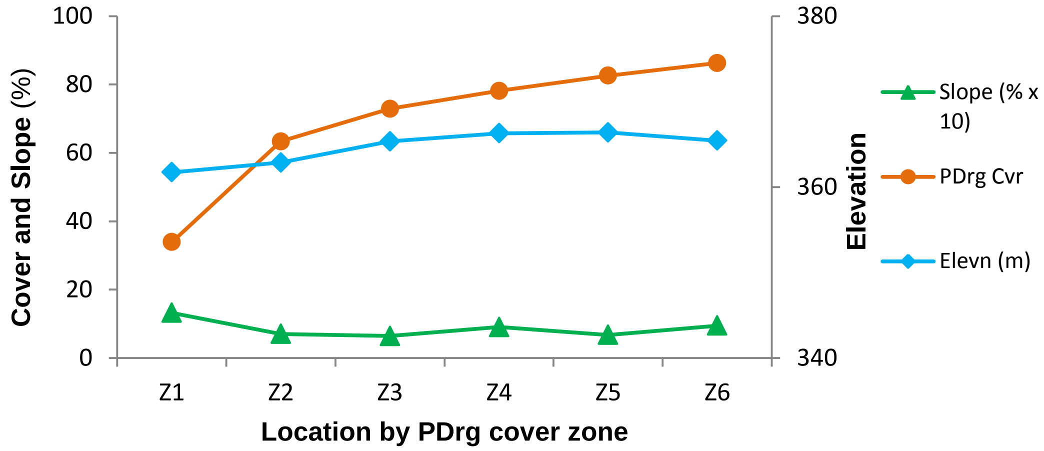

Figure 7.76 Cover, slope and elevation of the PDrg cover zones

Elevation was lowest in the lower PDrg cover zones and rose to a plateau as the PDrg cover increased from 33.8% to 86.3%.Slope remained relatively constant in all PDrg cover zones.

Four levels of change in cover (treatments) were made to each of these zones. Table 7-17 contains both the zonal characteristics as well the values used to adjust the level of cover in each zone for both the net increase and no net increase scenarios.

Table 7-17 PDrg Cover zone adjustment values (continued)

Zone	Total	Z1	Z2	Z3	Z4	Z5	Z6
Description	Whole	lowest	low medium	medium	above medium	high medium	highest
Area (ha)	5890.44	1034	994	925	1186	796	955
Elevation (m)	364.6	361.9	366.0	367.1	367.3	367.0	358.8
Slope (%)	2.5	1.4	1.0	0.9	0.9	1.1	1.3
Pixel No.	94,247	16,542	15,904	14,802	18,982	12,739	15,278
∑ zone Cover	6,489,081	560,262	1,007,598	1,079,081	1,483,112	1,051,775	1,318,136
Mean Cover %	68.9	33.9	63.4	72.9	78.1	82.6	86.3
Cover Range%	10.9 - 88.2	10.9 - 52	53.7 - 70.2	70.5 - 74.9	75.6 -80.3	81.5 -83.9	84.7 - 88.2

Added (% of catchment)	No cover offset scenario (increase in cover per pixel)					
1.5	5.88	6.12	6.57	5.12	7.64	6.37
3.0	11.76	12.24	13.15	10.25	15.28	12.74
6.0	23.53	24.48	26.30	20.51	30.56	25.48
12.0	47.07	48.96	52.60	41.02	61.12	50.96

Table 7-17 (co ntinued) PDrg Cover zone adjustment values

Zone	Total	Z1	Z2	Z3	Z4	Z5	Z6
Added cover (%)		**Percent increase in cover by zone (%)**					
1.5		17.4	9.7	9.0	6.6	9.3	7.4
3.0		34.7	19.3	18.0	13.1	18.5	14.8
6.0		69.5	38.6	36.1	26.3	37.0	29.5
12.0		139.0	77.3	72.2	52.5	74.0	59.1
Decrease (% of catchment)		**Cover offset scenario (decrease in cover per pixel)**					
1.5		-1.25	-1.24	-1.22	-1.29	-1.19	-1.23
3.0		-2.50	-2.48	-2.45	-2.58	-2.38	-2.46
6.0		-5.01	-4.97	-4.90	-5.17	-4.77	-4.93
12.0		-10.02	-9.93	-9.80	-10.34	-9.55	-9.86
Decreased cover (%)		**Percent decrease in cover by zone (%)**					
1.5		-1.6	-1.8	-1.8	-1.9	-1.8	-1.9
3.0		-3.3	-3.6	-3.6	-3.9	-3.6	-3.8
6.0		-6.6	-7.1	-7.2	-7.8	-7.2	-7.5
12.0		-13.1	-14.2	-14.4	-15.6	-14.3	-15.1

No Cover Offset

Figure 7.77 and Figure 7.78show the effect on catchment leakiness of increasing PDrg cover in each cover zone by 1.5% to 12% of the catchment cover. The additional cover has not been offset by any reduction in cover elsewhere in the catchment. This is a different pattern of response from the SAVI response (Figure 7.70 and Figure 7.71).

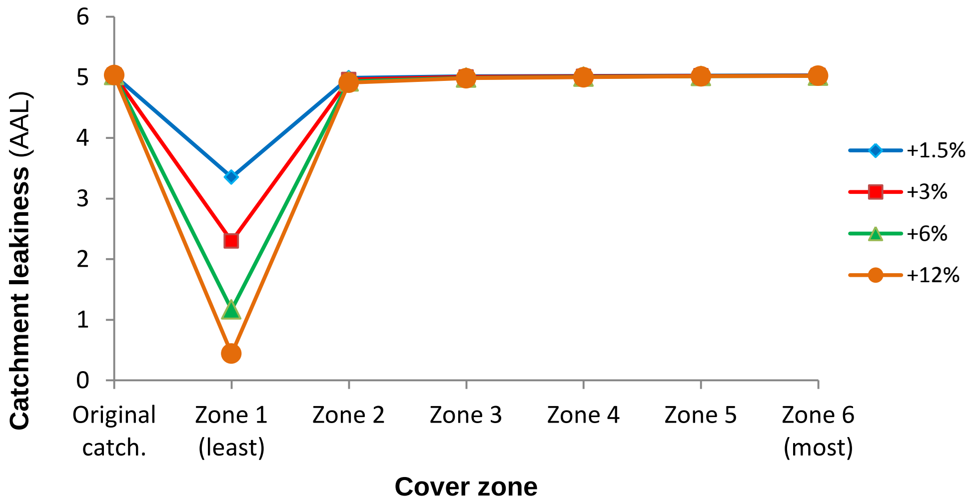

Figure 7.77 Amount of catchment leakiness due to increase in PDrg cover in different original PDrg cover zones (net increase in catchment cover).

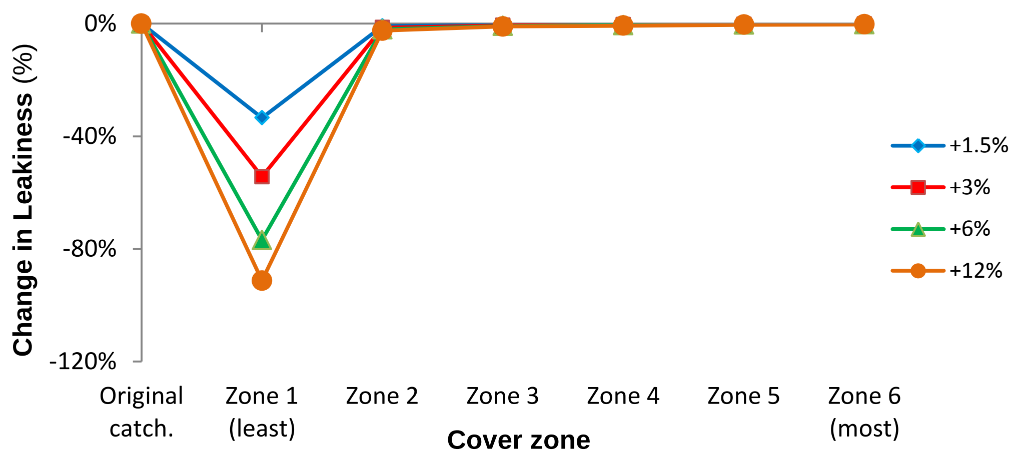

Figure 7.78 Change in catchment leakiness due to change in PDrg cover of original PDrg cover zones (net increase in catchment cover).

The preceding figures show that when PDrg cover was added to the catchment it was effective at reducing leakiness only when added to the zone with the least original cover (Zone 1) and its addition to all other zones did not decrease catchment leakiness. Addition of SAVI cover also decreased leakiness the most in the zone with the least original cover but it also decreased leakiness in the other zones, to a lesser extent.

Figure 7.79 shows the preceding results displayed on a zonal basis rather than on a percent cover basis. This shows that only zone 1 responded to added cover and this was in the expected negative curvilinear manner. Unit response was greatest for small amounts of added cover.

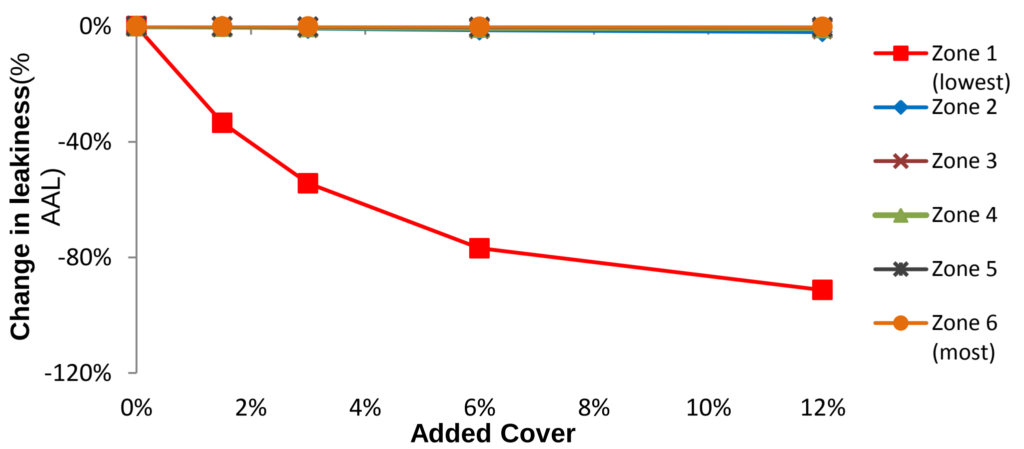

Figure 7.79 Response of catchment leakiness to addition of PDrg cover of original PDrg cover zone (net increase in catchment cover).

Cover Offset

Figure 7.80 and Figure 7.81show the effect on leakiness of increasing cover in each PDrg cover zone by 1.5% to 12% of the catchment while holding the overall catchment cover constant.

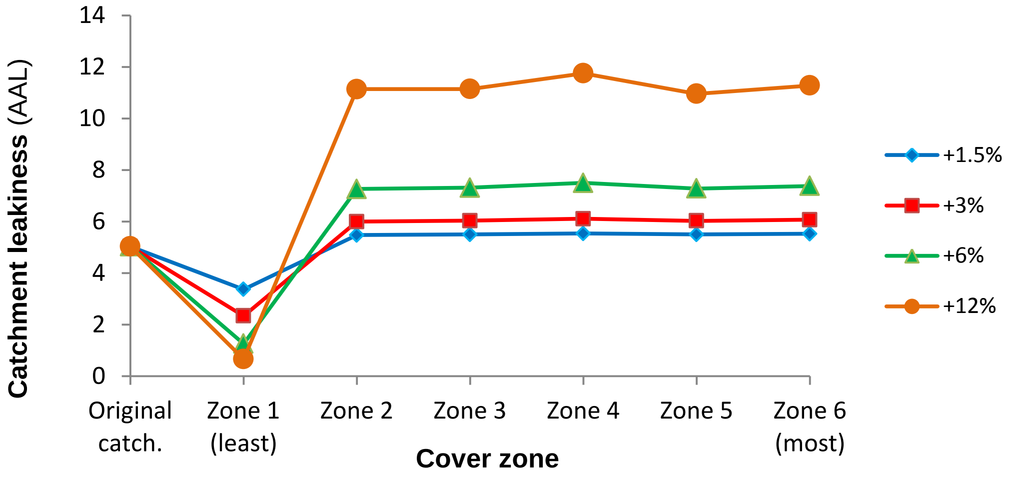

Figure 7.80 Amount of catchment leakiness due to change of PDrg cover by original PDrg cover zone (no net increase in catchment cover).

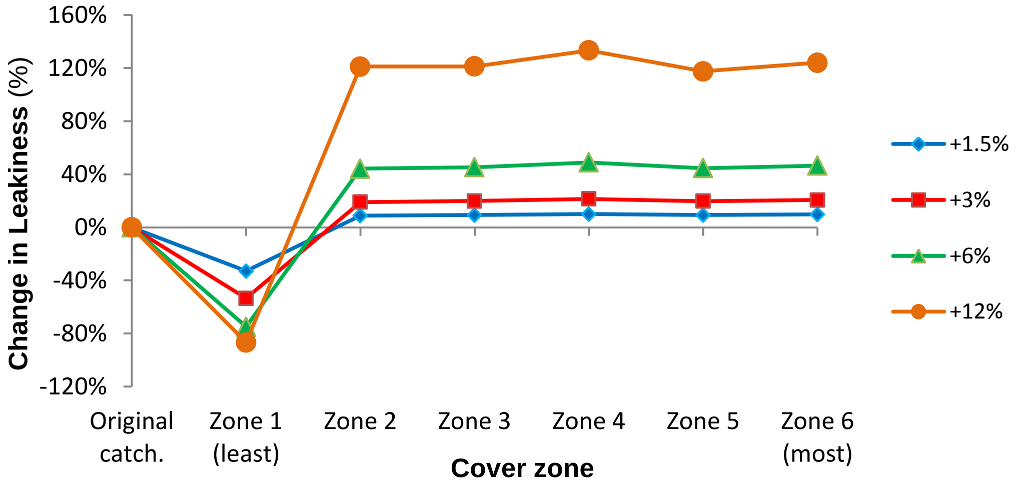

Figure 7.81 Change in catchment leakiness due to change of PDrg cover by original PDrg cover zone (no net increase in catchment cover).

These results show that leakiness decreases initially when cover is added to the Zone 1 (lowest original cover) when this additional cover is offset by reducing cover evenly across the rest of the catchment. However, when cover is added to any of the other cover zones, and the addition is offset by decreasing cover over the rest of the catchment, the leakiness increases to a plateau and remains constant across all other zones. The level to which the leakiness increases depends on the amount of PDrg cover added.

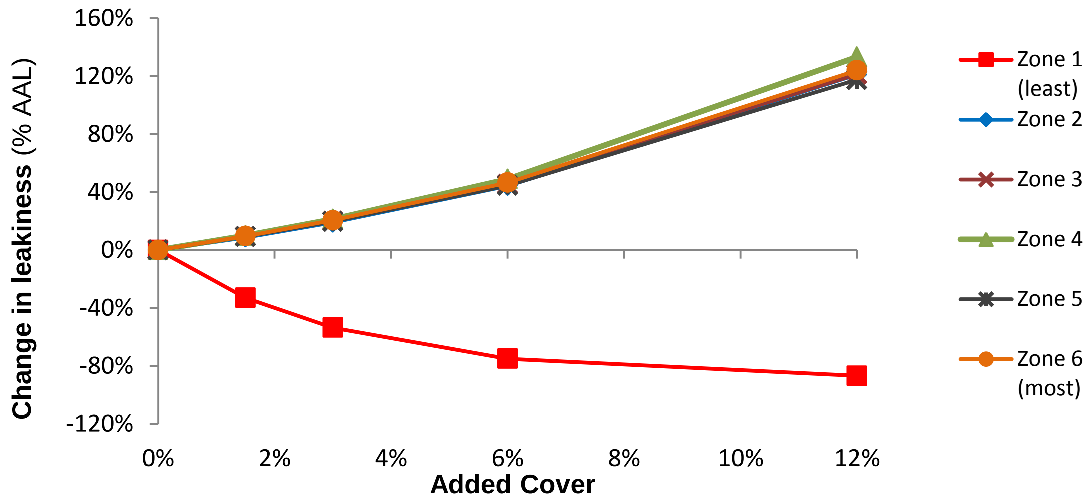

Figure 7.82 Response of catchment leakiness to addition of PDrg cover by original PDrg cover zone (net increase in catchment cover).

Figure 7.82 shows the preceding results displayed on a zonal basis, rather than on a percent basis. This confirms that the biggest decrease occurs when cover is added to Zone 1. Addition of cover to all other zones on a net offset basis causes the same amount of increase in leakiness. A maximum reduction in leakiness is achieved with the addition of 12% cover to Zone 1.

7.4. Discussion

This section discusses and explains the results of the effect of changing the amount of cover on different areas of the catchment on its leakiness. It does not cover changing the scale of the cover patches. To investigate this, the amount of cover was changed in a systematic way in each of the features and the effect of this on catchment leakiness was calculated using the LC. The performance of the LC was tested at the beginning of the analysis and the results (Table 7-3and Figure 7.15) showed that it was working in accordance with the published criteria. The exponential negative response of leakiness to increased catchment cover is consistent with the results reported by Ludwig, J. and G. N. Bastin *et al.* (2007). The use of standardised settings in the LC may jeopardise the leakiness calculations for some zones and favour the leakiness calculations for other areas but it was necessary so as to generate comparable results across all trials.

The results of varying the coverage within each feature are discussed, followed by a discussion of the overall pattern of leakiness response to cover location.

7.4.1. Drainage Line Distance (DLD) Zones

Both the No Cover Offset and the Cover Offset scenarios show that cover was most effective at reducing leakiness when it was added to areas that were farthest from drainage lines (Section 7.3.2). Decrease in leakiness was exponentially negative in response to increase in cover and small increments of cover had more effect per unit of cover than larger increments. The pattern of response was the same for both SAVI and PDrg types of cover.

These results appear to contradict both the conventional wisdom about priority for revegetation along watercourses as well as published research results. It is possible that the conventional wisdom about the importance of riparian vegetation in protecting water quality by filtration of cross flow drainage, stabilising stream banks against erosion and providing wildlife habitat (Munro and Lindenmayer 2011) are different issues from the issue of the best place to increase cover to reduce resource loss. However, CSIRO research in the dry tropics of North Queensland (Bartley and Corfield *et al.* 2010; Bartley and Toth *et al.* 2006; Bartley and Wilkinson *et al.* 2010) found that fine scale cover at the bottom of hillslope catchments reduced sediment transport more than if the cover was of a coarse scale. These results were based on only one catchment but the catchment was sufficiently large (5,889 ha) to include many small catchment and to constitute a representative sample of catchments in the Burdekin River drainage basin.

Figure 7.16 shows the elevation, slope and SAVI and PDrg cover for each DLD zone in the catchment. Both measures of cover are fairly constant for all zones. This precludes the enhanced response of catchment leakiness resulting from adding cover to the farthest DLD zones being due to lower cover (and by analogy larger exposed areas) in the more distant zones. The elevation increases consistently from the zone closest to the drainage line (DLD Zone 1) to the zone farthest from the drainage line (DLD Zone 6) and it is used in the LC calculation to determine the hydraulic head in the pixel-to-pixel flow distribution equation. This may contribute to the increased leakiness from the farthest zone(s). Slope also increases consistently from the closest zone to the farthest zone from the drainage lines but it is not used in the LIC calculation.

This result is also not consistent with the mode of leakiness reduction demonstrated by Ludwig and Eager *et al.* (2006) in the course of their development of the Cover based Directional Leakiness Index (CDLI). The CDLI model demonstrated that increasing the cover values of cells in the flow path closer to the bottom of the flow column (simulated closer to drainage line) reduced leakiness more than a like increase in cover to cells farther away from the bottom of the flow column. The CDLI model clearly demonstrated that

> "*columns with high cover pixels near the outflow (were) much less 'leaky' than those with high cover pixels near the top of the column*" .

The CDLI uses the loss term $l_{i,j} = 1 - C_{i,j}/100$, which defines a negative linear relationship. The LC uses the loss term $l_{i,j} = e^{-b \times c_{i,j}}$ where *b= - 0.065* which defines a negative exponential relationship. The test results for the LIC in Table 7-3 and Figure 7.15 confirm that the LC generates leakiness results that have a negative exponential relationship with cover.

These results lead to the conclusion, that at least for this catchment, added cover reduces the leakiness most, when added to areas farthest from the drainage lines This maybe because (i) the LC generates a different network of flow channels from ArcHydro and that the cells that are distant from the ArcHydro channels are closer to the LC flow channels, and/or (ii) the higher slope of the zones farther from the drainage lines, increases the flow of resources due to the higher hydraulic head and the downslope cover is not sufficient in quantity or fineness to retain the increased flow of resources.

The scenario in which the addition of cover to one zone was offset by an equivalent loss of cover spread proportionally across all other zones (Section7.3.2) showed that catchment leakiness increased for all zones compared to the original leakiness, except if the cover was added to only the farthest zone from the drainage lines (the most effective zone at reducing leakiness). As Figure 7.20 and Figure 7.21 show, the overall effect was an increase in leakiness compared to the no-offset scenario Figure 7.17 and Figure 7.18. This finding implies that adding cover in one zone to compensate for the loss of cover in another zone may or may not be an effective strategy in reducing catchment leakiness. The outcome depends on the relative efficacy of the zones where the cover is added or lost, at reducing leakiness. In the absence of additional data this may need to be tested on a catchment-by-catchment basis.

7.4.2. Elevation Zones

The No Cover Offset and Cover Offset scenarios for both SAVI and PDrg cover showed a similar pattern of change in leakiness with the addition of cover by elevation zone to the DLD zone results. Addition of cover was most effective at reducing leakiness when it was added to the highest elevation zones (Section 7.3.3). Decline in leakiness was exponentially negative with small additions of cover reducing leakiness more than larger additions per unit of cover (Figure 7.32, Figure 7.35, Figure 7.38 and Figure 7.41). These results are consistent with the DLD zone results because the higher elevation zones are further from the defined drainage lines (Arc Hydro) than the lower elevation zones (Figure 7.5). However, they continue to be inconsistent with the CSIRO group’s results as described in the previous subsection.

Figure 7.29 shows that elevation, slope and SAVI and PDrg cover follow a similar pattern for Elevation zones to that for DLD zones (Figure 7.16). Both elevation and slope are more accentuated (start lower, end higher) for elevation zones than for DLD zones. Both types of cover are fairly constant between all zones except that PDrg cover increases in the higher elevation zones.

The absence of increased response to SAVI cover in higher elevation zones precludes lack of cover being the cause of greater catchment leakiness response in these zones. Elevation increased consistently from the lowest zone to the highest zone and is used in the LC calculation to determine the hydraulic head in the pixel-to-pixel flow distribution equation. This may contribute to the enhanced leakiness response from the highest elevation zone(s). Slope also increased consistently from the lowest zone to the highest zone but is not used in the LC calculation.

Figure 7.30, Figure 7.31, Figure 7.36 and Figure 7.37show that adding cover (both SAVI and PDrg) to elevation Zones 1-4 (lower elevation) reduced leakiness by approximately the same amount for each zone. Adding cover to Zone 5 reduced leakiness more with the largest reduction occurring when cover was added to Zone 6 (highest elevation).

As with the DLD zones, offsetting the addition of cover for all zones except Zone 6, increased catchment leakiness while adding cover to Zone 6 reduced leakiness. Adding cover to Zone 6 reduced leakiness. This was because the reduction in leakiness in Zone 6 was large enough to offset the increase in leakiness from the other zones over which cover had been reduced. This suggests that higher elevation zones may be contributing disproportionally more to leakiness than lower elevation zones and that adding cover to them (e.g. revegetation) may be more effective at reducing resource loss per unit of added cover than revegetating lower elevation zones. Testing whether this pattern holds true in other catchments is necessary before any generally applicable guidelines can be agreed upon.

7.4.3. Slope Zones

Addition of cover to slope zones produced a different pattern of results from DLD and elevation zone results. Most reduction in leakiness occurred when cover was added to the lowest sloping zones (Zone 1 in Figure 7.43, Figure 7.44, Figure 7.46 and Figure 7.47). Figure 7.42 shows the elevation, slope and SAVI cover for each slope zone. Cover remains constant (within 1 unit) for all slope zones and its small variation is unlikely to be the reason for the leakiness response of Zone 1 to added cover. The elevation increased consistently from the lowest sloping zone to the highest sloping zone and is used in the LC calculation as explained previously. Slope also increased consistently from the lowest sloping zone to Zone 5 and then increased rapidly for Zone 6 but is not used in the LC calculation.

These results are consistent with the CSIRO findings (Bartley and Toth *et al.* 2006) and Boer and Puigdefabregas (2005) in which cover closer to drainage lines reduces leakiness more than the addition further from drainage lines because the low slope areas tend to be closer to drainage lines. They are also consistent with the CDLI model results (Ludwig and Eager *et al.* 2006). As found previously, incremental additional cover caused an exponentially negative response in catchment leakiness (Figure 7.45 and Figure 7.48).

These results are different from the DLD zone and elevation zone results in that the lower DLD zones (zones closer to the drainage lines) and the lower elevation zones have lower slopes. Sections 7.3.2 and 7.3.3 showed that the addition of cover to areas close to drainage lines and at lower elevations in these zones was the least effective area for reducing leakiness whilst the addition of cover to the lowest slope zones was the most effective area in reducing leakiness.

There are two reasons why added cover on lower sloping zones reduced leakiness more than addition of cover to higher sloping zones. Firstly, increased percent cover implies the cover has a finer spatial distribution (although not absolutely necessary). Boer and Puigdefabregas (2005) and Bartley and Toth *et al.* (2006) showed this was more effective at reducing sediment loss. Secondly, the loss term $l_{i,j} = e^{-b \times c_{i,j}}$ is acting on a larger input value coming from upslope drainage, which it reduces, and there is insufficient drainage path length in which to accumulate more sediment before discharge to the watercourse.

7.4.4. Aspect Zones

Addition of cover to different aspect zones showed a nearly equal reduction in leakiness for all zones (Figure 7.50, Figure 7.51, Figure 7.53 and Figure 7.54). Addition of small amounts of cover (1.5% of catchment cover) to each aspect zone, without offset, reduced leakiness by between 3-4% (Figure 7.51). As more cover was added (3% to 12% of catchment cover) addition of this added cover to Zones 1, 2 and 3 (eastern aspect zones) it reduced overall catchment leakiness more than its addition to Zones 4, 5 and 6 (western aspect zones). A similar response occurred when the added cover was offset by a reduction across the rest of the catchment. The offset caused an increase in leakiness rather than a reduction in leakiness (Figure 7.53 and Figure 7.54). As before, the unit response of leakiness to increase in cover was an exponentially negative reduction (Figure 7.52 and Figure 7.55).

Figure 7.49 shows that elevation, slope and cover were close to constant across all aspect zones. There was no variation in these values that might explain the progressively less effect that higher amounts of added cover (6 - 12%) had on leakiness as shown in Figure 7.50 and Figure 7.51. The absence of any clearly evident feature response is consistent with physical observations of the catchment in which there was no visual difference in the amount of cover on different aspects. However it suggests that the spatial distribution of cover was different on different aspects.

7.4.5. Topographic Zones

Addition of cover to all 6 land forms: Pit, Channel, Plain, Pass, Ridge and Peak (corresponding to Topo. Zones 1- 6) produced unique responses in catchment leakiness (Figure 7.57, Figure 7.58 Figure 7.60 and Figure 7.61). The pattern of response was similar for both SAVI and PDrg cover and the offset of added cover caused similar changes in leakiness to previous cover offsets.

Section 7.3.6.1 explains the different unit of measurement used in the analysis for this zone compared to other zones. Use of a normalised AAL ((AAL/cell)×10^6) allowed a similar pattern of comparison of the effect of added cover on leakiness for zones of markedly different cell numbers to each other. Addition of cover, reduced leakiness the most when added to Peaks (Figure 7.11) followed in declining order by Ridges, Passes, Plains, Channels and Pits for both SAVI and PDrg cover (Figure 7.57, Figure 7.58, Figure 7.63 and Figure 7.64). The elevation and slope of the different landforms (Figure 7.56) vary distinctly yet show no apparent correlation with the leakiness patterns as shown in Figure 7.57, Figure 7.58, Figure 7.60, Figure 7.61, Figure 7.63, Figure 7.64, Figure 7.66 and Figure 7.67.

This suggests that slope and elevation of landforms may not be the primary determinants of catchment leakiness. This would be unusual because of the widely accepted evidence that amount of cover and differences in elevation are the primary determinants of leakiness (Karfs and Abbott *et al.* 2009; Ludwig and Eager *et al.* 2002; O'Reagain and Brodie *et al.* 2005). It leaves the variables of patch size, Cross Scale Interaction (CSI) and Soil Surface Conditions (SSC) as the primary variables affecting the loss of resources in these types of catchments (North Queensland dry tropics). Ludwig and Eager *et al.* (2002) developed the “weighted mean patch size” index to describe patch structure. Wu and Sui (2001) used the lacunarity index to compare aggregation of landscape patch patterns. The circumstances under which these 5 variables contribute, and the extent of their contribution, remains to be resolved.

As before, unit reduction in leakiness was greater for small amounts of cover than for larger amounts of cover, for all zones that showed a response to added cover (all zones except Pits) with the largest unit response occurring for Peak landforms.

When the added cover was offset (Section 7.3.6) two differences in the pattern of leakiness response occurred. Firstly, offsetting of cover added to pit landforms reduced leakiness compared to offsetting cover added to channel landforms (Figure 7.60, Figure 7.61, Figure 7.66 and Figure 7.67). Cover addition to Pits with offset had nearly the same effect on leakiness as addition of cover to Plains with offset. This is likely to be due to the increase in leakiness caused by cover offset elsewhere in the catchment being greater for Pits than for Channels. The pattern was the same for both SAVI and PDrg cover. Secondly, additions of PDrg cover to Ridges that was offset reduced leakiness more than for Peaks (Figure 7.66, Figure 7.67). This did not occur with SAVI cover. The reason it occurred with PDrg cover and not SAVI cover is revealed by a close examination of Figure 7.66, Figure 7.67 (for PDrg) and Figure 7.57, Figure 7.58 (for SAVI). The PDrg figures show a faster rate of decline in Leakiness from Pass to Ridge than Ridge to Peak while the SAVI leakiness response occurs at the same rate of decline from Pass to Ridge as Ridge to Peak. The change in relative rate of response of leakiness, to addition of offset cover, caused the offset of added cover to Ridges to reduce leakiness more than if it had been added to Peaks.

7.4.6. Cover Zones

Addition of cover to Cover zones showed that the zone with the least initial (native) cover produced the most reduction in leakiness. This applied to both SAVI and PDrg cover types (Figure 7.70 to Figure 7.80).

Addition of SAVI cover, without offset, yielded the most reduction in leakiness for the zone with the lowest initial cover (Zone 1). The decrease in leakiness became progressively less (i.e. it increased) as the amount of initial cover on the zone increased (Figures 7-70, 71). This is consistent with the findings of Ludwig, J. and G. N. Bastin *et al.* (2007) in which leakiness decreases exponentially with added cover.

Addition of PDrg cover, without offset, produced a different result. The lowest PDrg initial cover zone (Zone 1) reduced catchment leakiness when PDrg cover was added to it (Figure 7.77 and Figure 7.78) and the unit response was exponentially negative (Figure 7.79). In this respect added PDrg cover caused a similar response to added SAVI cover. The difference from SAVI occurred when PDrg cover was added to each of the other cover zones (2-6) where it did not reduce leakiness (Figure 7.76 and Figure 7.77). The possibility that this was an erroneous result was carefully investigated and ultimately rejected because (i) these results came from the same geoprocessing model (See Sections 7.2.2 and 7.2.3) used to generate the other analyses, and (ii) the processing steps were redone individually and checked after each operation and they yielded the same results as the automated geoprocessing procedure.

Both SAVI and PDrg cover zones had essentially similar elevations and slopes but the pattern of cover differed. The SAVI cover zone had a similar, although slightly rising level of cover on each zone. On the other hand the PDrg cover zones had an exponentially increasing level of cover. The lowest PDrg cover zone had an initial cover of 33.89% and the other cover zones had initial covers above 63% (Table 7-17). These results indicate that increasing PDrg type cover above 63% does not reduce leakiness any further and that the catchment with an average of 68.65% PDrg cover (Table 7-17) was at its lowest leakiness. This suggests that the use of PDrg cover for measuring leakiness may have a leakiness saturation value equal to or less than 63.35%. This does not mean that such a catchment cannot conserve more resources but rather that the use of the PDrg Index as a measure of cover in well covered savannah catchments records high cover levels at spatial locations in the catchment, such that addition of further cover at these locations does not reduce leakiness any further. These results are based on only one experimental study catchment and need to be tested on other catchments. They also suggest that, despite the merits of the PDrg Index as a measure of cover, it might have limitations for use as a measure of cover for resource leakiness analysis using the LC in well covered (>63%) savannah catchments.

When the cover added to each zone was offset elsewhere in the catchment the leakiness shifted in the customary way for both SAVI and PDrg cover. The zone with the most leakiness response to the added cover, Zone 1, declined in leakiness and the rest of the zones increased in leakiness (Figure 7.73, Figure 7.74, Figure 7.80 and Figure 7.81). This is because addition of cover to only the least covered zone produced enough decrease in leakiness to offset the increase in leakiness from the rest of the catchment. In the case of PDrg cover offset, the response was similar for cover Zone 1, but the leakiness increased for all other zones with the largest amount of added cover causing the largest increase (Figure 7.80 and Figure 7.81).

Added SAVI cover (both offset and no-offset scenarios) produced an exponentially negative unit response in leakiness indicating the most response per unit of cover to the lowest amount of added cover (Figure 7.72 and Figure 7.75). Added PDrg cover also produced an exponentially negative response of leakiness for Zone 1 and no response for the other zones (Figure 7.79). This may be due to leakiness cover saturation in these zones. When added PDrg cover was offset it produced a characteristic negative exponential response for Zone 1 (Figure 7.82) but very similar positive exponential responses for the other 4 zones.

7.4.7. Summary

The preceding results establish a pattern of responses as summarised in Table 7-18. This shows which zones are the most effective in reducing leakiness by the addition of cover. The zones are the same for both SAVI and PDrg cover types, both with and without offset, except for Ridge and Peak zones where Ridges are more effective in offsetting PDrg cover loss while Peaks are more effective at offsetting SAVI cover loss.

Table 7-18 Summary of zones in which cover is most effective in reducing catchment leakiness

Feature	No-cover Offset zone scenario		Cover Offset zone scenario	
	SAVI	PDrg	SAVI	PDrg
Drainage Line Distance	Most distant	Most distant	Most distant	Most distant
Elevation	Highest	Highest	Highest	Highest
Slope	Lowest	Lowest	Lowest	Lowest
Aspect	East	East	East	East
Topo feature	Peak	Peak	Peak	Ridge
Cover	Least	Least	Least	Least

Table 7-19 provides an overall summary of the response of catchment leakiness to added cover by different zones using three parameters:

(a) zone in which leakiness is reduced the most,

(b) response of intermediate zones, and
(c) response of leakiness to the addition of each unit of cover.

Collectively, these results show that:

i. The zones, which exhibit the most sensitivity to conserving catchment resources (the ones that reduce the leakiness the most), depend on how the zones are established.
ii. Response of intermediate zones varies in an exponentially negative manner between the most responsive leakiness zone and the original catchment leakiness condition, and,
i. Unit response of leakiness to cover is exponentially negative with small units of cover giving greater unit responses of leakiness for all types of zones.

Table 7_19 Overall Summary of Response of Leakiness to cover added by feature zones

Feature	Cover Type	Scenario	Response parameters					
			Most leakiness reduction		Intermediate leakiness values		Leakiness unit cover response	
			Number	Description				
Drainage Line Distance	SAVI	No offset	Zone 6	Most distant	Negative exponential Above zero	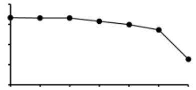	Negative exponential below zero	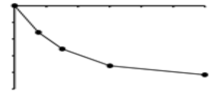
		Offset	Zone 6	Most distant	Curved, above zero	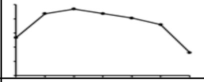	Positive exponential> above and below zero	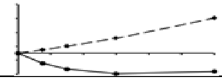
	PDrg	No offset	Zone 6	Most distant	Negative exponential, above zero	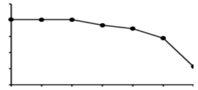	Negative exponential below zero	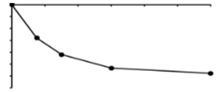
		Offset	Zone 6	Most distant	Curved, above zero	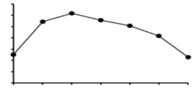	Positive exponential> above and below zero	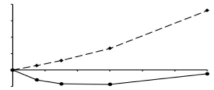
Elevation	SAVI	No offset	Zone 6	Highest	Initial decrease>negative exponential	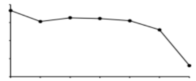	Negative exponential below zero	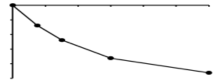
		Offset	Zone 6	Highest	Curved, above zero	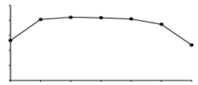	Positive exponential> above and below zero	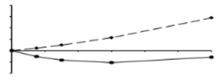
	PDrg	No Offset	Zone 6	Highest	Initial decrease>negative exponential	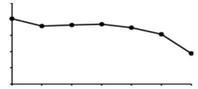	Negative exponential below zero	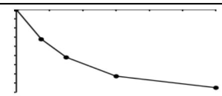
		Offset	Zone 6	Highest	Curved, above zero	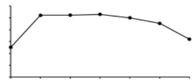	Positive exponential> above and below zero	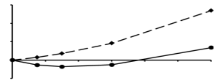
Slope	SAVI	No offset	Zone 1	Lowest	Initial decrease>positive exponential	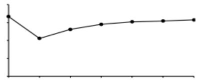	Negative exponential below zero	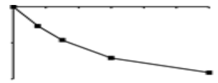
		Offset	Zone 1	Lowest	Static>positive exponential	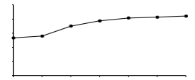	Positive exponential> above and below zero	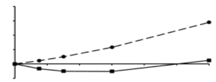

Table 7-19 (continued) Overall Summary of Response of Leakiness to cover added by feature zones

Feature	Cover Type	Scenario	Response parameters			
			Most leakiness reduction		Intermediate leakiness values	Leakiness unit cover response
			Number	Description		
Aspect	SAVI	No offset	No difference	Same response	Initial decrease, above zero>gradual increase 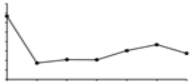	Negative exponential below zero>decreasing unit response 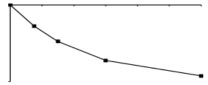
		Offset	No difference	Same response	Initial increase, above zero>gradual increase 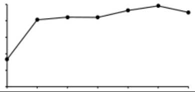	Positive exponential, above zero 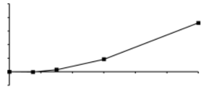
Topographic	SAVI	No offset	Peak	Crest of rise	No initial response>negative exponential 	Initial decrease >below zero>linear increase 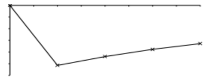
		Offset	Peak	Crest of rise	Increases to a peak>declines to below zero 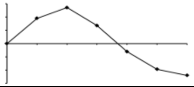	Initial decrease >below zero>linear increase 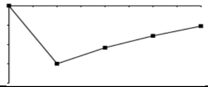
	PDrg	No Offset	Peak	Crest of rise	Negative exponential below zero 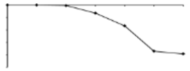	Initial decrease >below zero>linear increase 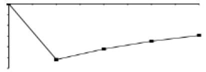
		Offset	Ridge	Top of ridgeline	Increases to a peak>declines to below zero>then increases 	Initial decrease >below zero>linear increase 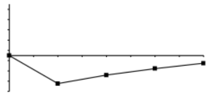
Cover	SAVI	No offset	Lowest	Least original cover	Initial decrease >above zero> positive exponential 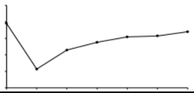	Negative exponential below zero>decreasing unit response 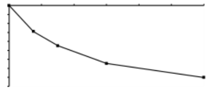
		Offset	Lowest	Least original cover	Static>Positive exponential 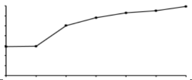	Positive exponential> above and below zero 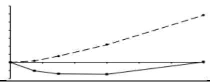
	PDrg	No Offset	Lowest	Least original cover	Initial decrease, below zero>return to original values 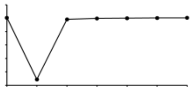	Negative exponential below zero>decreasing unit response 
		Offset	Lowest	Least original cover	Initial decrease, below zero>return to original values 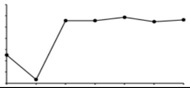	Positive exponential> above and below zero 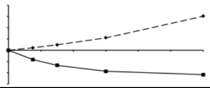

7.5 Conclusion

The results yield numerically consistent responses of change in leakiness to addition of vegetation cover however a number of patterns of response are different from intuitive expectations. It was expected that addition of cover to zones of pre-existing least cover and of lower slopes would reduce leakiness more than adding cover to zones already high in cover and having greater slopes. However, the zones with the lowest slopes also had the lowest elevations and these showed the lowest leakiness response to the addition of cover. Likewise the areas closest to the major drainage channels were at a lower elevation and had a lower slope than areas further from the drainage channels and they showed less reduction in leakiness than areas further from the drainage channels which had a higher elevation and a higher slope. Thus the response of leakiness to the position of cover in relation to drainage channels is consistent with its response to elevation but not to slope.

Adding cover to eastern facing areas reduced leakiness a little more than adding it to other aspects although the trend was not strong. Eastern facing areas would be comprised of both steep and gentle sloping areas at high and low elevations. Adding cover to peaks and ridges reduced leakiness more than adding them to other landforms. This response is consistent with the response to elevation because peaks and ridges were at higher elevations. However, it is inconsistent with the response to slope because these areas had higher slopes while lower adding cover to lower slopes reduced leakiness more than adding it to higher slopes.

The conundrum created by these finding will take more investigation to unravel. An indication of the nature of the solution may exist in the findings by Ludwig and Bartley *et al.* (2007). They found that large patches of low ground cover areas further from drainage lines contributed proportionally greater amounts of erosion sediment than similar amounts of bare areas arranged in smaller patches closer to drainage lines. This suggests that a more detailed analysis of the location of ground cover patches by size within a catchment is necessary to explain the response of leakiness to added cover. Such an approach could reinforce the need to revise the cover input variable to the Leakiness Calculator to get more responsive results

CHAPTER 8

CONCLUSION

8.1. Introduction

This section addresses accomplishment of the research objectives by bringing together the different findings about the behaviour of vegetation cover indices at different observation resolutions, about leakiness derived from the cover indices at different resolutions, about the effect of resolution on image structure and about the relationship between image variance and leakiness. Finally, the effect on leakiness of adding additional cover at different positions in a catchment is presented.

The main findings from this research are:

- The need for a new metric for comparing the leakiness of multi-scale catchments of different sizes (Research Objective B),
- That cover index values vary by resolution for spatially and temporally coincident images (Research Objective A1),
- That high resolution images cannot be upscaled to yield leakiness comparable with low resolution images (Research Objective A2),
- Both resolution and variance based scalograms can accurately predict the leakiness of upscaled images (Research Objective A2 and B),
- There are image specific relationships between the type of vegetation cover, its scale and its structure (variance) that affect leakiness in a predictable manner (Research Objective A3), and
- The position of added cover in a catchment produces unexpected patterns of change in leakiness (Research Objective C).

8.2. Findings

8.2.1. Adjusted Average Leakiness Metric

A new metric, the *Adjusted Average Leakiness (AAL)* was developed in this study for use in conjunction with output from the CSIRO Leakiness Calculator. It was used in place of the conventional Leakiness Index (LI) derived from the Calculated Leakiness (Lcalc).Its advantages are that it is not sensitive to cell number or cell size.

This allows easier comparison of leakiness from multi-scale imagery and for catchments of different cell numbers and sizes. The following findings are expressed in terms of both Lcalc and AAL.

8.2.2. Cover and Leakiness

Different vegetation cover indices from the same satellite image vary widely in value. The magnitude of the cover values has a primary influence on leakiness values because of the inverse relationship between cover and leakiness The same indices of the same scene at different resolutions also vary widely in value.

Overall, band ratio cover values showed the largest variance, while the Perpendicular Distance for red over green ($PD_{rg)}$ index values had the smallest variance with resolution. PD_{rg} values were also the most consistently close to the widely used Ground Cover Index (GCI) values.

Lcalc decreased with decrease in resolution because of its dependence on the number of pixels. It was more sensitive to low levels of cover at high resolution than to high levels of cover at low resolution. This means that better results for Lcalc can be obtained by using high resolution imagery in areas of low vegetative cover than would be obtained by using lower resolution imagery. Leakiness calculated from PD_{rg} indices produced more statistically stable Lcalc values than leakiness from the other cover indices.

AAL increased with decrease in resolution from 10 to 25 m and then either increased or stayed the same with further decrease in resolution from 25 to 250m except when calculated from PD_{rg} and PD_{rn} indices. For these two PD indices it decreased with decrease in resolution beyond 25m. AAL was also more sensitive to low levels of cover at high resolution than to low levels of cover at low resolution.

There was a high degree of correlation between leakiness calculated from vegetation cover indices with similar formulae. Leakiness from PD_{rg} cover did not correlate with any other type of cover index except the Perpendicular Distance for red over SWIR (PD_{rs}) cover. This indicates the independence of PD_{rg} from non-PDI cover indices. PD_{rg} and PD_{rn} had the highest negative correlation values with vegetation cover across all three resolutions.

Based on these results, the PD_{rg} index appears to be the most reliable cover index of the eight indices tested at all three resolutions for assessing landscape leakiness at multiple scales. The use of this index is limited by its dependence on generation of a soil line separate from a vegetation line, something that can be widely done for the arid and semi-arid areas of Australia because of the predominance of soils with a red chroma.

8.2.3. Leakiness Scaling Functions

It was not possible to predict the leakiness of lower resolution observation scale images by upscaling high-resolution images because of the structural decay and reorganisation of image features that occurs in the upscale resampling process.

Resolution based scaling functions (Scalograms) however were developed that accurately predicted upscaled leakiness (Lcalc and AAL) for upscaled images in the range of 10-250m resolution. The increase in AAL with decrease in resolution is moderated by the type of vegetation cover on which it is based. Leakiness responds differently to different cover indices in upscaling. Predictions are more accurate at lower resolutions (> 25m) than at higher resolutions. Thus it may be advisable to use scalograms specifically developed for high resolutions (<25m) when working with high resolution upscaling rather than using scalograms developed for a broader range of resolutions (10-250m).

The results also showed that upscaling can be used to find the best resolution for expression of the most Spatially Correlated Variance (SCV) for each type of vegetative cover index. This feature can be used to guide selection of the type of cover index to use for a particular resolution and a given landscape environment.

Sill Variance (SV) of upscaled images changes in a precise and predictable image-specific way with resolution. AAL also exhibits a precise and image-specific relationship with resolution. These two relationships were used to create Variance Scalograms that allow direct calculation of leakiness from image variance without reference to the underlying resolution. This relationship has the potential for use in developing a method to predict catchment leakiness from measurement of image Sill Variance without needing to know the resolution.

The form of the variance scalograms shows that evenly distributed vegetation cover results in less leakiness than the same amount of more variably distributed cover. This is because of the lower auto-correlation lag in evenly distributed cover versus less evenly distributed cover.

8.2.4. Scaling Effect on Image Structure

All three vegetation cover observation scale images had natural log variograms at 10 and 25m resolution. This changed at 250m resolution where SAVI and STVI exhibited quartic variograms and PDrg had a cubic variogram. Each of these is a bounded variogram with a characteristic Nugget, Sill and one or more Ranges.

The precise form of the variograms and their relationship to each other at different upscale resolutions was used to determine the structure of the images. Image structure decayed progressively with increased upscaling. The First Range of the upscaled images remained relatively close to the First Range of the observation scale images; however the Nugget Variance and Sill Variance increased and the Spatially

Correlated Variance (SCV) decreased relative to observation scale images at most upscaling levels. The change in Variance caused by upscaling indicates the decay and reorganising of the original pattern of patches of vegetation cover that determine leakiness. Equations that modelled image variance as contour plots and as surfaces were used to quantify the difference in behaviour between observation and upscaled image variances.

Variance surfaces of observation scale images take the form of 2-variable quadratic expressions. Upscaled SAVI and STVI images had variance surfaces of a similar form but the PDrg upscaled image variance is a 2-variable cubic expression. This difference is explained by SAVI and STVI images detecting one type of feature while PDrg images detect two types of features.

No variance measurements consistently explained the leakiness for all 3 native scale images; however a number of variance indices correlated well with Lcalc for the 3 upscaled images. Two variogram indices each increased linearly with decrease in resolution and have the potential for use in characterising the leakiness of catchment images at intermediate resolutions.

These results confirm the difference in image structure between different cover indices and their systematic change with image upscaling. They show that different cover indices vary in effectiveness at measuring spatial diversity at different resolutions and that this difference carries over in upscaled images. These factors combine to suggest that the performance of different cover indices should be compared before settling on a particular index to use in an extended catchment leakiness management program.

8.2.5. Position of Cover in Catchment

The effect of position of increased cover in the experimental catchment was tested as a way of identifying which areas were the most effective for adding revegetation cover to reduce leakiness. The analysis yielded an unusual pattern of results.

The addition of cover to areas distant from streams reduced leakiness more than the addition of cover closer to streams. The addition of cover to higher elevation zones reduced leakiness more than when it was added to lower elevation zones. These findings are consistent with each other because higher elevation areas are mostly located further from streams than near to streams. However, both of these results were unexpected and cannot be explained without further investigation. The results suggest that, at least in catchments like the experimental catchment, adding cover to elevated areas away from the streams needs to be given priority. This is different from the conventional practice of adding cover to lower elevated areas and areas adjoining streams.

The addition of cover to lower sloping zones decreased leakiness more than when it was added to higher sloping zones. This is the expected pattern of response; however it appears inconsistent with the preceding pattern of response because lower slope zones are generally closer to streams and exist at lower elevations. The addition of cover to each of the 6 aspects of the catchment made little difference to catchment leakiness. Cover added to topographic zones reduced leakiness the most when added to Peaks followed in declining order of effectiveness by addition to Ridges, Passes, Plains, Channels and Pits. Analysis of the slope and elevation of these landforms disclosed no systematic correlation with reduction in leakiness. Addition of cover to areas with the lowest original cover reduced leakiness more (expected) than addition to higher original cover areas. These results fit the expected pattern of leakiness response to added cover. SAVI and PDrg vegetation cover patterns responded similarly to each other in almost all scenarios.

Leakiness decreased in an exponentially negative manner with the addition of cover at all positions in the catchment. This means that leakiness can be reduced more by small additions of vegetation (grass) cover over wider areas of the catchment than by concentrating the same amount of added cover in specific localised areas within a catchment.

Taken together, these findings suggest that:

a. Areas of a catchment, which reduce leakiness the most in response to added cover, are not necessarily the areas that conventional practice would lead us expected to reduce leakiness the most.
b. Areas in which added cover reduce leakiness the most require catchment-by-catchment analysis to identify them.
c. Addition of cover is more effective if applied at lower rates over larger areas than by concentrating it in smaller areas.
d. Identification of the best areas for cover to reduce leakiness in grazing catchments could be used to guide management decisions such as tree clearing, subdivision fencing patterns, location of stock watering points, timing of grazing pressure and grassland revegetation.

8.3. Future Research

These results showed different responses from previous research findings in the areas of upscaling on image variance and on the position of cover within a catchment on reducing leakiness. They need to be repeated for different vegetation types in different catchments to find out if they are one-off findings or if they reoccur and the conditions under which they reoccur.

To realise the potential of satellite imagery for management of land condition in savannah grazing catchments, futurther research is needed to:

a. Determine the most reliable way of measuring vegetation cover and the optimal image resolution for calculating leakiness in rangeland catchments at management scales.
b. Compare the AAL with other landscape metrics to evaluate its relative usefulness as an indicator of landscape function at different scales and over a range of vegetation types subjected to different types of disturbances.
c. Evaluate the benefits or otherwise of inclusion of a Soil Surface Condition factor and a Vegetation Textural Analysis factor in the Leakiness Calculator algorithm.
d. Develop practical applications and guidelines for using variance leakiness scalograms
e. Determine the effect of different upscale resampling techniques on vegetation cover index behaviour and leakiness analyses, including variance-weighted techniques.
f. Develop a systematic and easily repeatable way of analysing grazing catchments to identify the best locations to add or retain cover to guide property management decisions.

REFERENCES

Abbott, BN and JP Corfield undated, Putting PATCHKEY into practice-Investigating landscape scale patchiness., CSIRO.

Abrahams, AD, AJ Parsons and S Luk 1988, 'Hydrologic and sediment responses to simulated rainfall on desert hillslopes in southern Arizona', *Catena*, vol. 15, pp. 103-17.

Adams, JB, DE Sabol, V Kapos, RA Filho, DA Roberts, *et al.* 1995, 'Classification of multispectral images based on fractions of endmembers: application to land-cover change in the Barzilian Amazon', *Remote Sensing of the Environment*, vol. 52, pp. 137-54.

Addink, EA, SM deJong and EJ Pebesma 2007, 'The importance of scale in object oriented mapping of vegetation mparameters with hyperspectral imagery.', *Photogrammetric Engineering and Remote Sensing*, vol. 73, pp. 905-12.

Armston, JD, RJ Denham, TJ Danaher, PF Scarth and TN Moffiet 2009, 'Prediction and validation of foliage projective cover from Landsat-5 TM and Landsat-7 ETN+ imagery', *Journal of Applied Remote Sensing*, vol. 3, no. 033540, pp. 1-28.

Atkinson, PM and NJ Tate 2000, 'Spatial Scale Problems and Geostatical Solutions: A Review', *Professional Geographer*, vol. 52, no. 4, p. 607, EBSCOhost, aph, item: 4023271.

Balaguer, A, LA Ruiz, T Hermosilla and JA Recio 2010, 'Definition of a comprehensive set of texture semivariogram features and their evaluation for object-oriented image classification', *Computers & Geosciences*, vol. 36, no. 2, pp. 231-40.

Bannari, A, D Morin, F Bonn and AR Huete 2009, 'A review of vegetation indices', *Remote Sensing Reviews*, vol. 13, no. 1-2, pp. 95-120.

Bartley, R, SN Wilkinson, AA Hawdon, BN Abbott and DA Post 2010, 'Impacts of improved grazing land management on sediment yields. Part 2: Catchment response', *Journal of Hydrology*, vol. 389, no. 3-4, pp. 249-59, item: WOS:000280976600002.

Bartley, R, JP Corfield, BN Abbott, AA Hawdon, SN Wilkinson, *et al.* 2010, 'Impacts of improved grazing land management on sediment yields, Part 1: Hillslope processes', *Journal of Hydrology*, vol. 389, no. 3–4, pp. 237-48.

Bartley, R, CH Toth, J Ludwig, D McJannet, AC Liedloff, *et al.* 2006, 'Runoff and erosion from Australia's tropical semi-arid rangelands: influence of ground cover for differing space and time scales', *Hydrological Processes*, vol. 20, no. 15, pp. 3317-33.

Bastin, G 2008, *Rangelands 2008 - Taking the pulse*, National Land and Water Resources Audit, ACRIS Management Committee, Canberra,<.

Bastin, G and V Chewings 2003, *Calculating PD54 index of vegetation cover*, CSIRO, Alice Springs, NT, Australia,<.

Bastin, G, B Abbott and V Chewings 2008, *Validating a remotely sensed index of Landscape Leakiness in the Burdekin Dry Tropics*, CSIRO, Queensland,<.

Bastin, G, B Abbott, V Chewings and J Wallace 2007, *Metrics of landscape health for suitable grazing in the Burdekin dry tropics, Queensland*, CSIRO, Canberra,<.

Bastin, G, JA Ludwig, RW Eager, VH Chewings and AC Liedloff 2002, 'Indicators of landscape function: comparing patchiness metrics using remotely-sensed data from rangelands', *Ecological Indicators*, vol. 1, no. 4, pp. 247-60.

Beeton, R, K Buckley, G Jones, D Morgan, R Reichelt, *et al.*, *Vegetation: Independent report to the Australian Government minister for the Environment and Heritage*, 2006, DoEa Heritage, Australian Government, Canberra.

Bian, L and R Butler 1999, 'Comparing effects of aggregation methods on statistical and spatial properties of simulated spatial data', *Photogrammetric Engineering and Remote Sensing*, vol. 65, no. 1, pp. 73-84.

Bock, M, J Bohner, R Kothe and A Ringeler 2010, *System for Automated Geoscientific Analysis (SAGA).*

Boer, M and J Puigdefabregas 2005, 'Effects of Spatially structured vegetation patterns on hillslope erosion in a semiarid Mediterranean environment: a simulation study', *Earth Surface Processes and Landform*, vol. 30, pp. 149-67.

Bradshaw, GA and MJ Fortin 2000, 'Landscape Heterogeneity Effects on Scaling and Monitoring Large Areas Using Remote Sensing Data', *Annals of GIS*, vol. 6, no. 1, pp. 61-8.

Carroll, C, D Waters, S Vardy, DM Silburn, S Attard, *et al.* 2012, 'A Paddock to reef monitoring and modelling framework for the Great Barrier Reef: Paddock and catchment component', *Marine Pollution Bulletin*, vol. 65, no. 4–9, pp. 136-49.

Chen, WR and GM Henebry 2009, 'Change of spatial information under rescaling: A case study using multi-resolution image series', *ISPRS Journal of Photogrammetry and Remote Sensing*, vol. 64, no. 6, pp. 592-7.

Cimmery, V 2010, *User Guide for SAGA,(version 2.0.5)*, <http://sourceforge.net/projects/saga-gis/files/SAGA%20-%20Documentation/SAGA%202%20User%20Guide/SAGA_User_Guide_Vol1_Cimmery_version_2.0.5_20100823.pdf/download?use_mirror=aarnet>.

Coakes, SJ, L Steed and C Ong 2010, *SPSS, Analysis without Anguish, Ver 17.0 for Windows*, John Wiley and Sons, , Queensland, Australia.

Collins, JB and CE Woodcock 1999, 'Geostatistical estimation of resolution dependent variance in remotely sensed images', *Photogrammetric Engineering and Remote Sensing*, vol. 65, no. 1, pp. 41-50.

Corfield, JP, BN Abbott, A Hawdon and S Berthelsen 2006, 'PATCHKEY: a patch classification frameworkfor the upper Burdekin and beyond.', in Proceedings of the Australian Rangeland Conference: *proceedings of theProceedings of the Australian Rangeland Conference*.

Csillag, F, MJ Fortin and J Dungan 2000, 'On the limits and extensions of the definition of scale', *Bulletin of the Ecological Society of America*, vol. 81, pp. 231-2.

Danaher, T, J Armston and L Collett, *A regression model approach for mapping woody foliage projective cover using Landsat imagery in Queensland, Australia*, 2004, QDNRM&E, Brisbane.

DeCola, L 1994, 'Simulating and mapping spatial cpomplexityusing multiscale techniques', *International Journal of Geographic Information Systems*, vol. 8, pp. 411-21.

DOE 2014, *Outback Australia-the rangelands*, viewed 4 November 2014, <http://www.environment.gov.au/land/rangelands>.

Edzer, JP and CG Wesseling 1998, 'GSTAT: A program for geostatistical modelling, prediction and simulation', *Computers and Geoscience*, vol. 34, no. 1, pp. 17-31.

Eiswerth, ME and JC Haney 2001, 'Maximizing conserved biodiversity: why ecosystem indicators and thresholds matter', *Ecological Economics*, vol. 38, no. 2, pp. 259-74.

ERDAS 2006, *Leica Photogrammetry Suite Automatic Terrain Extraction*, Leica, Norcross, GA, USA.

ERDAS 2010, *ERDAS Field Guide*, vol. II, ERDAS.

ESRI 2012, *ArcGIS Resource Center*, viewed 5 Dec 2012, <http://help.arcgis.com/en/arcgisdesktop/10.0/help/index.html#//00590000001m000000>.

ESRI 2014, *ArcGIS 9.2 Desktop Help*, viewed 22 March 2014, <http://webhelp.esri.com/arcgisdesktop/9.2/index.cfm?id=1666&pid=1644&topicname=Resample%20(Data%20Management)&>.

Exelis 2012, *Exploring ENVI*, Excelis Visual Information Solutions, Boulder, CO,<.

Eyre, T, A Kelly and V Neldner, *BioCondition: A Terrestrial Vegetation Condition Assessment Tool for Biodiversity in Queensland. Fied Assessment manual.*, 2006, QEp Agency, Brisbane.

Garrigues, S, D Allard and J Barer 2008, 'Multivariate quantification of landscape spatial hetereogeneity using variogram models', *Remote Sensing of Environment*, vol. 112, pp. 216-30.

Gibbons, P and D Freudenberger 2006, 'An overview of methods used to assess vegetation condition at the scale of the site', *Ecological Management & Restoration*, vol. 7, pp. S10-S7.

Gill, TK and S Phinn 2008, 'Estimates of bare ground and vegetation cover from Advanced Spaceborne Thermal Emission and Reflection Radiometer (ASTER) short-wave-reflectance imagery', *Journal of Applied Remote Sensing*, vol. 2, pp. 1-19.

Gill, TK and SR Phinn 2009, 'Improvements to ASTER-Derived Fractional Estimates of Bare Ground in a Savanna Rangeland', *Geoscience and Remote Sensing, IEEE Transactions on*, vol. 47, no. 2, pp. 662-70.

Goodin, DG and GM Henebry 2002, 'The effect of rescaling on fine spatial resolution NDVI data: a test using multi-resolution aircraft sensor data', *International Journal of Remote Sensing*, vol. 23, no. 18, pp. 3865-71, EBSCOhost, iih, item: 7288072.

Goulevitch, BM, TJ Danaher, AJ Stewart, DP Harris and LJ Lawrence 2007, 'Mapping woody vegetation cover over the State of Queensland using Landsat TM and ETM+ imagery', in 11 th Australasian Remote Sensing and Photogrammetry Conference: *proceedings of the11 th Australasian Remote Sensing and Photogrammetry Conference*.

Guerschman, JP, MJ Hill, LJ Renzullo, DJ Barrett, AS Marks, *et al.* 2009, 'Estimating fractional cover of photosynthetic vegetation, non-photosynthetic vegetation and bare soil in the Australian tropical savanna region upscaling the EO-1 Hyperion and MODIS sensors', *Remote Sensing of Environment*, vol. 113, no. 5, pp. 928-45.

Gullberg, J 1997, *Mathematics: From the Birth of Numbers*, W. W. Norton and Company, New York.

Hall, W, B Bruget, J Carter, G Mckeon, J Yet, *et al.* 2001, *Australian Grassland and Rangeland Assessment by Spatial Simulation *Aussie GRASS)*, Queensland Department of Natural Resources and Mines, Brisbane,<.

Hay, GJ and KO Nieman 1996, 'Selecting the most appropriate upscaling algorithm: A muti-scale approach', *Proceedings of the International Symposium on Remote Sensing of Environment*, vol. 26, pp. 435-8.

Hay, GJ, KO Niernann and DG Goodenough 1997, 'Spatial thresholds, image-objects, and upscaling: A multiscale evaluation', *Remote Sensing of Environment*, vol. 62, no. 1, pp. 1-19.

Hermosilla, T 2013, *Fetex 2.0 demo version*, viewed 12 May 2013, <http://cgat.webs.upv.es/bigfiles/fetex2web/>.

Huete, AR 1988, 'A Soil-adjusted vegetation index(SAVI)', *Remote Sensing of Environment*, vol. 25, pp. 295-309.

Huete, AR, C Justice and H Liu 1994, 'Development of vegetation and soil indices for MODIS-EOS', *Remote Sensing of Environment*, vol. 49, no. 3, pp. 224-34.

Huete, AR, HQ Liu, K Batchily and W van Leeuwen 1997, 'A comparison of vegetation indices over a global set of TM images for EOS-MODIS', *Remote Sensing of Environment*, vol. 59, no. 3, pp. 440-51.

IBM 2010, 'IBM SPSS Statistics for Windows, Version 19.0', in IBM Corp, Armonk, NY.

Industry Commission 1998, *A Fully Repairing Lease: Inquiry into ecologically sustainable land management. (Industry Commission) Report No 60*, Canberra,<.

Intergraph 2014, *Imagine Photogrammetry*, viewed October 2011, <http://www.hexagongeospatial.com/products/imagine-photogrammetry/ProductLiterature.aspx>.

Jafari, R, MM Lewis and B Ostendorf 2007, 'Evaluation of vegetation indices for assessing vegetation cover in southern arid lands in South Australia', *The Rangeland Journal*, vol. 29, no. 1, pp. 39-49.

Jensen, JR 2007, *Remote Sensing of the Environment: An Earth Resource Perspective*, 2nd edn, Pearson Prentice Hall, Upper Saddle River, NJ.

Jones, HG and RA Vaughan 2010, *Remote Sensing of Vegetation*, Oxford University Press, Oxford.

Karfs, RA 2002, 'Rangeland Monitoring in Tropical Savannah Grasslands, Northern Territory, Australia: Relationship Between Temporal Satellite Data and Ground Data.', Masters thesis, James Cook University, Townsville.

Karfs, RA, BN Abbott, PF Scarth and JF Wallace 2009, 'Land condition monitoring information for reef catchments: a new era', *The Rangeland Journal*, vol. 31, no. 1, pp. 69-86.

Karl, JW and BA Maurer 2010, 'Spatial dependence of predictions from image segmentation: A variogram-based method to determine appropriaqte scales for producing land management information', *Ecological Informatics*, vol. 5, pp. 194-202.

Kaufman, YJ and D Tanre 1992, 'Atmospherically resistant vegetation index (ARVI) for EOS-MODIS', *IEEE Transactions on Geoscience and Remote Sensing*, vol. 30, no. 2, pp. 261-70.

Kerry, R and M Oliver 2008, 'Determining Nugget:sill ratios of standardised variograms from aerial photographs to krige sparse soil data.', *Precision Agriculture*, vol. 9, pp. 33-56.

King, AW 1991, 'Translating models across scales into landscape', in MGaRHG Turner (ed.), *Quantitative Methods in Landscape Ecology*, Springer-Verlag, New York, pp. 479-517.

Knight, D 1987, 'Parasites, lightning, and vegetation mosaic in wilderness landscapes. In M. G. Turner (ed.)', in *Landscape Heterogeneity and Disturbance* Springer-Verlag, New York, pp. 59-83.

Kravchenko, AN 2003, 'Influence of spatial structure on accuracy of interpolation methods', *Soil Science Society of America Journal*, vol. 67, pp. 1564-71.

Krummel, JR, RH Gardner, G Sugihara, RV O'Neill and PR Coleman 1987, 'Landscape patterns in a disturbed environment.', *Oikos*, vol. 48, pp. 321-4.

Kutt, A, T Eyre, A Fisher and L Hunt 2009, *A Biodiversity Monitoring Program for Australian Rangelands*, Department of the Environment, Wate, Heritage and the Arts, Canberra,<.

Landres, PB, P Morgan and FJ Swanson 1999, 'Overview of the use of natural variability concepts in managing ecological systems', *Ecological Applications*, vol. 9, pp. 1179-88.

Landsberg, J and G Crowley 2004, 'Monitoring Rangeland Biodiversity: Plants as Indicators', *Austral Ecology*, vol. 29, pp. 59-77.

Landsberg, J, CD James, SR Morton, TJ Hobbs, J Stol, *et al.* 1997, 'The Effect of Artificial Sources of Water on Rangeland Biodiversity', *Biodiversity Technical Paper No 3*, p. 203.

Lausch, A, M Pause, D Doktor, S Preidl and K Schulz 2013, 'Monitoring and assessing of landscape heterogeneity at different scales', *Environmental Monitoring and Assessment*, vol. 185, no. 11, pp. 9419-34, item: WOS:000325116500049.

Leica 2009, *Orientation Management Software*, Norcross, GA. USA, <http://www.leica-geosystems.com/en/Leica-ORIMA_86819.htm>.

Leitao, AB, J Miller, J Ahern and K McGarigal 2006, *Measuring Landscapes: A Planners Handbook*, Island Press, Washington DC.

Leite, EP and CRdS Filho 2009, 'TEXTNN- A MATLAB program for textural classification using neural networks', *Computers and Geosciences*, vol. 35, pp. 2084-94.

Liedloff, AC 2007, *CSIRO Leakiness Calculator: Basic Instructions for Use*, CSIRO, Darwin, Australia,<.

Lillesand, TM, RW Keifer and JW Chipman 2008, *Remote Sensing and Image Interpretation*, 6th edn, John Wiley and Sons, Hoboken, NJ.

Lloyd, CD 2010, *Spatial data Analysis: An Introduction for GIS Users*, Oxford University Press, Belfast.

Ludwig, J and DJ Tongway 1995, 'Spatial organisation of landscapes and its function in semi-arid woodlands, Australia', *Landscape Ecology*, vol. 10, no. 1, pp. 51-63.

Ludwig, J and D Tongway 1996, 'Rehabilitation of Semiarid Landscapes in Australia. II. Restoring Vegetation Patches', *Restoration Ecology*, vol. 4, no. 4, pp. 398-406.

Ludwig, J and D Tongway 1997, *A Landscape Approach to Rangeland Ecology, in 'Landscape Ecology, Function and management: Principles from Australia's Rangelands' (Eds J. Ludwig, D. Tongway, D Freudenberger, J.C. Noble and K. Hodgkinson)*, CSIRO, Melbourne.

Ludwig, J, D Tongway and S Marsden 1999, 'Stripes, strands or stiples: modelling the influence of three landscape n]banding patterns on resourdce capture and productivity in semi-arid woodlands, Australia', *Catena*, vol. 37, pp. 257-73.

Ludwig, J, JA Wiens and DJ Tongway 2000, 'A Scaling Rule for Landscape Patches and How it Applies to Conserving Soil Resources in Savannas', *Ecosystems*, vol. 3, pp. 84-97.

Ludwig, J, DJ Tongway, GN Bastin and CD James 2004, 'Monitoring ecological indicators of rangeland functional integrity and their relation to biodiversity at local to regional scales', *Austral Ecology*, vol. 29, no. 1, pp. 108-20.

Ludwig, J, G Bastin, J Wallace and TR McVicar 2007, 'Assessing landscape health by scaling with remote sensing: when is it not enough?', *Landscape Ecology*, vol. 22, no. 2, pp. 163-9.

Ludwig, J, R Eager, G Bastin, V Chewings and A Liedloff 2002, 'A leakiness index for assessing landscape function using remote sensing', *Landscape Ecology*, vol. 17, no. 2, pp. 157-71.

Ludwig, J, BP Wilcox, DD Breshears, DJ Tongway and CI Anton 2005, 'Vegetation Patches and Runoff-Erosion as Interacting Ecohydrological Processes in Semiarid Landscapes', *Ecology*, vol. 86, no. 2, pp. 288-97.

Ludwig, J, RW Eager, AC Liedloff, GN Bastin and VH Chewings 2006, 'A new landscape leakiness index based on remotely sensed ground-cover data', *Ecological Indicators*, vol. 6, no. 2, pp. 327-36.

Ludwig, J, GN Bastin, VH Chewings, RW Eager and AC Liedloff 2007, 'Leakiness: A new index for monitoring the health of arid and semiarid landscapes using remotely sensed vegetation cover and elevation data', *Ecological Indicators*, vol. 7, no. 2, pp. 442-54.

Ludwig, J, GN Bastin, RW Eager, R Karfs, P Ketner, *et al.* 2000, 'Monitoring Australian rangeland sites using landscape function indicators and ground- and remote-based techniques', *Environmental Monitoring and Assessment*, vol. 64, no. 1, pp. 167-78.

Ludwig, JA, R Bartley, AA Hawdon, BN Abbott and D McJannet 2007, 'Patch configuration non-linearly affects sediment loss across scales in a grazed catchment in north-east Australia', *Ecosystems*, vol. 10, no. 5, pp. 839-45, item: WOS:000249969200013.

Mabutt, JA and PC Fanning 1987, 'Vegetation Banding in Arid Western Australia', *Journal of Arid Environments*, vol. 12, pp. 41-59.

Maidment, D and S Morehouse 2002, *ArcHydro: GIS for Water Resources (DVD-ROM)*, ESRI, Redlands, CA.

Martin, P and M Verbeek 2002, 'Property Rights and Property Responsibility', in *Property: Rights and Responsibilities. Current Australian Thinking.*, Land and Water Australia, Canberra, ch 1, pp. 1-12.

Mas, J-F, Y Gao and JAN Pacheco 2010, 'Sensitivity of landscape pattern metrics to classification approaches', *Forest Ecology and Management*, vol. 259, no. 7, pp. 1215-24.

Mather, P 2004, *Computer Processing of Remotely-Sensed Images*, John Wiley, West Sussex.

McElhinny, C, P Gibbons, C Brack and J Bauhus 2005, 'Forest and woodland stand structural complexity:its definition and measurement.', *Forest Ecology and Management*, vol. 218, pp. 1-24.

Muir, J, M Schmidt, D Tindall, R Trevithick, P Scarth, *et al.*, *Field measurement of fractional ground cover: A technical handbook supporting ground cover monitoring for Australia*, 2011, ABARES, Canberra.

Munro, NT and DB Lindenmayer 2011, *Planting for wildlife: A practical guide to restoring native woodlands*, CSIRO Publishing.

N L W R A 2001, *Rangelands - Tracking Change: A Summary of the Proposal for Monitoring Australia's Rangelands,*, Commonwealth of Australia, viewed 23 Sept 2006, <http://www.nlwra.gov.au/atlas>.

NASA 2010, *MODIS Product Description*, (National Aeronatics and Space Administration), viewed 20 October 2010

<http://modis.gsfc.nasa.gov/data/dataprod/pdf/MOD_02.pdf>.

NASA 2014a, *Land Processes Distributed Active Archive Center*, viewed 12 November, <http://ladsweb.nascom.nasa.gov/index.html>.

NASA 2014b, *Land Processing Details*, viewed 19 November, <http://landsat.usgs.gov/Landsat_Processing_Details.php>.

Niyogi, D, M Koren and C Arbuckle 2007, 'Stream communities along a catchment land-use gradient:Subsidy-stress responses to pastoral development', *Environmental management*, vol. 39, pp. 213-25.

O'Neil, A 1996, 'Satellite derived vegetation indices applied to shrublands in Australia', *Australian Geographer*, vol. 27, pp. 185-99.

O'Reagain, P, J Brodie, G Fraser, J Bushell, C Holloway, *et al.* 2005, 'Nutrient loss and water qualityunder extensive grazing in the upper Burdekin river catchment , North Queensland', *Marine Pollution Bulletin*, vol. 51, pp. 37-50.

Oliver, I 2003, *Maximising your Biodiversity Benefits Index*, NSW Department of Infrastructure, Planning and Natural resources, Parramatta,<.

Ostendorf, B and JF Reynolds 1993, 'Relationships between a terrain based hydrologic model and patch scale vegetation patterns in an arctic tundra landscape.', *Landscape Ecology*, vol. 8, no. 4, pp. 229-37.

Parkes, D, G Newell and D Cheal 2003, 'Assessing the quality of native vegetation: The 'habitat hectares' approach', *Ecological Management and Restoration*, vol. 4 Supplement.

Pegler, K, *GRASS Check,* 1997, QDoN Resources, Queensland Department of Natural Resources, GPO, Brisbane.

Pickup, G, VH Chewings and DJ Nelson 1993, 'Estimating changes in vegetation cover over time in arid rangelands using landsat MSS data', *Remote Sensing of Environment*, vol. 43, no. 3, pp. 243-63.

Pickup, G, G Bastin and VH Chewings 1994, 'Remote sensing-based condition assessment for non-equilibriumrangelands under large scale commercial grazing', *Ecological Applications*, vol. 4, pp. 497-517.

Pratap, R 2010, *Getting Started with MATLAB*, Oxford University Press, New York.

Pringle, HJR and J Landsberg 2004, 'Predicting the distribution of livestock grazing pressure in rangelands', *Austral Ecology*, vol. 29, no. 1, pp. 31-9.

Productivity Commission 1999, *Implementation of Ecologically Sustainable Development by Commonwealth Departments and Agencies, Report No 5*, Canberra,<.

Purvis, JR 2004, 'Practical Biodiversity. ', in 'Living in the Outback' Conference: *proceedings of the'Living in the Outback' Conference*, G Bastin, Walsh, D., Nicholson, S. (Eds) (ed.), Australian Rangeland Society, Northam, Western Australia, pp. 209-10.

QGRAZE, *Monitoring the Condition of Queenslands Rangelands*, 1992, QDPI, QDPI Brisbane.

Qi, J, F Cabot, MS Moran and G Dedieu 1995, 'Biophysical parameter estimations using multifitectional spectral measurements', *Remote Sensing of Environment*, vol. 54, pp. 71-83.

Qi, Y and JG Wu 1996, 'Effects of changing spatial resolution on the results of landscape pattern analysis using spatial autocorrelation indices.', *Landscape Ecology*, vol. 11, pp. 39-49.

Richardson, A and C Wiegand 1977, 'Distinguishing vegetation from soil background', *Photogrammetric Engineering and Remote Sensing*, vol. 43, pp. 1541-52.

Rouse, J, R Haas, J Schell and D Deering 1974, 'Monitoring vegetation systems in the Great Plains with ERTS', in Proceedings , Third Earth Resources Technology Satellite-1 Symposium: *proceedings of theProceedings , Third Earth Resources Technology Satellite-1 Symposium* NASA, Greenbelt MD USA, pp. 3010-7.

Rouse, JW, RH Haas, JA Schell and D Deering 1974, 'Monitoring vegetation systems in the Great Plains with ERTS', in ProceedingsThird Earth Resources Technology Satellite-1 Symposium: *proceedings of theProceedingsThird*

Earth Resources Technology Satellite-1 Symposium NASA SP-351, Greenbelt, MD, pp. 3010-7.

Ruiz, LA, JA Recio, A Fernández-Sarría and T Hermosilla 2011, 'A feature extraction software tool for agricultural object-based image analysis', *Computers and Electronics in Agriculture*, vol. 76, no. 2, pp. 284-96.

Sakurambo 2009, *Airy-2d drawing (Point Spread Function)*, <http://en.wikipedia.org/wiki/File:Airy-3d.svg>.

Salkind, NJ 2007, *Statistics for People Who Hate Statistics*, The Excel Edition edn, Sage Publications, London.

Saura, S 2002, 'Effects of minimum mapping uniton landcover dataspatial configurationand composition. ', *International Journal of Remote Sensing*, vol. 23, pp. 4853-80.

Scarth, P, A Roder and M Schmidt 2011, *Tracking Grazing Pressure and Climate Interaction - The Role of Landsat Fractional Cover in Time Series Analysis*. PS figshare.

Scarth, PF, M Byrne, T Danaher, B Henry, R Hassett, *et al.*, *State of the Paddock: monitoring condition and trend ground cover across Queensland*, 2006, QDoEaR Management, Brisbane.

Scarth, PF, M Byrne, T Danaher, B Henry, R Hassett, *et al.*, *State of the Paddock: monitoring condition and trend ground cover across Queensland*, 2008, QDoEaR Management, Brisbane.

Schmidt, M and P Scarth 2009, 'Spectral Mixture Analysis for Ground-Cover Mapping', *Lecture Notes in Geoinformation and Cartography: Innovations in Remote Sensing and Photogrammetry*, pp. 349-59,

Schmidt, M and R Trevithick 2010, 'Seasonal groundcover monitoring with Landsat time series data in the grazing lands of the Great Barrier Reef catchment', in Proceedings of the 15th Australasian Remote sensing and Photogrammetry Conference: *proceedings of theProceedings of the 15th Australasian Remote sensing and Photogrammetry Conference* Alice Springs.

Schmidt, M, R Denham and P Scarth 2010, 'Fractional ground cover monitoring of pastures and agricultural areas in Queensland', in 15th Australasian Remote Sensing and Photogrammetry Conference: *proceedings of the15th Australasian Remote Sensing and Photogrammetry Conference* Alice Springs.

Schmidt, M, D Tindall, K Speller, P Scarth and C Dougall 2010, *Ground cover management practices in cropping and improved pasture grazing systems:ground cover monitoring using remote sensing.*, Bureau of Rural Sciences, Canberra,<.

Schumm, S 1977, *The Fluvial System*, Wiley-Interscience, New York.

Sheffield, K 2009, 'Multi-spectral remote sensing of native vegetation condition ', Research thesis, RMIT, Melbourne.

Tanser, FC and AR Palmer 1999, 'The application of a remotely-sensed diversity index to monitor degradation patterns in a semi-arid, heterogeneous, South African landscape', *Journal of Arid Environments*, vol. 43, no. 4, pp. 477-84.

Tanser, FC and AR Palmer 2000, 'Vegetation mapping of the Great Fish River basin, South Africa: Integrating spatial and multi-spectral remote sensing techniques', *Applied Vegetation Science*, vol. 3, no. 2, pp. 197-204.

Thackway, R and R Lesslie 2006, 'Reporting vegetation condition using the Vegetation Assets, States and Transitions (VAST) framework', *Ecological Management and Restoration*, vol. 7, no. S1, pp. s53-s62.

Thenkabail, PS, AD Ward, JG Lyon and CJ Maerry 1994, 'Thematic mapper vegetation indices for determining soybean and corn growth parameters', *Photogrammetric Engineering and Remote Sensing*, vol. 60, pp. 437-42.

Tongway, D and JA Ludwig 1990, 'Vegetation and soil patterning in semi-arid mulga lands of Eastern Australia.', *Australian Journal of Ecology*, vol. 15, pp. 23-34.

Tongway, D and JA Ludwig 1996, 'Rehabilitation of Semiarid Landscapes in Australia. I. Restoring Productive Soil Patches', *Restoration Ecology*, vol. 4, no. 4, pp. 388-97.

Tongway, D and N Hindley, *Landscape Function Analysis: Procedures for Monitoring and Assessing Landscapes*, 2004, CSIRO Sustainable Ecosystems, Canberra ACT.

Tongway, D and N Hindley 2004, 'Landscape function analysis: a system for monitoring rangeland function', *African Journal of Range & Forage Science*, vol. 21, no. 2, pp. 109-13.

Tongway, DJ, C Valentin and J Seghieri 2012, *Banded Vegetation Patterningin Arid and Semiarid Environments*, Springer.

Tothill, JC, JNG Hargreaves, RM Jones and CK McDonald 1992, *BOTANAL: A comprehensive sampling and computing procedure for estimating pasture yield and composition. I Field sampling*, CSIRO, Division of Tropical Crops and Pastures, Canberra, Australia,<.

Trevithick, B 2013, *Fractional Cover- Landsat joint remote sensing research program algorithm, Australia coverage*, viewed 26 November 2013, <http://data.auscover.org.au/xwiki/bin/view/Product+pages/Landsat+Fractional+Cover#HAlgorithmsummary>.

Turner, MG, RH Gardner and RV O'Neill 2001, *Landscape Ecology: Pattern and Process*, Springer, New York.

Turner, MG, RV O'Neill, RH Gardner and BT Milne 1989, 'Effects of changing spatial scale on the analysis of landscape pattern', *Landscape Ecology*, vol. 3, no. 3, pp. 153-62.

USDOI 2012a, *Global Visualization Viewer (GLOVIS)*, US Geological Survey, viewed 16 November <http://glovis.usgs.gov/>.

USDOI 2012b, *Land Processes Distributed Active Archive Center (LP DAAC)*, NASA and USGS, viewed 12 November, <https://lpdaac.usgs.gov/data_access/data_pool>.

USGS 2014, *Global Visualization Viewer*, Us Department of the Interior, viewed 12 November, <http://glovis.usgs.gov/index.shtml>.

Westboy, M, B Walker and I Noy-Meir 1989, 'Opportunistic management for rangelands not at equilibrium', *Journal of Range Management*, vol. 42, no. 4, pp. 266-74.

Whitehead, B 2001, *Developing an analytical framework for monitoring biodiversity in Australia's rangelands, a report by the Tropical Savannas Cooperative research Centre*, Darwin,<.

Wiens, JA 1989, 'Spatial scaling in ecology', *Functional Ecology*, vol. 3, pp. 385-97.

Wilcox, BP, DD Breshears and CD Allen 2003, 'Ecohydrology of a resource-conserving semiarid woodland: Effects of scaling and disturbance.', *Ecological Monographs*, vol. 73, pp. 223-39.

Wilkinson, C and J Brodie 2011, *Catchment Management and Coral Reef Conservation: a practical guide for coastal resource managers to reduce damage from catchment areas based on best practice case studies.*, Global Coral reef Monitoring network and Reef Rainforest Research Center, Townsville, Australia,<.

Woinarski, J, R Fensham, P Whitehead and A Fisher 2000, *Developing an Analytical Framework for Monitoring Biodiversity in Australia's Rangelands: A review of Changes in Status and Threatening Processes.*, National Land and Water Resources Audit, Darwin,<.

Wu, J 2004, 'Effects of changing scale on landscape pattern analysis: scaling relations', *Landscape Ecology*, vol. 19, no. 2, pp. 125-38.

Wu, J, W Shen, W Sun and P Tueller 2002, 'Empirical patterns of the effects of changing scale on landscape metrics', *Landscaape Ecology*, vol. 17, pp. 761-82.

Wu, X and D Sui 2001, 'An initial exploration of lacunarity based segregation measure.', *Environment and Planning B: Planning and Design*, vol. 28, pp. 433-46.

Xiao, J and A Moody 2005, 'A comparison of methods for estimating fractional green vegetation cover within a desert-to-upland transition zone in central New Mexico, USA', *Remote Sensing and Environment*, vol. 98, pp. 237-50.

Zhang, X, C Liao, J Li and Q Sun 2012, 'Fractional vegetation cover estimation in arid and semi0arid environments usin HJ-1 satellite hyperspectral data', *International Journal of Applied Earth Observation and Geoinformation*.

APPENDICES

Appendix 1 Sub-catchment details at 3 resolutions

Sub-catchments	Perim_km	Area_ha	Slope_avg
10m Catchment			
2	20.05	696.40	3.602
3	12.92	391.80	3.789
4	20.24	709.30	3.080
5	11.46	409.80	3.041
6	17.52	590.00	2.473
7	14.68	451.10	3.763
8	15.20	335.60	2.245
9	20.98	1003.00	4.323
10	19.60	790.70	4.088
11	15.78	521.10	3.906
Whole	53.51	5898.80	3.719
25m Catchment			
2	18.25	649.70	2.555
3	11.70	413.00	2.610
4	20.05	742.80	2.266
5	10.35	396.90	2.272
6	15.65	616.10	2.006
7	12.75	466.30	2.566
8	13.75	285.70	1.460
9	18.60	962.80	2.932
10	19.25	812.40	2.827
11	15.80	544.80	2.899
Whole	49.90	5890.50	2.565
250m Catchment			
2	21.21	1947.39	1.13
3	12.59	582.65	1.28
4	10.06	245.18	0.44
5	17.58	962.07	1.45
6	11.20	540.02	0.88
7	11.43	565.69	1.01
8	13.22	911.30	1.20
Whole	35.74	5754.31	1.214

Appendix 2: Stereo Aerial Photo details

Air Photo details	
Collection by	Australian Mapping Service
Exposure date	18 march 1993
Flying height	4210 m ASL
Camera Focal length	152.53 mm
Approx. Photo scale	1:25000
Scanning resolution	1.5e-005
Pixel size	0.375m
Purchased from	Qld. Dept. of Natural. Resources

Air Photo Number	
QAP5157_200.tif	QAP5786_008.tif
QAP5157_201.tif	QAP5786_009.tif
QAP5157_202.tif	QAP5786_010.tif
QAP5161_029.tif	QAP5786_011.tif
QAP5161_090.tif	QAP5786_012.tif
QAP5161_091.tif	QAP5786_058.tif
QAP5784_246.tif	QAP5786_059.tif
QAP5784_247.tif	QAP5786_060.tif
QAP5784_248.tif	QAP5786_061.tif
QAP5784_249.tif	QAP5786_062.tif
QAP5786_005.tif	QAP5786_063.tif
QAP5786_006.tif	QAP5786_144.tif
QAP5786_007.tif	QAP5786_145.tif

Appendix 3: Data Dictionary for GCP and PSM data collection

```
"Ch Twrs Ref Feat ", Dictionary, version, 6
"GCP", point, "GCP", None, 20, Code
   "Intersection", menu, normal, "Intersection", normal, Label1
      "Rd"
      "Track"
      "Rd c Crk"
      "Rd c Rwy "
      "Tree on Rd"
   "Building", menu, normal, "Building", normal
      "SW Cnr"
      "NW Cnr"
      "NE Cnr"
      "SE Cnr"
   "Photo", numeric, 0, 1, 1000, 999, normal, "Photo", normal
   "Date", date, auto, dmy, manual, normal, "Date", normal
   "Time", time, auto, 24, manual, normal, "Time", normal
   "Separator", caption, normal, "Separator", normal, expanded

"PSM", point, "PSM", None, 20, Code
   "Urban", menu, normal, "Urban", normal, Label1
      "Elevn"
      "Direct Posn"
      "Estim Posn"
   "Rural", menu, normal, "Rural", normal, Label2
      "Elevn"
      "Direct Posn"
      "Estim Posn"
   "Photo", numeric, 0, 1, 1000, 99, normal, "Photo", normal
   "Date", date, auto, dmy, manual, normal, "Date", normal
   "Time", time, auto, 24, manual, normal, "Time", normal
   "Separator", caption, normal, "Separator", normal, expanded
```

Appendix 4. Trimble Nomad and ProXH used for field data collection

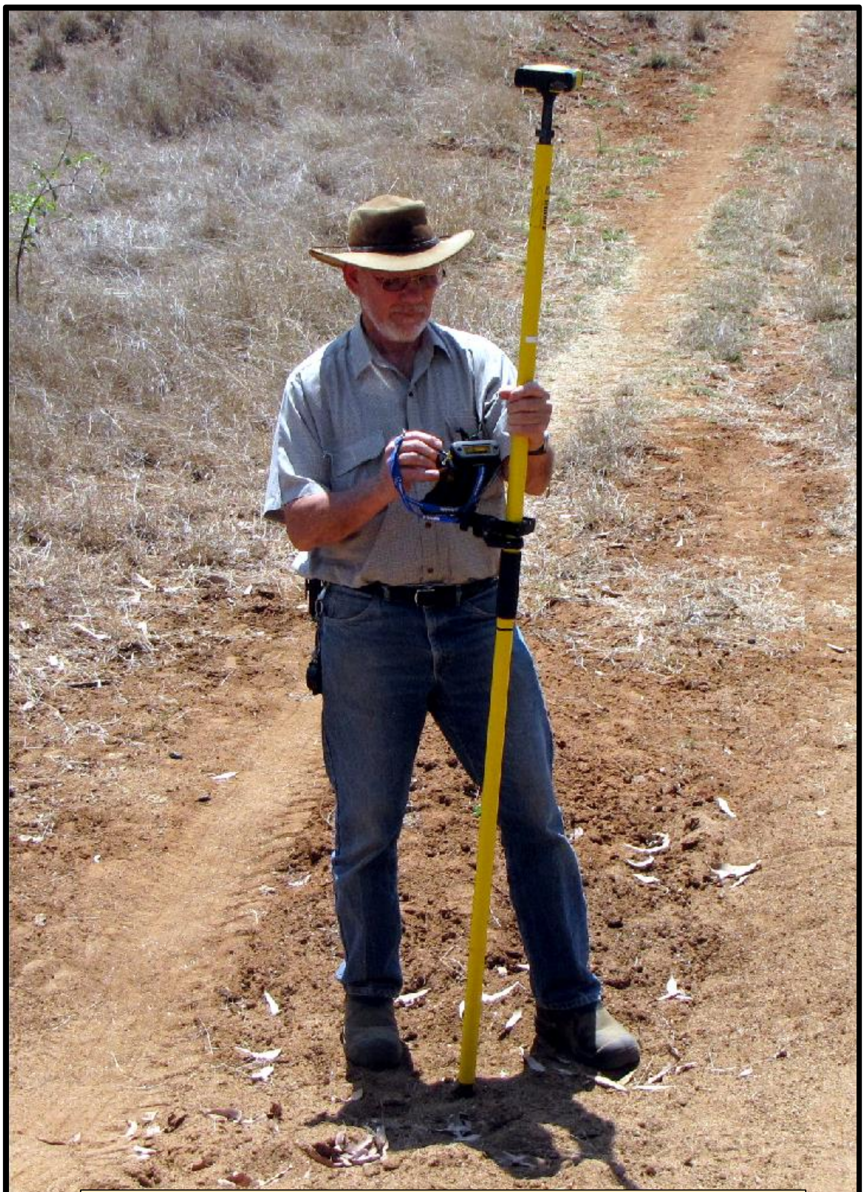

Trimble Nomad and ProXH antennae collecting ground reference control points, SW of Charters Towers, N Qld. J E Dunwoody (photo credit Assoc. Prof. A. Apan)

Appendix 1. Elevation comparison between Geoid (WGS 84) and Ellipsoid (GRS 1980)

PSM Registered No	GPS_Date	GPS_Time	GNSS Height	Surv Ht (AHD m)	Diff (m)	Vert_Prec	Horz_Prec	GNSS Easting	Surv. East.	Diff East (m)	GNSS Northing	Surv. North.	Diff North (m)
193	25/09/2011	07:37:16am	366.468	310.144	56.324	0.40	0.20	422548.899	422548.986	0.087	7780891.3102	7780891.551	0.241
702728	30/09/2011	11:04:03am	476.618	420.638	55.980	0.30	0.20	421836.0954	421836.487	0.392	7778496.5933	7778496.649	0.056
92192	3/10/2011	06:17:08pm	344.356	na	na	0.70	0.30	426361.0519	426361.000	0.052	7777826.9655	7777828.000	1.035
40050	4/10/2011	04:33:26pm	412.067	356.398	55.669	0.40	0.30	416674.2062	416674.031	0.175	7762852.1784	7762852.396	0.218
40048	4/10/2011	05:43:18pm	357.820	301.107	56.713	0.60	0.30	429921.3965	429921.308	0.088	7777489.5169	7777489.686	0.169
Mean					56.171					0.159			0.344

Appendix 6. Field Ground Reference Point Records

FID No	Easting	Northing	GPS_Date	GPS_Time	GNSS_ Height	Vert_ Prec	Horz_ Prec	Description
0	407287.951	7752761.788	3/10/2011	12:04:04pm	426.434	0.7	0.5	lge islated iron bark tree sth side of rd
1	409032.948	7753047.440	3/10/2011	12:46:05pm	438.068	1.0	0.5	lge tree sw cnr crk x rd
2	409055.873	7753050.852	3/10/2011	12:44:08pm	434.341	0.7	0.4	rd nd crk isection
3	409658.060	7753216.790	3/10/2011	01:45:43pm	436.419	0.4	0.3	rd nd flora crk isection
4	408144.710	7753224.813	3/10/2011	12:27:41pm	434.711	0.6	0.3	grid, fence xs rd
5	409639.978	7753227.362	3/10/2011	02:04:06pm	436.095	0.5	0.5	dark green tree ln crk line
6	408161.049	7753229.698	3/10/2011	12:34:29pm	435.639	0.4	0.3	3 way isection short cut
7	408205.712	7753233.015	3/10/2011	12:29:24pm	437.231	0.8	0.2	
8	408196.587	7753247.830	3/10/2011	12:31:13pm	436.602	0.5	0.2	Tree nth of isection
9	408166.044	7753251.231	3/10/2011	12:32:51pm	435.689	0.4	0.2	3way short cut at isection
10	407771.078	7753701.439	4/10/2011	09:12:38am	428.488	0.2	0.2	3 way fence isection
11	407784.989	7753720.003	4/10/2011	09:10:54am	429.002	0.2	0.2	3 way fence isection
12	407811.784	7753750.353	4/10/2011	09:05:08am	428.773	0.6	0.3	large blood wood tree sse of rd nd fence isection
13	407800.817	7753767.819	4/10/2011	09:03:13am	428.273	0.3	0.3	rd nd fence isection
14	410414.609	7753803.271	3/10/2011	02:11:33pm	432.673	0.4	0.4	big blue gum cnr of rd
15	407649.246	7754494.625	1/10/2011	08:22:19am	420.376	0.7	0.3	
16	407375.326	7754536.764	1/10/2011	08:27:18am	416.295	1.2	0.6	
17	406491.899	7754536.791	27/09/2011	01:54:28pm	411.608	0.4	0.2	pt 38 west pt 5 way intersection
18	405290.630	7754579.477	27/09/2011	02:05:30pm	397.707	0.4	0.3	pt 37 sharp bend in rd

Appendix 6. Field Ground Reference Point Records (continued)

FID No	Easting	Northing	GPS_Date	GPS_Time	GNSS_ Height	Vert_ Prec	Horz_ Prec	Description
19	407613.562	7754622.730	1/10/2011	08:16:56am	420.016	1.0	0.4	
20	407588.704	7754655.844	1/10/2011	08:13:30am	417.629	1.8	0.5	
21	407589.729	7754656.818	1/10/2011	08:15:44am	419.302	1.0	0.5	
22	411223.107	7755163.993	3/10/2011	02:22:01pm	442.858	0.5	0.4	prominent iron bark sw of grid on rd
23	411209.559	7755189.594	3/10/2011	02:19:12pm	443.136	0.5	0.5	grid where fence xs rd
24	407927.333	7755358.727	4/10/2011	09:46:05am	413.229	0.4	0.2	sq intersection of yard corner
25	407988.516	7755386.318	4/10/2011	09:52:48am	413.043	0.6	0.3	sw cnr of tank
26	407959.266	7755398.940	4/10/2011	09:49:05am	412.590	0.5	0.2	nw cnr of yards
27	408335.283	7755565.067	4/10/2011	02:24:37pm	420.380	0.4	0.4	big tree se side of dam nr yards
28	408553.513	7755727.514	4/10/2011	02:11:29pm	426.964	0.3	0.4	rocky outcrop
29	408572.571	7755813.261	4/10/2011	02:09:05pm	422.872	0.3	0.3	rocky outcrop
30	414357.161	7756391.368	3/10/2011	02:29:45pm	448.436	0.3	0.3	
31	403820.607	7757569.312	27/09/2011	03:20:22pm	382.186	0.3	0.2	track and Yd fence intersection
32	408772.264	7757717.668	4/10/2011	10:54:12am	396.515	0.7	0.4	sw cnr of tank
33	403869.426	7757747.859	27/09/2011	03:14:44pm	382.625	0.3	0.2	3 way intersection
34	403897.172	7757751.114	27/09/2011	03:11:48pm	383.371	0.3	0.2	sw cnr of small shed
35	402706.306	7758273.801	30/09/2011	04:37:03pm	382.154	0.6	0.3	intersecn fence w sandy crk
36	402636.505	7758335.164	30/09/2011	04:33:45pm	383.137	0.4	0.2	sandy creek
37	408492.139	7758714.526	4/10/2011	12:57:07pm	404.099	0.5	0.3	bend in fence line

Appendix 6. Field Ground Reference Point Records (continued)

FID No	Easting	Northing	GPS_Date	GPS_Time	GNSS_ Height	Vert_ Prec	Horz_ Prec	Description
38	408508.256	7759131.662	4/10/2011	11:30:56am	398.469	0.5	0.4	3 way fence isection nr dam
39	408476.396	7759168.043	4/10/2011	11:33:22am	397.344	0.5	0.4	sw cnr tank nr dam
40	408551.195	7759306.739	4/10/2011	11:37:13am	397.466	0.3	0.3	tree a ne cnr of main dam
41	403261.446	7760907.417	27/09/2011	01:13:14pm	397.919	0.4	0.3	creek and track
42	405638.100	7761010.455	29/09/2011	04:35:45pm	407.545	0.6	0.3	
43	414982.461	7761021.345	2/10/2011	11:12:36am	430.459	0.6	0.4	15 mile entrance grd
44	414977.462	7761021.698	2/10/2011	11:15:26am	430.396	0.5	0.3	fifteen mile turn off gdr
45	414507.098	7761081.640	2/10/2011	11:53:54am	435.777	0.3	0.3	cnr of fence w trk on east side
46	402818.959	7761109.139	27/09/2011	01:08:31pm	407.891	0.5	0.4	
47	402819.298	7761109.560	29/09/2011	04:08:00pm	407.191	0.5	0.2	
48	414514.400	7761173.165	2/10/2011	11:51:28am	436.011	0.3	0.3	fence xing rd
49	401692.253	7761209.833	27/09/2011	12:29:01pm	418.874	0.4	0.3	pt 26 trk intersection
50	414103.841	7761223.441	2/10/2011	12:56:59pm	422.391	0.8	0.4	intersecn 2 small gullies
51	414015.492	7761464.628	2/10/2011	01:13:57pm	419.170	0.5	0.3	15 mile rd x crk
52	412653.637	7762313.940	2/10/2011	01:29:43pm	410.820	0.6	0.4	trk xing crk
53	412631.560	7762320.788	2/10/2011	01:27:55pm	410.296	0.5	0.3	trk nd fence
54	412497.178	7762379.043	2/10/2011	01:37:40pm	413.540	0.4	0.3	house
55	407393.484	7762391.643	25/09/2011	02:58:02pm	425.214	0.3	0.2	3 way bdry pt
56	412510.884	7762395.311	2/10/2011	01:36:17pm	412.531	0.4	0.3	shed cnr

Appendix 6. Field Ground Reference Point Records (continued)

FID No	Easting	Northing	GPS_Date	GPS_Time	GNSS_ Height	Vert_ Prec	Horz_ Prec	Description
57	407318.465	7762399.480	25/09/2011	02:43:13pm	427.551	0.3	0.2	cnr 2 fence lines
58	405634.347	7762580.391	25/09/2011	02:12:29pm	415.969	0.3	0.2	fence cnr
59	405525.674	7763109.384	25/09/2011	01:51:18pm	418.712	0.4	0.2	fence cnr
60	411914.856	7763429.638	2/10/2011	04:14:05pm	406.948	0.5	0.3	old house
61	411706.534	7763437.880	2/10/2011	04:24:14pm	406.102	0.5	0.3	sandy creek
62	411909.040	7763442.280	2/10/2011	04:12:49pm	406.845	0.6	0.5	newer shed
63	411877.914	7763474.361	2/10/2011	04:09:46pm	406.488	0.3	0.2	water tank
64	411684.030	7763547.513	2/10/2011	04:39:26pm	407.263	0.7	0.5	
65	411826.265	7763580.109	2/10/2011	04:18:08pm	404.734	0.3	0.2	rd x crk nr old hse
66	405863.325	7763655.646	25/09/2011	01:44:25pm	430.010	0.4	0.2	
67	412256.039	7764429.112	2/10/2011	03:35:23pm	407.831	0.7	0.3	fence nd trk together
68	412011.036	7764445.429	2/10/2011	03:41:51pm	409.830	0.5	0.2	swer isection w fence
69	411369.823	7764487.682	2/10/2011	03:48:55pm	416.621	0.5	0.2	trk nd fence isect

Appendix 7 Additional modifications made to PDI calculation procedure.

The following steps reflect further modifications made to the PDI calculation procedure in this research.

1. Scatter plots of the respective bands for each image were made using ERDAS Imagine 2011>Supervised Classification>Feature space

2. The soil line and vegetation lines were fitted and required measurements made using ERDAS Imagine 2011>Supervised Classification>Feature space>Editor

3. The gain, offset and distance parameters required by the following step (4) in ERMapper were calculated in an MS Excel spreadsheet

4. The PD54 algorithm (Eqn. 4-7) supplied by CSIRO was used in ERMapper to produce each PDI image.

$$PD_{rz} = \left(\frac{abs\big((-V_1 * Band\ z * V_2) + Red\ Band - V_3\big)}{\sqrt{V^2}+1}\right) * 254/V_4 \qquad (4\text{-}7)$$

where V_1 = -1 (a constant)
V_2 = gain (slope of the soil line)
V_3 = offset (y intercept)
V_4 = max. vertical distance between vegetation line and soil line
z = Green, NIR and SWIR bands respectively

Appendix 8. Effect of upscaling the image versus upscaling the SAVI thematic cover layer

Resoln (m)	Cell count	Average Cover (%)		Experimental Calculated Leakiness (Lcalc)		Experimental Adjusted Average Leakiness (AAL)	
		Image resample	Thematic Raster resample	Image resample	Thematic Raster resample	Image resample	Thematic Raster resample
10	589913	44.81	44.19	79.10	81.99	1.34	1.39
15	262200	44.68	44.19	50.82	51.68	1.94	1.97
25	94416	44.68	44.18	26.41	27.31	2.80	2.89
30	65541	44.82	44.21	19.85	20.49	3.03	3.13
40	36920	44.61	44.21	14.42	14.85	3.90	4.02
50	23595	44.81	44.20	11.04	11.73	4.68	4.97
60	16374	44.58	44.19	9.30	9.46	5.68	5.78
70	12029	44.84	44.23	8.36	8.53	6.95	7.09
80	9233	44.57	44.16	8.25	8.49	8.93	9.20
90	7289	44.77	44.17	5.84	5.99	8.01	8.22
100	5892	44.58	44.19	4.59	4.77	7.79	8.10
110	4849	44.82	44.23	3.98	4.29	8.21	8.84
120	4098	44.65	44.24	3.94	4.04	9.62	9.85
130	3489	44.86	44.20	3.55	3.73	10.16	10.69
140	2981	44.65	44.28	2.73	2.75	9.14	9.21
150	2603	44.78	44.16	2.70	2.81	10.38	10.79
160	2269	44.50	44.12	2.19	2.21	9.64	9.73
170	2022	44.72	44.09	2.20	2.34	10.87	11.58
180	1798	44.48	44.11	2.08	2.13	11.56	11.82
190	1612	44.90	44.29	1.89	2.07	11.72	12.83
200	1461	44.59	44.19	1.77	1.82	12.10	12.46
210	1324	44.78	44.26	1.75	1.73	13.21	13.07
220	1208	44.71	44.30	1.81	1.86	14.98	15.39
230	1108	44.95	44.33	1.76	1.83	15.92	16.51
240	1016	44.46	44.04	1.45	1.49	14.23	14.69
250	942	44.82	44.22	1.72	1.77	18.24	18.83
Avg.		44.71	44.20	16.96	17.52	8.73	9.03
Std. Dev.		0.13	0.06	37.68	38.96	4.63	4.78

Appendix 9. Effect of upscaling the image versus upscaling the STVI thematic cover layer

Resol n (m)	Cell Count	Average Cover (%)		Experimental Calculated Leakiness		Experimental Adjusted Average leakiness	
		Image resample	Thematic raster resample	Image resample	Thematic raster resample	Image resample	Thematic raster resample
10	589913	56.44	56.44	33.94	33.94	0.58	0.58
15	262200	56.42	56.43	21.72	21.71	0.83	0.83
25	94416	56.41	56.43	11.39	11.38	1.21	1.20
30	65541	56.44	56.44	8.55	8.55	1.30	1.30
40	36920	56.43	56.45	6.25	6.25	1.69	1.69
50	23595	56.46	56.46	4.91	4.91	2.08	2.08
60	16374	56.42	56.43	4.06	4.08	2.48	2.49
70	12029	56.44	56.44	3.68	3.68	3.06	3.06
80	9233	56.42	56.44	3.66	3.65	3.96	3.96
90	7289	56.40	56.40	2.62	2.62	3.60	3.60
100	5892	56.40	56.42	2.05	2.05	3.48	3.48
110	4849	56.44	56.44	1.79	1.79	3.70	3.70
120	4098	56.48	56.50	1.78	1.77	4.33	4.33
130	3489	56.51	56.51	1.60	1.60	4.58	4.58
140	2981	56.45	56.47	1.23	1.23	4.12	4.11
150	2603	56.46	56.46	1.22	1.22	4.69	4.69
160	2269	56.35	56.38	0.98	0.98	4.31	4.31
170	2022	56.46	56.44	1.00	1.02	4.94	5.05
180	1798	56.33	56.37	0.93	0.94	5.17	5.23
190	1612	56.46	56.46	0.86	0.86	5.35	5.35
200	1461	56.44	56.45	0.79	0.77	5.41	5.24
210	1324	56.40	56.44	0.78	0.78	5.91	5.85
220	1208	56.44	56.43	0.80	0.78	6.63	6.47
230	1108	56.54	56.47	0.79	0.81	7.17	7.27
240	1016	56.31	56.37	0.67	0.67	6.55	6.63
250	942	56.41	56.41	0.77	0.77	8.18	8.18
Avg.		56.43	56.44	7.30	7.30	3.91	3.91
Std. Dev.		0.05	0.03	16.00	15.99	2.10	2.10

Appendix 10.Transformed and Predicted values for SAVI Image Leakiness

Experimental Image Leakiness	Experimental Image Leakiness transformed	Predicted Image Leakiness	Differences
79.10	0.34	134.88	55.78
50.82	0.48	67.73	16.91
26.41	0.70	29.98	3.57
19.85	0.76	22.77	2.92
14.42	0.98	14.99	0.58
11.04	1.17	11.00	-0.04
9.30	1.42	8.61	-0.69
8.36	1.74	7.04	-1.32
8.25	2.24	5.94	-2.31
5.84	2.01	5.12	-0.72
4.59	1.95	4.50	-0.09
3.98	2.05	4.01	0.03
3.94	2.41	3.61	-0.33
3.55	2.54	3.28	-0.26
2.73	2.29	3.01	0.29
2.70	2.60	2.78	0.08
2.19	2.41	2.58	0.39
2.20	2.72	2.40	0.21
2.08	2.89	2.25	0.17
1.89	2.93	2.12	0.23
1.77	3.03	2.00	0.23
1.75	3.31	1.89	0.14
1.81	3.75	1.80	-0.01
1.76	3.98	1.71	-0.05
1.45	3.56	1.63	0.19
1.72	4.56	1.56	-0.16

Appendix 11.Transformed and predicted values for STVI Image leakiness

Experimental Image Leakiness	Experimental Image Leakiness transformed	Predicted Image Leakiness	Differences
33.94	0.14	57.32	23.38
21.72	0.21	28.93	7.21
11.39	0.30	12.91	1.52
8.55	0.33	9.83	1.28
6.25	0.42	6.50	0.25
4.91	0.52	4.78	-0.12
4.06	0.62	3.75	-0.30
3.68	0.76	3.08	-0.60
3.66	0.99	2.60	-1.06
2.62	0.90	2.25	-0.38
2.05	0.87	1.97	-0.08
1.79	0.92	1.76	-0.03
1.78	1.08	1.59	-0.19
1.60	1.15	1.44	-0.15
1.23	1.03	1.32	0.10
1.22	1.17	1.22	0.00
0.98	1.08	1.14	0.16
1.00	1.24	1.06	0.06
0.93	1.29	0.99	0.06
0.86	1.34	0.93	0.07
0.79	1.35	0.88	0.09
0.78	1.48	0.84	0.05
0.80	1.66	0.79	-0.01
0.79	1.79	0.75	-0.04
0.67	1.64	0.72	0.06
0.77	2.05	0.69	-0.08

Appendix 12. PDrg calculated Leakiness values

Resoln (m)	Cell count	Average cover (%)	Expt. Image Lcalc	Image Lcalc trans-formed	Projected Lcalc		Differences	
					Linear soln.	Cubic soln.	Linear soln.	Cubic soln.
10	589913	71.05	82.97	0.35	152.62	78.29	69.65	-4.69
15	262200	68.72	42.18	0.40	70.07	50.39	27.88	8.20
25	94416	70.55	25.68	0.68	26.84	27.64	1.15	1.95
30	65541	68.93	19.83	0.76	19.20	21.93	-0.64	2.10
40	36920	69.99	15.86	1.07	11.43	14.83	-4.43	-1.03
50	23595	70.91	7.40	0.78	7.72	10.64	0.32	3.24
60	16374	69.51	6.52	1.00	5.64	7.91	-0.88	1.39
70	12029	69.97	7.65	1.59	4.35	6.02	-3.30	-1.63
80	9233	71.48	7.62	2.07	3.49	4.66	-4.14	-2.97
90	7289	71.63	2.98	1.02	2.88	3.65	-0.10	0.66
100	5892	70.77	3.04	1.29	2.43	2.88	-0.61	-0.16
110	4849	71.64	1.80	0.93	2.09	2.29	0.29	0.49
120	4098	71.07	1.74	1.07	1.83	1.84	0.08	0.10
130	3489	71.93	1.23	0.89	1.62	1.50	0.38	0.26
140	2981	70.58	1.12	0.95	1.45	1.23	0.32	0.10
150	2603	72.55	0.79	0.76	1.30	1.03	0.51	0.24
160	2269	70.87	0.69	0.76	1.19	0.88	0.50	0.19
170	2022	71.94	0.56	0.70	1.09	0.78	0.52	0.21
180	1798	71.44	0.77	1.07	1.00	0.71	0.23	-0.06
190	1612	71.58	0.83	1.29	0.92	0.68	0.09	-0.16
200	1461	71.96	0.82	1.41	0.86	0.67	0.04	-0.15
210	1324	71.06	0.57	1.09	0.80	0.68	0.23	0.10
220	1208	71.48	0.75	1.56	0.75	0.71	0.00	-0.04
230	1108	70.99	1.03	2.34	0.71	0.76	-0.33	-0.28
240	1016	71.86	0.48	1.19	0.67	0.82	0.19	0.34
250	942	72.43	0.91	2.43	0.63	0.90	-0.28	-0.01
Avg.		71.07	16.10	1.10	33.85	14.88	17.74	-1.22
Std. Dev.		0.98	40.56	0.54	115.55	33.53	76.06	8.32

Appendix 13. Comparison of experimental and predicted SAVI AAL values

Resoln	Cell count	Experimental AAL	Predicted AAL	Difference (Expt.- Pred.)
10	589913	1.34	2.25	-0.91
15	262200	1.94	2.54	-0.60
25	94416	2.80	3.12	-0.32
30	65541	3.03	3.41	-0.39
40	36920	3.90	4.00	-0.09
50	23595	4.68	4.58	0.10
60	16374	5.68	5.16	0.52
70	12029	6.95	5.75	1.20
80	9233	8.93	6.33	2.60
90	7289	8.01	6.91	1.10
100	5892	7.79	7.49	0.29
110	4849	8.21	8.08	0.13
120	4098	9.62	8.66	0.96
130	3489	10.16	9.24	0.92
140	2981	9.14	9.83	-0.69
150	2603	10.38	10.41	-0.03
160	2269	9.64	10.99	-1.35
170	2022	10.87	11.58	-0.71
180	1798	11.56	12.16	-0.60
190	1612	11.72	12.74	-1.02
200	1461	12.10	13.32	-1.22
210	1324	13.21	13.91	-0.70
220	1208	14.98	14.49	0.49
230	1108	15.92	15.07	0.85
240	1016	14.23	15.66	-1.42
250	942	18.24	16.24	2.00

Appendix 14. Comparison of experimental and predicted STVI AAL values

Resoln (m)	Cell Count	Experimental AAL	Predicted AAL	Difference (Expt.- Pred.)
10	589913	0.58	0.96	-0.39
15	262200	0.83	1.10	-0.27
25	94416	1.21	1.36	-0.15
30	65541	1.30	1.49	-0.19
40	36920	1.69	1.76	-0.07
50	23595	2.08	2.02	0.06
60	16374	2.48	2.29	0.19
70	12029	3.06	2.55	0.50
80	9233	3.96	2.82	1.14
90	7289	3.60	3.08	0.51
100	5892	3.48	3.35	0.13
110	4849	3.70	3.61	0.08
120	4098	4.33	3.88	0.46
130	3489	4.58	4.14	0.44
140	2981	4.12	4.41	-0.29
150	2603	4.69	4.67	0.02
160	2269	4.31	4.94	-0.63
170	2022	4.94	5.20	-0.26
180	1798	5.17	5.47	-0.30
190	1612	5.35	5.73	-0.38
200	1461	5.41	6.00	-0.59
210	1324	5.91	6.26	-0.35
220	1208	6.63	6.53	0.10
230	1108	7.17	6.79	0.37
240	1016	6.55	7.06	-0.51
250	942	8.18	7.32	0.86

Appendix 15. Comparison of experimental and predicted PDrg AAL values

Resolution (m)	Cell count	Average cover (%)	Experimental Leakiness	Experimental AAL	Predicted AAL		Difference (Expt. AAL – Pred. AAL)	
					Linear	Cubic	Linear	Cubic
10	589913	71.06	82.98	1.41	2.54	1.31	-1.14	0.10
15	262200	68.73	42.19	1.61	2.63	1.89	-1.02	-0.28
25	94416	70.56	25.69	2.72	2.79	2.88	-0.07	-0.16
30	65541	68.93	19.83	3.03	2.87	3.29	0.15	-0.26
40	36920	70.00	15.86	4.30	3.04	3.96	1.26	0.34
50	23595	70.91	7.40	3.14	3.21	4.44	-0.07	-1.30
60	16374	69.51	6.52	3.98	3.37	4.77	0.61	-0.78
70	12029	69.98	7.65	6.36	3.54	4.95	2.82	1.41
80	9233	71.49	7.62	8.26	3.70	5.03	4.55	3.23
90	7289	71.63	2.98	4.09	3.87	5.02	0.22	-0.92
100	5892	70.78	3.04	5.17	4.04	4.94	1.13	0.23
110	4849	71.65	1.81	3.73	4.20	4.83	-0.48	-1.10
120	4098	71.07	1.75	4.26	4.37	4.69	-0.11	-0.43
130	3489	71.94	1.24	3.55	4.53	4.57	-0.99	-1.02
140	2981	70.59	1.13	3.79	4.70	4.48	-0.91	-0.69
150	2603	72.56	0.79	3.04	4.87	4.44	-1.83	-1.40
160	2269	70.87	0.69	3.05	5.03	4.49	-1.99	-1.44
170	2022	71.94	0.57	2.81	5.20	4.63	-2.38	-1.82
180	1798	71.45	0.77	4.29	5.36	4.91	-1.08	-0.62
190	1612	71.59	0.83	5.16	5.53	5.34	-0.37	-0.18
200	1461	71.97	0.82	5.62	5.70	5.94	-0.08	-0.32
210	1324	71.06	0.58	4.34	5.86	6.75	-1.52	-2.40
220	1208	71.49	0.76	6.25	6.03	7.77	0.22	-1.52
230	1108	71.00	1.04	9.35	6.19	9.05	3.16	0.30
240	1016	71.86	0.48	4.74	6.36	10.60	-1.62	-5.85
250	942	72.43	0.91	9.69	6.53	12.44	3.17	-2.75
Avg.		71.07	16.10	4.39	4.39	5.11	0.00	-0.72
Std. Dev.		0.98	40.56	2.16	1.28	2.53	1.73	1.55

Appendix 16. Effect of upscaling on percent cover

Resoln	Cover (%)		
	SAVI	STVI	PDrg
10	44.81	56.44	71.06
15	44.68	56.42	68.73
25	44.68	56.41	70.56
30	44.82	56.44	68.93
40	44.61	56.43	70.00
50	44.81	56.46	70.91
60	44.58	56.42	69.51
70	44.84	56.44	69.98
80	44.57	56.42	71.49
90	44.77	56.40	71.63
100	44.58	56.40	70.78
110	44.82	56.44	71.65
120	44.65	56.48	71.07
130	44.86	56.51	71.94
140	44.65	56.45	70.59
150	44.78	56.46	72.56
160	44.50	56.35	70.87
170	44.72	56.46	71.94
180	44.48	56.33	71.45
190	44.90	56.46	71.59
200	44.59	56.44	71.97
210	44.78	56.40	71.06
220	44.71	56.44	71.49
230	44.95	56.54	71.00
240	44.46	56.31	71.86
250	44.82	56.41	72.43
Avg.	44.71	56.43	71.07
Std. Dev.	0.13	0.05	0.98

Appendix 17. Calculated and Adjusted Average Leakiness for 3 types of cover

Resoln	Calculated Leakiness			Adjusted Average Leakiness		
	SAVI	STVI	PDrg	SAVI	STVI	PDrg
10	79.10	33.94	82.98	1.34	0.58	1.41
15	50.82	21.72	42.19	1.94	0.83	1.61
25	26.41	11.39	25.69	2.80	1.21	2.72
30	19.85	8.55	19.83	3.03	1.30	3.03
40	14.42	6.25	15.86	3.90	1.69	4.30
50	11.04	4.91	7.40	4.68	2.08	3.14
60	9.30	4.06	6.52	5.68	2.48	3.98
70	8.36	3.68	7.65	6.95	3.06	6.36
80	8.25	3.66	7.62	8.93	3.96	8.26
90	5.84	2.62	2.98	8.01	3.60	4.09
100	4.59	2.05	3.04	7.79	3.48	5.17
110	3.98	1.79	1.81	8.21	3.70	3.73
120	3.94	1.78	1.75	9.62	4.33	4.26
130	3.55	1.60	1.24	10.16	4.58	3.55
140	2.73	1.23	1.13	9.14	4.12	3.79
150	2.70	1.22	0.79	10.38	4.69	3.04
160	2.19	0.98	0.69	9.64	4.31	3.05
170	2.20	1.00	0.57	10.87	4.94	2.81
180	2.08	0.93	0.77	11.56	5.17	4.29
190	1.89	0.86	0.83	11.72	5.35	5.16
200	1.77	0.79	0.82	12.10	5.41	5.62
210	1.75	0.78	0.58	13.21	5.91	4.34
220	1.81	0.80	0.76	14.98	6.63	6.25
230	1.76	0.79	1.04	15.92	7.17	9.35
240	1.45	0.67	0.48	14.23	6.55	4.74
250	1.72	0.77	0.91	18.24	8.18	9.69
Avg.	16.96	7.30	16.10	8.73	3.91	4.39
Std. Dev.	37.68	16.00	40.56	4.63	2.10	2.16

Appendix 18. Normalised calculated Leakiness values

Resoln	SAVI Lcalc transformed	STVI Lcalc transformed	PDrg Lcalc transformed
10	0.336	0.144	0.352
15	0.485	0.207	0.403
25	0.700	0.302	0.681
30	0.758	0.326	0.757
40	0.977	0.424	1.075
50	1.171	0.520	0.785
60	1.421	0.620	0.997
70	1.739	0.764	1.592
80	2.235	0.991	2.066
90	2.005	0.900	1.024
100	1.948	0.871	1.293
110	2.053	0.925	0.932
120	2.406	1.084	1.066
130	2.543	1.146	0.888
140	2.287	1.030	0.948
150	2.596	1.175	0.760
160	2.413	1.079	0.762
170	2.719	1.236	0.704
180	2.893	1.294	1.073
190	2.934	1.340	1.291
200	3.028	1.353	1.406
210	3.305	1.480	1.087
220	3.749	1.659	1.564
230	3.984	1.793	2.340
240	3.561	1.638	1.187
250	4.564	2.048	2.425
Avg.	2.185	0.979	1.099
Std. Dev.	1.158	0.525	0.540

Appendix 19. Comparison of experimental and projected leakiness values

Resoln	SAVI		STVI		PDrg		
	Lcalc experi-mental	Lcalc projected	Lcalc experi-mental	Lcalc projected	Lcalc experi-mental	Lcalc projected (linear)	Lcalc projected (cubic)
10	79.10	134.88	33.94	57.32	82.98	152.62	78.29
15	50.82	67.73	21.72	28.93	42.19	70.07	50.39
25	26.41	29.98	11.39	12.91	25.69	26.84	27.64
30	19.85	22.77	8.55	9.83	19.83	19.20	21.93
40	14.42	14.99	6.25	6.50	15.86	11.43	14.83
50	11.04	11.00	4.91	4.78	7.40	7.72	10.64
60	9.30	8.61	4.06	3.75	6.52	5.64	7.91
70	8.36	7.04	3.68	3.08	7.65	4.35	6.02
80	8.25	5.94	3.66	2.60	7.62	3.49	4.66
90	5.84	5.12	2.62	2.25	2.98	2.88	3.65
100	4.59	4.50	2.05	1.97	3.04	2.43	2.88
110	3.98	4.01	1.79	1.76	1.81	2.09	2.29
120	3.94	3.61	1.78	1.59	1.75	1.83	1.84
130	3.55	3.28	1.60	1.44	1.24	1.62	1.50
140	2.73	3.01	1.23	1.32	1.13	1.45	1.23
150	2.70	2.78	1.22	1.22	0.79	1.30	1.03
160	2.19	2.58	0.98	1.14	0.69	1.19	0.88
170	2.20	2.40	1.00	1.06	0.57	1.09	0.78
180	2.08	2.25	0.93	0.99	0.77	1.00	0.71
190	1.89	2.12	0.86	0.93	0.83	0.92	0.68
200	1.77	2.00	0.79	0.88	0.82	0.86	0.67
210	1.75	1.89	0.78	0.84	0.58	0.80	0.68
220	1.81	1.80	0.80	0.79	0.76	0.75	0.71
230	1.76	1.71	0.79	0.75	1.04	0.71	0.76
240	1.45	1.63	0.67	0.72	0.48	0.67	0.82
250	1.72	1.56	0.77	0.69	0.91	0.63	0.90
Avg.	16.96	30.32	7.30	12.90	16.10	33.85	14.88
Std. Dev	37.68	92.08	16.00	38.89	40.56	115.55	33.53

Appendix 20. Fine upscale cover and leakiness values

Resoln (m)	Avg. cover	Expt. Lcalc	Proj. Lcalc	Differences
SAVI				
10	44.81	79.10	134.88	55.78
15	44.68	50.82	67.73	16.91
25	44.68	26.41	29.98	3.57
30	44.82	19.85	22.77	2.92
STVI				
10	56.44	33.94	57.32	23.38
15	56.42	21.72	28.93	7.21
25	56.41	11.39	12.91	1.52
30	56.44	8.55	9.83	1.28
PDrg cubic				
10	71.06	82.98	78.29	-4.69
15	68.73	42.19	50.39	8.20
25	70.56	25.69	27.64	1.95
30	68.93	19.83	21.93	2.10
PDrg linear				
10	71.06	82.98	152.62	69.65
15	68.73	42.19	70.07	27.88
25	70.56	25.69	26.84	1.15
30	68.93	19.83	19.20	-0.64

Appendix 21. Leakiness and semivariance for upscaled SAVI and STVI

Resolution (m)	Adjusted Average Leakiness		Semivariance	
	SAVI	STVI	SAVI	STVI
10	2.25	0.96	16.2	18.1
15	2.54	1.10	16.1	19.1
25	3.12	1.36	16.1	21.3
30	3.41	1.49	16.2	22.5
40	4.00	1.76	16.8	25.3
50	4.58	2.02	17.8	28.5
60	5.16	2.29	19.2	32.1
70	5.75	2.55	21.0	36.1
80	6.33	2.82	23.2	40.5
90	6.91	3.08	25.8	45.3
100	7.49	3.35	28.8	50.5
110	8.08	3.61	32.2	56.1
120	8.66	3.88	36.0	62.1
130	9.24	4.14	40.2	68.5
140	9.83	4.41	44.8	75.3
150	10.41	4.67	49.8	82.5
160	10.99	4.94	55.2	90.1
170	11.58	5.20	61.0	98.1
180	12.16	5.47	67.2	106.5
190	12.74	5.73	73.7	115.3
200	13.32	6.00	80.7	124.5
210	13.91	6.26	88.1	134.1
220	14.49	6.53	95.9	144.1
230	15.07	6.79	104.1	154.5
240	15.66	7.06	112.7	165.3
250	16.24	7.32	121.7	176.5

Appendix 22. Leakiness and semivariance for upscaled PDrg images

Resolution (m)	Adjusted Average Leakiness	Semivariance
10	1.31	224.54
15	1.89	234.27
25	2.88	250.89
30	3.29	257.86
40	3.96	269.36
50	4.44	277.90
60	4.77	283.84
70	4.95	287.54
80	5.03	289.36
90	5.02	289.66
100	4.94	288.80
110	4.83	287.14
120	4.69	285.04
130	4.57	282.86
140	4.48	280.96
150	4.44	279.70
160	4.49	279.44
170	4.63	280.54
180	4.91	283.36
190	5.34	288.26
200	5.94	295.60
210	6.75	305.74
220	7.77	319.04
230	9.05	335.86
240	10.60	356.56
250	12.44	381.50

Appendix 23. Native DEM semivariance matrix

Lag Interval	Resolution (m)											
	0	5	25	50	75	100	125	150	175	200	225	250
1	0.20	0.23	-0.23	-0.23	-0.23	-0.23	-0.23	-0.23	-0.23	-0.23	-0.23	-0.23
5	1.29	0.31	3.60	8.49	13.38	18.27	23.16	28.05	32.94	37.83	42.72	47.61
10	1.99	0.36	9.77	21.54	33.30	45.06	56.82	68.59	80.35	92.11	103.87	115.64
15	3.28	0.84	17.29	37.85	58.42	78.98	99.55	120.11	140.68	161.24	181.81	202.37
20	4.99	1.08	25.39	55.78	86.16	116.55	146.93	177.32	207.70	238.09	268.47	298.86
25	3.54	3.60	32.13	67.79	103.45	139.11	174.78	210.44	246.10	281.76	317.43	353.09
30	6.58	2.93	40.95	88.48	136.01	183.54	231.07	278.60	326.13	373.66	421.19	468.72

Appendix 24. Reconstructed DEM semivariance matrix

Lag Interval	Resolution (m)							
	1	5	25	50	100	150	200	250
5	-0.94	0.15	5.60	12.41	26.03	39.65	53.27	66.89
10	-1.45	0.88	12.56	27.15	56.34	85.53	114.72	143.91
15	-4.57	-0.66	18.90	43.35	92.26	141.16	190.07	238.97
20	-5.93	-0.50	26.67	60.63	128.56	196.48	264.41	332.33
25	-3.90	2.67	35.55	76.64	158.82	241.01	323.19	405.38
30	-2.19	5.54	44.20	92.53	189.18	285.83	382.48	479.13
35	-6.15	3.60	52.36	113.31	235.21	357.11	479.01	600.91

Appendix 25. LC Settings and Batch Settings

Settings	
CoverToLIFunction	perennial tall tussock grasses
Name	Batch Project
OnPitDetection	Warning
OutputFile	sc2_pdrg_topo_netincr_nd_nonetincr_Lmax200.out
OutputPath	M:\2 4 Zone correln data\3 Topo zones\3 Analysis\PDrg\LI results

DEM settings

File Details	
Errors	
Filename	M:\2 4 Zone correln data\3 Topo zones\2 Rasters\PDrg\1 Native value\sc2_box_dem_25m.hdr
Header	LI.MapHeader
Bands	1
BandStorageType	Sequential
BitOrder	LSBFirst
Bits	32
Cellsize	25
Columns	520
DataFile	M:\2 4 Zone correln data\3 Topo zones\2 Rasters\PDrg\1 Native value\sc2_box_dem_25m.FLT
DataType	FloatingPoint32Bit
HeaderSource	ESRI_FLOAT
NullCellValue	-9999
Offset	0
Rows	520
ULX	402080
ULY	7764880
MapType	DEM
Modified	25/02/2013 10:11 PM
Sorted	True
Settings	
ID	PDrg_topo
Lmin	0
LossConstC	-0.065
Name	sc2_box_dem_25m
Power	3
UseBand	1

Mask settings

Settings	
band	1
bandLabel	
ID	sc2_b
Lmax	200
maskLabel	
maskValue	1
Name	sc2_box_1catch_25m

Cover settings

Settings	
band	1
bandLabel	
ID	sc2_b
Name	sc2_box_PDrg_25m_resc
NullPixelCover	0